THE GEOLOGICAL EVOLUTION OF TIBET

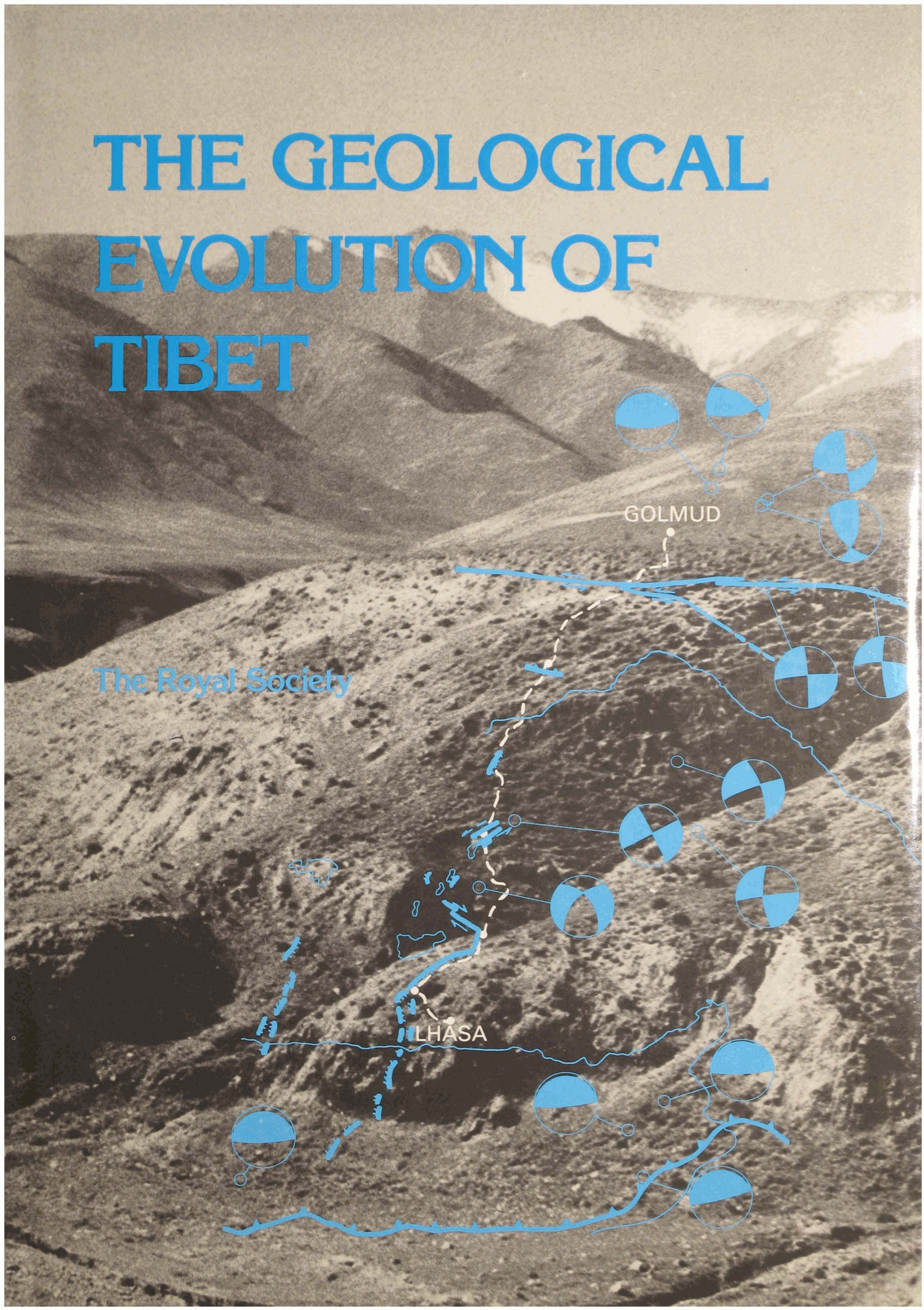

The Royal Society

THE GEOLOGICAL EVOLUTION OF TIBET

The Tibetan Plateau is a region that, because of its remoteness, elevation and mystery, has excited adventurers and explorers for centuries. It has also fascinated Earth scientists, who have regarded it as the type example of collision tectonics: collision between the Indian and Eurasian continents. This book presents the results of a two-month Geotraverse made in 1985 through cooperation between Academia Sinica and the Royal Society. Data from a wide range of geological methods are presented, along with a geological map of the region traversed. The final chapter gives our conclusions about the geological evolution of the plateau by successive accretion of terranes to the Eurasian continent, the collision of the Indian and Eurasian continents, the doubling in thickness of the Tibetan crust and the dramatic Recent uplift of the plateau.

The photograph on the cover was taken by John Dewey, and shows fluvial incision on the northern flank of the southern Kunlun Mountains. The Kunlun Mountains, forming the northern ranges of the Tibetan Plateau, have undergone strong uplift in the past 5 Ma, resulting in deeply eroded river valleys with terraces perched high on valley sides. The superimposed map, from the paper by Bill Kidd and Peter Molnar, shows the main road from Lhasa to Golmud, with rivers, faults and lower-hemisphere projections of fault plane solutions of earthquakes.

ISBN 0 85403 362 9

THE GEOLOGICAL EVOLUTION OF TIBET

REPORT OF
THE 1985 ROYAL SOCIETY – ACADEMIA SINICA
GEOTRAVERSE OF
THE QINGHAI – XIZANG PLATEAU
LED BY
CHANG CHENGFA,
ROBERT M. SHACKLETON, F.R.S.,
JOHN F. DEWEY, F.R.S., AND YIN JIXIANG

LONDON
THE ROYAL SOCIETY
1988

Printed in Great Britain for the Royal Society
by the
University Press, Cambridge

ISBN 0 85403 362 9
First published in *Philosophical Transactions of the Royal Society of London*,
series A, volume 327 (no. 1594), pages 1–413

The text paper used in this publication meets the minimum requirements of American National Standard for Information Sciences–Permanence of Paper for Printed Library Materials, ANSI Z39.48-1984.

British Library Cataloguing in Publication Data

Royal Society – Academia Sinica
Geotraverse of the Qinghai–Xizang Plateau
(1985).
The geological evolution of Tibet.
1. Tibet. Geological features
I. Title
555.1'5

ISBN 0-85403-362-9

Published by the Royal Society
6 Carlton House Terrace, London SW1Y 5AG

CONTENTS

[Sixteen plates and one pullout; two microfiches and map in pockets inside back cover]

PREFACE

The Tibetan Plateau is a unique feature of the Earth's surface. Its elevation, 5 km above sea level, and a crust twice the normal thickness, have long been recognized as resulting from the collision of the Indian and Eurasian continents. The region is regarded as the prime example of collision tectonics. However, because Tibet was for long virtually inaccessible to geologists from the rest of the world, the mechanism by which the Plateau evolved and by which the crust was doubled in thickness, remained speculative.

During the past two decades, Chinese geologists have explored and systematically mapped much of this vast and largely uninhabited region; Academia Sinica mounted a series of geological expeditions. The results of this and other work were presented at an international symposium on the Qinghai–Xizang (Tibet) Plateau in Beijing in 1980 and demonstrated on a traverse through southern Tibet from Lhasa to Kathmandu.

The excitement generated by this introduction to the geology of Tibet led Professor Gansser, Professor Molnar and me to the idea of a Geotraverse, based on the newly completed road from Lhasa to Golmud across central and northern Tibet. Chinese colleagues were enthusiastic. Because the Royal Society and Academia Sinica had an agreement for scientific cooperation, I submitted our proposal to the Society and an agreement was eventually signed.

Chinese geologists chosen for the project prepared for the Geotraverse by making detailed geological strip maps of the region to be covered and locating significant outcrops. In June 1985, the geologists, ten from the Royal Society side and fifteen from Academia Sinica, assembled in Lhasa. The next two months were spent working across the Plateau.

The Chinese took complete responsibility for the logistics. A fleet of lorries and jeeps, loaded with supplies, was driven into Tibet across the mountains and gorges from Chengdu. After acclimatization in Lhasa, and work from there, we set off northwards towards Golmud. Along the road, we stayed in military posts and, off it, in tents. Access to exposures was by jeep as far as they could go (heavy rains had made much of the area a morass) then on foot. Rarely, we used horses and yaks. Most of the food had to be brought in from outside.

We worked in small specialist groups, so understanding and friendships developed quickly. The thorough preparation by the Chinese geologists meant that little time was wasted.

The large collections of rocks and fossils were divided between ourselves and our Chinese colleagues for analysis and identification. Work on all this material is not yet complete; the results so far obtained are presented in this volume. The conclusions were discussed at an exceptionally successful conference in Beijing in 1986, followed by another geological traverse from Lhasa to Kathmandu.

The 1985 Geotraverse was inevitably only a reconnaissance. Many important unsolved problems remain. We hope that this is only the start of a collaboration between ourselves and our Chinese colleagues, which has led already not only to the results presented here but also to close and lasting friendships.

We acknowledge the wise and experienced leadership of Professor Chang Chengfa of the Chinese team, the linguistic and organizational skills of Freddie Sun Yiyin and the remarkable feats of the drivers of the jeeps. We thank Dr Peigi Wallace for editing the volume. Finally, we thank the Royal Society and Academia Sinica for enabling us to carry out this project.

April 1988 ROBERT SHACKLETON

Note

In reading the papers in this volume, reference should be made to the coloured geological map (1:125000) in the pocket at the end of the volume, and to the microfiche copies of the 1:100000 maps on which all localities mentioned in the text are plotted, together with structural and other field data. Copies of these maps, as well as satellite imagery and other materials, will be housed in the British Museum of Natural History, where they are available for study. Any type specimens of fossils will be preserved in Nanjing; duplicates of many of them will be housed in the B.M.(N.H.).

Meanings of a few commonly used Chinese and Tibetan words may be useful: Co, Tso (Tibetan), Hu (Chinese) = lake; Jiang = large river; Qu, He = river; Heyan = source of river; Datan = valley; -gou = valley; -quan = spring (as in Wenquan: hot spring, Budongquan: not-quite-frozen spring); Shan = mountains; Tagh = mountains; Tsangpo = Zangbo; Jinsha = Yangtze = Yangzi.

Phil. Trans. R. Soc. Lond. A **327**, 5–52 (1988)

Printed in Great Britain

The Tibetan plateau: regional stratigraphic context and previous work

By Yin Jixiang[1], Xu Juntao[2], Liu Chengjie[1] and Li Huan[1]

[1] *Institute of Geology, Academia Sinica, P.O. Box* 634, *Beijing, People's Republic of China*

[2] *Nanjing Institute of Geology & Palaeontology, Academia Sinica, Nanjing, People's Republic of China*

[One pullout]

A preliminary stratigraphic subdivision and correlation along the Qinghai–Xizang (Tibet) highway from Lhasa to Golmud and its adjacent areas is presented in this paper. The data used here are mainly observations on the 1985 Royal Society–Academia Sinica Geotraverse, together with published and unpublished accounts.

1. Introduction

Investigation of the stratigraphy along the Qinghai–Xizang (Tibet) highway from Golmud to Lhasa and its adjacent area started in the early 1950s. Field work in such a rugged and elevated region is extremely difficult, hence the level of understanding of the stratigraphy is obviously not comparable to that of other regions of China. This paper presents a preliminary stratigraphic subdivision and correlation along the Qinghai–Xizang (Tibet) highway from Lhasa to Golmud and its adjacent areas, as shown in the pullout (figure 23).

The data used here are mainly observations on the 1985 Royal Society–Academia Sinica Geotraverse, together with published and unpublished accounts. Some published and unpublished data from outside the area surveyed are briefly introduced where necessary. Unpublished data come from the following sources.

(1) The Bureau of Geology and Mineral Resources of Qinghai Province, 1981; Report on the Survey of Regional Geology, attached to the Geological Map of Qinghai Province (scale 1:200,000), People's Republic of China: Golmud City Sheet, J-46-(35); Naij Tal Sheet, I-46-(5); Zhidoi Sheet, I-46-(24); *ibid.* 1982; Aikengdeleisite Sheet, I-47-(1); Zadoi Sheet, I-46-(30); *ibid.* 1983; Dongwenquan Sheet, I-46-(6); Shanglaxiu Sheet, I-47-(25). The positions of these seven sheets and of the traverse routes are shown in figure 1.

(2) Explanatory notes to the Geological Map of Qinghai Province (scale 1:1,000,000) (Zhang Qizhen & Zhang Yifu 1981).

Fossil locality numbers, e.g. B60, refer to Smith & Xu, this volume, Appendix, to which reference should be made for faunal lists.

2. Stratigraphy

Three major provinces can be recognized along the Geotraverse route: from north to south the Kunlun Terrane, the Qiangtang Terrane and the Lhasa Terrane. Figure 2 is a sketch map of the geology of the northern part of the Kunlun Terrane. For an alternative interpretation of the geology of this and other areas, see Leeder *et al.* (this volume) and the map of the Geotraverse compiled by Kidd *et al.* (this volume, Map, in pocket).

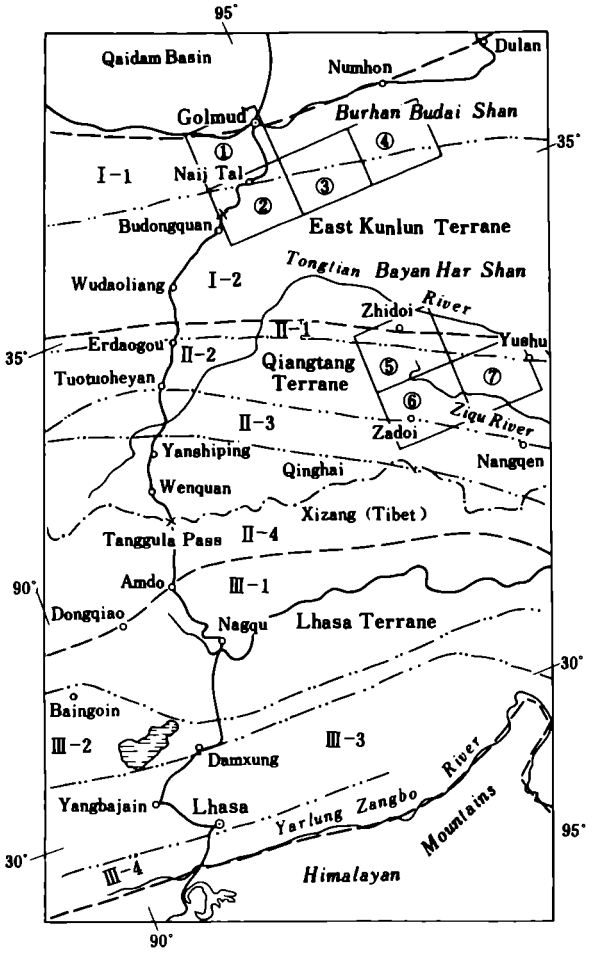

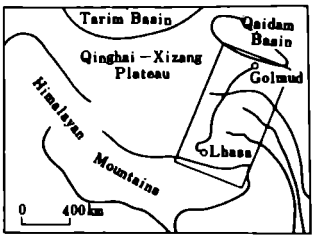

I. Stratigraphical Province of Kunlun: I-1, Burhan Budai sub-Region; I-2, Bayan Har sub-Region. II. Stratigraphical Province of Qiangtang: II-1, Zhidoi-Yushu sub-Region; II-2, Tuotuoheyan-Ziqu sub-Region; II-3, Kaixinling-Nangqen sub-Region; II-4, Tanggula Pass sub-Region. III. Stratigraphical Province of Lhasa: III-1, Dongqiao–Nagqu sub-Region; III-2, Baingoin-Nam Co sub-Region; III-3, Doilungdeqen-Lhunzhub sub-Region; III-4, Sangri sub-Region.

FIGURE 1. Stratigraphical provinces along the Qinghai–Xizang (Tibet) highway from Lhasa to Golmud and adjacent areas. 1–7 indicate the areas referred to in the unpublished reports relevant to this paper: 1. Golmud City Sheet, J-46-(35); 2. Naij Tal Sheet I-46-(5); 3. Dongwenquan Sheet I-46-(6); 4. Aikengdeleisite Sheet I-47-(1); 5. Zhidoi Sheet I-46-(24); 6. Zadoi Sheet I-46-(30); 7. Shanglaxiu Sheet I-47-(25).

3. Late Precambrian and Cambro–Sinian

The main development of supposed late Precambrian metamorphic rocks along the Geotraverse is in the Golmud–Naij Tal district in the Burhan Budai Mountains (figure 1). Sporadic occurrences of metamorphosed rocks here referred to the Cambro–Sinian are exposed in the southwestern Nyainqentanglha Mountains and south of Amdo (both in the Lhasa Terrane).

In the northern Burhan Budai Mountains, the lower unit, the Jinshuikou Group, is composed of medium-grade metamorphic rocks. The upper part, the Binggou Group, consists of medium to low-grade metamorphic rocks. They can be correlated with basement strata in the area of the Qaidam Basin and the Altun Mountains (Wang Yunshan & Chen Jiniang 1984). In the Daobangou Valley, 20 km south of Golmud, an incomplete section of the Binggou Group is unconformably overlain by Upper Devonian basal conglomerates; it is at least 1800 m thick. The lower part consists of grey and darkish-purple pebbly lithic greywackes, sericite-schists and phyllites with subordinate marbles, while the upper part consists mainly of laminated marbles, brecciated dolomitic marbles and dolomites with subordinate phyllites. The uppermost part of

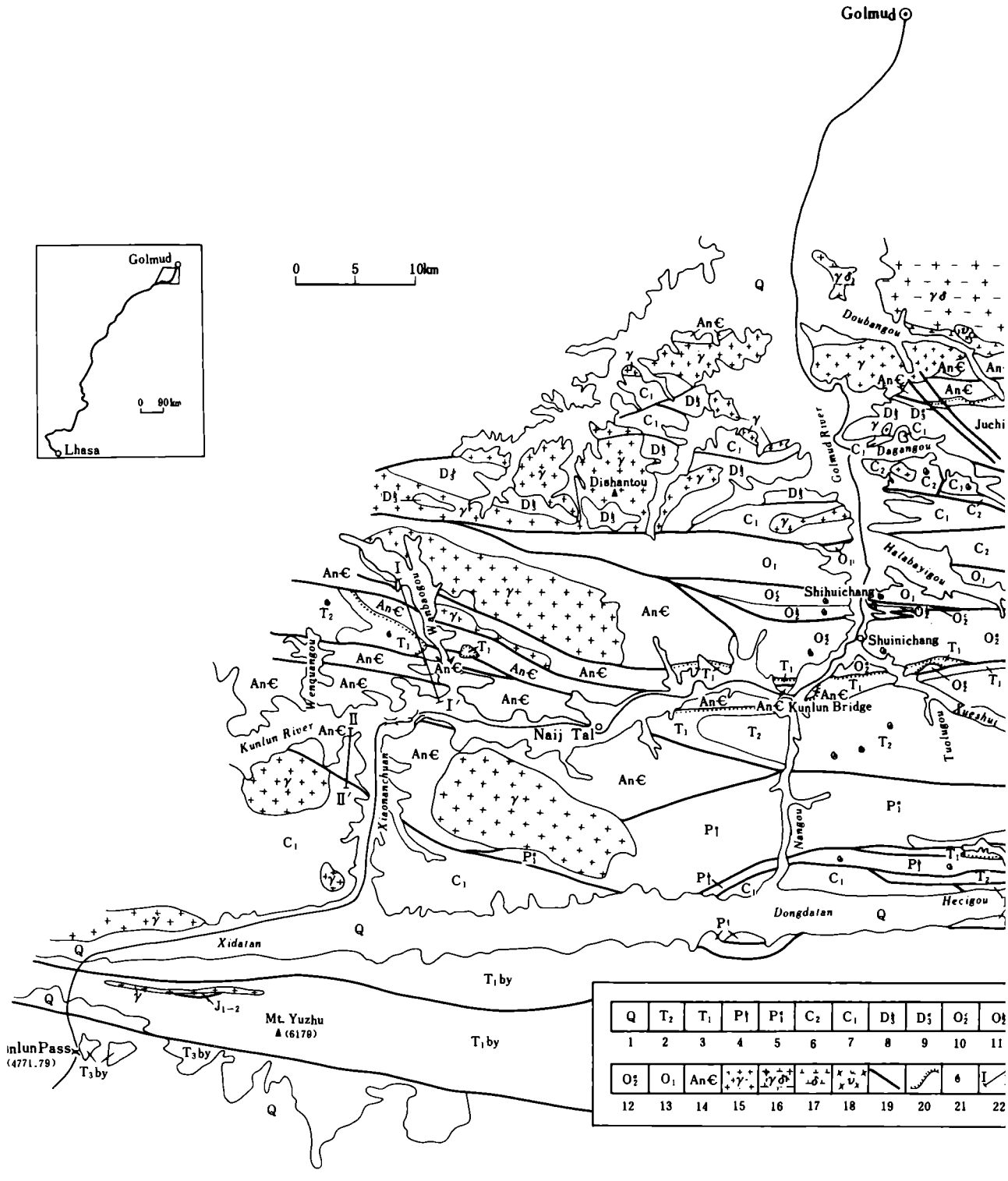

FIGURE 2. A sketch map of the geology of the Golmud–Naij Tal district showing the stratigraphy (modified from Golmud City Sheet and Naij Tal Sheet). 1. Quaternary (Q); 2. Naocangjianggou Formation (T_2); 3. Hongshuichuan Formation (T_1); 4. Carbonate Formation (P_1^b); 5. Clastic Formation (P_1^a); 6. Diaosu Formation (C_2^1), Sijiaoyanggou Formation (C_2^2); 7. Dagangou Formation (C_1); 8. Upper Member (Volcanics Member) of Juchishan Formation (D_3^b); 9. Lower Member (Clastics Member) of Juchishan Formation (D_3^a); 10. 'Fluxoturbidite Formation' (O_2^c); 11. Shihuichang Formation (O_2^b); 12. Shuinichang Formation (O_2^a); 13. Halabayigou Formation (O_1); 14. Binggou Group, Wanbaogou Group (An€); 15. Granite; 16. Granodiorite; 17. Diorite; 18. Gabbro; 19. Fault; 20. Unconformity; 21. Fossil localities; 22. Positions of sections.

the Group is intruded by granites. Stromatolites found nearby to the east suggest that the Binggou Group may be late Precambrian in age.

(*a*) *Wanbaogou Group*

In the southern Burhan Budai Mountains, possible late Precambrian belonging to the Wanbaogou Group is only locally exposed in the Naij Tal district. Its stratigraphy, age and correlation are all debatable because of the structural complexity and lack of fossil evidence in the type section in Wanbaogou Valley, 15 km NW of Naij Tal (Zhu Zhizhi *et al.* 1985; Li Guangcen & Lin Baoyu 1982). From our observations of the type section (figure 3 I–I′) and the principal reference section in Xiaonanchuan 20 km southwest of Naij Tal (figure 3 II–II′), the Wanbaogou Group is preliminarily divided into five formations in descending order as follows:

Fault

5. Clastic Formation (more than 1615 m in thickness)
4. Carbonate Formation (more than 330 m)
3. Green Schist Formation (235 m)
2. Volcanic Formation (more than 400 m)
1. Haematite-bearing Clastic Formation (more than 250 m)

Fault

(i) *Haematite-bearing Clastic Formation*

This formation is exposed only locally in the central Wanbaogou Valley. Its base is truncated by faulting; the topmost grey-white laminated marbles are conformably overlain by the Volcanic Formation. It consists mainly of phyllitic slates alternating with thin-bedded or lenticular dark grey marbles, greywackes and subordinate interbedded haematite-bearing clastics in the upper part. The haematite-bearing clastics include, in ascending order, feldspar-rich lithic greywackes, reddish-grey impure siliceous rocks, banded haematite-bearing quartzites, banded oolitic haematite units 3–5 cm in thickness, silty slates and red, silicified, dolomitic crystalline limestones as well as banded haematite-bearing calcite–quartz schists.

(ii) *Volcanic Formation*

In the Naij Tal district, the Volcanic Formation is repeated by folding and faulting. Dark grey basic volcanics and subordinate andesites dominate the lower part. In Xiaonanchuan (figure 3 II–II′), the formation has a conformable upper contact with the Green Schist Formation and the basal part is obscured by Quaternary deposits.

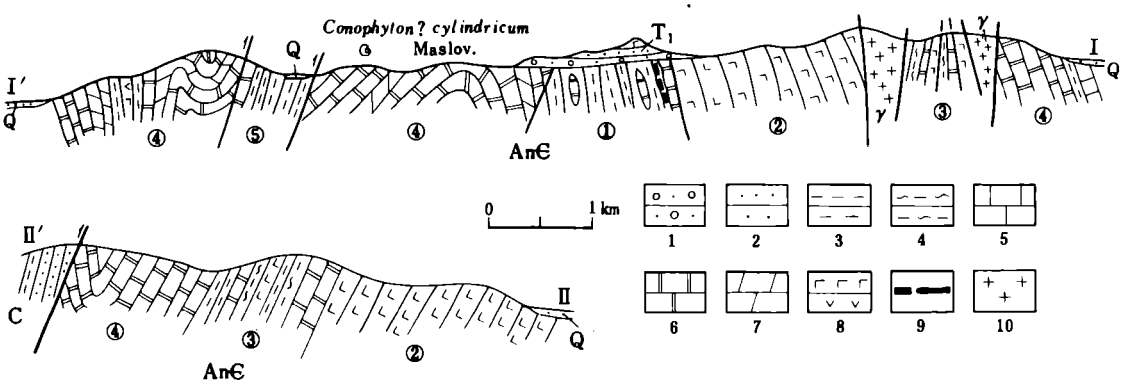

FIGURE 3. A section of the Wanbaogou Group in Wanbaogou, Xiaonanchuan, Naij Tal District and Golmud County (I–I′ Wanbaogou section, II–II′ Xiaonchuan section as shown in figure 2). 1. Conglomerate; 2. Sandstone; 3. Slate; 4. Green Schist; 5. Limestone; 6. Marble; 7. Dolomite; 8. Upper Basic volcanic rocks, Lower: Andesite; 9. Hematite; 10. Granite.

(iii) *Green Schist Formation*

The formation is well exposed in the Xiaonanchuan section and consists of grey-white laminated marbles, silicified marbles and ferruginous dolomitic marbles in the lower 80 m; grey-green laminated chlorite–quartz–schists and dark green actinolite–epidote–schists intercalated with basic volcanics in the middle 140 m; grey-green slate and subordinate laminated marbles form the upper 15 m.

(iv) *Carbonate Formation*

In Wanbaogou, the formation consists mainly of grey-white silicified marbles, calcareous dolomites, silicified dolomitic marbles and calcareous pisolitic micritic dolomites intercalated with subordinate quartzites. The basal and upper contacts are faulted. In the Xiaonanchuan, the top of the formation is overthrust by grey sandstones and slates of Carboniferous age, whereas the basal part is conformable on the Green Schist Formation.

(v) *Clastic Formation*

The lower and middle parts of the formation in Wanbaogou consist mainly of arenaceous slates intercalated with feldspar-rich lithic greywacke. The upper 30 m comprise dark grey thin cherts interbedded with siltstones and silicified marbles alternating with dark lenticular cherts and banded chert-bearing marbles as well as marbles with sparse, angular pebbles up to 40 cm in diameter of dark, yellowish pink and brown crystalline limestone. These represent debris flow deposits. The top and base are truncated by faulting.

The stromatolites *Conophyton ? cylindricum* Maslov, *Conophyton* cf. *miloradovici* Raaben and *Conophyton* sp. have previously been recorded from the Carbonate Formation in the Wanbaogou section (Zhu Zhizhi *et al.* 1985), who referred the Group to the late Precambrian. Similar fossils were also found in the same formation east of the Xiaonanchuan and north of Naij Tal, and suggest that the Wanbaogou Group may be roughly correlated with the Binggou Group. See discussion on the age of these beds, however, in Smith & Xu (this volume).

(*b*) *Nyainqentanglha Group*

A suite of paragneisses (the Nyainqentanglha Group) is best exposed in the southwestern Nyainqentanglha Shan. It is composed mainly of coarse-grained porphyritic–mica–gneiss and garnet–biotite granitic gneiss with subordinate amphibolite or hornblendite, reaching amphibolite facies (Li Pu 1955), locally decreasing to green schist facies. The age of the latest metamorphism of the Group, determined by whole rock Rb–Sr method, is 40–50 Ma, while the inherited age of zircon, determined by U–Pb method, is 1200–2000 Ma (Xu Ronghua, pers. comm.). It is assumed that the age of the main part of the Nyainqentanglha Group is Precambrian or, though with no geochronological evidence, Cambro–Sinian; the possibility of a part being younger cannot be ruled out (see Harris, Xu, Lewis, Hawkesworth & Zhang, this volume).

(*c*) *Amdo Schists*

A suite of thick meta-sediments, informally named the Amdo Schists, outcrops for 40 km along the traverse route between Amdo and Nagqu. The zircon age of metamorphosed granodiorites intruded into this Schist, determined by U–Pb method, is 531^{+5}_{-6} Ma (Xu Ronghua *et al.* 1985). This magmatism is possibly comparable with the Pan-African Event in Africa and Arabia (Gass 1982).

4. Ordovician

The Ordovician, seen only around Naij Tal in the Kunlun Shan, was originally divided into two formations, the Shuinichang Formation (lower Upper Ordovician) and the Shihuichang Formation (upper Upper Ordovician) by Li Guangcen & Lin Baoyu (1982). New fossil evidence and structural interpretations lead us to propose the following revised subdivision (figure 4):

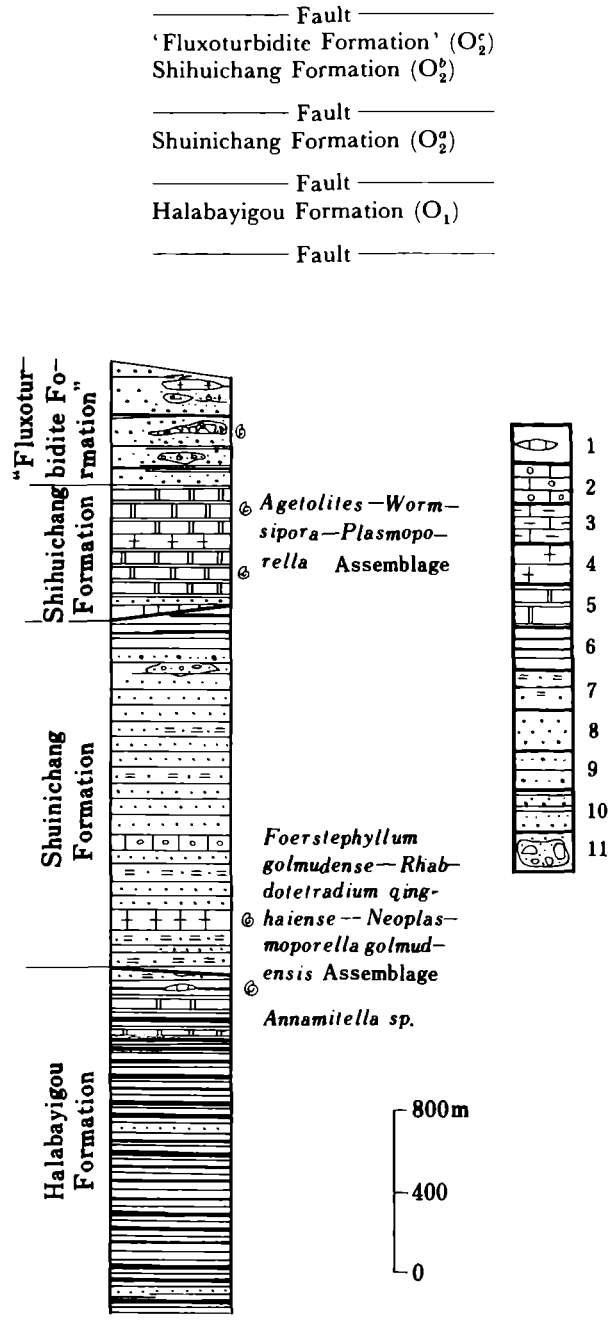

Figure 4. Generalized columns of the Ordovician in the Naij Tal district, Golmud County. 1. Lenticular limestone; 2. Oolitic limestone; 3. Argillaceous limestone; 4. Crystalline limestone; 5. Marble; 6. Slate; 7. Phyllite; 8. Graywacke, sandstone; 9. Pebbly sandstone; 10. Sandy turbidite; 11. Fluxoturbidite.

(i) *Halabayigou Formation* (O_1)

In the type section, situated on the eastern bank of the Golmud River north of Shihuichang, the main part of the formation is dominated by a monotonous flyschoid succession of grey slates alternating with thin-bedded sandstones. The upper part (about 150 m) is composed of phyllites and slates intercalated with subordinate dark limestones, oolitic limestones and marls as well as schistose brecciated marbles. The lower contact of the formation is not exposed and the upper contact is faulted. Li Guangcen & Lin Baoyu (1982) considered the Halabayigou Formation to be Silurian in age. However, one poor fragment of trilobite from the dark limestones at the top of the Formation indicates a possible early Ordovician age for these beds (loc. B100).

(ii) *Shuinichang Formation* (O_2^a)

The formation is best exposed along both banks of the Golmud River between Kunlun Bridge and Shihuichang; it is faulted against the Shihuichang Formation to the north and the Triassic or older sequences to the south (figure 2). The lower part of the formation is dominated by greywackes and phyllites intercalated with subordinate oolitic marbles, laminated marbles and dark grey crystalline limestones, they yield abundant corals (the '*Foerstephyllum golmudense* – *Rhabdotetradium qinghaiense* – *Neoplasmoporella golmudense* Assemblage'), dated as early late Ordovician (Li Guangcen & Lin Baoyu 1982; Lin Baoyu 1985). The middle part consists mainly of grey schistose feldspar-rich lithic greywackes and meta-lithic quartz greywackes intercalated with subordinate phyllites; the upper part consists of pebbly grits and feldspar-rich lithic greywackes interbedded in the topmost sequence with slates and schistose fluxoturbidites (50 m).

(iii) *Shihuichang Formation* (O_2^b)

This formation outcrops to the west of Shuhuichang and near the western bank of the Golmud River where it is mainly composed of laminated marbles and bioclastic crystallised limestones; some pyrite-bearing lithic quartz sandstones, arenaceous shales and silicified limestones are interbedded in the lower part. The contact with the overlying 'Fluxoturbidite Formation' in the north is conformable.

The limestones yield corals, bivalves and crinoids, some of which are poorly preserved indicating that they are not *in situ* fossils. The corals have affinities with the '*Agetolites–Wormispora–Plasmoporella* Assemblage'. Their age is late late Ordovician (Li Guangcen & Lin Baoyu 1982; Lin Baoyu 1985).

(iv) '*Fluxoturbidite Formation*' (O_2^c)

Along the western bank of the Golmud River, a suite of clastics with subordinate submarine mass-flow deposits, informally named the 'Fluxoturbidite Formation', rests conformably on the Shihuichang Formation. The lower sandy turbidites are intercalated with pebbly feldspar-rich lithic greywackes and calcareous shales with fragments of crinoid stems; the middle of the formation consists of fluxoturbidites and sandy turbidites. Two layers of thin-bedded crystallised limestone in the lower part yield a few corals and conodonts (B102). The top is faulted against Carboniferous strata to the north.

For a detailed sedimentalogical and palaeoenvironmental description of the Ordovician, see Leeder *et al.* (this volume).

Generally speaking, the Ordovician in the Naij Tal district has undergone low-grade metamorphism and strong deformation and has few fossil-bearing horizons. No section showing the complete sequence through the Ordovician has yet been established. The fossiliferous Upper Ordovician observed in this area may be correlated in lithology and fossils with the Tieshidasi Group in the Qimantage Mountains southwest of the Qaidam Basin and the Tanjianshan Group of the northern part of the Qaidam Basin (Xu Xian *et al.* 1982).

5. Silurian

No proven Silurian is found in the eastern Kunlun Terrane or the Qiangtang Terrane except in the 'Yidun–Zhongdian district' in the eastern part of the Qiangtang Terrane, where Middle and Upper Silurian strata are present. Outcrops of Silurian strata are, however, widespread in the Xainza district west of Nam Co in the Lhasa Terrane. The lower limestones yield corals, nautiloids, gastropods, stromatoporoids, brachiopods, bryozoa and crinoid stems of early and mid Silurian age. The upper part is mainly composed of sericite–chlorite phyllites alternating with quartzites. It is unfossiliferous but may be late Silurian in age as it rests conformably on the underlying Lower and Middle Silurian.

In the Xainza district, about 150 km SSW of Dongqiao, the Lower Silurian is represented by graptolitic shale and the Middle and Upper Silurian mainly by carbonates bearing cephalopods, corals and conodonts. It rests conformably on an Ordovician sequence and is disconformably overlain by the Devonian (Lin Baoyu 1983*a*; Xu Hankui *et al.* 1981).

6. Devonian

Devonian deposits along the Geotraverse route may be divided into two facies: terrestrial sediments cropping out at Daobangou 20 km south of Golmud in the Kunlun Terrane and marine deposits sporadically found to the west of Dongqiao in the northern part of the Lhasa Terrane. Only the former was observed.

(*a*) *Juchishan Formation*

Unmetamorphosed terrestrial clastic and volcanic rocks seen at Daobangou and Dishantou along the eastern and western banks of the Golmud River are here designated the Juchishan Formation after the Juchi Mountains south of Daobangou. The lower part of the Formation comprises basal conglomerate, slate, arenaceous mudstone, lithic feldspar-rich sandstone with subordinate siltstone intercalated with amygdaloidal andesite and meta-trachybasalt; the upper part is dominantly andesite intercalated with basalt and dacite, followed by purple massive rhyolite or perlitic rhyolite with subordinate sandstone, volcanic breccia and tuff. The basal conglomerate of the formation in the Daobangou section rests unconformably on the Precambrian Binggou Group while the volcanic rocks of the upper part (see Pearce & Mei, this volume) pass disconformably upward into the coarse clastic rocks or volcanic rocks of the Lower Carboniferous. The Juchishan Formation, whose age is inferred to be late Devonian (figure 5), can be roughly correlated, in sequence and lithology, with the Harzha Group in the Qimantage Mountains northwest of Golmud (Xu Xian *et al.* 1982).

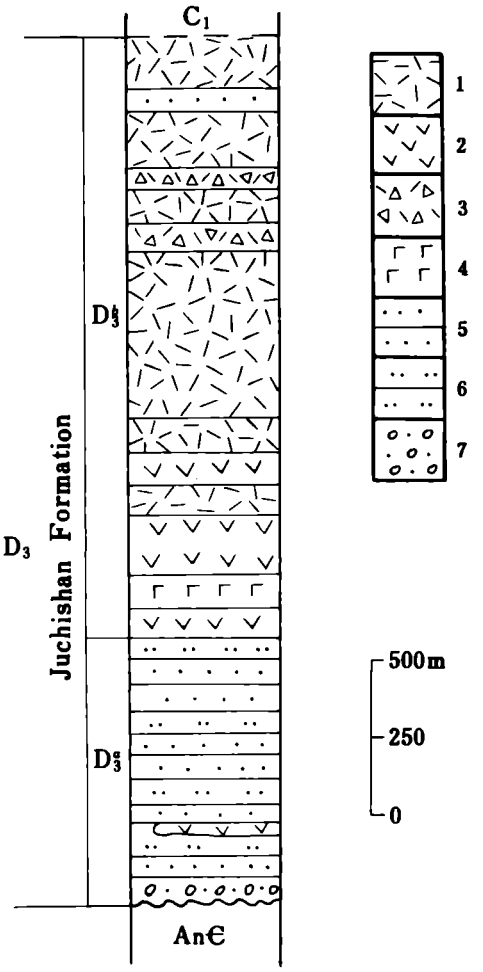

FIGURE 5. Columnar section of the Juchishan Formation at Juchi Mountain, south of Daobangou, Golmud County. 1. Rhyolite, perlitic rhyolite; 2. Andesite, dacite; 3. Volcanic breccia; 4. Basalt; 5. Sandstone; 6. Siltstone; 7. Conglomerate.

7. CARBONIFEROUS

Carboniferous strata are widespread in the Kunlun, Qiangtang and Lhasa Terranes.

(*a*) *Golmud District, Kunlun Terrane*

Good sections of fossiliferous Carboniferous rocks are exposed near Dagangou and Halaguole in the mid Burhan Budai Mountains, though only the Dagangou section was examined (figures 6 and 7).

(i) *Dagangou Formation* (C_1)

The Dagangou section lies to the east of the Golmud River. The lower part of the formation (1012 m thick), consists mainly of terrestrial sandstones with subordinate rhyolite, basalt and tuff at different horizons. Some shallow-water sedimentary structures including cross-bedding and ripple marks were observed. The middle part is composed of white, medium- to thick-bedded quartzose sandstone, purple siltstone with subordinate pebbly sandstone and fine-grained conglomerate; medium-scale cross-bedding in sandstones of fluvial facies is common.

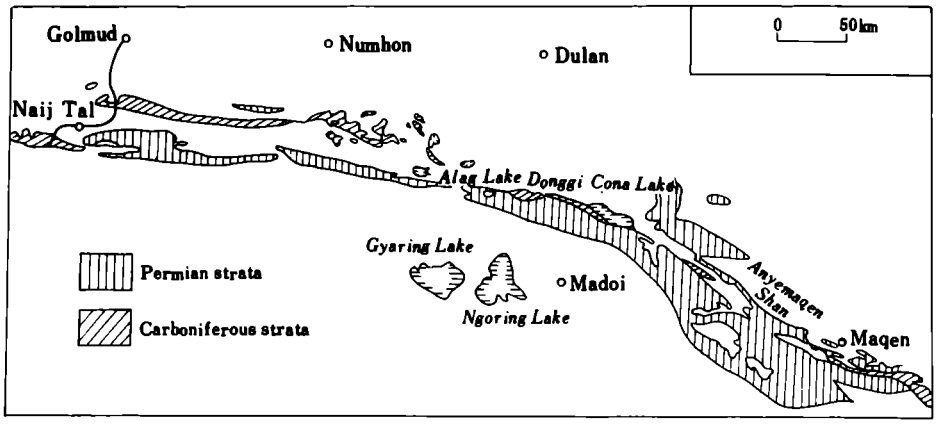

FIGURE 6. Sketch map of the distribution of the Carboniferous and the Permian in the Burhan Budai Mountains.

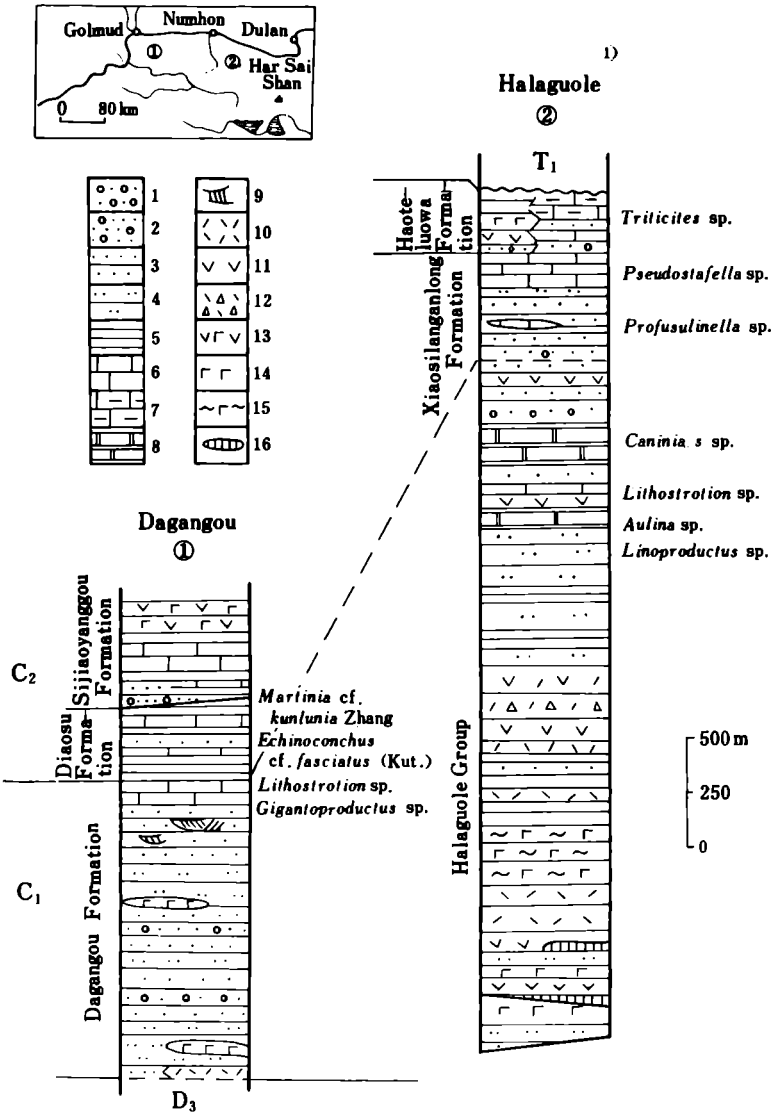

FIGURE 7. Correlation of columnar sections of the Carboniferous in the Burhan Budai Mountains. 1) Modified from Aikengdeleisite Sheet. 1. Conglomerate; 2. Pebbly sandstone; 3. Sandstone; 4. Siltstone; 5. Shale; 6. Limestone; 7. Argillaceous limestone; 8. Marble; 9. Cross-bedding; 10. Rhyolite; 11. Andesite; 12. Tuffaceous breccia; 13. Andesite-basalt; 14. Basalt; 15. Metamorphosed intermediate-basic volcanic rocks; 16. Siliceous rock.

The upper part, about 60 m thick, consists of grey, medium-bedded limestones, with sporadic reefs intercalated with subordinate carbonaceous shale or thin coal seams yielding brachiopods, corals and a few trilobites and crinoid stems (loc. B108) indicating a late Visean age.

(ii) *Diaosu Formation* (C_2^1, 380 m)

The Diaosu Formation rests conformably on the Dagangou Formation. The lower 140 m consists of arenaceous shale interbedded with thin-bedded sandstone, carbonaceous shale and thin-bedded bioclastic limestones yielding brachiopods (loc. B108); the upper part is characterised by a rhythmic succession which is in turn succeeded upwards by a succession of thin-bedded conglomerate, sandstone, shale and limestone intercalated with subordinate rhyolite at higher levels. The succession yields brachiopods, corals, fusilinaceans and conodonts (loc. B108, first limestone unit).

The Carboniferous succession in the Dagangou section is in turn succeeded upwards by a sequence of terrestrial, alternating marine and terrestrial and neritic deposits representing a transgressive succession. The fossil assemblages of the Dagangou Formation are predominantly benthonic and fixed fauna, while those of the Diaosu Formation and the Permian Sijiaoyanggou Formation include larger benthic foraminifera.

A flyschoid sequence exposed in Xiaonanchuan southwest of Naij Tal shows a southward increase in metamorphic grade from greenschist in the north to low amphibolite facies in the south (near the Xidatan Fault). The sequence has tectonic contacts both to the north and to the south and the thicknesses seen is estimated at over 2000 m. Some spores and pollen, the '*Laevigatosporites–Reinshospora* Assemblage', have been reported, although not described or figured, from the lower part of the sequence in Xiaonanchuan. Based on this assemblage, the age is considered to be 'Middle and Late Carboniferous' (Zhu Zhizhi *et al.* 1985). Lithologically the sequence is roughly similar to the Halaguole Group to the east near Numhon, so it is taken to be early Carboniferous in age, although it may be Cambro–Ordovician (see Leeder *et al.*, this volume).

(*b*) *Tuotuoheyan–Zadoi District, Qiangtang Terrane*

Carboniferous strata are mainly developed in the Zadoi and Qamdo districts east of the traverse route. However, a tectonic slice, previously referred to the Lower Permian, was discovered at Kaixinling. The strata, about 300 m thick, consist of thick-bedded or massive limestones with fusulinaceans (loc. B60). *Quasifusulina longissima* is a species found in the Mapingian in Hunan, Guizhou, Zhejiang, Gansu and Ningxia Provinces; it is also found at the top of the Taiyuan Formation in Shanxi Province. The fusuline-bearing strata are referred to the late Carboniferous of Chinese workers (mid Lower Permian of non-Chinese workers).

Several good Permo–Carboniferous sections are found in the Zadoi and Qamdo districts. To the west of Qamdo, the Lower Carboniferous is composed mainly of carbonates in the lower part and thick coal-bearing clastic rocks in the upper part. The Permian is carbonates; the contact of the Lower Carboniferous with the underlying Devonian is conformable, that of the early Permian with the overlying late Permian disconformable (Dong Deyuan & Mu Xinan 1984). In the Zadoi district, between Kaixinling and Qamdo, the Lower Carboniferous is composed of limestones intercalated with coal, gypsum and purple clastics with intermediate-acidic volcanics at different levels; it yields early Carboniferous corals and brachipods. The early Permian (late Carboniferous of Chinese workers) consists mainly of purple clastic rocks intercalated with subordinate carbonates with intermediate-basic and intermediate-acidic

volcanic rocks and bears Lower Permian fusulinaceans (Zadoi Sheet). The Carboniferous is disconformable on the underlying Devonian; the contact with the overlying Permian is obscure.

(c) *Lhasa District, Lhasa Terrane*

Carboniferous sediments are widespread in the Lhunzhub district and are also sporadically exposed to the south of Jang Co in the north of the Lhasa Terrane. So far, fossiliferous Lower Carboniferous has only been found in the Maizhokunggar district 60 km northeast of Lhasa where it is composed mainly of quartzose sandstones alternating with slates and subordinate limestones bearing the coral *Kueichowphyllum* sp. It is over 600 m thick (Li Pu 1955).

The type section of the Pondo Group at Urulung village west of Pondo is predominantly composed of diamictites, i.e. pebbly arenaceous mudstone, pebbly siltstone and pebbly sandstone intercalated with siltstone, mudstone and lenticular conglomerate. The basal part is intruded by granites and the topmost part grades conformably into the early Permian Urulung Formation; it is more than 1000 m thick. Pebbles within the diamictites are of diverse composition, dominantly quartzite with subordinate limestone, slate and granite. The diamictites generally appear to be massive and structureless but some sedimentary structures including bioturbation, graded bedding and pseudo-dropstones may be seen, suggesting that part of the

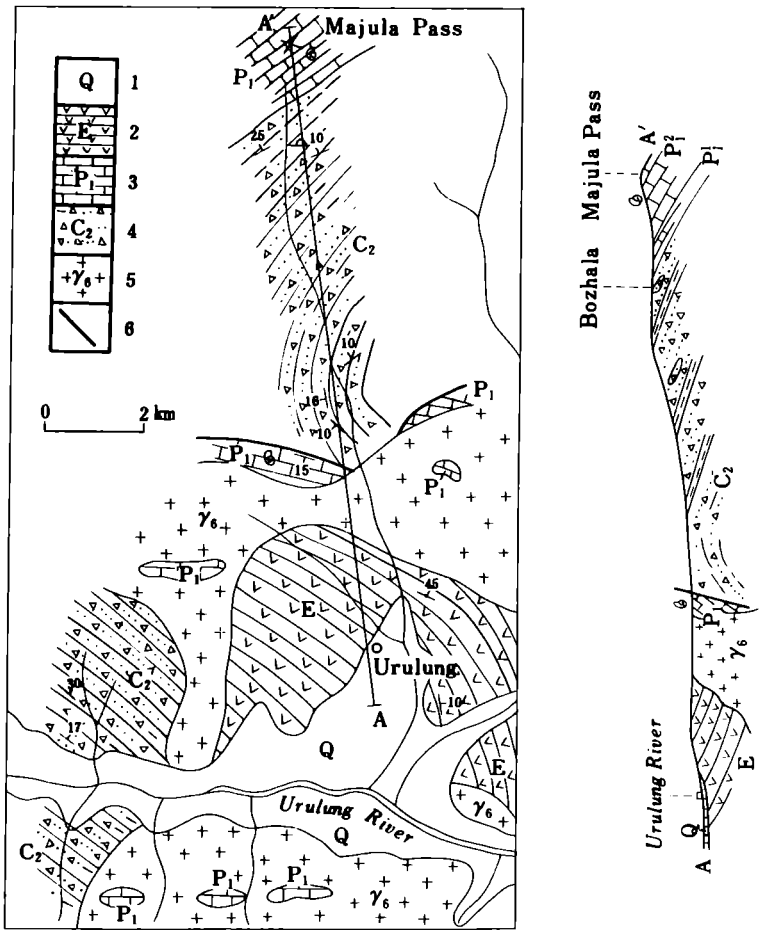

FIGURE 8. A section of the Pondo Group at Urulung village, west of Pondo town, Lhunzhub County. (From Yin Jixiang & Wan Chuanfen, in press.) 1. Quaternary deposits; 2. Volcanic rocks (Linzizong Formation); 3. Limestone (Urulung Formation and Lobadoi Formation); 4. Diamictite (Pondo Group); 5. Granite; 6. Fault.

diamictites originated as submarine gravity current deposits. Fossils from the upper part, on the whole, belong to the '*Bandoproductus* Fauna' which may be compared, in horizon and characteristics, with the '*Stepanoviella* Fauna' which occurs in Kashmir and Australia (Chen Chuzhen & Wang Yujing 1984). Exposures of the Pondo Group on the East Hill of Damxung City, 26 km northwest of Urulung village, are fossiliferous (locs. B17–21); the fossils suggest a late Carboniferous/early Permian age (figure 8).

8. Permian

Permian strata are widespread in the Kunlun, Qiangtang and Lhasa Terranes.

(*a*) *Golmud District, Kunlun Terrane*

(i) *Sijiaoyanggou Formation*

The base of this formation was not observed. However, other work indicates that it lies conformably on the Diaosu Formation (The Compiling Group of the Charts of Stratigraphical Units Sequences of Qinghai 1980). The lower part of the formation, exposed on the southern bank of the lower Dagangou Valley near the Golmud River, mainly consists of siltstone and pebbly sandstone intercalated with carbonates. The top is truncated by a fault; about 284 m is seen. The upper part is dominantly composed of andesitic basalts. The age of these basalts is questionable: for an alternative interpretation, see Smith & Xu, and Leeder *et al.*, this volume.

(*b*) *Naij Tal District, Kunlun Terrane*

The Permian forms an E–W trending belt in the western part and a NW–SE trending belt in the southeastern part of the southern Burhan Budai Mountains and is developed immediately to the south of the Carboniferous. It forms the bulk of the strata exposed in the Anyemaqen Mountains between Alag Lake and Maqen and extends westwards to Naij Tal (figure 6). In the eastern part of the outcrop, between Alag Lake and Maqen, the Permian sequence is associated with a number of small ultramafic bodies which have long been believed to be ophiolites; this belt has been regarded as the Southern Kunlun Suture (Li Baotian 1984). In the western part of the outcrop, between Alag Lake and Naij Tal, the Permian contains a great deal of basic, intermediate-basic and intermediate-acid volcanic rocks; no ultramafic rocks have been found. In the Naij Tal district, the Lower Permian succession is well-exposed at Nangou south of Kunlun Bridge, along the southern bank of the Xueshui River and the Tuolugou as well as along both banks of the Dongdatan Valley, while fossiliferous Upper Permian is found only along the Upper Xueshui River and in the Xugui district to the east of the Geotraverse route. No true flysch sediments typical of deep water facies have been found in the Permian of the Kunlun Shan despite its tremendous thickness (figure 9). A generalized Permian sequence in the Naij Tal district is as follows.

Overlying beds	Neogene red beds
	Unconformity
Upper Permian (after 'Dongwenquan Sheet')	
Upper Part	Carbonates and calcirudite intercalated with tuff; carbonates yield early late Permian Araxoceratid ammonoids and the brachiopods *Neophricodothyris* cf. *asiatica* (Chao), *Waagenites* sp. and *Buxtonia* sp.
Lower Part	Conglomerate and pebbly sandstone with subordinate thin-bedded limestone.

Paraconformity

Lower Permian (after 'Dongwenquan Sheet' and 'Naij Tal Sheet')

Carbonate Rock Formation (P_1^b) or (P_2^a)	Bioclastic limestone intercalated with subordinate calcareous shale and quartzose sandstone, limestone yielding fusulinaceans: *Verbeekina*, *Schwagerina*, *Neoschwagerina* and *Sumatrina*; corals: *Iranophyllum* and *Wenzelella* etc. (log. M855/7). The sequence is generally intensely deformed. (This formation is considered by non-Chinese workers to be of early late Permian age on forams.)
Clastic Rock Formation (P_1^a)	
Upper Part	Limestone alternating with slate and phyllite intercalated with lenticular conglomerate and thin-bedded limestone.
Lower Part	Schistose sandstone and conglomerate, schistose rhyolitic brecciated lava, rhyolite and tuff intercalated with siltstone, pebbly sandstones and subordinate dolomite.

Fault

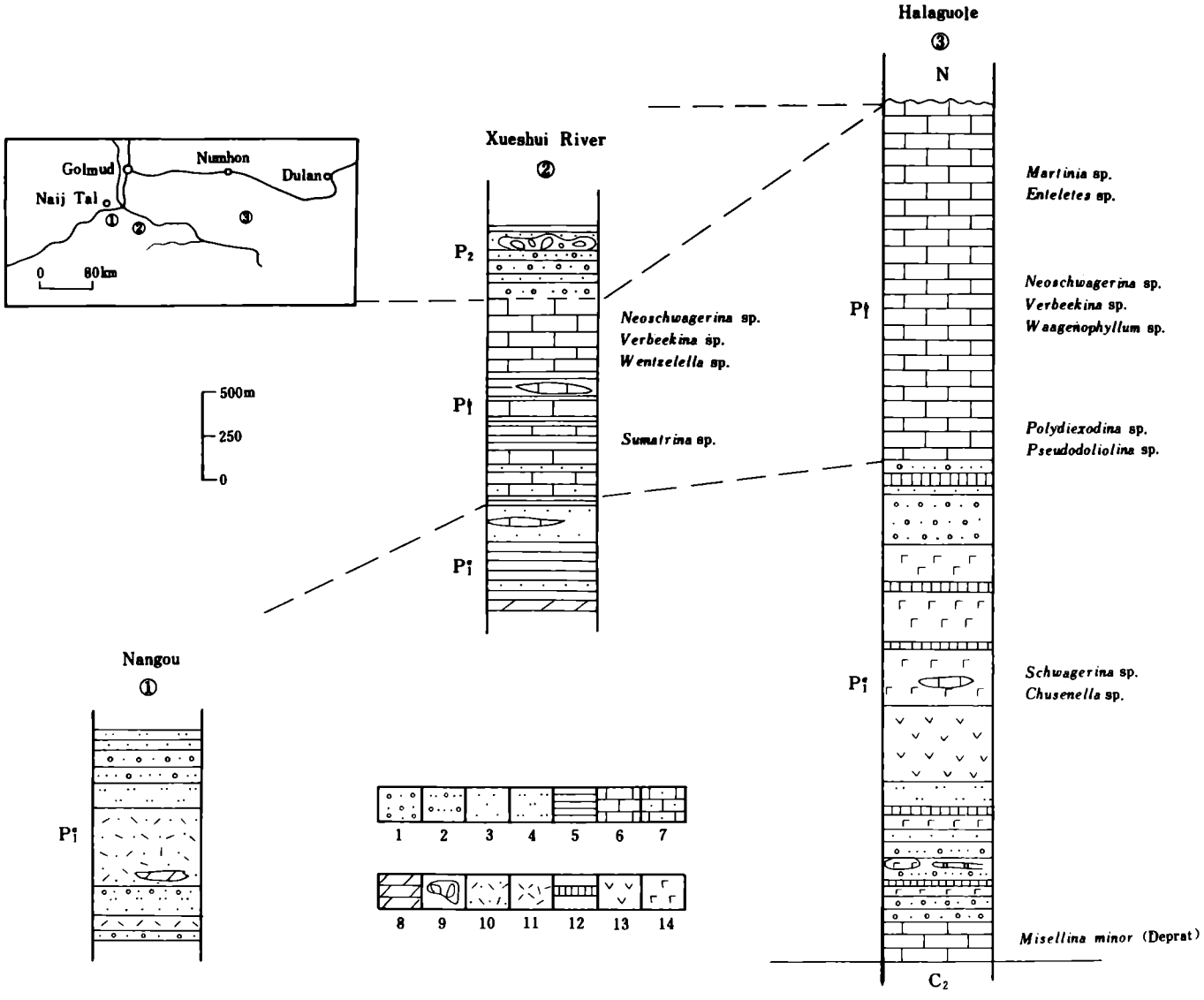

FIGURE 9. Correlation of the Lower Permian in the Burhan Budai Mountains. (1) After Naij Tal Sheet; (2) After Dongwenquan Sheet; (3) After Aikengdeleisite Sheet. 1. Conglomerate; 2. Pebbly sandstone; 3. Sandstone; 4. Siltstone; 5. Slate; 6. Limestone; 7. Arenaceous limestone; 8. Dolomite; 9. Calcirudite; 10. Tuff; 11. Rhyolite; 12. Siliceous rocks; 13. Andesite; 14. Basalt.

In the Halaguole district to the south of Numhon, the Lower Permian is predominantly basic and intermediate volcanic rocks. The fossiliferous limestone at the bottom the upper Lower Permian rests conformably on the fossiliferous topmost limestone of the lower Lower Permian (of non-Chinese usage).

(c) *Wuli–Kaixinling District, Qiangtang Terrane*

The core of the Kaixinling–Nangqen anticlinorium is formed of Permian. Good sections mostly occur in the Zadoi or Nangqen districts east of the Geotraverse route. However, several small, incomplete and faulted sections of the same strata are exposed in the Wuli–Kaixinling district (figure 10).

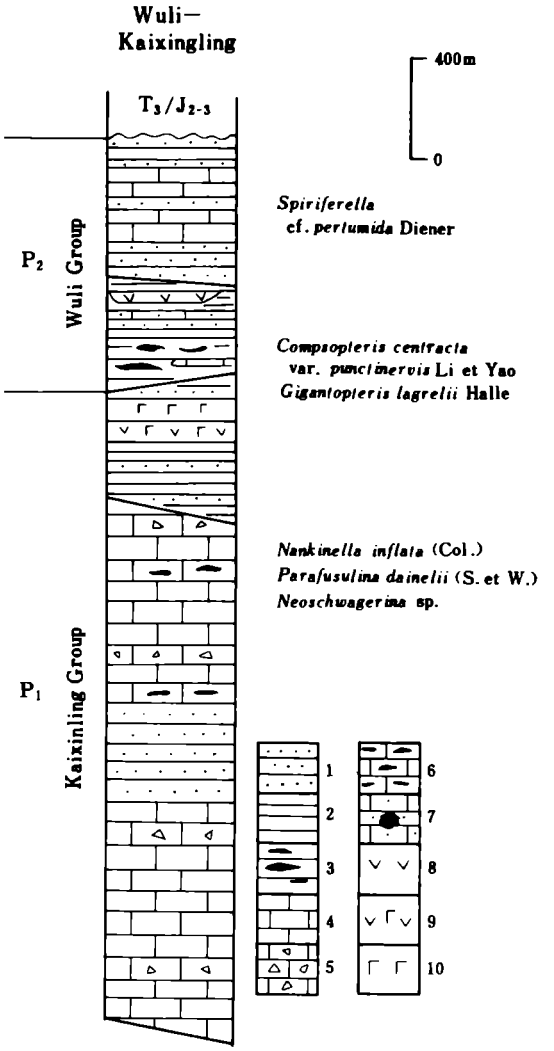

FIGURE 10. Columnar section of the Permian in the Wuli–Kaixinling district. 1. Sandstone; 2. Shale, mudstone; 3. Coal series; 4. Limestone; 5. Brecciated limestone; 6. Arenaceous limestone; 7. Cherty limestone; 8. Andesite; 9. Intermediate-basic volcanics; 10. Basalt.

(i) *Kaixinling Group* (P_1) or (P_2^a)

The Kaixinling Group includes the lower Carbonate Rock Formation which is faulted against the upper Volcanic Rock Formation. The limestones and sandstones of the thick Carbonate Rock Formation bear fusulinaceans (loc. 60), suggesting a Lower Permian (Chinese usage) or lower Upper Permian (non-Chinese usage) age. Among them, *Verbeekina verbeeki*,

Neoschwagerina haydeni, *N. craticulifera* and *Parafusulina multiseptata* belong to the *Neoschwagerina* and *Yabeina–Neomisellina* zones of the Maokouan stage; the age is inferred to be late early Permian (early late Permian of Western authors). The Volcanic Rocks Formation (at least 380 m) is composed of grey, green and purple basic and intermediate volcanic rocks in the lower part and amygdaloidal basalts intercalated with sandstone and slate in the upper part.

(ii) *Wuli Group* (P_2)

The lower Coal-bearing Clastic and Volcanic Rock unit of the Group is 288–534 m thick at Kaixinling coal mine and at the East Hill of Wuli and is dominantly composed of carbonaceous shale intercalated with coal, sandstone, andesite, bioclastic calcareous sandstone and dark grey thin-bedded limestone as well as silty mudstone at different levels. Carbonaceous sandstones from the East Hill of Wuli yield brachiopods, bivalves and gastropods (loc. B59). In addition, some brachiopods, bivalves and plant fossils were collected from Kaixinling (loc. B66). The following plant fossils from the same locality have previously been reported: *Gigantopteris nicotianaefolia* Schenk, *G. largrelii* Halle, *Lobatannularia ensifolia* Halle, *Calamites* cf. *gigae* Brogn., *Asterophyllites* sp., *Pecopteris arborescens* Goeppert, *P.* (*Ptychocarpus*) *ascuata* Halle, *Cladophlebis* sp., *Taeniopteris multinervis* Weiss, etc. (Pan Guan 1957). Brachiopods from both Wuli and Kaixinling belong to the same fauna but the horizon of the fossils from Wuli is probably slightly lower than that of the same fossils from Kaixinling. The fauna suggests a late Permian age.

The limestones, sandstones and shales of the overlying Carbonate Rocks Unit exposed to the east of Wuli is conformable on the Coal-bearing Clastic and Volcanic Rocks Unit; it reportedly yields the brachipods *Perigegarella* cf. *castellata* Wang and *Spiriferella* cf. *pertumida* Diener (The Compiling Group of the Charts of Stratigraphic Units Sequences of Qinghai 1980).

The Permian of the Kaixinling–Wuli district is comparable in fauna and lithology to that of the Qamdo district to the east except that the upper part of the Upper Permian exposed at Wuli is mainly composed of carbonates while it is volcanic in Qamdo. The palaeofloral assemblage of the Wuli Group is essentially allied to that of the Tuoba Formation in the Qamdo (Li Xingxue *et al.* 1982) and the Yushu districts (He Yuanliang & Zhang Shanzhen 1984) as well as that of the Ryaggor Caka Formation to the west in the Amugang-Mayingangri region. All may be referred to the late Permian Cathaysian flora (Li Xingxue & Yao Zhaoqi 1983).

(*d*) *Lhasa District, Lhasa Terrane*

Lower Permian strata are widespread in the Lhasa district and are unconformably overlain by Mesozoic strata. The Lower Permian may be divided into two formations, the lower Urulung Formation (limestones and sandstones) and the overlying Luobadoi Formation. The Lielonggou Formation is Upper Permian. These formations have been investigated in detail by the Scientific Expedition to the Xizang (Tibet) Plateau of the Chinese Academy of Sciences in the 1970s and a summary of these formations from published data is as follows.

(i) *Urulung Formation* (P_1^1)

This formation (40 m) has yielded Artinskian brachiopods, corals and bryozoa: *Fluctuaria* cf. *mongolica* (Denier), *Transennatia gratiosus* (Waagen), *Cancrinella cancriniformis* (Tsch.) (brachiopods), *Praewentzelella* cf. *multiseptata* (Enderle) (coral).

(ii) *Luobadoi Formation* (P_1^2)

The formation (about 640 m thick) is conformable on the Urulung Formation and is composed of limestones intercalated with subordinate siltstone and marble; it has yielded the Kungurian fusilinaceans *Neoschwagerina globularis* Wang, Sheng et Zhang, *N. margaritae* Deprat, *Yabeina shiraiwensis* Ozawa, and the corals *Iranophyllum minor* Wu and *Ipciphyllum percicum* (Douglas) (Chen Chuzhen & Wang Yujing 1984). The upper part of the formation is absent.

(iii) *Lielonggou Formation* (P_2)

The lower part of the formation is truncated by faulting. The upper part passes conformably into or is paraconformable with the overlying Chaqupu Group of early and mid-Triassic age. It is mainly composed of sandstone intercalated with thin-bedded or lenticular andesite and andesite–basalts at different levels. The grain size of the sandstone increases upward in the upper part of the sequence and fragments of plant fossils appear representing a prograding sequence. It contains brachiopods, bivalves and bryozoa (loc. B11); the formation has been referred to the Upper Permian by Sun Dongli *et al.* (1981).

A coal-bearing clastic rock sequence more than 700 m thick exposed in the Xiagangjiang district (84° 15′ E, 30° 26′ N) in the western part of the Lhasa Terrane has been reported as displaying a 'mixed flora' of the Eurasian and Gondwanan Continents (Li Xingxue *et al.* 1985). However, neither typical elements of the Gondwanan flora nor those of the Cathysian flora were found in the 'mixed flora', which showed both features unique to the Lhasa Terrane and features relating the Terrane to the Cathaysian palaeolandmass to the northeast and Gondwanaland to the south.

9. Triassic

Triassic sediments are widely distributed in the Kunlun and Qiangtang Terranes but occur only sporadically in the Lhasa Terrane (figure 11).

(*a*) *Naij Tal Region, Kunlun Terrane*

(i) *Burhan Budai Subregion*

This subregion lies to the north of the major Xidatan–Xugui–Maqen fault. The Lower Triassic Hongshuichuan Formation, 1346 m in thickness (figure 12), has a lower part mainly composed of conglomerate, lithic feldspathic sandstone, pebbly sandstone and siltstone reportedly resting unconformably on Ordovician and Precambrian (Wanbaogou Group) sediments. The reputed basal conglomerate, 100 m thick, consists of pebbles and boulders of sandstone, tuff, quartzite, limestone and granite; they range in diameter from 4 cm to 1 m and are well-rounded or subrounded. The upper part is calcareous. The Middle Triassic Naocangjiangou Formation is over 2000 m thick. The lower part is composed of quartzose feldspathic sandstone intercalated with siltstone and slate, the upper part is mainly composed of slate with siltstone and sandstone interlayers, the top is unseen. Thick intermediate-acid volcanics are intercalated in the middle part of the Hongshuichuan Formation and in the lower part of the Naocangjiangou Formation about 150 km east of Golmud.

The early Triassic brachiopod *Pseudospiriferina* cf. *tsinghaiensis* Yang et Ti has been reported

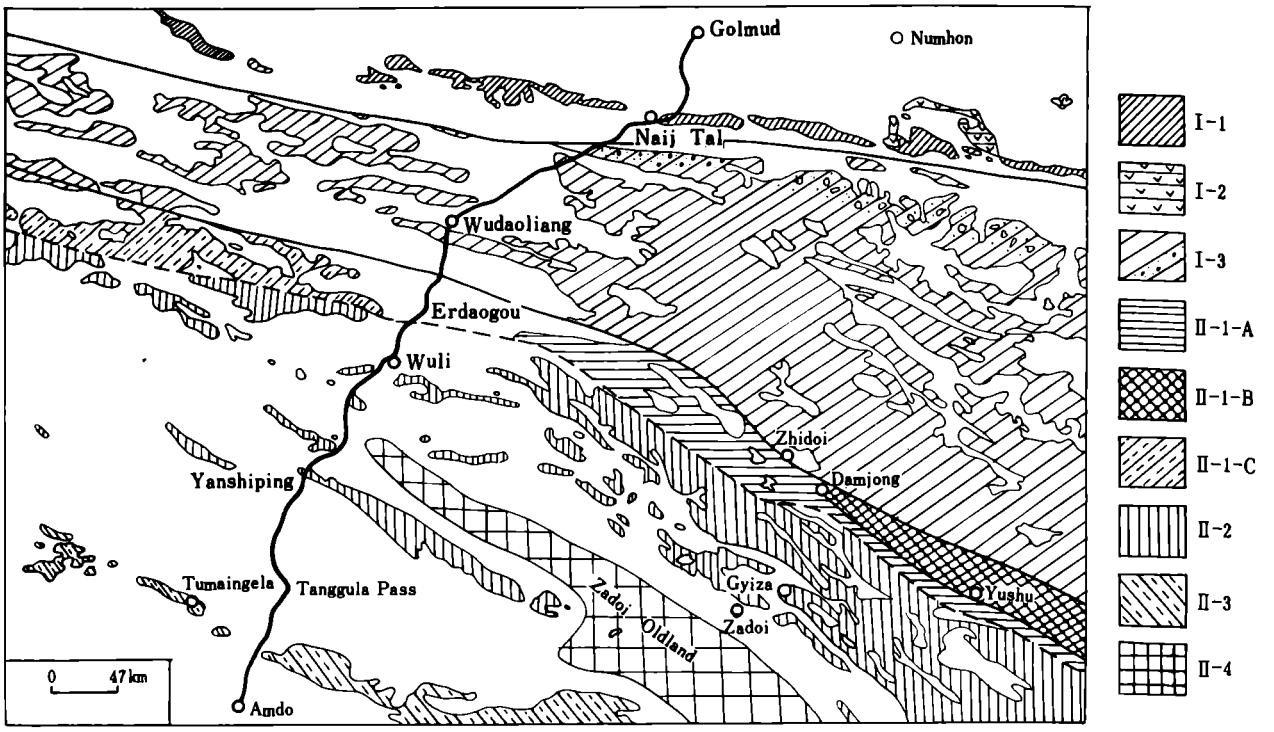

FIGURE 11. Distribution of Triassic sediments in the Kunlun and the Qiangtang Terranes. I. The East Kunlun Terrane: I-1, The Lower to Middle Triassic marine sediments in Burhan Budai Mt.; I-2, The Triassic terrestrial sediments–Babaoshan Group in Burhan Budai Mt.; I-3, The Triassic flysch–Bayan Har Group in Burhan Budai Mt. II. The Qiangtang Terrane: II-1-A, The Triassic Baitang Group is dominated by calc-alkaline volcanics; II-1-B, 'Ophiolite-Island arc complex belt'; II-1-C, Alterations of terrestrial and marine coal-bearing clastics (island arc belt); II-2, Triassic sediments in 'Back-arc basin'–Gyiza Group; II-3, Alternations of terrestrial and marine coal-bearing clastics–Tumain-gela Formation at the southern margin of Qiangtang Terrane; II-4, The uplift region–'Zadoi oldland' during Triassic.

from the upper part of the Hongshuichuan Formation in the West Hill of Wanbaogou Valley. The Anisian bivalve *Posidonia* cf. *bosniaca* Bittner and the ammonoid *Leiophyllites* sp. were previously found from the Naocangjiangou Formation 10 km west of Wanbaogou. Ladinian sediments have not yet been found from the Burhan Budai Mountains (see Naij Tal Sheet). Abundant brachiopods, bivalves and ammonoids were found in supposed equivalents of the Hongshuichuan and the Naocangjiangou Formations in the eastern Burhan Budai Mountains; the assemblages display features of a mixture of typical Tethyan and Boreal faunas (Sun Dongli & Ye Songling 1982; The Research Group on the Triassic of the Wuhan Geological College and Qinghai Institute of Geology 1979; Yin Hongfu & Ling Qiuxian 1986; He Yuanliang & Yin Jiarun 1983; Wang Yigang & Chen Guolong 1984). Late Permian brachipods were collected (loc. B91) during the Geotraverse from greyish-white limestone probably equivalent to the middle part of the original Hongshuichuan Formation.

The terrestrial coal-bearing clastics (Babaoshan Group) yield abundant plant fossils similar to the late Triassic '*Dictyophyllum–Clathropteris* flora' of South China (Wu Shunqing & Wu Xiangwu 1982; Wu Shunqing 1983) and the brackish water bivalve *Utschamiella*, suggesting that a brief late Triassic transgression took place in this area.

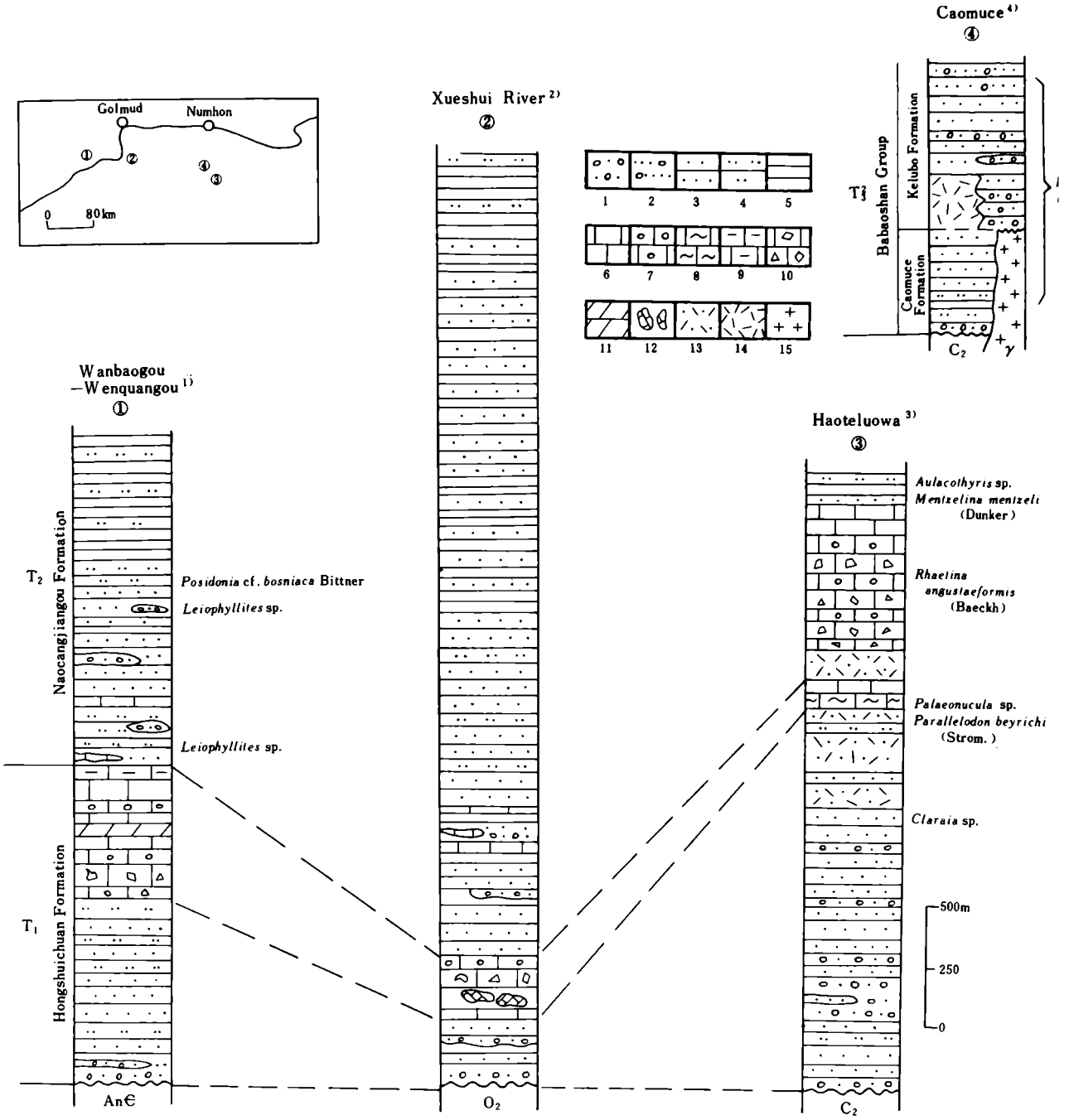

FIGURE 12. Correlation of columnar sections of Triassic sediments in the Burhan Budai Mountain area. 1) Modified from Naij Tal Sheet, Wanbaogou section and Wenquangou section. 2) *Ibid.*, Xueshuihe section. 3) and 4) Modified from Aikengdeleisite Sheet. 1. Conglomerate; 2. Pebbly sandstone; 3. Sandstone; 4. Siltstone; 5. Shale, slate; 6. Limestone; 7. Oolitic limestone; 8. Argillaceous banded limestone; 9. Argillaceous limestone; 10. Brecciated limestone; 11. Dolomite; 12. Calcirudite; 13. Tuff; 14. Rhyolite; 15. Granite.

(ii) *Bayan Har Subregion*

The Bayan Har Subregion is situated between the Qiangtang Terrane, the Yangtze Terrane and the Burhan Budai-West Qinling Mountains. The Triassic sediments in the subregion are composed mainly of fairly monotonous sandstones and shales. They outcrop sporadically over

150 km in the area from Budongquan to Beiluheyan along the Geotraverse route and are well represented by the sections at Coal-mine Valley and on the northern side of the Kunlun Shan Pass. On the southern side of the Xidatan, the sequence contains 'exotic blocks' of sandstone, limestone, granite, conglomerate and slate, which range in diameter from several cms to tens of metres; they are arranged mainly along the schistosity. Some limestone blocks are reported to bear Carboniferous–Permian fossils similar to those from the Burhan Budai Mountains. Break-ups are seen between the blocks and the matrixes suggesting later structural deformation (Li Guangcen & Lin Baoyu 1982; Zhu Zhizhi *et al.* 1984; see also Coward *et al.*, this volume, figure 4). These we interpret as olistostromes. A previous discovery of the ammonoids *Meekoceras* and *Mesohedenstroemia* from an equivalent horizon in the East Wenquan region close to the east of Xidatan indicates that these olistostrome-bearing strata of mid–late early Triassic age represent the lower Bayan Har Group in the northern part of the 'Bayan Har Fold System' (see Naij Tal Sheet).

The bivalve *Halobia* has been found from the sandstone and slates of the Upper Bayan Har Group in the Wudaoliang area (The Compiling Group of the Charts of Stratigraphical Units Sequences of Qinghai 1980). The Triassic sediments at the southern margin of the 'Bayan Har Fold System' in the Zhidoi area are composed mainly of distal turbidites with a typical Bouma sequence intercalated with cherts and pelagic limestones yielding *Halobia*. They are thrust southward on the Upper Triassic Baitang Group (Yin Jixiang, unpublished field mapping, 1967).

The 'Bayan Har Fold System' is a thick Triassic terrigenous sequence of clastic turbidites (Zou Dingbang *et al.* 1984) without volcanics. Small granitoid intrusives (213 Ma K–Ar age for the granodiorite at Wudaoliang) occur. The major fauna recorded is Tethyan-type planktonic thin-shelled bivalves and other plankton. The paraconformity between the lower Bayan Har Group and the Upper Permian has been seen only south of Maqen (The Research Group on the Triassic of Wuhan Geological College and Qinghai Institute of Geology 1979; Wang Yigang & Sun Dongli 1985). Based on the aeromagnetic survey (Cai Zhenjing 1984), magmatism and deep faulting are not well-developed in the region where Triassic sediments occur, implying a hardened basement. It is probable that there is a Palaeozoic basement in the northern part of the Bayan Har Fold System, while in its southern part, nearer to the 'Litian Lake–Jinsha River Suture Zone', there is an accretion prism or subduction complex. The asymmetry of the Triassic sedimentation in the Bayan Har and Songpan–Garze fold systems, with shallow-water characteristics in the north and northeast and abyssal or bathyal deposits to the south (Zhang Qinwen 1981; Liu Baotian 1984) suggests that the Bayan Har Group represents a forearc basin.

(*b*) *Tuotuoheyan–Zadoi District, Qiangtang Terrane*

(i) *Zhidoi–Yushu Subregion*

This subregion, 18–45 km in width, lies at the northern or northeastern margin of the Qiangtang Terrane. In its western part, west of Erdaogou towards Xijir Ulun Lake, thick Triassic sandstones and siltstones with carbonaceous shale and coal seams are exposed; they are associated with serpentinised ultrabasic rock in Chawuma Mountain 60–70 km west of Beiluheyan (Zhang Qizhen & Zhang Yifu 1981). Late Triassic bivalves and plants have been reported.

The Triassic in the Zhidoi area (the middle part of the subregion) is called the Baitang

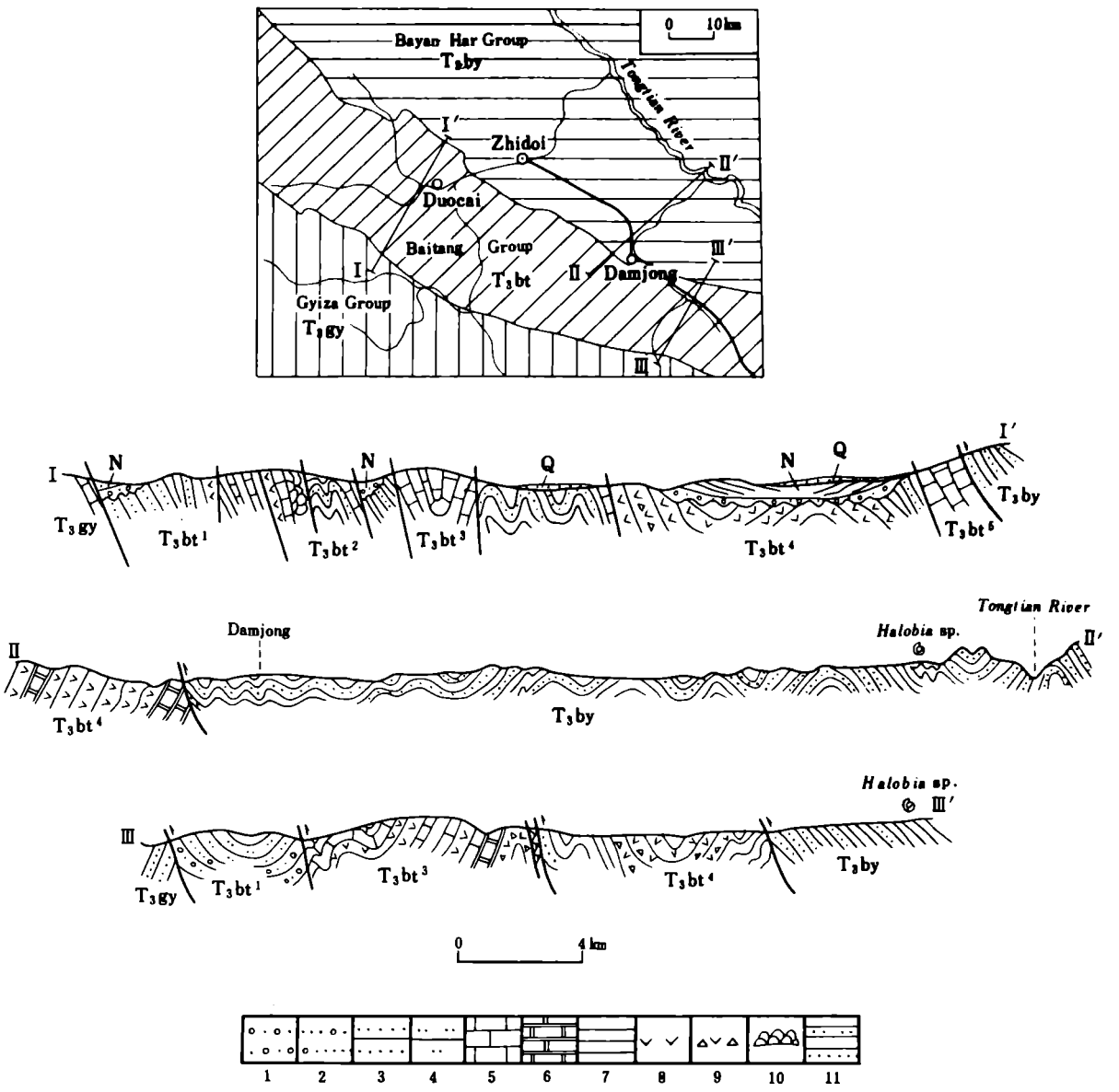

FIGURE 13. Sections of the Baitang Group in Duocai–Damjong, Zhidoi County, Qinghai Province. 1. Conglomerate; 2. Pebbly sandstone; 3. Sandstone; 4 Siltstone; 5. Limestone; 6. Marble; 7. Shale and slate; 8. Andesite; 9. Volcanic breccia; 10. Pillow lava; 11. Flysch.

Group; it has yielded late Triassic brachiopod, bivalve, coral, ammonoid and gastropod faunas of Tethyan type (Zhao Rongli 1982). The Group contains enormous amounts of volcanics and outcrops around Damjong–Duocai in Zhidoi County, where it was surveyed by some Chinese stratigraphers after the Joint Geotraverse (figure 13).

At Duocai (figure 13, I–I′), the Baitang Group can be subdivided into five suites separated from each other by faults; the first four of these occur in the Songmorong–Yangzhilong section at Damjong village (figure 13, III–III′). These sections suggest that the volcanic component increases and carbonates decrease eastwards (figure 14).

The five suites of the Baitang Group represent five sedimentary associations; from bottom to top and south to north: (1) variegated clastic; (2) intermediate-basic volcanic (including

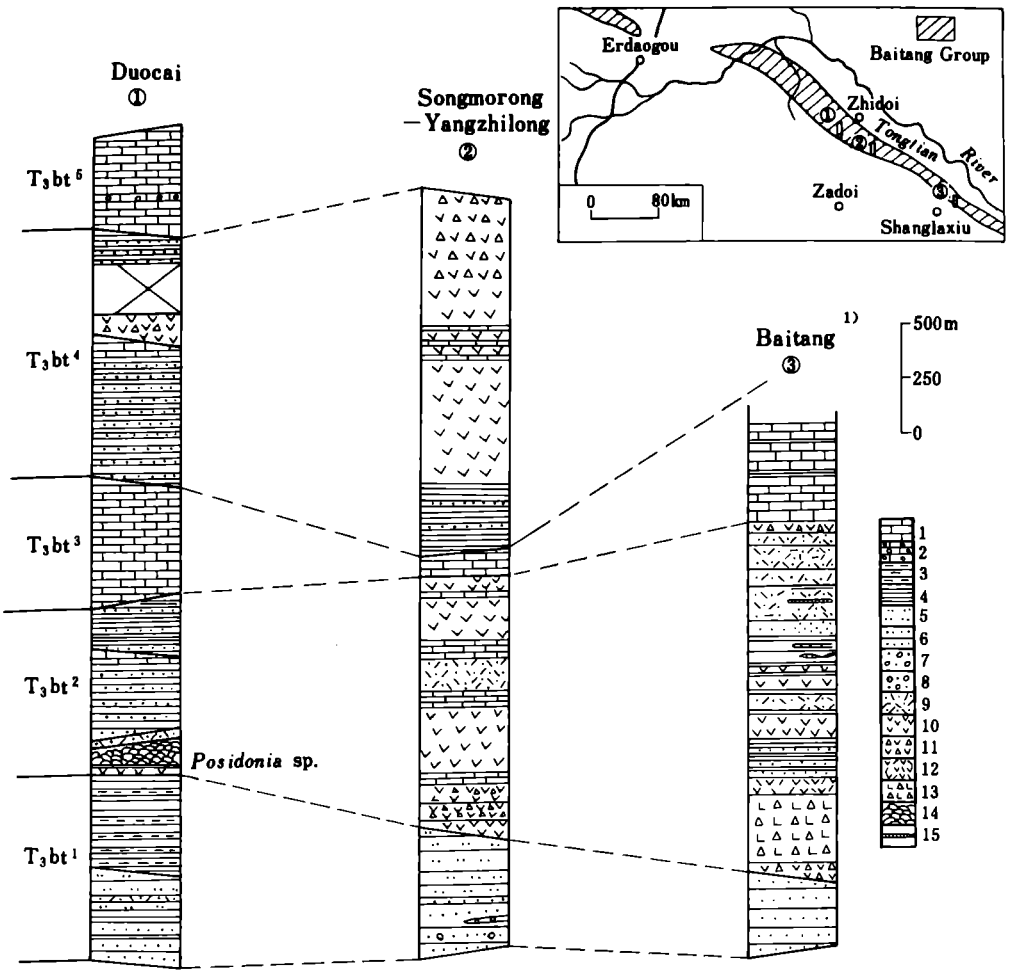

FIGURE 14. Correlation of columnar sections of the Baitang Group in the Zhidoi–Yushu subregion. 1) Ref. Shanglaxiu Sheet. 1. Crystalline limestone, limestone; 2. Oolitic limestone; 3. Calcareous mudstone; 4. Shale and slate; 5. Siltstone; 6. Sandstone; 7. Pebbly sandstone; 8. Conglomerate; 9. Tuff; 10. Andesite; 11. Intermediate-acidic volcanics; 12. Dacite; 13. Basalt; 14. Pillow lava; 15. Jasper.

pillow lavas); (3) carbonate; (4) intermediate-acidic and flysch; and (5) carbonate. 'The southern volcanic rock belt' (association 2) extends along the strike to the Baitang district south of Yushu, while the 'northern volcanic rock belt' (association 4) extends along strike to Chumda, north of Yushu, and joins with the 'Ophiolite–island arc complex belt'. Chemical analyses (85YR16a, 85YR18) indicate that the calc-alkaline pillow lavas of association 2 are comparable with island arc volcanics (Zhao Rongli 1982).

Flute casts and graded bedding are found in the greywackes of suite 4. The angular and ill-sorted lithic clasts are composed mainly of volcanics and subordinate chert indicating that they were deposited rapidly near the source region. The carbonates of suites 3 and 5 are made up mainly of micritic bioclastic limestone and a little oolitic limestone. They yield numerous bivalves and brachiopods at some horizons and display platform and platform-margin slope facies. Judging from the alternating layers of lower neritic clastics passing up into submarine basic lava, platform carbonates and sandstone and slate of flysch facies, it appears that the Baitang Group was deposited in a mobile tectonic setting. Widespread intrusions of grano-

diorite and the occurrence of a few small ultrabasic and gabbro bodies suggest that the Baitang Group represents a late Triassic mature island arc.

The outcrop of the upper part (suites 4 and 5) of the Baitang Group at Damjong widens gradually eastwards to 20–40 km around Chumda–Xiwu north of Yushu. Here the rocks have undergone low grade metamorphism. The thickness of the volcanics is over 2500 m. There are more than ten small tectonic lenses of ophiolite, mainly serpentinite, gabbro and pillow lava and basic dyke swarms, such as the ophiolites in Gala village, only 150–200 m in width. The ophiolites are commonly intruded by granodiorites, granites and quartzose diorite. This series extends southeastwards to the Garze and Litang areas of western Sichuan Province, joining the ophiolitic melange of MORB type there (Jiang Yaoming 1984). The authors interpret these ophiolitic associations as an 'Ophiolite–island arc complex belt' rather than as another stratigraphic unit as some authors have suggested.

Thus the rocks exposed in the Zhidoi–Yushu region where the 'Litian Lake–Jinsha Suture Zone' passes through vary greatly in lithology, metamorphism and tectonic deformation and form a complicated collision zone (figure 15).

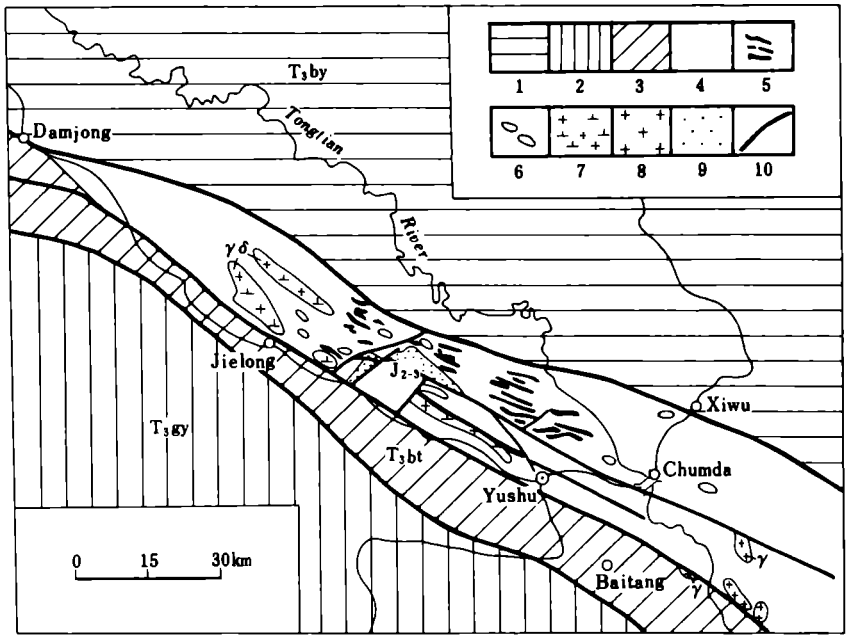

FIGURE 15. Sketch map of the ophiolite-island arc complex belt in Damjong–Yushu. 1. Bayan Har Group (T_{3by}); 2. Tuotuoheyan–Ziqu fold zone (Middle–Upper Triassic and part of the Palaeozoic sediments); 3. Southern volcanic rock belt of the Baitang Group; 4. Ophiolite-island arc complex belt; 5. Diabase dykes; 6. Ultramafic rock (or ophiolite); 7. Granodiorite; 8. Granite; 9. Yanshiping Group (J_{2-3}); 10. Fault.

(ii) *Tuotuoheyan–Ziqu Subregion*

The Gyiza Group (Middle and Upper Triassic) is intermittently exposed between Wuli and Yanshiping. At Zakongjian, 30 km southeast of Wuli, the variegated clastics of the Dongmaolong Formation and the Xiaoqiaco Formation carbonates are exposed. These are equivalent to the lower and middle parts respectively of the Gyiza Group (the stratotype) south of Yushu. The Dongmaolong Formation, 630 m thick, rests unconformably on the Lower Permian

volcanics. Its lower part consists of fluvial pebbly sandstone, coarse lithic quartzose sandstone and grey conglomerate. The clasts are of quartzite, andesite, tuff and cherts originating from the island arc to the north. The upper part consists of dark calc-alkaline to alkaline purple andesites and basalts, chemically similar to those of the Baitang Group. The conformably overlying Xiaoqiaco Formation, over 370 m thick, is covered by Tertiary red beds. This comprises grey medium- to thick-bedded limestone with chert bands in the lower part and bioclastic limestone above. Late Triassic fossils (brachipods, bivalves, foraminifers, conodonts, crinoids etc.) indicate a mid Norian age (loc. B67).

The Gyiza Group (Middle to Upper Triassic) outcrops in the Ziqu River Valley, southern Yushu, south of the Geotraverse route, where it reaches over 4000 m in thickness. The lower Dongmaolong Formation of purple clastics with inter-layers of iron-bearing deposits, carbonaceous shale, thin-bedded limestone and gypsum yields fossil plants and marine bivalves. Such Anisian ammonoids as *Balatonites gracilis* Arthaler, *Paraceratites trinodosus* (Mojs.) and Anisian to Ladinian bivalves, foraminifers and brachiopods collected from the Dongmaolong Formation (Chen Chuzhen, personal communication) indicate a complete Middle Triassic sequence. The upper Dongmaolong Formation yields early Carnian brachipods, bivalves, foraminifers, etc. (Ma Fubao *et al.* 1984). The Carnian–Norian ammonoids *Trachyceras* cf. *aon* (Munster), *Tropites* sp. and *Pseudocardioceras* sp. have been recorded from the Xiaoqiaco Formation, which is mainly composed of dolomites and limestones representing platform and platform-marginal slope facies.

The Jiagenda Formation, conformable on the Xiaoqiaco Formation, is composed of alternate terrestrial–marine coal-bearing clastics, bioclastic limestones and intermediate-acidic tuffs. The sandstone and shale are intercalated with gypsum and show shallow water ripple-marks and cross-bedding near the 'Zadoi oldland' (Ma Fubao *et al.* 1984; Zheng Yanzhong 1984).

The Tumaingela Formation on the southern slope of the Tanggula Mountains is composed of terrestrial–marine coal-bearing clastics of late Triassic age and is laterally equivalent to the upper part of the Gyiza Group (Wu Xiangwu 1982).

The Anisian–Norian marine invertebrate fauna from the Gyiza Group is Tethyan while the *Clathropteris meniscioides–Pterophyllum minutum* plant assemblage belongs to the *Dictyophyllum–Clathropteris* Norian flora of South China (Chen Guolong *et al.* 1982; Yin Hongfu & Ling Qiuxian 1986; Wu Shunqing 1983; Ma Fubao *et al.* 1984) (figure 16).

No Lower Triassic sediments have yet been discovered in southern Qinghai. The Middle–Upper Triassic sediments of the Gyiza Group are very similar to those in the Burhan Budai Mountains (Kunlun Terrane), overlapping or unconformable on older rocks. They represent back arc deposits related to tensional tectonics.

(*c*) *Lhasa District, Lhasa Terrane*

Fossiliferous Triassic sediments in the Lhasa Terrane are found at Quesangwenquan in Doilungdeqen County and at Mailonggang and Qibunong in Lhunzhub County. The East Hill section of Quesangwenquan provides the best exposures. Despite previous work on this section (Chen Guoming *et al.* 1980; Sun Dongli *et al.* 1981; Gu Qingge *et al.* 1980), the classification, age and lithological description are still confused. Based on the observations of Yin Jixiang and Sun Yiyin in 1981 and fieldwork during this Geotraverse, the following sequence has been deduced from this section (figure 17).

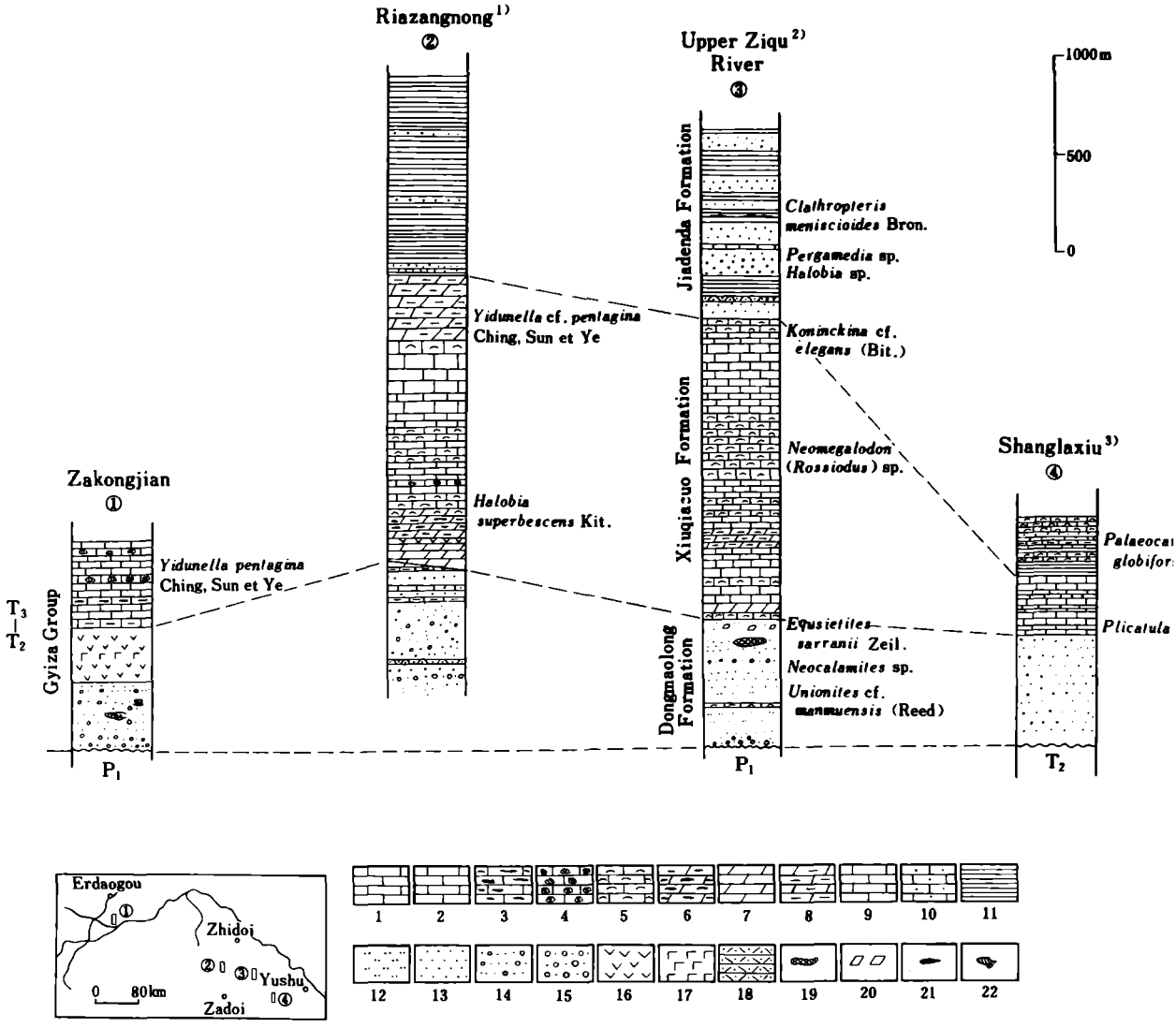

FIGURE 16. Correlation of the Gyiza Group in the Tuotuoheyan–Zadoi region. 1) After Zhidoi County Sheet; 2) After Zadoi County Sheet; 3) After Shanglaxiu Sheet. 1. Limestone; 2. Argillaceous limestone; 3. Banded chert limestone; 4. Shelly limestone: 5. Bioclastic limestone; 6. Banded chert dolomite; 7. Dolomite; 8. Dolomitic limestone; 9. Marble; 10. Arenaceous limestone; 11. Shale and slate; 12. Siltstone; 13. Sandstone; 14. Pebbly sandstone; 15. Conglomerate; 16. Intermediate volcanics; 17. Basic volcanics; 18. Tuff; 19. Iron Formation; 20. Gypsum; 21. Coal; 22. Cross-bedding.

Overlying strata: Jurassic sandstone and conglomerate (Quesangwenquan Formation)

Unconformity

'Yeba Formation' (T_3):

Ferruginous, chamosite-cemented sandstone and thin-bedded sandstone with plant fragments (13 m thick) in the lower part: variegated andesite, altered andesite basalts with basic tuff, brecciated basalt and tuffaceous pebbly sandstone interlayers in the middle and upper parts.

Paraconformity

Chaqupu Group (T_{1-2}):

Upper Formation (T_2^2): Intermediate-basic welded breccia in the lower and middle parts with haematite lenses at the base, 66 m thick; medium- to thin-bedded limestone, oolitic lime-

stone interlayered with banded shelly limestone and arenaceous shale in the upper part yielding bivalves, gastropods and crinoids; bivalves:? *Leptochondria* cf. *michaeli* Assman, ? *Pseudocorbula* sp., *Myophoriopsis* aff. *lineata* (Munster), *Modiolus* sp., *Myophoria* (*Costatoria*) *curvirotris* Schlotheim emend. Seeb, *Entolium* sp.

Paraconformity

Middle Formation (T_2^1): Medium to thick-bedded grey limestone with layers of argillaceous limestone, altered tuff, with 5 m thin-bedded altered volcanics at the base, yielding crinoids, ammonoids, brachiopods and bivalves from the argillaceous limestone; Bivalves:? *Lima* sp. aff. *L. tarnowitzensis* Assmann, *Myophoria* (*Elegantinia*) sp., *M.* (*Neoschizodus*) *laevigata* (Zeithen), *Entolium subdemissum* (Munster), *Pleuromya* cf. *fassaensis* Wissm., *Plagiostoma* sp. 81 m.

Lower Formation (T_1): 1.7 to 2 m thick arenaceous limestone intercalated with epidotic marble at the base and brachiopod-bearing limestone and oolitic limestone in the middle and upper parts. 125 m.

Conformity

Underlying strata: Upper Permian Sandstone (Lielonggou Formation)

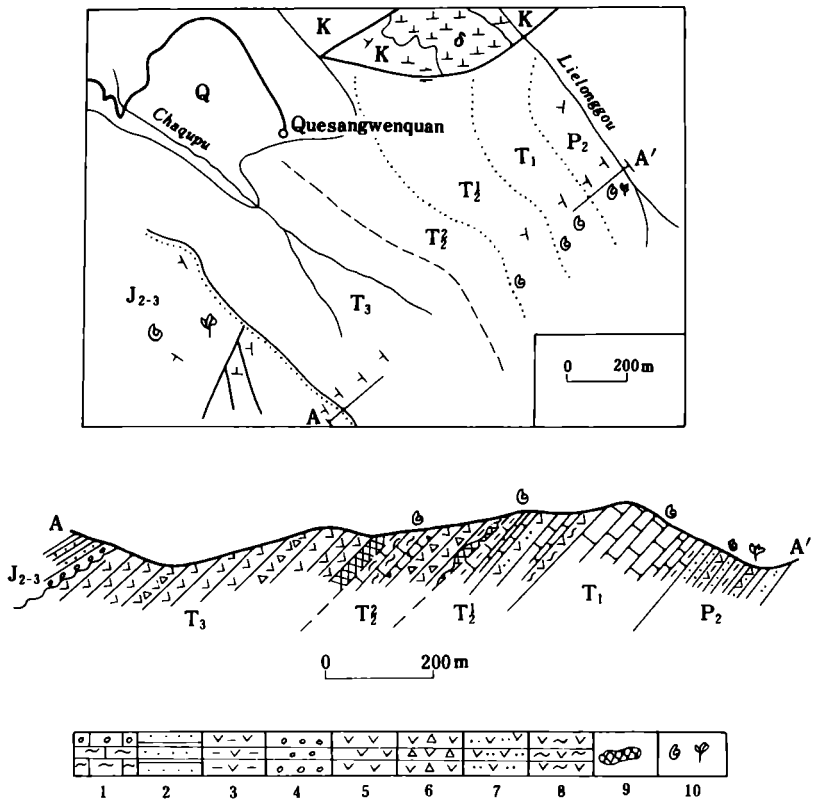

FIGURE 17. The Triassic section at Quesangwenquan in Doilungdeqen County. 1. Oolitic and shelly limestone; 2. Alternating siltstone and arenaceous shale; 3. Tuffaceous mudstone intercalated with altered andesite and andesitic basalt; 4. Conglomerate; 5. Intermediate-basic lava, tuff and volcanic breccia; 6. Intermediate-basic welded breccia; 7. Altered ignimbrite; 8. Altered volcanics – 'greenstone'; 9. Hematite lens and ferruginous sandstone; 10. Fossil localities.

Fossils previously reported from the Lower Triassic in the Himalayas and the Far East Coastal Province of the U.S.S.R. were collected from the limestones of the Chaqupu Group, such as the brachiopods *Neowellerella lielonggouensis* Sun, *Abrekia chaqupuensis* Sun, *Paranorellina duilongdeqingensis* Sun, the conodont *Neospathodus homeri* (Bender) and the gastropod *Natica* cf. *subtilistriata* Frech (Sun Dongli *et al.* 1981). Anisian brachiopods and ammonoids have been

collected from the middle Chaqupu Group; this assemblage resembles the late Anisian Palaeotethyan ammonoid fauna of northern Tibet and the Alps more closely than the Neotethyan ammonoid fauna of the same age in the Himalayas (Gu Qingge *et al.* 1980). Most fossils from the upper formation are Middle Triassic genera, only *Myophoriopsis* aff. *lineata* is similar to *M. lineata* commonly seen in the Ladinian in Europe. These bivalve-bearing strata could be Ladinian as the underlying strata are late Anisian. The volcanics of the 'Yeba Formation' are interposed between fossil-bearing Middle Jurassic sandy conglomerate and the Chaqupu Formation, so a late Triassic age is ascribed to them. Similar volcanics are found near Dagze. The Multidisciplined Survey of the Bureau of Geology and Mineral Resources of Tibet named them the 'Yeba Formation' in 1979 based on the sequence observed at Yeba. The Yeba Formation is deduced to be late Triassic since it is unconformably capped by Jurassic limestone and *Thecosmilia* was found from strata equivalent to the lower part of the Yeba Formation elsewhere in the Lhasa region. Chinese and French geologists previously took the Yeba Formation to be Upper Cretaceous because they believed it to be faulted against the overlying Upper Jurassic Duodigou Formation and to rest conformably on the Lower Cretaceous (Wang Naiwen 1983). As the relations of the volcanics are still obscure and the volcanics may be of different ages, further study is needed. However, palynomorphs indicate a late Carboniferous or Permian age.

10. Jurassic

Fossiliferous marine Jurassic strata are restricted to the Qiangtang and Lhasa Terranes. The Kunlun Terrane was mountainous during Jurassic times: a small amount of coal-bearing clastics was deposited in fault basins.

(*a*) *The Southern Mountain of Xidatan, Kunlun Terrane*

The coal-bearing strata of the abandoned coal mine near Xidatan in the Bayan Har subregion form a 65 m thick and 1 km long wedge-like slab which is bounded by faults and surrounded by the Lower Bayan Har Group. The clastics contain five or six layers of poor-quality coal seams (about 10 cm thick) containing early to mid Jurassic plant fossils, such as *Eborasia lobifolia* (Phillips) Thomas and *Ciliatopteris pectinata* Wu (see Naij Tal Sheet).

(*b*) *Yanshiping–Amdo Region, Qiangtang Terrane*

From Yanshiping south to Amdo, Jurassic strata are dominant, forming a synclinorium centred on the Tanggula Mountains. Despite previous studies of this area (Sun Dongli & Zhang Binggao 1979; The Compiling Group of Charts of Stratigraphical Units Sequence of Qinghai 1980; Li Guangcen & Lao Xiong 1982; Jiang Zhongti 1983), the classification, correlation and age of the units are still confused. Here we assign the 'Yanshiping Group' to the suite of alternating terrestrial/marine molasse on the basis of the data published in the Stratigraphical Charts of Qinghai Province.

Based on field observations at Wenquan and data from Jiang Zhongti (1983), the Yanshiping Group is divided into five suites, in which four clastic-carbonate rhythms are observed (figure 18). The total thickness attains 5021 m. For a detailed sedimentological description, see Leeder *et al.*, this volume. The sequence in ascending order is as follows.

Suite 1 (1000 m). This is truncated by a fault at the bottom. The lower and middle parts are

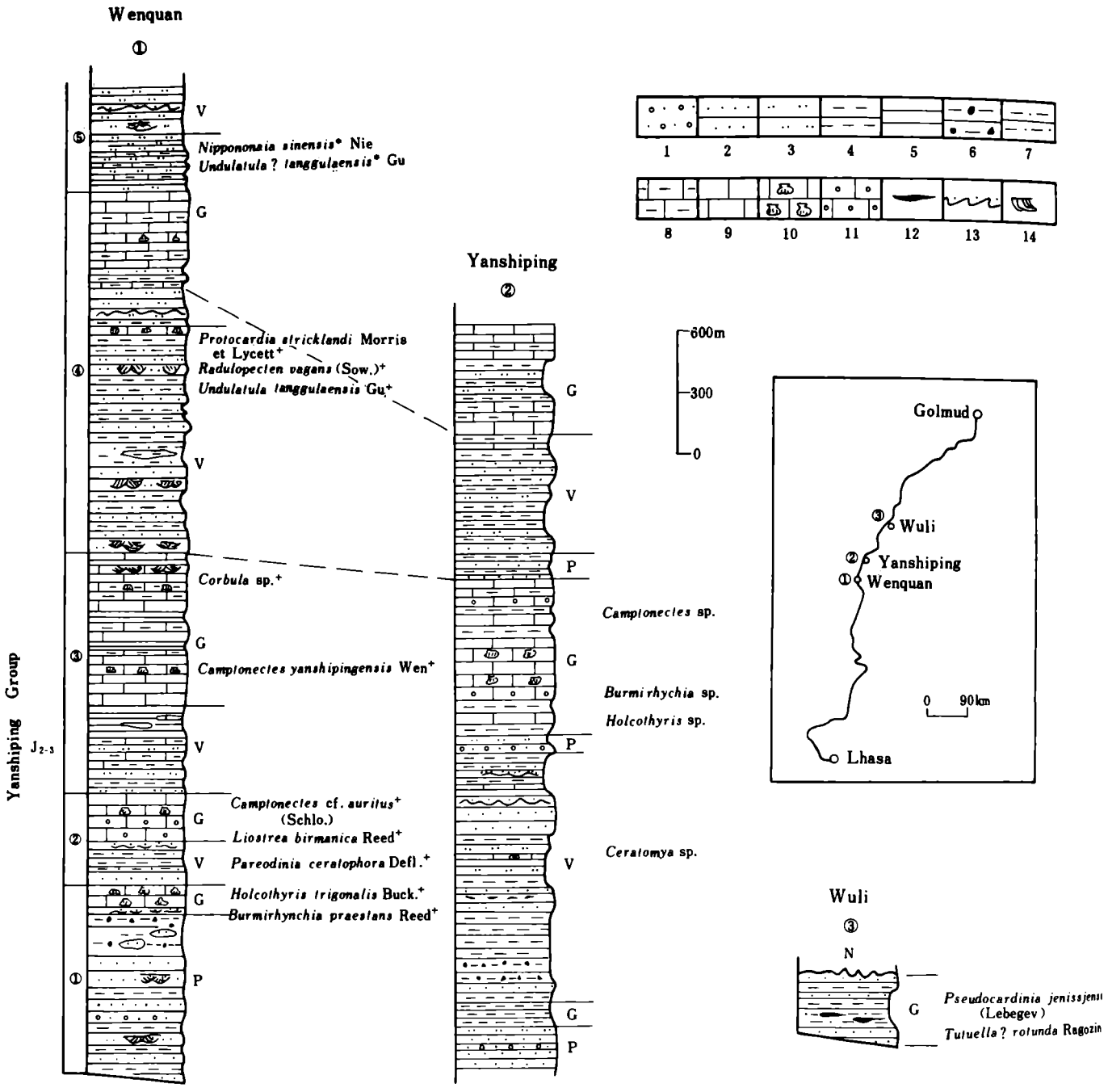

FIGURE 18. Correlation of the Jurassic on the northern slope of the Tanggula Mountains. ① and ② Modified from the 'Wenquan Section' and the 'Yanshiping Section' by Jiang Zhongti (1983, pp. 92–96). 1. Conglomerate; 2. Sandstone; 3. Siltstone; 4. Mudstone; 5. Shale; 6. Clay-boulder mudstone; 7. Arenaceous shale; 8. Muddy limestone; 9. Limestone; 10. Bioclastic and shelly limestones; 11. Oolitic limestone; 12. Coal seams; 13. Ripple marks; 14. Cross-bedding.

purplish-red mudstone, siltstone interbedded with sandstone and conglomerate lenses (888 m). Cross- and convolute-bedding are very common in the sandstone and the palaeocurrents were southwards. The upper part is composed of fossiliferous limestone, argillaceous and shelly limestones, 122 m thick (loc. B57).

Suite 2 (437 m). The lower part is composed of variegated sandstone, arenaceous mudstone

and shale with dinoflagellates (loc. B58, lower shales) (184 m) with asymmetrical current ripple marks on the sandstone surfaces. The upper part is of oolitic limestone, shelly limestone and mudstone (253 m). Both are fossiliferous (loc. B58).

Suite 3 (1191 m). The lower part, 445 m thick, is composed of interbedded variegated sandstone, arenaceous shale and mudstone with thin-layered argillaceous limestone bands. Some cross-bedding and a few plant fragments are found in the red siltstone; the upper part, 746 m thick, consists of grey bioclastic and arenaceous limestone; some cross-bedding, wave-ripple marks and storm flow rollers are found in the medium-thick bedded limestone at the top. Palaeocurrents trend NW 320°. Fossil bivalves were collected from the limestone in the upper part (loc. B58, beds 37–45).

Suite 4 (1135 m). The lower part (472 m) consists of interbedded variegated arenaceous shale and siltstone with intercalations of mudstone and thin-bedded bioclastic limestone. The upper part, 663 m thick, is composed of limestone, marls and bioclastic limestone with siltstone and mudstone intercalations bearing fossil bivalves (loc. B58).

Suite 5 (599 m). The lower part is dominated by grey siltstone interbedded with micrites, while the upper part is brown and grey bivalve-bearing siltstone and fine sandstone intercalated with argillaceous siltstone.

The bottom of the Yanshiping section is covered but it is assumed that the Jurassic unconformably overlies the Middle and Upper Triassic Gyiza Group. Cupreous intermediate volcanics are intercalated in the red clastics in the lower part of the Yanshiping Group south of Yanshiping.

The Yanshiping Group on the northern slope of the Tanggula Shan is composed mainly of fine-grained clastics with channel sandstones and conglomerate lenses with abundant well-preserved shallow-water structures, such as cross-bedding, mud cracks and ripple marks. The carbonates are mainly bioclastic, shelly and oolitic limestones with some cross-bedding and storm flow rollers. These structures suggest that the Yanshiping Group was rapidly deposited in terrestrial, littoral and neritic environments.

The carbonates of the Yanshiping Group on the southern slope of the Tanggula Mountains are much thinner than those on the northern slope. The rhythmic clastics and carbonates seen in the Yanshiping and Wenquan sections are less evident on the southern slope. North of 114th Highway Maintenance Squad, the strata are mainly variegated red/grey clastics whereas further south the dominant rocks are limestones interbedded with grey clastics, implying increasingly marine conditions southwards.

Li Guangcen & Lao Xiong (1982) noted that the Jurassic in the Wenquan region is more than 5375 m thick, and thins both southwards and northwards, implying that this was the area of maximum subsidence. Changes in thicknesses of carbonate units, palaeocurrents and the thickness of the Yanshiping Group support the assumption that a Jurassic elevated belt of Palaeozoic strata in the present Tanggula Mountains area (from Wenquan to Amdo) influenced the adjacent sedimentary basins. It is concluded that the Yanshiping Group represents an overlapping sequence of foreland and neritic sediments in a paralic molasse basin at the northern margin of the Neotethys.

The age of the Yanshiping Group is mid- to late Jurassic. The lower part of Suite 2 in the Wenquan section yields dinoflagellates including *Pareodinia ceratophora*, a typical widely distributed Bajocian/Bathonian species, whereas the abundant brachiopod and bivalve fossils from Suites 1, 2 and 3 exhibit noticeable endemic features, i.e. most of the genera and species

are also elements of the Liuwan Formation in Western Yunnan and the Namyau series in North Burma, both mid-Jurassic. This represents a biogeographical subprovince at the northern margin of East Tethys during the Jurassic (Yin Jixiang & Fang Zhongjing 1973; Reed 1936; Buckman 1917). The abundant non-marine bivalves of Suite 4 are also found in the Upper Jurassic of Sichuan and Yunnan Provinces. Furthermore, *Peregrinoconcha*, reported from this formation (The Compiling Group of 'Bivalve Fossils of China' 1976; Zhang Zuoming *et al.* 1980) is typical of the 'Jingxing Fauna' of Yunnan; this fauna is generally taken as late Jurassic or late Jurassic/early Cretaceous. When discussing the age of the Yanshiping Group, Sun Dongli & Zhang Binggao (1979) noted the occurrence of the freshwater bivalves *Nippononaia sinensis* Nie and *Undulatula tanggulaensis* Gu in strata equivalent to Suite 5 of the Yanshiping Group. *Nippononaia sinensis* Nie is a key element of the Upper Jurassic fauna in western Liaoning Province. Thus the existence of the Upper Jurassic in the Yanshiping Group is certain. In the Wenquan area, Suites 4 and 5 are characterized by the *Undulatula* Fauna of late Jurassic age.

Four km west of the highway at Wuli, non-marine Jurassic bivalves were collected (loc. B64) from a coal series previously taken to be late Permian. From a section at Yanshiping, many individual bivalve fossils were also collected (loc. B56). Combined with the bivalve fossils *Lamprotula* (*Eolamprotula*) *cremeri* (Frech) and *L.* (*E.*) *subquadrata* Gu found in the Wenquan area (The Compiling Group of 'Bivalve Fossils of China' 1976, pp. 315–316), these fossils belong to the *Lamprotula* (*Eolamprotula*)–*Pseudocardinia* fauna widespread in Asia during the Jurassic.

The shales on the eastern bank of the Jiebu River, south of Tanggula Shan, yield dinoflagellates and the argillaceous limestone 80 m above this yields abundant poorly preserved ammonoids (loc. B50). The age of the dinoflagellate *Pareodinia ceratophora* from Suite 2 in the Wenquan section is early Bajocian. The ammonoid *Stephanoceras* is Upper Bajocian (i.e. the 'Middle Inferior Oolite' of Britain), hence, both fossil-bearing beds are Bajocian (but see loc. B60). The strata beneath the dinoflagellate-bearing beds are covered; ammonoid-bearing beds pass gradually up into medium- to thin-bedded limestones yielding Bathonian brachiopods and bivalves (loc. B51). In 1961, Yin Jixiang collected bivalves and gastropods of Bathonian age from the same limestone: *Astarte subcardiformis* Fan, *Protocardia lamellosa* Fan, *Grammatodon minutus* Fan, *Trigoria* sp. (Fan Jiasong 1965). These strata are however reported to yield late Jurassic ammonoids (Jiang Zhongti 1983). Bathonian brachiopod and bivalve fossils were also collected 4 km southwest of 114th Highway Maintenance Squad (loc. B49).

(*c*) *Lhasa Region, Lhasa Terrane*

The Jurassic may be divided on facies into three subregions, which are, from north to south: the Dongqiao–Nagqu Subregion, the Doilungdeqen–Lhunzhub Subregion and the Sangri Subregion.

(i) *Dongqiao–Nagqu Subregion*

The subregion is bounded to the north by the Banggong–Dongqiao–Nujiang fault zone which separates it from the Qiangtang Terrane. However, lithostratigraphical features seem to be transitional across this boundary. The southern boundary is a line from Qilingco–Duoba–Senco–Jiuzila–Sangba (i.e. the northern marginal fault of the Nyainqentanglha Shan). The Jurassic in this region is intensely deformed constituting a synclinorium with destroyed limbs. The lithofacies changes notably, both across and along strike; it is associated with

ophiolites. The stratigraphy is complicated and despite several geological surveys and the discovery of early to late Jurassic fossils, the basic stratigraphy remains uncertain (Li Pu 1955; Wang Mingzhou & Cheng Liren 1980; Jiang Zhongti 1983; Han Tonglin 1983, 1984; Wang Naiwen 1983, 1985).

The early Jurassic fossiliferous strata are restricted to a small, narrow area from the Lunpola Basin eastward to the east of Amdo in the northern part of the subregion. Early and middle Jurassic ammonoids and bivalves were collected from the grey argillaceous limestone, shale and nodular shale in the 'Zhamunaqu' (the present 'Raoqinlongbaqu') section, 19 km northeast of Amdo (loc. B45). The fossiliferous strata are 200–300 m thick and situated on the southern limb of a syncline; they grade gradually upward into shale and bioclastic limestones. *Grammoceras* is a zone indicator of the European Toarcian stage (Yeovilian of Britain), and *Soninia* (*Soninia*) a zone indicator of the Upper Bajocian ('Middle Inferior Oolite' of Britain), suggesting that the fossiliferous strata are upper Lower Jurassic to lower Middle Jurassic. The bivalve *Hippopodium ponderosum* (Gu Zhiwei 1982) and the ammonoids *Giveliceras* and *Arnioceras* (Jiang Zhongti 1983), zone fossils of the European Sinemurian stage, are an earlier fauna, from a horizon probably lower than that from which fossils were collected during the 1985 Geotraverse.

The Sinemurian ammonoids *Baucaulticeras* cf. *baucaultianum* (d'Orbigny), *Angulticeras* cf. *lacunatum* (Backman) and the fossil plant *Cladophlebis* sp. were recorded (Wen Shixuan 1984) from pelites and shales at the northern and southern margins of the Lunpola Basin, 60 km west of Dongqiao. These neritic sediments are a westward extension of the Lower Jurassic from the northeast of Amdo. The underlying strata are concealed; upwards these strata cannot be distinctly separated from the Middle Jurassic fossil-bearing strata.

The flysch series widely distributed in the lake region from Dongqiao to Jang Co has been variously named (Wang Mingzhou & Cheng Liren 1980; Wang Naiwen 1983). These names are abandoned here because there are no appropriate stratotype sections and the precise timing for these units is uncertain. Here the name 'Lake Area Flysch' is temporarily substituted for the previous names.

Some pillow lavas dipping southwestward crop out at Luobuzhong Hill 8 km southeast of Dongqiao and grade upward into a flysch sequence, both being intensely deformed. Grading in the flysch in Erong valley south of Luobuzhong Hill suggests the sequence near the lava is inverted. A detailed sedimentological description is given by Leeder *et al.*, this volume.

The transitions from volcanoclastic and argillo-calcareous to arenaceous-argillaceous flysch, and from pelitic to neritic bioclastics upwards to terrestrial clasts represent environmental changes from pelagic to continental slope. The occurrence of olistostromes implies a steep slope and unstable sedimentary environment.

The 'Lake Area Flysch' elsewhere is composed of intercalations or lenses of limestone turbidites, intermediate-basic volcanics, fine-grained conglomerates, pebbly sandstones, and neritic bioclastic limestones attaining a thickness of over 4000 m.

The argillaceous graywacke on the northern bank of Jang Co yields abundant orientated gastropods and other fossils showing a southward palaeocurrent (loc. B32). The strata, previously regarded as Triassic, yield the coral *Stylosmilia* (Middle Jurassic to early Cretaceous). The faunal assemblage indicates these strata are Upper Jurassic.

From the slate and limestone in the west hill of Murong, Jiaqiong village at the western bank of the Daru Co, previous workers have collected Middle Jurassic bivalves: *Inoceramus* cf. *kudoi*,

Protocardia cf. *hepingxiangensis*, *P. strichlandi*, *Astarte* sp., *Camptonectes* (*Camptonectes*) sp., *Grammatodon* (*Indogrammatodon*)? sp. Late Jurassic fossils found in limestone interlayers north of the Luoertai–Regala area, southeast of Luobuzhong, include hexacorals, hydroid stromatopora: *Enallhelia?* sp., *Microsolena agariaformis*, *Epismilia?* sp., *Actinarea* sp., *Spongiomorpha* (*Heptastylopsis*) *asiatica*, *Parastromatopora delicata* (Wang Mingzhou & Cheng Liren 1980). In the limestone 3 km north of 26th Highway Maintenance Squad (E 91° 47′, N 31° 43′) north of Nagqu, the top Jurassic gastropod assemblage *Nerinea*, *Nerinella*, *Ptygmatis* and *Pseudomelania* was found (Yin Jixiang 1964). Late Jurassic ammonoids *Himalayites*, *Pseudocadoceras*, *Lilloetia*, the gastropod *Aptyriella* and some bivalves were found at Guishan (Jienu) on the northern bank of the Xiaqiong Co (Liao Weihua & Chen Tingen 1984). The above fossils found at various localities in the lake area verify that the 'Lake Area Flysch' is of mid-late Jurassic age. North of Dongqiao, there is a series of ophiolitic clastic rocks. A limestone sequence unconformably overlying the ophiolites yielded late Jurassic to early Cretaceous plant fossils, stromatopora and bivalves (Wang Mingzhou & Cheng Liren 1980; Wen Shixuan 1984). Hence, the upper age limit of the 'Lake Area Flysch' should be earlier than late late Jurassic.

The lithofacies of the 'Lake Area Flysch' changes remarkably eastward towards the upper Nujiang River. Fossiliferous Middle Jurassic with a red conglomerate at the base overlies the Amdo Schists and the Upper Triassic (Tumaingela Formation). The upper Middle Jurassic, 1130 m thick, comprises oolitic limestone, mudstone and bioclastic limestone interlayered with andesite and volcanic breccia without flysch structures. The base of the Upper Jurassic consists of red and grey conglomerates and granitoid conglomerates, also resting on Amdo schists and the Middle Jurassic northwest of Xiaqiuka. The middle and upper parts are arenaceous slate interlayered with nodular slate, fine conglomerate and pebbly sandstone of flysch facies. The late Jurassic ammonoids *Virgatosphinctes*, *Aspidoceras* and *Berriasella* are reported from the nodules. The Upper Jurassic is more than 2300 m thick (Han Tonglin 1983).

(ii) *Doilungdeqen–Lhunzhub Subregion*

This subregion is separated from the Sangri subregion to the south by a line between Doilungdeqen and Lhasa. The Jurassic here lies in three roughly E–W trending belts. The northern belt runs from the southeast of Nam Co–Deqen, east through Doilungdeqen County, passing south of Nam Co to Sangba; the middle and southern belts lie north and south of the Cretaceous red bed basin north of Lhasa. The middle and northern belts are separated by the Carboniferous–Permian and Nyainqentanglha metamorphic rocks.

The Jurassic in the northern belt is well developed near Deqen. According to Han Tonglin (1983, 1984), the unfossiliferous lower part, 1200 m thick and unconformable on Permian, consists of basal conglomerate, tuffaceous and pebbly sandstone. The middle part, 800 m thick, comprises intermediate-basic volcanics with tuffaceous sandstone, siltstone and conglomerate, yielding the ostracodes *Damonella* and *Lycopterocypris*, the foraminifers *Quinqueloculina*, *Textularia* and *Endothyranella*, the coral *Goniopora* sp., bivalves, brachipods and crinoids. The ostracodes and foraminifers from the middle and upper parts are of late Jurassic age.

The Jurassic in the middle belt, well-exposed at Quesangsi (figure 19), was studied by Yin Jixiang and Sun Yiyin in 1981 and later by the Chinese–French geologists. The lower part of the Middle Jurassic, the Quesangwenquan Formation, unconformable on Triassic volcanics, is 33 m of interbedded volcanic conglomerate. The middle part is 85 m of interbedded sandstone and shale with amygdaloidal andesite intercalations and yielded the bivalves *Protocardia* aff.

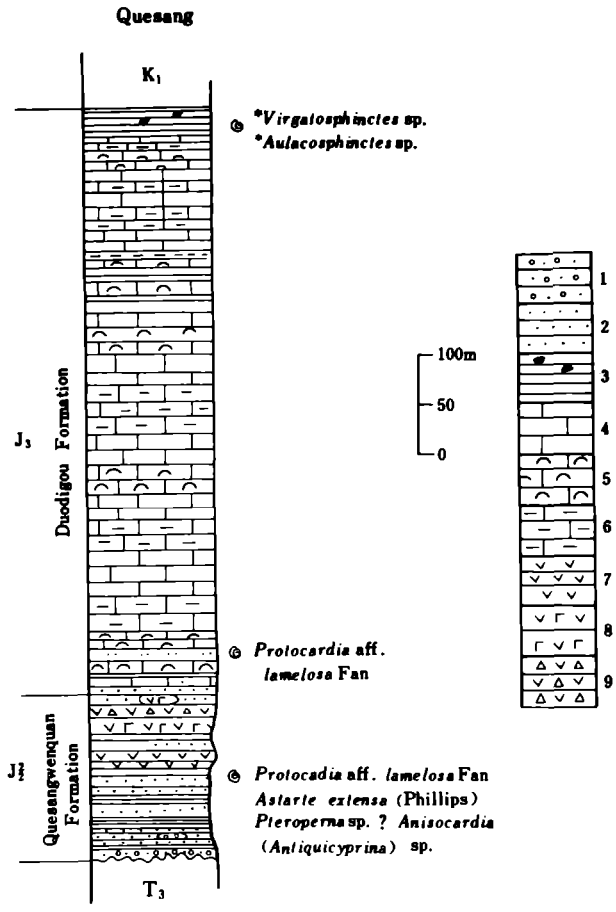

FIGURE 19. Columnar section of the Jurassic at Quesangsi. * The fossil list of ammonoids is from Wang Naiwen *et al.* (1983). 1. Conglomerate; 2. Sandstone; 3. Shale, nodular shale; 4. Limestone; 5. Shelly limestone and bioclastic limestone; 6. Argillaceous shale; 7. Andesite; 8. Andesitic basalt; 9. Volcanic breccia.

lamellosa Fan, *Astarte extensa* (Phillip), *Pleuromya* sp., *P. uniformis* (Sowerby), *Pteroperna* sp., and ? *Anisocardia* (*Antiquicyprina*) sp. The upper 40 m comprises greyish-purple and green andesite basalts and volcanic breccia. Chinese and French geologists recorded the bivalves *Astartoides dingriensis* Wen, *A. gambaensis* Wen & Lan and *Pleurotomaria spitiensis* Spitz, and also the plant fossils *Ptilophyllum* sp. and *Zamites* sp. from the Quesangwenquan Formation. The bivalves recorded commonly occur in the Upper Jurassic, e.g. *Astarte extensa* in Basu, East Xizang (Tibet), *Astartoides dingriensis* and *A. gambaensis* from the Upper Jurassic in the Mt. Qomolangma (Everest) region; *Protocardia* aff. *lamellosa* has affinity with specimens from the Bathonian at 114th Highway Maintenance Squad in the Qiangtang Terrane.

The Upper Jurassic (Duodigou Formation) is 580 m in thickness, the lower 60 m argillaceous limestone interbedded with shale, shelly limestone and fine sandstone yielding *Protocardia* sp.; the upper 468 m limestone and bioclastics with argillaceous limestone layers; the topmost beds (52 m) are nodular limestones and siltstones with minor thin-bedded limestones which gradually pass upwards into the Lower Cretaceous Linbuzong Formation. From the top shale of the Duodigou Formation, *Virgatosphinctes* sp. and *Aulocosphinctes* sp. (Wang Naiwen *et al.* 1983) indicating a Berriasian (latest Jurassic of Chinese workers, early Cretaceous of others) age, were found.

Faulting and magmatism obscure the Jurassic in the southern belt; Duodigou Formation limestones dominate the Upper Jurassic near Lhasa. Gastropods (*Nerinea*, *Cossmannea*) and corals are recorded from them.

The primary Jurassic sequence in the subregion is basal conglomerate, interbedded sandstone shale and carbonate-shale, representing a complete transgression-regression cycle. The Jurassic thickens northwards. Flexural folds caused by sea-bottom slumping in the Duodigou limestone and volcanics in the strata equivalent to the Quesangwenquan Formation imply deposition in an unstable shallow-water environment (figure 19).

(iii) *Sangri Subregion*

This subregion is bounded by the Yarlung–Zangbo Suture Zone to the south. The fossiliferous Jurassic and the overlying inseparable Cretaceous mainly occur north of the Yarlung–Zangbo River, especially in the Oin region of Sangri and Nedong County. The Jurassic–Cretaceous beds mainly occur as caps and country rocks to the granitoids and are variably metamorphosed. A suite of andesites/quartz andesites grading into metasiltstones, hornstone skarns, marbles and calcirudites, over 650 m thick, occurs immediately north of the Yarlung–Zangbo Suture Zone east of Zetang and represents the lower part of the Sangri Group. From the marble, the Second Geological Surveying Team of Xizang Autonomous Region collected gastropods, bivalves, corals etc., among which the gastropod *Ptygmatis nodosa* Voltz is widely spread in the Kimmeridgian of Europe and *Elegantella conoidalis* Peel is also found in the Ruac Series in the Crimea, U.S.S.R. Hence, the fossiliferous strata are late Jurassic (Yang Shengqiu & Wang Huiji 1985). The Sangri Group resembles the Doudigou Formation in sequence and lithology, except that it contains enormous amounts of calc-alkali volcanics, which implies that the Sangri Group was deposited under the influence of the Gangdise island arc at the southern margin of the Lhasa Terrane.

11. Cretaceous

The marine Cretaceous in the Tibetan Plateau is restricted to the Lhasa Terrane. The Terrane is divided into three subregions.

(*a*) *Pangkog–Nam Co Subregion*

This area lies west of Nagqu in the lake region from Nam Co to Pangkog Co. Two major sedimentary facies of the early early Cretaceous are found. Firstly, terrestrial beds with marine intercalations, the Douba Formation are distributed around the southern margin of the Baingoin Basin and extend westwards to the west of Nam Co. Secondly, in the lake area north of the Bangoin Basin, the lowest Cretaceous, the Xiaqiongco Formation, is mainly composed of marine clastics and volcanics while the Langshan Formation is composed of neritic carbonates of late early to early late Cretaceous age (Ma Xiaoda 1981; Wang Naiwen 1983).

(i) *Duoba Formation*

The base of the Douba Formation on the northern slopes of Langshan Mountain in the Douba region, Baingoin County, is thrust southwestward over Tertiary pebbly sandstone. The lower part is composed of purple arenaceous conglomerate-pebbly sandstone–siltstone–mudstone rhythms. The middle part is formed of rhythms of grey or greyish-green grits–

siltstone–mudstone and the upper part of rhythms of interlayered grey or purple fine sandstone–siltstone–mudstone. The whole sequence fines upward. Individual beds of the lower sandstone and conglomerate are commonly 10–15 m in thickness and 50–80 m in length with fluvial facies cross-bedding. Pebbles in the conglomerate are well-rounded and sorted and composed of mudstone, limestone, granite and occasional mafic rock. The lower part of the Duoba Formation on the southern slope of Langshan Mountain is grey sandstone and conglomerate intercalated with nodular shale. Derived *Orbitolina* are found in the calcareous sandstone. The thickness of the Duoba Formation is over 1300 m; it is faulted against the underlying Qusongbo Formation (Han Xiangtao *et al.* 1983). The Duoba Formation passes lithologically into the Xiaqiongco Formation to the north.

(ii) *Xiaqiongco Formation*

The Xiaqiongco Formation occurs in the Guiya–Raibadange–Gushan area of Xiaqiong Lake, north of Pangkog Lake, and is composed mainly of rhythmic alternations of variegated fine-grained calcareous sandstone, mudstone and quartzose sandstone interlayered with purple and green siliceous mudstone, amygdaloidal basalt and bioclastic limestone. It passes upward into the Langshan Formation. The base is covered; only some 300 m of strata can be seen. The lower part has yielded the ammonoids, *Neocosmoceras*, *Spiticeras*, *Neocomites*, *Calliphylloceras*, *Thurmaniceras*, *Killianella*, *Sarasinella*; the corals *Acrosmilia*, *Montlivaltia*, and bivalves, gastropods, foraminifers and echinoids as well as a few plant fossils such as *Zamiophyllum*. The age of the fossil-bearing beds is Berriasian–Hauterivian (Han Xiangtao *et al.* 1983; Liang Shousheng & Xia Jinbao 1983; Wang Naiwen 1983). North of Gushan, east of Xiaqiong Lake, palaeontological collections were made from equivalent beds (locs. B29–32).

(iii) *Langshan Formation*

The Langshan Formation forms the core of a syncline in the Duoba region and is composed mainly of grey limestones and biolithites with argillaceous limestone, siltstone and mudstone intercalations, up to 700–900 m thick. The upper part is absent in the section. The biolithites consist of Orbitolina limestone, rudist bioclastic limestone and calcareous algal limestone yielding abundant fossils (Zhang Binggao *et al.* 1981; Han Xiangtao *et al.* 1983; Liang Shousheng & Xia Jinbao 1983; Yu Wen & Xia Jinbao 1985). During the Geotraverse, extensive fossil collections were made (loc. B28). The nerineid (gastropod) species are all common in the Aptian of Europe and the Middle East. Most of the foraminifers are found in the Albian. If the previous identification of *Orbitolina concava* is reliable, the age range should extend to the Cenomanian (but see Smith & Xu, this volume). The bivalves and other fossils may range from early to late Cretaceous. Equivalent strata near Xungmai, Xainza County, west of Langshan Mountain, also yield *Orbitolina* (*O.*) *birmanica* associated with an Albian–Cenomanian brachiopod assemblage (Liao Weihua & Chen Tingen 1984). Since the uppermost part of the Langshan Formation is absent in the Langshan section, the Langshan Formation may extend into the Cenomanian, although the sequence may be inverted.

The Cretaceous sections along Gushan–Hongyashan and the northern bank of Xiaqiong Lake have been worked on previously but the stratigraphy is still confused. The authors agree with Ma Xiaoda (1981) that these sequences are equivalents of the Langshan Formation, because of their lithological and palaeontological similarities. The Cretaceous on the northern bank of Xiaqiong Lake is more than 1600 m thick and is composed mainly of limestone and

biolithites in the lower and upper parts, interlayered with quartzose sandstone, siltstone and bioclastic limestone in the middle part. At Hongyashan, the upper limestone is unconformably overlain by Tertiary red beds. The Cretaceous in this region yields abundant corals, brachiopods, foraminifers and echinoids, but no *Orbitolina* (foraminifera), despite its common occurrence in the Langshan Formation, which might either suggest a difference in biofacies between the two regions during Cretaceous times, or, alternatively, a different age. The limestone of the uppermost Langshan section supposedly yields rudists similar to those from the late Cretaceous in the Mount Qomolangma (Everest) region (Wang Naiwen 1983). However, the fossils associated with the rudists, especially the brachiopods *Orbirhynchia*, *Lunpolaia*, *Trochifera* and *Yuezhuella*, are very similar to those of the Langshan Formation at Xungmai southwest of the Baingoin Basin (Ye Songling & Yang Shengqiu 1979), hence the Cretaceous sequence on the northern bank of Xiaqiong Lake seems to be no younger than Cenomanian (see also Smith & Xu and Leeder *et al.*, this volume).

Around Dongqiao, a series with ophiolitic sandstone and conglomerate at the bottom, picotite-bearing sandstone, siltstone and carbonaceous shale in the lower part and interbedded bioclastic limestone and thin-bedded sandy conglomerates in the upper part unconformably overlies the ophiolites south of Zige Tang Lake. The clastics in the lower part yield the plants *Ptilophyllum*, *Podozamites*, *Cladophlebis*, *Baiera* and *Nilssonia*: the limestone in the upper part yields the stromatopora *Milleoporella*, *Milleporidium*, *Parastromatopora*, *Cladocoropus* and *Astrorhizopora*, and the bivalves *Pterinella*, *Mytilus*, *Placunopsis* and *Protocardia*. These fossils range from latest Jurassic to earliest Cretaceous (Wen Shixuan 1984; Wang Mingzhou & Cheng Liren 1980).

(*b*) *Doilungdeqen–Lhunzhub Subregion*

The Cretaceous around Lhunzhub, Lhasa region, has been studied in detail previously; the sequence is as follows.

(i) *Linbuzong Formation*

The Linbuzong Formation, of which coal-bearing terrestrial clastics form the major part, is 300–1000 m thick and conformably overlies the Upper Jurassic Duodigou Formation. In Quesangsi, it yields plant fossils (loc. B69). From the same locality, Wang Naiwen *et al.* (1983) collected *Weichselia reticulata* (Stockes & Webb) Ward and *Onchyopsis* sp. This assemblage is similar to that of the Wealden Stage in Europe and is correlatable with the plant assemblages from the Duoni Formation, Nujiang River (Duan Shuying *et al.* 1977; Li Pu 1955). Both represent fossil plant assemblages of a swamp environment along the continental margin or the central uplift region of the Lhasa Terrane.

(ii) *Chumulong Formation*

Succeeding the Linbuzong Formation, the Chumulong Formation (700–1000 m) is composed mainly of terrestrial quartzose sandstone, conglomerate with variegated arenaceous shale and some irregularly distributed andesites and andesitic ignimbrites.

(iii) *Takena Formation*

Succeeding the Chumulong Formation and overlain unconformably by volcanics of the Linzizong Formation, the Takena Formation is divided into two members, the lower Penbo

Member and the upper Lhunzhub Member. The Penbo Member, interbedded grey marine limestone, siltstone and argillaceous limestone, is 170–300 m thick. Aptian-Albian fossils such as the foraminifers *Orbitolina* (*Mesorbitolina*) *texana* (Roemer), *O.* (*Eorbitolina*) *prisca* Zhang, *O.* (*Columnorbitolina*) *tibetica* Cotter, *O.* (*Columnorbitolina*) *pengboensis* Zhang, the ammonoids *Acanthohoplites* sp., *Uhligella* cf. *chansayensia* (Jacob), *Paracycloceras?* sp., *Parahoplites* cf. *melchioris* Anthula and echinoids, gastropods, bivalves, marine vertebrates, shrimps and crabs have been recorded from it (Wang Naiwen *et al.* 1983; Chen Chuzhen & Wang Yujing 1984).

The Lhunzhub member, 600–1000 m thick, consists mainly of interbedded marine and terrestrial variegated siltstones and mudstones intercalated with argillaceous limestone, irregularly distributed andesite and ignimbrites. The bivalve *Amphidonte* reported from the argillaceous limestone is supposed to be Cenomanian in age.

(*c*) *Sangri Subregion*

The Sangri Group is developed along the southern margin of the Lhasa Terrane, immediately neighbouring the Yarlung–Zangbo Suture Zone. It is an unsubdivided Upper Jurassic to Lower Cretaceous stratigraphical unit over 4500 m thick. The principal components of the Lower Cretaceous part of the Group are rhythmic alternations of volcanics, clastics and carbonates. The volcanics pass from intermediate-basic upward into intermediate-acidic and further into acidic rocks. Bivalves, corals and gastropods are recorded from the limestone (Xu Baowen *et al.* 1982); the nerineid gastropods are similar to those from the lower part of the Langshan Formation in the Baingoin district (Yang Shengqiu & Wang Huiji 1985).

The marine Cretaceous of the Lhasa Terrane is restricted to the lake area west of Nagqu; east of Nagqu, along the middle Nujiang River, there are only Lower Cretaceous marine bands in a non-marine sequence, and further east or southeast only terrestrial Cretaceous beds crop out. The uppermost Cretaceous marine beds in the eastern part of the lake area and the Lhasa area are similar in age, i.e. Aptian to Cenomanian. The Cretaceous east of the lake area is characterised by 'platform' neritic clastics and carbonates which overlie the Middle to Upper Jurassic flysch and indicate the beginning of the decline of the Banggong Lake–Dongqiao–Nujiang River 'back-arc basin'. The Cretaceous in the Lhasa area is dominated by terrestrial deposits indicating fluvial, lacustrine or neritic environments in the central uplifted area of the Lhasa Terrane. The thick calc-alkaline volcanics associated with sediments in the Sangri area are interpreted as deposits at the frontal margin of the Gangdise magmatic island arc (figure 20).

12. Tertiary

The Tertiary in the Geotraverse region is represented by fluviatile, lacustrine and piedmont sediments. Due to the scarcity of fossils and strong deformation, it is difficult to reconstruct the morphology or recognise lateral facies changes in the Tertiary basins or correlate them. Hence the Tertiary period is the most poorly understood stratigraphically in the Tibetan Plateau. From the northern slope of the Tanggula Mountains to the Bayan Har Mountains, the Tertiary is represented by the Fenghuoshan Group and in the Nyainqentanglha Mountains southward to the Yarlung–Zangbo Suture zone by the Linzizong Formation.

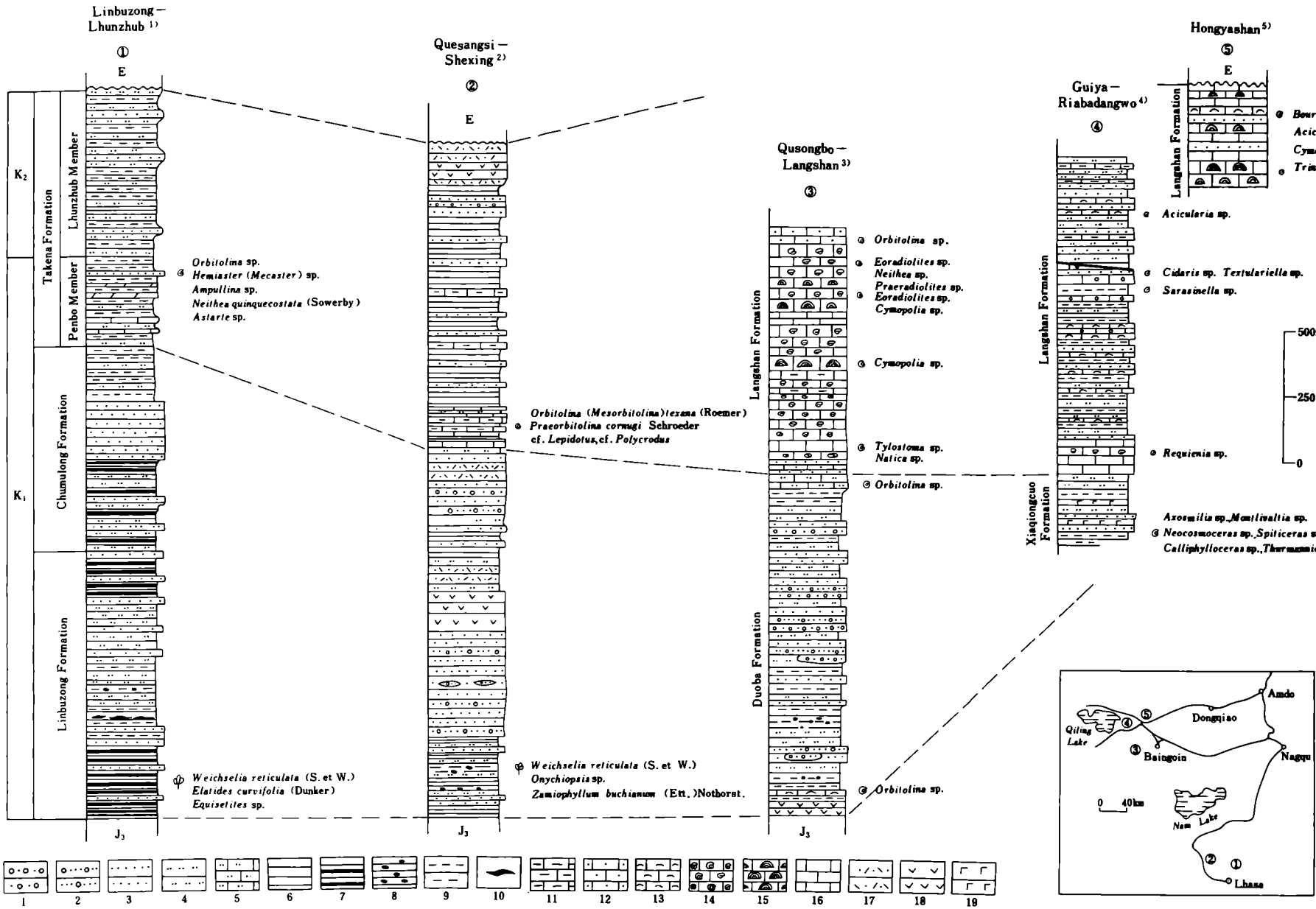

FIGURE 20. Columnar sections of the Cretaceous in the central part of the Lhasa Terrane. 1) Modified from Chen Chuzhen & Wang Yujing (1984). 2) Modified from Wang Naiwen *et al.* (1983). 3) Modified from Han Xiangtao *et al.* (1983). 4) Modified from Liang Shousheng & Xia Jinbao (1983). 5) Modified from Wang Naiwen (1983). 1. Conglomerate; 2. Pebbly sandstone; 3. Sandstone; 4. Siltstone; 5. Calcareous sandstone; 6. Shale; 7. Slate; 8. Nodular shale; 9. Argillaceous rock; 10. Coal; 11. Argillaceous limestone; 12. Arenaceous limestone; 13. Bioclastic limestone; 14. Orbitolina limestone; 15. Calcareous algal limestone; 16. Limestone; 17. Tuff; 18. Andesite; 19. Basalt.

(*a*) *Fenghuoshan Basin*

From Tongtianheyan northward to Budongquan (about 220 km), the Tertiary was deposited in a single basin in two suites of red beds, separated by an unconformable contact. The lower red beds, the Fenghuoshan Group, are widely distributed around the Tuotuo River, Erdaogou and Fenghuoshan, dipping steeply with many folds. They form high mountains, and are more than 3000 m thick. The lower part, composed of interbedded purple-red mudstones with quartzose sandstones, unconformably overlies older rocks with a basal conglomerate; the middle part is composed of dark purple quartzose sandstone and siltstone with mudstone intercalations; the upper part is purple sandstone. A cupreous sandstone layer occurs at the boundary of the lower and middle parts. Some irregularly distributed gypsum and shallow water sedimentary structures such as cross-bedding, ripple and rill marks are frequently found in the sandstones. From the argillaceous limestone of the lower part on the northern slope of the Fenghuoshan west of Erdaogou, a fossil assemblage was collected (loc. B69), which indicates an early Palaeogene, i.e. Palaeocene and/or early Eocene age.

The upper red beds, unconformable on the Fenghuoshan Group, are called the Chabaoma Group. The Chabaoma Group, in contrast to the complexly deformed Fenghuoshan Group, dips very gently and is more than 300 m thick. The base is a soil-coloured sandy conglomerate; the lower part consists of interbedded yellowish-brown or grey mudstone and fine-grained sandstone; the upper part is grey mudstone and shale with argillaceous limestone intercalations. Palynomorphs (loc. M216) indicate a Neogene age.

(*b*) *Lunpola Basin*

The Lunpola Basin is roughly 200 km long and 15–20 km wide, elongated east–west. The Tertiary Lunpola Group in the basin is up to 3800 m thick. The lower Niubao Formation and the upper Dengqen Formation are conformable.

The Niubao Formation, 450 to 2700 m thick, rests unconformably on the Cretaceous. The lower part is mainly composed of purple-red conglomerates and sandstones intercalated with purple-red mudstone; the middle part has interbedded grey mudstone and shale with arenaceous conglomerates and crystal tuffaceous intercalations; the upper part is interbedded mudstone, argillaceous limestone, siltstone and fine-grained sandstone. Abundant Palaeogene ostracods, spores and pollen, charophyta and gastropods are found.

The Dengqen Formation is 300–1100 m thick; the lower part is composed mainly of mudstone, shale and fine-grained sandstone with oolitic sandstone and argillaceous limestone interlayers; the middle part is grey shale and mudstone with oil shale, siltstone and tuffaceous intercalations; the upper part is mudstone, shale, argillaceous limestone and siltstone alternating with brown mudstone and tuff yielding abundant Neogene ostracods, spores and pollen and some gastropods, fishes and insects (Wang Kaifa *et al.* 1975; Xia Jinbao 1983; Wu Yimin 1983).

(*c*) *Linzizong Basin*

The Linzizong Basin extends from Pengbo Farm to Doilungdeqen and westward to the north of Lhasa City. The Tertiary in the Basin comprises calc-alkaline volcanics interbedded with purple-red sandstones, conglomerates and siltstones unconformably overlying the Cretaceous. The volcanics, dated at 40–70 Ma, formed in the eastern part of the Gangdise magmatic arc (Wang Songchan 1984; Yin Jixiang *et al.* 1980).

13. Discussion and summary

It is quite probable that the Jitang Group of the Hengduan Mountains, the Jiayuqiao Group of the Lhorong–Dengqen district (southeastern part of the Qiangtang Terrane) and the Amugang Group in the west of that terrane may all be correlated with the 'Amdo Schists' and the Nyainqentanglha Group of Cambro–Sinian age (but see Harris, Xu, Lewis, Hawkesworth & Zhang, this volume) in the Lhasa Terrane. All the rocks mentioned above may be part of the basement formed by the 'Pan-African Event' of Gondwanaland during late Precambrian times. The late Precambrian metamorphic rocks in the Burhan Budai Mountains in the Kunlun Terrane, long referred to the basement series of Laurasia, differ markedly from the rocks mentioned above.

The lithological and palaeontological characteristics of the Ordovician in the Lhasa Terrane are similar to the Ordovician in the Himalayas (Lin Baoyu 1983*a*) but slightly different from those in the Qiangtang Terrane. The Lower Ordovician in the Qiangtang Terrane is disconformably or unconformably overlain by Middle Devonian (Dong Deyuan & Mu Xinan 1984). The Ordovician sequences of both the Qiangtang and the Lhasa Terranes are lithologically and faunally diverse compared with that of the Kunlun Terrane.

It is interesting that no fossil-bearing Silurian sequence is found in the Kunlun Terrane or the central and western parts of the Qiangtang Terrane. The Silurian of the Lhasa Terrane has a similar fauna to that of the Himalayas but contrasting lithology.

Complete Devonian sequences, conformable or paraconformable on Silurian, have been reported from the Lhasa and Himalayan Terranes. No Lower Devonian occurs in the Qiangtang Terrane except in the eastern Yidun–Zhongdian region, where a complex sequence through the Devonian has long been known. It consists of carbonate rocks closely resembling those of South China or the Yangtze region. The Middle and Upper Devonian of the Qiangtang Terrane are characterised by a regressive sequence with subordinate intermediate volcanic rocks. The basal, coarse, clastic rocks of molasse facies lie unconformably on the Lower Ordovician sequence or low grade Cambro–Sinian metamorphics. In the Kunlun Terrane, only terrestrial Upper Devonian deposits occur, molasse facies in the lower part and an enormous amount of basic to acidic volcanics in the upper part. They rest unconformably on Precambrian metamorphics. The Upper Devonian in the Qimantage Range northwest of the Burhan Budai Mountains, mainly composed of alternations of terrestrial and marine deposits, also unconformably overlies Lower Ordovician. Thus the Devonian strata of the Qiangtang and Kunlun Terranes shows common characters in their sedimentary history as the first sediments of the tectono-stratigraphic phase which stretched from mid- or late-Devonian to late Triassic.

The widespread Carboniferous succession of the Lhasa and western Qiangtang Terranes is characterised by flyschoid sediments (especially in the Upper Carboniferous), intermediate-basic volcanics, diamictites and a 'cold water fauna', while the Carboniferous in the Kunlun Terrane and the central and eastern parts of the Qiangtang Terrane is characterized by enormous amounts of basic to acidic volcanics intercalated with coal-bearing clastic rocks and yielding a fauna like that of South China or the Yangtze Province. In both the Qiangtang and Kunlun Terranes, the Lower Carboniferous is far thicker than the Upper Carboniferous.

The Permian sequences in the Qiangtang and Kunlun Terranes have common characteristics.

(1) The Permian sequence is well-developed in both Terranes.

(2) The preserved thickness of the Lower Permian is far greater than that of the Upper Permian and the total thickness of the Permian and Carboniferous strata in each terrane reaches 8000 m and more.

(3) Voluminous basic and intermediate-acid volcanics occur at different levels, associated with shallow-sea flyschoid clastics and carbonates. No typical deep-water flysch deposits are found.

(4) The Permian is generally overlain unconformably or paraconformably by Mesozoic strata except in the western part of the Qiangtang Terrane, where Upper Permian coal-bearing clastics grade conformably into Lower Triassic strata.

(5) The Qiangtang Terrane, with its *Gigantopteris* flora in the Upper Permian coal-bearing series, and the Kunlun Terrane are referred to one biogeographical province with a Cathysian flora.

In the Lhasa Terrane, Lower Permian strata are unconformably overlain by Mesozoic deposits. In a small outcrop northwest of Lhasa the Upper Permian grades upwards into the Lower Triassic. The early Permian faunas from the Lhasa Terrane are similar to those of the Tethyan Himalayas, so-called 'cold water faunas'. At the beginning of the late early Permian, the sedimentary environments in these regions changed rapidly and the Tethyan fauna appeared, replacing the 'cold water fauna'. From late early Permian times, the Lhasa Terrane began to share sedimentary features with synchronous sediments in the Qiangtang, Kunlun and South China Terranes (Ching Yukan *et al.* 1977; Lin Baoyu 1983*b*). A so-called 'mixed flora' in the Lower Permian was reported from the western part of the Lhasa Terrane (Li Xingxue *et al.* 1985) but typical elements of the Gondwanan or the Cathaysian flora were not discovered in it. Some elements of the so-called 'cold water fauna' were also reported from the western part of the Qiangtang Terrane in early Permian strata resembling those of the Tethyan Himalayas.

Along the Geotraverse route, Triassic deposits, widespread in the Kunlun and Qiangtang Terranes, have been identified as representing a trench-island arc system at the continental margins of the northern and southern parts of Palaeotethys respectively. The Jielong Group (T_2) and the Baitang Group (T_3) are characterised by enormous amounts of calc-alkaline volcanics, tentatively attributed to an island arc environment at the northern margin of the Qiangtang Terrane, whereas the Gyiza (T_{2-3}) and Tumaingela (T_3) Groups outcropping to the south of the Baitang Group are platform-type sediments. These are succeeded by variegated clastics, carbonates and coal-bearing clastics, with subordinate calc-alkaline volcanics and are preliminarily interpreted as back-arc basin deposits behind the Baitang island arc. The Bayan Har Mountains are mainly formed of the Bayan Har Group, referred to the fore-arc basin at the southern margin of the Kunlun Terrane. The Lower and Middle Triassic marine strata in the Burhan Budai Mountains, of platform-type, are succeeded by coarse clastics, carbonates and flyschoid clastics with calc-alkaline volcanics, whereas the terrestrial Upper Triassic strata in the eastern part of the Burhan Budai Mountains, east of the Geotraverse route, are mainly coal-bearing clastics and an enormous amount of calc-alkaline volcanics, tentatively interpreted as back-arc basin deposits. However, the nature and location of the island arc there needs further exploration. The Triassic strata widespread in the Kunlun and Qiangtang Terranes commonly overlap or unconformably overlie Palaeozoic or late Precambrian strata. We believe that this unconformity is related to tensional tectonics resulting in the emergence and development of

the Palaeotethyan rift system or embryo ocean. Triassic strata in the Lhasa Terrane may represent deposits along the passive continental margin of the northern Neotethyan ocean.

Along the Geotraverse route, marine Jurassic deposits are restricted to the Lhasa and Qiangtang Terranes. In the Qiangtang Terrane, the Middle and Upper Jurassic lies unconformably on Triassic or Palaeozoic and comprises alternating terrestrial and marine sediments. They may be regarded as a result of repeated deposition of molasse in a foreland basin in the southern part of the Bayan Har fold belt or Palaeotethyan orogenic belt and marine transgression of the Tethyan ocean. It is suggested that the Sangri Group (J_3–K_1) in the south, the Quesangwenquan Formation (J_2) and Duodigou Formation (J_3) in the central area, and the 'Lake Area flysch' (J_{2-3}) in the north may represent the deposits of the Gangdise island arc, inter-arc basin or transitional belt, and back-arc basin of the northern Neotethys respectively.

Marine Cretaceous is restricted to the Lhasa Terrane. The highest marine horizon in the northern part of the Lhasa Terrane is the Langshan Formation, late Aptian to Cenomanian in age. The Cretaceous in the central and northern parts of the terrane represents post-flysch deposits in the back-arc basin. These are succeeded by coarse clastic and carbonate associations of platform-type. The lower Cretaceous exposed in the southern part of the terrane contains voluminous calc-alkaline volcanics and represents deposits of the Gangdise island arc belt. No fossiliferous Cretaceous strata have been found along the Geotraverse route in the Qiangtang Terrane, but early Cretaceous terrestrial sediments may occur beyond the Geotraverse route.

The Tertiary continental red beds are mainly developed in the central and northern parts of the Lhasa, Qiangtang and Kunlun Terranes. Marine Palaeogene sediments are found only in the 'Xigaze fore-arc basin' south of the Gangdise island arc of the Lhasa Terrane. The foraminifer-bearing early Eocene of the Zhongba district, 450 km WNW of Xigaze City, may represent the highest marine beds in the Lhasa Terrane.

Based on the foregoing, the evolution of the Palaeotethys and Banggong Lake–Dongqiao–Nujiang River back-arc basin has been deduced as follows.

Three stages can be recognized in the pre-Jurassic evolution of the Palaeotethyan domain in the Kunlun and Qiangtang Terranes: pre-Ordovician, Ordovician and Devonian-Triassic (figure 21). The late Palaeozoic evolution of the Palaeotethyan Ocean in the Tibetan Plateau may itself be divided into stages.

I. Middle and late Devonian to early Permian ($D_{2\ 3}$–P^1_1).
The Pangaean basement was broken up, producing the 'Kunlun rift system'; further splitting led to the emergence of new oceanic crust and sedimentation in symmetric rim basins.

II. Late early Permian to late Permian (P^2_1–P_2); the sea-floor spreading stage.
Palaeotethys expanded rapidly.

III. Early Triassic to Middle Triassic (T_1–T_2); the sea-floor consumption stage.
The Palaeotethyan oceanic crust was subducted along two subduction zones towards both the southern margin of the northern continent and the northern margin of the Xizang (Tibet) microcontinent (Qiangtang–Lhasa Terrane) respectively, resulting in the emergence of two mobile continental margins facing each other.

IV. Early late Triassic to middle late Triassic (T^1_3–T^2_3); the shrinking stage.
The Palaeotethyan ocean narrowed rapidly and was completely consumed by subduction until only a narrow relict shallow sea was left.

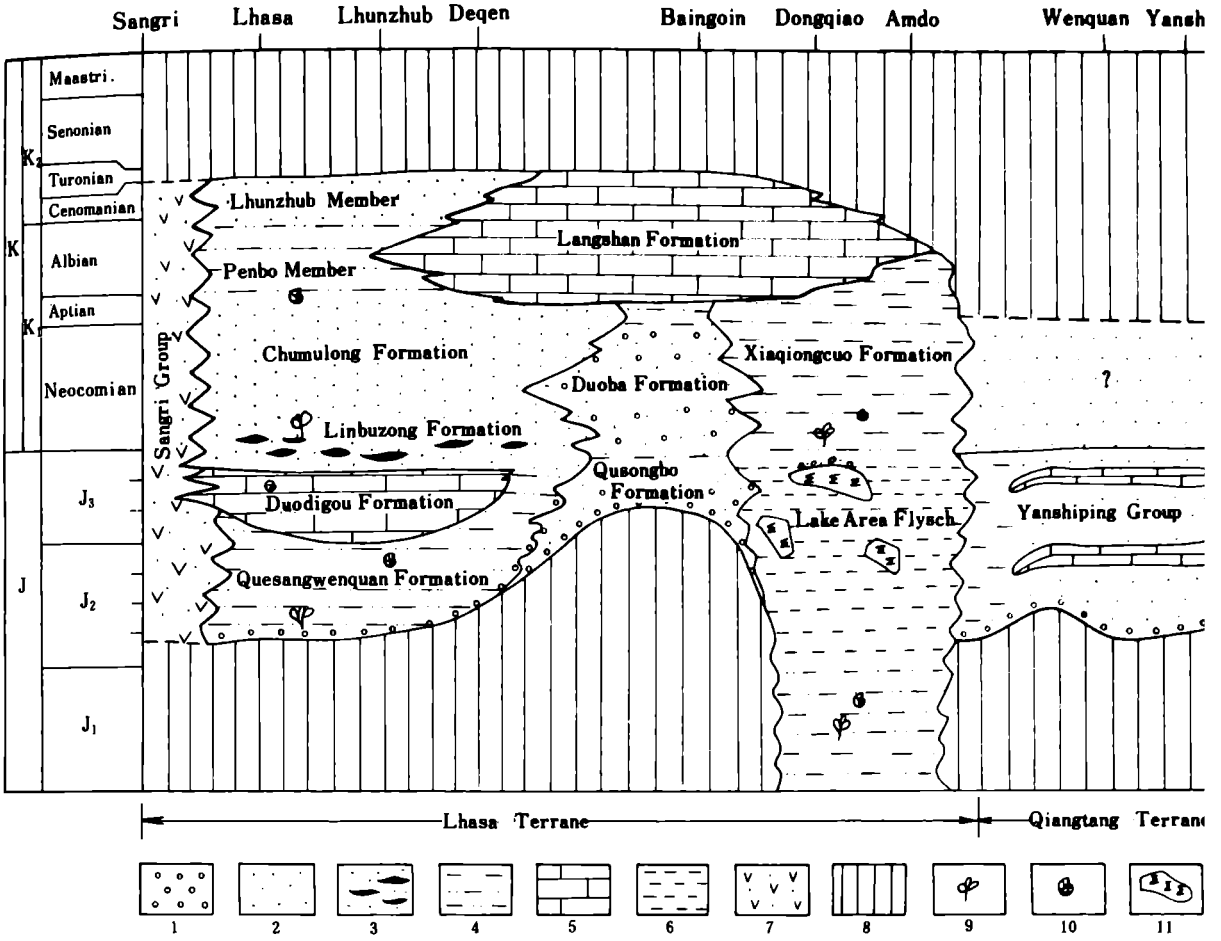

FIGURE 21. Map of the Jurassic and the Cretaceous in the Lhasa and the Qiangtang Terrane. 1. Terrestrial sandstone and conglomerate; 2. Terrestrial fine-grained clastics; 3. Terrestrial coal-bearing clastics; 4. Marine fine-grained clastics; 5. Carbonate; 6. Flysch-series; 7. Flyschoid clastics and calc-alkaline volcanics; 8. No deposition; 9. Plant fossils; 10. Animal fossils; 11. Ophiolite.

V. Late Triassic to early Jurassic (T^3_3–J_1); the initial collision stage.
The relict sea eventually vanished and the Xizang (Tibet) microcontinent collided with the northern continent and accreted into a united ancient Asian continent. The junction of these two continents is called 'Litian Lake–Jinsha River Suture Zone'.

VI. Middle and late Jurassic (J_{2-3}); the strong collision and deformation stage.
The collision and accretion of the Xizang (Tibet) microcontinent with the northern continent persisted into the late Jurassic, resulting in intense folding, thrusting and magmatic activity and the gradual uplift of the present Kunluns including the Bayan Har Mountains and the Tanggula Mountains. This created the Palaeotethyan or Indosinian orogenic belt. Foreland-type molasse basins were developed in the southern part of the orogenic belt and overlapped the marginal basins of the northern continent.

As a result of the disappearance of the Palaeotethyan ocean in the Qinghai–Xizang (Tibet) Plateau in the latest Triassic, the western part of the present Qiangtang Terrane rotated clockwise and separated in an opposite direction from the present Lhasa Terrane. This led, in the early Jurassic, to the formation of a wedged rift system, widening westward and closing eastward. Because of spreading behind the Gangdise arc, caused by early subduction of the

Neotethyan ocean in the mid-Jurassic, the rift system extended eastwards and southeastwards as far as western Burma, leading to a mature back-arc basin along the Banggong Lake–Dongqiao–Nujiang River line. The continuous marine environments from late Triassic to early late Cretaceous, and Jurassic emplacement of ophiolites, are restricted to the central belt of the back-arc basin west of Dengqen. East and southeast of Dengqen, in the middle and lower reaches of the Nujiang River and western Burma, no marine early or late Jurassic or Cretaceous sequences have been found.

The evidence that the Banggong Lake–Dongqiao–Nujiang River back-arc basin developed from a rift system at the continental margin is as follows.

(1) Basic and acidic volcanics are best developed along the central axial line of the back-arc basin in the Middle and Upper Jurassic.

(2) The transition from continental to marine deposits in the Middle Jurassic has been found in the lake region of northern Xizang (Tibet) and along the Nujiang River.

(3) A distinct regional unconformity between Middle or Upper Jurassic strata and the underlying strata occurs at both the northern and southern continental margins of the back-arc basin.

(4) Jurassic evaporites (gypsum) and continental red beds are widespread in the Tanggula and Hengduan Mountains in the northeast, while contemporaneous coal-series occur only in the Gangdise–Nyainqentanglha Mountains in the south.

(5) After the disappearance of the back-arc basin in early late Cretaceous times, Tertiary red molasse developed in these basins (figure 22).

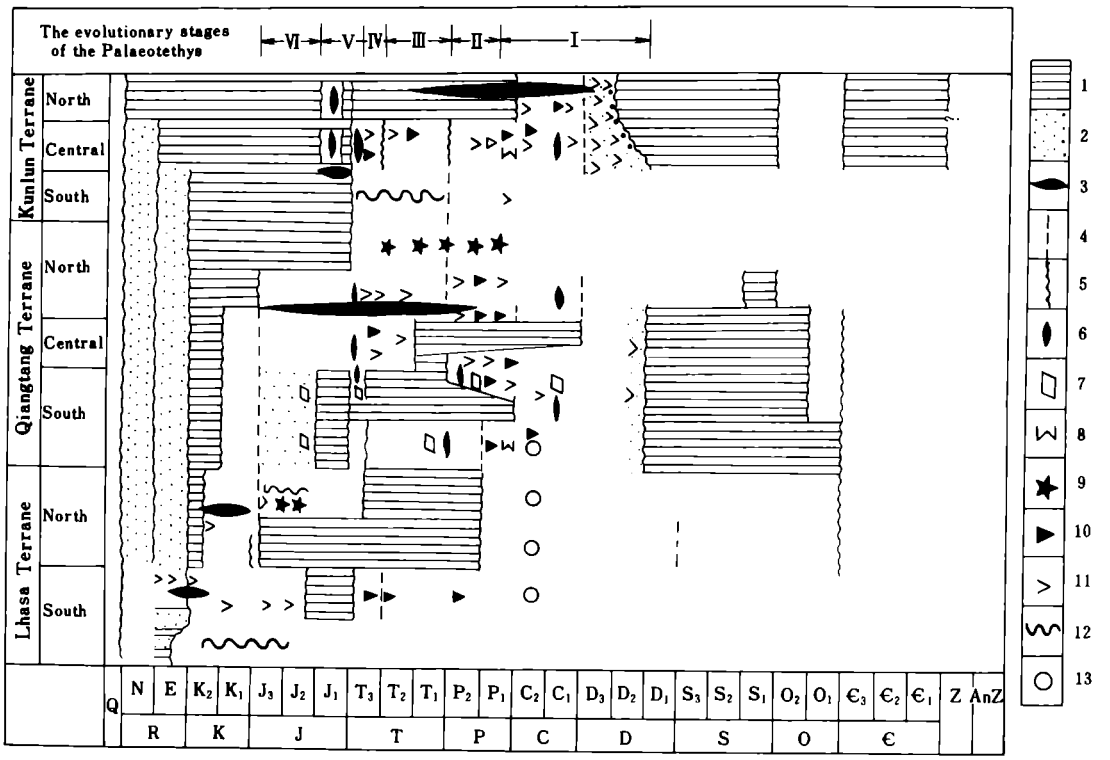

FIGURE 22. Diagram of the major geological events along the Qinghai-Xizang (Tibet) Highway from Lhasa to Golmud and its adjacent area. 1. No available geological record; 2. Molasse; 3. Plutonic rocks; 4. Paraconformity; 5. Unconformity; 6. Coal; 7. Gypsum; 8. Ultramafic rocks; 9. Ophiolites; 10. Basic volcanics; 11. Intermediate-acidic volcanics; 12. Flysch; 13. Diamictites.

DIVISION AND CORRELATION OF THE STRATA ALONG QINGHAI-XIZANG HIGHWAY FROM LHASA TO GOLMUD AND ADJACENT REGIONS

		Lhasa Terrane				Qiantang Terrane				East Kunlun Terrane	
		Sangri	Doilungdeqen-Lhunzhub	Baingoin-Nam Lake	Dongqiao-Nagqu (East Part of Lake Region)	Amugang-Mayigangri	Tuotuoheyan-Zadoi	Qamdo-Jomda	Yidun-Zhongdian	Bayan Har Mountains	Burhan Budai Mountains
		1	2	3	4	5	6	7	8	9	10
Q											
N			Sandstones, andesites, rhyolites, coal-bearing clastics, pebbly sandstones. Pl. > 2955m	Conglomerates	**Bulong Fm.** Sandstones. *Hipparion* > 50m **Lunpola Group** **Dengqen Fm.** P. & Ost. 300-1100m **Niubao Fm.** Variegated clastics S. & P., Ost. 450-2700m	**Chabaoma Gp.** Grey-yellow arenaceous marls, brick-red siltstones and pale fine sandstones. 900m		**Mencheng Fm./Lawula Fm.** Coal-bearing sandstones, siltstones and mudstones. Variegated coal-bearing sandstones, conglomerates and volcanics. Pl. >760-1250m		**Chabaoma Group**	Variegated sandstones and conglomerates.
E			**Linzizong Fm.** Andesites, rhyolites intercalated with red beds. Ver. > 1500m	**Jinzhushan Fm.** > 3000m		**Fenghuoshan Gp.** Purple argillaceous siltstones, sandstones, conglomerates intercalated with mudstones, copper-bearing sandstones and gypsum. S. & P., Ost. 400-1600m		**"Konjo Group"** Red sandstones, conglomerates intercalated with mudstones, salts and gypsum. Ins., S & P. 2753m		**Fenghuoshan Group**	
K	Maestrich										
	K_2 Senonian										
	Turonian										
	Cenom		**Takena Fm.** Lhunzhub Mem. -643m **Penbo Mem.** For., Biv., Amm., Gas., Ech. -335m	**Langshan Fm.** Limestones. *Orbitolina* spp. 700-900m	**Langshan Fm.** 700-900m Limestones, shales *Orbitolina* spp.						
	Albian	**Sangri Gp.** Clastics, intermediate-acid volcanics and limestones. Gas., Biv., Coral > 5269 m	**Liuvu Fm.** Limestones, sandstones, andesites, For., Biv. 500m **Niedang Fm.** Clastics. Amm. 500m		Xiaqiongco Fm. (= Dongqiao Fm.) Ophiolitic sandstones, carbonaceous shales and limestones. *Spiticeras* sp. *Milleoporella* spp.	Argillaceous rocks, sandstones intercalated with marls and conglomerates. Pl., Gas. 240m	Terrestrial Sediments	Xiangdui Group Purple quartz sandstones and siltstones intercalated with conglomerates. > 2575m			
	K_1 Aptian		**Chumulong Fm.**	**Duoba Fm.** Conglomerates, sandstones 1300-1600m	> 300m						
	Neocomian		**Linbuzong Fm.** Coal-bearing siltstones, shales and argillaceous rocks. Pl. 1006m **Potala Fm.** Slates alternating with marls and limestones. Biv., Bele. > 750m		"Lake Area Flysch" Biv., Bra., Gas., Amm. > 4000m	**Yanshiping Group.** (in descending order) Grey purple sandstones; Limestones intercalated with siltstones; Variegated siltstones intercalated with marls; Limestones and siltstones intercalated with marls; Purple sandstones, conglomerates, limestones intercalated with andesites and gypsum. Bra., Biv. >5000m					
J	J_3		**Duodigou Fm.** Limestones, shales. Amm., Biv., Coral. > 700m	**Qusongbo Fm.** Amm. 700m		**Sewa Fm.** Shales 950m		**Chaya Group** Red sandstones, purple siltstones intercalated with marine bioclastic limestones 1636-2698m *Quensteidia* sp. *Volsella* sp. *Liostrea birmanica* (Reed) *Tibetodus gyroides*			
	J_2		**Quesangwenquan Fm.** Clastics. Biv., Pl. 148m		Shales, clayey and argillaceous limestones. Biv., Pl., Amm., Bra. > 2000m					Coal Series. *Eboracia lobifolia* (Phillip) Thomas Pl. >65m	Sandstones and conglomerates intercalated with coal.
	J_1				**Tumaingela Fm.** Coal-bearing shales intercalated with sandstones. Biv. Pl. 2270m	Clastics intercalated with intermediate basic volcanics and limestones. Biv., > 2000m Limestones and sandstones. Amm. 100m Limestones interbedded with shales Biv. 453m Coal-bearing sandstones. Biv. 310m	**Gyiza Gp.** Clastics, limestones. Coal-bearing shales. Biv., Amm., Pl. >4000m **Baitang Gp.** Volcanics, limestones Bra. >3500m **Jielong Gp.** Sandstones Amm. >2767m	Coal series with marine shales. Pl. 565-1770m Limestones and marbles. 500m Red sandstones, shales and volcanics. Biv., Bra. 2161m Sandstones interbedded with shales, andesites. Amm., Biv. 2739m Oolitic limestones, siltstones, conglomerates and tuffaceous lava. Biv., Gas. 902m Andesites, mudstones, siltstones. Fus., Biv., Coral. 590-1790m **Tuoba Fm.** Pl. 880m Volcanic clastics, tuffs and limestones. Fus., Coral. 400m	Sandstones, slates intercalated with basalts and intermediate-acid volcanics, limestones and coal-bearing shales. Amm., Biv. > 6000m Sandstones, slates and phyllites, volcanics. 1000-4800m Sandstones, siltstones intercalated with basic volcanics and siliceous rocks. Con. 700-1500m Limestones intercalated with slates, sandstones and basalts. 115-2130m Basalts, slates. 152-3800m Limestones, basalts, tuffs, sandstones, cherts. 500-3600m Basalts, phyllites, cherts and tuffs. 200-2157m	**Bayan Har Group** Terrigenous clastic turbidites. Biv., Amm. 7,000-10,000m Massive limestones and some sandstones, siltstones at the base. Bra., Coral. 1156m Crystalline limestones, banded chert limestones. > 2075m Sandstones, greywackes, slates and andesites. 536-3462m	**Babaoshan Gp.** Coal series intercalated with intermediate-acid volcanics. Biv., Pl. 1019m **Naocangjiangou Fm.** Sandstones, slates and tuffs. Amm., Bra. > 856-2967m **Hongshuichuan Fm.** Limestones in the upper. Conglomerates, sandstones, tuffs in the lower. Biv. 1629m Conglomerates, sandstones, calciradites and bioclastic limestones. Bra. > 1390m Dolomites, conglomerates, slates and bioclastic limestones, intermediate-basic volcanics. Fus. >1755-4916m
	T_3	**Yeba Fm.** Intermediate-basic volcanics. 300-1000m **Mailonggang Gp.** Limestones, slates. > 500m									
T	T_2	**Chaqupu Gp.** Limestones intercalated with ignimbrites and hematites. ? *Leptochondria* cf. *michaeli* Assmann *Myophoria* (*Elegantinia*) sp. *Paraceratites trinodosus* (Mojs.)									
	T_1	300m									
P	P_2	**Lielonggou Fm.** Sandstones, siltstones and andesites. *Guizhoupecten* cf. *regularis* Chen *Spinomarginifer* sp. > 108m									
	P_1	**Luobadoi Fm.** Limestones, bioclastic limestones. Fus. > 640m **Urulung Fm.** Argillaceous limestones, shales. Bra. 40m		**Xiala Fm.** Limestones *Iranophyllum* sp. *Chusenella* sp. 523m							
C	C_2	**Pondo Gp.** Diamictites, mudstones and sandstones. *Bandoproductus hemiglobicus* Cheng et Sun *Syringothyris* cf. *nagmargensis* Bion *S. lyddekeri* Diener > 1000m		Diamictites, interbedded with sandstones *Neospirifer fasciger* var. *paucicostulata* (Reed) *Stepanoviella* sp. *Syringothyris nagmargensis* Bion 1582m	Diamictites.	Diamictites, sandstones, siltstones and sandy limestones. Coral 200m Sandstones, siltstones, bioclastic limestones intercalated with brecciated limestones. Coral, Bra., Amm., Tri. 1885m	Sandstones, slates intercalated with limestones. Bra., Bry., Coral. 134m Andesites intercalated with conglomerates. 594m	Limestones, marls and dolomites. Bra., Coral., Stro. 479-880m Limestones, marls, dolomites and purple clastics intercalated with limestones. Bra., Coral. 55-395m	**Talipo Fm.** Limestones, oolitic limestones. Bra., Coral. 368-1200m **Cangna Fm.** Dolomites, limestones. Bra. 400-900m **Qiongcuo Fm.** Limestones. 286-500m **Gerong Fm.** Limestones in the north, sandstones, slates in the south. Coral, Bra. 500m		**Haoteluowa Fm.** Limestones, volcanics, sandstones. 673m **Xiaoxilangannong Fm.** Clastics, limestones, volcanics 491m **Halaguole Gp.** Basic-acidic volcanics and clastics 3210m ?	**Sijiaoyanggou Fm.** Volcanics, clastics >284m **Diaosu Fm.** Sandstones, shales, rhyolites Coral, Bra., Fus. >380m **Dagangou Fm.** Volcanics, clastics, limestones. 1298m **Juchishan Fm.** Clastics and volcanics 3366m
	C_1	**Lading Fm.** Sandstones intercalated with slates, limestones and tuffs. *Kuzichouphyllum* sp. > 900m		Variegated sandstones, siltstones and wormkalks. Amm., Bra., Con., Coral. 853m	Quartz sandstones.				Yongren Fm. Dolomitic limestones interbedded with dolomites. 270m **Sanze Fm.** Carbonate rocks 600m Carbonate rocks, volcanics and clastics 470m			
D	D_3	F		Limestones, bioclastic limestones and wormkalks. 850m	F	Bioclastic limestones, marls, purple crystalline limestones intercalated with brecciated limestones. Bra., coral 200m					
	D_2			Oolitic limestones, limestones. Con. 226m	Crystalline limestones and sandstones. *Favosites* sp. *Hermatostroma* sp. > 200m						
	D_1			Quartz sandstones, bioclastic limestones and sandy limestones. Coral, Ten., Bra. 741m							
S	S_3			Limestones. Con.	F Phyllites alternating with quartz schists. > 700m **Donka Fm.** Crystalline limestones, bioclastic limestones and dolomitic limestones. *Palaeofavosites felix* Sokolov *Allanoceras xizangensis* Chen > 900m				Aofuochipu Fm. Purple marls, sandstones, and dolomites. 160-585m		**Naij Tal Gp.** Greywacke, limestones,fluxoturbidites. 4489m
	S_2										
	S_1			Shales intercalated with limestones. *Climacograptus rectangulari* s(M. Coy). 257m							
O	O_2			Limestones, banded limestones and bioclastic limestones. Grap., Orth., Tri. 867m	F Crystalline limestones, argillaceous rocks and sandstones. *Cryptophragmus* sp. 500m		Sandstones, argillaceous intercalated with siliceous rocks and limestones. Grap.	Qingnidong Fm. Variegated shales, quartz sandstones and limestones. *Didymograptus* sp. 1560m	Liuranka Fm. Dolomitic limestones, dolomites. Orth. 800m **Banggui Fm** ibid. 700m		**Halabayigou Fm** Clastics, limestones. > 1619m
	O_1										
ε		**Nyainqentanglha Group** Granitic gneiss and hornblendites. > 1000 m			"Amdo Schists" Paragneisses and green schists.	"Amugang Group" Gneisses, schists, slates and intermediate-basic volcanics. >5000m	"Jitang Group" Gneisses, green schists, slates., phyllites and metamorphosed volcanics intercalated with marbles.	"Jiayuqiao Group" (= "Jitang Group")	Slightly metamorphosed clastic rocks, basic volcanics, crystalline limestones and marbles. > 7000m		**Wanbaogou Gp.** Clastics, volcanics, marbles St. > 2936m
$An_ε$											**Binggou Gp.** Marbles, phyllites, sandstones. St. >1800m

Notes

1. Modified from Wen Chuanfen and Yin Jixiang (in press); Wang Naiwen *et al.* (1983); Xu Baowen *et al.* (1982).
2. Modified from Yin Jixiang *et al.* (eds.) (1980); Geng Guocang (1984).
3. Lin Baoyu (1983); Yang Shipu & Fan Yingnian (1982); Han Xiangtao *et al.* (1983); Liang Shousheng & Xia Jinbao (1983).
4. The authors: Liang Shousheng & Xia Jinbao (1983); Liao Weihua &Chen Tingen (1984); Lin Baoyu & Qiu Hongrong (1983); Han Tonglin (1983); Xia Jinbao (1983); Wu Yimin (1983).
5. Wen Shixuan (1979, 1984); The Bureau of Geology and Mineral Resource of Xizang, Explanatory Notes of the Geological Map, the People's Republic of China, (1/1,000,000), "Gerze Sheet". I-45, (in press).
6. The authors; Jiang Zhongti (1983); Wen Shixuan (1984); Zhao Rongli (1982); The Bureau of Geology and Mineral Resource, Qinghai Province, The Reports of the Regional Geological Survey of the People's Republic of China, (1/2,000,000), "Zhidoi Sheet", I-46-(24), (1981); "Zadoi Sheet", I-46-(30), (1982); "Shanglaxiu Sheet", I-47-(25), (1983); Ma Fubao *et al.* (1984).
7. Dong Deyuan & Mu Xinan (1984).
8. Ji Ping (1984); Zhu Zhanxiang (1982); Institute of Geology and Mineral Resources of the Bureau of Geology, Sichuan Province, Explanatory Notes of the Geological Map of Nujiang River-Lancang River-Jinsha River of the People's Republic of China, (1/1,000,000), (in press).
9. Zhang Qizhen & Zhang Yifu (eds.) (1981).
10. The authors; Li Guangcen & Lin Baoyu (1982); Zhu Zhizhi *et al.* (1985); Wang Yunshan & Cheng Jiniang (1984). The Bureau of Geology and Mineral Resource, Qinghai Province, The Reports of the Regional Geological Survey of the People's Republic of China (1/2,000,000), "Golmud City Sheet", I-46-(5), (1981); "Aikangdeleste Sheet", I-47-(1), (1982); "Naij Tal Sheet", I-46-(1), (1981); "East Wenquan Sheet", I-46-(6), (1983).

Gp. = Group; Fm. = Formation; Mem. = Member

Amm. = Ammonoids; Bele. = Belemnites; Biv. = Bivalve; Bra. = Brachiopoda; Ch. = Charophyta; Con. = Conodonts; Ech. = Echinoderm; For. = Foraminifera; Fus. = Fusulinaceans; Gas. = Gastropoda; Grap. = Graptolites; Ins. = Insect; Orth. = Orthoceras; Ost. = Ostracoda; S&P = Spores and Pollen; Pl. = Plant; Ra. = Radiolaria; St. = Stromatolit; Stro. = Stromatopora; Ten. = Tentaculites; Tri. = Trilobites; Ver. = Vertebrates

Unconformity; Disconformity; Unknown; F — Fault

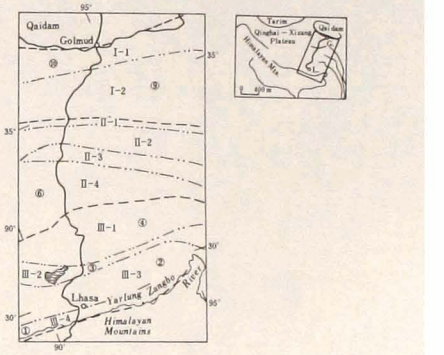

The Stratigraphical Provinces along the Qinghai-Xizang (Tibet) Highway from Lhasa to Golmud and the Adjacent Regions.

I. Stratigraphical Province of East Kunluns
- I-1 Burhan Budai Subregion;
- I-2 Bayan Har Subregion.

II. Stratigraphical Province of Qiangtang
- II-1 Zhidoi-Yushu Subregion;
- II-2 Tuotuoheyan-Ziqu Subregion;
- II-3 Kaixinling-Nangqen Subregion;
- II-4 Tanggula Pass Subregion.

III. Stratigraphical Province of Lhasa
- III-1 Dongqiao-Nagqu Subregion;
- III-2 Baingoin-Nam Lake Subregion;
- III-3 Doilungdeqen-Lhunzhub Subregion;
- III-4 Sangri Subregion.

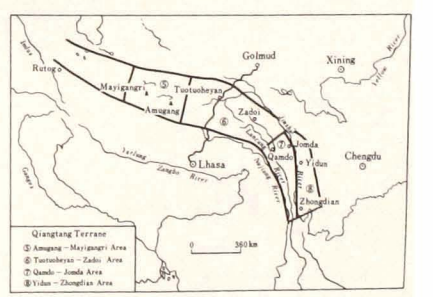

The Subdivision of the Qiangtang Stratigraphical Province

FIGURE 23. Division and correlation of the strata along the Qinghai–Xizang Highway from Lhasa to Golmud and adjacent regions.

(*Facing p.* 48)

Thus the tectono-stratigraphical evolution of the Banggong Lake–Dongqiao–Nujiang River back-arc basin may be suggested.

I. Late Triassic to early Jurassic (T_3–J_1); Early evolutionary stage.
A change from continental rifting to initial expanding, resulting in the emergence of a narrow gulf closing towards the east.

II. Middle Jurassic to mid Late Jurassic (J_2–J^2_3); Sea-floor spreading–shrinking stage.
Deposition of flysch and new oceanic crust in the central belt of the back-arc basin and contemporaneous subduction and obduction of oceanic crust were in progress; ophiolites were dismembered and sandwiched into the flysch sequences.

III. Late Jurassic to early late Cretaceous (J^3_3–K^1_2); initial collision stage.
As a result of the collision of the Gangdise arc with the northern continent, flysch and oceanic deposition ended to be replaced by shallow sea sedimentation in the relict sea.

IV. Late Cretaceous to Palaeogene (K^2_2–E); the collision and deformation stage.
After the disappearance of the marine facies, continental sedimentation of red molasse soon occurred. The welded line of the northern continent and the Gangdise arc is called the Banggong Lake–Dongqiao–Dengqen Suture Zone.

References

Buckman, S. S. 1917 The brachiopods of the Namyau Beds, Northern Shan States, Burma. *Pal. Indica* N.S. **3** (2).

Cai Zhenjing 1984 The explanation of the regional geological structure by aeromagnetism in eastern Xizang, western Sichuan and southern Qinghai. *Contr. Geol. Qinghai–Xizang (Tibet) Plateau* **15**, 189–200.

Chen Chuzhen & Wang Yujing 1984 Stratigraphy of the Lhasa subregion. In *Stratigraphy of Xizang (Tibetan) Plateau*, 141–155. Beijing: Science Press.

Chen Guolong, He Guoxiong & Wang Yigang 1982 New knowledge of the Zezha Group in southern Qinghai. *J. Strat.* **6**, 307–309.

Chen Guoming, Han Tonglin & Zhu Zhizhi 1980 Preliminary analysis of the tectonic framework of eastern Xizang (Tibet). *Bull. Chinese Acad. geol. Sci.* ser. 1, **2**, 47–58.

Ching Yukan, Liang Xiluo & Wen Shihhsuan 1977 Additional material of fossil animals from the Permian deposits on the northern slope of Mount Qomolangma Feng. *Scientia geol. Sinica* **3**, 236–249.

Dong Deyuan & Mu Xinan 1984 Stratigraphy of the Qamdo region. In *Stratigraphy of Xizang (Tibet) Plateau*, 237–287. Beijing: Scientific Press.

Duan Shuying, Chen Yen & Keng Kuochang 1977 Some early Cretaceous plants from Lhasa, Tibetan Autonomous Region, China. *Acta bot. Sinica* **19**, 114–119.

Fan Jiasong 1965 On some Middle Jurassic lamellibranchiata from northern Tibet. *Acta palaeont. Sinica* **13**, 248–257.

Gass, I. G. 1982 Upper Proterozoic (Pan African) calc-alkaline magmatism in north-eastern Africa and Arabia. In *Andesites* (ed. R. S. Thorpe), 591–609. Chichester, John Wiley.

Geng Guocang 1984 Upper Tertiary. In *Stratigraphy of Xizang (Tibetan) Plateau*, 379–396. Beijing: Science Press.

Gu Qingge, He Guoxiong & Wang Yigang 1980 Discovery of Late Anisian *Paraceratites trinodosus* fauna (Ammonoidea) from Doilungdeqen, Tibet and its significance. *Acta palaeont. Sinica* **19**, 343–356.

Gu Zhiwei 1982 *The Jurassic and Cretaceous of China*. Beijing: Science Press.

Han Tonglin 1983 Discussion on the Mesozoic succession in northeast Xizang. *Contr. Geol. Qinghai–Xizang (Tibet) Plateau* **3**, 21–46.

Han Tonglin 1984 The characteristics of the geological structures of the Xainza–Baingoin area, Xizang (Tibet). *Contr. Geol. Qinghai–Xizang (Tibet) Plateau* **15**, 53–72.

Han Xiangtao, Lunzhu Jiaco & Li Cai 1983 Subdivision of the marine Cretaceous of the Baingoin area in the Lakes region of North Xizang (Tibet). *Contr. Geol. Qinghai–Xizang (Tibet) Plateau* **3**, 194–209.

He Yuanliang & Yin Jiarun 1983 A preliminary discussion on the Triassic stratigraphy, palaeontological characteristics and distribution in Qinghai. *Contr. Geol. Qinghai–Xizang (Tibet) Plateau* **3**, 47–56.

He Yuanliang & Zhang Shanzhen 1984 Late Permian fossil plants around the Shanglaxiu District of Yushu County, Qinghai Province and their geologic significance. *Contr. Geol. Qinghai–Xizang (Tibet) Plateau* **14**, 115–124.

Ji Ping 1984 The Indosinian movement in the northern part of the Sanjiang region as related to the southern part. *Contr. Geol. Qinghai–Xizang (Tibet) Plateau* **15**, 157–171.

Jiang Yaoming 1984 Geochemical characteristics of basalt at Zhidoi, Litang and their meaning in geologic structure. *Contr. Geol. Qinghai–Xizang (Tibet) Plateau* **14**, 235–252.

Jiang Zhongti 1983 Some problems on the Jurassic stratigraphy of Qiangtang region. *Contr. Geol. Qinghai–Xizang (Tibet) Plateau* **3**, 87–112.

Li Guangcen & Lao Xiong 1982 Some geological characteristics of the Wenquan region in the Tanggula, China. *Contr. Geol. Qinghai–Xizang (Tibet) Plateau* **1**, 80–95.

Li Guangcen & Lin Baoyu 1982 On some geological problems in Eastern Kunlun Mountain. *Contr. Geol. Qinghai–Xizang (Tibet) Plateau* **1**, 28–48.

Li Pu 1955 A preliminary recognition on the geology of eastern Xizang (Tibet). *Kexue Tongbao* **7**, 62–71.

Li Xingxue, Wu Yiming & Fu Zaibin 1985 Preliminary study on a mixed Permian flora from Xiangangjiau of Gerze district, Xizang and its palaeobiogeographical significance. *Acta palaeont. Sinica* **24**, 150–170.

Li Xingxue, Yao Zhaoqi & Deng Longhua 1982 An early late Permian flora from Toba, Qamdo district, eastern Xizang. In *Palaeontology of Xizang* **5**, 17–44. Beijing: Scientific Press.

Li Xingxue & Yao Zhaoqi 1983 Carboniferous and Permian floral provinces in East Asia. In *Palaeobiogeographic Provinces of China*, 74–82. Beijing: Science Press.

Liang Shousheng & Xia Jinbao 1983 Marine Cretaceous of the Baingoin area, north Xizang (Tibet). *Contr. Geol. Qinghai–Xizang (Tibet) Plateau* **3**, 181–193.

Liao Weihua & Chen Tingen 1984 Stratigraphy of Shiquanhe–Shenzha region. In *Stratigraphy of Xizang (Tibet) Plateau*, pp. 127–140. Beijing: Science Press.

Lin Baoyu 1983*a* Palaeozoic stratigraphy in Xainza, Xizang (Tibet). *Contr. Geol. Qinghai–Xizang (Tibet) Plateau* **8**, 1–14.

Lin Baoyu 1983*b* Lower Permian stratigraphy and coral faunas from both flanks of the Yarlung Zangbo River in central-southern Xizang (Tibet). *Contr. Geol. Qinghai–Xizang (Tibet) Plateau* **8**, 69–181.

Lin Baoyu 1985 Geographic and geologic distribution of Palaeozoic tabulate corals of Qinghai Province. *Contr. Geol. Qinghai–Xizang (Tibet) Plateau* **16**, 107–114.

Lin Baoyu & Qiu Hongrong 1983 The Silurian System in Xizang (Tibet). *Contr. Geol. Qinghai–Xizang (Tibet) Plateau* **8**, 15–28.

Liu Baotian 1984 The geological tectonic character of fold system from Bayanhar to Kunlun and its evolution. *Contr. Geol. Qinghai–Xizang (Tibet) Plateau* **15**, 101–112.

Ma Fubao, Wang Xiulin & Che Yi 1984 Subdivision of the 'Gyiza Group' in the southern part of Yushu County, Qinghai Province. *Contr. Geol. Qinghai–Xizang (Tibet) Plateau* **14**, 147–163.

Ma Xiaoda 1981 Cretaceous marine sediments of central Xizang. *J. Strat.* **5**, 133–138.

Pan Guan 1957 The finding of the *Gigantopteris* flora in Qinghai–Xizang (Tibet) Plateau. *Kexue Tongbao* **11**, 341.

Reed, F. R. C. 1936 Jurassic lamellibranchs from the Namyau series, Northern Shan States. *Ann. Mag. Nat. Hist.* ser. 10, **18** (103).

Sun Dongli, Hu Zhaoxun & Chen Tingen 1981 Discovery of the Upper Permian strata in Lhasa, Xizang. *J. Strat.* **5**, 139–142.

Sun Dongli & Ye Songling 1982 Middle Triassic brachiopods from the Tosu lake area, Central Qinghai. *Acta palaeont. Sinica* **21**, 153–173.

Sun Dongli & Zhang Binggao 1979 Some problems of the marine Jurassic strata of the Karakorum–Tanggula area. *Acta strat. Sinica* **3**, 317–321.

The Compiling Group of Charts of Stratigraphic Units Sequence of Qinghai 1980 Qinghai. In *Charts of Regional Stratigraphic Units Sequences of Northwest China*. 277 pp. Beijing: Geol. Publ. House.

The Compiling Group of Nanjing Institute of Geology and Palaeontology 1976 *Bivalve Fossils of China*. 522 pp. Beijing: Science Press.

The Research Group on the Triassic of the Wuhan Geological College and Qinghai Institute of Geology 1979 The characteristics of the Triassic stratigraphy and palaeontology on Qinghai Province. In *Contrib. to the Geology for International Exchanges, Stratigraphy and Palaeontology*, pp. 124–142. Beijing: Geol. Publ. House.

Wang Kaifa, Yang Jiaowen, Li Zhe & Li Zengrui 1975 On the Tertiary sporo-pollen assemblages from the Lunpola Basin of Xizang, China and their palaeogeographic significance. *Scientia geol. Sin.* **4**, 366–374.

Wang Mingzhou & Cheng Liren 1980 New discovery and recognition of the Mesozoic strata in the Dongqiao–Jiangcuo district of north Xizang (Tibet). *J. Changchun Geol. Coll.* **3**, 14–20.

Wang Naiwen 1983 Development of the Mesozoic formations in the Lakes region, north Tibet, and its plate tectonics implications. *Contr. Geol. Qinghai–Xizang (Tibet) Plateau* **8**, 29–40.

Wang Naiwen 1985 The Jurassic of the Tanggula and Lhasa subregion. In *The Jurassic System of China*, pp. 138–151. Beijing: Geol. Publ. House.

Wang Naiwen, Wang Sien, Liu Guifang, Bassoulet, J., Cochen, M., Mascle, L. & Jaeger, J. 1983 The Juro-Cretaceous marine-terrestrial alternating formations in the Lhasa area, Xizang (Tibet). *Acta geol. Sinica* **1**, 83–95.

Wang Songchan 1984 The features of the Linzizong volcanic series in the eastern section of the Gangdise volcanic arc in Xizang (Tibet). In *Sino-French Co-operative Investigation in the Himalayas* (ed. Li Guangxen and J. L. Mercier), pp. 305–320. Beijing: Geol. Publ. House.

Wang Yigang & Chen Guolong 1984 The Triassic ammonoid horizons in Qinghai Province. *Contr. Geol. Qinghai–Xizang (Tibet) Plateau* **14**, 137–144.

Wang Yigang & Sun Dongli 1985 The Triassic and Jurassic palaeogeography and evolution of the Qinghai–Xizang (Tibet) Plateau. *Can. J. Earth Sci.* **22**, 195–204.

Wang Yunshan & Chen Jiniang 1984 The formation and development of the Qaidam landmass. *Contr. Geol. Qinghai–Xizang (Tibet) Plateau* **14**, 27–40.

Wen Chuanfen & Yin Jixiang 1988 Petrologic characteristics of the Triassic at Tulong section, Nyalam County of Mount Qomolangma region and at Qubsang section, Doilungdeqen County of Lhasa region in Xizang. *Mem. Inst. Geol. Acad. Sinica* **3**, 55–72.

Wen Shixuan 1979 New material of biostratigraphy in the Qiangtang Province. *Acta strat. Sinica* **3**, 150–156.

Wen Shixuan 1984 Stratigraphy of Mugagangri region and Tanggula region. In *Stratigraphy of Xizang (Tibetan) Plateau*, pp. 186–189, 202–236. Beijing: Science Press.

Wu Shunqing 1983 On the late Triassic, Lower and Middle Jurassic floras and phytogeographic provinces of China. In *Palaeobiogeographic Provinces of China*, pp. 121–130. Beijing: Science Press.

Wu Shunqing & Wu Xiangwu 1982 The Triassic plant-bearing strata in China. In *Stratigraphic Correlation Charts in China with Explanatory Text*, pp. 206–222. Beijing: Science Press.

Wu Xiangwu 1982 Fossil plants from the Upper Triassic Tumaingela Formation in Amdo–Baqen area, northern Xizang. *Palaeontology of Xizang* **5**, 59–101.

Wu Yimin 1983 The Tertiary of Xizang (Tibet). *Contr. Geol. Qinghai–Xizang (Tibet) Plateau* **3**, 224–232.

Xia Jinbao 1983 Cenozoic of Baingoin and its borders, Xizang (Tibet). *Contr. Geol. Qinghai–Xizang (Tibet) Plateau* **3**, 243–253.

Xu Baowen, Badeng Zhu & Zhang Yizhi 1982 Preliminary study of the gigantic Yarlung–Zangbo structural zone. *Contr. Geol. Qinghai–Xizang (Tibet) Plateau* **1**, 237–249.

Xu Hankui, Ni Yunan & Chen Tingen 1981 The Silurian and Devonian of Xainza area, northern Xizang. *J. Strat.* **5**, 316–320.

Xu Ronghua, Scharer, U. & Allègre, C. J. 1985 Magmatism and metamorphism in the Lhasa block (Tibet): a geochronological study. *J. Geol.* **93**, 41–57.

Xu Xian, Wei Zhengsheng, Chen Guoen & Jiao Shengrui 1982 *Charts of Regional Stratigraphic Units Sequence in the Qinghai–Xizang (Tibet) Plateau.* Beijing: Geol. Publ. House. 163 pp.

Yang Jingzhi & 8 others 1982 Classification and correlation of the Carboniferous in China. In *Stratigraphical Correlation Charts in China with explanatory notes*, 124–136. Beijing: Science Press.

Yang Shengqiu & Wang Huiji 1985 Jurassic–Cretaceous Nerinea from Xizang. *Acta palaeont. Sinica* **24**, 403–411.

Yang Shipu & Fan Yingnian 1982 Carboniferous strata and fauna in Shenza district, northern Xizang (Tibet). *Contr. Geol. Qinghai–Xizang (Tibet) Plateau* **10**, 46–69.

Ye Songling & Yang Shengqiu 1979 Brachiopods from the Bagon (Pangkog) Lake series, northern Tibet. *Acta palaeont. Sinica* **18**, 64–72.

Yin Hongfu & Liang Qiuxian 1986 Triassic palaeobiogeographic provincialisation of China. In *Selected Papers from the 13th and 14th Conventions of the Palaeontological Society of China.* Anhui Science and Technology Publishing House, pp. 189–204.

Yin Jixiang 1964 On the occurrence of Nerinea in northern Tibet. *Acta palaeont. Sinica* **10**, 524–531.

Yin Jixiang & Fang Zhongjing 1973 Marine Jurassic in western Yunnan. *Scientia geol. Sinica* **3**, 217–237.

Yin Jixiang & Wen Chuanfen 1988 Diamictites of the Carboniferous and Lower Permian in Xizang, their stratigraphical characteristics and origin. *Mem. Inst. Geol. Acad. Sinica* **3**, 26–54.

Yin Jixiang & 13 others 1980 Geology and geophysics. In *A Scientific Guidebook to South Xizang (Tibet).* Organising Committee, Symposium on Qinghai–Xizang (Tibet) Plateau. Academia Sinica, pp. 17–104.

Yu Wen & Xia Jinbao 1985 Late Jurassic–Early Cretaceous Nerineids from northern Xizang. *Acta palaeont. Sinica* **24**, 640–650.

Zhang Binggao, Sun Dongli, Yang Shengqiu & Ye Chuanhui 1981 New observations on the Cretaceous of Baingoin and Xainza areas, northern Xizang. *J. Strat.* **5**, 313–315.

Zhang Qinwen 1981 The sedimentary features of the flysch formation of the Xikang Group in the Indosinian–Songpan–Garze geosyncline and its geotectonic settings. *Geol. Rev.* **27**, 405–412.

Zhang Qizhen & Zhang Yifu (eds) 1981 Explanatory notes to the geological map of Qinghai Province (scale 1:1000000). Unpubl. data, Qinghai Inst. Geol.

Zhang Zuoming, Lu Yiju & Wen Shixuan 1980 Lamellibranchiata. In *Palaeontologic Atlas of Northwestern China.* Qinghai Fasc. **1**, 225–314. Beijing: Geol. Publ. House.

Zhao Rongli 1982 About the Upper Triassic Batang Group in Yushu district, Qinghai. *Contr. Geol. Qinghai–Xizang (Tibet) Plateau* **10**, 98–104.

Zheng Yanzhong 1984 Geological structures and evolutional characteristics of continental accretion in Tuotuo River–Yushu area. *Contr. Geol. Qinghai–Xizang (Tibet) Plateau* **4**, 73–84.

Zhu Zhanxiang 1982 On the late Triassic formation in Yidun area, western Sichuan. *Contr. Geol. Qinghai-Xizang (Tibet) Plateau* **10**, 85–97.

Zhu Zhizhi, Zhao Min & Shi Lixin 1984 The Xidatan melange in the southern margin of the east Kunlun Mountains. *Bull. Chinese Acad. Geol. Sci.* **10**, 129–135.

Zhu Zhizhi, Zhao Min & Zhang Jiankang 1985 The dismembering of the Nachitai Group and the establishment of the Wanbaogou Group in the middle of the East Kunlun Mountains. *Contr. Geol. Qinghai-Xizang (Tibet) Plateau* **16**, 1–14.

Zou Dingbang, Rao Rongbiao, Chen Yongming & Chen Lukun 1984 On the Triassic turbidite in the southern Burhan Budai Mountains region. *Contr. Geol. Qinghai-Xizang (Tibet) Plateau* **15**, 27–42.

Phil. Trans. R. Soc. Lond. A **327**, 53–105 (1988) [53]
Printed in Great Britain

Palaeontology of the 1985 Tibet Geotraverse, Lhasa to Golmud

By A. B. Smith[1] and Xu Juntao[2]

[1] *Department of Palaeontology, British Museum (Natural History), Cromwell Road, London SW7 5BD, U.K.*

[2] *Institute of Geology and Palaeontology, Academia Sinica, Chi-ming-ssu, Nanjing, People's Republic of China*

[One plate]

Palaeontological collections made on the 1985 Geotraverse are used to date the associated strata and provide information about palaeoenvironments. A biostratigraphical and palaeoenvironmental framework for the Tibetan plateau is constructed. The crucial stratigraphical and palaeontological evidence for dating volcanic sequences, flysch basins, open oceanic sediments, latest marine sediments and terrestrial red beds in each terrane is reviewed. A quantitative palaeobiogeographical analysis from the Carboniferous to early Triassic is presented for the Tibetan fauna and flora, to establish the biotic relationships between the various terranes. This is based largely on coral, brachiopod and fusulinid distributional data, but other groups have also been analysed, including the Permian terrestrial flora. This analysis demonstrates a clear diversity gradient from equatorial or sub-equatorial biotas in the north to temperate biotas in the south during the late Palaeozoic. No suture line consistently marks the position of a faunal/floral break during the late Palaeozoic and there appears to have been no physical barrier (such as a large ocean) to biotic dispersal between Tibetan terranes at this time. Climate is seen as the most likely factor dominating biotic distribution in this region and the early Permian glaciation had a profound effect on marine faunal distributions in Tibet.

1. Introduction

Palaeontology provides three kinds of evidence which are crucial to our understanding of Tibetan geology. *Firstly, fossils provide a biostratigraphical framework.* Competent taxonomists can use the stratigraphical succession of evolving biotas to construct a highly resolved and refined time framework, without which it would be more or less impossible to place data from other geological subdisciplines in relative context. The time resolution achievable using fossils, even in remote parts of the world such as Tibet, is generally in the order of 5 Ma, and may sometimes be considerably less. *Secondly, fossils provide a great deal of evidence concerning palaeoenvironments.* By using a knowledge of an organism's functional morphology, trace fossil data and general concepts of community structure, a considerable amount can be deduced about the palaeoenvironment in which the fossils once lived. A knowledge of palaeoenvironments is important in making palaeogeographical reconstructions and therefore in placing constraints on plate tectonic models. Usually the palaeontological data are combined with facies analysis of the sediments to build up a detailed picture of the evolution of environments, as we have done here. Leeder *et al.* (this volume) combine palaeontological evidence concerning palaeoenvironments with sedimentological data to provide an overall synthesis. *Thirdly, fossil distributions provide*

biogeographical data. The geographical distribution of fossil taxa can be analysed rigorously to determine the degree of effective biotic exchange between regions; this places constraints on palaeogeographical and palaeomagnetic reconstructions and plate tectonic models.

2. Biostratigraphical framework

Details of the regional biostratigraphical setting have largely been outlined by Yin *et al.* (this volume), but a few additional points are worth stressing here. Approximately 2500 specimens of macrofossil and several hundred microfossil samples were collected during this expedition. These have been studied in both the Nanjing Institute of Palaeontology and in the British Museum (Natural History) and, indeed, work is still proceeding on the mammoth task of identifying this material. The Appendix lists those fossils that have been identified to date, together with notes on their occurrence and palaeoenvironmental setting. The approximate position for all localities for which palaeontological data have been collected is shown later in figure 15. Some age-diagnostic Permian and Cretaceous foraminifera are shown in plate 1.

The geological subdivisions that have been adopted in this chapter follow Harland *et al.* (1982), with the exception of the Permian. International correlation of Permian strata has been problematic until recently, but there is now emerging a general broad consensus of opinion (viz. Waterhouse 1976; Kanmera *et al.* 1976; Iranian–Japanese research group 1981; Ross 1970, 1982*a*; Toriyama 1984; Dickins 1985*b*). In the Chinese literature, the Asselian and Sakmarian stages are placed as Upper Carboniferous, whereas throughout Europe and North America the Permian is considered to start at the base of the Asselian with the first appearance of the fusulinid *Pseudoschwagerina* as a useful marker. Higher stages in the Permian are often referred to Russian type sections, but there is still some dispute as to their correlation outside Russia. In this paper, therefore, we have adopted the Chinese subdivisions of the Permian, since there is a broad similarity between the total fauna of China and Tibet, and because these stages have been widely applied in the Chinese literature of this region. There are four stages, the Qixian, Maokouan, Longtanian and Changxinian, defined largely on the larger benthic foraminifera (see Wang, Sheng & Zhang 1981). Broadly speaking, the Qixian is equivalent to the Artinskian, the Maokouan to the Ufimian and Kungurian, the Longtanian to the Kazanian and the Changxinian to the Tartarian. In figure 1, each of the four stages is given the nominal duration of 5 Ma.

For the aims of this expedition, there are certain rocks whose dating is more critical than others for constructing plate tectonic models. These are volcanic sequences, flysch sequences, oceanic sediments, fluviatile red beds and the latest marine sediments present in each terrane. The evidence for dating these strata is outlined below.

Volcanic strata

(*a*) *Lhasa Terrane*

(i) *Dagze volcanics*. A relatively thick sequence of sheet-flow basalts and pyroclastics with interbedded mudrocks is found to the south of Lhasa towards the southern margin of the Lhasa Terrane. The interbedded mudrocks have yielded simple fern palynomorphs (see Appendix: locality M15) indicating a late Carboniferous or Permian age. Previously, these volcanics had been considered as probably Triassic in age.

(ii) *Chisan volcanics*. In the Chisan district, north of Lhasa, volcanics overlie a sequence of

limestones, which at one horizon yield a late Anisian (Triassic) marine fauna of ammonoids (Gu, He & Wang 1980; see also Appendix, loc. B12). This would suggest a Ladinian (Middle Triassic) age for these volcanics.

(iii) *Takena Formation.* In the northern part of the Lhasa Terrane, around Naqu, Amdo and Jang Co, there is an extensive sequence of volcanics and associated intrusive sheets. These have been dated radiometrically as between 110 and 75 Ma (i.e. Upper Cretaceous) by Coulon *et al.* (1986).

(iv) *Jienong Group.* Wang (1983*a*) has recorded the presence of andesitic volcanics interbedded in the Jienong Group, dated as Lower to Middle Jurassic on the evidence of ammonites. We have not been able to confirm this as the only volcanics of Jurassic age that we examined were in the Damqiao area associated with oceanic chert beds.

(v) *Sangri Group.* This is a thick 'eugeosynclinal' sequence found along the southern margin of the Lhasa terrane. The stratigraphical sequence is complex and includes thick and extensive volcanics. Interbedded sediments have yielded Tithonian to Aptian (latest Jurassic to Lower Cretaceous) faunas (Yang & Wang 1985). This sequence was not examined by our expedition.

(vi) *Linzizong Formation.* North of Lhasa a sequence of calcalkaline volcanics is interbedded with continental clastics. There is no fossil evidence for the age of these red beds, but the succession unconformably overlies folded and eroded Upper Cretaceous strata of the Takena Formation and can be no older than latest Cretaceous. Radiometric dating of the interbedded volcanics (Maluski *et al.* 1982) suggests a late Cretaceous/early Palaeocene age.

(*b*) *Qiangtang Terrane*

(i) *Kaixinling Group.* Basaltic and andesitic flows within this sequence at Kaixinling lie within a sequence that includes limestones yielding Maokouan fusulinids (early Upper Permian) and a fluvial sequence with an Upper Permian flora [see Appendix, locs B59 and B60]. This suggests that the volcanics are late Permian in age. Volcanics are found at a similar horizon in the Qamdo region further to the east (Dong & Mu 1984).

(ii) *Batang Group.* At Zhakongjian, in the northern part of the Qiangtang terrane, there is a thick sequence of andesitic volcanics overlying a fluvial sequence of conglomerates and sandstones and themselves directly overlain by a marine clastic and carbonate sequence of Norian age (Upper Triassic) [see Appendix, loc. B67]. These volcanics are probably therefore early late Triassic (Carnian or early Norian) in age.

(iii) *Yanshiping Group.* Near Wenquan, just north of the Tanggula Pass, there is a sequence of basaltic volcanics which lies at the base of an enormously thick fluviatile red bed sequence. Within this red bed sequence there are occasional marine incursions which date the succession as Bathonian/Callovian (Middle Jurassic). The age of the volcanics is therefore likely to be early mid Jurassic.

(*c*) *Kunlun Terrane*

(i) *Juchishan and Dagangou Formations.* In the Dagangou valley, to the north of Naij Tal in the northern Kunlun Shan, there is a series of volcanic outcrops that has been mapped previously as two formations, one Devonian in age, the other Carboniferous. Although there is a fossiliferous sequence of late Visean/early Namurian (mid Carboniferous) fluvio-deltaic sediments [see Appendix, loc. B108], the stratigraphical relationship between this fossil-bearing sequence and both groups of volcanics is problematic. The 'Devonian' volcanic sequence appears to

underlie a thick basal sequence of conglomerates and arkosic sandstones which themselves are conformably overlain by the fossiliferous mid Carboniferous strata, suggesting that there is a genuine late Devonian or early Carboniferous volcanic sequence here. However, the so-called 'Carboniferous' volcanics show fault-bounded contacts with the Carboniferous sequence where examined by us and we suspect them to be fault-bounded blocks of Devonian volcanics. Alternatively, they may be younger volcanics (?Permo-Triassic) downfaulted into this area.

(ii) *Permian Volcanics.* In the north Kunlun Mountains a number of local stratigraphical names has been applied to early Permian (Asselian–Sakmarian) volcanics that are found interbedded with fusulinid-bearing limestones (Qinghai Stratigraphical Working Group 1980: see also Yin *et al.*, this volume). Unfortunately, no volcanics interbedded with dateable Permian sediments were seen by our expedition. However, we suspect that the thick sequence of volcanics seen to the southeast of Naij Tal (the Wanbaogou Group) may be Permian in age.

The Wanbaogou Group, outcropping from Wanbaogou in the west to the Kunlun bridge in the east, comprises a thick sequence of resedimented tuffs and basaltic volcanics, with occasional crystalline limestones. This sequence has been attributed to the pre-Cambrian on account of the discovery of *Conophyton*, a supposedly pre-Cambrian stromatolite, within one of the limestones in the Wanbaogou valley (Zhu, Zhao & Zheng 1985). However, this identification needs confirmation since in the same paper they assign a Jurassic/Cretaceous age to Upper Ordovician strata on the misidentification of platyceratid gastropods as Mesozoic bivalves. At one locality (B88 – see Appendix), one of these limestones contained badly recrystallized crinoidal debris indicating an age no older than Ordovician. As this sequence of resedimented tuffs, volcanics and limestones appears to grade up into late Permian limestones in the Wanbaogou valley, they are tentatively assigned to the early Permian.

Flysch basins

(*a*) *Lhasa terrane*

(i) Flysch type sequences interbedded with volcanics (the Jienong Formation) occur in the Jang Co region in the northern part of the Lhasa Terrane. Wang (1983*a*) records ammonites from this succession which range in age from Sinemurian to Callovian (Lower to Middle Jurassic) while Girardeau *et al.* (1984) report an Aalenian (Middle Jurassic) age on the basis of gastropods. Our sparse evidence suggests a slightly younger age. At locality B48, near Amdo close to the line of the Banggong Suture, we logged a continuous sequence which commenced with shallow fluvio-marine sediments, with periodic bands of *Cladocoropsis*, mostly broken and transported. This graded upwards into a fine sand/shale turbiditic flysch sequence containing derived nerineid gastropod and other shelf faunas, similar to those occurring at Jang Co (locs B32 and B33). The occurrence of *Cladocoropsis* (Upper Jurassic) in the underlying beds places this flysch sequence as late Jurassic or possibly even early Cretaceous.

(ii) In the very south, adjacent to the Zangbo Suture, flysch-type sediments are intermixed with volcanics (the Sangri Formation). From these sediments Yang & Wang (1985) have discovered latest Jurassic (Tithonian) to Lower Cretaceous (Aptian) fossils.

(*b*) *Qiangtang and Kunlun Terranes*

(i) *Bayan Kala Group.* A thick sequence of turbidites and contourites occurs extensively over the northern part of the Qiangtang Terrane. Its precise thickness is impossible to gauge due

to the considerable repetition produced by tectonic slicing. No fossil evidence was found by us to date this sequence. However, further to the east, previous Chinese geological teams have been more successful (He & Yin 1983). According to their work, the sequence commences with sandstone-dominated clastics that have yielded species of the bivalve *Claria* indicative of an early Induian age (basal Triassic). Proper flysch-type sedimentation does not appear to have commenced until slightly later, in the late Induian or Olenian. Fossil evidence for a mid Triassic age has also been found; the highest beds in this sequence have yielded the bivalves *Halobia* and *Daonella* and are late mid Triassic or early late Triassic in age. Thus the whole flysch sequence appears to be entirely Triassic in age.

Oceanic sediments

(*a*) *Zangbo Suture*

Distal fan turbidites and radiolarian cherts are found along the line of the Zangbo Suture, but were not examined by our expedition. Wang & Sheng (1982) have described Upper Triassic radiolaria from cherts associated with deep water clastics in the Gyirong district, as well as Upper Jurassic radiolaria from shales with lentiform limestones in the Gyangze district. Wu & Li (1982) and Wu (1984, 1986, and unpublished manuscript) have described latest Jurassic (Tithonian), Berriasian, late Valanginian and late Albian–?Cenomanian (all Cretaceous) radiolaria from cherts along this suture. Deep water clastics of Valanginian and Albian to Cenomanian age have also been proved (Wu 1984, 1986). The formation of the olistostrome associated with the Zangbo Suture has been dated on the basis of radiolaria in the sedimentary matrix as Turonian (Upper Cretaceous) (Wu *et al.* 1982), but there may also have been olistrostrome formation as late as Maastrichtian to produce the intermixing of *Globotruncana*-bearing limestones of Campanian/Maastrichtian age and Triassic strata. It is, however, not yet clear whether this is syndepositional or post-depositional mixing.

There is thus evidence for oceanic sediments associated with the Zangbo Suture from the late Triassic to the end of the early Cretaceous (the majority being early Cretaceous in age). There is also evidence that ophiolite emplacement and olistostrome formation had started by the Turonian (Upper Cretaceous).

(*b*) *Banggong Suture*

Oceanic cherts and fine clastics associated with the Dongqiao ophiolite sequence along the Banggong Suture were examined, but unfortunately samples collected proved to have no determinable radiolaria. However, Wang (1984) reported a radiolarian assemblage from these cherts which he suggested was probably late Jurassic in age and Li (1986) has recently described an early Tithonian (Upper Jurassic) radiolarian fauna from cherts in this suture zone.

The timing of obduction for the ophiolite and chert sequence is bracketed by an apparently conformable (though faulted) sequence just to the west of Dongqiao (loc. B41) previously described by Girardeau *et al.* (1984). Here the ophiolite suite is overlain unconformably by a three metre palaeosol followed by a fluviomarine sequence with the alga *Cladocoropsis* and other fossils. This dates the overlying sediments as Upper Jurassic and no later than Tithonian (latest Jurassic).

At another locality near Dongqiao (loc. B39), a deep water clastic sequence with thin limestones contains a melange horizon with chert, pillow lava and limestone olistoliths. The age of the clastic sequence is unknown, since only indeterminate radiolaria were collected, but the

limestone blocks in the melange are fossiliferous and yield a fauna of corals, stromatoporoids and echinoid spines, including *?Pseudocidaris maresi* (Cotteau). The fauna from these limestone blocks exactly matches that found from late Jurassic (Kimmeridgian) to early Cretaceous (?Valanginian) reef limestones of the Xiaqiong Co region to the west [see Appendix, locs B28–B30]. Erosion of emplaced ophiolitic material was obviously taking place after lithification of this late Jurassic/early Cretaceous limestone, possibly in the latter part of the Lower Cretaceous.

Latest marine strata

Dating of the latest marine strata in each terrane helps to bracket the timing of final closure of epicontinental seas following collision. There is a progressive increase in the age of the latest marine strata from south to north.

(*a*) *Himalayan Terrane*

South of the Zangbo Suture, in the Himalayan Terrane, the youngest marine strata appear to be Lutetian (early mid Eocene), to judge by the occurrence of foraminifera including *Orbitolites complanatus* (Zhang 1981, Wang 1983*a*). Pan *et al.* (1984) report Palaeogene marine sediments from immediately north of the Zangbo Suture to the west of our traverse, but this clearly represents deposition associated with the closing seaway along this suture zone.

(*b*) *Lhasa Terrane*

In the Lhasa Terrane, strata as young as Maastrichtian (uppermost Cretaceous) have been reported from the Bange region (Wang 1983*b*; Wang & Bassoullet 1984; Pan 1985), but this is decidedly questionable. The one locality that our expedition visited from which Wang (1983*b*) reported Upper Cretaceous fauna (loc. B31 – see Appendix) turned out to have Albian/Cenomanian orbitoline foraminiferans, and the gastropods described by Pan (1985) are not by themselves convincing evidence for a late Cretaceous age. The highest marine strata in this region are therefore late early Cretaceous in age, though there is the possibility that marine conditions may have continued into the lower Upper Cretaceous. Previous suggestions that the Langshan Formation extended into the Cenomanian have recently been shown to be wrong (Zhang 1986).

(*c*) *Qiangtang Terrane*

In the Qiangtang Terrane, the youngest fully marine strata found are seen around Amdo and are late Jurassic (Kimmeridgian) in age [Appendix, loc. B50]. Marine incursions into a predominantly continental red bed sequence occurred in the Middle and possibly Upper Jurassic of the Amdo region, but to the north of Yanshiping no marine strata younger than Norian (Upper Triassic) are found, suggesting that the marine incursions were coming from the south. This deduction is supported by sedimentary studies (Leeder *et al.*, this volume).

(*d*) *Kunlun Terrane*

Finally, in the Kunlun Terrane, the oldest marine beds encountered by our expedition are late Permian in age. The section in the Wanbaogou Valley, west of Naij Tal, originally considered to be early Triassic in age (e.g. Li & Lin 1982; Chang *et al.* 1986) is now known to have an Upper Permian fauna (Appendix, loc. B91). It is clear that there are outcrops of Induian to Anisian (Lower to Middle Triassic) marine strata to the north in the South Qilian

Mountains, where a diverse ammonoid and brachiopod fauna has been reported (Yang *et al.* 1983). Whether similar aged beds exist in the Kunlun Shan remains to be proved.

The record of marine Mesozoic (Jurassic or Cretaceous) by Zhu, Zhao & Zheng (1985) has also been disproved by our expedition, as these beds are late Ordovician in age (see Appendix, loc. B98).

Continental red beds

These are the most difficult to date accurately.

(*a*) *Lhasa Terrane*

(i) *Linbuzong Formation.* Extensive fluvial red bed sequences with occasional marine incursions occur to the north of Lhasa [e.g. Appendix, loc. B16]. Fossils from these marine to brackish horizons indicate a latest Jurassic (Tithonian) to early Cretaceous age (Bassoullet *et al.* 1984, Wang & Sun 1983) near the base of this sequence. Plant fossils from higher in the sequence [Appendix, loc. B16a] suggest an early Cretaceous age. The whole succession is overlain by clastics and limestones yielding Aptian to Albian (upper Lower Cretaceous) orbitoline foraminiferans, the transition being seen in the Baingoin district by our expedition.

(ii) *Lhunzhub Member of the Takena Formation.* The major marine incursion of Aptian/Albian age, the Pembo Group, which overlies the Linbuzong Formation, is itself overlain by a sequence of variegated clastics known as the Lhunzhub Member. As these are folded and overlain uncomformably in turn by the possibly Palaeocene Linzizong Formation, they are likely to be early late Cretaceous in age, although we have no internal faunal or floral data to support this.

(iii) *Linzizong Formation.* These volcanics, with intercalated red beds, unconformably overlie the Upper Cretaceous Takena Formation. There is no independent fossil evidence as to their age, but radiometric dating of some basal volcanics suggests they are Palaeocene (see Maluski *et al.* 1982).

(*b*) *Qiangtang Terrane*

(i) *Kaixinling Group.* In the Kaixinling district of the central Qiangtang Terrane, a sequence of continental clastics overlies limestones with a Maokouan (early Upper Permian) fauna of fusulinid foraminiferans [Appendix, locs B59 and B60] and themselves contain an Upper Permian plant flora. These red beds, which have intercalated volcanics, are late Permian in age.

(ii) *Batang Group.* At Wuli, near the northern margin of the Qiangtang Terrane, a thick sequence of Upper Triassic volcanics is underlain by a red clastic sequence of continental origin. A precise age for these beds cannot be proposed, but their conformable relationship with overlying Norian strata suggests that they are probably early late Triassic (Carnian) in age. Late Upper Triassic (Norian) red beds cap the sequence and have yielded plant fossils from further east around Qamdo (Wu 1982).

(iii) *Yanshiping Group.* From around Amdo to just north of Wenquan, on either side of the Tanggula Mountains, there is an extensive sequence of red beds (over 2 km in thickness) with occasional brackish to marine incursions. The fauna from the marine horizons ranges in age from Bathonian to Kimmeridgian [Appendix, locs B49, B50, B51, B56, B57 and B58]. A probable equivalent succession is seen at Wuli, to the north, where continental clastics with thin coal seams, previously attributed to the Permian, yielded Middle Jurassic non-marine bivalves belonging to the genus *Pseudocardinia*.

(iv) *Fenghuoshan Group*. Around Erdaogou, to the north of the Qiangtang Terrane, is another thick sequence of continental red beds. There are no marine incursions within this sequence, but thin lacustrine limestones yielded charophytes and palynomorphs [Appendix, locs B69 and B74] which indicate a ?Palaeocene or early Eocene age for these beds.

(*c*) *Kunlun Terrane*

(i) *Juchishan Formation*. In the region of Dagangou, in the northern Kunlun Mountains, red siltstones and fine sands are overlain by fluviatile arkosic sandstones and gravels. These reach several kilometres in thickness and are conformably overlain by a marine limestone/shale sequence of latest Visean or early Namurian age (mid Carboniferous) [Appendix, loc. B108]. They are therefore most likely to be early Carboniferous in age.

(ii) Lower Jurassic red beds are also reported from this region (Qinghai Stratigraphical Working Group 1980), based on the identification of palynomorphs. However, no positive evidence for Jurassic red beds was found by our team. A sizeable outcrop of continental clastic sediments was examined in the north Kunlun Shan, at localities B103 and B104. No fossils were obtained from these strata to provide a clue as to their age, but they are probably post-Carboniferous, since they are not cut by any dykes or sills, in stark contrast to the immediately adjacent Carboniferous sequence. These have previously been mapped as Jurassic, but are best considered as late Palaeozoic or Mesozoic.

(iii) A small outcrop of continental, plant-bearing clastic sediments is found in the Xidatan valley at locality B88. There are no diagnostic palynormorphs in our samples and the macrofossil material is scrappy. However, it does hint at a Mesozoic rather than Palaeozoic age for these beds.

The biostratigraphical data is summarized in figure 1. This shows the distribution of broad

---

FIGURE 1. Biostratigraphy of the Tibetan plateau. This diagram summarizes the distribution of broad rock types and facies from Carboniferous to Recent across the Tibetan plateau. Areas left blank represent time spans for which there is no record of deposition.

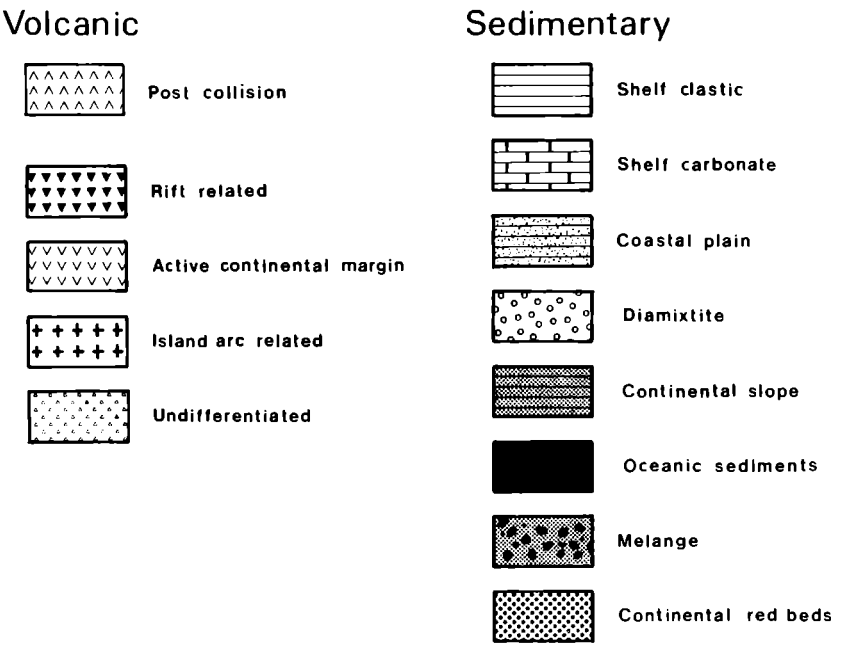

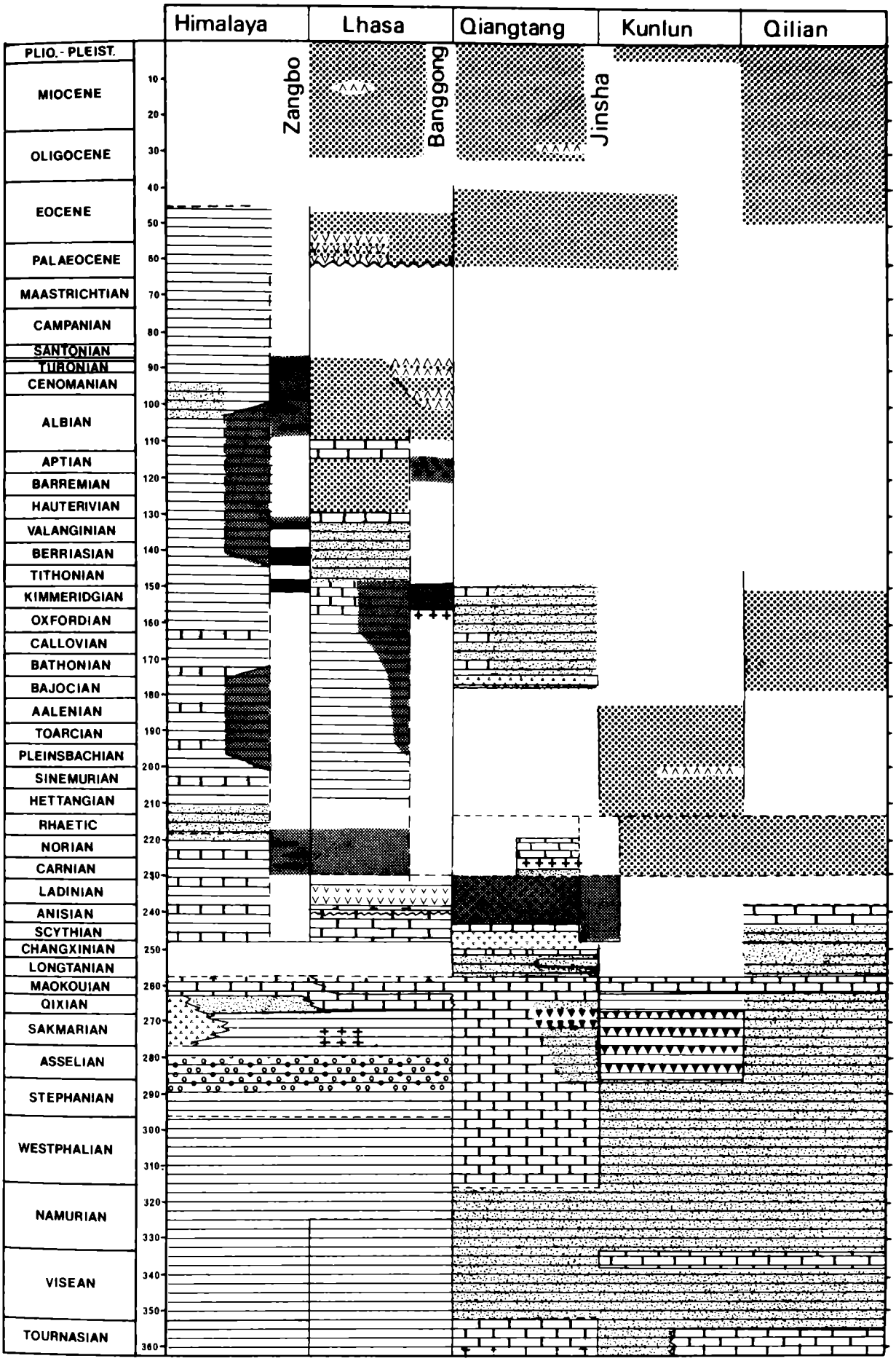

FIGURE 1. For description see opposite.

palaeoenvironments and rock types across the Tibetan plateau and has been compiled from our own observations, supplemented where necessary with data from published sources. Facies are distinguished on faunal and lithological grounds, and divided into the following types: fluviatile; coastal plain; clastic marine shelf; carbonate marine shelf; continental rise and oceanic. Volcanics are separated into rift, active continental margin and post collisional on the basis of data presented by Pearce (this volume). Palaeoenvironments and geological history are discussed more fully by Leeder *et al.* (this volume).

3. Biogeographical Analysis

In principle it should be possible to use a knowledge of the distribution of fossil biotas to set some constraints on palaeogeographical reconstructions. The underlying rationale is that, in comparing the biotas from a number of regions, those with many members in common come from areas which maintain (or maintained until relatively recently in the past) a large degree of biotic exchange and migration with one another, whereas conversely those with few members in common have been isolated from one another for a relatively greater length of time. Temperature also plays a role in restricting the distribution of taxa and distributions of fossil taxa may help define climatic belts.

However, in practice several problems enter into any biogeographical analysis which make the task much less simple than would first appear, and which are sometimes overlooked. First there is the problem of the vagaries of the fossil record. For example, the absence of a fossil taxon from one region may be genuine, or may be a pseudo-absence produced by collection failure or the absence of exposures of rocks of the right facies. This is clearly a particularly pressing problem in palaeobiogeographical studies of poorly studied regions of the world such as Tibet.

A second problem arises because all taxa are to a greater or lesser extent facies-restricted. Within the same region, adjacent facies may support quite different biotas. To avoid this problem, either the region's biota must be sampled over as broad a range of facies as possible, or the biotas of very specific facies only must be compared. In practice, because of the sheer impossibility of recognizing subtle, yet important, differences in habitat within the fossil record, by far the best approach is to sample as widely as possible within one broad habitat (such as 'shallow marine' or 'terrestrial').

A third problem arises from diversity gradients. In most rigorous methods of analysis, variation in biotic diversity for whatever cause (genuine diversity gradient or sampling problems) will affect the result. Thus evidence of a depleted biota is not sufficient by itself to establish provinciality; only endemicity is significant.

Finally, there are very many different methods of analysis which do not necessarily produce the same results. The more rigorous and explicit the method, the easier it is for others to assess.

Biogeographical analysis of the fossil biota of the Tibetan plateau is particularly difficult for the following three reasons.

(1) Despite the tremendous effort over the last decade, primarily by Chinese scientists, to understand the geology of the Tibetan plateau and record its fossil biota, our knowledge of the fossil fauna and floral of this region is still at an elementary stage. A great deal of field and laboratory work remains to be done.

(2) Consequently, there remain some fairly serious problems in correlation both within the

region and also with other parts of the world. A broad picture has emerged over the last decade but the biostratigraphical time scale in many places is still very coarse and in need of refinement.

(3) Because fossil taxa from this region are generally neither abundant nor well preserved, there are serious taxonomic difficulties. The small sample sizes mean that variation within populations is rarely established, which has had the unfortunate result that there has been a great deal of taxonomic oversplitting at all levels. Poor preservation also makes systematic determinations difficult. We have strong reservations about the quality of the taxonomic data, but have expertise in only a small proportion of the Tibetan fauna and flora. Published taxonomic determinations have therefore had to be taken on trust without the possibility of checking for accuracy or consistency.

Because of the numerous problems mentioned above, one might wonder whether it was not premature to attempt a biogeographical analysis in a region such as Tibet where sampling is poor and taxonomy uncertain. Whether or not this is correct, there have already been numerous attempts to define past biogeographical provinces and reconstruct palaeogeographies on the data that is available, (viz. Allègre *et al.* 1984; Dickins 1985*b*; Dickins & Shah 1981; Fan 1985; Gu *et al.* 1980; He & Zhang 1984; Jin 1985; Li, Yao & Deng 1982; Liang & Wang 1983; Liao & Xia 1985; Lin 1983, 1984; Liu 1981; Liu & Cui 1983; Ross & Ross 1985; Wang 1984; Wang & Mu 1984; Waterhouse & Bonham Carter 1975; Xia 1983; Yang & Fan 1983; Zhang & He 1985; Zhang & Wu 1983; Zhang *et al.* 1985). These have largely been descriptive and anecdotal in form and for this reason are difficult to assess or compare with rival hypotheses. Furthermore, in many cases it has been only a small proportion of the total biota that has been used. It is therefore necessary to undertake a more rigorous analysis of the data as it stands, with all its inconsistencies and limitations, in order to discover precisely what the available data really does imply about Tibetan palaeogeography. This analysis must be considered as a very preliminary attempt to investigate Tibetan palaeobiogeography.

4. Approach

Our primary interest is to discover the historical pattern of relationships of the biotas from the three strip-like terranes that constitute the Tibetan Plateau, with respect to biotas of the Indian and Eurasian plates between which they now lie sandwiched. We specifically wish to ask the question 'at a particular time, is the biota of terrane *x* closer in character to that of the Himalayas (Indian Terrane) or of the Qilian (Eurasian Terrane)?'

Methods of biogeographical analysis currently employed to probe such questions in a rigorous way are vicariance biogeography, multivariate analysis and parsimony analysis of endemism. Unfortunately, vicariance biogeography is not an option in this case because the method requires a taxonomic group whose relationships have been determined cladistically and which has at least one species unique to each terrane. No single taxon from Tibet fulfils these criteria. Left with the choice of multivariate analysis or parsimony analysis of endemism, we have chosen to adopt the latter (for details of this method see Rosen & Smith (1988)). The advantage of parsimony analysis of endemism is that it produces a cladogram of sample areas directly interpretable in terms of relative recency of biotic contact between sample areas. The method nests sample areas hierarchically according to the taxa that are shared between them. A dichotomously branching tree is calculated relating the areas which requires the fewest reversals and parallelisms of data (maximum parsimony).

(*a*) *Choice of sample areas*

The often difficult and subjective choice of sample areas for analysis is made simple in this case because of the highly specific problem that we are investigating, namely the relationships of the three suture-bounded terranes that compose the Tibetan Plateau. Geological boundaries delimit our sample areas (figure 2). Thus the region to the south of the Zangbo Suture is the Himalayan Terrane (H); that between the Zangbo and Banggong Sutures, the Lhasa Terrane

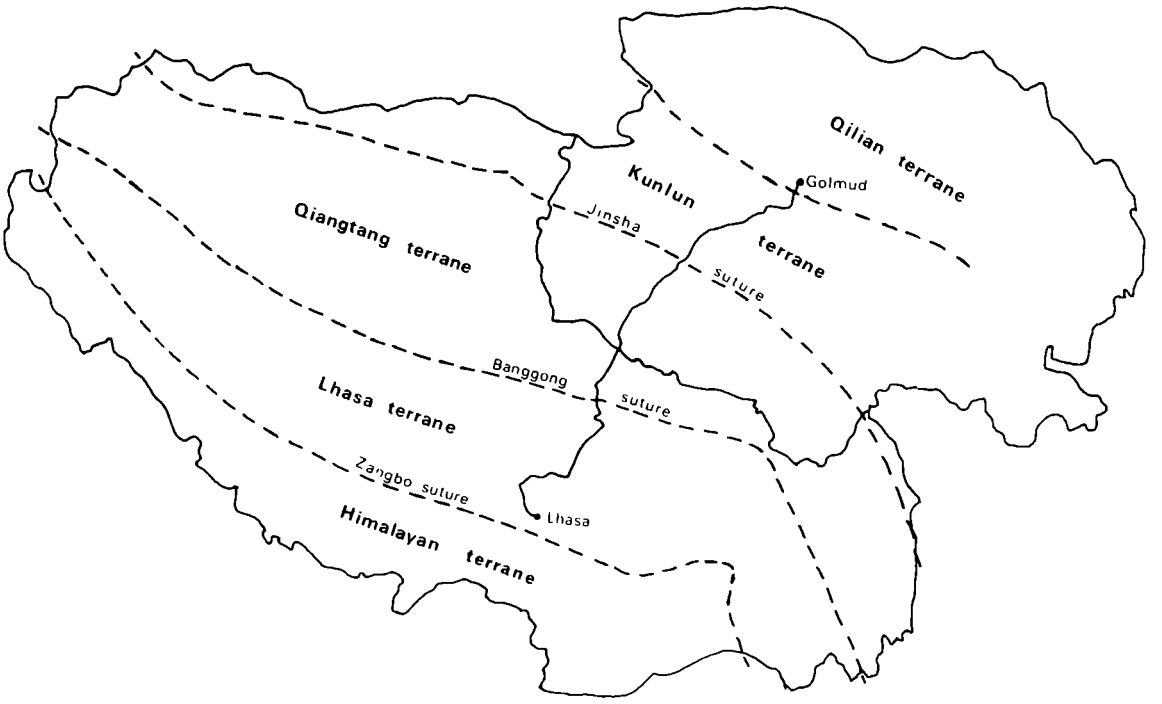

FIGURE 2. Outline map of Xizang and Qinghai provinces (Tibetan Plateau), China, showing the sample areas (terranes) used in the biogeographical analysis and their boundaries (suture zones).

(L); that between the Banggong and Jinsha Sutures, the Qiangtang Terrane (Qa); that between the Jinsha Suture and the major fault marking the northern margin of the Kunluns, the Kunlun Terrane (K); and the area to the north of the Qaidam basin in Qinghai Province, the Qilian Terrane (Qi). The biota within each terrane is treated as a single entity and data from different localities within it are amalgamated. Note that the western part of the Qiangtang Terrane of previous authors (e.g. Wen 1984: Rutog district, etc.) is omitted from consideration here, since it appears to be part of the Lhasa Terrane, both lithologically and faunally, and ought to be treated as a separate sample area in analysis.

(*b*) *Level of analysis and data set*

Biogeographical analyses were attempted for biotas from the Lower Carboniferous through to the Middle Triassic. No analyses were attempted for geological periods before the Lower Carboniferous because rocks of the appropriate ages are not represented in each terrane. The pattern of plates after the Triassic is little disputed and there is sufficient independent evidence

on which to base palaeogeographical reconstruction. Thus the prime aim of this analysis is to establish the relationships of terranes prior to the establishment of a large Tethyan ocean represented now by the Zangbo Suture. Faunal and floral lists of genera were compiled for specific geological periods (generally a single stage) for each terrane, based largely on the published Chinese literature, but supplemented wherever possible with our own data. We chose to work at the taxonomic level of genus for practical reasons. As noted above, species level taxonomy appeared to us to be oversplit, with few species apparently found outside their type area, let alone in more than one terrane. Genera appeared to be somewhat more consistently used and provided sufficient endemism to be of use.

Taxa that are unique to just one terrane are uninformative about how that area relates to others. It is only those taxa that are recorded from two or more terranes that can provide the necessary data from which to assess area relationships. The full taxonomic lists for each sample area were thus culled to remove all taxa unique to a single area. In practice only a few major groups were abundant enough to analyse with this method.

(*c*) *Interpolation of ranges*

Because our knowledge of the fossil biota of Tibet is still very preliminary, the problem of pseudo-absences in the data is acute. In order to try to minimize this, we have made one assumption, namely that the five sample areas remain in their same relative positions through time. Although major barriers to biotic exchange could appear and disappear between adjacent terranes, it is assumed that no terrane switched position ('leap-frogged') relative to its neighbours along the north/south transect. This seems eminently reasonable since the three terranes form long narrow strips running east/west. Accepting this, then a taxon's range can be interpolated between its most southerly and northerly records. Where a taxon is present in two non-adjacent terranes, then its absence in the intervening terranes is ascribed to collection failure or absence of the appropriate facies.

The culled data set of taxonomic ranges was then analysed following the parsimony analysis of endemism method outlined by Rosen & Smith (1988). For each time period analysed, only a few major groups were used, those being the most important and best studied. The results for each taxonomic group were kept separate and then compared to check for congruence. Where there is a high degree of congruence between the results from different taxonomic groups then more reliance can be placed on the results. In most cases the data matrixes were small enough to carry out a parsimony analysis empirically, without the aid of computer programs.

5. Results

(*a*) *Late Dinantian (Visean)*

(i) *Correlation*

This is the first period for which there is a good record of fossiliferous marine strata across the plateau. Correlation within the Qiangtang, Kunlun and Qilian Terranes is well established on the brachiopod and coral faunas (Jin & Sun 1981; Chen 1984), which are closely comparable in all three regions. Correlation into the Lhasa and Himalayan Terranes is less well established and no detailed stratigraphy is yet available.

(ii) *Corals* (figure 3)

The Qiangtang, Kunlun and Qilian Terranes share a very similar coral fauna dominated by Eurasian elements. It is a high diversity fauna dominated by compound rugose corals or large solitary rugose corals with complex dissepimentation, typical of a shallow marine carbonate shelf environment. Stromatoporoids and chaetetids are also common. Many of the genera are part of a fairly cosmopolitan equatorial fauna (e.g. *Lithostrotion*, *Lonsdaleia*), but there are also genera which are found only in the South China Block (e.g. *Yunnanophyllum*, *Kueichophyllum*).

There is a marked drop in diversity to the south of the Qiangtang Terrane and corals from the Lhasa and Himalayan Terranes are on first sight very different. This is solely due to the loss of compound genera. The sparse fauna of small solitary rugose corals without dissepiments or thickened axial edges and of tabulate corals is composed of genera that have also been reported as present in the Qiangtang–Kunlun–Qilian biota. Notably, there are no endemic forms unique to the Lhasa–Himalaya region.

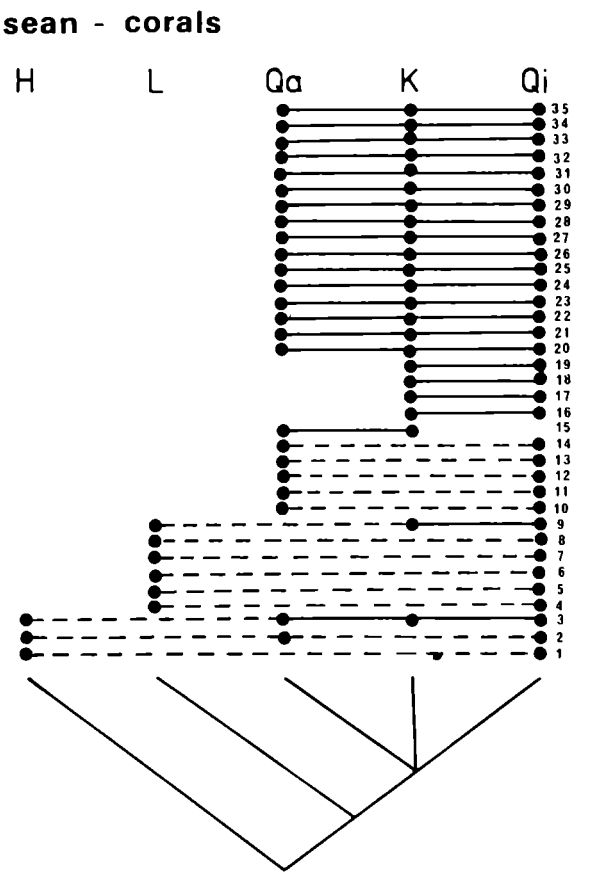

FIGURE 3. Taxon/area matrix of late Dinantian coral distribution across the Tibetan Plateau. H = Himalayan Terrane; L = Lhasa Terrane; Qa = Qiangtang Terrane; K = Kunlun Terrane; Qi = Qilian Terrane. Only genera found in two or more terranes are included: each line represents the range of a genus; black circles = presence recorded; dashed lines = interpolation of range through a terrane from which the taxon has not yet been recorded. Summary cladogram of sample areas is shown at the base. Data from many sources. Taxa are as follows: 1, *Zaphrentoides*; 2, *Caninophyllum*; 3, *Caninia*; 4, *Cyathaxonia*; 5, *Barrandeophyllum*; 6, *Meniscophyllum*; 7, *Zaphrentites*; 8, *Rhopalolasma*; 9, *Amplexus*; 10, *Zaphriphyllum*; 11, *Neoclisiophyllum*; 12, *Clisiophyllum*; 13, *Stelechophyllum*; 14, *Lophophyllum*; 15, *Hunanoclisia*; 16, *Qinghaiphyllum*; 17, *Chaetetes*; 18, *Michelinia*; 19, *Ekvasophyllum*; 20, *Kueichouphyllum*; 21, *Kueichoupora*; 22, *Lithostrotion*; 23, *Heterocaninia*; 24, *Syringopora*; 25, *Hexaphyllia*; 26, *Dibunophyllum*; 27, *Lonsdaleia*; 28, *Aulina*; 29, *Palaeosmilia*; 30, *Syphonophyllia*; 31, *Carcinophyllum*; 32, *Gangamophyllum*; 33, *Arachnolasma*; 34, *Yunanophyllum*; 35, *Diphyphyllum*.

(iii) *Brachiopods* (figure 4)

The brachiopod data produce a result congruent with that from corals. Brachiopods are rather more widespread in their distribution, with a less marked drop in diversity between the Qiangtang and Lhasa Terranes. As with corals, there appears to be a continuous decline in diversity from north to south, with no genus endemic to the Lhasa–Himalaya region.

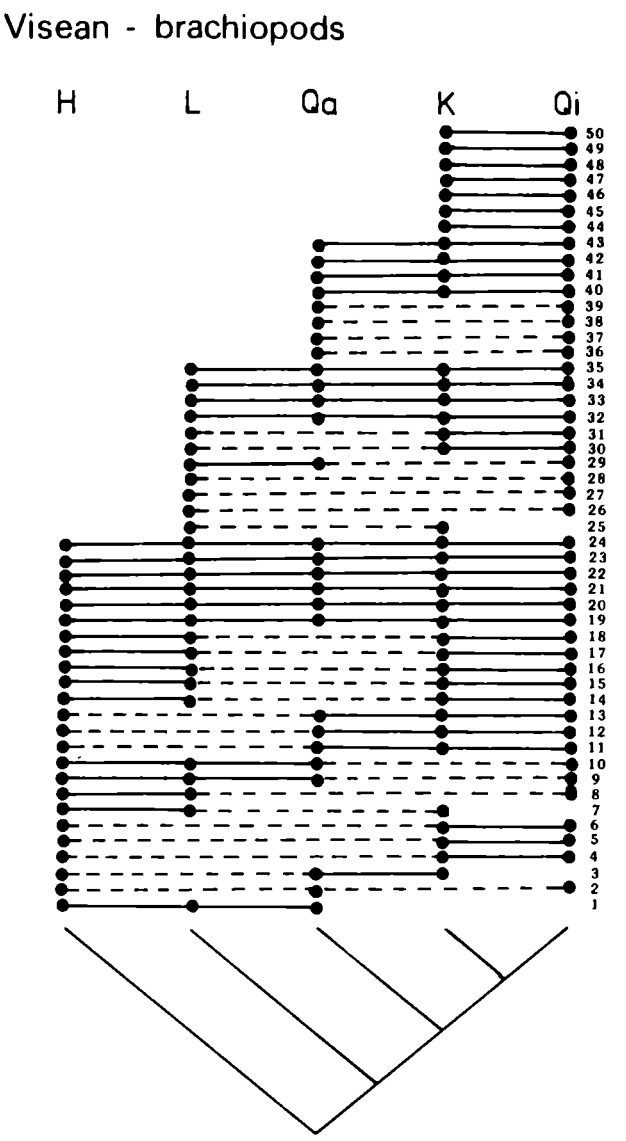

FIGURE 4. Taxon/area matrix and cladogram of late Dinantian brachiopods. Symbols as in figure 2. Taxa are as follows: 1, *Fusella*; 2, '*Chonetes*'; 3, *Waagenoconcha*; 4, *Pugilis*; 5, *Delepinea*; 6, *Schuchertella*; 7, *Rotaia*; 8, *Balakhonia*; 9, *Tylothyris*; 10, *Ectochoristites*; 11, *Striatifera*; 12, *Gigantoproductus*; 13, *Linoproductus*; 14, *Syringothyris*; 15, *Ovatia*; 16, *Neospirifer*; 17, *Marginatia*; 18, *Composita*; 19, '*Spirifer*'; 20, *Eomarginifera*; 21, *Dictyoclostus*; 22, *Dielasma*; 23, *Buxtonia*; 24, *Brachythyris*; 25, *Marginifera*; 26, *Pugnax*; 27, *Hustedia*; 28, *Fluctuaria*; 29, '*Productus*'; 30, *Plicatifera*; 31, *Rhipidomella*; 32, *Punctospirifer*; 33, *Phricodothyris*; 34, *Martinia*; 35, *Overtonia*; 36, *Schellwienella*; 37, *Semiplanus*; 38, *Crurithyris*; 39, *Camaratoechia*; 40, *Megachonetes*; 41, *Echinoconchus*; 42, *Cleiothyridina*; 43, *Antiquatonia*; 44, *Uncinella*; 45, *Rugosochonetes*; 46, *Pustula*; 47, *Leptagonia*; 48, *Kansuella*; 49, *Grandispirifer*; 50, *Cancrinella*.

(iv) *Interpretation*

The marine fauna of this period can be divided into a highly diverse, shallow carbonate shelf community dominated by compound rugose corals, solitary rugose corals with dissepiments, stromatoporoids and brachiopods in the north, and a low diversity, deeper water clastic community dominated by brachiopods, fenestellid bryozoans, crinoids and small simple solitary rugose corals to the south. Clearly the faunas of the Qiangtang, Kunlun and Qilian Terranes are closely comparable, and indeed show the same detailed biostratigraphical succession. The coral data suggest that these three areas also maintained a close connection with the South China Block at this time.

The differences between the two faunas are striking but cannot be taken as evidence for there being a major palaeogeographical break coincidental with the Banggong Suture at this period as some have suggested (e.g. Fan 1985). This is because different facies are being compared (offshore deeper shelf clastics with shallow subtidal carbonates). What is clear from this analysis is that there is a decrease in diversity southwards and that in both taxonomic groups the Lhasa Terrane shares more fauna in common with areas to the north than it does with the Himalayan region. This may be a genuine latitudinal effect, with the progressive loss of tropical/subtropical faunas southwards into more temperate regions. But it is equally possible that it is a depth-related phenomenon, with diverse shallow water communities being replaced to the south by reduced diversity deeper water communities. In particular, the absence of a single genus endemic to the Lhasa–Himalaya region at this time argues strongly against there being a separate 'Gondwanan' province south of the Banggong Suture. Faunal analysis provides no evidence for there having been provinciality of biotas across this region at this time.

(*b*) *Early Permian*

(i) *Correlation*

Where they occur, we have used the occurrence of fusulinids belonging to the *Pseudoschwagerina* assemblage to define this period. In the Lhasa and Himalayan Terranes, there are no larger benthic foraminiferans and correlation has been done on the basis of brachiopod faunas (Wang & Mu 1984).

(ii) *Fusulinids* (figure 5)

Fusulinids are found only in the Qiangtang, Kunlun and Qilian Terranes. They are generally thought to be shallow water and tropical to warm temperate in distribution (Ross 1982*b*). Many of the genera are also shared with the South China Block. Their distribution matches that seen for Visean compound rugose corals. Although there are slightly more genera shared in common between the Kunlun and Qiangtang Terranes, there is no real evidence for separation of these three areas.

(iii) *Corals*

The number of coral genera known from this period is relatively small and few genera are known from more than one terrane, therefore no quantitative analysis is possible. Broadly speaking, however, coral distribution appears much as it was in the Visean, with compound rugose corals restricted to the Qiangtang, Kunlun and Qilian Terranes and small solitary

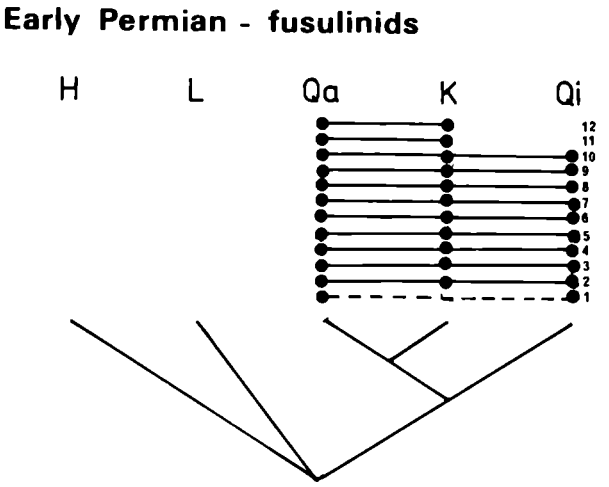

FIGURE 5. Taxon/area matrix and cladogram of early Permian (Asselian/Sakmarian) fusulinid genera. Symbols as in figure 2. Data from many sources. Genera are as follows: 1, *Paraschwagerina*; 2, *Schwagerina*; 3, *Schubertella*; 4, *Pseudofusulina*; 5, *Quasifusulina*; 6, *Ozawainella*; 7, *Triticites*; 8, *Rugosofusulina*; 9, *Eoparafusulina*; 10, *Pseudoschwagerina*; 11, *Boultonia*; 12, *Sphaeroschwagerina*.

rugose corals dominating in the Lhasa and Himalayan Terranes. Simply on number of taxa, there does appear to have been a southward shift in peak coral diversity from the Qilian Terrane in the mid Carboniferous to the Qiangtang Terrane in the early Permian. This may be due to collection failure or may be genuine and result from the increasingly more fluviatile conditions that apparently developed towards the north.

(iv) *Brachiopods* (figure 6)

Only relatively few taxa are recorded from the Qiangtang–Kunlun–Qilian region making interpretation of results difficult. The Lhasa Terrane has a fauna that has shared elements both

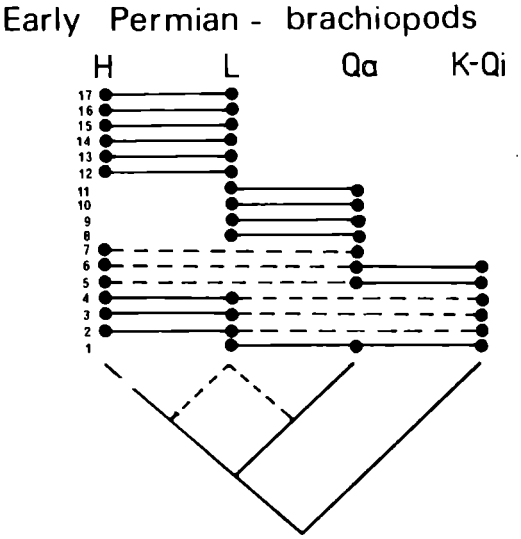

FIGURE 6. Taxon/area matrix and cladogram of early Permian brachiopods. Symbols as in figure 2. Data from many sources. Taxa are as follows: 1, *Dictyoclostus*; 2, *Neospirifer*; 3, *Linoproductus*; 4, *Martinia*; 5, *Cancrinella*; 6, *Orthotetes*; 7, *Orthotichia*; 8, *Marginifera*; 9, *Chaoiella*; 10, *Choristites*; 11, *Punctospirifer*; 12, *Stenoschisma*; 13, *Stepanoviella*; 14, *Brachythryis*; 15, *Syringothyris*; 16, *Trigonotreta*; 17, *Paekmannella*.

with the Himalayan Terrane to the south (six genera) and with terranes to the north (five genera). Clearly Lhasa holds an intermediate position with the possibility of faunal exchange in both directions.

(v) *Interpretation*

The dichotomy between shallow carbonate marine communities to the north of the Banggong Suture and deeper water shelf clastics communities to the south seen during the Carboniferous continues here into the early Permian. Our sparse knowledge of the fauna from north of the Banggong Suture hampers interpretation of the biogeography at this time, but there is at least some hint of faunal similarity between Lhasa and the Himalayas.

(c) *Qixian*

(i) *Correlation*

Larger benthic foraminiferans provide a sound basis for correlation between most regions, the only exception being the Himalayan Terrane, from which they are absent. Here brachiopods are once again used, although the precise correlation is somewhat tentative.

(ii) *Fusulinids*

For the first time fusulinids extend into the carbonate facies of the Lhasa Terrane (*Parafusulina*, *Pseudofusulina*, *Nankinella*, etc.). They are most diverse in the Qiangtang Terrane, becoming less numerous further north, possibly because of the predominance of near-shore fluvio-deltaic conditions.

(iii) *Corals* (figure 7)

Here we find corals are relatively uncommon in the Qiangtang–Kunlun–Qilian region; those that are present are predominantly compound rugose forms (e.g. *Wentzellophyllum*, *Polythecalis*) or large solitary rugose corals with well developed dissepimentation (e.g. *Caninia*). Some small solitary rugose forms also occur. To the south, in the Lhasa and Himalayan Terranes, there are many genera of small, solitary rugose corals, (though this may to some extent be a product of taxonomic oversplitting), some of which are not present to the north.

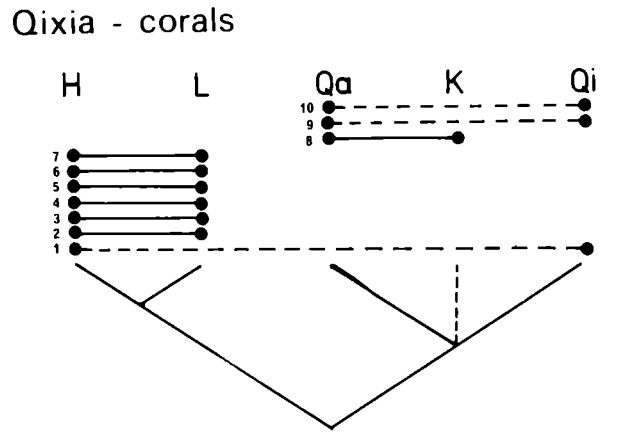

FIGURE 7. Taxon/area matrix and cladogram of Qixian coral genera: data from many sources. Symbols as in figure 2. Genera are as follows: 1, *Lophophyllidium*; 2, *Wannerophyllum*; 3, *Cyathocarina*; 4, *Verbeekiella*; 5, *Trachylasma*; 6, *Plerophyllum*; 7, *Lytvolasma*; 8, *Protomichelinia*; 9, *Sechuanophyllum*; 10, *Yatsengia*.

(iv) *Brachiopods* (figure 8)

As for the corals, there appears to be close links between the brachiopods of the Lhasa and Himalayan regions at this time, with several genera and even species (e.g. *Calliomarginata*, *Costiferina indica*, *Stenoschisma purdoni*) uniquely shared between these two regions. There are also a couple of genera shared uniquely between the Qiangtang, Kunlun and Qilian Terranes (*Uncinunella*, *Neoplicatifer*), though the fauna of this area is still relatively poorly known.

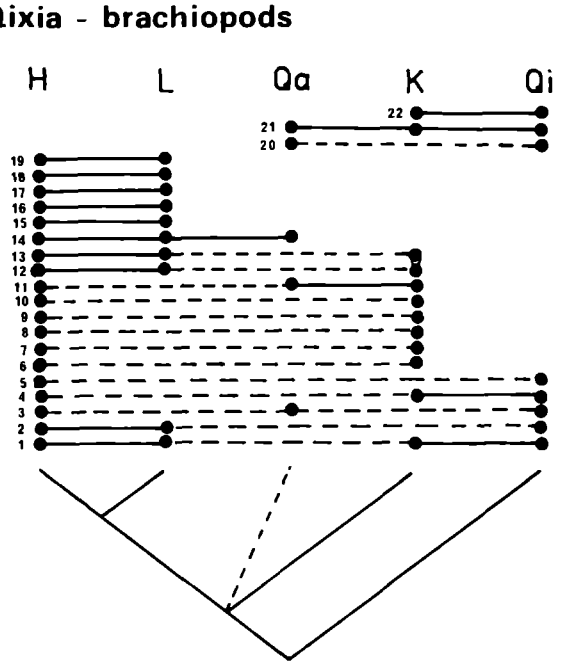

FIGURE 8. Taxon/area matrix and cladogram of Qixian brachiopods: data from many sources. Symbols as in figure 2. Genera are as follows: 1, *Dielasma*; 2, *Spiriferellina*; 3, *Streptorhynchus*; 4, *Linoproductus*; 5, *Squamularia*; 6, *Waagenoconcha*; 7, *Punctospirifer*; 8, *Dictyoclostus*; 9, *Marginifera*; 10, *Cancrinella*; 11, *Athyris*; 12, *Martinia*; 13, *Neospirifer*; 14, *Stenoschisma*; 15, *Costiferina*; 16, *Stepanoviella*; 17, *Cleiothyridina*; 18, *Caliomarginata*; 19, *Anadanthus*; 20, *Neoplicatifera*; 21, *Uncinunella*; 22, *Haydenella*.

(iv) *Interpretation*

The marine fauna of the Qixian provides some good evidence from coral and brachiopod data in support of a faunal tie between the Lhasa and Himalayan Terranes. This, however, is unsupported by the distribution of fusulinids. This suggests that the Lhasa Terrane occupied a somewhat intermediate position between the Himalayas and the Qiangtang–Kunlun–Qilian regions, and the faunal distribution pattern is probably best explained as a product of latitudinal gradient, or facies change.

(*d*) *Maokouan*

(i) *Correlation*

The larger benthic foraminiferans provide the key to correlation from the Lhasa Terrane northwards (*Verbeekina* assemblage), but once again correlation into the Himalayan Terrane is somewhat tentative and based on brachiopods.

(ii) *Fusulinids* (figure 9)

As in the Qixian, fusulinids occur from the Lhasa Terrane northwards, though they are most abundant and diverse in the Qiangtang–Kunlun terranes. There is a hint that the fauna from the Qiangtang and Kunlun Terranes is more closely comparable than either is to the Qilian Terrane at this time.

(iii) *Corals* (figure 10)

Compound rugose corals (e.g. *Wentzellites*, *Lonsdaleastraea*) and larger solitary rugose corals with complex dissepimentation (e.g. *Iranophyllum*), generally considered to be part of the Tethyan equatorial reefoidal fauna, are widely distributed at this time. They are present to the north of the Banggong Suture, but are also now known from the Lhasa Terrane, where a diverse

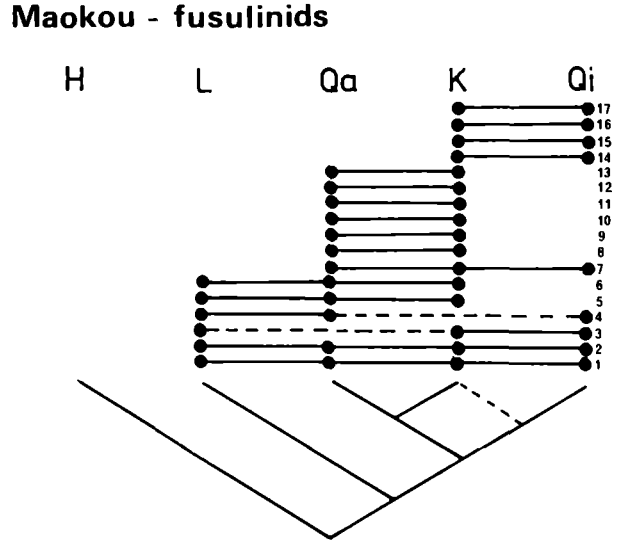

FIGURE 9. Taxon/area matrix and cladogram of Maokouan fusulinids: data from many sources. Symbols as in figure 2. Genera are as follows: 1, *Verbeekina*; 2, *Neoschwagerina*; 3, *Rugososchwagerina*; 4, *Chusenella*; 5, *Yangchienia*; 6, *Nankinella*; 7, *Sumatrina*; 8, *Yabeina*; 9, *Schubertella*; 10, *Parafusulina*; 11, *Pseudofusulina*; 12, *Ozawainella*; 13, *Khalerina*; 14, *Monodiexodina*; 15, *Polydiexodina*; 16, *Schwagerina*; 17, *Afghanella*.

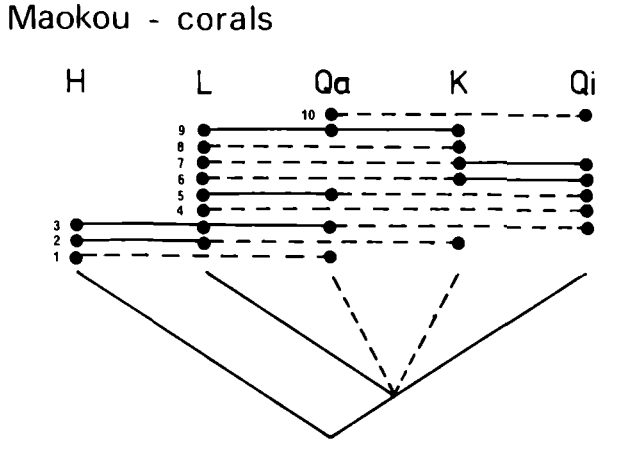

FIGURE 10. Taxon/area matrix and cladogram of Maokouan coral genera: data from many sources. Symbols as in figure 2. Genera are as follows: 1, *Wannerophyllum*; 2, *Amplexocarina*; 3, *Trachylasma*; 4, *Tomasiphyllum*; 5, *Wentzelella*; 6, *Waagenophyllum*; 7, *Iranophyllum*; 8, *Syringopora*; 9, *Ipciphyllum*; 10, *Duplophyllum*.

reefoidal community has been described by Lin (1983, 1984). This fauna is accompanied by other corals and stromatoporoids. In the Himalayan Terrane only small solitary rugose corals without dissepimentation are known (e.g. *Trachylasma*, *Lytvolasma*), some of which are also found in the more diverse faunas to the north. The affinities of the Lhasa Terrane at this period lie clearly with the Qiangtang Terrane and the South China Block.

(iv) *Brachiopods* (figure 11)

The brachiopod fauna is relatively large and the analysis shows a rather complex mosaic of overlapping ranges. However, the predominant clustering suggests that the strongest faunal affinity lies between the Lhasa, Qiangtang and Kunlun Terranes. This region has several

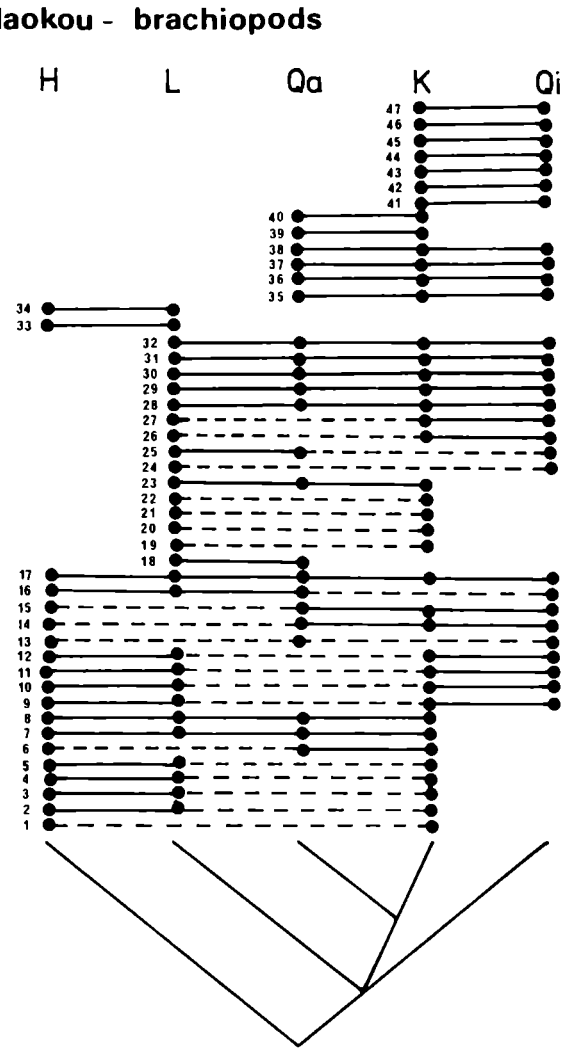

FIGURE 11. Taxon/area matrix and cladogram of Maokouan brachiopod genera: data from many sources. Symbols as in figure 2. Genera are as follows: 1, *Chonetes*; 2, *Phricodothyris*; 3, *Waagenoconcha*; 4, *Stenoschisma*; 5, *Neospirifer*; 6, *Anidanthus*; 7, *Spiriferella*; 8, *Chonetella*; 9, *Haydenella*; 10, *Dielasma*; 11, *Marginifera*; 12, *Martinia*; 13, *Orthotetina*; 14, *Linoproductus*; 15, *Streptorhynchus*; 16, *Spiriferellina*; 17, *Leptodus*; 18, *Composita*; 19, *Spirigerella*; 20, *Chonetinella*; 21, *Terebratuloidea*; 22, *Notothyris*; 23, *Hustedia*; 24, *Cancrinella*; 25, *Spinomarginifera*; 26, *Waagenites*; 27, *Derbyia*; 28, *Araxathyris*; 29, *Neoplicatifera*; 30, *Dictyoclostus*; 31, *Squamularia*; 32, *Enteletes*; 33, *Costiferina*; 34, *Calliomarginata*; 35, *Oldhamia*; 36, *Compressoproductus*; 37, *Neowellerella*; 38, *Uncinunellina*; 39, *Gefonia*; 40, *Tyloplecta*; 41, *Alexania*; 42, '*Echinoconchus*'; 43, *Urushtenia*; 44, *Punctospirifer*; 45, *Buxtonia*; 46, *Megaderbyia*; 47, *Compressoproductus*.

genera in common (e.g. *Spinomarginifera*, *Neoplicatifera*, *Araxathyris*). There are also some genera restricted to the Qiangtang–Kunlun–Qilian region. Diversity is lower both in the Qilian and the Himalayan Terranes. Apart from *Cleiothyridina*, there is no evidence for taxa shared uniquely between the Lhasa and Himalayan terranes.

(v) *Interpretation*

There is little doubt that the faunal affinities of the Lhasa Terrane now lie strongly with the region north of the Banggong Suture, and with the South China Block, where a similar coral and fusulinid fauna is recorded. The brachiopod data also support this, although the distribution of taxa is much less internally congruent.

(*e*) *Permian flora*

(i) *Floral distributions* (figure 12)

The Permian flora has been much used in biogeographical analysis, but suffers from the same sorts of problems as are encountered in the marine faunas. The material from the Tibetan Plateau, though sometimes well preserved in detailed structure, is generally rather scrappy,

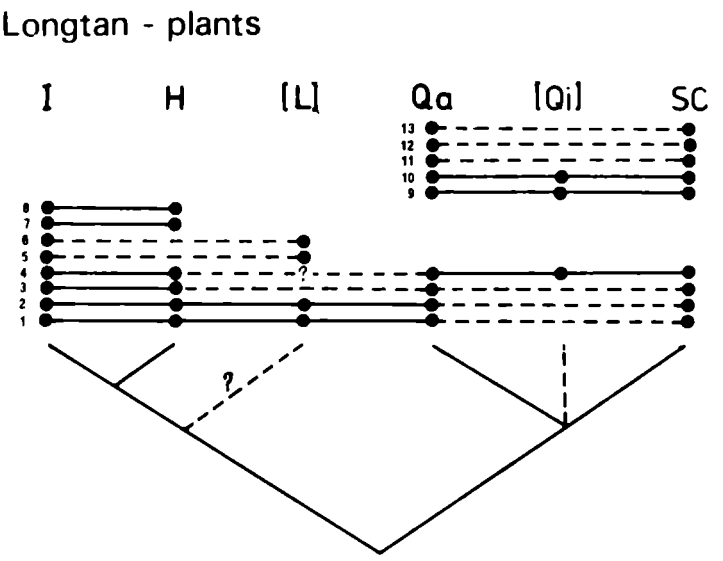

FIGURE 12. Taxon/area matrix and cladogram of early Upper Permian plant genera; see table 1 for sources of data. Symbols as in figure 2. Genera are as follows: 1, *Pecopteris* s.l.; 2, *Chladophlebis*; 3, *Sphenophyllum*; 4, *Lobatannularia*; 5, *Phyllotheca*; 6, *Noeggerathiopsis*; 7, *Glossopteris*; 8, *Gangamopteris*; 9, *Lobitannularia sinensis*; 10, *Lepidodendron*; 11, *Gigantopteris*; 12, *Gigantonoclea*; 13, *Rajahia*.

making determination difficult. There is also the general problem of correlating non-marine beds. Thus there has been a tendency to talk about the Permian flora as a whole without ensuring that more or less contemporary floras are being compared. Floral lists for the principal localities are listed in table 1. From this it is seen that the Gondwanan flora of the Himalayas is Qixian in age, whereas the Cathaysian floras of Qiangtang and Qilian are Longtanian or later in age. However, there is a reasonable flora reported from the Mamal Formation (= Kazanian; early Upper Permian) of Kashmir that can be compared (Singh *et al.* 1982).

The results of the analysis are presented in figure 12. This suggests that the Qiangtang flora

TABLE 1. PERMIAN FLORA (GENERA) OF THE QINGHAI–XIZANG PLATEAU AND ADJACENT REGIONS

(Regions and source for data are as follows: 1, South China Block (a = Longtanian: b = Changxinian); Li, Yao & Deng 1982. 2, Qilian Mountains (Longtanian); Liu 1984. 3, Qiangtang Terrane (a = Maokouan, b = Changxinian); He & Zhang 1984, Li, Yao & Deng 1982, this expedition. 4, Lhasa Terrane (stage uncertain); Li *et al.* 1985. Southern Tibet, S of Zangbo suture (Qixian); Li 1983; 6 Kashmir (a = Qixian, b = Maokouan); Singh *et al.* 1982.)

	Regions								
	1		2	3		4	5	6	
	a	b	.	a	b	.	.	a	b
Lepidodendron	×	×	×	×	.	.	.	.	.
Sphenophyllum	×	×	.	×	×	.	×	.	×
Annularia	.	×	.	×	×	.	.	.	.
Paracalamites	.	.	.	×	.	.	.	×	×
Lobatannularia	×	×	×	×	×	.	.	.	×
Schizoneura	×	.	.	×	?	.	.	×	.
Rajahia	×	×	.	×	×	.	.	.	×
'*Pecopteris*'	×	×	.	×	×	×	×	×	×
Chladophlebis	.	.	.	×	×	.	?	.	.
Fascipteris	×	×	×	×	×	.	.	.	.
Compsopteris	×	×	.	×	×	.	.	.	.
Gigantopteris	×	×	.	×	×	.	.	.	.
Gigantonoclea	.	×	.	×	×	.	.	.	.
Sphenopteris	.	.	.	×	.	×	×	×	.
Taeniopteris	×	.	.	.	.	.	.	.	.
Rhizamopteris	×	.	.	×	×	.	.	.	.
Rhipidopsis	×	×	.	×	.	.	.	.	.
Selaginellites	.	.	.	.	×	.	.	.	.
Alethopteris	.	.	.	.	×	?	.	.	.
?Neuropteridium	.	.	.	×	×	.	.	.	.
?Pterophylum	.	.	.	.	×	.	.	.	.
Calamites	.	.	×	.	.	.	.	.	.
Cordaites	.	.	×	.	.	.	.	.	.
Glossopteris	.	.	.	.	.	.	×	×	×
Gangamopteris	.	.	.	.	.	.	.	×	×
Stellotheca	.	.	.	.	.	.	×	.	.
Noeggerathiopsis	.	.	.	.	.	×	.	.	.
?Plagiozamites	.	.	.	.	.	×	.	.	.
Cardiocarpus	.	.	.	.	.	×	.	.	.
Carpolithus	.	.	.	.	.	×	.	.	.
Phyllotheca	.	.	.	.	.	×	.	.	.
Odontopteris	.	.	.	×	.	.	.	.	.

at this time shared a number of elements in common with the Qilian Terrane and the South China Block. Thus we find *Rajahia*, *Compsopteris*, *Gigantopteris* and *Gigantonoclea* in Qiangtang, all of which are considered to be elements of the south Cathaysian flora (see He & Zhang 1984). The sparse flora reported from Qilian has taxa that are either widespread or suggest Cathaysian affinities.

In the Himalayas there is a reduced diversity flora with *Gangamopteris* and *Glossopteris* as endemic elements of a Gondwanan flora. Some taxa are common to both areas (*Pecopteris s.l.*, *Sphenopteris*, *Sphenophyllum*) and are cosmopolitan in distribution. *Lobatannularia* is generally considered to be a Cathaysian genus, but Singh *et al.* (1982) has reported this genus from Kashmir, and Li *et al.* (1985) have suggested that *Stellotheca* from the Himalayan region of Tibet is also synonymous with *Lobatannularia*. *Lobatannularia* does not extend southwards into more typical Gondwanan floras of India.

The reported flora from the Lhasa Terrane (Li *et al.* 1985) is very poorly preserved and determinations are tentative. It includes none of the characteristic elements of either the Gondwanan or Cathaysian floras and is therefore difficult to place. Li *et al.* (1985) interpreted some elements of the flora as *Noeggerathiopsis* and *Phyllotheca*, which are elements of the Indian Gondwanan flora. They also claimed that there were Cathaysian elements in the flora, namely *Pecopteris* spp., but this form genus is best considered as more cosmopolitan in distribution. The remainder of the flora is inconclusive as to its affinities.

(ii) *Interpretation*

The floral distribution supports the hypothesis that the Qiangtang Terrane and areas to the north were in close biotic contact at this time with the South China Block. Clearly some genera are more restricted in their range (e.g. *Gigantopteris*) while others have a broader range (e.g. *Lobatannularia*) and are less geographically restricted. This flora is considered by palaeobotanists to be characteristic of humid tropical to subtropical regions. The Himalayan Terrane flora on the other hand is characteristic of the more southern temperate regions. The flora from the Lhasa Terrane may have closer affinities with the Gondwanan flora, but the evidence for this is at present exceedingly tenuous and cannot be relied upon. The clear dichotomy in terrestrial flora between India to the south and the Qiangtang Terrane to South China Block region to the north may well have been maintained by the broad shelf sea that existed across the Lhasa Terrane at this time.

(*f*) *Upper Anisian ammonoids*

Ammonoids form the basis for subdividing the Triassic in the Tibetan Plateau and there is no real problem in correlating across this region. The Lhasa Terrane has only an Upper Anisian fauna, and so the analysis is restricted to this time period. No marine fauna of this age is known from the Qilian region and the Kunlun fauna comes from the Bayan Kala Group (see He & Yin 1983). The analysis (figure 13) shows clear evidence for the Lhasa Terrane sharing closer faunal relations with the Qiangtang and Kunlun Terranes rather than with the Himalayan

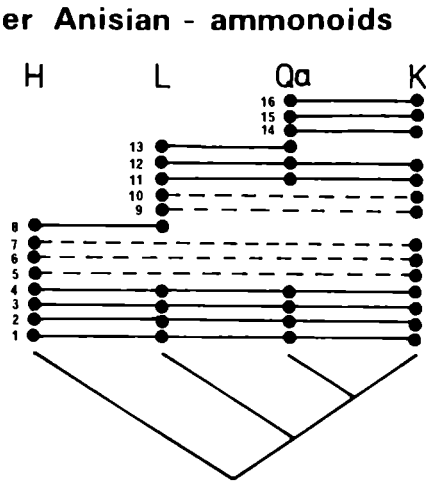

FIGURE 13. Taxon/area matrix and cladogram of Upper Anisian (Middle Triassic) ammonoids: data from many sources. Symbols as in figure 2. Genera are as follows: 1, *Gymnites*; 2, *Hollandites*; 3, *Leiophyllites*; 4, *Japonites*; 5, *Buddhaites*; 6, *Anagymnites*; 7, *Ussurites*; 8, *Anacrocordiceras*; 9, *Paraceratites*; 10, *Reiflingites*; 11, *Balatonites*; 12, *Acrochordiceras*; 13, *Aristoptychites*; 14, *Paracrochordites*; 15, *Procladiscites*; 16, *Cuccoceras*.

Terrane. Xia & Liao (1986) have previously suggested that the Qiangtang ammonoids are European in appearance, and a similar conclusion has been drawn from coral data (Xia & Liao 1986). The ammonoid fauna from Lhasa also shows a preponderance of European (Tethyan) genera and species, with more similarity to the faunas of the Alps than to those of the Himalayan region (Gu, He & Wang 1980).

6. Discussion and interpretation

The analyses presented above, covering the period from early Carboniferous to Middle Triassic, provide a rigorous assessment of the available taxonomic data on the biotic relationships of the Tibetan terranes. The changes in area relationships through time are summarized in figure 14, and what now remains to be done is a synthesis of this data to provide an overall picture.

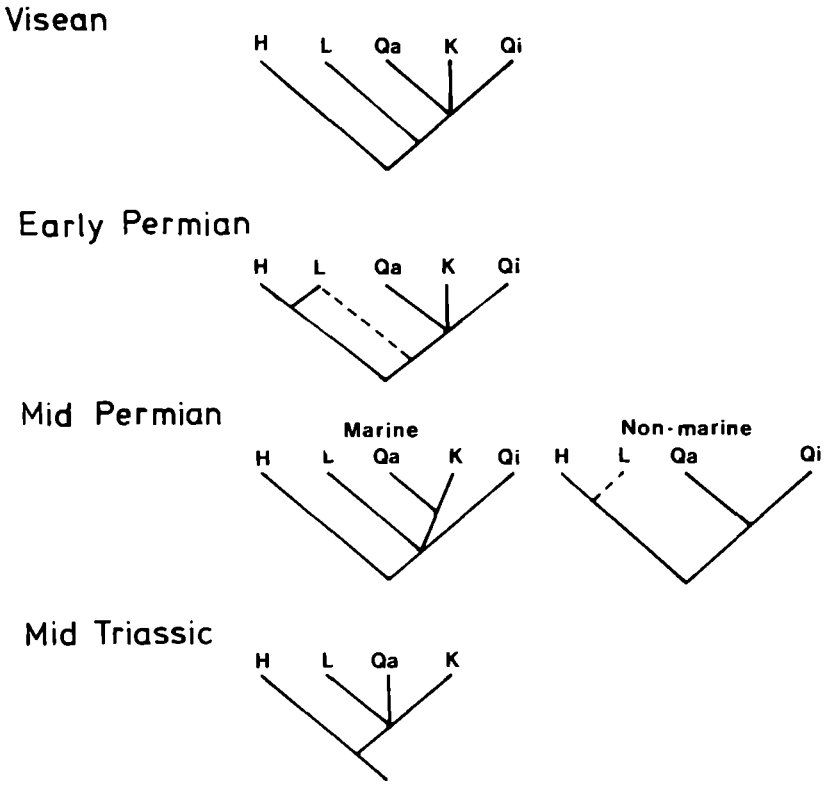

Figure 14. Summary diagram of area cladograms showing the changing relationships of sample locality areas through time. Note the change in position of the Lhasa Terrane in the early Permian. Symbols as in figure 2. For further discussion see text.

Firstly, what undoubtedly stands out is the cohesiveness of the Qiangtang–Kunlun–Qilian region throughout the late Palaeozoic. In the later part of the Permian, the Kunlun–Qilian biotic connection appears to become less strong, but this is just as likely to be due to sampling problems as to any genuine biogeographical divergence between these regions. The overall similarity of the biota is demonstrated by marine coral, brachiopod and fusulinid data, and by non-marine plant data. Furthermore, the fauna and flora of this large region also have close

connections with that found in the South China Block, as demonstrated by the shared endemic genera of corals.

What is also clear is that for most of the late Palaeozoic there was a diversity gradient in the marine fauna from north to south, with taxa becoming progressively lost southwards. In the Permian there is an unambiguous dichotomy in the flora between the temperate flora of the Himalayas and the more humid equatorial flora of Qiangtang and Qilian, but the position of the Lhasa Terrane remains unclear.

Less clear is the question of whether there was a significant faunal break coincidental with one of the sutures that might indicate the presence of an oceanic barrier. Different workers have at different times argued that one or other of the suture zones represent the remains of a large Prototethyan ocean. For example, initially the Zangbo Suture zone was considered to mark the northern margin of Gondwanaland, but Chinese work to the north of this suture in the 1970s has tended to disprove this theory. Currently, argument seems to centre around whether the Banggong Suture or the Jinsha Suture marks the Palaeotethys Ocean (viz. Yang & Fan 1983; Wang 1984).

A major oceanic break could only be positioned at either the Zangbo Suture or the Banggong Suture if we accept the Qiangtang–Kunlun–Qilian region as a cohesive biotic region. Previous claims as to the position of this disjunction have been based almost entirely on comparisons of faunas from different facies (shallow water carbonate facies with deeper water clastic facies). Thus although facies differences are potentially significant, the apparent differences in marine faunas could just as easily be attributed to, for example, changes in depth across a broad continental shelf. The absence of any evidence for two centres of endemism in marine faunas across the Tibetan Plateau, except possibly in the early part of the Permian (Asselian to Qixian), does not support the idea that there was a significant oceanic barrier to biotic exchange in the late Palaeozoic. The supposedly characteristic Gondwanan marine fauna of the southern terranes is simply a reduced diversity fauna in a clastic facies.

The problem is most acutely demonstrated by the apparent switch in faunal affinities of the Lhasa Terrane during the late Palaezoic. In the earliest Permian, the marine fauna of Lhasa shows strongest ties with the Himalayan Terrane. By the Qixian there is evidence of mixed faunal affinities and by the Maokouan the fauna of the Lhasa Terrane shows unambiguous links with the Qiangtang Terrane and the South China Block. This well established fact (see for example Lin 1984; Dickins 1985*b*) has posed a significant problem to those searching for a place in Tibet to insert a major ocean during the late Palaeozoic, since the boundary appears to migrate with time: from the Banggong Suture in the early Permian, to the Zangbo Suture by the late Permian.

However, the change in marine faunas and their affinities is also correlated with a change in lithofacies. Where offshore clastic facies like those of the Himalayan region prevail, the fauna resembles that of the Himalayan region, but with the onset of carbonate ramp toe conditions a mixed fauna is found. The establishment of shallow water carbonate shelf facies in the Lhasa Terrane, similar to contemporary facies in the Qiangtang Terrane, results in similar faunas being present in these two areas. A double oscillation in affinities is also demonstrated within a single section in the Ali district of the southern Karakoram Mountains (Liang *et al.* 1983) where it again appears to be facies-related.

What then are the possible explanations to account for the distribution of faunas in the late Palaeozoic, and for the change in affinities of the biota of the Lhasa Terrane in particular? We

think that there are three possibilities worth considering; plate migration, sea level changes, and shifts in climatic belts.

(i) *Plate migration*

Under this model the Lhasa Terrane is initially part of the marginal shelf platform of the Gondwanan complex during the early Permian, and then migrates northwards during the Qixian stage to become part of the Qiangtang–Kunlun complex by the Maokouan.

This model can be rejected on several grounds. There is no independent evidence to suggest that subduction and collision took place between the Lhasa and Qiangtang Terranes during the Permian; all available evidence suggests that the Banggong Suture was a Jurassic creation. Furthermore, it is more or less impossible to explain why the Qiangtang Terrane should have both kinds of facies/faunas under this model (mixtites and Himalayan fauna to the west around Rutog and Ali, shelf carbonates with a diverse 'warm water' fauna in central and eastern Xizang). Even if we assume that the western portion of the Qiangtang Terrane is in reality part of the Lhasa Terrane and that the Banggong Suture has been wrongly traced eastwards in Xizang, there is still the problem of the double oscillation of faunal affinities noted in Ali.

(ii) *Sea level changes*

Under this model a southward-prograding shore face would bring a carbonate platform across the continental shelf producing a migration of depth-related facies southwards. Only when suitable shallow water conditions were established were diverse coral/brachiopod/stromatoporoid communities able to flourish.

Although there may be some evidence that marine conditions were progressively lost through the Carboniferous and Permian in the northern part of the Tibetan Plateau, and that shelf carbonate platforms were initiated in the Lhasa region in the Permian (see Leeder *et al.*, this volume), this model cannot explain all the features. Clearly the fauna is to some extent depth-related, but there is evidence of tidally-influenced clastic sediments at Chisan Ka (see Leeder *et al.*, this volume) which show that it is not a simple dichotomy between deep water and shallow water communities, and thus the model is rejected.

(iii) *Shift in climatic belts*

Under this model the faunas would be controlled to a large extent by latitudinal variation in climate (which would also control the development of carbonate shelf facies). During the end-Carboniferous glaciation the climatic gradient would be at a maximum and the equatorial belt of high diversity faunas would be relatively restricted, but with amelioration of conditions the gradient would decrease and the equatorial high diversity belt expand southwards. Dickins (1977, 1978, 1984, 1985*a*, *b*, *c*) has provided a very strong case in favour of significant climatic changes taking place during the late Carboniferous and Permian.

This is to some extent supported by the observation that the maximum evidence for regionalization of the marine fauna coincides with the period of glaciation and that immediately following. It could also account for variation within a single plate, for example, by assuming that the Qiangtang region is orientated at a high angle to the climatic belts during the Permian (Wang 1984) or by invoking an appropriate pattern of oceanic circulation. [A more simple explanation, however, would be that the mixed fauna in the Qiangtang Terrane during the Permian reflects bathymetric differences across the region.] It would also explain the diversity gradient so obviously picked up in the biogeographical analysis outlined above.

This last explanation, probably in conjunction with sea level changes, is our favoured model. Note then that this carries with it certain implications about late Palaeozoic palaeogeography.

(i) The various terranes from Qilian to northern India extended from an equatorial or subequatorial position in the north to a temperate position in the south during the late Palaezoic. This is based on diversity gradients of the total fauna, coral distribution and floral distribution, but also receives independent confirmation from the limited palaeogeomagnetic data available (see Lin & Watts, this volume, who place the Kunlun Shan at approximately 20° south of the palaeoequator) and from the occurrence of late Carboniferous/early Permian glacio-marine facies in the southern block (see Leeder *et al.*, this volume).

(ii) The boundary between these two climatic regions fluctuated through time across the Qiangtang and Lhasa Terranes according to global conditions. There can be little doubt that significant changes in climate were taking place in the late Palaeozoic (see Dickins 1984, 1985*a*, *b*, *c*) which affected the distribution of the biota.

(iii) Because the biotas from equatorial and temperate zones appear to cross terrane boundaries (suture zones) without impediment as global climatic conditions changed, no single suture zone can be recognized as the location of a 'Palaeotethyan' ocean on faunal (or facies) evidence.

(iv) The overlapping nature of faunal and lithological ranges through time (e.g. the extension of a compound rugose coral fauna into the Lhasa Terrane in the Maokouan; the extension of mixtite facies into the Qiangtang Terrane in the Asselian) suggests that there was no consistent physical barrier other than climate across this region. Specifically, we see no evidence for significant oceanic barriers within this region during the late Palaeozoic. The continuity of both faunas and lithofacies across suture zones at different times is more in keeping with the idea of a continuous epicontinental shelf. The alternative of having a series of island terranes is possible, but less appealing because of the absence of firm evidence of continental rise or deep ocean sediments of this age on any of the terranes. Whatever break there was between island terranes under this model was not significant enough to affect the fauna and left no record in the sedimentary succession.

Wang (1984) has previously suggested that the regions to the south of the Jinsha Suture all formed one large continuous plate with India (the Qingzangindia Plate), and recently Dickins (1985*b*) and Dickins & Shah (1981) have also hinted that the Tibetan Plateau was all one region continuous with India in the late Palaeozoic. Our evidence not only supports this view, but also raises doubts about supposing that any major oceanic barrier existed between the Qilian/South China Block and India in the late Palaeozoic. This view was also put forward by Crawford (1974) who argued that the entire Tibetan Plateau was contiguous with India and Gondwanaland and that the boundary lay to the north along the Tien Shan.

7. Summary

1. The late Palaeozoic biota ranged from equatorial or sub-equatorial in the north to temperate (southern) in the south.

2. Climatic fluctuation on a global scale controlled the distribution of the biota of this region during the late Palaeozoic and no suture zone can be identified as a consistent boundary between 'Gondwanan' (i.e. temperate southern) and 'Cathaysian' (i.e. equatorial) biotas.

3. It is therefore suggested that either the whole region formed one continuous shelf region

at this time, or that, under an island terrane model, the terranes formed 'island' platforms spread out across the region more or less uniformly. There is no evidence for any consistent dichotomy at one particular suture zone, nor for any one suture zone marking a significant barrier to faunal dispersal.

4. There is no evidence for any Upper Palaeozoic continental rise or oceanic sediments on the Tibetan plateau. The earliest evidence is of early Triassic turbidites and late Triassic radiolarian cherts. This is contrary to the expectations of an island terrane model.

5. The breakup of this region may date from the Permian.

References

Allègre, C. J. *et al.* 1984 Structure and evolution of the Himalaya-Tibet orogenic belt. *Nature, Lond.* **307**, 17–22.

Bassoullet, J. P., Colchen, J. P., Mascle, G. & Wang Naiwen 1984 Les ensembles sédimentaires de la zone du Tsangpo (Lhaze, Lhasa, Linzhu). In *Mission Franco-Chinoise au Tibet* (ed. J. L. Mercier & Li Guangcen), pp. 133–153. Paris: Editions du Centre National de la Recherche Scientifique.

Bayliss, D. D. 1966 Foraminifera from the Bau Limestone Formation, Sarawak, Malaysia. *Ann. Rept Malaysia Geol. Surv., Borneo Reg., Kutching 1965*, pp. 173–195, pls 51, 52.

Baski, S. K. 1971 On the palynological biostratigraphy of Bengal basin. In *Proceedings of the Seminar on Paleopalynology and Indian Stratigraphy*, pp. 188–206. Calcutta University.

Boulter, M. C. & Riddick, A. 1986 Classification and analysis of palynodebris from the Palaeocene sediments of the Forties Field. *Sedimentology* **33**, 871–886.

Chang Chengfa *et al.* 1986 Preliminary conclusions of the Royal Society and Academia Sinica 1985 geotraverse of Tibet. *Nature, Lond.* **323**, 501–507.

Chen Chuzhen 1984 Carboniferous. In *Stratigraphy of Xizang (Tibetan) plateau*, pp. 311–317. Beijing: Scientific Press [in Chinese].

Coulon, C., Maluski, H., Bollinger, C. & Wang, S. 1986 Mesozoic and Cenozoic volcanic rocks from central and southern Tibet: ^{39}Ar–^{40}Ar dating, petrological characteristics and geodynamic significance. *Earth planet. Sci. Lett.* **79**, 281–302.

Crawford, A. R. 1974 The Indus suture line, the Himalayas, Tibet and Gondwanaland. *Geol. Mag.* **111**, 369–380.

Dickins, J. M. 1977 Permian Gondwana climate. *Chayanica Geologica* **3**, 11–21.

Dickens, J. M. 1978 Climate of the Permian in Australia: the invertebrate faunas. *Palaeogeog. Palaeoclimat. Palaeoecol.* **23**, 33–46.

Dickens, J. M. 1984 Evolution and climate in the Upper Palaeozoic. In *Fossils and climate* (ed. P. Brenchley), pp. 317–327. London: J. Wiley & Sons.

Dickens, J. M. 1985*a* Late Palaeozoic climate with special reference to invertebrate faunas. *C. R. Neuvième Congrès Internat. Strat. Géol. Carbonifère.; Washington & Champaign–Urbana, 1979*, **5**, 394–402.

Dickens, J. M. 1985*b* Palaeobiofacies and palaeobiogeography of Gondwanaland from Permian to Triassic. In *The Tethys, her paleogeography and paleobiogeography from Paleozoic to Recent* (ed. K. Nakazawa & J. M. Dickens), pp. 83–92. Tokyo: Tokyo University Press.

Dickens, J. M. 1985*c* Late Palaeozoic glaciation. *B.M.R. J. Austral. Geol. Geophys.* **9**, 163–169.

Dickens, J. M. & Shah, S. S. 1981 Permian paleogeography of peninsular and himalayan India and the relationships with the Tethyan region. In *Gondwana five: the 5th International Gondwana Symposium, Wellington, New Zealand, 1980* (ed. M. M. Cresswell & P. Vella), pp. 79–83. Rotterdam: A. A. Balkema.

Dong Deyuan & Mu Xinan 1984 Qamdo region. In *Stratigraphy of Xizang (Tibetan) plateau*, pp. 237–287. Beijing: Scientific Press [in Chinese].

Duan Shuyin, Chen Yeh & Keng Kuochang 1977 Some early Cretaceous plants from Lhasa, Tibetan Autonomous Region, China. *Acta Bot. Sinica* **19**, 114–119.

Fan Yingnian 1985 A division of zoogeographical provinces by Permo-Carboniferous corals in Xizang (Tibet). *Contribs Geol. Qinghai–Xizang Plateau* **16**, 87–106 [in Chinese with English abstract].

Girardeau, J., Marcoux, J., Allègre, C. J., Bassoullet, J. P., Tang Youking, Xiao Xuchang, Zao Yougong & Wang Xibin 1984 Tectonic environment and geodynamic significance of the Neo-Cimmerian Dongqiao ophiolite Banggong–Nujiang suture zone, Tibet. *Nature, Lond.* **307**, 27–31.

Gu Qingge, He Guoxiong & Wang Yigang 1980 Discovery of Late Anisian *Paraceratites trinodosus* fauna (Ammonoidea) from Doilungdeqen, Tibet and its significance. *Acta Palaeont. Sinica* **19**, 343–356 [in Chinese with English abstract].

Harland, W. B., Cox, A. V., Llewellyn, P. G., Pickton, C. A. G., Smith, A. G. & Walters, R. 1982 *A geological time scale*. 131 pp. Cambridge: Cambridge University Press.

Harris, T. M. 1979 *The Yorkshire Jurassic Flora, V: Coniferales*. British Museum (Natural History), London.

He Yuanliang & Yin Jiarua 1983 A preliminary discussion on the Triassic period stratigraphy, palaeontological characteristics and its distribution in Qinghai. *Contribs Geol. Qinghai–Xizang Plateau* **3**, 47–56 [in Chinese].

He Yuanliang & Zhang Shanzhen 1984 Late Permian fossil plants around Shanglaxiu District of Yushu County, Qinghai Province and their geological significance. *Contribs Geol. Qinghai–Xizang Plateau* **14**, 115–124 [in Chinese with English abstract].

Iranian–Japanese Research Group 1981 The Permian and the Lower Triassic systems in Abadeh Region, Central Iran. *Mem. Fac. Sci. Kyoto Univ. Ser. Geol. Mineral.* **47**, 61–133.

Jansonius, J. & Hills, L. V. 1976 Genera file of fossil spores. *Sp. Publ. Dept. Geol. Univ. Calgary.*

Jin Yugan 1985 Permian Brachiopoda and paleogeography of the Qinghai–Xizang (Tibet) plateau. *Palaeontologica Cathayana* **2**, 19–71.

Jin Yugan & Sun Dongli 1981 Palaeozoic brachiopods from Xizang. In *Palaeontology of Xizang* **3**, 127–176. Beijing: Scientific Press [in Chinese with English abstract].

Kanmera, K., Isu, K. & Toriyama, R. 1976 The evolution and extinction patterns of Permian fusulinaceans. *Geol. Palaeont. S.E. Asia* **17**, 129–154.

Li Guangcen & Lin Baoyu 1982 On some geological problems in Eastern Kunlun Mountain. *Contribs Geol. Qinghai–Xizang Plateau* **1**, 28–48 [in Chinese with English abstract].

Li Hongsheng 1986 Upper Jurassic (early Tithonian) radiolarians from Southern Banggong Lake, Xizang. *Acta micropal. Sinica* **3**, 297–315.

Li Xingxue 1983 Notes on three new species of *Glossopteris* flora from Qubu Formation, S. Xizang (Tibet), with a discussion on the age of the Formation. *Acta Palaeont. Sinica* **22**, 130–138 [in Chinese with English abstract].

Li Xingxue, Yao Zhaoqi & Deng Longhua 1982 An early Late Permian flora from Toba, Qamdo district, eastern Xizang. In *Palaeontology of Xizang* **5**, 17–44. Beijing: Scientific Press [in Chinese with English abstract].

Li Xingxue, Wu Yiming & Fu Zaibin 1985 Preliminary study on a mixed Permian flora from Xiagangjiang of Gerze district, Xizang and its palaeobiogeographical significance. *Acta Palaeont. Sinica* **24**, 140–170 [in Chinese with English abstract].

Li Xingxue, Yao Zhaoqi, Zhu Jianan, Duan Shuying & Hu Yufan 1982 Late Permian plants from northern Xizang. In *Palaeontology of Xizang* **5**, 17–44. Beijing: Scientific Press [in Chinese with English abstract].

Liang Dingyi & Wang Weipin 1983 Preliminary discussion on the Carboniferous–Permian systems and its fauna at Kangmar district and Qushiam Lhaza, Xizang (Tibet). *Contribs Geol. Qinghai–Xizang Plateau* **2**, 226–236 [in Chinese with English abstract].

Liang Dingyi, Nei Zetong, Guo Tieying, Zhang Yizhi, Xu Baiwen & Wang Weipin 1983 Permo-Carboniferous Gondwana-Tethys facies in southern Karakoram, Ali, Xizang (Tibet). *Earth Sci. J. Wuhan Coll. Geol.* **19**, 9–28 [in Chinese with English abstract].

Liao Weihua & Xia Jinbao 1985 Upper Jurassic and Lower Cretaceous Scleractinia from Baingoin district of northern Xizang (Tibet). *Mem. Nanjing Inst. Geol. Palaeontol. Acad. Sinica* **21**, 119–164 [in Chinese with English abstract].

Lin Baoyu 1983 Lower Permian stratigraphy and coral faunas from both flanks of the Yarlung–Zangbo River in central-southern Xizang (Tibet). *Contribs Geol. Qinghai–Xizang Plateau* **8**, 69–181 [in Chinese with English abstract].

Lin Baoyu 1984 Les strates du Permien inférieur de la faune corallienne de part et d'autre du Yarlung-Zangbo dans la région centre-sud du Tibet. In *Mission Franco-Chinoise au Tibet* (ed. J. L. Mercier & Li Guangcen), pp. 77–107. Paris: Editions du Centre National de la Rechérche Scientifique.

Liu Benpei & Cui Xinsheng 1983 Discovery of *Eurydesma* fauna from Rutog, Xizang (Tibet) and its biogeographical significance. *Earth Sci. J. Wuhan Coll. Geol.* **1**, 79–92 [in Chinese with English abstract].

Liu Guangcai 1984 On the strata of the Permian period in the area near the Buha River of Tianjun County, Qinghai Province. *Contribs Geol. Qinghai–Xizang Plateau* **14**, 125–136.

Liu Jingling & Tang Lingyu 1980 Pollen analysis of the Nihewan Formation. *Paper for the Fifth International Palynological Conference, Nanjing.* 1–8. Nanjing Institute of Geology and Palaeontology, Academia Sinica.

Liu Xiaoliang 1981 Twenty four Early Permian Ectoprocta (Bryozoa) from Xizang (Tibet) with reference to their geographical division. *Ann. Rept. Chinese Acad. Geol. Sci.* [1981], (abstract only).

Liu Zhengqian *et al.* 1984 A preliminary study on the northern boundary and the evolution of Gondwana and Tethys in the light of new data on Qinghai–Xizang (Tibet) plateau. *Contribs Geol. Qinghai–Xizang Plateau* **12**, 11–24.

Ma Fubao, Wang Xiulin & Che Yi 1984 Subdivision of the "Gyiza Group" in the southern part of Yushu County, Qinghai Province. *Contribs Geol. Qinghai–Xizang Plateau* **14**, 147–163 [in Chinese with English abstract].

Maluski, H., Proust, F. & Xiao, X.-C. 1982 First results on ^{39}Ar-^{40}Ar dating of the Trans-Himalayan calc-alkaline magmatism of southern Tibet. *Nature, Lond.* **298**, 152–154.

Oishi, S. 1940 The Mesozoic flora of Japan. *J. Fac. Sci. Hokkaido Imp. Univ.*, series IV, **5**, 123–480.

Pan Guitang, Jiao Shupei, Wang Peisheng, Xu Yaorong & Xiang Tianxiu 1984 The geological events at the Eocene–Oligocene boundary and its tectonic implications, Qinghai–Xizang Plateau. *Contribs Geol. Qinghai–Xizang Plateau* **15**, 147–155 [in Chinese with English abstract].

Pan Yuntang 1985 Late Cretaceous gastropods in Bange County, Xizang (Tibet). *Contribs Geol. Qinghai–Xizang Plateau* **17**, 183–196 [in Chinese with English abstract].

Qinghai Stratigraphical Working Group (Bureau of Geology, Qinghai Province) 1980 *Regional Stratigraphical Tables of Northwest China: the stratigraphy of Qinghai province.* Beijing: Geological Publishing House Mineral Resources, Qinghai Province [in Chinese].

Rosen, B. R. & Smith, A. B. 1988 Tectonics from fossils? Distribution of reef corals and sea urchins from Late Cretaceous to Recent using a new method. In *Gondwana and Tethys* (eds M. G. Audley-Charles and A. Hallam), pp. 275–306. Oxford: Oxford University Press.

Ross, C. A. 1967 Development of fusulinid (Foraminiferida) faunal realms. *J. Paleont.* **41**, 1341–1354.

Ross, C. A. 1970 Concepts in Late Paleozoic correlations. *Geol. Soc. Amer. Spec. Pap.* **124**, 7–36.

Ross, C. A. 1982*a* Paleozoic Foraminifera – fusulinids. In *Foraminifera – notes for a short course* (ed. T. W. Broadhead). *Univ. Tennessee Dept. Geol. Sci., Studies in Geology* **6**, 163–176.

Ross, C. A. 1982*b* Paleobiology of fusulinaceans. *Proc. Third N. American Paleont. Convention* 441–445.

Ross, C. A. & Ross, J. R. P. 1985 Carboniferous and early Permian biogeography. *Geology* **13**, 27–30.

Salaj, J., Borza, K. & Samuel, O. 1983 *Triassic foraminifers of the West Carpathians. Geologický Ustav Dionyza Stura*, Bratislava. 213 pp, 157 pls.

Shroeder, R. 1975 General evolutionary trends in Orbitolinas. *Revista española de Micropaleontologia*, Special Publication for 1975, pp. 117–28.

Singh, G., Maithy, K. & Bose, M. N. 1982 Upper Palaeozoic floras of Kashmir Himalayas. *Palaeobotanist* **30**, 185–232.

Song Zhichen 1981 *Cretaceous-Tertiary palynological assemblages from Jiangsu.* Beijing: Geological Publishing House, 269 pp. [in Chinese].

Song Zhichen, Guan Xueting, Zheng Yahui, Li Zengrui, Wang Weiming & Hu Zhongheng 1985 *A research on Cenozoic palynology on the Longjing structural area in the shelf basin of the East China Sea (Donghai) region.* Anhui: Anhui Science and Technology Publishing House, 209 pp. [in Chinese with English abstract].

Sun Xiangjun 1981 In *Tertiary palaeontology of north continental shelf of South China Sea* (ed. South Sea Branch of the Petroleum Corporation of P.R.C.), pp. 1–58. Guangdong: Guangdong Science and Technology Press [in Chinese].

Toriyama, R. 1984 Summary of the fusuline faunas in Thailand Malaysia. *Geol. Palaeont. S.E. Asia* **25**, 137–147.

Wang Naiwen 1983*a* The tethyan Jurassic stratigraphy of China. *Contribs Geol. Qinghai–Xizang Plateau* **3**, 62–86 [in Chinese with English abstract].

Wang Naiwen 1983*b* The tethyan Cretaceous stratigraphy of China. *Contribs Geol. Qinghai–Xizang Plateau* **3**, 148–180 [in Chinese with English abstract].

Wang Naiwen 1983*c* Development of the Mesozoic formations in the Lakes region, north Tibet, and its plate tectonic implications. *Contribs Geol. Qinghai–Xizang Plateau* **8**, 29–40 [in Chinese with English abstract].

Wang Naiwen 1984 Le paléocontinent qingzangindien et sa suturation avec le paléocontinent cathaysien. In *Mission Franco-Chinoise au Tibet* (ed. J. L. Mercier & Li Guangcen), pp. 33–54. Paris: Editions du Centre National de la Recherche Scientifique.

Wang Naiwen & Bassoullet, J. P. 1984 Les systèmes du Jurassique et du Cretacé dans la région de Lhasa au Tibet. In *Mission Franco-Chinoise au Tibet* (ed. J. L. Mercier & Li Guangcen), pp. 155–166. Paris: Editions du Centre National de la Recherche Scientifique.

Wang Yigang & Sun Dongli 1983 A survey of the Jurassic system of China. *Canad. J. Earth Sci.* **20**, 1646–1656.

Wang Yujing & Mu Xinan 1984 Permian. In *Stratigraphy of Xizang (Tibetan) Plateau*, pp. 318–339. Beijing: Scientific Press [in Chinese].

Wang Yujing & Sheng Jingzhang 1982 Fossil radiolarians from Gyirong and Gyangze districts of southern Xizang. In *Palaeontology of Xizang* **4**, 81–96. Beijing: Scientific Press [in Chinese].

Wang Yujing, Sheng Jinzhang & Zhang Linxin 1981 Fusulinids from Xizang, China. In *Palaeontology of Xizang* **3**, 1–80. Beijing: Scientific Press [in Chinese with English abstract].

Waterhouse, J. B. 1976 World correlations for Permian marine faunas. *Pap. Dept. Geol. Univ. Queensland* **7**, (2) 1–232.

Waterhouse, J. B. & Bonham Carter, G. F. 1975 Global distribution and character of Permian biomes based on brachiopod assemblages. *Canad. J. Earth Sci.* **12**, 1085–1146.

Wen Shixnan 1984 General report of stratigraphical provinces. In *Stratigraphy of Xizang (Tibetan) Plateau*, pp. 6–8. Beijing: Scientific Press [in Chinese with English abstract].

Wu Haoruo 1984 The Congdu Formation – Cretaceous deep-sea deposits in southern Xizang (Tibet) and its significance. *Scientia Geologica Sinica* **1**, 26–33 [in Chinese with English abstract].

Wu Haoruo 1986 Some new genera and species of Cenomanian radiolaria from southern Xizang (Tibet). *Acta Micropal. Sinica* **3**, 347–360.

Wu Haoruo & Li Hongsheng 1982 Radiolaria from the olistostrome of the Zongzhuo Formation, Gyangze, southern Xizang (Tibet). *Acta Palaeont. Sinica* **21**, 64–71 [in Chinese with English abstract].

Wu Haoruo, Yin Jixiang & Sun Yiyin 1982 Melange in the Zombe district, Lhaze county, southern Xizang. *IGAS 1982 Research on Geology*, pp. 34–41.

Wu Xiangwu 1982 Late Triassic plants from eastern Xizang. In *Palaeontology of Xizang* **5**, 63–103. Beijing: Scientific Press [in Chinese with English abstract].

Xia Daixiang 1983 Palaeozoic stratigraphy of Xianza area, northern Xizang (Tibet). *Contribs Geol. Qinghai–Xizang Plateau* **2**, 106–120 [in Chinese with English abstract].

Xia Jinbao & Liao Weihua 1986 Some scleractinian corals of Procyclolitidae from Lhasa. *Acta Palaeont. Sinica* **25**, 37–47 [in Chinese with English abstract].

Yang Shengqiu & Wang Huiji 1985 Jurassic–Cretaceous Nerinea from Xizang. *Acta Palaeont. Sinica* **24**, 403–411 [in Chinese with English abstract].

Yang Shipu & Fan Yingnian 1983 Carboniferous brachiopods from Xizang (Tibet) and their faunal provinces. *Contribs Geol. Qinghai–Xizang Plateau* **11**, 265–289 [in Chinese with English abstract].

Yang Zunyi, Yin Hongfu, Xu Guirong, Wu Shunbao, He Yuanliang, Liu Guangcai & Yin Jiarun 1983 *Triassic of the South Qilian Mountains*. Beijing: Geological Publishing House, 224 pp, 29 pls.

Zaninetti, L. & Whittaker, J. E. 1980 New records of Triassic Foraminifera from the Shan States, Eastern Burma. *Notes du Laboratoire de Paléontologie de l'Universite' de Genève* **6**, 29–35.

Zhang Binggao 1981 Latest marine sediments in Xizang and process of early Tertiary regression. In *Geological and ecological studies of the Qinghai–Xizang Plateau* **1**, 329. Beijing: Scientific Press.

Zhang Lipie 1986 Early Cretaceous orbitolinids from Xainza and Baingoin. *Bull. Nanjing Inst. Geol. Palaeont. Acad. Sinica* **10**, 101–122.

Zhang Lipie & Wu Rangyong 1983 Early Permian brachiopods from Xainxa district, Xizang (Tibet). *Contribs Geol. Qinghai–Xizang Plateau* **7**, 103–121.

Zhang Shanzhen & He Yuanliang 1985 Late Palaeozoic palaeophytogeographic provinces in China and their relationships with plate tectonics. *Palaeontologica Cathayana* **2**, 77–86.

Zhang Zhenggui, Chen Jirong & Yu Hongjin 1985 Early Permian stratigraphy and character of fauna in Xianza District, Northern Xizang (Tibet). *Contribs Geol. Qinghai–Xizang Plateau* **16**, 117–137 [in Chinese with English abstract].

Zheng Yahui, Zhou Shanfa, Liu Xiangqi, Wang Lianyuan, Xu Shujian & Wang Xianzhen 1981 Neogene sporo-pollen grains from northern Jiangsu and South Yellow Sea Basin. *Bull. Nanjing Inst. Geol. Palaeont. Acad. Sinica* **3**, 1–90 [in Chinese with English summary].

Zhu Zhizhi, Zhao Ming & Zheng Jiankang 1985 The dismembering of the Nachitai Group and the establishment of the Wanbaogou Group in the Middle of East-Kunlun Mountains. *Contribs Geol. Qinghai–Xizang Plateau* **16**, 1–14.

Appendix 1. Palaeontological data

The following determinations represent the combined work of a large number of experts, not only in the British Museum (Natural History) and Nanjing Institute of Palaeontology, but also in Universities and Research Establishments of Britain, Europe and the United States of America. These experts and their addresses are listed beneath. The initials of each expert are given wherever appropriate to indicate the source of the determination and any comments that may accompany it.

The localities are not listed in stratigraphical order, rather for each prefix letter they are in order of collection during the expedition, starting with localities in the south and ending with those in the north. The alphabetical prefixes identify the various working groups of the expedition. Figure 15 shows the approximate position for all localities for which we have collected palaeontological data. The map names and grid references refer to the 1:100000 scale geographical maps used as field maps during the expedition. A set of these is lodged in the British Museum (Natural History). No field maps were available for the Baingoin region and reference should be made to our field maps (Kidd *et al.*, this volume: microfiche 2 in pocket) for precise locations of fossil samples.

Each locality number generally refers to a section that was logged. In many cases simplified stratigraphical logs of these sections are presented in Leeder *et al.*, this volume) where the precise horizons from which samples were collected are sometimes marked. In other cases, where the section is small or unimportant, there is no accompanying sketch log to consult. Where fossils were found from more than one horizon in the section, individual sample numbers are also given, thus, for example, under **locality B50** there are a number of sample horizons, each one designated by its bed number in the field logs (e.g. B50.118).

For each entry there is a brief statement about geographical locality, age, and, where appropriate, palaeoenvironment. Many determinations, such as those of Foraminifera, are at a provisional (generic) level pending further work. In other cases (notably amongst the corals) the work of identifying the material has only just commenced and only the occurrence of such material is noted. Some age-diagnostic Permian and Cretaceous foraminifera are illustrated in plate 1.

A complete suite of macrofossils from this expedition is housed in the Nanjing Institute of Palaeontology, Academia Sinica, Nanjing, China, together with micropalaeontological samples determined by Chinese workers. Where duplicate material was collected a representative sample is also housed in the British Museum (Natural History), London, where there is also a complete set of micropalaeontological samples determined by British scientists. A duplicate set of palynological samples is held by the British Geological Survey, Keyworth, Nottinghamshire.

List of contributors

ABS Dr Andrew B. Smith, BM(NH).
BRR Dr Brian R. Rosen, BM(NH).
CHCB Dr C. H. C. Brunton, BM(NH).
CP Dr Colin Patterson, BM(NH).
CPP Mr C. P. Palmer, BM(NH).
CRH Dr C. R. Hill, BM(NH).
CS Dr Colin Scrutton, Department of Geology, University of Newcastle upon Tyne, NE1 7RU, U.K.
EAP Professor E. A. Pessagno, Department of Geology, University of Texas at Dallas, Box 688, Richardson, Texas 75080, U.S.A.
FZZ Dr Fang Zongzie, Nanjing Institute of Palaeontology.
GW Dr G. Warrington, British Geological Survey, Keyworth, Nottingham, U.K.
JBR Dr J. B. Riding, British Geological Survey, Keyworth, Nottingham, U.K.
JC Mr J. Collins, 63 Oakhurst Grove, London SE22 1AH, U.K.
JEPW Dr J. E. P. Whittaker, BM(NH).
JWN Professor J. W. Neale, Department of Geology, The University, Hull, HU6 7RX, U.K.
LXX Professor Li Xingxue, Nanjing Institute of Palaeontology.
MCB Dr M. C. Boulter, Palynology Research Unit, North East London Polytechnic, Romford Road, London E15 4LZ, U.K.
MDS Dr M. D. Simmons, BP Research Centre, Sunbury on Thames, Middlesex TW16 7LN, U.K.
MF Dr Monique Feist, Departement de Géologie, Université de Montpellier, Montpellier, France.
MKH Dr M. K. Howarth, BM(NH).
NJM Dr N. J. Morris, BM(NH).
PDT Dr P. D. Taylor, BM(NH).
PV Pamela Vaughan, Department of Geology, The Open University, Milton Keynes, MK7 6AA, U.K.
PS Dr P. Skelton, Department of Geology, The Open University, Milton Keynes, MK7 6AA, U.K.
RAF Dr R. A. Fortey, BM(NH).
RHW Dr R. H. Wagner, Jardin Botanico de Córdoba, Apartado de Correos 3048, Córdoba, Spain.
RJC Mr R. J. Cleevely, BM(NH).
RO Dr R. Owen, The National Museum of Wales, Cardiff.
RW Dr Rachel Wood, Institut fur Palaontologie (WE 3), Freie Universitat Berlin, F.R.G.
SDL Dr Sun Dongli, Nanjing Institute of Palaeontology.
SFM Mr S. F. Morris, BM(NH).
WCY Dr Wang Chengyuan, Nanjing Institute of Palaeontology.
WHR Wu Haoruo, Institute of Geology, Academia Sinica, Beijing.
WSX Wen Shixuan, Nanjing Institute of Palaeontology.
WZ Wang Zhen, Nanjing Institute of Palaeontology.

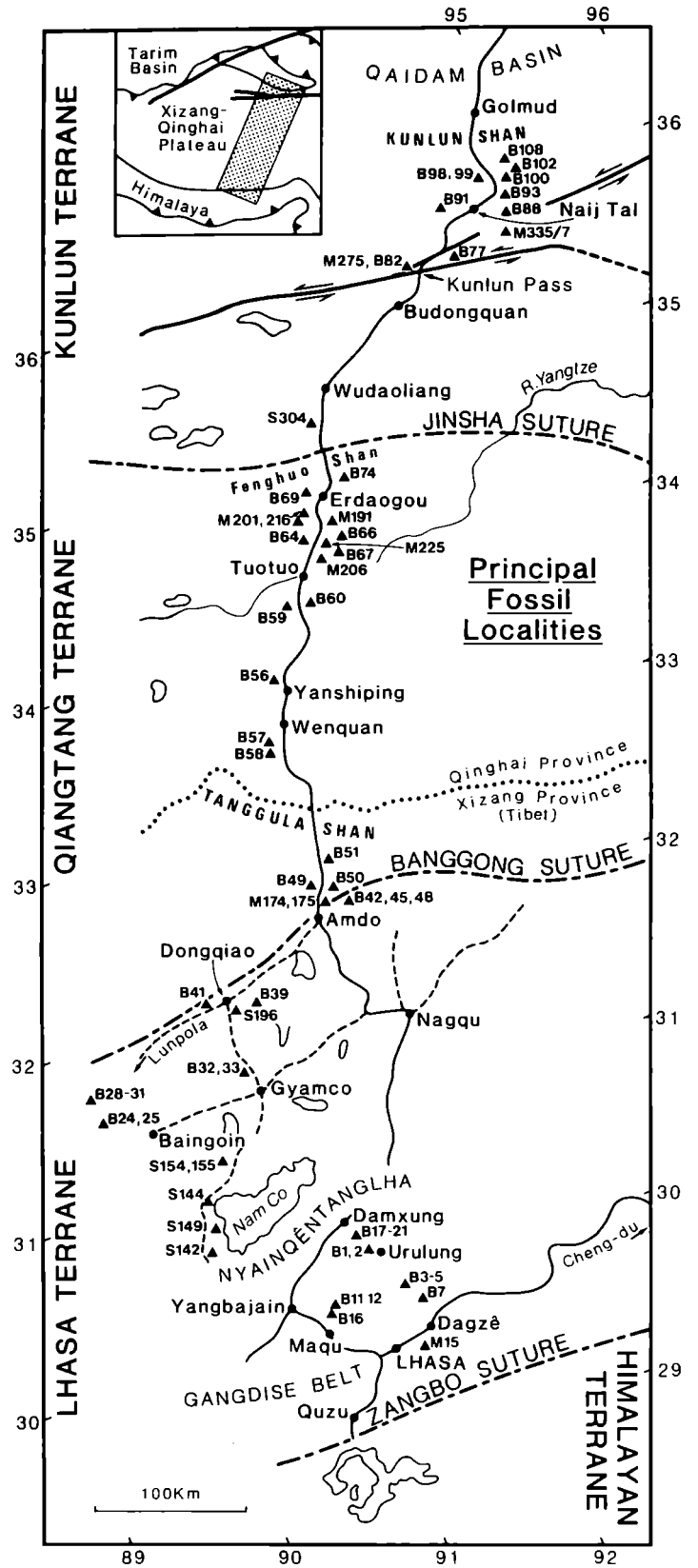

FIGURE 15. Strip map of the Geotraverse route showing the principal fossil localities listed in the Appendix.

XJT Dr Xue Juntao, Nanjing Institute of Palaeontology.
YCH Dr Ye Chunhuei, Nanjing Institute of Palaeontology.
YW Dr Yu Wen, Nanjing Institute of Palaeontology.
ZLJ Dr Zhang Lujing, Nanjing Institute of Palaeontology.
ZLX Dr Zhang Linxin, Nanjing Institute of Palaeontology.
ZZK Dr Zhu Zhikang, Nanjing Institute of Palaeontology.

Locality B1. Section at Urulung, north east of Lhasa (Pangduo sheet, grid ref. 63,328E 33,624N). Near the top of the Pondo Group: Early Permian (Asselian/Sakmarian). The fossils come from a thin calcareous sandstone bed and represent an allochthonous assemblage probably of storm deposit origins at or near wave base.

Brachiopoda (CHCB)
Mucrospiriferinella cf. *undulosa* Waterhouse
cf. *Cancrinelloides monticulus* Waterhouse
cf. *Chonetes ambiensis* Waagen

Locality B2. Section at Urulung, north east of Lhasa (Pangduo sheet, grid ref. 66,324E 33,626N).

B2.11. Thin storm deposit bed of allochthonous bryozoan debris within the Urulung Formation: Qixian Stage, Lower Permian. About 50 m below base of limestones.

Bryozoa (PDT)
Meekopora sp.
Goniocladia sp.
?Girtypora sp.
Streblotrypa sp.
Polypora sp.
'*Fenestella*' sp.

Loose limestones derived from the Lobadoi Formation which here forms a steep cliff face: *Neoschwagerina* Zone, Maokoan, Upper Permian. These are micritic limestones with a sparse derived fauna of corals and fusulinids, interpreted as carbonate ramp facies.

Foraminifera

'Contains the fusu ine *Rugososchwagerina* (see plate 1, figures 1, 6) and specimens of the smaller benthic foraminifer, *Pachyphloia*. Species of the former have previously been recorded from Tibet by Wang *et al.* (1981) from the Lobadoi Formation (Majula Member) and the Ombo Formation. According to Kanmera *et al.* (1976), *Rugososchwagerina* is restricted to the *Neoschwagerina* Zone of the Maokouan 'tage' (JEPW).

(ZLX)
Rugososchwagerina x zangica (Wang, Sheng & Zhang)
Nankinella inflata (Colani)
Schwagerina sp.

Corals

Locality B3. Exposures near the roadside approximately 1 km south of the village of Qibulung, Lhasa Terrane (Pangduo sheet, grid ref. 63,3' 2E 33,306N). Limestone/shale turbidite sequence interpreted as shelf-basin or shelf-margin facies. Qibulung Formation, Chaqupu Group; ?Carnian, Upper Triassic.

Bivalves (NJM)
Halobia cf. *charlyana* Mojsisovics (probably Carnian but just possibly Lower Norian: common).

Locality B4. 600 m south of locality B3. Well bedded micritic limestones with shales. Allochthonous fauna includes recrystallised branched ?stromatoporoid, crinoidal debris, micromorphic gastropods, fragmentary pieces of scleractinian coral and bivalve. Interpreted as carbonate ramp facies. Mailonggang Formation; Carnian, Upper Triassic.

Crinoids (ABS)
'*Isocrinus*' *candelabrum* Bather (columnals); a species from the Carnian of southern Europe.

Locality B5. 1 km south of locality B3. Limestone/shale sequence with transported shelf fauna of corals and bivalves, probably shelf basinal facies. Mailonggang Formation; Carnian/Norian, Upper Triassic.

Bivalves and Corals

Locality B11. Outcrops on the hillside approximately 500 m east of Chisan Ka hot springs, Lhasa Block: (Maqu sheet, grid ref. 62,882E 33,255N). See Leeder *et al.* (this volume) figure 6 for logged section. Here Permian cross-bedded sands of shoreface facies are overlain by thick-bedded sparsely fossiliferous micritic limestones.

B11, bed 9: Tuffaceous quartz sand, slightly calcareous within cross-bedded sand unit interpreted as distal shoreface sand. ?Urulung Formation, Lower Permian.

Brachiopods (CHCB).
Badly preserved productacean; marginiferid
?Chaoiella latisinuata Jing & Sun
?Rectimarginifera sp.

Bryozoans (PDT)
Indet. fenestellids

B11, bed 23: Basal bed of limestone sequence. Permo-Triassic.

Indeterminate crinoid stem fragments.

B11, bed 37: Thick bedded fossiliferous micritic limestone approximately 40 m above the base of the limestone sequence.

Foraminifera (JEPW)
'A dolomite with abundant macrofossil shell fragments [mostly rhynchonellids, but also some ostracodes and crinoid debris]. There are a few, poorly preserved foraminifera belonging either to *Angulodiscus* or *Glomospira*. Age, probably Triassic.'

Locality B12. Outcrop on hillslope 100 m east of Chisan Ka hot springs, Lhasa Terrane (Maqu sheet, grid ref. 62,876E 32,256N). Black micritic limestone overlying prominent disconformity; Chaqupu Group, Upper Anisian, lower Middle Triassic.

Ammonoids (MKH)
Paraceratites elegans Mojsisovics

Brachiopods (SDL)
Nudirostralina substrinodosi (Yang & Xu)
Costirhynchopsis cf. *sinensis* (Yang & Xu)

Bivalves (NJM)
Indet. pteriomorph

Locality B16. Outcrops forming cliff to the south of Chisan monastery, Lhasa Terrane (Maqu sheet, grid ref. 62,850E 33,236N). Plant-bearing sandstones in a fluviatile red bed sequence; Lingbuzong Formation, late Jurassic or early Cretaceous.

B16; near the base of the succession.

Plants (CRH)

'*Ptilophyllum cutchense* Morris. There is no exact match in the regional literature, but very similar leaves also referred to this species are known from the Jurassic of Kazakhstan. *P. caucasicum* Doludenko & Svanidze from the Upper Jurassic of Georgia, U.S.S.R., is very similar and has preserved cuticles, but the venation appears to be much more dense. The Japanese Upper Jurassic to Lower Cretaceous specimens figured by Oishi (1940, pl. 32 figs 1–3) as *P. pecten sensu lato* also look very similar and have a comparable vein density. The Indian type material described by Morris includes a broader range of leaf and pinna form than this Tibetan collection but amongst them are some more or less identical leaves.

'*P. cutchense* is a broadly defined and probably rather artificial species, now used mainly as a catch-all for material with short pinnae of which the cuticle is unknown. It is a suitable provisional determination for the Tibetan specimens until much larger samples showing more detail become available. Age: Mesozoic. The most closely comparable material from elsewhere ranges from Middle Jurassic through to Lower Cretaceous.

'*Ptilophyllum* sp. A, cf. *P. cutchense* Morris. Differs from the above species mainly in its smaller size. Broadly similar material from the Gondwanan Mesozoic has been referred directly to *P. cutchense* Morris. Material from the Jurassic of the Kazakhstan, also refered to *P. cutchense*, is more similar than the Gondwanan material but is larger. Age: Middle Jurassic to Lower Cretaceous.

'?*Ptilophyllum* sp. B: leaf fragment. The general appearance of the pinnae is of *Pterophyllum* but the pinna base (based solely on one or two of the better preserved pinnae) appears rounded acroscopically and slightly decurrent basiscopically, as in *Ptilophyllum*. I know of no other species of *Ptilophyllum* which exactly resembles this leaf and none referred to *Pterophyllum* that resembles it closely. Age; Permian to Middle(?) Cretaceous. The most similar material comes from the late Triassic and Lower Cretaceous.

'Indeterminate bennettitalean leaf fragments. Though often described as *Ptilophyllum* or *Zamiophyllum*, leaf fragments such as these are not sufficiently well preserved to identify securely to genus or species.

'*Pagiophyllum* sp. A, cf. *P. astrachanense* Doludenko. Similar material has been identified in the Chinese literature as *Sphenolepis* sp., a characteristically Cretaceous genus, but there is an equal or greater resemblance to several other species worldwide that have been given various generic names with little justification. Because of lack of epidermal detail and absence of attached or associated cones the present material is placed in the form genus *Pagiophyllum* following Harris (1979). This species lies at or near the boundary of *Pagiophyllum* with *Geinitzia*, but has a leaf shape closer to the former. The genus ranges from Triassic to Recent but is most characteristic of Jurassic and Lower Cretaceous floras.

'*Geinitzia* sp. A. Branching coniferous shoots of which the epidermal details are unknown. Shoots of this form are typical of the Mesozoic taxodiaceous genus *Elatides*. *E. harrisii* Zhou from the Lower Cretaceous of Liaoning differs in its longer and straighter leaves. Similar material from East Asia has been named *E. curvifolia* (Dunker), but full comparison of the Tibetan material with other species is precluded by the lack of epidermal detail. Age (of genus) Late Triassic to Lower Cretaceous.

'**Age of the flora.** Duan *et al.* (1977) previously recorded from this locality the fern *Weichselia reticulata*, a highly characteristic member of Lower Cretaceous floras worldwide, but extending back into the Middle Jurassic in some localities. The advanced fern *Onychiopsis*, also recorded by them, is similarly characteristic of Lower Cretaceous floras, but the photographs of this material (as published) are not entirely convincing. The present sample considerably augments botanical knowledge of the flora as a whole but adds little to estimating its age. The sample could equally on palaeobotanical grounds be ?Middle to Late Jurassic as well as Lower Cretaceous. In general the flora is composed of cosmopolitan elements, although if *Geinitzia* sp. A does turn out to be a species of *Elatides*, this genus has never previously been reported from Gondwana.'

B16b; approximately 100 m above the base.

Plants (CRH)
'Indet. cycad or cycadophyte leaf: it could be *Nilssonia* (in which the pinnules do not meet over the rachis) or one of a number of bennettitalean genera such as *Pterophyllum* or *Zamiophyllum* seen from the abaxial surface. The material is insufficient to identify'.

Locality B17. Outcrops along track running southeast of Damxung, immediately southeast of the summit of the pass, 3 km southeast of Damxung, Lhasa Terrane (Damxung sheet, grid ref. 63,232E 33,772N). Cleaved mudrocks of offshore marine shelf facies. Pondo Group, beds within mixtite sequence; ?late Carboniferous – Asselian, Lower Permian.

Brachiopods (CHCB)
Punctospirifer cf. *tamugangensis* Zhang
?Phricodothyris sp. cf. *asiaticus* (Chao)
mucronate spiriferid – *?Alispirifer* sp.
large productacean – *?Chaoiella* cf. *grundwaldti* (Krotov)
?Linoproductid fragments
?Spinatrypa khalfini Alekseeva
Rhipidomellid

Bryozoans (PDT)
Fenestella s.l.
?Polypora sp.
?'Thamniscus'
Indet. trepostome bryozoans
Indet. rhabdomesine cryptostome bryozoans

Bivalves (NJM)
Paleyoldia sp. (common)

Gastropods (RJC)
Peruvispira sp.

Indet. crinoid debris

Locality B18. As above, 20 m southeast from the summit: at top of mixtites.

Brachiopods (CHCB)
Schuchertella sp.
A chonetid with no external ribbing – cf. *Tornquistia tropicalis* Grant
Mucronate spiriferid – *?Alispirifer* sp.
Lochengia [= *Cyrtospirifer*] sp. cf. *L. lochengensis* Grabau & Yoh
Davidsoniacean indet.

Bryozoans (PDT)
Fenestella sp. s.l.
?Reteporidra sp.
Indet. trepostome bryozoans

Bivalves (NJM)
Ptychopteria sp.

Indet. crinoid debris

Locality B19. As for locality B17, 50 m southeast of the summit. Beds within the mixtite unit.

Brachiopods (CHCB)
Large spiriferid – *?Alispirifer* sp.
Indet. Davidsonacean
cf. *Chaoiella grunwaldti* (Krotov)

Conulariid (ZZK)
cf. *Notoconularia tenuistriata* (McCoy)

Bivalves (NJM)
Deltopecten sp.

Indet. crinoid debris

Locality B20. Outcrops along valley side approximately 6 km southeast of Damxung along a trackway (Damxung sheet, grid ref. 63,260E 33,749N). Finely laminated mudrock with thin calcareous bands, interpreted as offshore clastic shelf facies. Pondo Group, ?Upper Carboniferous.

Brachiopods (CHCB)
Chonetid sp. – ?anopliid
Martiniid indet.
cf. *Crurithyris* sp.

Gastropods (RJC)
Peruvispira sp.

Locality B21. Outcrop forming small cliff on the northern side of the valley, 8.5 km southeast of Damxung, along the trackway running from Damxung southeastwards (Damxung sheet, grid ref. 63,275E 33,734N). Pondo Group, ?early Upper Carboniferous.

Brachiopods (CHCB)
Sculptospirifer cf. *acutiplicatis* (Su)
?Martiniid

Crinoids (ABS)
Cyphostelechinus sp. (columnals)
Indet. crinoid and bryozoan debris

Locality B24. Outcrop forming a steep cliff to the south of Duoba village, Baingoin District, Lhasa Block. Limestones and calcareous shales of shallow marine facies. Langshan Formation; Aptian/Albian, Lower Cretaceous. [The sequence is aparently inverted].

Foraminifera (JEPW & MDS) [From first massive limestone approximately 50 m above top of red beds].
'An *Orbitolina* Limestone which contains good large embryons with alveolae indicating the subgenus *O.* (*Mesorbitolina*). Other foraminifera include *Daxia*. Age; Early Cretaceous, Albian.' (see plate 1, figure 10).

Bivalves (NJM & PS) [B24, bed 99; approximately 25 m above start of limestones]
Praeradiolites sp.

Locality B25. Outcrops up the left bank of a north/south gulley in the north-facing Lang Shan scarp face, approximately 2 Km ESE of Duoba Village, Baingoin District, Lhasa Terrane. A thick sequence of shallow marine calcareous shales and limestones of lagoonal facies, with rudist reefs. There is one clastic horizon in the sequence that is ?hypomarine. The sequence is inverted, based on foraminiferan dating of the beds. Langshan Formation; Aptian/Albian, Lower Cretaceous. Individual beds are as follows:

B25, beds 15 & 17.

Foraminifera (JEPW & MDS)
'An *Orbitolina* limestone. The embryons show alveolae, which according to Shroeder (1975) would place them within the subgenus *Orbitolina* (*Mesorbitolina*). Other foraminifera include *Pseudocyclammina* and *Cuneolina*. Age; early Cretaceous, Middle to Late Albian.'

B25, bed 30.

Foraminifera (JEPW & MDS)
'An *Orbitolina* limestone with *O.* (*Mesorbitolina*). Other foraminifera include *Trochospira* and miliolids. Age; early Cretaceous, late Albian.'

B25, bed 32.

Gastropods (NJM & YW)
Tylostoma sp. (common)

Bivalves (NJM)
'Concentrically ribbed infaunal bivalves, badly preserved; possibly small Astartidae. Also a fragment of ?*Liopistha*.'

B25, bed 33.

Foraminifera (JEPW & MDS)
'An *Orbitolina* limestone with *O.* (*Mesorbitolina*) and *Palorbitolinoides*. Age; early Cretaceous, late Aptian to Albian.' (see plate 1, figure 7).

B25, bed 38.

Bivalves (NJM & PS)
Offneria sp. [top Lower Aptian]
'*Praeradiolites*' *hedini* Douville. This species was first described from Aksai Chin in Western Tibet, associated with orbitolines. On the basis of the general similarity of this species with *P. fleuriani* from the Cenomanian of Aquitaine, Douville suggested that this species might be Cenomanian. In fact the two species are hardly similar at all and there is no reason to believe that Douville was correct. Yang *et al.* described further material attributed to *Praeradiolites* from the Ngari area of western Tibet; it was here associated with Requenidae and again orbitolines. *P. hedini* was identified as occurring in Lower Albian to Cenomanian deposits, but it would appear that the Cenomanian age was based on Douville's assertion, rather than on independent evidence. In the area around Gilgit and another locality in Western Afghanistan '*Praeradiolites*' *gilgitensis* (a probable synonym of '*P*'. *hedini*) occurs with *Horiopleura lamberti*, a species restricted to near the Aptian - Albian boundary. There seems little doubt that all this material is of late Aptian to early Albian age.

B25, bed 44.

Bivalves (NJM & PS)
'*Praeradiolites*' *hedini* Douville

B25, bed 45.

Foraminifera (JEPW & MDS)
'An *Orbitolina* limestone. Good, very large embryons are preserved, suggesting *O.* (*Mesorbitolina*). Other foraminifera include *Ammobaculites* and *Palaeodictyoconus*. Age; early Cretaceous, probably Albian.'

Algae (MDS)
Neomeris budaense Johnson

B25, bed 54.

Foraminifera (JEPW & MDS)
'An *Orbitolina* limestone containing *O.* (*Mesorbitolina*) and *Praeorbitolina* and other foraminifera including *Cuneolina* and *Daxia*. Age; early Cretaceous, Aptian or Albian.' (See plate 1, figures 12.)

B25, bed 66.

Foraminifera (JEPW & MDS)
'An *Orbitolina* limestone. Good embryons are available and these show a primitive condition of the genus *O.* (*Mesorbitolina*). Other foraminifera include *Cuneolina* sp., *Vercorsella* and miliolids. Age; early Cretaceous, late Aptian.' (See plate 1, figures 9 and 11.)

B25, bed 72.

Foraminifera (JEPW & MDS)
'An *Orbitolina* limestone with *Eopalorbitolina*: an interesting find as this genus was thought to be endemic to western Europe. Age, early Cretaceous, Late Barremian'. (See plate 1, figure 8.)

B25, bed 77.

Foraminifera (JEPW & MDS)
'An *Orbitolina* limestone. The embryons are rather primitive and indicate *Praeorbitolina*. Age; early Cretaceous, early Aptian.'

B25, bed 87.

Foraminifera (JEPW & MDS)
'An *Orbitolina* limestone. Both matrix-free and random thin sections show good embryons referable to a primitive species of *O.* (*Mesorbitolina*). The foraminifer *Cuneolina* is also present. Age; early Cretaceous, Aptian.'

B25, upper beds (loose).

Gastropods
Trocharia sp. (YW): indet. nerineid (PV)

Locality B28. Outcrops on the north side of Xiaqiong Lake, approximately 50 km northwest of Baingoin, Lhasa Terrane (see Kidd *et al.*, field maps on microfiche; also logged section, Leeder *et al.* figure 9). Massive dolomitised limestones separated by siltstone sequences. Three main reefoidal limestones form prominent sharp features and are of immediately subtidal marine shelf facies. The interbedded siltstone facies represents back-reef mud flats and beachrock environments. Xiaqiongco Formation; late Jurassic (Upper Oxfordian/Kimmeridgian) to Lower Cretaceous (Valanginian).

First limestone

Foraminiferans (PDT)
Placopsilina – type encrusting species.

Sclerosponge (PDT)
Neuropora sp.

Chaetetid (BRR & RW) [from top bed]
Blastochaetetes angoulensis Fischer [Kimmeridgian species]

Scleractinian corals (BRR) [from top beds]
Pseudocoenia sp.
Fungiastraea arachnoides (Parkinson)
Stylosmilia cf. *michelini* Milne Edwards & Haime
Stylina bangoinensis Liao
Stylosmilia sp.
Myriophyllia cf. *rastellina* (Michelin): this coral differs from *M. rastellina* in being lamellar rather than massive.
'This fauna mostly indicates a Late Oxfordian or Kimmeridgian age.'

Octocoral (BRR)
?Polytremacis sp.

Bryozoans (PDT)
Berenicea sp.
?Discosparsa sp.
Proboscina sp.

Gastropods (PV)
Phaneroptyxis sp. (common)
Eunerinea sp.
Adicoptyxis sp. cf. *A. valdensis* (Pictet & Campiche). This genus is typically Lower Cretaceous.

Bivalves (NJM)
Indet. oysters

Echinoids (ABS) [from top bed]
Trochotiara sp.

Saleniid; either *Salenia* or *Hyposalenia*, but details of apical disc not seen and determination not possible. Age; Saleniids similar to this range from Kimmeridgian to late Cretaceous.

Second limestone
Brachiopods (terebratulids), stromatoporoids and bivalves.

Beachrock between second and third limestones

Serpulid-encrusted surface.

Third limestone

Stromatoporoids

Bivalves (NJM)
Lophid oyster, genus indet.

Echinoids (ABS)
Pseudocidaris ?maresi (Cotteau). Large, club-shaped spines similar to these have been reported from the Neocomian of Algeria, the Valanginian/Hauterivian of Portugal and the Bau Formation of Kutching, Borneo (Lower Cretaceous). They are also probably synonymous with spines reported as 'late Jurassic' from Japan, under the name *Firmacidaris neumayri* Nisiyama.

Locality B29. Outcrop of massive limestone 1 km to the southeast of locality B28. Xiaqiongco Formation, late Jurassic – early Cretaceous. For locality see field map (Kidd *et al.*, this volume: microfiche 2, in pocket). Shallow reefoidal limestone.

Chaetetids (BRR & RW)
Blastochaetetes angoulensis Fischer [Kimmeridgian species]

Coral (BRR)
Stylina bangoinensis Liao [late Jurassic species]

Locality B30. Siltstones above the main limestone sequence of locs B28 & B29, conformably underlying a fluviodeltaic sequence 1.5 km east of locality B28 and 0.5 km north of locality B29, north side of Xiaqiong Lake, Baingoin district, Lhasa Terrane (see field maps, Kidd *et al.*, this volume: microfiche 2, in pocket) for a log of this section see Leeder *et al.*, this volume, fig. 11). Very shallow back reef marine lagoonal facies, with strand-line deposits. Xiaqiongco Formation; Lower Cretaceous, Valanginian to Hauterivian.

Foraminifera (JEPW & MDS)
A fine sandstone containing a species of *Pseudocyclammina*. Age; Valanginian to ?Aptian. (See plate 1, figure 14.)

Serpulids (ABS)
Serpula sp. s.s.

Gastropods
Cryptaulax sp. (YW). 'The overall shell shape and lack of internal folds are characteristic of *Aphanoptyxis*'. (PV)

Echinoids (ABS)
Numerous specimens, all badly crushed and distorted, of a heart-shaped atelostomate echinoid. The apical disc is not seen in any specimen but appears to be compact rather than elongate, indicating it is a spatangoid, rather than a holasteroid. There are no fascioles developed thus it belongs to the family Toxasteridae. The frontal ambulacrum is sunken and shows no evidence of two forms of pore pairs (hence it is not *Heteraster*). The petals also are not sunken and the anterior pair are curved anteriorly. This is almost certainly *Toxaster* sp., closest to the Neocomian *T. cordiformis* Breynius. The unsunken nature of the petals is a primitive feature and suggests an earlier rather than later species within the range of this genus (Berriasian – Hauterivian).

Also plates and spines of a cidarid. The spines are very large (10 cm) and coarsely thorned, with a flattened shaft. These come from the genus *Rhabdocidaris* and are indistinguishable from those of *R. tuberosa* (Gras) from the Valanginian of southern Europe.

Locality B31. Scarp face exposures near base of hill approximately 5 km NNE of locality B28, on the north side of Xiaqiong Lake (see field map (Kidd *et al.*, this volume: microfiche 2, in pocket for locality). Biosparite limestones with shell beds of oysters, rudists and stromatoporoids, and with some terebratulids. Hanshan Formation [= Langshan Formation]; Albian, early Cretaceous.

Foraminifera (JEPW & MDS)
Orbitolina sp. Age; Albian – Cenomanian.

Stromatoporoids and Brachiopods

Bivalves (MDS)
'In thin section radiolitid rudist bivalve debris is seen. Age; must be Albian or younger.'

Locality B32. Cleaved mudrock with thin calcareous sandy horizons exposed on the end of a narrow spit extending from the northern margin into Jang Lake (Jang Co sheet, grid ref. 62,960E 34,984N). Continental slope turbidites with transported shallow shelf fauna. Lake Area Flysch; probably late Jurassic.

Fragmentary scleractinian compound corals and stromatoporoids including *Stylosmilia* sp. (LWH)

Gastropods
'There are at least three different genera present in this material. (1) *Aptyxiella* or *Nerinella* (long, thin tapering shells are characteristic of both genera and the fold structure which would distinguish between them is not seen). (2) *?Trochalia*. (3) *Eunerinea*.' (PV)

'*Aptyxis* sp.' (YW)

Bivalves (NJM)
Camptonectes sp. (badly distorted)

Cirripedes (SFM)
'A single valve of a scalpellid cirripede in which the lateral margins and apex are ill preserved. It can be identified as a tergum from the apico-basal ridge which is wide, flat and increases in width towards the basal angle. This is characteristic (though not exclusively so) of the genera *Archaeolepas* and *Eolepas*, both Upper Jurassic in age, and is much rarer at other times.'

Locality B33. As for locality B32; exposures along the north edge of Jang Lake (Jang Co sheet, grid ref. 62,955E 34,995N).

Algae (GE)
Indet. cyanophyte algae (common)

Gastropods
As at locality B32 (PV & YW)

Locality B39. Outcrop on the northwest side of a small valley 7 km southeast of Dongqiao village, Banggong Suture zone (Dongqiao sheet, grid ref. 63,045E 35,384N). Silts and fine sands with thin bedded calcarenitic limestones; ?distal fan turbidite shelf facies. Latest Jurassic or Lower Cretaceous.

Trace fossils (ABS) [in silts]
Chondrites (abundant)
Laminaria
Rhizocorallium

Radiolaria (EAP) [calcarenite]
'The single specimen appears to be a yet unnamed Jurassic/Cretaceous Spumellarian'

WHR records the following genera:
Paronaella
Pseudodictyomitra
Patulibrachium
Praeconocaryomma
Crucella
?Hemicryptocapsa
Archaeospongoprunum

Fauna from limestone blocks within a bedded olistostrome, composed predominantly of chert and basalt.

Stromatoporoids and Corals

Echinoids (ABS)
Large club-shaped spines identical to those found in the third limestone at locality B28, and referable to *?Pseudocidaris maresi* (Cotteau).

Locality B41. Outcrop on the hillside southwest of Zige Tang Lake approximately 10 km northwest of Dongqiao village, Banggong Suture zone (Zige Tang Co map, grid ref. 62,916E 35,504N). Sequence overlying ophiolite; for log see Leeder *et al.*, this volume, figure 9. Includes shore-facies shallow marine limestones at top. Late Jurassic.

B41, bed 19. [plant bed]

Plants (CRH)

'Gross form is poorly preserved but preservation of leaf cuticles is good. Material includes *Cyparissidium* sp., a poorly preserved, branching shoot fragment with needle-like leaves and poorly preserved shoots which most probably belong to *Brachyphyllum* but might possibly turn out to belong to *Pagiophyllum* or even *Cyparissidium*. These forms are most commonly found in Middle to Upper Jurassic floras.'

B41, beds 26–28.

Sclerosponge (BRR)
Cladocoropsis sp.

Corals

Gastropods (NJM & RJC)
Eunerinea sp.
Ampullella sp.
?Nerinea (*Ptygmatis*) sp.
Pseudomelanid genus indet.

Bivalves (NJM)
Arcomytilus sp.

'The bivalves and gastropods suggest a Middle or Upper Jurassic age.'

Locality B42. Outcrop forming prominent conical hill, approximately 15 km northeast of Amdo, Banggong Suture Zone (112th Station sheet, grid ref. 63,920E 35,888N). Oolitic limestones, shallow marine shelf facies. Zhamunaqu Formation; Lower/Middle Jurassic.

Basal oolitic/oncolitic limestone.

Brachiopods (CHCB)
Koninckinacean, *?Cadomella* sp.

Higher massive oolitic limestones.

Gastropods (RJC)
Procerithium (*Xystrella?*) sp.

Bivalves (NJM)
Pernopecten or *Propeamussium* sp. The distinguishing feature which is the ribbing on the inner shell surface of the latter is not exposed.

Crinoids (ABS)
Pentagonal isocrinid stem ossicles with smooth latera and simple petaloid crenulariae – *?Balanocrinus* or *Isocrinus*.

Locality B45. Outcrop along the floor of a small valley immediately to the south of the conical hill of loc. B42, approximately 15 km northeast of Amdo, Banggong Suture Zone (112th Station sheet, grid ref. 63,928E 35,868N). Black shale with thin bands of calcareous nodules, interpreted as offshore shelf basinal facies. Zhamunaqu Formation; Middle Jurassic (Bajocian; *sauzei* Zone in part).

Bivalves (NJM)
Ceratomya cf. *bajociana* d'Orbigny
Propeamussium sp.
Chlamys-like pectinacean
Astartidae sp. A: possibly *Nicaniella* sp.
Small *Gryphaea*-like oyster
?Gervillella sp. (fragment)
?Palaeonucula sp.
?Mesosacella sp.
?Isocyprina sp.
Corbulidae fragment resembling *Corbulamima* sp.

Ammonites (MKH)
Euhoploceras adicra (Waagen); Lower Bajocian, *discites* Zone or *sauzei* Zone.
Dorsetensia sp. indet. (2 small fragments); Lower Bajocian *sauzei* Zone.
Phylloceras sp. indet.

Fontannesia cf. *luculenta* Buckman; Lower Bajocian, *discites* Zone. [the precise location of this specimen within the sequence is uncertain. If it is much lower than the other specimens then it could be the Upper Toarcian *Dumortieria*].

Crustacean (JC)
Protocarcinus ?hebes Meyer: carapace

Locality B48. Outcrops along the east bank of a small stream, approximately 4 km southeast of the conical hill of loc. B42, some 15 km northeast of Amdo, Banggong Suture Zone (112th Station sheet, grid ref. 63,945E 35,852N). Cross-bedded sands with shale and thin bioclastic limestones of shallow fluvio-marine facies. ?Zhamunaqu Formation; Upper Jurassic.

Lower beds in sequence

Sclerosponge (BRR)
Cladocoropsis sp.

Stromatoporoid

Top beds at bend in stream: at start of flysch sequence.

Gastropods (PV)
Aptyxiella or *Nerinella*; similar to locality B32/33

Locality B49. Material excavated in a marmot burrow from immediately above a submarine lithified surface, outcropping on the hillside 800 m north of the road, approximately 17 km ENE of Amdo, Qiangtang Terrane (112th Station sheet, grid ref. 63,875E 35,918N). Yanshiping Group; Bathonian/Callovian, Middle Jurassic.

Gastropods (NJM)
Internal mould of a small ?Naticacea

Bivalves (NJM,WSX & XJT)
Lophid oyster, possibly *Actinostreon* sp.
Ceratomya concentrica (Sowerby)
Camptonectes yanshipingensis Wen
Modiolus imbricatus (Sowerby)
Pteroperna sp.
Arcomytilus sp.
?Catinula sp.
Indeterminate heterodont bivalve

Brachiopods (SDL)
Burmirhynchia sp. [Large numbers of specimens were collected attributable to the following nominal species – *B. asiatica* Buckman, *B.* cf. *lobata* Ching, Sun & Ye, *B. parva* Buckman, *B. luchingensis* Reed, *B. quinquiplicata* Ching, Sun & Ye, *B. nyainrongensis* Ching, Sun & Ye, *B. shanensis* Buckman, ?*B. namtuensis* Buckman, *B. lobata* Ching, Sun & Ye].

Echinoids (ABS)
Holectypus depressus (Leske) (Bathonian/Callovian)

Locality B50. Cliff outcrop on the east bank of the river, approximately 18 km northeast of Amdo, Qiangtang Terrane (112th Station sheet, grid ref. 63,895E 35,935N). Grey mudrock of shelf basinal facies; Sewa Formation, Kimmeridgian, Upper Jurassic.

Dinoflagellates (Nanjing Institute scientists) [from near the base of the section]
Pareodinia ceratophora Deflandre
Meiourogonyaulax rioultii Sarjeant
Ctenidodinium mosaicum Dodekova
Mendicodinium ? *reticulatum* Morgenroth
Dapcodinium (*Macodinium*) *semitabulatum* (Morgenroth) Dorhofer & Davies
Yalkapodinium (*Cyclomephelium*) cf. *areolatum* (Cookson & Eisenack) Morgan
Paragonyaulacysta ? *calloviensis* Johnson & Hills
?*Meiourogonyaulax valensii* Sarjeant
Ambonosphaera cf. *jurassica* Gitmez & Sarjeant
Subtilisphaera sp.
Dichadogonyaulax sellwoodii Sarjeant

Bivalves (NJM, WSX & XJT)
Pholadomya cf. *hemicaredia* Roemer
Entolium sp.
Arcticidae, genus indet.
Radulopecten sp.
Exogyriform oyster cf. '*Gryphaea*' *hennigi* Dietrich
Chlamys sp.
'*Exogyra*' cf. *forteaui*
Inoperna sp.
Actinostreon sp.

Brachiopods (SDL)
Indet. rhynchonellids

Ammonites (MKH)
'Many large fragments of indeterminate perisphinctids, probably Upper Jurassic. The largest specimen and the Kodachromes are probably *Torquatisphinctes* of Lower Middle Kimmeridgian age. The coarse ribbed and tuberculate ammonites are *Katroliceras* sp. indet. from the Middle Kimmeridgian.'

Locality B51. Roadside cutting by Highway Station 114, approximately 22 km northeast of Amdo, Qiangtang Terrane (112th Station sheet, grid ref. 63,907E 35,965N). Restricted marine sequence with black, fossiliferous shales, cross-bedded sands and a coalified plant bed. Yanshiping Formation; Middle Jurassic.

Bivalves (CPP)
Protocardia sp. cf. *stricklandi* (Morris & Lycett)
Tancredia? sp.
Corbulimima sp. cf. *attenuata* Lycett
Pleuromya sp.
Ceratomya sp. cf. *concentrica* Lycett
Thracia sp.

Locality B56. Exposures at the northeast end of the road cutting immediately to the northeast of Yanshiping village, Qiangtang Terrane (Yanshiping sheet, grid ref. 64,176E 37,232N). Fine sands and silts with rippled and mudcracked horizons indicative of very shallow lacustrine or hypomarine conditions. Lower part of the Yanshiping Group; Middle Jurassic (pre-Bathonian).

Bivalves (WSX)
Psilunio spp. including *P. ovalis* Mu, *P. chaoi* (Grabau), *P. thailandicus* (Hayami), *P. henanensis* Gu and *P.* aff. *guangyuanensis* Mu. ['The genus *Psilunio* as used in the Chinese literature is probably not the same as *Psilunio* Gabbe. Some smaller specimens within this sample show the sculpturing of *Protocardia*. This suggests that the beds may contain a mixture of non-marine and marginal marine forms. All are Middle Jurassic species.' (NJM)]

Locality B57. Outcrop in east/west valley just south of kilometre post 1000, approximately 3 km to the east of the road, 15 km south of Wenquan station, Qiangtang Terrane (Wenquan sheet, grid ref. 63,938E 36,825N). Brackish to marine limestones within a red bed fluviatile sequence (a lower and upper limestone sequence was studied). Yanshiping Group; Bathonian, Middle Jurassic.

Upper marine limestone.

Brachiopods (SDL)
Holcothyris sp. [conforming to the morphotypes *H. trigonalis* Buckman, *H. subovalis* Buckman and *H. acuminata* Buckman]
Burmirhynchia sp. [conforming to the morphotypes *B. praestans* Reed, *B. globulus* Buckman and ?*B. gutta* Buckman]
Cererithyris sp.

Gastropods (NJM)
Naticid gastropod

Bivalves (NJM)
Praeexogyra cf. *hebredica* (Forbes) [? = *Ostrea davaiacencis burmanica* Reed]. Probably Bathonian in age, though Tibetan and other Far Eastern occurrences could have a different range to those in Europe, where the species is not known outside the Bathonian. Marginal marine species.
Modiolus sp.
Camptonectes cf. *auritus* (Schlotheim)
Camptonectes sp. (smooth or exfoliate specimen)
?Sphaeriola sp.
Ceratomya sp.

Echinoids (ABS)
Badly preserved regular eucchinoid. Tall globular test with uniserial columns of ambulacral pores and one primary tubercle on each interambulacral plate. Ambulacra relatively narrow. Either an Acrosaleniidae or a Hemicidaridae.

Locality B58. A section logged through approximately 2 km of predominantly red bed facies exposed up the hill slope in a southwesterly directed valley approximately 3 km due west of the road near kilometre marker number 1004, 18 km south of Wenquan army station, Qiangtang Terrane (Wenquan sheet, grid ref. 63,935E 36,800N to 63,905E 36,793N). Coastal plain facies with marine incursions and some lacustrine horizons (for a log of this section see Leeder *et al.*, this volume, figure 9). Yanshiping Group; Middle Jurassic ?Bathonian/Callovian – Upper Jurassic, Kimmeridgian.

Dinoflagellates [from 'Lower Shales'] (Nanjing Institute scientists)
Pareodinia groenlandica Sarjeant
P. prolongata Sarjeant
P. ceratophora Deflandre
P. ceratophora var. *pachyceras* (Sarjeant) Lentin & Williams
Dapcodinium (*Mancodinium*) *semitabulatum* (Morgenroth) Dorhofer & Davies
Mendicodinium reticulatum Morgenroth
Wanaea ? digitata Cookson & Eisenack
Polysphaeridium sp.
Ctenidodinium aff. *arnatum* (Eisenack) Deflandre

Bivalves (NJM, WSX & XJT)

B58, beds 37/38
Camptonectes yanshipingensis Wen
Protocardia sp.
?Praeexogyra cf. *hebredica* (Forbes)

B58, beds 41 & 45
Corbula sp.
Protocardia sp. Here and in other beds *Protocardia* forms monospecific masses suggestive of low salinity environments. This form has clear ribbing on the corcelet not known on other taxa with comparable morphology except a single undescribed arcticacean from the Bajocian of Madagascar, and identification must remain slightly tentative until details of hinge structure can be determined.

B58, bed 59
Undulatula tanggulaensis Gu (an Upper Jurassic species in China).
Pseudocardinia or Neomiodontid
Protocardia sp.

B58, bed 63
Dinoflagellates (JBR)
Systematophora areolata Klemant. A Late Oxfordian to Kimmeridgian species.

Palynomorphs (GW)
Abundant organic debris with some spores, but largely indeterminate. Material includes a questionable circumpolles group pollen and *Cyadopites*.

B58, bed 71

Ostracods (YCH)
Darwinula sarytirmenensis Shanapova

Bivalves (NJM, WSX & XJT)

B58, bed 103

Protocardia sp.
Unionid

B58, bed 106

Undulatula tanggulaensis Gu (an Upper Jurassic species in China).
U. perlonga Gu
?Pseudocardinia sp.

B58, bed 118

Bivalves (NJM)
Radulopecten sp.
Protocardia sp.
?*Liostrea* sp.
?*Antiquicyprina* sp.

B58, bed 139

Bivalves (NJM)
Placunopsis sp.
Protocardia sp. (as before)
Radulopecten sp.
Anisocardia sp.
'*Modiolus*' sp.
?*Antiquicyprina* sp.

Gastropods (NJM)
Naticacean – ? *Ampullospira* sp.

Trace fossils (ABS)
Zoophycos

Locality B59. Outcrops at Kaixinling coal field, approximately 12 km southwest of Tuotuo station, Qiangtang Terrane (Tuotuo River sheet, grid ref. 64,404E 37,806N). Succession of fluvio-marine clastics with drift coal beds, overlain by thick-bedded micritic limestones; marginal marine to shallow marine shelf facies. Kaixinling Group; Maukouan, early Upper Permian.

From shales immediately underlying the drift coal beds.

Brachiopods (CHCB)
Orthotichia cf. *waterhousei* Grant
Davidsoniacean – cf. *Perigeyerella tricosa* Grant
new genus cf. *Bilotina*, superficially like *Spinomarginifera* in external form.

Bivalves (NJM & MD)
Leptodesma sp.
Aviculopecten sp.
?*Guizhopecten* sp.
?*Etheripecten* sp.
?*Pernopecten* sp.
?*Pseudomonotis* sp.
Aviculopectenid, genus indet.
Mytilus s.l.

Plants (LXX)
Compsopteris contracta Gu & Zhi var. *punctinervis* Li & Yao
Rajahia (*Pecopteris*) *calceiformis* Li & Yao
Pecopteris sp. cf. *P.? tobaensis* Li *et al.*
Pecopteris spp.
Gigantonoclea or *Gigantopteris* sp.

[RW also identified the following
Odontopteris sp.
Pecopteris orientalis Schenk]

Massive micritic limestone exposed above and immediately to the east of the coalfield.

Fusuline foraminifera (JEPW)
'Contains a large fusuline with schwagerinid wall structure, probably a *Parafusulina*. The range of the genus according to Kanmera *et al.* (1976) is *Cancellina* to *Lepidolina* Zone, Maokouan, Upper Permian.' (See plate 1, figure 2.)

(ZXL) recognized:
Parafusulina dainelis (Skinner & Wilde)
P. yabei Hanzawa
Nankinella sp. indet.
Staffella sp. indet.

Locality B60. Massive micritic limestone outcropping to the east of the road opposite the track leading to Kaixinling coal field, approximately 11 km WSW of Tuotuo River station (Tuotuo River sheet, grid ref. 64,460E 37,775N). Carbonate ramp facies. Maokouan, Upper Permian.

Fusuline foraminifera (JEPW)
'A fusuline limestone containing the genera *Verbeekina*, *Parafusulina* and *Nankinella*. According to Kanmera *et al.* (1976), *Verbeekina* is restricted to the Maokouan Stage.' (See plate 1, figures 3, 4.)

(ZXL) recognized the following:
Parafusulina gigantia (Deprat)
P. dainelii (Skinner & Wilde)
P. multiseptata (Schellwien)
Verbeekina verbeeki Geinitz
Neoschwagerina craticulifera (Schwager)
N. haydeni Dutkevich & Khabokov
N. sp. nov.
Yangchienia cf. *haydeni* Thompson

In addition an apparently older assemblage of fusulines, including
Schwagerina pseudocervicalis Sheng & Sun
Quasifusulina cf. *longissima* Moeller
Rugosofusulina cylindrica Sheng & Sun
Pseudofusulina sp.
were found in this vicinity. These were studied by ZXL and dated as Asselian/Sakmarian (early Permian).

Corals

Locality B64. Outcrop approximately 3 km west of the highway northwest of the abandoned '85th Service Station', approximately 25 km WSW of Erdaogou Station, Qiangtang Terrane (Erdaogou sheet, grid ref. 64,710E 38,130N). Fluviatile sequence with drift coal deposits and non-marine shales. Yanshiping Group (previously mapped as Permian); Middle Jurassic.

Bivalves (NJM & FZZ)
Pseudocardinia sp. cf. *P. jenissejensis* (Lebegev)
'*Tutuella*' ? *rotunda* Ragozin
Astartid, indet.
Unionid – *Unio* sp. s.l.

Locality B66. Outcrop to the southeast of a small lake, approximately 6 km southeast of '85th Service Station' (abandoned), some 25 km south of Erdaogou Station, Qiangtang Terrane (Erdaogou sheet, grid ref. 64,795E 38,075N). Shale/siltstone sequence with thin fossiliferous sandy packstone limestones interpreted as offshore (basinal) marine shelf facies. Wuli Group; Lower Permian.

Brachiopods (CHCB)
Orbiculoidea sp.
Davidsoniacean – ?*Streptorhynchus sulcatulum* Grant
Chonetinella cf. *convexa* (Yang & Fang) or *irregularis* (Lee & Sun)
?Rugosochonetid
Productacean – cf. *Bilotina acantha* Waterhouse & Piyasin
Productacean cf. *Avonia echidniformis* Chao
Perigeyerella sp.

Gastropods (NJM & RJC)
?*Naticopsis* sp.
Belleriphontidae (two species, both indet.)

Echinoids (ABS)
Large club-shaped spine with a relatively long shaft. ?Undescribed genus: nothing comparable has been described from the Palaeozoic, except *Nortonechinus*, which has much shorter spines.

Locality B67. Outcrops forming a low ridge, approximately 50 km east of the Highway near Zhakongjian, about 30 km due south of Erdaogou Station, Qiangtang Block (no map reference). Blue coloured biomicrites interpreted as carbonate platform facies, approaching shallow subtidal towards the top where large oncolitic structures are found. All four fossil horizons are near the top of the sequence. Batang Group; Norian, Upper Triassic.

From a limestone bed 25 m below the top.

Brachiopods (SDL)
Yidunella magna Ching, Sun & Ye
Aulacothyropsis sp.
Omolonella sp.
Amphiclina intermedia Bittner

From a limestone bed about 75 m below the top.

Brachiopods (SDL)
Yidunella pentagina Ching, Sun & Ye
Y. yunnanensis (Ching & Fang)
Amphiclina intermedia Bittern

From a bed 85 m below the top.

Brachiopods (SDL)
Yidunella yunnanensis (Ching & Fang)
Rimirhynchopsis sp.

Amphiclina intermedia Bittner
Lobothyris sp.

Bivalves (NJM)
Oxytomidae indet.

From a bed 10 m above the volcanics at the base of the limestone sequence.

Brachiopods (SDL)
Terebratuloids indet.

Corals

From limestones in the upper half of the main limestone.

Conodonts (WCY)
Diplodondella sp.
Neogondolella hallstattensis
N. cf. *steinbergensis*
N. sp.
Epigondolella postera
E. abneptis
Lonchoidina sp.
Enatignathoidus zeigleri

Foraminifera (JEPW)
'A fine grained bioclastic limestone with a few smaller benthic foraminifera which are difficult to determine with certainty. Similar to forms identified by Salaj *et al.* (1983) from the Norian of the West Carpathians and referred by them to the genera *Nodosaria*, *Agathammina*/*Ophthalmidium* and *Glomospirella*. Age; probably late Triassic.'

ZLX also identified *Plagioraphs* and *Ammodiscus*.

Locality B69. Outcrops on the south flank of the hill to the north of the valley leading northwestwards from Erdaogou, some 2.5 km northwest of Erdaogou Station (Erdaogou sheet, grid ref. 64,830E 38,382N). Shallow pond limestones in red bed sequence. Fenghuoshan Group; early Eocene.

Charophytes (MF)
'One species, belonging to the family Characeae, and genus *Stephanochara* (Lower Eocene to Recent). Species belonging to this genus with this type of ornamentation have not been found in beds younger than the Middle Oligocene. With reference to the numerous species described from the Palaeogene of China, this most closely resembles '*Naedleiella*' *nanxiangensis* Huang from the Lower Eocene.'

WZ identified the following:
Rhabdochara ? sp.
Peckichara subsphaerica? Lin & Z. Wang
Harrisichara yunlongensis? Z. Wang, Lin & S. Wang
These indicate an early Palaeogene (Palaeocene or Lower Eocene) age.

Locality B74. Outcrop on the east side of the highway at the northern end of the Fenghuoshan Range, approximately 28 km north of Erdaogou Station, Qiangtang Terrane (Fenghuoshan sheet, grid ref. 64,940E 38,522N). Thin limestones within a clastic sequence, interpreted as shallow freshwater pond deposits: Fenghuoshan Group, Palaeogene (Palaeocene/early Eocene)

Palynomorphs (ZLJ)
Triporopollenites? *nactonodus* Zhao, Sun & Wang
Polypodiaceaesporites sp.
Cyathidites sp.
Schizosporis sp.
Pediastrum sp.

(MCB) A single specimen of a well preserved bisaccate pollen (*Pityosporites sylvestris* type) and one specimen of a monolete spore (*Polypodiaceaesporites*) were found. Black debris is oxidized to amorphous matter and degraded bundles (see Boulter & Riddick 1986) suggesting an organic-rich freshwater deposit.

Charophyta (MF & WZ)
Gyrogoneae, gen. indet.

Ostracods (YCH)
Cypreid

Gastropods (YW)
Amnicola sp.
Bithynia sp.

Locality B77. Coal bed outcropping by a stream in the South Kunlun Shan, 9 km northeast of Kunlun Pass, Kunlun Terrane (63rd Station sheet, grid ref. 65,095E 39,548N). Interpreted as a allochthonous coal within a fluviatile sequence with volcanoclastic debris. Babaoshan Group; ?Triassic or Jurassic.

Plants (LXX & CRH)
Pecopteris s.l. or *Sphenopteris*. One badly preserved pinna of a fern, Permian or Triassic. The widely spaced pinnules suggest a Mesozoic age.

? Associated beds (XJT Collection)

Holothurian sclerites [indicative of a Triassic or younger age]
Theelia zawidzkae
Kuehnites spinioformius

Sponge sclerites

Locality B82. Finely laminated silts beneath a varve sequence, interpreted as lake beds. Pliocene/Pleistocene. Exposure 100 m to the west of the highway, 300 m north of the Kunlun Pass summit (63rd Station sheet, grid ref. 65,995E 39,495N).

Palynomorphs (MCB)
About 20 pollen were recovered and are either bisaccates, similar to modern *Pinus* species, or triporate, of the *Corylus – Myrica* type. Palynodebris is abundant and consists of cuticle and tracheids. This together with the evidence of a badly preserved *Pediastrum* colony, common in the Tertiary, shows that deposition was in a freshwater lake. With and without oxidation the plant cells are a pale yellow and very well preserved. The very limited palynological evidence supports a Plio-Pleistocene age.

Gastropods (YW)
Limnaea sp.

Ostracods (JWN)
Cyprideaidae

Locality B88. Outcrop forming a small mound on the north side of the Xidatan valley, approximately 20 km southwest of Kunlun bridge (along a trail leading southwards from beside the small works east of Naij Tal), central Kunlun Shan (Naij Tal sheet, grid ref. 66,775E 39,648N). Fluviatile red beds with silts; age uncertain – ?Mesozoic.

Plants (CRH)
'Sphenopsid stems – linear leaf and pinna fragments and cone scales which are indeterminate. Could be Permian, Triassic or younger.'

Locality B91. Limestones from relatively high in the thick carbonate sequence forming the higher outcrops on West Mountain, Wanbaogou valley, approximately 15 km westnorthwest of Naij Tal Station, North Kunlun Shan (Qingbanshisu sheet, grid ref. 65,250E 39,850N). Shelf carbonate facies. Hongshuichuan Formation; Upper Permian [originally considered to be Lower Triassic].

Brachiopods (CHCB)
'There are six or seven species in the sample. Two species show well preserved laminar shell, characteristic of strophomenaceans. One, with a wide hinge and strong ribs is the chonetid *Waagenites*, a characteristic Permian genus well-known from Timor, South Himalayas, Thailand, etc. Especially well known from late Lower Permian through to Upper Permian. The other strophomenacean might be a productid, such as a small marginiferid, not known above the Permian.

'A smooth-shelled, elongate, anteriorly folded species with impunctate coarse fibres is also present. This has internal structures suggestive of Stenoscismatacea and externally resembles *Camarophorina*, a Permian Timor/Malaysia genus extending up into the Upper Permian. There is also a ribbed stenoscismatacean, possibly *Stenoscisma* itself, a Carboniferous through to Late Permian genus.

'There is a ribbed, rounded species which externally looks like *Rhipidomella* (Carboniferous – Permian). The shell is poorly preserved and it is not possible to see the expected fine endopunctae of this genus, but it does not resemble any Triassic genus that I know.

'There are a couple of small, rounded specimens which might be *Crurithyris* sp., a long-ranging genus that extends into the Triassic.

'Finally, there is an (?)impunctate shell with a ventral median septum, low profile ribbing and a ?well developed ventral umbo. I think this is some sort of spire-bearer, but these few characters do not allow determination. In conclusion, the sample is Permian in age and probably Late Permian rather than early Permian.'

Locality B93. Large cliff face close to Shuinichang, just to the northeast of Naij Tal, on the north side of the river approximately 24 km eastnortheast of Naij Tal Station, Kunlun Shan (Naij Tal sheet, grid ref. 66,695E 39,820N). Massive micritic limestones of shelf facies. Shuinichang Formation (? = Shihuichang Formation); Upper Ordovician/Lower Silurian.

Stromatoporoids

Corals (CS)
?Pycnolithus sp. (Lower Silurian genus)

Gastropods

Locality B98. Outcrop to the north of a large valley, approximately 1 km west of the river and 2 km north of a working quarry, 24 km ENE of Naij Tal Station, Kunlun Shan (Naij Tal sheet, grid ref. 66,655E 39,860N). Micritic limestone bed with transported fossils of shelf facies. Shihuichang Formation; Upper Ordovician.

Stromatoporoids (CS)
Labechia sp.
Clathrodictyon sp.

Corals (CS)
Agetolites sp. cf. *A. raritabulatus* Lin – *A. aequabilis* Lin & Chow group

Gastropods (NJM)
?Lophospira sp.

?Lovonemetrida sp.
[specimens housed in Nanjing Institute of Palaeontology from this limestone proved to be platyceratid gastropods - ABS & XJT]

Locality B99. Limestone exotic block within a ?Triassic or younger sequence of tuffs and conglomerates, identical to the limestone exposed at locality B98. Outcrop on south face of small promontory ridge approximately 600 m west of the river and 3 km north of a working quarry some 24 km eastnortheast of Naij Tal (Naij Tal sheet, grid ref. 66,656E 39,868N). Derived from the Shihuichang Formation limestone, Upper Ordovician.

Stromatoporoids (CS)
Labechia sp.
Clathrodictyon sp.

Corals (CS)
Agetolites sp.
Wormsipora sp.

The corals suggest an Upper Ordovician age.

Locality B100. Oolitic limestone on the north slope of a ridge, 150 m east of the highway approximately 4 km due north of a working quarry and some 24 km east of Naij Tal Station, north Kunlun Shan (Naij Tal map, grid ref. 66,676E 39,876N). Shallow marine shelf, Halabayigou Formation; late Cambrian – early Ordovician.

Trilobite (RAF)
'A single cranidium which can be determined only as a leiostegiacean. I do not believe it is an *Annamitella* because the internal mould shows no sign of glabeller furrows. Elongate unfurrowed glabellae of this type are more usual among late Cambrian and early Ordovician (Tremadoc) leiostegiaceans. I would go no further on the basis of this specimen.'

Locality B102. Limestone exposed on the west side of a gulley on a prominent ridge of hills approximately 9 km northeast of a working quarry some 5.5 km east of a major loop in the highway across a dry gulley (Naij Tal sheet, grid ref. 66,742E 39,906N). ?Shihuichang Formation; Ordovician.

Conodonts (WCY)
Panderosus gracilis

Locality B108. Section up a north/south running dry gulley at Dagangou, north Kunlun Shan, approximately 10 km east of the highway and approximately 12 km eastnortheast of a large working quarry (Dishantuo sheet, grid ref. 66,760E 39,955N). Marine limestone units within a thick fluviatile sequence (For a log of this section see Leeder *et al.*, this volume, figure 2). Dagangou and Diaosu Formations; late Visean to early Namurian.

First Limestone unit, beds in lowest 3 m.

Conodonts (WCY)
Neognathodus dilatus

Stromatoporoids and chaetetids

Corals (LWH)
Lithostrotion
Dibunophyllum
Clisiophyllum

(BRR)
Actinocyathus floriformis crassiconus (McCoy)
Siphonodendron pauciradiale (McCoy)
Siphonodendron intermedium (Poty)

Bryozoans (PDT)
Fenestella sp. s.l.
?Septopora sp.
?Anisotrypid trepostome cystoporates

Brachiopods (CHCB)
'*Overtonia*' *transversus* (Wang)
cf. *Ovatia* sp.
cf. *Flexaria* sp.
?Rugosochonetes kansuensis Chao
?Cleiothyridina sp.
?Uncinella cf. *minor* Grabau
Rhipidomella cf. *plana* Yang
"*Gigantoproductus*" cf. *rectestrius* (Grabau)
Echinoconchus fasciatus (Kutorga) or *E. parafascifera* Wang
'*Antiquatonia*' cf. *taiguanfuensis* (Grabau)
Davidsoniacean cf. *Pseudorthotetes borodencovensis* Sokolskaya
?Punctospirifer tamugangensis Zhang
?Dielasma dieneri Grabau & Yoh
?Beecheria sp.
'*Echinoconchus*' *transversus* Wang

Protoniella sp.
Productacean – cf. *Diaphragmus* sp.
?Linoproductid fragments
cf. *Marginifera chuchuhuai* Grabau & Yoh
Reticulariacean – cf. *Martinia* sp.
?*Derbyia* sp.
Small ?spiriferellinids
?*Hystriculina* sp.
Small dictyclosid

Trilobite (RO)
Linguaphillipsia sp. (glabella & pygidium)

Limestone bed near the top of the section, just below fault contact with volcanics. Upper Carboniferous.

Corals

Brachiopods (CHCB)
cf. *Liraplecta richthofeni* (Chao)
Martinia cf. *kunlunia* Zhang
Coledium cf. *trigonalis* (Wang)
cf. *Choristites jigulensis* Stuckenberg

Limestone band towards the top of the section in a neighbouring gulley to that above. Upper Carboniferous.

Conodonts (WCY)
Idiognathoides corrugatus
I. cf. *sinuatus*
Neognathodus dilatus (Stauffer & Plummer)

Corals

Brachiopods (CHCB)
?*Rugosochonetes* sp.
Echinoconchus cf. *fasciatus* (Kutorga)
Hystriculina cf. *sinica* Wang
Martinia sp.
Pleuropugnoides wangenheimi (Pander)

Locality M15. Mudrock with volcanics intercalated outcropping at the base of a ridge 1.2 km south of the Lhasa–Dagze road on the east side of the valley which trends south from the main Kyu-Chu river valley: about 13 km ESE of Lhasa [Lhasa sheet, grid ref. 63,344E 32,345N]. From the base or within a thick volcanoclastic and volcanic sequence, ?Chaqupu Group, Dagze Formation; Late Palaeozoic: Upper Carboniferous or Permian.

Palynomorphs (GW)
Poorly preserved miospores, mostly trilete spores but also one poorly preserved bisaccate spore, indicative of a Late Palaeozoic age (Upper Carboniferous or Permian). Genera include:
Densosporites
Lycospora
?*Convolutispora*
?*Dictyotriletes*
?*Knoxisporites*

Locality M174. Grey shaly limestone outcrop in the east bank of the river 10 km WNW of the army station at Amdo [Amdo sheet, grid ref. 63,698E 35,781N]. Bioclastic limestone with almost monotypic accumulation of oyster shells, probably *Nannogyra* (NJM). Jurassic or Cretaceous brackish marine facies [?Zhamunaqu Formation].

Locality M175. As above, slightly upstream. Bioclastic limestone with large erect in situ colony of *Cladocoropsis* (BRR). Upper Jurassic ?Zhamunaqu Formation. Shallow but protected marine facies.

Locality M191.1. Tan mudstone blocks in pink marble outcrops in gullies above the east bank of the river adjacent to and below the thrust plate of red arenites 12.3 km SSW of Erdaogou Station [Erdaogou sheet, grid ref. 64,786E 38,242N].

Palynomorphs (MCB)
Osmundacidites, *Tsugaepollenites*, *Classopollis* and Mesozoic bisaccates suggest a Jurassic – early Cretaceous age.

Locality M201. Pale concretionary (?freshwater) limestones loose on the south slope of an east/west trending ridge, about 16 km SW of Erdaogou Station [Erdaogou sheet, grid ref. 64,786E 38,242N].

Locality M206.5. Low outcrops of pale sands and marls in gullies on west bank of dry stream bed 1.8 km due north of main Lhasa–Golmud road, 17 km NE of the bridge over the Tuotuo River [Yaxicuo sheet, grid ref. 64,625E 38,038N].

Locality M216. Pale concretionary (?freshwater) limestone forming a low outcrop adjacent to the west side of the main Lhasa–Golmud road on south slope of low hill, about 23.2 km WSW of Erdaogou Station [Erdaogou sheet, grid ref. 64,772E 38,071N]. All Neogene lake bed deposits, probably Pliocene in age.

Palynomorphs (MCB)
'These three samples are from different localities but are treated together here because their origin, preservation and taxonomic composition shows they are from the same sequence of deposition, though M201 has very few angiosperms. M216 has the most abundant pollen and the most diverse assemblage. Palynodebris is very rare in all three samples.

'More than 10 specimens of each of the following form genera have been identified in the oxidized preparations (see Jansonius & Hills 1976 for descriptions of these taxa):
Polypodiidites
Pityosporites spp.
Abiespollenites
Piceapollenites
Cedruspollenites
Tsugaepollenites
Inaperturopollenites
Cycadopites
Monocolpopollenites
Graminidites
Tricolpopollenites spp.
Ilexpollenites
Tricolporopollenites spp.
Polyvestibulopollenites
Trivestibulopollenites spp.
Myricipites spp.
Momipites spp.
Chenopodipollis spp.
Ericipites

'As indicated, some of these form genera are represented by many different form species, and there are rarer specimens of other form genera not listed. Comprehensive studies of Neogene pollen and spores have been published from two regions in Asia, N.E. India and eastern China. Though neither is sufficiently close to these Tibetan deposits for ideal geographical comparison, there is sufficient palynological similarity to suggest that these intervening Tibetan samples contain fossils from the same floristic province.

'The Indian and Chinese Neogene assemblages are described by Baski (1971) and Song *et al.* (1985) respectively. These Neogene assemblages have a temperate aspect, lacking sub-tropical taxa, and show surprising similarities with the relatively well described Neogene palynology of Europe. Although there is a distinct Neogene character to the palynology, and an absence of equally distinctive Palaeogene forms, most assemblages have a strong facies-related element, as might be expected for terrestrial deposits. These three deposits may record stages in the development of an inland lake deposit. Upland conifers whose bisaccate pollen were distributed by wind and rivers to the very young lake (M201) were later joined by pollen from plants growing at the edge of the larger lake (M206). It is in this sample that the most diverse assemblage of pollen is preserved. As well as numerous bisaccate pollen from the hinterland conifers, the assemblage includes pollen from plants such as the Taxodiaceae, Betulaceae, Fagaceae and Myricaceae, which may have grown at the edge of the lake.

'The multiporate pollen referred to here as *Chenopodipollis* is enigmatic within such a reconstruction, despite its abundance both in these samples and in those described by Liu & Tang (1980), Song (1981), Sun (1981) and Zheng *et al.* (1981). Zheng *et al.* (1981), Horowitz (personal communication) and others assign such fossil pollen to the Chenopodiaceae, a family whose 75 modern genera are nearly all halophytic. Such plants are abundant today on the salt steppes of eastern Asia and the Himalayas, usually in xerophytic conditions. This is an enigma, because plants from such environments are rarely fossilized. If *Chenopodipollis* really does come from plants of this family, either the pollen was transported some distance from the dry steppes to this lake bed or the Neogene species enjoyed wet habitats just as some modern species (e.g. *Chenopodium rudrum* and *C. botryodes*) do today.

'On the basis of this evidence any age determination more accurate than 'Neogene' is speculative. However, comparing the overall character of these samples with the results of recent Chinese work shows a clear similarity with Pliocene material. Assemblages described by Sun (1981), Liu & Tang (1980), Song (1981) and Song *et al.* (1985) also have a high proportion of Chenopodiaceae-type pollen, which these authors asign to the Pliocene, rather than the Miocene. If this feature is genuinely stratigraphical and not facies related, then it suggests that the above assemblage is also Pliocene in age.'

Locality M225. Grey limestone outcropping as loose fragments on the west shoulder of the hill on the east/west trending ridge, 2 km due south of the main Lhasa–Golmud road, about 32 km SW of Erdaogou Station [Erdaogou sheet, grid ref. 64,686E 38,071N].

Foraminifera (JEPW)
A dolomite with poorly preserved Triassic foraminifera, including *Angulodiscus* (*Involutina auct.*) and *Trochonella* (*Trocholina auct.*). Similar faunas are known from the late Triassic (Norian) of the West Carpathians (Salaj *et al.* 1983) and elsewhere. Age; late Triassic, probably Norian.

Locality M275. Pale lake bed marls outcropping in interfluve 17.5 km ESE of the Kunlun Pass (just south of the trace of the Kunlun Pass fault) [63rd Station map, grid ref. 66,170E 39,476N]. Probably Pliocene.

Palynomorphs (MCB)
'There is no palynodebris but there are single specimens of *Compositoipollenites*, *Pityosporites* and *Graminidites* present. These taxa are also present in the ?Pliocene assemblages of M201–M206 (see above) and may have come from the northern part of the same lake deposit.'

Locality M335/7. Loose limestone blocks derived locally from mountains 1–3 km to the north in a side valley on the north side of the Dongdatan, 56 km ESE of Naij Tal Station [Reshui sheet, grid ref. 67,007E 39,653N].

Foraminifera (JEPW)
'A bioclastic limestone with abundant smaller Permian foraminifera, including *Hemigordius*, *Pachyphloia*, and *Glomospira*. *Pachyphloia* is not known in earliest Permian and similar species to these are known in Murgabian or equivalent strata of the Tethyan realm. Age; Permian, probably Late Permian but of a different facies than the fusuline – bearing limestones.' (See plate 1, figure 5).

'Another sample contains the fusulines *Kahlerina* and *Nankinella* with an associated foraminiferal fauna including *Bradyina* and *Climacammina*. According to Ross (1967), *Kahlerina* is restricted to the Murgabian; similar species are figured from Tibet by Wang *et al.* 1981) from the Lasaila Limestone. Age; Late Permian, Murgabian [= Kazanian/Ufimian of western workers: = Maokouan of Chinese workers].'

Bryozoans (PDT)

'Thin sections show rhabdomesine cryptostomes, hexactinellid? cystoporates and fistuliporid cystoporates including – *Fenestella* sp. s.l., *Polypora* sp., *Streblotrypa* (*Streblotrypa*) sp. and a cystodictyonid cystoporate cf. *Filiramoporina*. This tends to indicate a Permian age, possibly Lower Permian'. [?Equivalent to the Wanbaogou valley Hongshuichuan Formation].

Locality N20.4. Outcrop of pale marls and silts on eroded eastern face of low hill, 200 m north of dirt road, about 76 km directly WSW of Dongqiao [Dongkaco sheet, grid ref. 62,230E 35,345N].

'Pharyngeal tooth of a Barbine fish, Family Cyprinidae' (CP) and indeterminate fresh water ostracods.

Locality S2.31. A biomicritic, slightly brecciated limestone overlying ophiolites to the west of Nam Lake and south of Gyanco village [no map reference]. In thin section a biomicrite wackestone with oyster and echinoderm debris (including echinoid spines), much of it algal coated and bored, and micromorphic gastropods.

Foraminifera (JEPW & MDS) – 'some large agglutinating foraminifera: a cyclamminid and/or *Haplophragmoides*, and algae. A second specimen contains the foraminifera *Buxicrenata*, *Neotrocholina* and a *Nautiloculina* similar to forms described by Bayliss (1966) from the Bau Limestone of Sarawak (late Jurassic – early Cretaceous).

This specimen also contains algae, determined by GFE and MDS. The algae are a profusion of a *Permocalculus* sp. (very uniform and finely pored, probably a new species), rare *Thaumatoporella parvovesiculifera* (Raineri) Pia and an indet. dasyclad, possibly *Salpingoporella* sp. Age: the algae suggest early Cretaceous but the top Jurassic cannot be ruled out. The foraminifera, on the other hand, support an early Cretaceous pre-Barremian age.'

Locality S2.33. Grey, fine-grained *Orbitolina* limestone 1 km north of the northwest edge of Nam Lake [no map reference]. Langshan Formation; Lower Cretaceous.

Foraminifera (JEPW & MDS)
'An *Orbitolina* limestone. Embryons are large and advanced with well developed alveolae suggesting *O.* (*Mesorbitolina*). Age: early Cretaceous, Albian.' (See plate 1, figure 13).

Locality S2.34. Grey, fine-grained *Orbitolina* limestone outcropping as a shore cliff on the northwestern corner of Nam Lake [no map reference]. Langshan Formation, Aptian/Albian, Lower Cretaceous.

Foraminifera (JEPW & MDS)
'An *Orbitolina*-limestone. Embryons of both *O.* (*Mesorbitolina*) and *O.* (*Orbitolina*) are present (species superficially similar to *O. concava*). Age: early Cretaceous, late Albian.'

Locality S2.43. Dense light grey conchoidally fractured limestone lenses in volcanics, probably of a melange type, 1 km south of Amdo.

Foraminifera (JEPW & MDS)
'Contains some foraminifera but preservation is poor; they are probably *Pseudocyclammina* and *Everticyclammina*. Age: late Jurassic or early Cretaceous.'

Locality S142. Limestone 'above' ophiolite in sequence of intersliced and imbricated units by track running N–S on western side of Nam lake [no map reference].

An algal-bound micritic limestone with numerous indeterminate ostracode valves, some indeterminate small foraminifera and algal fragments of *Halimeda* or a related genus (determination by GFE). Age: Not older than Lower Cretaceous.

Locality S144. Limestone near the northwestern corner of Nam lake [no map reference]. Late Jurassic.

A large *in situ* colony of *Cladocoropsis* (BRR).

Locality S149. Outcrop of limestone about 500 m to the east of the track running N–S approximately 5 km due west of Nam lake [no map].

Corals

Locality S154. Bioclastic limestone with foraminifera outcropping 3 km north of the NW edge of Nam Co, overlying red beds. Early Cretaceous: Albian.

Foraminifera (JEPW & MDS)

'An *Orbitolina* limestone containing *O.* (*Mesorbitolina*) and *O.* (*Conicorbitolina*). Other larger foraminifera include *Daxia*, *Cuneolina*, and *Buccicrenata*. Age: Early Cretaceous, late Albian.'

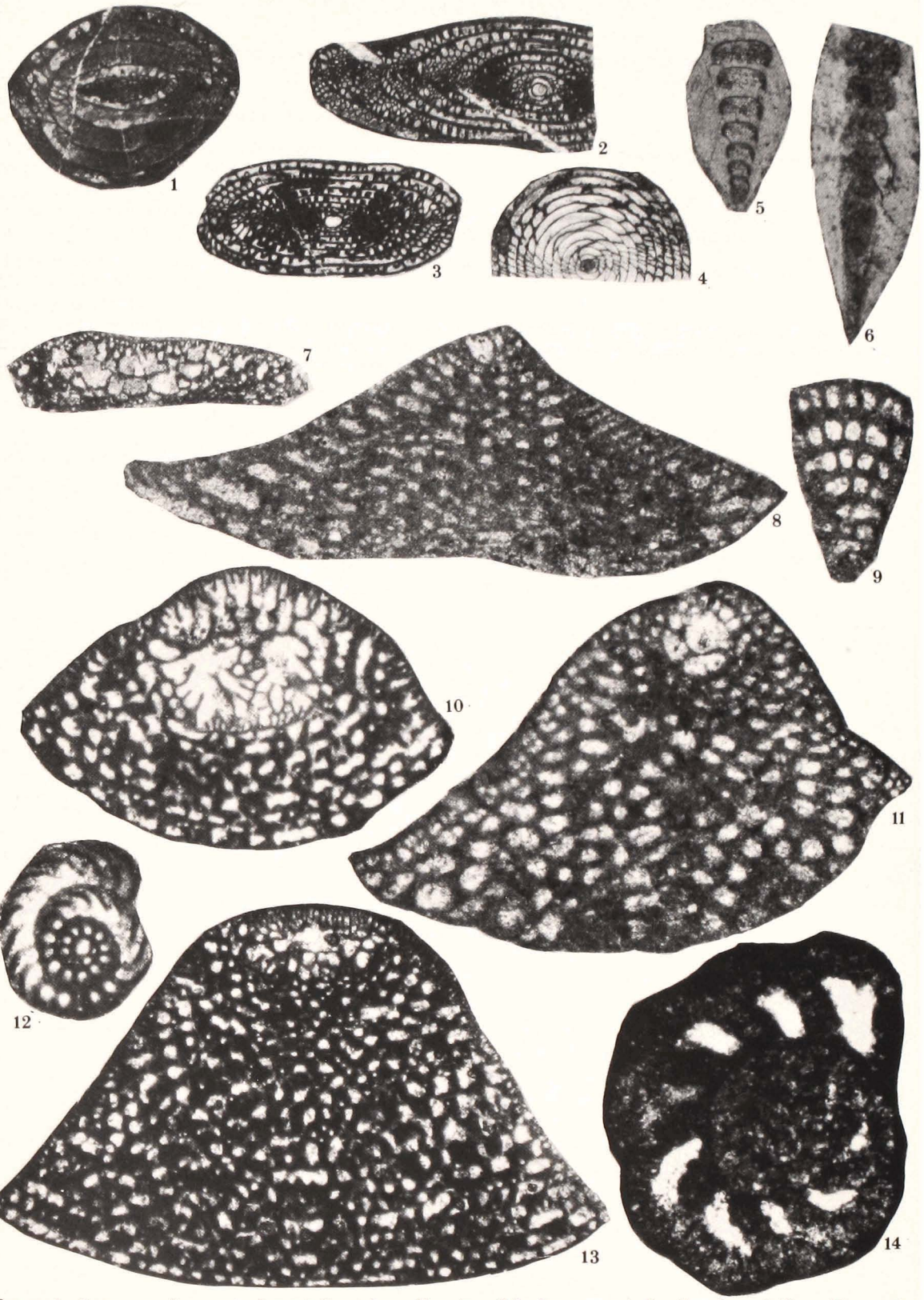

PLATE 1. Some age-diagnostic foraminifera. Late Permian (Maokoan stage) fusuline foraminifera. Figure 1. *Rugososchwagerina*. Lobadoi Formation, locality B2, × 5. Figures 2, 3. *Parafusulina* s.l. Kaixinling Group, localities B59 (fig. 2) and B60 (fig. 3), both × 5. Figure 4. *Verbeekina*. Kaixinling Group, locality B60, × 5. Smaller benthic foraminifera. Figure 5. *Pachyphloia*. Dongdatan Valley, Kunluns, locality M335/7, × 65. Figure 6. *Pachyphloia*. Lobadoi Formation, locality B2, × 65.

Some age-diagnostic Cretaceous (late Barremian to late Albian) foraminifera. Figure 7. *Palorbitolinoides*: (embryonic apparatus only). Langshan Formation, locality B25.33, × 32. Figure 8. *Eopalorbitolina*. Langshan Formation, locality B25.72, × 80. Figure 9. *Cuneolina*. Langshan Formation, locality B25.66, × 80. Figure 10. *Orbitolina (Mesorbitolina)*. Langshan Formation, locality B24, × 32. Figure 11. *Orbitolina (Mesorbitolina)*. Langshan Formation, locality B25.66, × 80. Figure 12. *Daxia*. Langshan Formation, locality B25.54, × 32. Figure 13. *Orbitolina (Mesorbitolina)*. Langshan Formation, Nam Co area, locality S2.33, × 32. Figure 14. *Pseudocyclammina*. Xiaqiongcuo Formation, locality B30, × 32.

(*Facing p.* 104)

Locality S155. Bioclastic limestone outcropping 6 km north of the NW edge of Nam Co lake and about 3 km south of She lake. Early Cretaceous.

Foraminifera (JEPW & MDS)
'An *Orbitolina* limestone; no embryons seen. Age, early Cretaceous.'

Locality S196. A dolomite containing many small foraminifera in a brecciated limestone sequence 4 km SE of Dongqia [Dongqiao sheet, grid ref. 63,020E 35,415N].

Foraminifera (JEPW)
'Abundant specimens of *Glomospira*. Although this genus has a long range, monotypic faunas like this are usually indicative o early or mid Triassic (see Zaninetti & Whittaker 1980). Age: early or mid Triassic, Scythian or Anisian.'

Locality S304. Outcrop of marl on the western side of the road at a low limestone ridge [Fenghuoshan sheet, grid ref. 65,014E 38,762N]. ?Pliocene lake beds.

Palynomorphs (MCB)
'The oxidized preparation yielded 10 badly preserved bisaccates, most likely Neogene, but no other palynomorphs and more o less no palynodebris. The unoxidized preparation yielded two well preserved specimens of Neogene *Pityosporites* and three or fou badly preserved palynomorphs of what may be reworked taxa.'

Phil. Trans. R. Soc. Lond. A **327**, 107–143 (1988) [107]
Printed in Great Britain

Sedimentology, palaeoecology and palaeoenvironmental evolution of the 1985 Lhasa to Golmud Geotraverse

By M. R. Leeder[1], A. B. Smith[2] and Yin Jixiang[3]

[1] *Department of Earth Sciences, University of Leeds, Leeds LS2 9JT, U.K.*
[2] *Department of Palaeontology, British Museum (Natural History), Cromwell Road, London SW7 5BD, U.K.*
[3] *Institute of Geology, Academia Sinica, P.O. Box* 634, *Beijing, People's Republic of China*

[Microfiche in pocket]

Vertical and horizontal measurements of almost 30 km of sections were made along the Geotraverse route at 113 localities ranging in age from Ordovician to Tertiary. Over 280 palaeocurrent measurements were taken and 200 thin sections were studied. Ordovician strata occur only in the Kunlun Terrane, where thick metamorphosed sequences of clastics and carbonates occur. These are tentatively interpreted as platform margin and slope deposits. During Carboniferous times in the Kunlun Terrane transgressive late-Dinantian marine limestones with tropical to subtropical Eurasian reefoidal faunas overlie fluviatile redbeds derived from an unroofed orogenic belt. The Lhasa Terrane contains shelf basin clastics with low-diversity faunas succeeded by thick late Carboniferous/early Permian glacio-marine mixtites deposited by iceberg meltout. Permian carbonate ramp and shelf facies with reefoidal developments occur over both the Lhasa and Qiangtang Terranes, with coal-bearing clastics and fluviatile redbeds also occurring in the latter. Permian sequences in the Kunlun Terrane comprise resedimented tuffaceous shelf basin clastics overlain by shelf carbonates. Triassic rocks are widely distributed. Those of the Lhasa Terrane are predominantly carbonate ramp and platform margin/slope facies showing evidence for shelf breakup due to extensional tectonics. Qiangtang sequences occur below and above a thick andesite lava development. Those below are mature fluviatile gravels derived from the north. The strata above the arc-related volcanics are typical shoaling-upwards carbonate ramp facies. Thick sequences in the southern Kunlun Terrane are tentatively ascribed to passive continental rise deposits of countourite drift aspects. Those in the northern areas are highly immature coarse clastics derived as alluvial fans from an Anisian–Carnian granitoid intrusive belt to the north. Jurassic sequences are unknown in the Kunlun Terrane. In the Qiangtang Terrane very thick (c. 5 km) sequences of clastic redbeds are interpreted as fluviatile and coastal plain molasse derived from the newly formed Kunlun orogen to the north. These intertongue southwards with marine shelf carbonates and clastics. The northern Lhasa Terrane contains thick clastic mudrocks and turbiditic sandstones of shelf basin aspects. Pelagic cherts and clastics overly oceanic pillow lavas, with ophiolitic ultrabasics capped by ferrosiallitic duricrusts and overlain by late Jurassic marine limestones. Cretaceous rocks are only known in the Lhasa Terrane. North of Lhasa they comprise northerly-derived fluviatile redbeds of molassic aspects which record the formation and uplift of the Jinsha/Banggong orogen. 300 km NW of Lhasa probable Neocomian fluviatile clastics are overlain by Lower Cretaceous marine carbonate buildup and lagoonal facies. Tertiary successions are almost entirely continental and record fluvio-lacustrine deposition in a number of basins which are thought to have originated as thrust-related features during major crustal shortening of the Tibetan Plateau in the Palaeogene and Neogene.

Introduction and methodology

Once sedimentary rocks have been dated palaeontologically (see Smith & Xu, this volume), they can yield much information of value to the tectonic interpretation of displaced terranes and collision orogenic belts like the Himalaya/Tibet Plateau. With the aid of palaeoecological data, facies analysis of the stratigraphic record of individual terranes enables the evolution of depositional environments to be deduced throughout time. This evolution can then be linked with other geological data to retrieve the basin and plate tectonic history. Critical to this approach is the accurate vertical and horizontal measurement of sedimentary sequences, with field records made of lithology, grain size, grain size trends, bed contacts, sedimentary structures, faunas and floras. During the Tibetan Geotraverse, almost 30 km of sections at 113 localities were logged in this way, albeit many at a rapid reconnaissance pace.

The evolution of a multiple-accreted terrane is usually accompanied by the periodic shedding of fluviatile molasse wedges into the subsiding continental margin or foreland basin of the youngest accreted terrane. Vital information concerning palaeoslope, orogenic vergence and unroofing trends is contained within such sequences and, once the fluviatile nature of the rocks is established, this data can be released by the complementary study of both palaeocurrents and petrography. Over 280 palaeocurrent measurements were taken. They are subdivided according to locality, age and the hierarchy of the measured structure in figure 17, see microfiche. In addition, over 200 thin sections were cut from sedimentary rocks and subjected to qualitative modal analysis, selected Carboniferous fluviatile sandstones being point-counted for 10 constituents. Field observations on pebble and boulder compositions are a more valuable indication of provenance than the sand-sized fraction and data of this kind are used wherever possible.

There are several kinds of evidence that the study of fossils can provide about palaeoenvironments. Trace fossils are rarely reworked and can therefore provide direct evidence of depositional setting, e.g. degree of sediment lithification, rates of sedimentation, environment of deposition. Taphonomic studies focus on the various processes that take place between death and discovery of the fossil assemblage. Critical information on the degree of reworking of an originally *in situ* community is essential for environmental analysis. Mode of life of individual species within a community structure can be deduced by a combination of functional morphology studies and comparison with extant communities. Valuable environmental constraints emerge from such studies

In the sections which follow, we discuss the sedimentary evolution of the Tibetan Geotraverse segment for successive geological periods, dividing each period between the Lhasa, Qiangtang and Kunlun Terranes. The emphasis is placed upon the factual record in each Terrane, followed by environmental and palaeogeographical deductions and hypotheses. In a later section we summarize the palaeogeographical evolution of the Tibetan Plateau (figure 16). The major sections of strata examined in each Terrane for the various geological periods are summarized in figures 1, 2, 6, 8, 9, and 11. For exact localities, see Kidd *et al.*, (this volume, field maps; see microfiche).

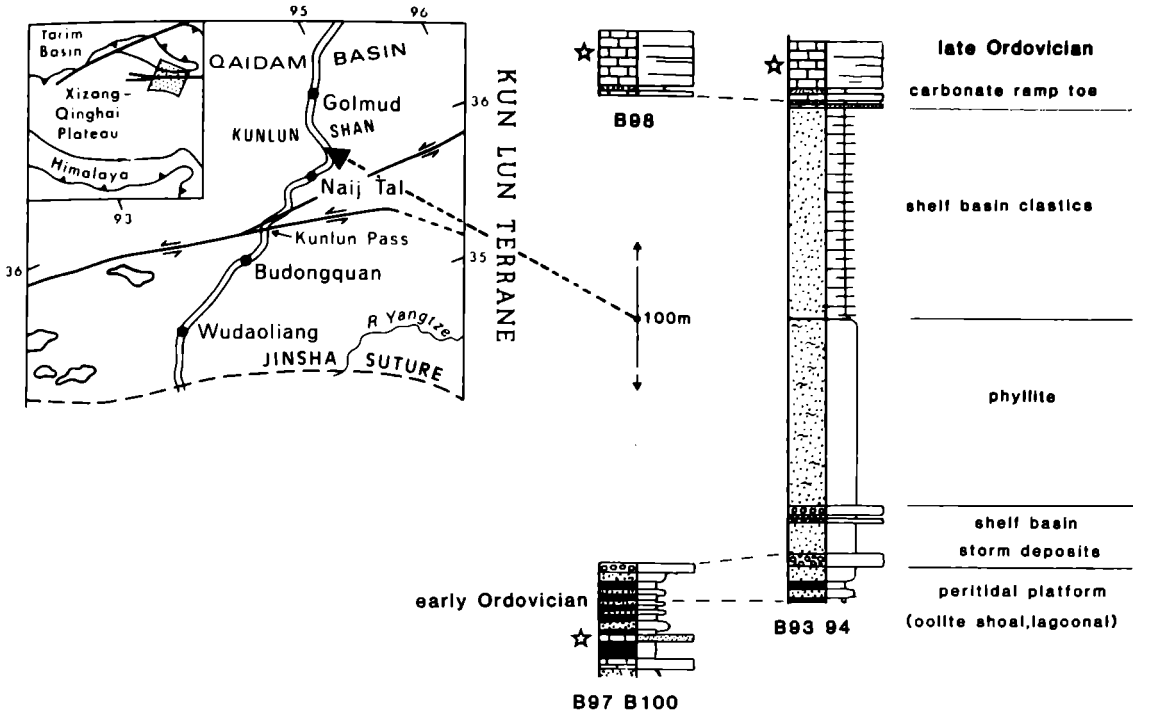

FIGURE 1. Ordovician lithofacies and tentative proposed correlations in the northern Kunlun Shan. B97, B98 etc. refer to localities.

ORDOVICIAN

Ordovician strata were encountered by us only in the Kunlun Shan where thick low-grade metamorphic sequences of clastics and carbonates were logged (figure 1). The considerable tectonic overprinting in this region has unfortunately destroyed almost all primary sedimentary features and much of the fossil content, making interpretation of these sequences difficult.

The best exposures were studied in the northern Kunlun Shan, close to Shuinichang just to the northeast of Naij Tal (localities B93, B101, figure 1). Here the oldest beds, dated as late Cambrian or early Ordovician on the strength of a unique trilobite fragment (locality B100, see Smith & Xu, this volume, Appendix), are dark blue or black graphitic phyllites interbedded with green quartz phyllites and three limestone beds, several metres in thickness, one of which is oolitic. The presence of organic-rich shales and oolitic limestones with trilobites suggests a platform margin origin for some of these facies. Above this comes quartz mica phyllite with two or three major (up to 60 cm thick) matrix-supported conglomerates. The highly-strained clasts, which are coarse and reach 30 cm diameter, are predominantly of white limestone and quartz, with subsidiary green and purplish sandy phyllite clasts. No igneous clasts were seen. The conglomerates may be debris flow deposits formed in a shelf-basin or on a platform slope. Next comes a thick succession of poorly bedded pale-green quartz mica phyllites, with no primary structures from which to interpret their facies. These grade up into well-bedded dark grey fine quartz wackes and slates which also lack primary sedimentary structures but which may be turbidites.

The topmost strata in the sequence are thick-bedded fossiliferous micritic limestones of late

Ordovician age (see Smith & Xu, this volume, Appendix, localities B93, B98). The fauna of shallow water corals and stromatoporoids appears to be allochthonous and restricted to possible storm deposit horizons; the sequence may have formed on the distal portion of a carbonate ramp.

Another belt of low grade metamorphosed sediments is found in the central Kunlun Shan. These were studied along the road section between the Xidatan and Wanbaogou, to the southwest of Naij Tal. There is no fauna from which to determine the age of this sequence, but the presence of spectacular quartz/white limestone conglomerates, identical with those described above from the northern Kunlun Shan, leads us to suspect a broadly similar age for the two successions. Near the base there are amphibole garnet schists of igneous origin; but whether intrusive or extrusive is impossible to determine. Most of this thick succession is made up of metamorphosed sandstones and mudrocks with occasional intercalations of thin-bedded and predominantly calcareous strata. Near the top of the sequence is a thick coarse conglomerate of quartz and white limestone pebbles, which we interpret as a debris flow.

The highly tentative correlation of the two sequences suggests that the central Kunlun Shan succession is Cambro-Ordovician in age. This is based on the assumption that the white limestone conglomerates are approximately equivalent and that most of the central Kunlun Shan succession lies stratigraphically below that seen to the east of Naij Tal.

Carboniferous (figure 2)

Carboniferous sedimentary rocks are known from the Lhasa and Kunlun Terranes along the Traverse route (figure 2). No exposure of Carboniferous in the Qiangtang Terrane was studied by us but sequences with facies and faunas similar to those of the Lhasa Terrane are known far to the west in the southern Karakoram Mountains (Norin 1946; Liang *et al.* 1983). In addition facies and faunas of Kunlun aspect are reported to the east around Qamdo (Dong & Mu 1984) as well as just to the west of our traverse route in Zhado County (Dong & Mu 1984).

(*a*) *Lhasa Terrane*

Stratigraphic sequences, comprising parts of the Pondo Group, were logged in detail at three localities; the columns in figure 2 summarize the major characters of the successions. The predominating mudrocks and siltstones are generally deformed and strongly cleaved, features preventing an accurate estimate of thickness. The whole Carboniferous section may exceed 1 km in thickness.

The lithofacies of the Pondo Group are dominated by dark grey mudrocks of shelf-basin origins. These contain abundant late Carboniferous fenestellid bryozoans, bivalves, brachiopods and crinoid debris, as at localities B19/B20 near Damxung. The crinoidal debris occurs in thin, sharp-based and sometimes graded laminae and is clearly allochthonous, probably of storm origins. The well-preserved bryozoan fronds are almost certainly preserved *in situ* and are indicative of a low energy environment, probably below all but storm wave base. Shallower shelf-basin facies, deposited above wave base, are represented by mudrocks with interlaminated siltstones and lenticular siltstone and fine sandstones with wave-ripple formsets and sparse-to-common bioturbation.

These fine-grained sequences are succeeded by a spectacular mixtite horizon which may be

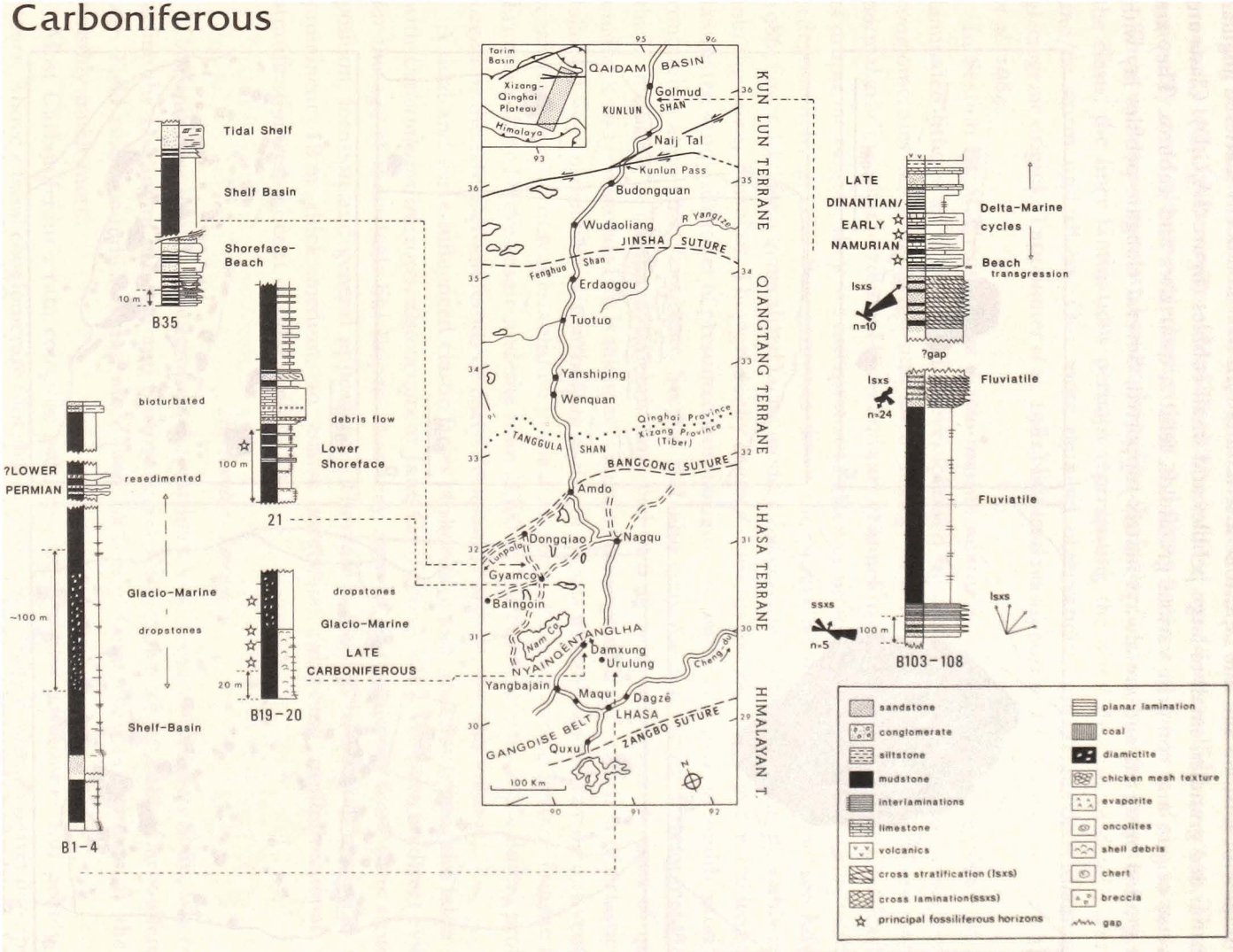

FIGURE 2. Distribution of Carboniferous measured sections, their lithofacies, environmental interpretations, age determinations and palaeocurrent distributions. See text for discussion and further data. Inset provides general key for this and subsequent diagrams.

up to 100 m thick, although given the poor degree of exposure and correlation there may be several such horizons. Fossils place the age of the mixtite close to the Carboniferous–Permian boundary (Smith & Xu, this volume). The mixtite lithofacies comprises silty mudrocks, sometimes with siltstone and fine sandstone interlaminations in which occur scattered angular to subrounded granules, small to large pebbles and small cobbles (figure 3A,C,D). Clasts are of diverse origins and comprise various granitoids, felsites, quartzites and gabbros. They are never graded or sorted and are always matrix-supported. Several elongate pebbles lay with

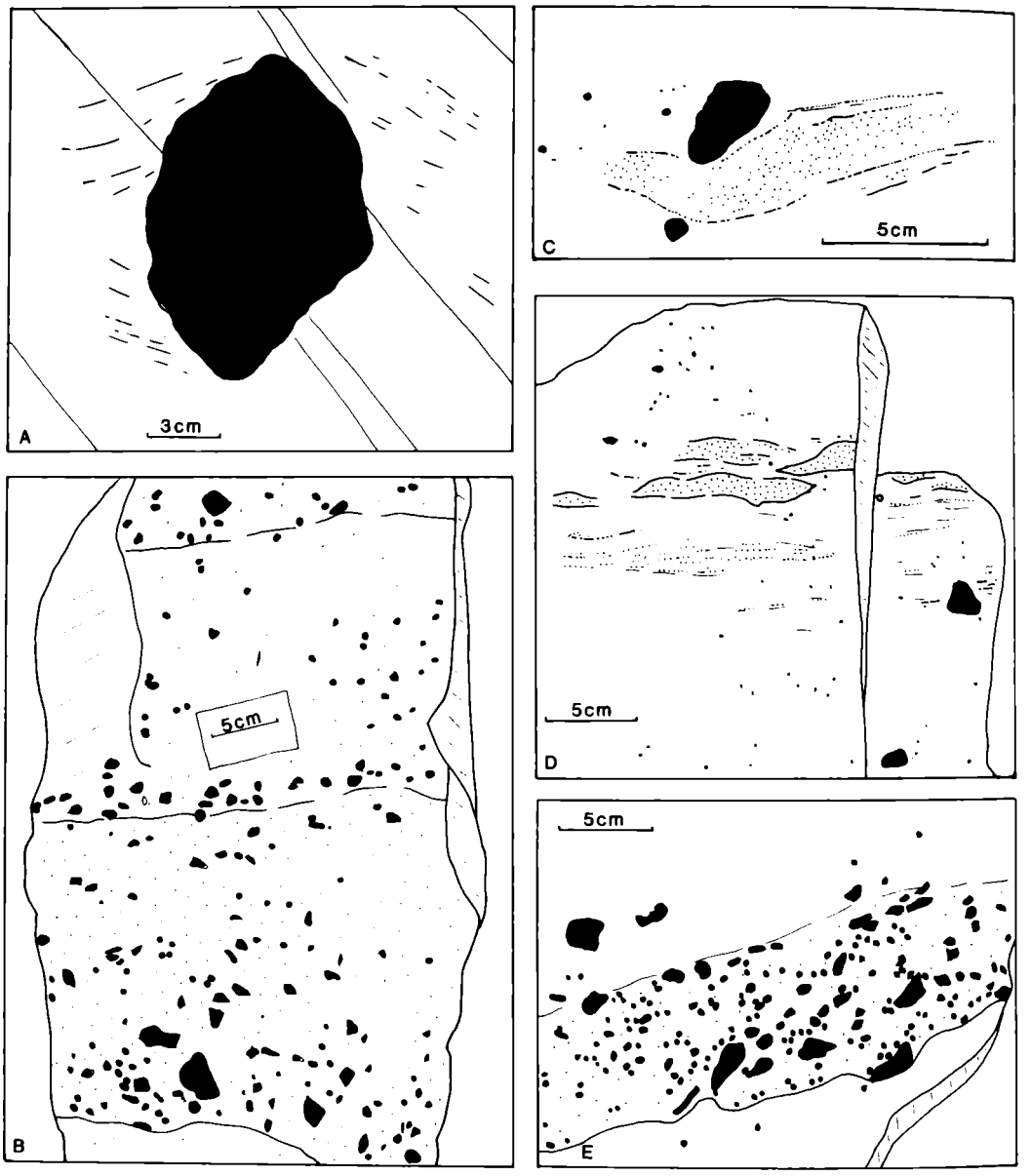

FIGURE 3. Sketches from photographs and field observations to show various late Carboniferous glacio-marine facies in the Lhasa Terrane. 3A Large andesitic dropstone observed to cut faint lamination traces in cleaved mudrock. NW SE lines represent cleavage planes. Locality B34, 3B Resedimented pebbly sandstones showing crude grading and well defined internal bedding contacts. Locality B1, 3C, D Small dropstone clasts in laminated mudrocks. Locality B1, 3E Channelized pebbly sandstone lens with sharp basal contact overlying mudrock, possibly a resedimented product of turbidity flow. Locality B1.

their long axes at a high angle to the bedding. Three examples were seen where pebbles had apparently cut across pre-existing siltstone interlaminations (figure 3A). Two showed fine multiple striations on their surfaces. At localities B19/B20 the lower contact between the clasts defining the mixtite and the underlying mudrocks is sharp, with the clasts occurring in close proximity to an *in situ* community of brachiopods, bivalves and fenestellid bryozoans. There are noticeably more siltstone interlaminations and fewer bryozoa at the base of the mixtite.

These various features are best explained on the basis of a glacio-marine dropstone origin for the clasts, the finer laminations perhaps representing the distal deposits of density currents and/or storm underflows. Our more detailed observations support previous diagnoses of glaciogenic origins (Tapponnier *et al.* 1981) but lend no support to alternative theories (Allègre *et al.* 1984).

In Section B1 at Urulung the glacio-marine mixtite is succeeded by a sequence of interlaminated lithofacies as described above, followed by pebbly coarse-grained sandstones and conglomerates showing grain-supported clasts, well-developed bed boundaries, internal normal grading, sharp erosional bases and rare channel-like forms (figures 3B, 3E). Clearly not of dropstone origins, they are interpreted as glaciogenic sediment from subaqueous moraines, redeposited by gravity flow processes down the proglacial depositional slope (see Edwards 1986, figure 13.6 for a generalized facies model). Successions above these units probably extend into the Lower Permian. They gradually coarsen upwards through wave-generated lenticular-laminated sandy siltstones of presumed storm origin into highly bioturbated muddy sandstones containing abundant *Teichichnus*. Section B21 also contains a limestone development (20 m thick) including a spectacular debris flow bed (1.5 m) with cobble-sized clasts of quartz, mudrock and limestone. This is taken as evidence for the gradual progradation of a clastic slope followed by construction of a carbonate platform bypass margin in a nearby area. Eventually a carbonate platform was established in the area north of Lhasa during Permo–Triassic times. Eruption of the Dagze basalt–andesite suite (1500 m; see Pearce & Mei, this volume) probably began in the late Carboniferous or early Permian (Smith & Xu, this volume).

A tidal and wave-influenced clastic facies of shoreface and tidal flat origin, the latter facies with *Diplocraterion* burrows, also occurs at Jang Co (Section B35). We have no direct evidence for the age of these beds but suspect that they may be Carboniferous from their structural position, location and general appearance. They are succeeded by 50 m of mudrocks and a prominent 12 m thick medium to coarse sandstone exhibiting multidirectional cross-stratification reminiscent of tidal sand facies.

(*b*) *Kunlun Terrane*

Carboniferous sequences outcrop in the northern foothills of the Kunlun Shan, where they define the Dagangou, Teqosu and Sijiaoyanggou Formations, all probably Carboniferous in age. Field evidence indicates that more than 1500 m of Carboniferous is present in the area, possibly much more.

Most Carboniferous strata comprise red-coloured siltstones, sandstones and pebbly sandstones. Above a basal conglomerate (not shown on figure 2) there is overall coarsening-upwards from siltstone to pebbly sandstones. Beds of coarser clastics, from 0.5–10 m thick, usually show sharp erosional lower contacts with either sandstone or siltstone. In the lower half of the succession fine-grained lithologies predominate (figure 2), comprising dull red silty mudrocks and thin (0.5–1.0 m), sharp-based, lithic and feldspathic sandstones with upper phase plane-

bed laminations, climbing ripple cross-laminations and rare wave-modified current ripple formsets. Palaeocurrent measurements indicate a northwest vector mean transport direction, the sediment probably having been deposited by sheet floods on low gradient alluvial cones. The red pigment is assumed to be early diagenetic.

The upper half of the sequence (figure 2, B103–108) is first dominated by thick red multistorey lithic and feldspar-rich sandstones and pebbly sandstones which show well-developed trough cross-stratification and variable palaeocurrents with a SSW vector mean. They are interpreted as of fluviatile channel origin. Clasts include feldspars, basic volcanics, marbles and quartz. One marble clast resembling nearby Ordovician lithologies has well-developed foliation. The topmost clastics show marked changes in facies and petrography. White pebbly sandstones contain more abundant quartz clasts, usually well-rounded, and only rare feldspar sand grains. Other structures resemble those of the pebbly sandstones beneath and are again attributed to fluvial channel activity. Palaeocurrents from the southwest support the deduction that a different dispersal system has now developed. Sandstone storeys are separated by up to 13 m of red mudrocks with thin horizons of calcite nodules resembling the 'cornstone' nodules of pedogenic calcrete common in the Upper Palaeozoic fluviatile redbed sequences of NW Europe and Appalachia.

The red mudrocks of the Kunlun Carboniferous are succeeded by a rapidly coarsening-upwards sequence culminating in grain-supported, imbricated quartz conglomerate. The clasts, up to 10 cm diameter, are well-rounded to sub-rounded and clearly record major reworking, probably on a marine shoreface. This is strongly supported by the overlying grey mudrocks which contain a marine fauna and a 6 m dark lime wackestone rich in crinoidal debris at the top. Succeeding strata comprise 20 m of alternating grey mudrocks and limestones before a prominent shaly coal appears. Then comes a high diversity shallow water community of brachiopods, compound rugose and large solitary rugose corals with extensive dissepimentation, broad-spreading stromatoporoids and bryozoans, all *in situ*. Compound corals are predominantly massive and tabulate. Further up the succession, in the more massive limestones, erect fasciculate coral colonies dominate, suggesting slightly deeper water. The fauna is latest Visean or early Namurian in age. The succeeding strata (> 200 m) comprise numerous cyclical alternations of marine limestones and clastics, the latter including facies of delta front and on-delta types (figure 4). These include coarsening-upwards cycles similar to modern inter-distributary bay fills; sharp-based, erosive, cross-stratified sandstones resembling crevasse or minor distributary channel deposits and thin coals and carbonaceous mudrocks of on-delta affinities. The fauna in the limestone beds is more restricted, but occasional echinoid and crinoid fragments and, less often, rugose corals confirm that fully marine conditions were periodically established from time to time throughout the entire succession.

The marine limestone/deltaic clastic cycles are remarkably similar to the late Dinantian/early Namurian 'Yoredale-cycles' that dominate the north British and North American (Kansas to Texas) successions of the Laurasian continental margins of Hercynia–Appalachia.

(*c*) *Carboniferous palaeogeography*

(i) *Lhasa Terrane*

The thick dropstone facies indicates that the Terrane lay on a continental margin within the iceberg fringe (perhaps extending to about 50° S by comparison with the Pleistocene) that

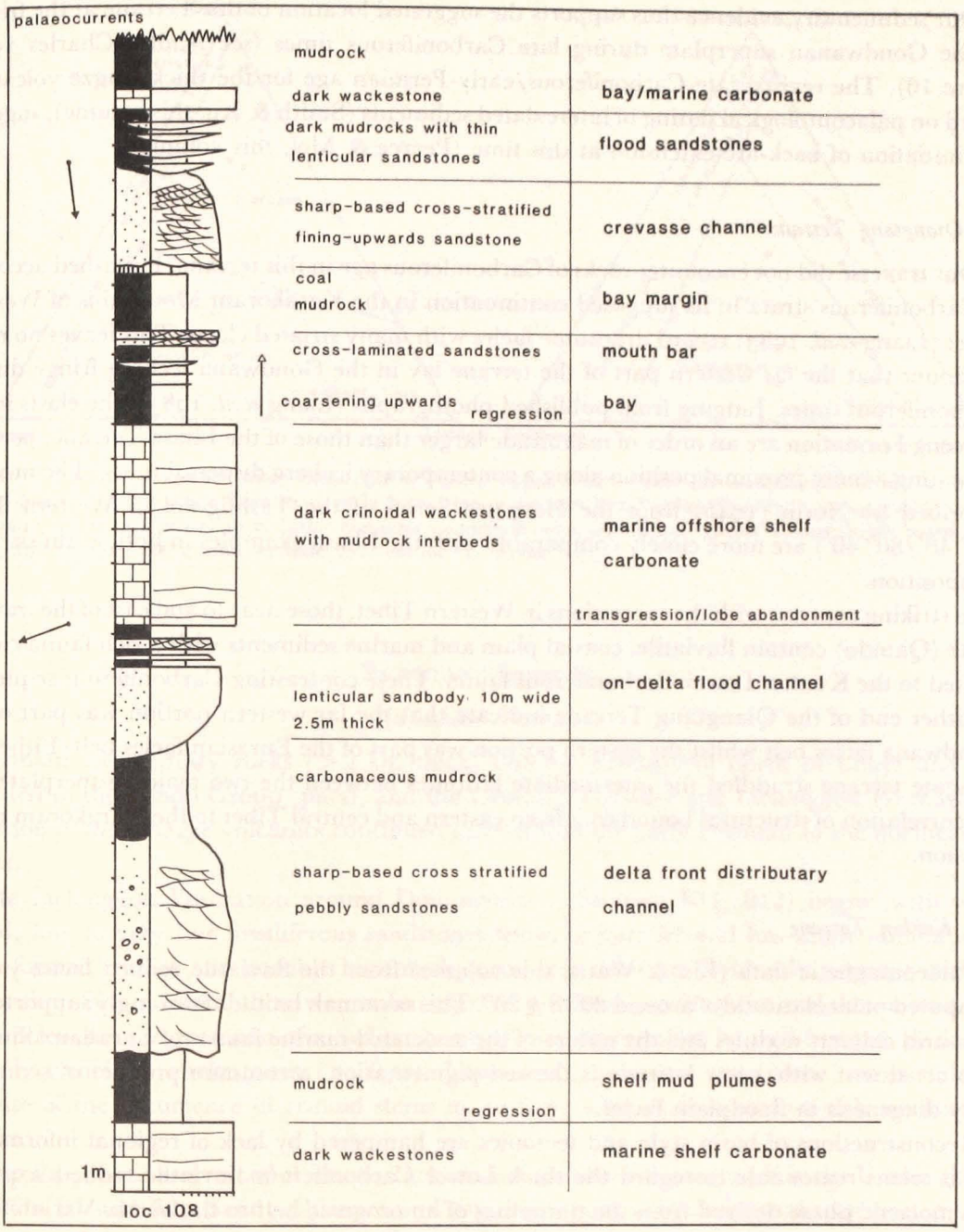

FIGURE 4. Log to show delta/marine cycles of Euro–North American 'Yoredale' aspect in the late Dinantian/early Namurian of the northern Kunlun Shan. Locality B108.

must have surrounded the icecap responsible for Permo–Carboniferous tillite deposition in South America, South Africa, North Arabia (Oman), North India and Australia (see Frakes 1979; Braakman *et al.* 1982; Powell & Veevers 1987). Our observations on clast compositions suggest a hinterland rich in granitoids and metamorphics but we have no directional structures indicating where these lay in terms of present day co-ordinates.

Our sedimentary evidence thus supports the suggested location of this Terrane at the fringes of the Gondwanan superplate during late Carboniferous times (see Audley-Charles 1984; figure 16). The revised late-Carboniferous/early-Permian age for the thick Dagze volcanics, based on palaeontological dating of intercalated sediments (Smith & Xu, this volume), suggests the initiation of back-arc extension at this time (Pearce & Mei, this volume).

(ii) *Qiangtang Terrane*

Our traverse did not encounter rocks of Carboniferous age in this terrane. Published accounts of Carboniferous strata in its supposed continuation in the Karakoram Mountains of Western Tibet (Liang *et al.* 1983) record dropstone facies with many striated clasts. This leaves no room for doubt that the far western part of the terrane lay in the Gondwana iceberg fringe during Carboniferous times. Judging from published photographs (Liang *et al.* 1983), the clasts in the Cameng Formation are an order of magnitude larger than those of the Lhasa Terrane, perhaps indicating a more proximal position along a contemporary iceberg dispersal route. The mixtites described by Norin (1946) from the Herpatso Series of the Tashlig-kol in Western Tibet (34° 40′/80° 40′) are more closely comparable with the Lhasa examples in both grain size and composition.

In striking contrast with the successions in Western Tibet, those near to and east of the traverse route (Qamdo) contain fluviatile, coastal plain and marine sediments with a rich fauna closely related to the Kunlun Lower Carboniferous fauna. These contrasting Carboniferous sequences at either end of the Qiangtang Terrane indicate that the far western portion was part of the Gondwana facies belt whilst the eastern portion was part of the Eurasian facies belt. Either the elongate terrane straddled the intermediate latitudes between the two major 'superplates' or the correlation of structural boundaries from eastern and central Tibet to the Karakoram needs revision.

(iii) *Kunlun Terrane*

Palaeomagnetic data (Lin & Watts, this volume) from the fluviatile redbed facies yield a computed palaeolatitude of around 20° S ± 20°. This savannah latitude is strongly supported by semi-arid calcrete nodules and the nature of the associated marine faunas of Eurasian affinities. Also consistent with a low latitude is the red pigmentation, a common product of semi-arid early diagenesis in floodplain facies.

Reconstructions of basin style and tectonics are hampered by lack of regional information but it seems reasonable to regard the thick Lower Carboniferous fluviatile redbed sequence as a molassic phase derived from the unroofing of an orogenic belt to the north. Variability of the palaeocurrents may indicate deposition in extensional or strike-slip basins. Petrographic data suggests derivation of the detritus from basic to intermediate volcanics (possibly Devonian in age) of island arc type and from granitoid/gneiss terranes (figure 5). A major marine transgression, possibly eustatic, during the late Dinantian was accompanied by a radical change of drainage system and establishment of a mature quartz-rich hinterland in the southwest.

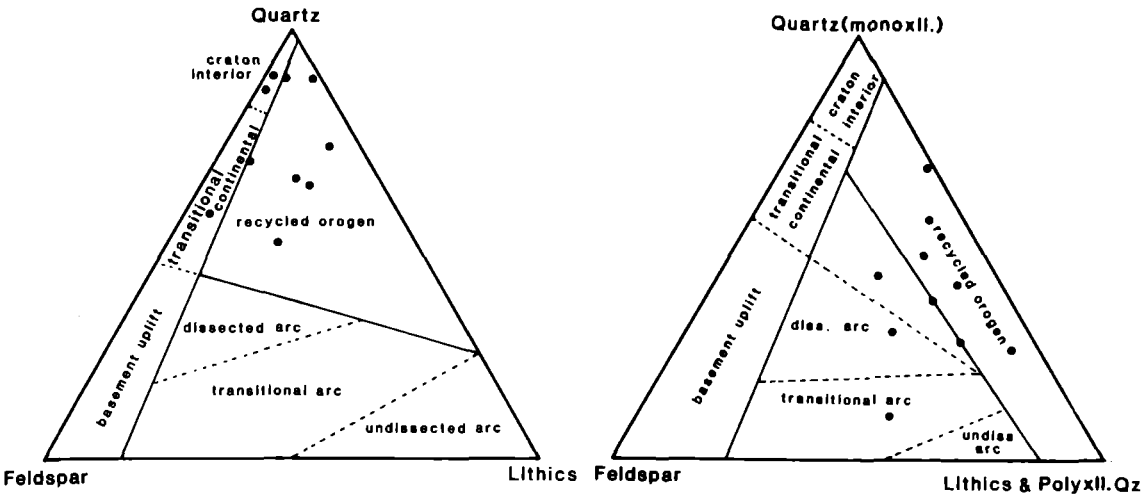

FIGURE 5. Ternary diagrams (after Dickinson & Suczek 1979) to show that the compositions of fine to coarse sandstones from the late Dinantian/early Namurian of the northern Kunlun Shan indicate a recycled orogen and volcanic arc provenance. Lithic components include common volcanic grains. Compositions based upon point counting 200 grains per slide. See text for discussion.

PERMIAN (figure 6)

(*a*) *Lhasa Terrane*

Permian sedimentary rocks (> 1 km thick) outcrop extensively north of Lhasa and are included in the Pondo Group (pars), and the Urulung, Lobadoi and Lielonggou Formations. Eruption of the Dhagze volcanics continued at least into the early Permian to the northeast of Lhasa.

The Lielonggou Formation around Doilungdeqen (Sections B11, B12) begins with well-sorted, fine to very fine fossiliferous sandstones showing parallel and low-angle laminations, wave-formed ripples and possible hummocky cross-stratification. Evidently subtidal mid- to upper-shoreface in origin, these were submerged by a relative sea level rise and thereafter acted as a nucleus for the accretion of a carbonate ramp now represented by well-bedded, dark and sparsely crinoidal wackestones (> 50 m). Low-energy ramp-toe conditions are postulated because of the occurrence of crinoid stems up to 2 cm long set in a carbon-rich wackestone matrix.

A similar, but finer-grained clastic-to-carbonate transition is documented in the Urulung area (Sections B1 and B2). Sandy siltstones and fine sandstones with occasional transported shell beds of possible storm origin are overlain by unfossiliferous, black, carbonaceous mudrocks. Higher in the sequence come occasional thin (0.5–1.0 cm) grainstones composed of bryozoan fragments. These are also probably storm deposits. The mudrocks are followed by a thick carbonate sequence which was not examined in detail. The carbonates are sparsely fossiliferous wackestones (with fusulinids and corals) and are interpreted as low-energy ramp-toe and offshore shelf facies.

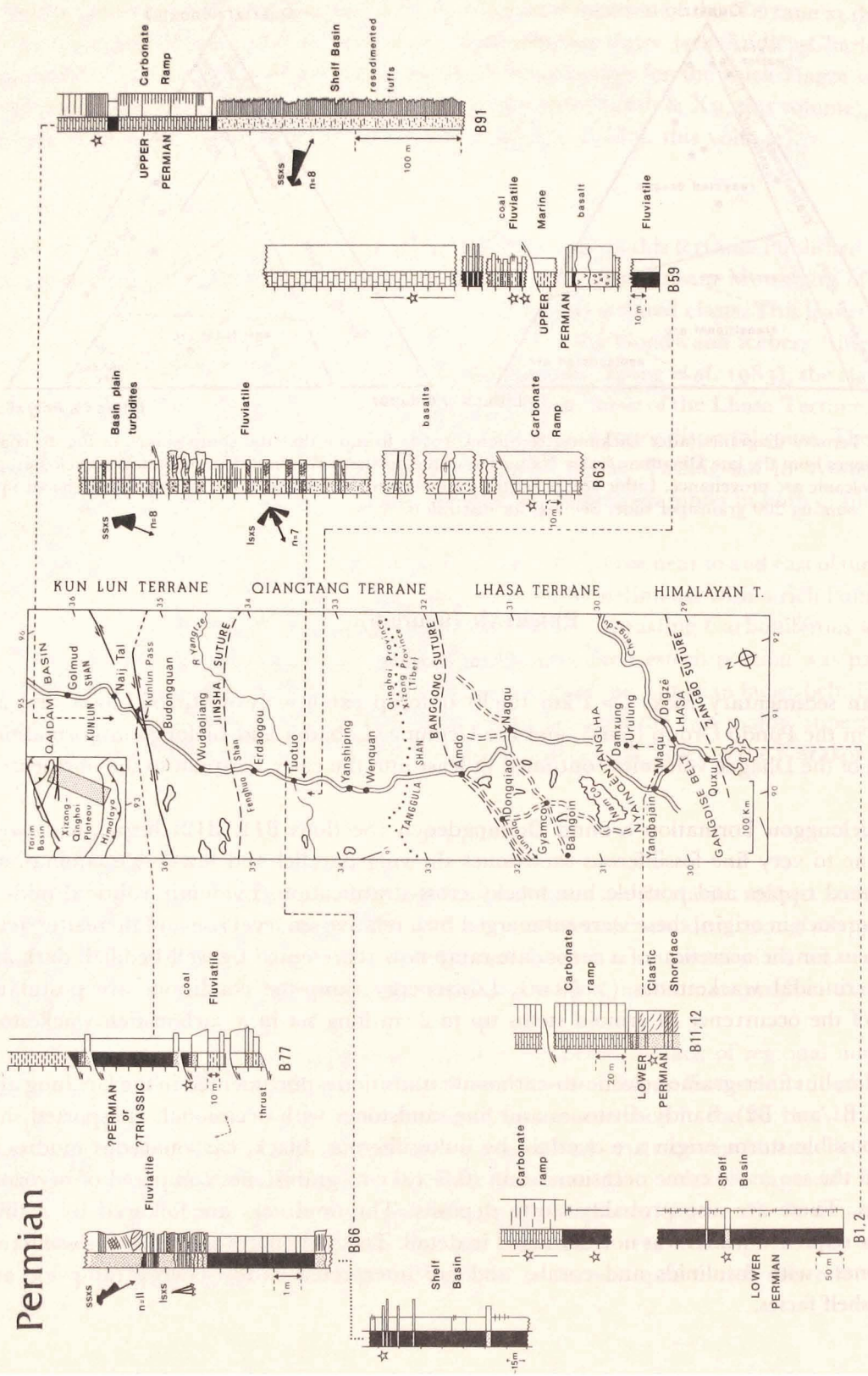

FIGURE 6. Distribution of Permian measured sections, their lithofacies, environmental interpretations, age determinations and palaeocurrent distributions. See text for discussion and further data. Key in figure 2.

(*b*) *Qiangtang Terrane*

Very thick sequences of Permian deposits crop out in the northern part of the Qiangtang Terrane around the Tuotuo River. They are included in the Kaixinling and Wuli Groups which may total over 6 km in thickness.

Section B59, south of the Tuotuo River, begins with undated variegated red/green mudrocks and thin purple sandstones of presumed continental (possibly well-drained floodplain) origin. These are succeeded by about 40 m of possibly subaerially erupted agglomerates, tuffs and basalt flows. The thick middle basalt flow shows fine vertical to subvertical tufa veins, perhaps recording a lengthy period of weathering prior to the eruption of the overlying tuffs. The volcanics are succeeded by 40 m of coal-bearing clastics with marine bands near the base dated as Longtanian (Upper Permian). The clastic lithofacies include dark grey carbonaceous mudrocks, a pale grey mudrock with well-defined vertical rootlets, 10–80 cm coals, finely interlaminated, silty-streaked mudrocks and 5–20 cm sharp-based possibly tuffaceous medium/coarse lithic-rich sandstones. This facies assemblage is inferred to have evolved from marginal marine to a sheltered bay/lake complex bounded by vegetated wetlands. The periodic sandy influxes are probably products of floods originating from distant distributary channels. A major transgression evidenced in Section B59 is recorded by a rapid upward transition via shoal-water algal packstones to thinly interbedded mudrocks and lapilli-bearing limestones. Finally a continuous spread of carbonate developed, now represented by dark, irregularly bedded fusulinid wackestones (> 200 m) with frequent horizons of chert nodules. The carbonates, dated as early Upper Permian (Smith & Xu, this volume, Appendix, Locality B59), indicate the construction of a carbonate ramp.

In an adjacent section, (B60, B61), similar fusulinid/crinoidal wackestones with abundant chert nodules are seen in faulted contact with four andesitic volcanic flows (> 60 m) of extensional rift affinities (Pearce & Mei, this volume). The lavas are interbedded with continental clastics (up to 8 m) showing southwest-directed, small-scale cross-stratification. One flow shows an irregular and highly vesiculated top capped with finely laminated chert. Succeeding thick fluviatile red beds are of uncertain age but the occurrence of possibly Permian limestone pebbles in them suggests a Triassic (or younger) age. Sedimentary structures record a palaeoflow towards the southwest. These redbeds are faulted in turn against turbiditic sandstones and grey mudrocks of uncertain age (section B62).

Section B66 exposes the Upper Permian Wuli Group where fossiliferous shelf-basin mudrocks and thin limestones coarsen upwards into a thick sequence (> 150 m) of rapidly alternating unfossiliferous fine sandstones and muddy siltstones. The sheet-like sandstones show sharp, often erosional, bases and internal upper phase plane-bed lamination, climbing ripple cross-lamination and rare large-scale cross-stratification (sets up to 65 cm thick). Grading is commonplace and convolute laminae and overturned foresets are occasionally seen. We interpret these lithofacies as sheet flood deposits on a low-gradient alluvial cone. Palaeocurrent data indicate a persistent flow to the southeast.

(*c*) *Kunlun Terrane*

Permian sections in the northern Kunlun Terrane around Naij Tal contrast dramatically with those described above. Around Wanbaogou Shan (Locality B91) the Hongshuichan Formation (Upper Permian) includes a thick lava sequence at the base, overlain by > 200 m

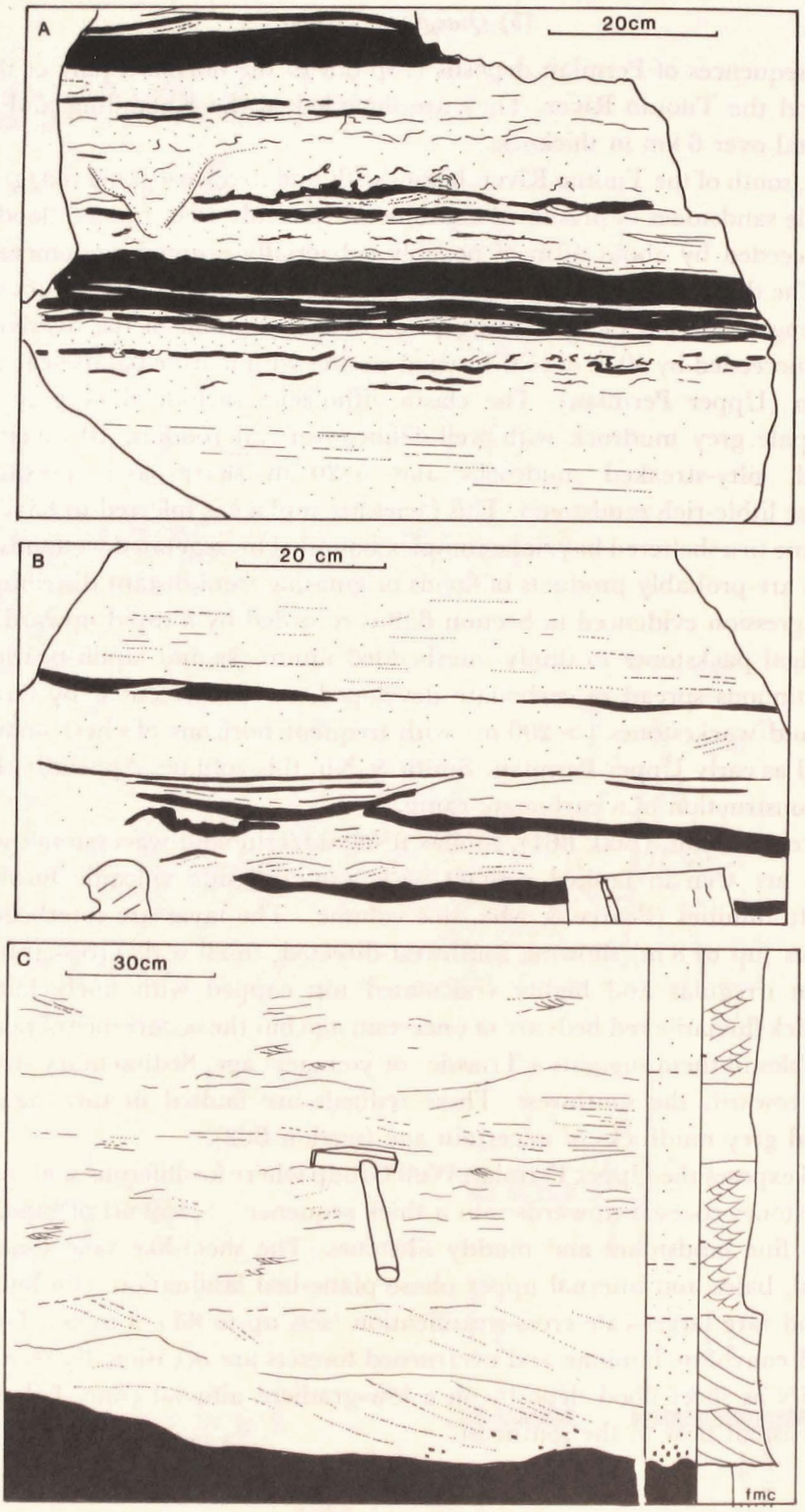

FIGURE 7. 7A/7B – Sketches from photographs and field observations of Permian resedimented tuffaceous fine sandstones and muddy siltstones (black shading). Note sharp-based sandstones with scoured basal contacts, wave-modified current ripple formsets and frequent lenticular muddy drapes. Locality B91. 7C – Field sketch and summary log to show possibly Permian fluviatile facies of sheet flood origin. Wuli Group, Lower Permian. Locality B66.

of chloritic fine to medium tuffaceous sandstones and siltstones. The sandstones are thinly bedded (5–25 cm) and frequently show grading, parallel lamination, cross-lamination and current-ripple formsets (figure 7). Scoured basal contacts, sometimes channelised, are typical. These features indicate that the sandstone and siltstone units probably consist of resedimented tuffs and other detritus, possibly representing the distal portion of a shelf-basin storm deposit or shelf-basin fan. Current structures prove flow to the ESE in the resedimented units. The clastic sequence is overlain by a thick (> 800 m) limestone succession. This includes skeletal wackestones, pseudobreccias and thin calcitised chicken-mesh anhydrites, and is interbedded with tuffaceous sands at the base. Cross-stratified grainstones with crinoidal debris follow quickly, interpreted as shallow, shore-face facies. Cross-stratification indicates transport to the southeast. Higher beds are thin-bedded fine calcareous silts and limestones, often with regular centimetre banding disrupted periodically by bioturbation. They are completely unfossiliferous and represent deposition either on shallow mud-flats or in a distal shelf-basin. The succession continues with unfossiliferous massive-bedded white limestones and then thinner-bedded limestones, often red. The whole succession is in excess of 200 m thick. The red limestones are fossiliferous, with layers of brachiopod shells and crinoid debris. The brachiopods prove a late Permian age for the sequence.

(*d*) *Permian palaeogeography* (figure 16)

(i) *Lhasa Terrane*

Permian sequences record the major progradation and development of a carbonate ramp over much of the southern part of the Lhasa Terrane (and indeed over much of Tibet), in an area that was previously shelf-basinal in character. No evidence was seen during our expedition of contemporaneous shelf-break or oceanic facies, but some extensional tectonic effects upon basin evolution are suspected because of the continued eruption of the possible back-arc Dhagze volcanics (see Pearce & Mei, this volume).

(ii) *Qiangtang Terrane*

As for the Carboniferous, we have no palaeomagnetic control on the palaeolatitudes of this terrane. The Wuli Group represents a Lower Permian shelf-basin which was filled by fluviatile clastics derived from the northwest. Following the coastal plain wetland facies of the Kaixinling coal basin, carbonate ramps developed in mid-Permian times, succeeded by an interval of basaltic/andesitic volcanism of extensional rift affinities.

(iii) *Kunlun Terrane*

Resedimented tuffaceous sandstones of the Wanbaogou Shan are interpreted as storm deposits in a shelf basin. Cessation of volcanism was followed by carbonate ramp development.

Triassic (figure 8)

Triassic rocks are widely distributed over Tibet, being present on all three terranes.

(*a*) *Lhasa Terrane*

Sequences at Doilungdeqen northwest of Lhasa define the Chaqupu Group (300 m). Ammonites above an internal disconformity date them as Upper Anisian (Middle Triassic, see

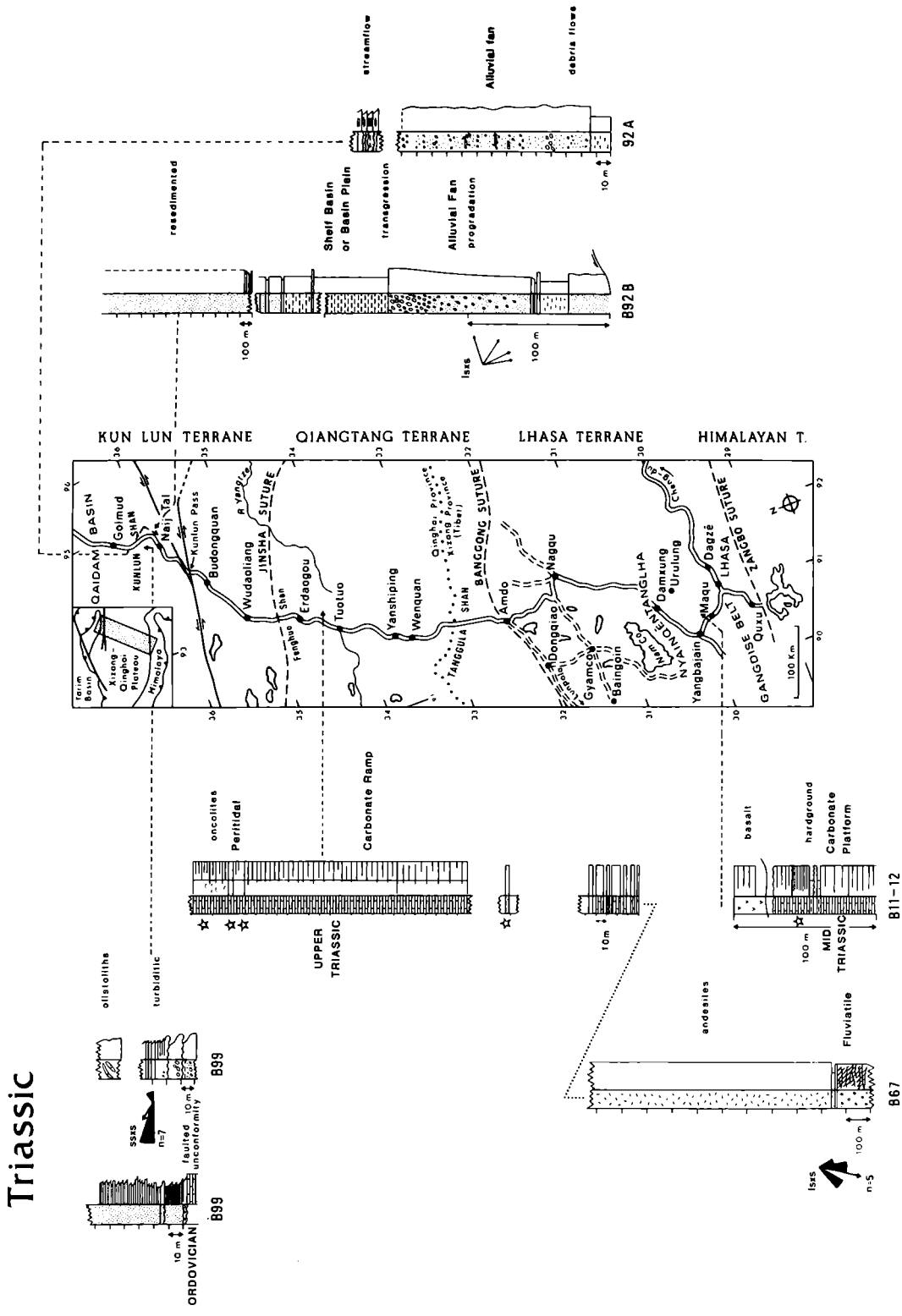

FIGURE 8. Distribution of Triassic measured sections, their lithofacies, environmental interpretations, age determinations and palaeocurrent distributions. See text for discussion and further data. Key in figure 2.

Smith & Xu, this volume, Appendix, locality B12). The Chaqupu Group is predominantly dark lime wackestone deposited on the lower slopes of a carbonate ramp. About halfway up the logged sequence there is a prominent bed with fissures (up to 40 cm deep) coated by 20 cm of dark ferruginous crust. Overlying chlorite-rich spherulitic mudrocks rest with slight angular discordance on the fissured horizon and pass upwards into ammonoid-bearing Upper Anisian limestones with occasional haematitic crusts on bedding planes. The topmost (6 m) limestone horizon is a grainstone with molluscan fragments and deep fissures and encrustations as before. The encrusted and fissured horizons are interpreted as products of periodic carbonate ramp fragmentation, probably caused by extensional faulting which generated local unconformities due to differential tilting. It is interesting to note that rapid water deepening, fracturing and exhalative mineralisation are characteristic features of Tethyan carbonate platform break-up in European Triassic sequences (Bernoulli & Jenkyns 1974). The sequence is overlain by 300–1000 m of basalt and andesitic lavas (Pearce & Mei, this volume).

Exposures of late-Triassic rocks are seen in the Qibulung area southeast of Urulung (Localities B3, B4) in a series of thrust-related folds. Wackestones with scattered bivalve and crinoid fragments occur in one thrust slice. A section to the north reveals thinly-bedded (15–30 cm) skeletal grainstones alternating with silty clastic mudrocks. The grainstones show faint internal parallel laminations and are interpreted as resedimented limestone turbidites of basin-plain origin. They provide additional evidence for carbonate platform break-up in late Triassic times, with the development of marked platform margins, perhaps fault-bounded. Other outcrops of limestone turbidites occur, as at locality B23, approximately 50 km northwest of Damxung (see Kidd *et al.*, this volume, field slips; Microfiche, in pocket), but have not been dated palaeontologically.

(*b*) *Qiangtang Terrane*

As described below, the central and southern parts of the Qiangtang Terrane are dominated by an extraordinary thickness of Jurassic strata. In the north, extensive and important outcrops of Triassic rocks occur in the Zhakongjian Mountains (Locality B67). Here, > 150 m of pebbly, cross-stratified coarse sandstones make up the lowest strata exposed. The sandstones are apparently multistorey with frequent erosion surfaces separating trough cross-stratified units up to 5 m thick. Cross-stratification azimuths indicate flow to the south. The 0.5–3 cm sub-rounded granules and pebbles are predominantly of quartz and black/green chert. Modal analyses prove mature quartz arenite compositions with high proportions of metamorphic polycrystalline quartz and sedimentary chert in the sand-size fraction. A thin possibly marine limestone caps the sequence and underlies a series of thick (> 800 m) porphyritic andesite flows of island arc affinities (Pearce & Mei, this volume).

The andesites are overlain by at least 200 m of limestones, but the contact is not exposed. These limestones are well bedded (30–40 cm), pale, sparsely skeletal wackestones of carbonate ramp aspect. The lowermost are rich in chert nodules. Ammonoids occur in the topmost units. Conodonts date the sequence as Norian (Upper Triassic; Smith & Xu, this volume, Appendix, locality B67). Several horizons in the upper part of the sequence show well developed algal oncolites and other stromatolitic laminations. Sometimes algal laminae coat the brachiopod valves. The upper part of the sequence thus records gradual shallowing-upwards into peritidal environments as the carbonate ramp prograded seawards.

(*c*) *Kunlun Terrane*

A highly deformed sequence of clastic strata, the Bayan Har Group, outcrops from the Jinsha Suture northwards to the Kunlun Pass. No faunas were discovered during the present expedition but fossils from areas to the east indicate a Triassic age (Smith & Xu, this volume). The deformation makes a thickness estimation extremely difficult but it may total several kilometres. Exposures are predominantly siltstone and mudrock, now deformed into slates. Some show rare thin (5–20 cm) very fine sandstone/coarse siltstone beds with sharp tops and bases. One example of small-scale cross-lamination indicated a palaeoflow to the west, similar to that deduced from microflute casts (*fide* J. F. Dewey). Most of these lithofacies are tentatively interpreted as continental rise deposits, possibly originating as contourites and accreted on to the southern margin of the Kunlun Terrane as an accretionary prism during the Triassic, an interpretation supported by structural data (Coward *et al.*, this volume).

Between the two strands of the Kunlun Fault along the southern margin of the Xidatan Valley, there are sections through a poorly dated succession which appears to be Permo-Triassic (the section, B77, is shown graphically with the Permian sections of figure 6). They occur at the junction between the low metamorphic grade slates of the Bayan Har Group to the south and the high grade rocks (garnet schists, phyllites and phyllenites) to the north. The rocks are highly thrust and intruded by sheared porphyritic granitoids dated (Rb/Sr) at 195 Ma (Lower Jurassic; Harris *et al.*, this volume). Section B77 (figure 6) is highly schematic and details of the true succession remain obscure. Undoubtedly, however, several sedimentary lithofacies occur in the various thrust slices. They include graded coarse wackes, dark mudrocks, carbonaceous mudrocks and at least one coal seam. The coarser clastic units contain angular acidic volcanic detritus. A mature quartzite unit (5 m thick) is also present. The variety of lithofacies is remarkable and it seems clear elsewhere (Localities M253, M245, M248; data of W. S. F. Kidd & J. F. Dewey) that individual thrust slices may represent olistolithic masses.

Sections of suspected Triassic age occur (B99) north of Naij Tal and show faulted and possibly erosive relationships with the underlying Ordovician. They must be younger than Anisian–Carnian because of the 240–224 Ma ages obtained from the Golmud batholith to the northeast (Harris *et al.*, this volume, Isotope Geochemistry, Locality G273), clasts of which are common in the sections. A late Triassic or early Jurassic age is therefore likely. Thick (> 200 m) polymict conglomerates and granule grade sandstones contain a large variety of clasts, some up to 1.5 m in apparent maximum diameter. Sedimentary structures are absent from the conglomerates, the large clasts of which are frequently matrix-supported. We interpret them as debris flows. The granule-grade units and sandstones occasionally show normal grading, cluster bedforms and parallel laminations, indicating streamflow origins. An upward trend to finer grain sizes is seen in section B92A, but B92B shows part of a coarsening-upwards sequence overlying an unfossiliferous limestone bed. Cross-stratification is seen in finer-grained sandstones in both sections, giving a flow direction towards the southeast. Crude imbrications of the larger boulders confirms this. The many types of clast in the conglomerates include various granitoids, microgranite, quartz porphyry, rhyolite, basic volcanics, gabbro, micaceous wackes, white limestone, dolomitic marble, purple-brown sandstone and quartz. The granites and limestone clasts are usually the largest. In all the sections the predominant clast type changes upwards from quartz to limestone to granitoid. Some exposures (eg B99) show large (> 20 m) olistoliths of possibly Upper Ordovician limestones. Depositional environments are interpreted

as subaerial alluvial fans and fan deltas draining a hinterland exposing Ordovician 'basement' and newly unroofed Triassic granitoids.

The conglomeratic sequences are overlain by thick (2 km) successions of indeterminate origins, including pale quartzitic sandstone, highly cleaved fine-grained wackes and greenish tuffaceous (possibly resedimented) fine to medium sandstones.

(*d*) *Triassic palaeogeography* (figure 16)

(i) *Lhasa Terrane*

No palaeomagnetic results are available for the Triassic from the Lhasa Terrane. Fragmentation of the Lhasa carbonate platform by extensional tectonics is envisaged, with eventual mantle melting to produce the Quesang volcanics above a back-arc attentuation zone (Pearce & Mei, this volume). These magmo-tectonic processes caused marked bathymetric differences during late Triassic times.

(ii) *Qiangtang Terrane*

The Yaxico/Zhakongjian andesites yield a palaeolatitude (Lin & Watts, this volume) of around $29° \pm 14°$ N for the Terrane in Triassic times. Accepting the andesites as arc-related (Pearce & Mei, this volume), the underlying mature fluviatile clastics imply uplift of basement in the northern Qiangtang Terrane prior to southerly subduction of Jinsha ocean crust. Cessation of subduction was followed by submergence of the arc and establishment of a carbonate platform.

(iii) *Kunlun Terrane*

The coarse clastic rocks of the northern Kunlun represent subaerial and possible subaqueous fans derived from the Triassic plutonic/volcanic arc to the north (Golmud batholith etc) but their ages cannot be directly determined. The sedimentological data suggest that they represent unroofing molasse and thus probably postdate active subduction and possibly collision. The Bayan Har Group repesents deposition along a former continental margin lying at the southern margin of the Kunlun Terrane.

Jurassic (figure 9)

Jurassic rocks are present in the Lhasa and Qiangtang Terranes, but probably do not occur north of the Jinsha suture in the Kunlun Terrane.

(*a*) *Lhasa Terrane*

Kimmeridgian carbonates and siltstones are well-exposed at Xiaqiong Lake (Localities B28, B29). The latter area lies close to the supposed line of the Banggong Suture and may possibly be of Qiangtang Terrane origins. In the lower part of the succession three massive (10–20 m) limestones with abundant stromatoporoids and occasional coral patch reefs are separated by dolomitic siltstones. The siltstones contain interbedded, thin sharply-based sandstones with wave-ripples and flat laminations interpreted as lagoonal washover deposits. Nerinaceid gastropods and thick-spined echinoids in the limestones indicate shallow sublittoral conditions. Beach strand concentrations of foraminiferans are found in the dolomitic siltstones and at least

one serpulid-encrusted beachrock horizon occurs. Marine infaunal spatangoids occur at one level.

Around Gyamco (localities B32, B33), in the northern part of the Lhasa Terrane, a thick (> 1.3 km) succession of late Jurassic to ?early Cretaceous clastic sediments is present. The succession begins with monotonous black basinal mudrocks containing subordinate resedimented carbonates rich in molluscs and derived from nearby shallow shelf environments, judging from the abundance of nerinaceid gastropods and rare compound scleractinian coral fragments. Higher up 0.1–0.3 m graded wackes are common, interbedded in thicker (2–5 m) mudrocks with rare wacke units up to 1 m. The wackes are very fine to fine-grained and show sedimentary structures indicative of Bouma A to E divisions. One C division yielded a palaeocurrent towards the west. A divisions frequently contain molluscan debris. These lithofacies are interpreted as basin-plain turbidites probably derived, at least in part, from a colonised shelf which may have lain to the east.

South of Dongqiao, at Loubochong (locality B38), there is an inverted succession of possibly Upper Jurassic sedimentary rocks which stratigraphically overlie vesiculated pillow lavas of oceanic arc affinities (Pearce & Mei, this volume). The topmost pillow lavas are veined by red cherts and overlain by a massive red brecciated and mineralized chert horizon up to 1.5 m thick. This may have an exhalative origin. An overlying bedded greenish chert is succeeded by 5 m of siliceous mudrocks containing thin tuffs and 50 m of silty mudrocks with thin interbedded lenticular cherts. The mudrocks contain the trace fossil *Chondrites*. The topmost horizon contains thin silicified graded beds of turbiditic aspect, with Bouma A–C divisions occasionally present. These lithofacies resemble deposits of resedimented cherts and may have formed on an oceanic arc slope in an area of high oceanic water productivity.

West of Dongqiao, there are outcrops which constrain the age of obduction of the oceanic arc crust previously inferred. At locality B41 a thrust mass of ophiolitic serpentinite is succeeded by 2 m of nodular rock rich in chalcedonic silica and overlain by a yellowish, clayey pisolitic deposit. We interpret this as a silcrete duricrust developed on the thrust serpentinite during a lengthy period of pedogenesis under a seasonally humid climate. An overlying detrital interval, with large chromite-rich clasts and angular reworked chert fragments is succeeded by a second soil horizon of red pisolite-rich mudrock (3.5 m) and a goethite-rich boxstone layer (1.5 m) both rich in chert. This is interpreted as a ferrosiallitic soil, developing perhaps under a more humid climate than the silcrete below. Both soil horizons are succeeded by clastic sediments deposited in hollows upon the underlying duricrust surface. Micaceous muddy siltstones with plant fragments (2.5 m) are cut by thin sharp-based and cross-laminated very fine sandstones of crevasse aspect. The whole sequence is capped by siltstones and mudrocks rich in rootlets, with one thin ferruginous soil horizon. These products of an encroaching, low-energy, coastal plain are succeeded by poorly exposed granule conglomerates rich in very angular chert and limestone clasts and, significantly, chromite grains. The latter indicate continued reworking of serpentinite masses. The fluviatile clastics are overlain by a 0.5 m calcareous very fine sandstone with cross-cutting low angle laminations and numerous escape burrows. This apparently transgressive beach facies is succeeded by > 3.5 m of richly fossiliferous shallow marine limestones with abundant *in situ* colonies of *Cladocoropsis* which, with occasional scleractinian corals, forms a primary framework. The corals date the underlying beds as no younger than Tithonian (late Jurassic).

(*b*) *Qiangtang Terrane*

Thick (5 km) Jurassic successions occur over much of the southern half of this Terrane, from Amdo northwards through the Tanggula Shan to Yanshiping. In the north continental clastics predominate, while marine limestones become increasingly important southwards.

The northernmost proven Jurassic that we encountered lies south of the Tuotuo River, where a coal-bearing sequence of deltaic aspect occurs. Channel sandstones yield evidence of flow towards the south.

In the thick Middle and Upper Jurassic successions exposed around Yanshiping (figures 9, 10) the clastic lithofacies include:

(1) Variegated red/green mudrocks with suncracked surfaces and thin (< 1 m) horizons of calcitic nodules resembling calcretes. These are interpreted as deposits of well-drained, periodically-arid floodplains subjected to periods of slow sedimentation which encouraged soil formation.

(2) Thin red/green mudrocks as above, with thin fine sandstone interbeds (figure 10B). These are sharp-based and often graded. They show planar laminations and internal current-ripple cross-laminations capped by symmetrical, flat-topped and interference ripple trains. They are interpreted as flood crevasse/overbank splays introduced into shallow lakes or bays subject to wave and possibly tidal action prior to desiccation.

(3) Thicker (usually < 4 m) erosive-based fine to medium sandstones show well-developed internal cross-stratification, basal scour marks and rare lateral accretion surfaces (figure 10A). They are interpreted as the deposits of sluggish, possibly meandering, river channels traversing the lower reaches of the Yanshiping coastal plain. Palaeocurrent structures indicate flow to the south and southwest. Some sandbodies yield non-marine bivalves in lag deposits.

(4) Aggregates of thin siltstone and very fine to fine sandstone form coarsening-upward sequences that pass up from green floodplain/lacustrine mudrocks (figure 10C–10D). Internally these are dominated by small-scale cross-lamination of current ripple origin, but with frequent modifications due to waves. Sometimes the coarsening-upwards sequences are capped by thin limestones. The sequences are interpreted as shallow lacustrine infills by small crevasse deltas. Structures indicate flows predominantly towards the west.

(5) Dark grey mudrock alternating with muddy dark molluscan coquinas rich in monotypic *Liostrea* or corbulid bivalves. Occasional algal nodules occur. At least one karstified bedding plane with abundant isocrinoid columnals and ribbed bivalves is present. These are interpreted as the products of brackish-to-marine bay/lagoons that periodically became fully marine. Analogous present-day biofacies occur along the Texas Coast.

As noted, the southern outcrops of Jurassic rocks include more marine carbonates, with common peritidal grainstones (including oolites) and lower-to-mid ramp packstones and wackestones. An oyster-encrusted hardground of shallow subtidal aspects was discovered at locality B49. The overlying beds yield an abundant and varied fauna of bivalves, brachiopods and echinoids of Bathonian or Callovian age (Middle Jurassic; Smith & Xu, this volume, Appendix). Kimmeridgian (Upper Jurassic) calcareous mudrock of shelf-basin origin occurs at locality B50.

These various marine lithofacies frequently interdigitate with fine-grained red alluvial coastal plain mudrocks in the southern area. At several localities thick evaporites are exposed as halokinetic domes and pillows. Close examination of section B51 reveals red/purple

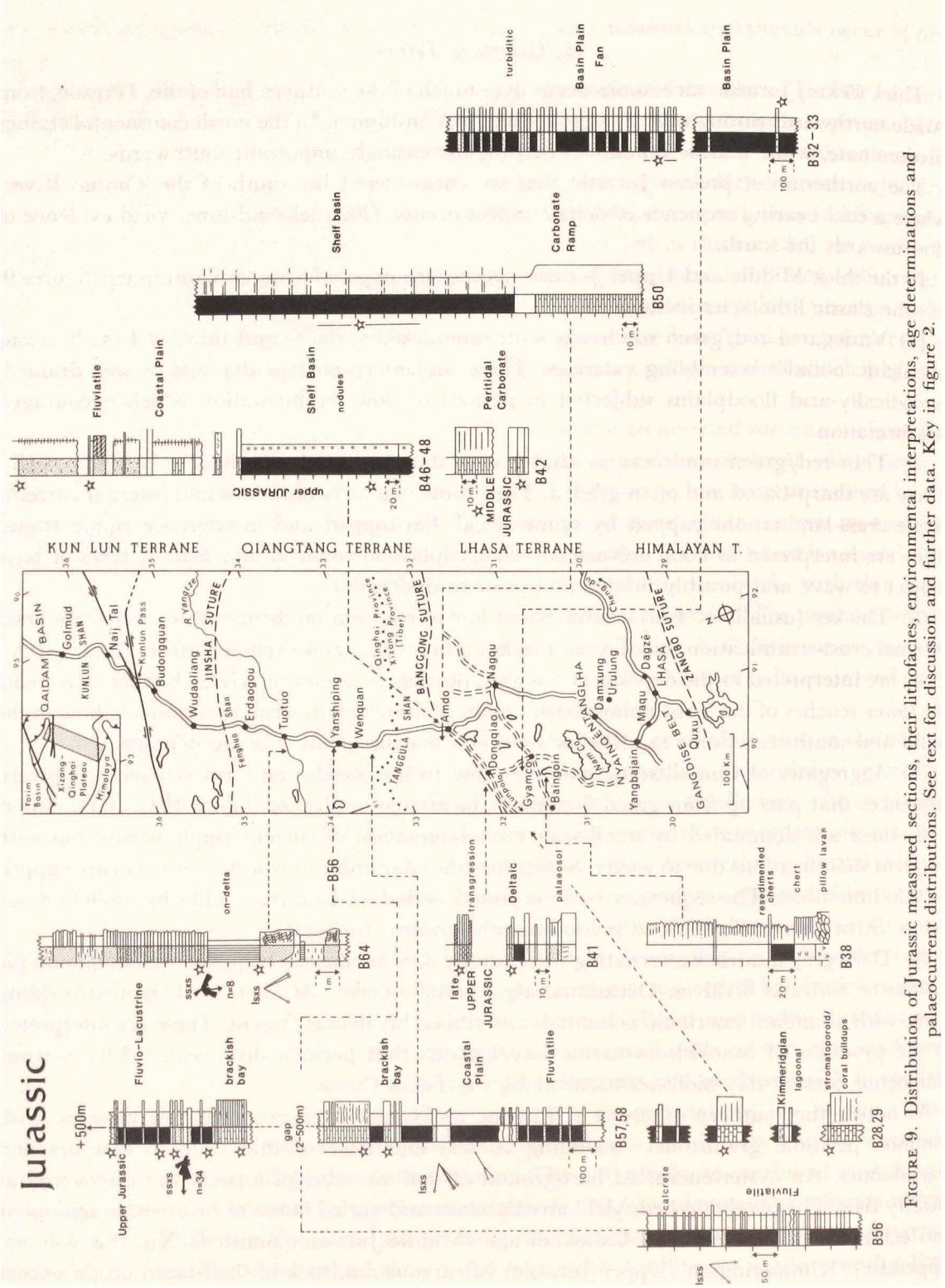

FIGURE 9. Distribution of Jurassic measured sections, their lithofacies, environmental interpretations, age determinations and palaeocurrent distributions. See text for discussion and further data. Key in figure 2.

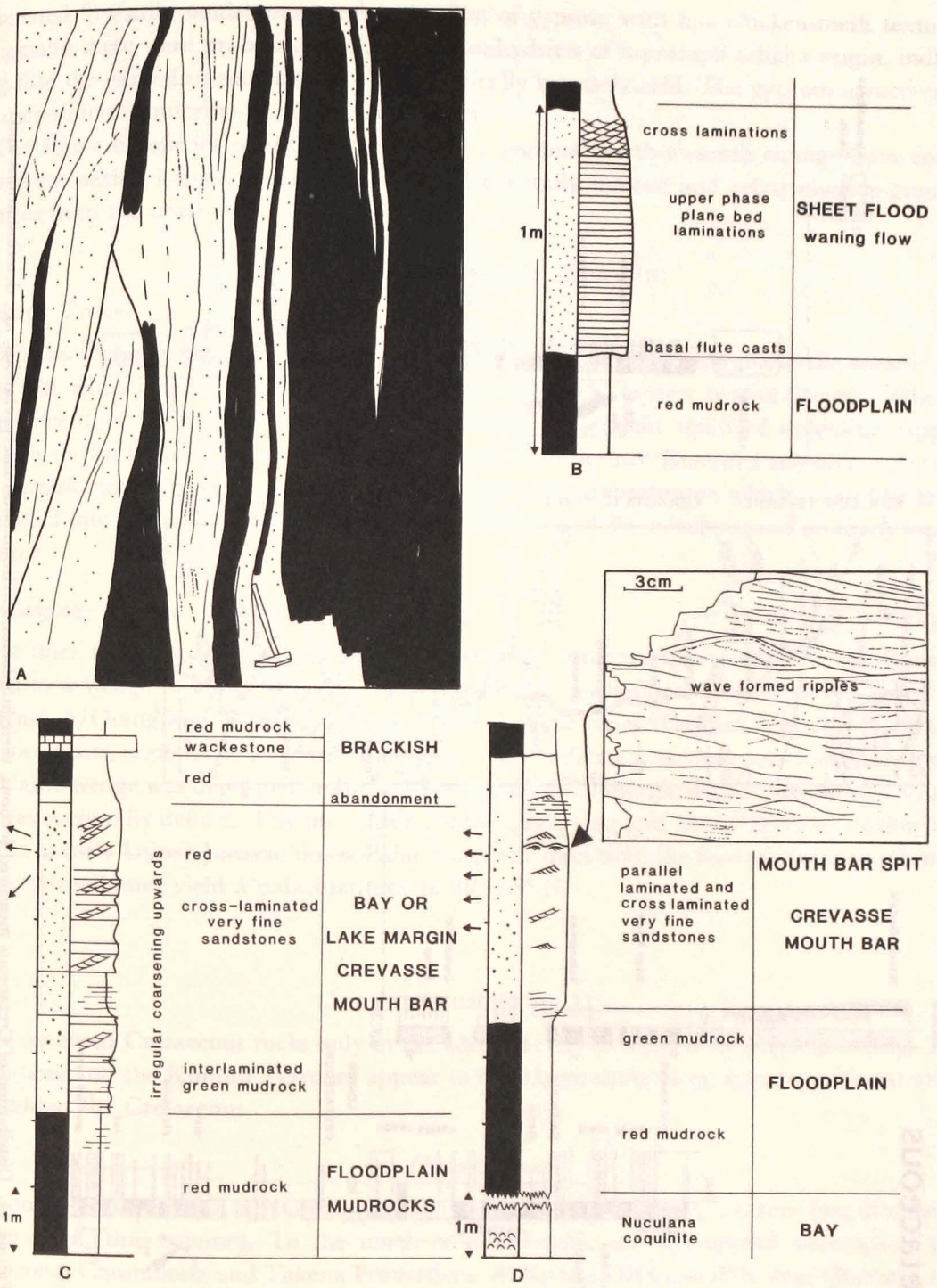

FIGURE 10. Field sketches and logs to illustrate the commoner Middle Jurassic lithofacies of the Qiangtang Terrane around Yanshiping/Wenquan. 10A – Tectonically-vertical bedded fluviatile shallow channel sandstones and floodplain mudrocks. The beds young from right to left. The sandbody to the left of the hammer (shaft is 35 cm long) contains well-developed lateral accretion surfaces of probable point bar origins. Locality B57. 10B – Log to show sheet flood facies. Locality B57. 10C/10D – Logs to show bay/lake infill cycles. Arrows show palaeocurrent azimuths. Locality B58.

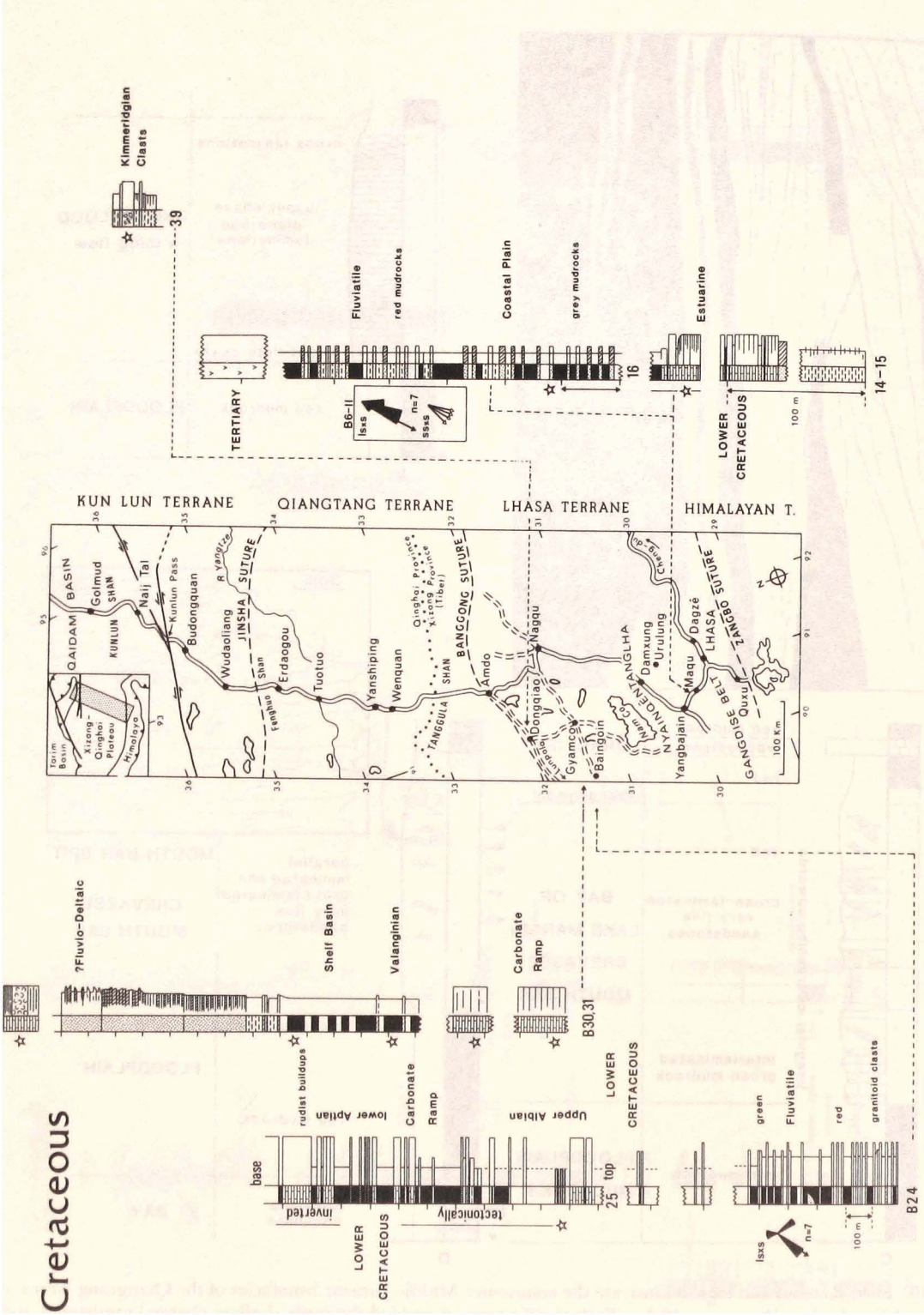

FIGURE 11. Distribution of Cretaceous measured sections, their lithofacies, environmental interpretations, age determinations and palaeocurrent distributions. See text for discussion and further data. Key in figure 2.

laminated fluviatile sandstones overlain by 8 m of gypsum with fine chicken-mesh textures. Originally these were probably chicken-mesh anhydrites of supratidal sabkha origin, indicating that the early Jurassic climate was periodically intensely arid. The gypsum is succeeded by unfossiliferous micrites of uncertain pedigree.

The above lithofacies relationships indicate a regional north-to-south change from continental to marine influences and derivation of generally mature and relatively fine-grained detritus from the north.

(*c*) *Jurassic palaeogeography* (figure 16)

(i) *Lhasa Terrane*

Deposits of the former Banggong oceanic tract indicate development of a fertile oceanic arc slope with extensive cherts. The clastic successions of 'flysch' aspects around Gyamco indicate development of continental margin environments. Subsequent uplift of ophiolitic-capped basins is shown by the development of thick residual duricrusts. Renewed subsidence in very late Jurassic times accompanied several phases of marine transgression which, as will be seen, continued into early Cretaceous times over several parts of the northern and southern Lhasa Terrane.

(ii) *Qiangtang Terrane*

The thick fluviatile Middle to Upper Jurassic of the southern Qiangtang Terrane is interpreted as a wedge of clastic molasse derived from the newly-fused orogenic belt formed by the Kunlun/Qiangtang Terrane collision in late Triassic times (Coward *et al.*, this volume). Palaeocurrents, regional facies trends and fining trends indicate a north to northeast derivation. The clastic wedge was deposited on the southern continental margin of the Qiangtang Terrane and was eventually deformed by the collision of the Qiangtang and Lhasa Terranes during late Middle to early Upper Jurassic times. Palaeomagnetic data from the fluviatile redbeds (Lin & Watts, this volume) yield a palaeolatitude of $39° \pm 8°$ N.

Cretaceous (figure 11)

We observed Cretaceous rocks only in the Lhasa Terrane, where they outcrop widely. The Qiangtang and the Kunlun Terranes appear to have been upstanding non-depositional areas throughout the Cretaceous.

(*a*) *Lhasa Terrane*

No fossiliferous rocks of late Cretaceous age are known in the Lhasa Terrane (see discussion of Yin *et al.*, this volume). To the north of Lhasa there are widespread outcrops of the Linbuzong, Chumulong and Takena Formations. At Sections B14 and B15, near Quesang, the sequence begins with alternating dark carbonaceous muddy siltstones and thinly-bedded (10–50 cm) fine-medium sandstones (> 50 m). The sandstones are sharp-based and faintly cross-laminated. The fine intervals may contain siderite nodules and vertical rootlets. These features indicate a poorly-drained floodplain.

Above a significant exposure gap comes a cross-stratified sandstone followed by alternating limestones, cross-stratified sandstones and mudstones. These yield a hyposaline to mesohaline

fauna of oysters, gastropods and ostracods, with occasional horizons of possibly restricted-marine coarse-ribbed bivalves. The limestones are dark wackestones with scattered quartz grains. The sequence is interpreted as bay or estuarine, oscillating between oyster- and gastropod-dominated benthos suggesting fluctuating salinities.

Overlying the limestones is a great thickness (> 1 km) of clastics, belonging to the Takena Formation (figure 12). The lower half of these comprises alternating mudstone, siltstone and fine to medium grained sandstones. The fine beds contain siderite nodules, carbonaceous fragments and siltstone interlaminae. The coarse members range up to 5 m in thickness and are usually sharp-based. The latter are sometimes strongly erosional, with overlying 'lag' concentrates of exotic and intraformational pebbles. Large scale cross-stratification sets are common, sometimes lying between even larger sigmoidal bedding surfaces of lateral accretion origin (figure 12). These lithofacies are interpreted as fluvio-distributary channels which meandered to the southeast through poorly-drained floodplains. The upper half of the succession is similar, but with prominent red colouration suggesting that the floodplains became well-drained, allowing early vadose oxidation. Other outcrops of the Takena redbed facies were examined around Ganpa (localities B6–B11) to the north of Lhasa. These have yielded palaeocurrents generally towards the south. A coarsening-upwards sequence is seen (> 200 m), with increasing amounts of cross-stratified multistorey channel sandstones higher up (figure 12C). If it proves to be part of a regional coarsening-upwards trend then a southwards shift in facies belts is indicated. P. Allen (pers. comm. 1987) has observed similar multistorey pebbly and non-pebbly cross-stratified sandstones of fluviatile origins (possibly of braided channel facies) north of Lhasa at Lhunzhub. Palaeocurrent data suggest that these were deposited by south-flowing rivers.

Thick Cretaceous sequences were also examined around Duba, near Baingoin, some 300 km northwest of Lhasa. Here the probable Neocomian clastics (> 700 m) of the Duba Formation are faulted against Tertiary redbeds (figure 14). Dominated by red/green siltstone and mudrock of floodplain aspects, they contain thin calcrete profiles in places. Scattered throughout are feldspathic sandstones and pebbly sandstones, respectively of sheet-flood and channel origins. Both lithofacies are frequently cross-stratified and indicate a mean flow direction to the southwest. The pebbles include abundant granitoids, cherts and hornfelses. These are thought to have been derived from the nearby Baingoin granitoid pluton, dated at around 121 ± 2 Ma (Harris *et al.* this volume) i.e. middle Neocomian. Above come alternating limestones and mudrocks of the Aptian to Albian Longshan Formation (> 200 m). The inverted sequence at locality B25 begins with several massive rudist limestones of early Aptian age, in which the rudists form primary reefs alternating with orbitolinid-bearing mudrocks. Further up there is a brief phase of fine clastics with a mesohaline community of gastropods and bivalves replacing the orbitolinids. Finally, the sequence passes up into a late-Albian limestone/mudrock sequence in which mudrocks predominate. Abundant orbitolinids indicate shallow lagoonal conditions. The entire sequence was deposited in extremely shallow marine environments with rudist patch reefs and back reef lagoons in which the orbitolinids thrived.

The succession at Xiaqiong Lake (figure 11, localities B30–B31; see also Smith & Xu, this volume, Appendix) also comprises non-marine clastics. It overlies Kimmeridgian stromatoporoid/coral buildups and dolomitic siltstones which may extend up to the Jurassic/Cretaceous boundary. Above there is a rapid change to Berriasian/Valanginian siltstones and ripple cross-laminated and cross-bedded sands. The sands are thin at first (1–5 cm) alternating

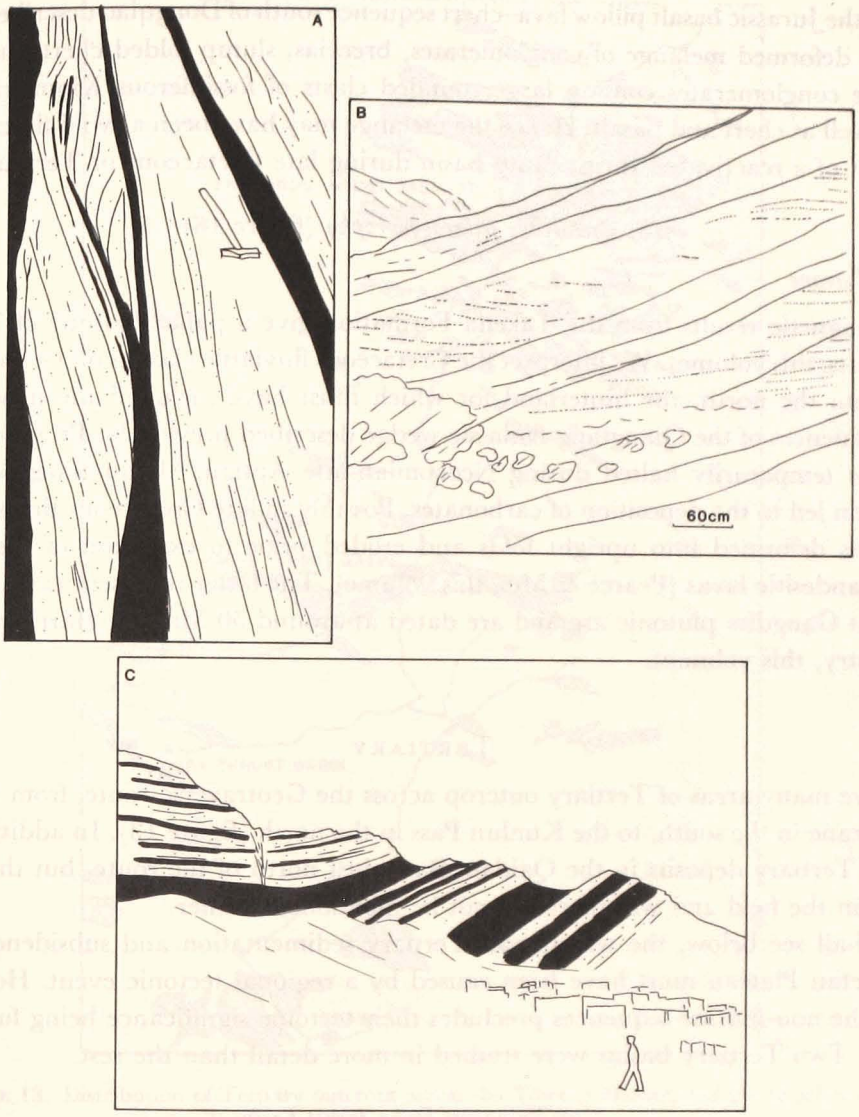

FIGURE 12. Sketches from photographs and field observations to illustrate fluviatile lithofacies of the Takena Formation in the Lhasa Terrane. 12A – Tectonically-vertical bedded fluviatile channel sandstones with well-developed lateral accretion surfaces of point bar origins. Mudrocks and siltstones of floodplain and channel-fill origins are shaded. The beds young from right to left. Locality B16. 12B – Cross-stratified medium-grained sandstones forming part of a thick multistorey sandbody of channel origins. Locality B6. 12C – Sketch of hillside exposures behind the village of Gampa (looking east) to show a coarsening-upward sequence of fluviatile facies some 150 m thick. Fine-grained units of floodplain origin are shaded black. Locality B7.

with mudstone, but up the sequence thicker (up to 1 m) cross-bedded units predominate, often with sharp-based erosional lower surfaces. These lithofacies are interpreted as fluvio-distributary channel sediments. The upper part of the sequence is dominated by siltstones and fine sandstones with periodic cross-bedded sandstones (20–60 cm) of possible floodplain origins. After a considerable exposure gap, thick-bedded bioclastic packstone limestones with abundant oysters are seen. These have orbitolinid foraminiferans that are Aptian/Albian in age and record a return to shallow marine or restricted marine conditions.

The most northerly outcrop of Cretaceous (locality B39) is also the most difficult to interpret.

Overlying the Jurassic basalt pillow lava–chert sequence south of Dongqiao described previously is a highly deformed melange of conglomerates, breccias, slump folded cherts and turbiditic flysch. The conglomerates contain large rounded clasts of fossiliferous Kimmeridgian limestones, as well as chert and basalt. Hence the melange may have been a 'wild flysch' deposited at the front of a reactivated thrust ramp basin during late Cretaceous or Tertiary times.

(*b*) *Cretaceous palaeogeography* (figure 16)

(i) *Lhasa Terrane*

Palaeomagnetic results from the Takena Formation give a palaeolatitude of $7.6° \pm 3.5$ °N (Lin & Watts, this volume). We interpret the Cretaceous fluviatile clastics of the area as molasse derived from the north, the hinterland for which must have included the newly-deformed Jurassic sequences of the Qiangtang molassic wedge described previously. Progradation of the clastics was temporarily halted during Neocomian-late Aptian/Albian times when marine transgression led to the deposition of carbonates. Possibly in late Cretaceous times the Takena molasse was deformed into upright folds and eroded prior to extrusion of the arc-related Linzizong andesitic lavas (Pearce & Mei, this volume). The latter represent extrusive portions of the great Gangdise plutonic arc and are dated at around 50 Ma (see Harris *et al.*, Isotope Geochemistry, this volume).

Tertiary

There are many areas of Tertiary outcrop across the Geotraverse route, from the northern Lhasa Terrane in the south, to the Kunlun Pass in the north (figure 13). In addition there are very thick Tertiary deposits in the Qaidam Basin just north of the route, but these were not examined in the field and will therefore not be mentioned further.

As we shall see below, the widespread Tertiary sedimentation and subsidence across the entire Tibetan Plateau must have been caused by a regional tectonic event. However, poor dating of the non-marine sequences precludes their tectonic significance being fully exploited at present. Two Tertiary basins were studied in more detail than the rest.

(*a*) *Baingoin/Duba thrust basin*

As shown in figures 13 and 14, this is bounded by a major NW–SE backthrust, which defines the great scarp of the Lang Shan as the Cretaceous hangingwall to the basin. The hangingwall exposes a lower clastic sequence overlain conformably by Aptian/Albian marine orbitolinid limestones (see above). Our fieldwork showed that the fluviatile, possibly Lower Cretaceous, clastics are thrust onto a Tertiary footwall of clastic redbeds.

Adjacent to the thrust (figure 14) there is a poorly-sorted conglomeratic unit containing abundant angular clasts of orbitolinid limestone. The conglomerates are folded into a footwall syncline with a highly developed cleavage on the southwestern limb adjacent to the backthrust. The clasts are identical with the Aptian/Albian limestones outcropping on Lang Shan immediately to the southwest. The conglomerates (> 100 m thick) comprise unstratified, ungraded and matrix-supported units up to 5 m thick, occasionally separated by thin (0.2 m) muddy sandstones. These are interpreted respectively as debris flow deposits with thin impersistent streamflow lithofacies, both presumed to have been deposited on alluvial fans draining to the northeast i.e. away from the thrust hangingwall.

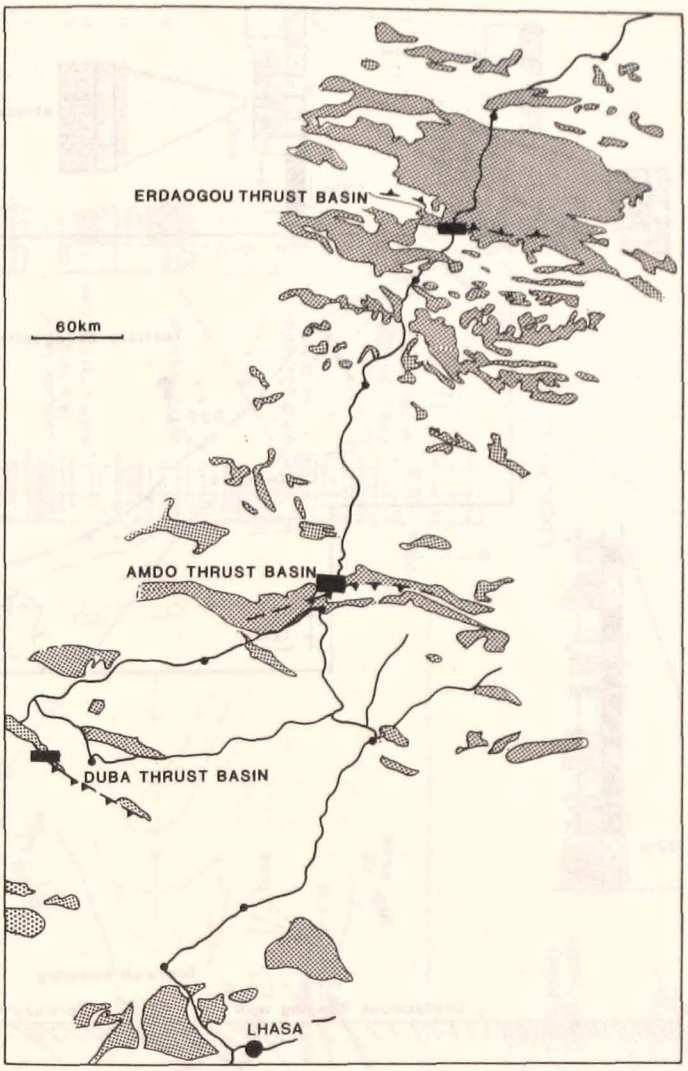

FIGURE 13. Distribution of Tertiary outcrops across the Tibetan Plateau and the location of Tertiary sections studied by us in detail.

Below the conglomerates is a calcareous cross-stratified medium to coarse sandstone member (> 250 m thick) of obvious stream flow origin. Palaeocurrent directions in the northwest of the area are parallel to the line of the thrust, whereas in central areas they run oblique to the thrust outcrop. Cross-stratified sets range from 20–70 cm thick and are predominantly tabular. They occur in stacked sandstone storeys separated by persistent erosion surfaces. The sandstones are interpreted as river channel deposits, probably of sand-bed braided rivers that flowed roughly parallel to the line of the contemporary thrust front. They gradually coarsen-up into the debris flow facies described above, suggesting that alluvial fans from the hangingwall prograded into the axial basin. Clasts of Cretaceous limestones are absent from this sequence, but several large, well-rounded clasts of exotic ignimbrites were found along one erosion surface. These are presumed to have been derived from the Linzizong Group (see Pearce & Mei, this volume).

The oldest sediments, which are not well exposed, include relatively fine-grained siltstones

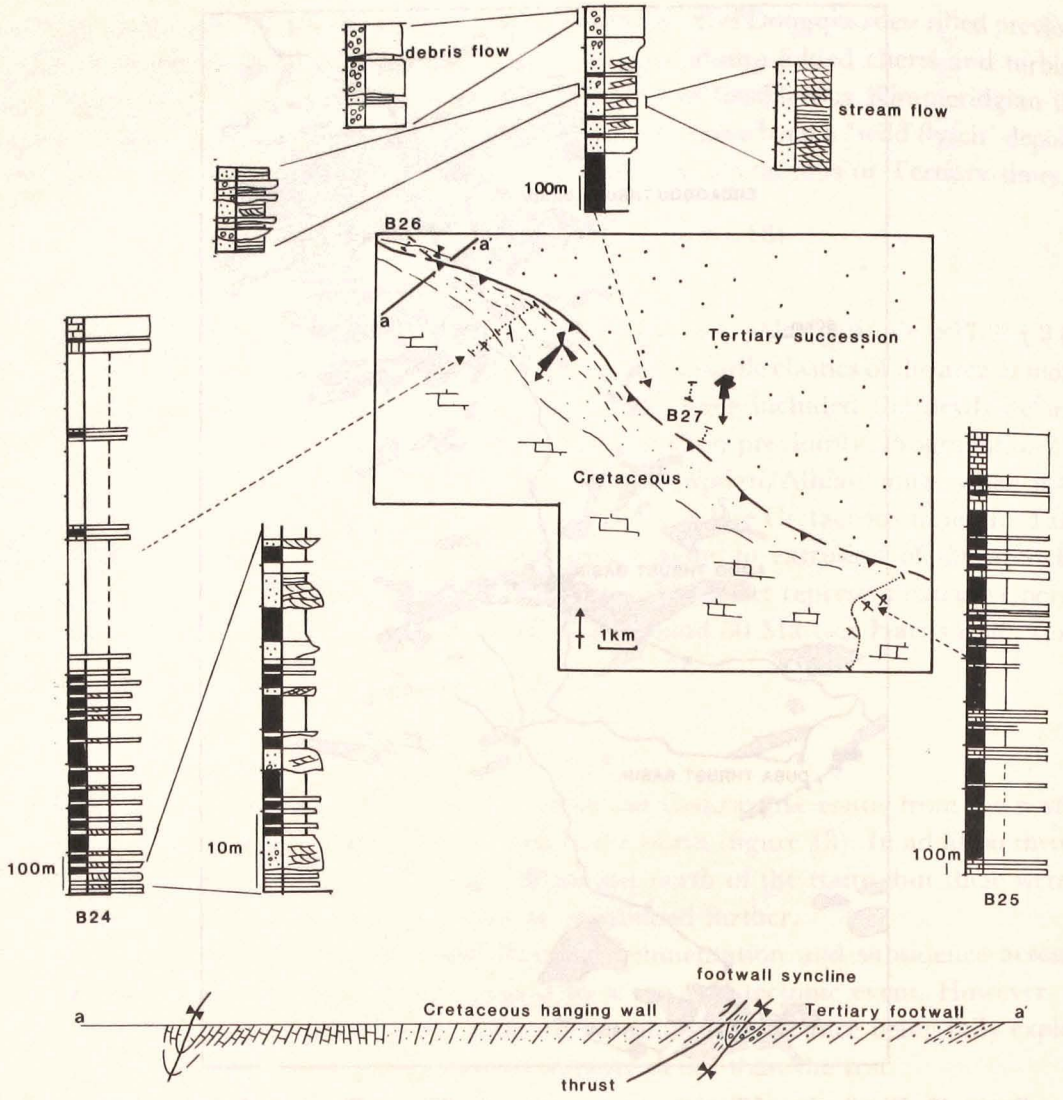

FIGURE 14. Sketch map, logs and section to illustrate the stratigraphy, sedimentology and structure of the Duba thrust basin. Note that the section for B25 is now known to be inverted and is described in true order of deposition in the Cretaceous section of the accompanying text. Rose diagrams indicate palaeocurrent distributions (see Appendix, microfiche, for details). Sketch geological section ignores topography. Localities B24–27.

with sandstone and conglomerate stringers. The latter contain well-rounded micritic pebbles, but with no sign of the distinctive Lang Shan orbitolinid limestone.

The arrangement of the above continental lithofacies strongly suggests that they were generated by a progressively northward-moving thrust fault and growth fold. We visualise the thrust front as eventually cutting out the Mesozoic sequence along its footwall and progressively overriding the alluvium, leading to the observed facies and grain-size trends. Unfortunately we have obtained no fauna or flora from the post-Albian sequence of clastics and thus we cannot be certain about the age of sedimentation and thrusting, save that the possible Linzizong ignimbrite clasts prove a Tertiary age for the sequence.

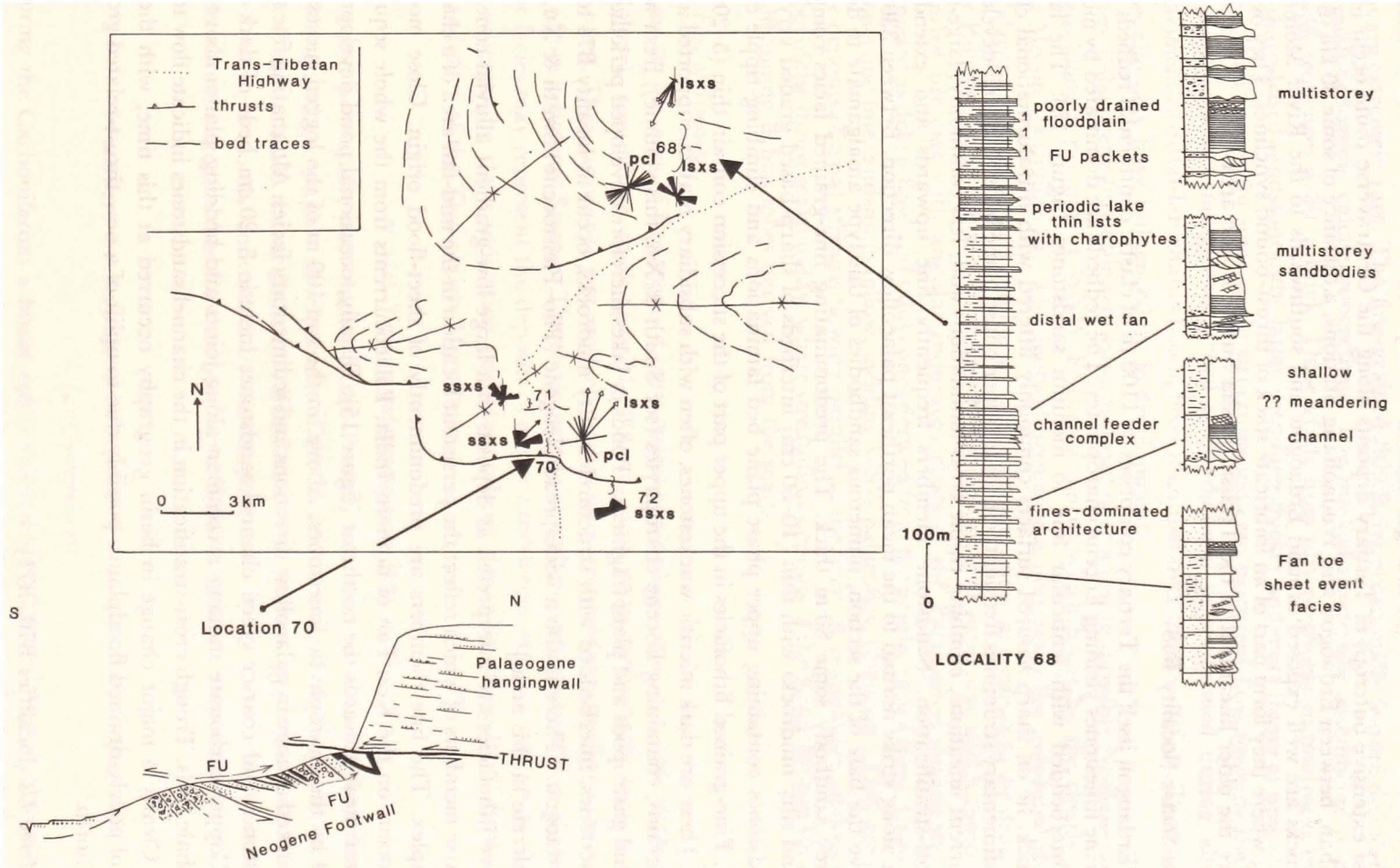

FIGURE 15. Sketch map (data of MPC, RMS, JFD, WSFK) of structure and bed traces around the Erdaogou Tertiary basin complex. Logs and sketch section show the character of the local Palaeogene succession in the hangingwall of the major thrust at Locality B70. Rose diagrams indicate palaeocurrent distributions. ssxs – small scale cross-stratification; lsxs – large scale cross-stratification; pcl – primary current lineations. Fu – firing upwards.

(b) Erdaogou thrust basin complex

The most extensive outcrops of Tertiary deposits along the Geotraverse route occur in the Fenghuo Shan, between Erdaogou and Wudaoliang Stations, a distance of some 80 km (figure 13). The rocks are well exposed around Erdaogou and southwards to the River Moron Us (figure 15), where they form part of an imbricate stack of thrust-bound synclines. They overlie and obscure the older lineament of the Triassic Jinsha Suture in the area.

(i) *Erdaogou Station* (locality B68)

Around Erdaogou itself the Tertiary comprises > 1100 m of clastic continental redbeds with rare lacustrine limestones yielding Eocene charophytes. The redbeds are dominated by muddy siltstones interbedded with lenticular fine to medium sandstones (figure 15). The latter, 0.5–3 m thick, lie on sharp scoured surfaces commonly littered with intraformational clasts. Internal sedimentary structures frequently include upper phase plane beds with well-developed primary current lineations, climbing ripple cross-laminations and, less commonly, large-scale trough cross-stratification. Sandstone members frequently fine upwards and extend for 100–400 m along strike normal to the mean northeast palaeoflow direction. Between 330 and 400 m above the base of the section, numerous sandbodies of this type amalgamate to define a multistorey sandbody some 80 m thick. The predominating fine-grained facies comprise siltstones and silty mudrocks with thin (10–50 cm) interbeds of sharp-based graded very fine to fine sandstones containing upper phase plane bed laminations and climbing-ripple cross-lamination. Fine-grained lithofacies in the upper part of the succession contain thin (5–20 cm) limestones. These are dark micritic wackestones, often with subsidiary matrix-supported angular quartz grains, containing Eocene charophytes (see Smith & Xu, this volume), fresh water ostracods and gastropods and plant fragments. Ponds or lakes therefore developed periodically. Similar limestones, interbedded with structureless silty mudrocks, occur at locality B74 to the north of Erdaogou. [There is also a widespread Neogene (Plio–Pleistocene; Smith & Xu, this volume) calcrete in this area.]

The above lithofacies are interpreted as deposits of a large low-gradient alluvial cone, the stacked coarse members of which reflect the persistent location in the mid-fan area of a channel feeder complex. The fine members are predominently of sheet-flood origin. Close modern analogues occur on the Kosi Fan of nothern India. Palaeocurrents from the whole sequence yield a vector mean towards the northeast (figure 15). Distally, occasional pond development is indicated by the charophytic limestones. Above, in the top 100 m of the logged succession, there is a marked change in palaeoflow directions and sedimentary facies. Alternating fine sheet flood sandstones and coarser green channel sandstones include 5–20 cm beds of dark grey mudrock. Copper carbonate staining is common along joints and bedding planes above and below the shale beds. Trough cross-stratification in the channel sandstones indicate flow to the southwest. Clearly a major change in basin geography occurred at this time, with the development of poorly-drained floodplains, possibly due to uplift of a new thrust-related growth fold in the north.

(ii) *River Moron Us* (localities B70, B71)

A thick (> 500 m) succession here is dominated by sheetflood lithofacies similar to those described above. Waning-flow sequences are common, with occasional wave-formed modi-

fications on the sandstones' upper surfaces. Channel sandstones and sandstones thicker than 1.5 m are extremely rare. The fine-grained lithofacies occasionally feature desiccation cracks and small pedogenic calcite concretions. The most characteristic assemblage is coarsening-upwards sequences 5–30 m thick. These grade from silty mudrocks to mudrocks interbedded with sharp-based sandstones, the latter becoming thicker and more frequent upwards. Palaeocurrent directions from small-scale structures indicate persistent flow towards the northeast. The sandstones are thought to record progradational pulses formed during alluvial cone development as distal-fan channel complexes migrated over the fan surface. Tectonic/climatic factors also may have influenced cycle development.

These Palaeogene fluviatile redbeds are thrust over a young (possibly Neogene) sequence of redbeds along a prominent WNW–ESE escarpment which is cut by the clearly antecedent River Moron Us (figure 15). This footwall sequence is noticeably less indurated than that on the Palaeogene hangingwall and has a brick red colouration, in contrast to the drab red-brown of the Palaeogene. It contains some crudely fining-upwards sequences which comprise matrix-supported breccias with angular indurated clasts of the Palaeogene sandstones. These are interpreted as debris flow and talus cones derived from the nearby thrust front. Cross-laminated siltstones and fine sandstones follow, yielding WSW palaeoflow directions. They are interpreted as the deposits of axial streams flowing parallel to the front. A remarkable analogue is seen at the foot of the thrust scarp today, where streamflow deposits of the River Moron Us are eroding and offlapping debris lobes derived from the scarp.

(iii) *East of Erdaogou*

Some 20 km east of Erdaogou a very coarse grained facies occurs (*fide* W. S. F. Kidd & P. Molnar), comprising thick (possibly 200 m) grain-supported conglomerates and coarse sandstones. These appear to rest erosively within finer-grained facies similar to those described above from Erdaogou Station. The clasts include abundant limestone and rare silicic volcanics. These facies may represent the deposits of major axial-feeder channel systems to large alluvial cone systems, the clasts indicating possible southerly derivation from the Triassic limestones and andesites of the Zhakonjian Mountains.

(*c*) *Tertiary palaeogeography* (figure 16)

As noted previously, poor dating of the Tertiary sections precludes a full understanding of the timing and geographic development of the basins. Nevertheless the two examples studied in detail show clearly that sedimentary lithofacies development, provenance and stratigraphic sequences were closely controlled by contemporaneous Palaeogene, Neogene and, indeed, Recent thrust tectonics (see Coward *et al.* and Kidd & Molnar, this volume).

Synopsis of palaeoenvironmental history (figure 16)

(*a*) *Carboniferous*

During the Carboniferous a broad epicontinental sea extended from northern India to the Qilian Shan in the north. The faunas decrease in diversity from north to south, with tropical to subtropical Eurasian reefoidal faunas in the Kunlun Terrane (succeeding fluviatile redbeds derived from the north), and shelf-basin clastics with low diversity faunas in the Lhasa Terrane.

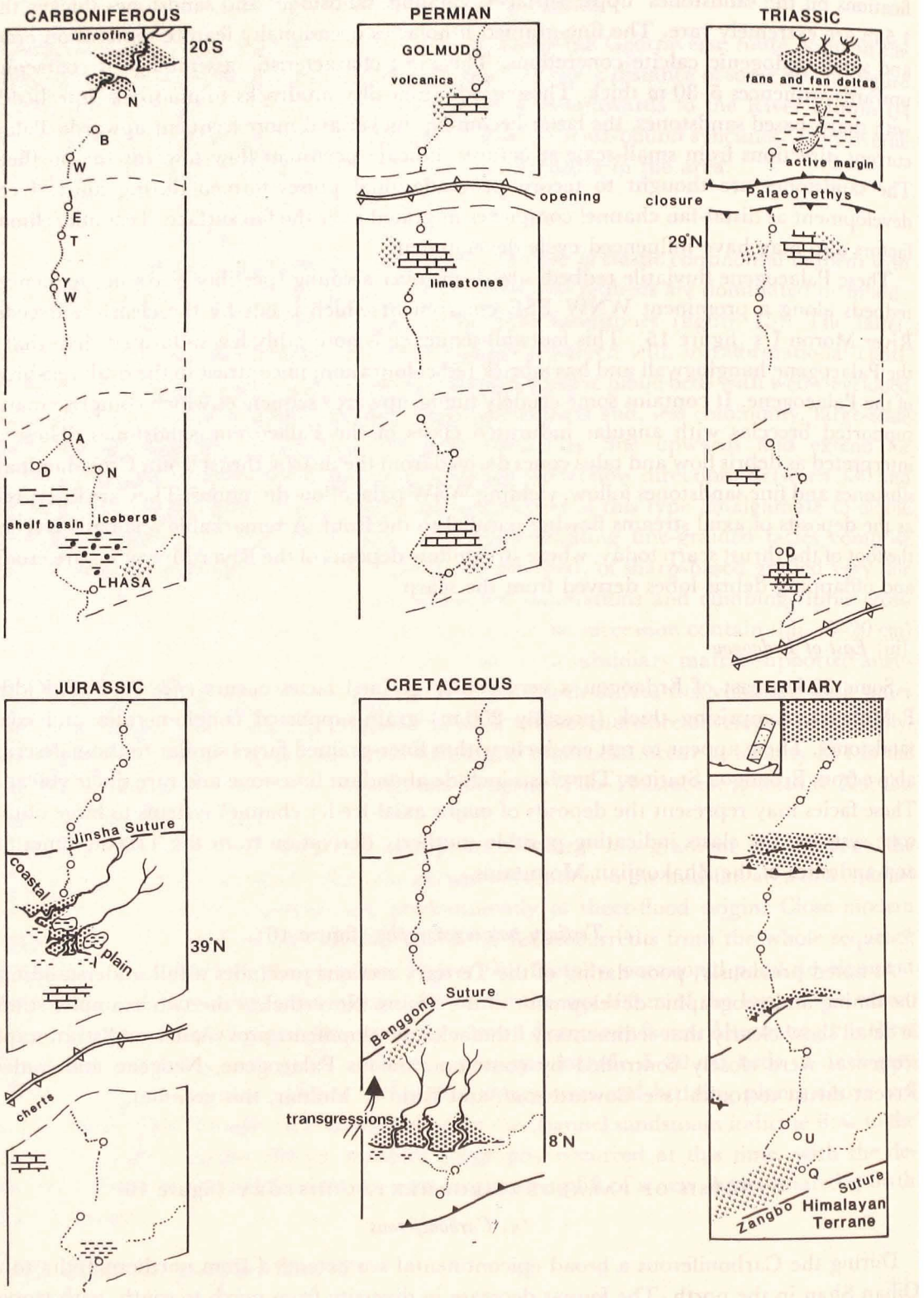

FIGURE 16. Series of very generalised diagrams to show the major lithofacies patterns and palaeogeography of the Tibetan Terranes from Carboniferous to Tertiary times. See the palaeogeographic sections of each geological system in the text for a summary discussion.

A late Dinantain marine transgression is well marked in the Kunlun Shan, with evidence from the underlying fluvial clastics for the unroofing of an orogenic belt to the north. Palaeomagnetic data indicates a latitude of $20° \pm 20$ °S for the Kunlun Terrane.

(*b*) *Late Carboniferous/early Permian*

Toward the end of the Carboniferous the climate had become significantly cooler, with the result that climatic belts narrowed. Thus deposition of shallow water carbonates with large benthic forams and compound corals continued in the north whilst thick mixtite deposits were laid down on the Lhasa Terrane, indicating that it lay within the iceberg belt. Glaciomarine deposition probably continued into the Sakmarian, contemporaneous with the tillites and other evidence of glaciation elsewhere on the Gondwanan superplate. Thick volcanics northeast of Lhasa are of possible back-arc extensional origins (Pearce & Mei, this volume) and may herald the initiation of breakup of Gondwanaland.

(*c*) *Permian*

The climate appears to have warmed up again during the Qixian (Artinskian) causing the facies and faunal belts to expand. This brought prograding carbonate ramps into the Lhasa region, together with large benthic forams and compound corals. Possibly at this time, and certainly during the early Permian, the first extensive rift volcanics were extruded in the Kunlun Shan. They may signal the beginning of rifting along Palaeo–Tethys.

The Maokouian (early Upper Permian) saw extensive development of shallow shelf carbonates with reefoidal developments reaching as far south as the Lhasa Terrane. Rifting continued throughout the Permian, recorded for example in the Kaixinling Group of the Qiangtang block.

By the late Permian the Palaeo–Tethys was presumably an ocean of significant size. Much of the land to the south appears to have been undergoing erosion at this time as no definite deposits of this age are known.

(*d*) *Triassic*

During Triassic times a major fore-arc accretionary prism of clastics built up along the northern margin of Palaeo–Tethys in response to north-directed subduction. Along the southern margin an extensive early Upper Triassic back-arc volcanic system (the Batang Group) developed. This was relatively short-lived because Norian shelf limestones lie across it, suggesting also that southward subduction had ceased along the Jinsha Suture.

There is evidence in the Lhasa Terrane of renewed Middle Triassic rift volcanics and breakup of the widespread carbonate platform during the Anisian. In the Carnian and Norian, extensive shelf basinal carbonate turbidites developed, and the first oceanic radiolarian cherts are found associated with the Zangbo suture, indicating the initiation and development of a major oceanic rupture.

(*e*) *Jurassic*

North of the Qiangtang Terrane, no marine Jurassic was deposited and the whole area appears to have undergone erosion at this time. A very thick fluviatile/coastal plain sequence of mid-Jurassic age in the southern Qiangtang Terrane represents a molassic wedge derived from the newly-fused orogenic belt formed by the Kunlun/Qiangtang Terrane collision. In the

northern part of the Lhasa Terrane marine incursions from a southern shelf penetrated into the coastal plain sequence occasionally. Upper Jurassic cherts and pillow lavas along the line of the Banggong Suture show that this was the site of a possibly minor ocean tract. Ophiolites had been emplaced and flysch basins developed by the end of Jurassic times, but final shortening does not appear to have occurred until well into the early Cretaceous.

(*f*) *Cretaceous*

The area north of the Banggong Suture was progressively uplifted and eroded as a result of the collision between the Lhasa and Qiangtang Terranes, producing the extensive Cretaceous molasse of the Lhasa region. There was also extensive post-collisional volcanism in the northern part of the Lhasa Terrane in Takena Formation times. A major marine transgression from the south during Aptian to early Cenomanian times temporarily halted the deposition of fluviatile clastics over the Lhasa Terrane. Deformation and erosion ensued towards the end of the Cretaceous, but its cause is uncertain.

In the Zangbo suture tract, open ocean sedimentation continued until the Turonian. Olistostromes then formed, marking the onset of obduction.

(*g*) *Tertiary*

Marine sedimentation continued along the Zangbo tract until mid Eocene times. Around Lhasa and at many localities to the north, molassic sedimentation persisted into the early Palaeogene. Thick arc-related volcanic sequences were erupted onto folded and eroded Upper Cretaceous molasse. Thick fluviatile facies accumulated in thrust-bound basins during the Eocene and later, indicating the onset of pervasive crustal shortening.

We thank Perce Allen, F.R.S., for his helpful comments on our work and its presentation. Thanks also to Roy Boud for drafting the complex figures 2, 6, 8, 9 and 11. We also express our gratitude for the herculean labours undertaken by the Chinese logistical support team, particularly to our willing and careful B-group drivers.

References

Allègre, C. J., Courtillot, V. and 33 others 1984 Structure and evolution of the Himalaya-Tibet orogenic belt. *Nature, Lond.* **307**, 17–22.

Audley-Charles, M. G. 1984 Cold Gondwana, warm Tethys and the Tibetan Lhasa block. *Nature, Lond.* **310**, 165.

Bernoulli, D. & Jenkyns, H. C. 1974 Alpine, Mediterranean and Central Atlantic Mesozoic facies in relation to the early evolution of the Tethys. In *Modern and ancient geosynclinal sedimentation* (ed. R. H. Dott & R. H. Shaver) SEPM Spec. Publ. No. 19, pp. 129–160. Tulsa.

Braakman, J. H., Levell, B. K., Martin, J. H., Potter, T. L. & Vilet, A. van. 1982 Late Palaeozoic Gondwana glaciation in Oman. *Nature, Lond.* **299**, 48–50.

Dickinson, W. R. & Suczek, C. A. 1979 Plate Tectonics and sandstone composition. *Bull. Am. Ass. Petrol. Geol.* **63**, 2164–2182.

Dong Deyuan & Mu Xinian 1984 Qamdo Region. In *Stratigraphy of Xizang (Tibet) Plateau*, pp. 237–287. [In Chinese.] Beijing Scientific Press.

Edwards, M. 1986 Glacial Environments. In *Sedimentary Environments and facies* (ed. H. G. Reading), pp. 445–470. 2nd Edn. Oxford: Blackwells.

Frakes, L. A. 1979 *Climates throughout geological time.* Amsterdam: Elsevier.

Liang Dingyi, Nie Zetong, Guo Tieying, Xu Baiwen, Zhang Yizhi & Wang Weipin 1983 Permo-Carboniferous Gondwana-Tethys facies in southern Karakoram Ali, Xizang (Tibet). *Earth Sci. Journal Wuhan College Geology* **19**, 9–26. [In Chinese with English abstract.]

Norin, E. 1946 Geological Explorations in western Tibet. *Sino-Swedish Exped. Publ.* 29. Stockholm: Aktiebolaget Thule, 214 pp.

Powell, C. McA. & Veevers, J. J. 1987 Namurian uplift in Australia and South America triggered the main Gondwanan glaciation. *Nature, Lond.* **326**, 177–179.

Tapponnier, P., Mercier, J. L. and 28 others 1981 The Tibetan side of the India-Eurasia collision. *Nature, Lond.* **294**, 405–410.

Phil. Trans. R. Soc. Lond. A **327**, 145–168 (1988) [145]
Printed in Great Britain

Plutonic rocks of the 1985 Tibet Geotraverse, Lhasa to Golmud

By N. B. W. Harris[1], Xu Ronghua[2], C. L. Lewis[1] and Jin Chengwei[2]

[1] *Department of Earth Sciences, Open University, Walton Hall, Milton Keynes MK7 6AA, U.K.*
[2] *Institute of Geology, Academia Sinica, P.O. Box* 634, *Beijing, People's Republic of China*

[Microfiche in pocket]

Two large east-trending granitic batholiths are exposed on the plateau of Central Tibet. In the southern Lhasa Terrane, north of the Zangbo Suture, the Gangdise Belt is a calc-alkaline composite batholith dominated by monzodiorites, tonalites, granodiorites and monzogranites. Trace elements indicate that strongly fractionated melts were emplaced at an active continental margin; deeper crustal levels of the batholith are exposed in the crustally-derived Nyainqentanglha orthogneiss. Along the northern edge of the plateau, a syn-tectonic calcic to calc-alkaline suite of tonalites, granodiorites and monzogranites forms the Kunlun batholith with post-tectonic granites emplaced to the south. The Kunlun intrusions are derived from anatexis of a garnet-bearing source at intermediate crustal depths above an active or recently active continental margin.

Between these two batholiths, a bimodal suite of metaluminous tonalite-granodiorite and peraluminous two-mica granite is exposed in the northern Lhasa Terrane, indicative of melting both in the upper crust and at deeper levels in the crust or upper mantle. This association suggests a post-collision setting.

1. Introduction

The Sino–British Geotraverse of Tibet identified three continental fragments which now comprise the Tibetan Plateau; the Lhasa, Qiangtang and Kunlun Terranes (Chang *et al.* 1986). Plutonic magmatism exposed along the route is largely restricted to three major regions; an east-trending batholith in the southern Lhasa Terrane, a broad belt of discrete plutons in the northern Lhasa Terrane and a second east-trending batholith in the Kunlun Mountains. The exposures in the Qiangtang and southern Kunlun Terranes are almost entirely restricted to volcano-sedimentary units but stream samples of granitoids suggest that a plutonic belt may be exposed along the Tanggula Shan both east and west of the Geotraverse route. This paper describes the petrology, geochemistry and petrogenesis of the three plutonic belts from south to north along the Geotraverse route.

2. Techniques and data collection

Major element analyses were determined by energy dispersive X-ray fluorescence on fusion discs at the Open University, and by wet chemical techniques at the Institute of Geology, Beijing (Academia Sinica). Trace elements (Rb, Sr, Ba, Y, Zr, Nb, Th and U) were determined by XRF analysis of pressed pellets and also by neutron activation analysis (U, Th, Ta, Hf, REE) at the Open University and computed using the methods of Potts *et al.* (1981). Trace

elements (Sr, Ba, Zr, Y, La) were determined in the Institute of Geology, Beijing (Academia Sinica) by ICP.

Selected analyses of Open University data are given in tables 1–3. The complete data-set of 110 analyses with the provenance of the data is available on microfiche (in pocket).

3. Plutonism of the southern Lhasa Terrane

(*a*) *The Gangdise Belt*

The southern edge of the Lhasa Terrane is intruded by a 3000 km long east-trending belt of magmatic rocks known as the Gangdise Belt, sometimes referred to as the Trans-Himalaya batholith in earlier publications. The plutonic complex is emplaced immediately north of the Zangbo Suture which defines the southern limit of the Lhasa Terrane and intrudes both its volcanic cover and folded Mesozoic sediments. The geochemistry of the belt has been the subject of numerous studies which have concentrated on four areas (figure 1); North Kohistan and Karakoram (Debon *et al.* 1987; Petterson & Windley 1985), Ladakh (Honnegar *et al.* 1982), Kailas (*ibid*) and the Lhasa–Zangbo Traverse (Debon *et al.* 1986; Jin & Xu 1980). It is the Lhasa–Zangbo Traverse which has been the area of further investigation in this study.

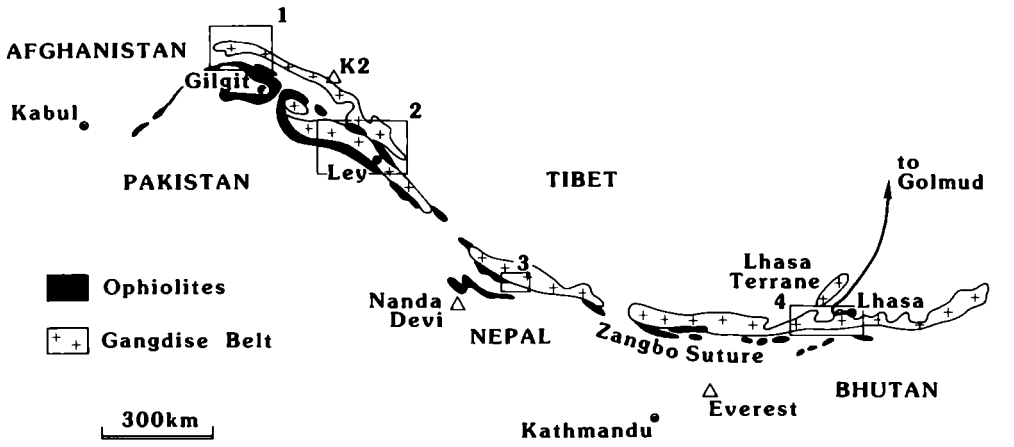

FIGURE 1. Sketch-map of distribution of granitoids from the Gangdise Belt intruded north of the Zangbo ophiolite. Localities of published geochemical data: 1. North Kohistan and Karakorum. 2. Ladakh. 3. Kailas. 4. Lhasa-Zangbo traverse. For references see text.

The northern limit of the Gangdise Belt to the north of Lhasa is equivocal. Previously it has been defined 30 km beyond the northern limit of the Lhasa–Gurong pluton (which lies about 50 km north of the Zangbo Suture) and includes a small granite body east of Yangbajain (Debon *et al.* 1986). In this study the belt is extended to include the extensive granitoids of the Nyainqentanglha Mountains, 10 km north-west of Yangbajain, on the basis of geochemical and isotopic similarities of these rocks with those exposed in the southern Gangdise Belt (figure 2).

(*b*) *Field relations and Petrology*

From the Zangbo Suture to 20 km north of Lhasa a suite of plutonic rocks emplaced into volcanics and Mesozoic sediments is known as the Quxu, Dagze and Lhasa–Gurong intrusions.

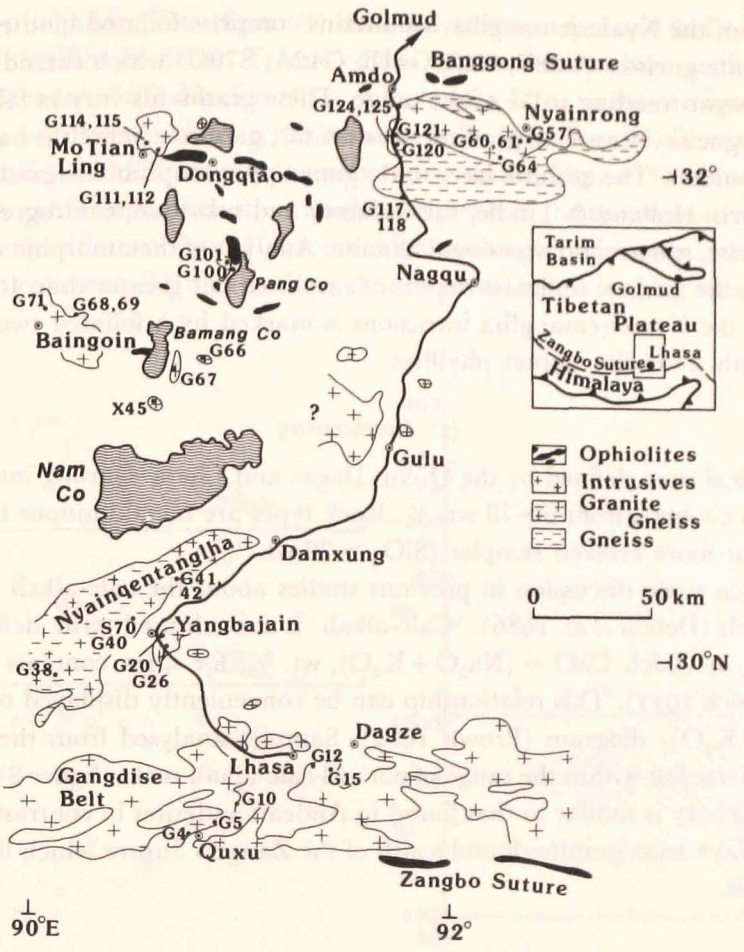

FIGURE 2. Sample location map for geochemical samples from the Lhasa Terrane.

The boundaries between these bodies are gradational and since petrological variation within any one 'intrusion' is considerable they are here described as a composite plutonic complex, representative of the southern Gangdise Belt. The igneous suite is characterized by olivine gabbro (< 5% of exposed outcrop), hornblende quartz diorite, hornblende–biotite monzodiorite (G4, G5), tonalite (G15A), biotite–hornblende granodiorite (G12) and biotite monzogranite (G10). The Streckeisen (1976) petrological classification is used throughout this study. No deformation is observed towards the core of these bodies, but a foliation is frequently developed towards their margins. Contacts with non-plutonic rocks are sharp and contact metamorphism is developed locally. For example, along the northern contact of the Lhasa body diopside and idocrase occur within Jurassic limestone and along its western margin it intrudes volcanics from the Linzizong Formation within which pinite replacement of cordierite is developed close to the contact.

The Yangbajain intrusion (6 × 10 km in outcrop area) contains two plutonic facies intruded into Carboniferous sandstone. A biotite-hornblende-sphene granite (G26) is intruded by a more leucocratic biotite granite (G20) containing large xenoliths of biotite gneiss and injection migmatites. Although no diagnostic metamorphic minerals have been found in these xenoliths, they strongly resemble pelitic gneiss exposed 20 km north in the Nyainqentanglha Mountains.

Exposures from the Nyainqentanglha Mountains comprise foliated biotite granites (G42B, S70D) and granite gneisses (G38E, G40, G41B, G42A, S70C) which extend for about 80 km along the north-east-trending strike of the range. These granitoids vary in fabric from slightly foliated to orthogneiss (but are all granites *sensu stricto*); gabbroic xenoliths have been found in some gneissic boulders. The granites have undergone upper amphibolite grade metamorphism (> 700 °C, Harris, Holland & Tindle, this volume) and subsequent retrogression resulting in chlorite, muscovite, sphene and occasional allanite. Analysis of metamorphic assemblages from xenoliths within the gneisses indicates depths of emplacement greater than 10 km. The north-eastern limit of the Nyainqentanglha intrusions is marked by a foliated two-mica granite in fault-contact with staurolite–garnet phyllites.

(*c*) *Geochemistry*

The petrological suite defined by the Quxu, Dagze and Lhasa–Gurong intrusions represent a range of silica contents from 50–73 wt. %. Rock types are metaluminous becoming slightly peraluminous for more evolved samples (SiO_2 > 70 wt. %).

There has been some discussion in previous studies about the calc-alkali characteristics of the Gangdise Belt (Debon *et al.* 1986). 'Calc-alkali' is a much used term, defined originally as a suite of rocks in which CaO = ($Na_2O + K_2O$), wt. %, for silica contents between 56 and 61 wt. % (Peacock 1931). This relationship can be conveniently displayed on a SiO_2 vs $\log_{10}$ ($CaO/(Na_2O + K_2O)$) diagram (Brown 1982). Samples analysed from the Zangbo–Nyainqentanglha traverse fall within the range of normal calc-alkali rocks (figure 3), and their major element geochemistry is similar to that found in Andean andesites in contrast, for example, to the High Himalaya leucogranites found south of the Zangbo Suture which lie well within the alkali-calcic field.

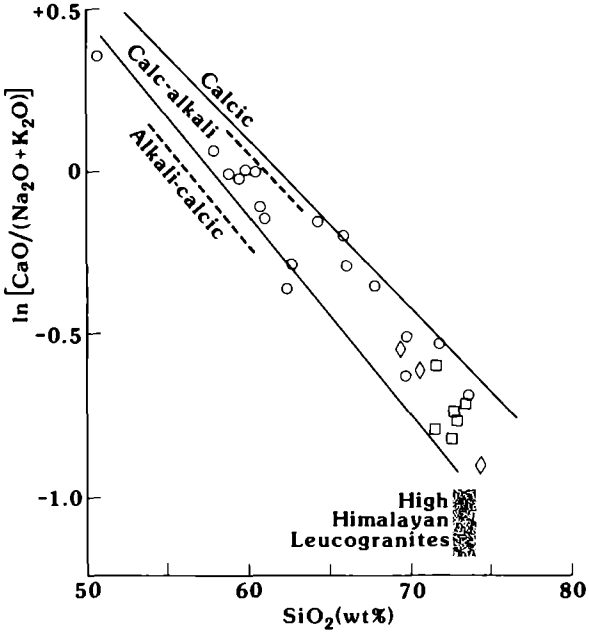

FIGURE 3. Plot of $\log_{10}(CaO/(Na_2O + K_2O))$ against SiO_2 for samples from Gangdise Belt (Zangbo–Nyainqentanglha traverse). Broken lines indicate boundaries of calc-alkali field. Solid lines define field of Andean andesites (Brown 1982). Data from Table 1 and Debon *et al.* 1986. ○ = Lhasa-Gurong-Quxu, ◇ = Yangbajain, □ = Nyainqentanglha.

Major element variation plots (figure 4) show a systematic decrease in Fe, Ca, Mg and an increase in K with silica contents. Trends of this type are an ambiguous indicator of fractionation, both because of the dilution effect of increasing SiO_2 on other major element oxides and because apparent trends could result from assimilation of a granitic end-member, but a general interpretation is that fractionating phases contain Fe, Mg and Ca, but not alkalis, such as hornblende. Amphibole fractionation would also result in the switch from metaluminous to peraluminous compositions observed in more evolved samples. However, trace element plots (figure 4) are less coherent. Rb and Sr show characteristic trends for plagioclase fractionation,

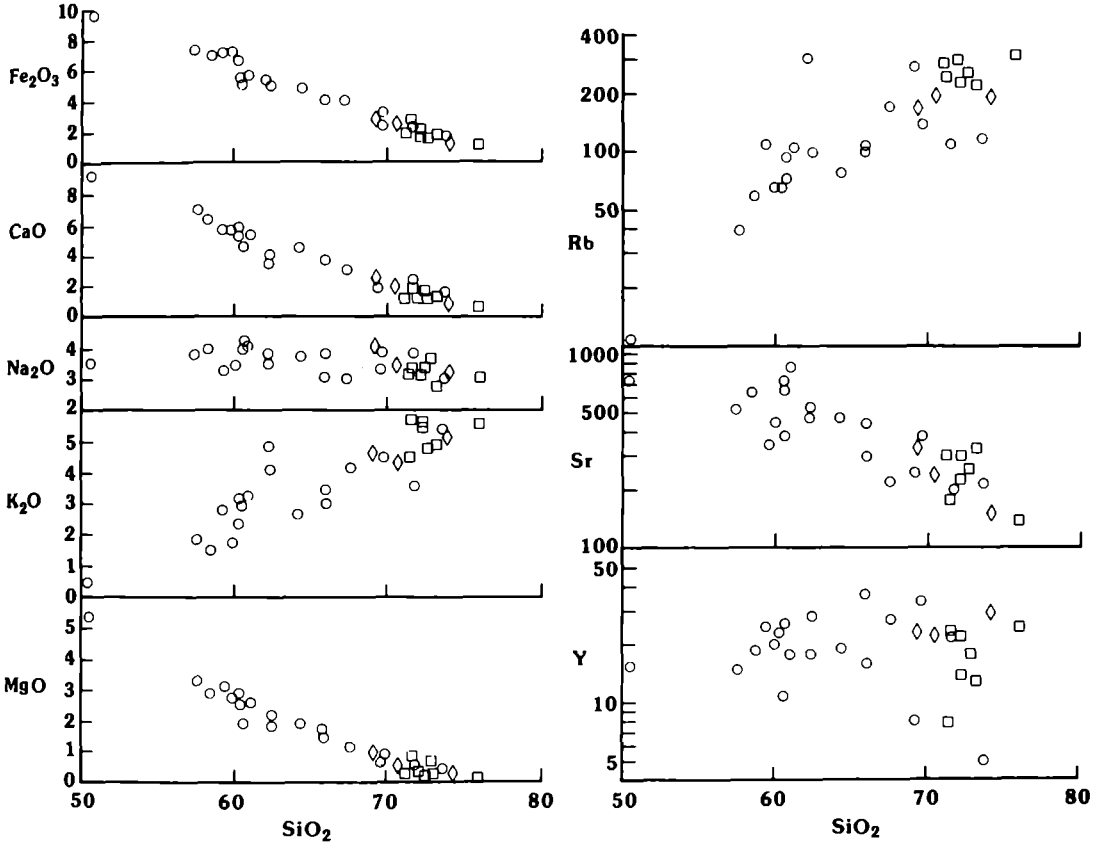

FIGURE 4. Silica variation diagrams for samples from Gangdise Belt (Zangbo-Nyainqentanglha traverse). Oxides in wt. %, trace elements in p.p.m. All Fe calculated as Fe_2O_3. Symbols and data sources as for figure 3.

but Y, a generally immobile element, shows a poor correlation with SiO_2. For $SiO_2 < 68$ wt. % there is a general increase with silica content indicating incompatible behaviour. More siliceous samples have widely ranging Y contents suggesting complex accessory phase fractionation.

To analyse the major phases responsible for fractionation within a restricted zone of the batholith, Rb/Sr vs Sr has been plotted from the Quxu–Lhasa section (figure 5). Fractionation trends for observed major phases are also plotted. This shows clearly that fractionation is controlled by feldspar rather than biotite, although hornblende fractionation would not be apparent on this plot. About 30 % feldspar fractionation is required to derive the granite (G10) from the monzodiorite (G5). However a second monzodiorite (G4), although lying close to this

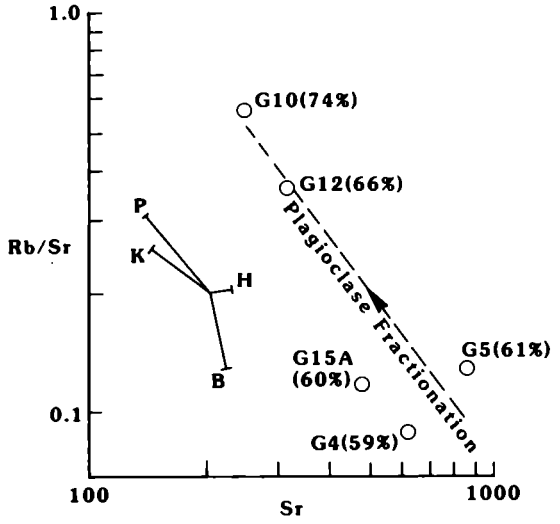

FIGURE 5. Rb/Sr against Sr for samples from the Quxu-Lhasa section of the Gangdise Belt. Approximate SiO_2 contents (wt. %) given in parentheses. Data from table 1. Vectors give change in magma composition from 10% fractionation of plagioclase (P), potassium feldspar (K), hornblende (H) and biotite (B).

trend, cannot result from the same magma batch due to its much lower K/Rb at similar SiO_2.

REE plots from the Quxu intrusion (figure 6*a*) show that the gabbro has a high LREE/HREE ratio, consistent with a garnet-bearing source. Evolution from gabbro (SiO_2 = 51 wt. %) to granodiorite (SiO_2 = 62 wt. %) require an increase in all REE except Eu – a indication of feldspar fractionation. However evolution to the granite (SiO_2 = 70 wt. %) requires fractionation of a HREE-enriched phase such as zircon or xenotime. This is mimicked, although less convincingly, in the SiO_2 vs Y plot of figure 4. Both trends are indicative of late-stage zircon or xenotime fractionation. The REE plot from the Dagze tonalite (G15a, figure 6*a*) indicates an

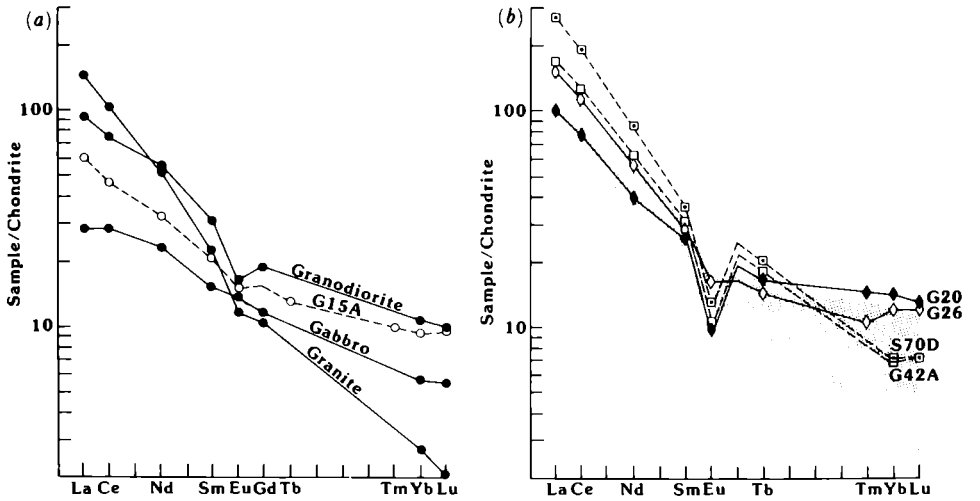

FIGURE 6. Chondrite normalized REE plots for Gangdise Belt intrusives. (*a*) solid lines indicate Quxu pluton (data from Debon *et al.* 1986). Broken line indicates Dagze tonalite (G15A). (*b*) Yangbajain granite (G20, G26), and Nyainqentanglha granite gneiss (G42A, S70D). Shaded region delineates range from Quxu intrusion. Data from table 1.

REE profile with a similar LREE/HREE to the Quxu granodiorite, but with a smaller Eu anomaly indicating a smaller degree of feldspar fractionation in the tonalitic magma.

In summary, geological evolution within the southern Gangdise Belt is dominated by feldspar and hornblende fractionation from gabbroic melts in the early stages, but also by minor phases in the more evolved samples. Isotopic constraints (Harris, Xu *et al.* this volume) require crustal assimilation to contribute to magmagenesis of tonalites and granites from the Gangdise Belt. Not all samples can be related to the same source, even within a restricted area such as Quxu.

The Rb vs (Nb+Y) and Rb vs (Ta+Yb) plots are useful indicators of tectonic setting for fresh equigranular granitic rocks (Pearce *et al.* 1984). Samples from throughout the Gangdise Belt fall within the volcanic arc/post-collision field in strong contrast to the syn-collision High Himalayan leucogranites found south of the Zangbo Suture (figure 7*a*), although since some of these samples represent the data-base from which the plots were derived, this is unsurprising. Since the publication of Pearce *et al.* (1984), it has been established that the high Rb-low HFS element field has encompassed not only syn-collision granites such as from the High Himalayas, but also post-collision crustal melts, such as the Alpine Novate intrusion (Harris *et al.* 1986). Moreover the geochemically similar Pyrenean leucogranites, although undoubtedly crustal melts, may have been generated in an extensional environment (Wickam & Oxburgh 1986). For these reasons the field has been relabelled 'upper crustal melt', which does not of course preclude granites with crustal components falling in other fields. It does however encompass those granites formed largely from melting of the upper crust due to anomalously high temperatures in that crust whether these are induced by collision or crustal thinning.

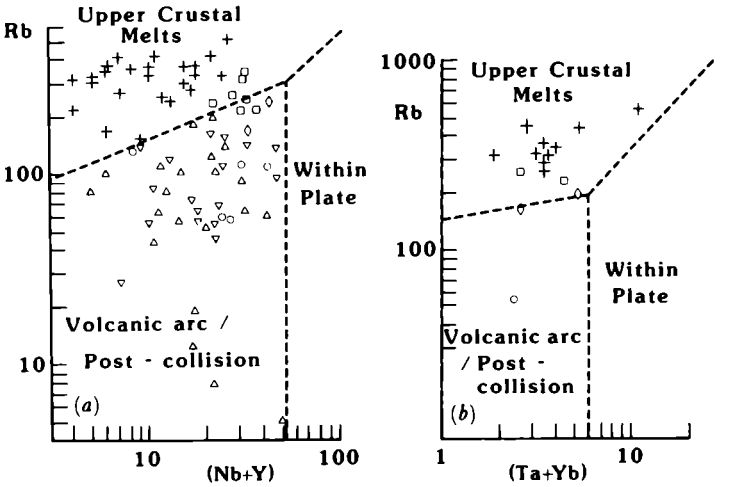

FIGURE 7. (*a*) Rb vs (Nb+Y) plot (*b*) Rb vs (Ta+Yb) plot for samples from Gangdise Belt and High Himalaya leucogranites (+, data from Dietrich & Gansser 1981, Harris *et al.* 1986). △ = Kohistan, ▽ = Ladakh. Other symbols as for figure 3. Field boundaries from Pearce *et al.* (1984).

The Yangbajain body is a metaluminous biotite–hornblende–sphene monzogranite intruded by peraluminous biotite granite. The metaluminous phase is indistinguishable from the granites exposed in the Lhasa–Quxu region to the south in both major and trace element plots. It is part of the calc-alkaline trend (figure 3), has a similar REE profile to the Quxu granodiorite (sample G26, figure 6*b*) and lies in the volcanic arc field in the tectonic discrimination diagrams (figure

7*a*, *b*). Spidergram plots of a range of trace elements (figure 8) indicates that the granite is virtually identical to Andean continental margin granites of similar SiO_2 contents. The younger peraluminous granite is more depleted in Eu than samples from the southern Gangdise Belt (sample G20, figure 6*b*) which implies either a small degree partial melt of feldspar-bearing source rock, or plagioclase fractionation.

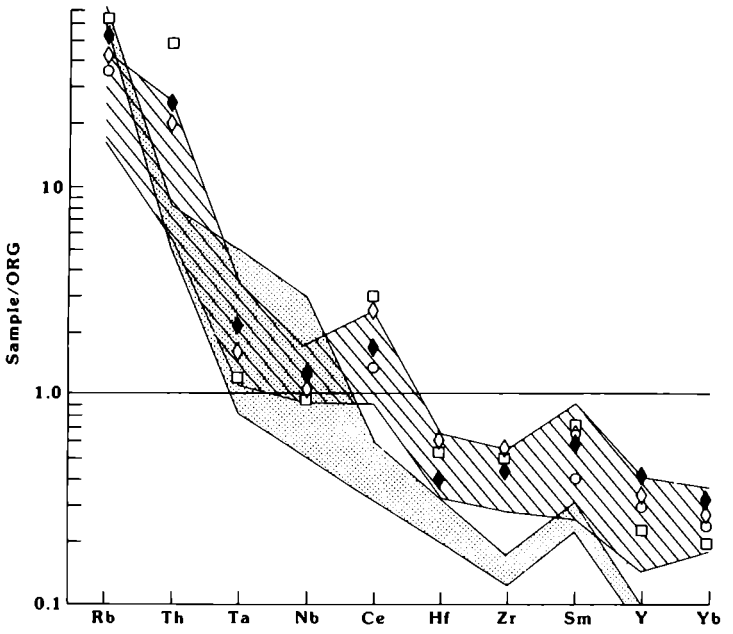

FIGURE 8. Geochemical patterns for granitic samples from the Gangdise Belt (SiO_2 = 68–75 wt. %) normalized against Ocean Ridge Granite (Pearce *et al.* 1984). Lined field = volcanic arc/post-collision granites, stippled field = High Himalayan leucogranites. ○ = Lhasa granite (Debon *et al.* 1986), ◇ = G26 (Yangbajain, metaluminous facies), ◆ = G20 (Yangbajain peraluminous facies), □ = S70D (Nyainqentanglha). Data from table 1.

The Nyainqentanglha samples are predominantly peraluminous biotite syeno-monzogranites. They are all highly evolved (SiO_2 > 71 wt %) and lie within a calc-alkali field (figure 3). They have somewhat lower Fe, Ca, Mg and Sr and higher K and Rb than the calc-alkaline rocks of the southern Gangdise belt (figure 4). The Nyainqentanglha samples are also LREE-enriched and show larger negative Eu anomalies compared to southern Gangdise samples (figure 6*b*). The uniformly high SiO_2 and Rb contents and strongly peraluminous compositions from samples across the Nyainqentanglha range are an indication that crustal melting was involved in their petrogenesis. Available Sr and Nd isotopic data (Harris, Xu, Lewis, Hawkesworth & Zhang, this volume) require a crustal source and preclude an origin by simple fractionation of amphibole and feldspar from calc-alkaline magmas now represented in the southern Gangdise Belt.

In the Rb vs (Nb+Y) plot (figure 7*a*) Nyainqentanglha samples straddle the volcanic arc/post collision and crustal melt fields. These granites however differ from crustal melts derived from collision-related anatexis such as the High Himalaya leucogranites (figure 8) in their much higher Th and LREE contents and their smaller depletions in HFS elements (Hf, REE, Y). Th enrichment in subduction-related magmas may be interpreted as a

component from subducted sediments (Pearce 1982) but Th contents in the Nyainqentanglha granites (28–78 p.p.m.) are much higher than those observed in magmatic arcs (< 20 p.p.m. Brown *et al.* 1984). U, with the exception of S70C which is a highly evolved granite (SiO_2 > 76 wt. %), is not enriched in the Nyainqentanglha granites. Th and LREE bearing phases observed in the granites include allanite and monazite.

The high Th and LREE contents of the Nyainqentanglha granites result from either late-stage accessory phase crystallization from the magma or entrainment of these phases into the magma from the source rock during anatexis, a process inferred from studies of other crustally-derived granites (Sawka *et al.* 1986). Microprobe studies of accessory phases are required to identify the dominant host phase of Th and LREE, but the discordant nature of some zircons from the granites provides evidence that this phase at least is inherited from the source region (Xu *et al.* 1985).

TABLE 1. SELECTED ANALYSES FROM SOUTHERN LHASA TERRANE

	Quxu		Lhasa		Dagze	Yangbajain		Nyainqentanglha		
	G4	G5	G10	G12	G15A	G20	G26	G42A	S70C	S70D
	MzD	MzD	Gr	Gd	Ton	Gr	Gr	Gr gn	Gr gn	Gr
SiO_2	58.73	61.00	73.76	65.96	60.00	74.25	69.30	72.23	76.05	72.87
TiO_2	0.71	0.70	0.22	0.75	0.83	0.19	0.43	0.31	0.11	0.26
Al_2O_3	17.18	16.85	14.20	15.41	16.86	14.14	15.77	15.46	13.75	14.52
Fe_2O_3	6.97	5.61	1.73	4.98	7.24	1.31	2.99	2.06	1.25	1.79
MnO	0.13	0.10	0.03	0.07	0.14	0.08	0.09	0.03	0.02	0.04
MgO	2.82	2.63	0.61	1.56	2.80	0.12	0.98	0.39	0.18	0.31
CaO	6.15	5.34	1.71	4.17	5.74	1.02	2.54	1.64	0.89	1.44
Na_2O	3.99	4.25	3.00	3.44	3.92	3.43	4.20	3.60	3.29	3.67
K_2O	2.55	3.27	5.53	3.16	1.84	5.18	4.66	5.53	5.71	4.81
P_2O_5	0.20	0.28	0.05	0.18	0.23	0.00	0.15	0.08	0.13	0.08
LOI	0.35	0.32	0.21	0.61	0.33	0.21	0.51	0.26	0.37	0.33
Total	99.78	100.35	101.05	100.29	99.93	99.93	101.63	101.59	101.75	100.12
ppm										
Rb	58	110	137	108	57	229	174	236	339	264
Sr	645	867	242	304	470	152	368	303	127	236
Ba	623	660	370	620	381	358	880	330	<210	750
Zr	127	174	99	208	101	119	190	225	118	175
Hf	—	—	—	—	3.9	3.8	5.5	6.9	—	5.3
Nb	6	13	3	7	7	13	10	8	17	10
Ta	—	—	—	—	0.44	1.6	1.2	3.0	—	0.92
Y	19	18	5	36	20	30	24	14	25	18
Th	6	27	21	6	4.0	21	17	7.3	55	43
U	< 3	6	4	< 3	1.0	3.0	3.4	8.9	31	6.3
La	—	—	—	—	21	34	53	90	—	54
Ce	—	—	—	—	41	69	101	167	—	108
Nd	—	—	14	—	21	26	36	54	38	38
Sm	—	—	1.7	—	4.3	5.6	6	7.2	8.1	6.3
Eu	—	—	—	—	1.2	0.77	1.3	1.0	—	0.83
Tb	—	—	—	—	0.68	0.89	0.75	1.1	—	0.95
Tm	—	—	—	—	0.34	0.52	0.36	—	—	—
Yb	—	—	—	—	2.1	3.3	2.8	1.5	—	1.6
Lu	—	—	—	—	0.34	0.46	0.42	0.25	—	0.25

MzD = monzodiorite, Gr = granite, Gd = granodiorite, Ton = tonalite, gn = gneiss.

4. Plutonism of the northern Lhasa Terrane

(*a*) *Field relations and petrology*

Between the Nyainqentanglha Belt and the Banggong Suture lies a 100 km wide east-trending belt of predominantly intrusive magmatism (figure 2). The intrusions display pre-kinematic fabric such as foliated margins or elliptical cordierite spots in the contact zones although many of the samples appear undeformed in outcrop.

The best exposed pluton in the belt outcrops south-east of Baingoin and is a composite body which comprises a biotite tonalite (G68) intruded by a two-mica tourmaline granite (G69, G71) with tonalite enclaves and cut by tourmaline-muscovite pegmatites. Contacts between the intrusion and the Carboniferous shales it intrudes are semi-concordant and within the metasediments a narrow garnet–tourmaline–topaz aureole is developed.

On the north-west banks of Pung Co, biotite granite (G100) is intrusive into both Jurassic sediments and a 1 km diameter plug of hornblende–hypersthene–biotite granodiorite (G101). Both intrusions post-date allochthonous gabbros associated with a dismembered sliver of Banggong ophiolite. A similar association of biotite granites and granodiorite–quartz monzonite is emplaced to the south-east of Bamang Co (G67, X45).

The largest known outcrop of intrusive rock in the northern Lhasa Terrane is the Nyainrong–Amdo batholith which covers an area at least 2000 km^2 south-east of Amdo. Exposed along the Nagqu–Nyainrong road, the dominant rock-type is a porphyritic biotite granite (G64), within which patches of strongly porphyritic (5–10 cm microcline megacrysts) hornblende–biotite granite are developed (G60, G61). The intrusion is transected by screens of biotite or hornblende gneiss and calc-silicates. Contact metamorphic skarns are observed in the calc-silicates containing diopside and idocrase. South of Amdo a biotite–hornblende granodiorite (G124) is locally strongly porphyritic and intrudes both amphibolite (G117) and biotite orthogneiss (G118).

Twenty kilometres north-west of Dongqiao, near Mo Tian Ling, Carboniferous shales are intruded by a 12 km diameter intrusion of biotite–hornblende–augite–sphene granodiorite (G111, G115) and biotite granite (G114). Regional structures indicate the Banggong Suture lies to the north of this intrusion which implies that the Mo Tian Ling pluton should be grouped with the intrusions of the northern Lhasa Terrane.

(*b*) *Geochemistry*

The northern Lhasa Terrane granitoids are characterized by a bimodal association of a peraluminous granite intruding a metaluminous granodiorite or tonalite. This relationship is exemplified at Baingoin by a biotite tonalite of strongly calcic geochemistry (figure 9) being intruded by a calc-alkaline peraluminous syeno-monzogranite. The high Rb and SiO_2 contents and strongly peraluminous character of the granite are indicative of a crustal component and the strong negative Eu anomaly (figure 10*a*) suggests a feldspar-bearing source. The associated tonalite (G68A) has a similar negative Eu anomaly which precludes fractionation of feldspar from the tonalite to generate the peraluminous granite. The Rb vs (Nb + Y) and Rb vs (Ta + Yb) plots (figure 11) indicate that the more calcic phase of the bimodal association lies in the volcanic arc/post-collision field whereas the peraluminous granite lies in the crustal melt field. On trace element grounds it has not been possible to distinguish 'volcanic arc' from some 'post-collision' intrusions. For example, most post-collision Alpine intrusions plot within

the volcanic arc field of figure 11. However the spatial and temporal association of 'volcanic arc' magmas and upper crustal melts is indicative of post-collision magmatism. In general, the 'volcanic arc' component is thought to be derived from near the base of the thickened crust in response to the transient geotherm and to rising mantle melts above the now defunct subduction zone (Harris *et al.* 1986). The crustal melts result from anatexis of the tectonically thickened crust in response to rising aqueous fluids from underthrust sediments. The abundance of tourmaline in many such granites suggests marine sediments as a possible boron source.

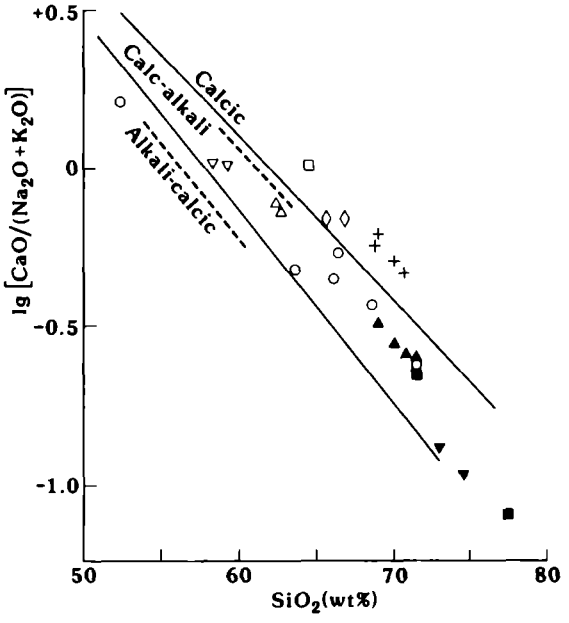

FIGURE 9. Plot of $\log_{10}(CaO/(Na_2O+K_2O))$ against SiO_2 for samples from northern Lhasa Terrane. Field boundaries as for figure 3. Data from table 2. ■ = Baingoin (granite), □ = Baingoin (tonalite), ▼ = Pung Co (granite), ▽ = Pung Co (granodiorite), ◇ = Bamang Co, ▲ = Nyainrong, △ = Amdo, ○ = Mo Tian Ling, + = basement south of Amdo.

The detailed geochemistry of the peraluminous granite however (figure 12) is distinct from the syn-collision melts of the High Himalayas. Like the Nyainqentanglha granites, Th and LREE are strongly enriched but HFS elements are only slightly depleted. These may be interpreted in one of two ways: either the magma contains a LIL-enriched component derived from the hydrated mantle wedge beneath the collision zone or the magma results from crustal anatexis under conditions where Th and LREE enter the melt. Since Th enrichment is more marked than for normal arc-related granites, and since Th enrichment is seen in the Eocene Nyainqentanglha intrusions to the south, it seems likely that the latter reason is appropriate and the Th is therefore probably crustally derived. However unlike the discordant zircons from the Nyainqentanglha gneiss, zircons and monazites of Cretaceous age from the Baingoin granite (121 ± 2 Ma) are virtually concordant (Xu *et al.* 1985). Preliminary microprobe analysis of accessory phases indicate that Th and LREE are concentrated in monazite ($ThO_2 = 6.3\%$, $Ce_2O_3 = 28.5\%$); other accessories include apatite, zircon and ilmenite. The refractory nature of monazite is critically dependent on the size of the crystals in the source rock and the water activity in the melt. For example at temperatures of 700–800 °C and under

hydrous conditions small monazites will be digested in the melt but larger crystals are residual (Rapp & Watson 1986). The concordant nature of the Baingoin monazites and zircons suggests crystallisation from the Cretaceous melt.

The Bamang Co intrusions have a higher alkali feldspar content than the Baingoin tonalite, but otherwise are geochemically similar; they are calcic rather than calc-alkaline (figure 9),

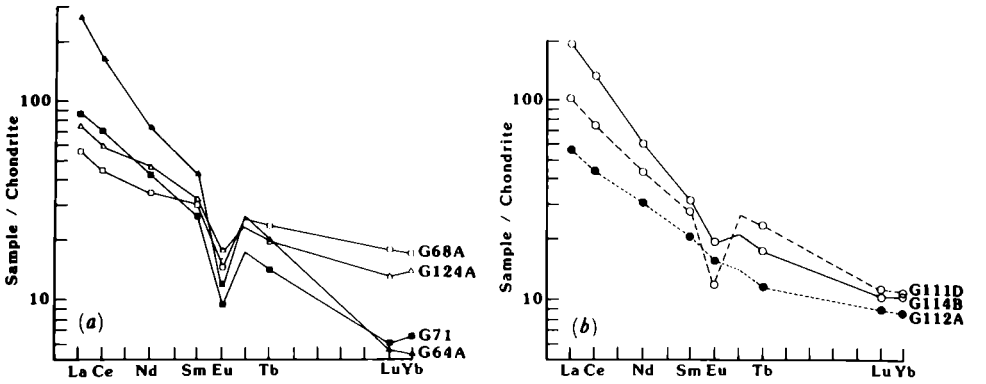

FIGURE 10. Chondrite normalized REE plots for samples from northern Lhasa Terrane. (*a*) Baingoin (G68A, G71) and Nyainrong-Amdo batholith (G64A, G124A). (*b*) Mo Tian Ling. Data from table 2.

and trace elements indicate a volcanic arc/post-collision origin (figure 11*a*). The two components of the Pung Co intrusion also show a close geochemical similarity to those from the Baingoin body. The granodiorite is metaluminous with a volcanic-arc/post-collision signature (figure 11*a*). The granite is peraluminous bridging the syeno-monzogranite boundary and trace elements (elevated Rb/HFS ratios) indicate a crustal melt origin.

The Nyainrong–Amdo batholith again reflects this bimodal association. The Amdo region is characterized by metaluminous, calc-alkaline granodiorite with trace elements indicating volcanic arc/post-collision field. Rare earth elements show a large LREE/HREE ratio and a strong negative Eu anomaly closely paralleling that of the Baingoin tonalite (G124A,

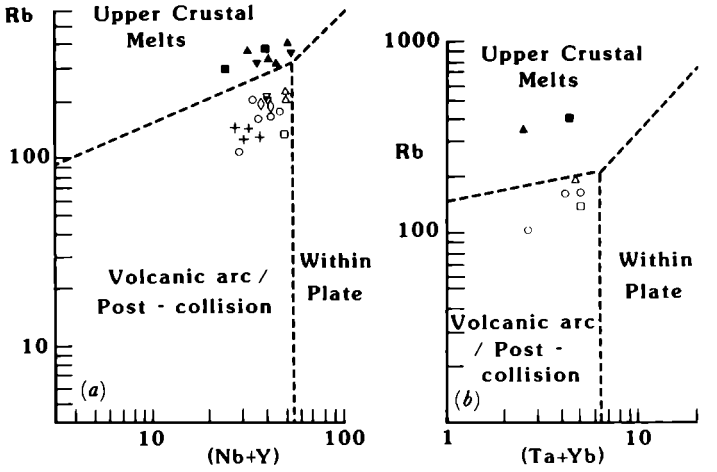

FIGURE 11. (a) Rb vs (Nb+Y) plot, (b) Rb vs (Ta+Yb) plot for samples from the northern Lhasa Terrane. Symbols as for figure 9. Field boundaries from Pearce *et al.* (1984).

figure 10). In the Nyainrong region a peraluminous monzogranite is rimmed by a metaluminous orthoclase–porphyritic monzogranite, both facies indicating a crustal melt origin (figure 11), although in the case of the strongly porphyritic phase this is inconclusive because alkalis have certainly been affected by post-crystallisation fluid mobility. The equigranular phase has trace elements similar to the Baingoin granite (figure 12) except that Th and LREE are even more enriched in the Amdo sample. Microprobe analysis of accessory phases indicate that the hosts for Th and LREE include allanite (ThO_2 = 8.8%, Ce_2O_3 = 13.8%) and thorite (ThO_2 = 63.0%).

The exposures of basement to the south of Amdo are predominantly tonalitic orthogneiss which the Nyainrong–Amdo batholith intrudes. The orthogneiss is calcic (figure 9) and lies in the volcanic arc field of figure 11*a*. Both Rb and Th are low indicative of an island arc, rather than an active continental margin. Low Th values make this gneiss an unlikely source for the crustal melt granites of the region, and this inference is supported by isotopic arguments (Harris, Xu, Lewis, Hawkesworth & Zhang, this volume).

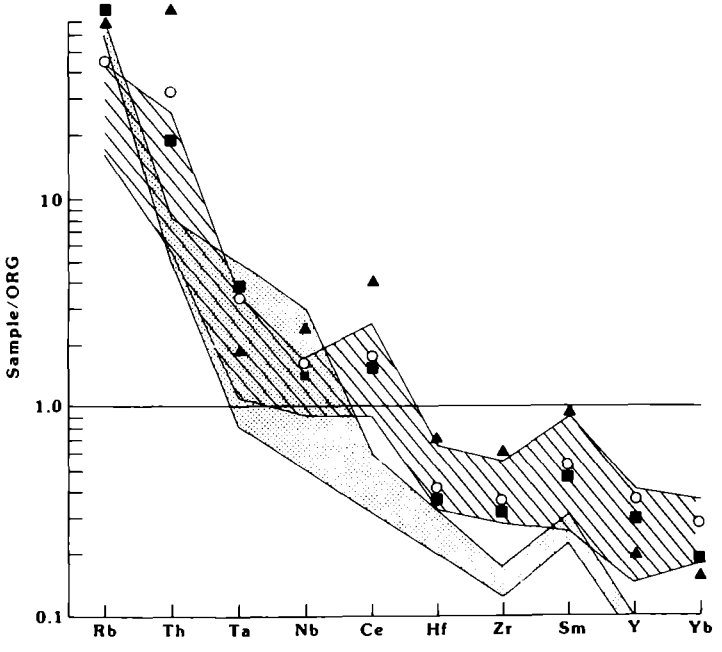

FIGURE 12. Geochemical patterns for granitic samples from the northern Lhasa Terrane (SiO_2 = 68–75 wt. %) normalised against Ocean Ridge Granite (Pearce *et al.* 1984). Lined field = volcanic-arc/post-collision granites, stippled field = High Himalaytan leucogranites. ■ = G71 (Baingoin), ▲ = G64A (Nyainrong), ○ = G114B (Mo Tian Ling).

The Mo Tian Ling intrusion is a granodiorite-granite which is calc-alkaline (figure 9) and lies well within the 'volcanic arc/post-collision' field of figure 11. The granodiorite (G111D) could be derived from a diorite source (G112A) since the strong negative Eu anomaly and increased REE contents of the granodiorite indicate feldspar fractionation (figure 10*b*). However, the monzogranite (G114B) has a much smaller Eu anomaly than the granodiorite, and, although the steeper LREE/HREE ratios could be modelled by fractionating a HREE-rich accessory phase such as zircon or xenotime, it is not possible to reduce substantially a negative Eu anomaly unless the granite incorporates cumulate feldspar. Therefore the REE plots

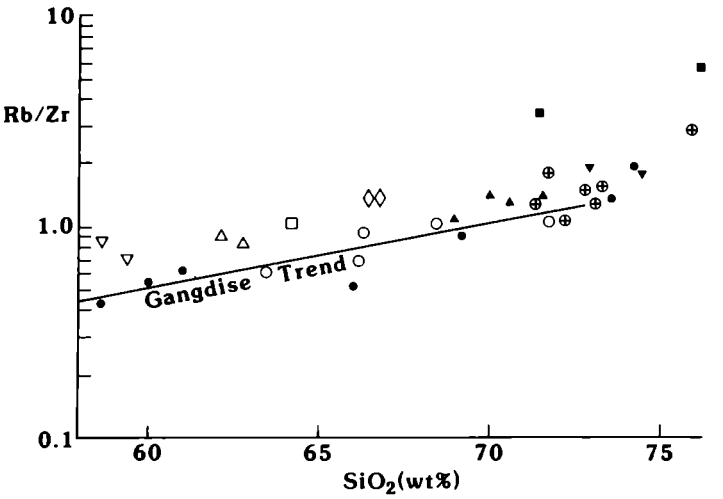

FIGURE 13. Rb/Zr vs SiO_2 for samples from the northern Lhasa Terrane compared with the Gangdise Belt (●) and the Nyainqentanglha (⊕). Other symbols as for figure 9.

TABLE 2. SELECTED ANALYSES FROM NORTHERN LHASA TERRANE

	Baingoin		Nyainrong-Amdo		Mo Tian Ling				Amdo Basement	
	G68A	G71	G64A	G124A	G111D	G112A	G114B	G115A	G118A	G118D
	Ton	Gr	por Gr	Gd	Gd	D	Gr	Gd	Ton gn	Ton gn
SiO_2	64.27	71.49	71.56	62.28	63.54	52.23	71.77	68.43	68.98	69.91
TiO_2	0.53	0.32	0.39	0.79	0.80	0.90	0.40	0.57	0.43	0.41
Al_2O_3	16.62	15.57	14.76	16.74	16.79	14.90	15.15	15.99	14.86	15.34
Fe_2O_3	5.19	3.24	2.16	5.49	4.25	8.22	2.15	3.16	4.53	3.87
MnO	0.10	0.07	0.04	0.09	0.07	0.13	0.04	0.06	0.08	0.08
MgO	2.43	1.08	0.50	2.76	1.88	8.73	0.85	1.49	1.47	1.25
CaO	5.21	1.63	2.02	4.42	3.80	7.79	2.06	2.93	3.30	3.05
Na_2O	2.55	2.85	3.28	3.89	4.35	2.83	3.65	4.06	3.74	4.39
K_2O	2.34	4.41	4.89	3.07	3.47	1.86	4.82	3.75	1.54	1.39
P_2O_5	0.13	0.17	0.10	0.16	0.23	0.21	0.13	0.16	0.10	0.08
LOI	0.75	0.88	0.57	0.88	0.59	2.34	0.34	0.47	0.76	0.39
Total	100.12	101.71	100.27	100.57	99.77	100.14	101.36	101.07	99.79	100.16
ppm										
Rb	130	391	353	198	156	103	156	201	140	129
Sr	301	112	227	262	387	311	223	287	168	137
Ba	< 310	< 270	< 280	450	580	780	320	340	410	< 280
Zr	126	119	246	212	255	116	145	171	156	137
Hf	4.2	3.7	6.8	6.7	5.9	2.9	3.8	—	—	—
Nb	10	16	19	16	18	9	16	16	11	14
Ta	0.98	2.7	1.3	1.7	1.5	0.60	2.5	—	—	—
Y	42	21	14	35	25	21	28	24	22	23
Th	7.3	17	81	14	27	5.8	37	26	17	14
U	3.1	2.9	7	7	3.2	1.1	2.4	< 4	< 3	< 3
La	19	29	90	25	64	19	34	—	—	—
Ce	40	61	147	52	114	39	65	—	—	—
Nd	23	27	48	29	39	20	29	—	34	22
Sm	6.2	5.4	9.2	6.6	6.5	4.3	5.9	—	5.7	4.5
Eu	1.1	0.74	0.97	1.4	1.5	1.2	0.93	—	—	—
Tb	1.2	0.75	1.1	1.0	0.92	0.61	1.2	—	—	—
Tm	—	—	—	—	—	—	—	—	—	—
Yb	3.9	1.4	1.3	2.9	2.4	2.0	2.5	—	—	—
Lu	0.58	0.23	0.19	0.49	0.38	0.30	0.38	—	—	—

Ton = tonalite, Gr = granite, Gd = grandiorite, D = diorite, gn = gneiss, por = porphyritic.

preclude simple fractionation from a single parent magma. The range of trace elements (figure 12) indicates a typical active continental margin or post-collision intrusion with some Th enrichment.

The high crustal component present in some post-collision magmas can not readily be demonstrated by trace elements in the absence of isotopic data. However, Rb/Zr has been used as an indicator of crustal melting (Harris *et al.* 1986), although its usefulness depends on zircon being residual during anatexis. This ratio does show that for virtually all northern Lhasa Terrane intrusives there is a shift to higher Rb/Zr for given SiO_2 contents relative to the Gangdise samples (figure 13). This may reflect the high contribution of crust found in post-collision magmagenesis compared with active continental margin processes.

In summary the northern Lhasa Terrane plutons are essentially bimodal and the two phases cannot be easily related in terms of single petrogenetic process. The earlier phase is a metaluminous, often calcic, tonalite or granodiorite. Geochemically, this phase is characteristic of an active continental margin although Rb/Zr ratios are somewhat higher. The subsequent phase is a peraluminous granite, commonly containing two micas and tourmaline. Although mineralogically similar to upper crustal melts such as the High Himalaya leucogranites, they differ geochemically in their strong Th enrichment and less-marked depletion in HFS elements. These characteristics may indicate more extensive anatexis such that accessory phases like zircon or monazite are not residual in the source rock. The association between the two distinct magma-types implies a post-collision environment in which early melts are derived from near the base of a thickened crust with crustal assimilation occurring during ascent whereas the younger melts have a predominantly upper crustal source in response to tectonic thickening.

5. Plutonism of the Qiangtang–southern Kunlun Terranes

(*a*) *Field relations and petrology*

The boundary between the Qiangtang and Kunlun Terranes is marked by the southern limit of Triassic shales south of the Kunlun Mountains, which roughly coincides with an east–west line through an ultramafic/gabbro complex to the west of the Geotraverse route (Chang *et al.* 1986). This boundary represents the Jinsha Suture marking a former northward-dipping subduction zone, the polarity being determined from the south-facing recumbency of the structures and Jurassic molasse, derived from the north, deposited south of the suture. From the Banggong Suture (which marks the southern limit of the Qiangtang Terrane), north to the Kunlun Mountains, a distance of about 500 km, there is little evidence of intrusive magmatic activity (figure 14). North of the Tanggula Pass, numerous stream samples of hornblende–hypersthene–biotite quartz monzodiorite and biotite granite (G136) have been found from an easterly source (Mt. Munai) and similar samples have been located from a westerly source in the Tuotuo River. It can be concluded that at least a small proportion of the Tanggula Mountains is underlain by granitic rocks of unknown age, but these are not exposed *in situ* along the Geotraverse route.

A small plug of phlogopite quartz microsyenite (2×1 km) is emplaced into late Cretaceous or early Tertiary sandstones of the Fenghuoshan Group in the north of the Qiangtang Terrane (G141). Fifteen kilometres south of Wudaoliang a small (3×1 km) hornblende–biotite tonalite is intruded into Triassic shales (G142). This tonalite is post-tectonic and homogeneous except for occasional dykes of peraluminous biotite granite (G143).

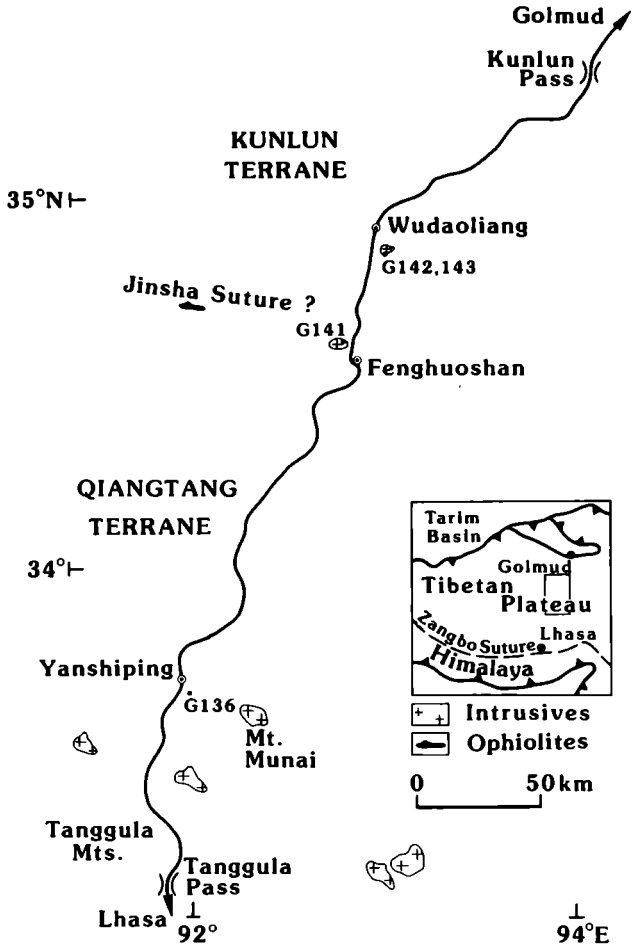

FIGURE 14. Sample location map for geochemical samples from the Qiangtang and southern Kunlun terranes.

(*b*) *Geochemistry*

The Fenghuoshan quartz microsyenite is a metaluminous alkalic body. This isolated plug intrudes Tertiary strata and must clearly be 'within plate' in tectonic setting in that no plate margin is known to be active in post-Cretaceous times within 1000 km of its emplacement. HFS element enrichment is a consistent indicator of within-plate sources, and its absence in the microsyenite may result from emplacement into anomalously thick continental crust which caused contamination by crustal melts with low HFS element concentrations. Crustal contamination is also supported by oxygen isotope data (Harris, Xu, Lewis, Hawkesworth & Zhang, this volume).

This Wudaoliang metaluminous tonalite is strongly calcic in composition. The calcic major element composition and arc-related trace element characteristics are shared by intrusions from the massive batholith of the Kunlun Mountains to the north. The Wudaoliang body represents a small post-tectonic pulse of magmatism emplaced into the accretionary prism north of the Jinsha Suture.

6. Plutonic magmatism of the Kunlun Mountains

(a) *Field relations and petrology*

The northern edge of the Tibetan Plateau is marked by the Kunlun Mountains which form an east-trending belt divided along the route of the geotraverse into a northern and southern range by the Xidatan Fault (figure 15).

Few plutonic bodies have been found intruding the Triassic phyllonites of the southern range of the Kunlun Mountains, south of the Xidatan fault. Five kilometres north of the Kunlun Pass, stream samples of granitoids include foliated two-mica granite, biotite granodiorite, hornblende–biotite quartz monzonite, hornblende diorite and pyroxenite (G204). Scree outcrops of foliated granitoids can be traced east along the ridge of the southern Kunlun. Numerous plugs or sills of post-tectonic plagioclase–quartz ± garnet porphyry have been located intruding shales on the northern slopes of the south Kunlun range.

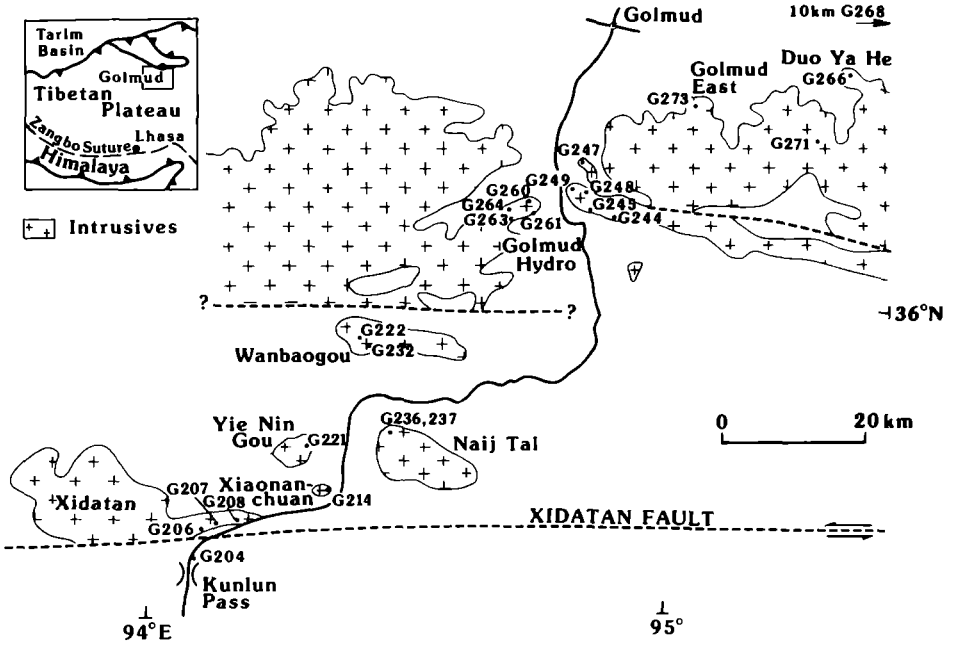

Figure 15. Sample location map for geochemical samples from the Kunlun Mountains.

Immediately north of the Xidatan Fault an orthogneiss is emplaced into phyllites with a strong penetrative fabric, parallel to the east-trending Xidatan Fault. The dominant rock-type is a porphyritic biotite granite gneiss (G206 A, B, G207, G208) interlayered with bands of a more leucocratic granite gneiss (G206 C, D, E). The Xidatan orthogneiss becomes weakly foliated to non-foliated as it is traced westwards.

Two kilometres north of the Xidatan Valley, west of the Lhasa–Golmud Highway, a small (2.5 km diameter) undeformed circular pluton intrudes phyllites. The intrusion, known as the Xiaonanchuan pluton (G214), is a high level post-tectonic granitoid with sharp contacts along which cordierite-bearing hornfels is developed. The pluton is a homogeneous and undeformed biotite ± sphene granite–granodiorite. A similar but larger intrusion, located 4 km north-west of the Xiaonanchuan pluton (Yie Nin Gou), is a homogeneous biotite–sphene granodiorite (G221) containing biotite-rich autoliths and calc-silicate xenoliths.

The third and largest intrusion in this group of post-tectonic granites is emplaced south-west of Naij Tal. The Naij Tal intrusion is a 20×10 km body of biotite $\pm$ hornblende granite granodiorite (G236, G237) with limestone xenoliths and dioritic enclaves. It is emplaced into limestones and shales and a sub-horizontal upper contact indicates that the intrusion is exposed close to the roof of the magma chamber.

Fourteen kilometres north of Naij Tal in the Wanbaogou valley, the southern margin of an intrusion is exposed with a porphyritic biotite granite core and a marginal muscorite-tourmaline granite facies (G222, G232). It is unclear on field evidence whether the Wanbaogou granite should be grouped with the three post-tectonic bodies to the south, or with the syn-tectonic Kunlun batholith to the north, but preliminary isotopic data suggest a significantly older intrusive age than either group of intrusions.

The Kunlun batholith, which extends for at least 1000 km along its east–west strike and marks the northern margin of the Tibetan Plateau, is exposed throughout the northern 30 km of the Kunlun Mountains. Along the Geotraverse route its southern expression is the Golmud Hydro granite which has a north–south dimension of 10 km and a minimum east–west extent of 18 km. It is comprised of a biotite granite core (G245) and cut by biotite pegmatites, and aplites. The marginal facies of the intrusion is a strongly porphyritic biotite granite (G244, G260, G261, G263, G264). Both facies are syn-tectonic, contain enclaves of diorite or granodiorite and are cut by abundant mafic dykes. Along the southern contact, the Golmud Hydro granite intrudes andesites and basalts and at the contact the volcanics are strongly hornfelsed and intruded by numerous aplites, quartz veins and granitic dykes. Along the northern contact the granite intrudes a hornblende granodiorite which often shows a pronounced fabric (G249) and an undeformed biotite granodiorite (G248) which is cut by dykes of the porphyritic phase of the Golmud Hydro granite. Five kilometres north of the granodiorite exposures, a biotite–hornblende tonalite (G247) showing local flow-banding forms an actively quarried inlier. The tonalite contains hornblende-rich autoliths and is cut by abundant garnet granite pegmatites.

Along the northern margin of the Kunlun Mountains, plutonic rocks are continuously exposed for several hundred kilometres both east and west of Golmud. Twenty kilometres south-east of Golmud, an active quarry exposes a biotite–hornblende granodiorite (G273, Golmud East). Further east the dominant rock-type is a hornblende–biotite tonalite–granodiorite (G271, G268) which intrudes a strongly foliated biotite granodiorite (G266, Duo Ya He). Apart from abundant basaltic dykes, mafic intrusives are restricted to a single outcrop of norite in this region of the Kunlun batholith.

There are some differences in interpretation amongst authors concerning the sub-division of intrusives in the northern Kunlun Terrane. Jin Chengwei suggests that to the north of the Golmud Hydro granite, a major east–west fault (the Daobangou Fault) separates a northern group of diorites, tonalites and granodiorites (which includes the Duo Ya He and the Golmud East bodies described in this study) from the Central Kunlun (which includes the granites and granodiorites of Golmud Hydro and Wanbaogou). Although not clearly identified along the Geotraverse route, the Daobangou Fault is reported several hundred kilometres to the east, with ultramafic bodies within the fault zone and this fault is identified by Jin Chengwei as a palaeosuture.

(*b*) *Geochemistry*

The fabric and field relations of the Kunlun batholith suggests that it may be divided into three facies, the strongly deformed Xidatan granite orthogneiss, the post-tectonic granites and granodiorites of Naij Tal, Xiaonanchuan and Yie Nin Gou, and the syn-tectonic composite batholith ranging from diorite to granite of the northern Kunlun. Geochemically the intrusions can not be categorized in this way (table 3). Major elements indicate that the leucogneiss facies of the Xidatan intrusion is siliceous, calc-alkali syenogranite (figure 16). Despite the high silica content of many samples (> 76 wt. %), modal compositions lie close to the granite eutectic implying a probable magmatic origin. The biotite gneiss from the Xidatan intrusion is similar in composition to the Golmud Hydro syn-tectonic intrusion; they are both monzogranites and lie on the boundary between calc-alkaline and calcic. The Naij Tal post-tectonic granite and the Golmud East and the Duo Ya He syn-tectonic granodiorites are all calcic in composition. There is therefore no obvious spatial or textural correlation with major element geochemistry.

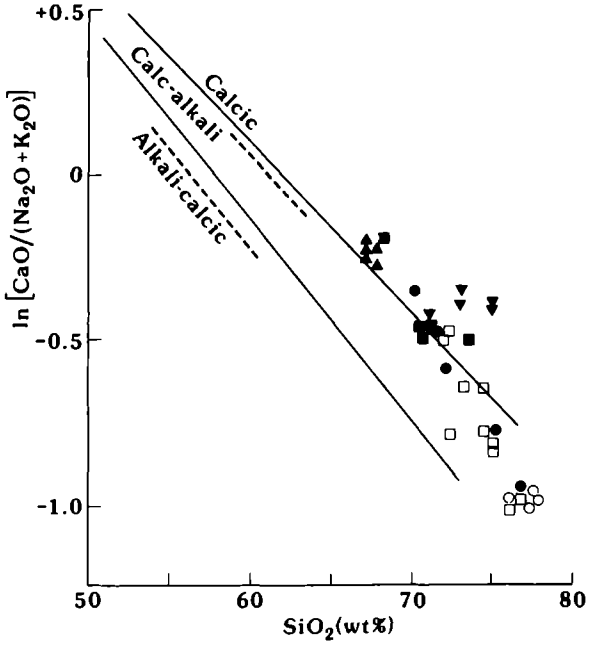

FIGURE 16. Plot of $\log_{10}(CaO/(Na_2O+K_2O))$ against SiO_2 for Kunlun samples. Field boundaries as for figure 3. Data from table 3. ● = Xidatan (biotite gneiss), ○ = Xidatan (leucogneiss), ■ = Naij Tal, □ = Golmud Hydro, ▲ = Golmud East, ▼ = Duo Ya He.

All samples analysed for Rb, Y and Nb lie well within the volcanic arc/post-collision field (figure 17). Granite suites lying in the calcic field of figure 16 often represent island arc magmas (that is volcanic arc magmas generated in the absence of upper crustal contamination) but both Sr and Nd isotopic data require considerable crustal involvement (see Harris, Xu, Lewis, Hawkesworth & Zhang, this volume). Partial melting of a quartz diorite or tonalite parent results in a melt of calcic characteristics (Tindle & Pearce 1983) and such a source is consistent with the Rb/Sr characteristics inferred from Sr–Nd studies. It is likely therefore that melts were

generated at either an active continental margin or in a post-collision setting but the crustal component came from sources of intermediate compositions which were igneous in origin.

The REE from the Kunlun granites fall into two distinct groups. Group A (figure 18*b*) have a high Ce/Yb ratio and a small negative Eu anomaly, as seen in samples from Naij Tal as well as from the Duo Ya He (G266) and Golmud East (G273) facies in the Kunlun batholith. Such

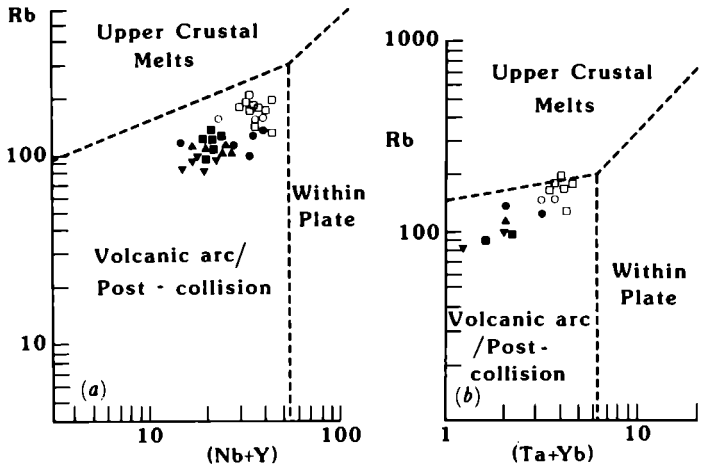

FIGURE 17 (*a*) Rb vs (Nb+Y) plot, (*b*) Rb vs (Ta+Yb) plot for Kunlun samples. Symbols as for figure 16. Field boundaries from Pearce *et al.* (1984).

REE are typical of magmas with a HREE-bearing phase such as garnet in the source, which have undergone limited feldspar fractionation. Group B (figure 18*b*) as seen in the Golmud Hydro intrusion, have flatter patterns but with a large negative Eu anomaly. Such patterns characterize feldspar-bearing but garnet-free crustal sources as seen in the High Himalaya leucogranites (Dietrich & Gansser 1981, Vidal *et al.* 1982) and the Palaeozoic intrusions of the North Himalayas (Debon *et al.* 1986). Interestingly both REE patterns are observed in the Xidatan orthogneiss, the biotite granites (G206A, B) showing steep group A patterns, but the leucogranite gneiss (G206C, D) showing flatter, group B, profiles.

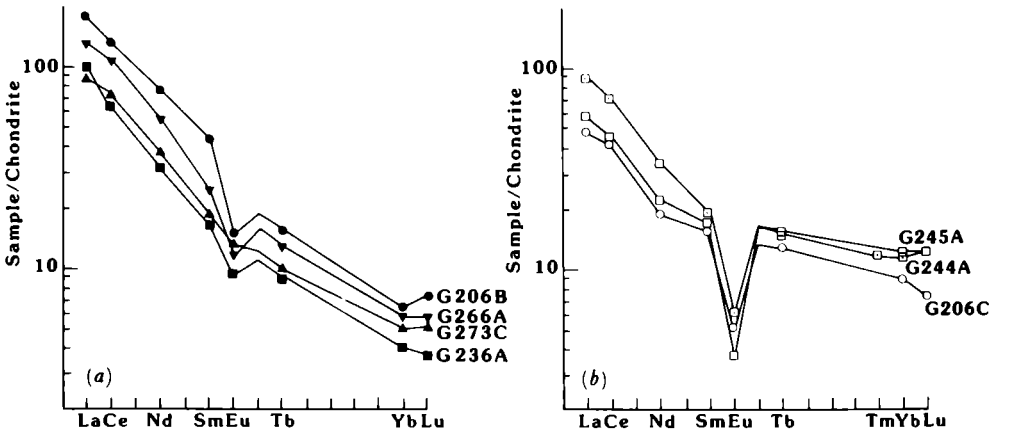

FIGURE 18. Chondrite normalized REE plots for Kunlun samples. (*a*) Group A, Xidatan biotite gneiss (G206B), Naij Tal (G236A), Golmud East (G273C) and Duo Ya He (G266A). (*b*) Group B, Xidatan leucogneiss (G206C) and Golmud Hydro (G244A, G245A).

The two groups can also be clearly distinguished on a Rb/Zr diagram (figure 19). Group B intrusions have elevated Rb/Zr indicative of a crustal source. Group A tend to have lower Rb/Zr than the calc-alkaline Gangdise Belt to the south. This indicates either a low crustal component, as in an island arc setting, or a crustal source of intermediate composition such as a tonalite or amphibolite.

The relationship between these two geochemical groups requires further study, but since they have similar Sr–Nd isotope characteristics in the source (Harris, Xu, Lewis, Hawkesworth

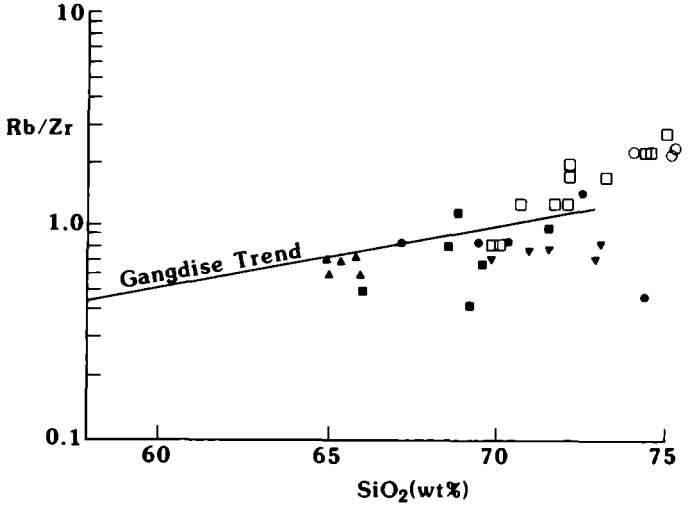

FIGURE 19. Rb/Zr vs SiO_2 for Kunlun samples compared with Gangdise Belt. Symbols as for figure 16. Note that closed symbols represent group A samples and open symbols group B.

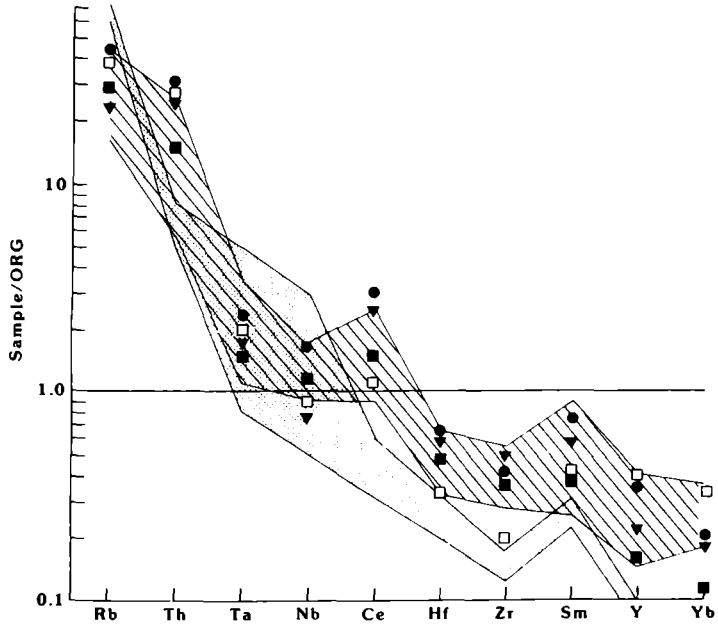

FIGURE 20. Geochemical patterns for granitic samples from Kunlun Terrane (SiO_2 = 71–74 wt. %) normalised against Ocean Ridge Granite (Pearce *et al.* 1984). Lined field = volcanic arc/post-collision granites; stippled field = High Himalayan leucogranites. ● = Xidatan biotite gneiss (G206B), ■ = Naij Tal (G236A), □ = Golmud Hydro (G245A), ▼ = Duo Ya He (G266A).

& Zhang, this volume) it is likely that they are related either by mineral fractionation or by crustal reworking. Although there is a general trend towards higher silica contents in group B intrusions, there is also considerable overlap in the range 72–75 wt. % SiO_2 (see figure 19). It is probable that the group B granites therefore do not result from simple fractionation of feldspar and a LREE-rich phase from a magma of group A geochemistry. If a wide range of trace elements are considered for the Kunlun intrusives (figure 20), the strong depletion of HREE and Y seen in the group A intrusives, and of Zr, Hf seen in group B intrusives indicates probable crustal anatexis. Sr–Nd isotopic constraints in fact require petrogenesis principally from crustal anatexis with only a limited mantle component (Harris, Xu, Lewis, Hawkesworth & Zhang, this volume). Both trace element and isotopic characteristics can be reconciled with a model which derives the group A intrusions from a garnet-bearing crustal source of intermediate composition, and group B from remelting the earlier plutonic suite resulting in predominantly highly siliceous partial melts with low LREE/HREE. Trace elements for both groups indicate either a volcanic arc or a post-collision setting, but the large scale of the batholith requiring a large and long-lived energy source is more characteristic of an active arc than a post-collision setting. A

TABLE 3. SELECTED ANALYSES FROM THE KUNLUN TERRANE

	Xidatan		Naij Tal		Golmud Hydro		Golmud E	Duo Ya He
	G206B	G206C	G236A	G236D	G245A	G244A	G273C	G266A
	Gr gn	Gr gn	Gr	Gd	Gr	por Gr	Gd	Gd
SiO_2	71.40	77.29	73.63	68.07	76.42	74.06	66.97	73.80
TiO_2	0.39	0.08	0.27	0.44	0.04	0.22	0.57	0.37
Al_2O_3	15.30	13.80	14.64	15.73	13.26	13.93	16.31	14.97
Fe_2O_3	2.61	0.84	1.75	2.68	1.13	2.42	3.97	2.49
MnO	0.06	0.03	0.04	0.04	0.04	0.06	0.06	0.03
MgO	0.88	0.15	0.75	1.30	0.18	0.44	1.44	0.83
CaO	2.57	0.93	2.35	3.63	0.83	1.78	4.10	2.91
Na_2O	3.83	3.61	3.96	4.27	3.86	3.92	3.81	3.81
K_2O	3.67	5.04	3.41	2.62	4.62	3.95	3.14	2.54
P_2O_5	0.14	0.08	0.08	0.21	0.04	0.07	0.20	0.12
LOI	0.51	0.11	0.58	0.50	0.40	0.35	0.72	0.06
Total	101.36	101.96	101.46	99.49	100.82	101.20	101.29	101.93
ppm								
Rb	125	152	135	93	178	170	114	102
Sr	300	65	291	492	53	132	500	245
Ba	663	171	711	719	219	767	895	575
Zr	143	63	132	177	74	129	162	136
Hf	5.1	2.6	4.1	4.7	3	3.9	4.6	4.84
Nb	16	16	11	11	9	8.7	9.8	7.9
Ta	1.6	1.6	1.1	0.79	1.5	0.93	0.82	0.58
Y	18	23	11	9	27	29	12	15
Th	23	16	12	11	21	22	12	20
U	1.6	3.2	3.0	3.0	3.0	3.0	4.0	4.0
La	60	13	32	42	19	29	30	44
Ce	114	28	57	73	40	62	64	95
Nd	40	11	20	26	14	22	26	35
Sm	6.6	3	3.4	4.2	3.5	3.9	3.9	5.5
Eu	1.1	0.40	0.74	1.1	0.29	0.70	1.0	0.90
Tb	0.81	0.68	0.49	0.44	0.79	0.84	0.52	0.68
Tm	—	—	—	—	—	0.45	—	0.20
Yb	1.4	2.0	0.91	0.71	2.7	2.7	1.1	1.3
Lu	0.25	0.25	0.13	0.10	0.43	0.43	0.18	0.20

Gr = granite, Gd = granodiorite, por = porphyritic, gn = gneiss.

possible interpretation is that the batholith represents anatexis of garnet amphibolite at intermediate crustal levels above an active continental margin. Some reworking of the igneous suite resulted from convective heat transfer at a destructive margin. The post-tectonic plutons to the south of the batholith are probably younger and were formed in a post-collision setting.

A modification of this model (Jin Chengwei) is that only intrusions along the northern margin of the Kunlun batholith result from active subduction. The Golmud Hydro body is therefore post-collisional in this model, the two groups being separated by a suture zone not clearly identified along the geotraverse route. Along the Golmud–Naj Tal traverse of the Kunlun batholith it is agreed that there is an apparent trend from intrusions of intermediate compositions along the northern margin, to more evolved granitic compositions to the south. However it is the contention of N.B.W.H. that although this could reflect southwards subduction from the north there is no compelling evidence for the location of a suture within the Kunlun Terrane along the geotraverse route.

7. Discussion and conclusions

Three plutonic provinces have been identified in the Tibetan Plateau, each of which can be related to tectonothermal processes at an active, or recently active, plate margin.

The Gangdise Belt is a composite calc-alkaline batholith emplaced along the southern margin of the Lhasa Terrane. Minor gabbroic components within the southern Gangdise Belt with a garnet-bearing, probably mantle source, represent primitive magmas from which more evolved compositions can be derived by fractionation and crustal assimilation. Trace elements are indicative of generation at an active continental margin and the Eocene ages of emplacement (Harris, Xu, Lewis, Hawkesworth & Zhang, this volume) imply formation above a north-dipping subduction zone at the southern margin of the Lhasa Terrane before the Himalayan collision. The northern Gangdise Belt (Nyainqentanglha Mountains) exposes uplifted orthogneisses representing crustal anatexis at deeper crustal levels of the continental margin.

Seven hundred kilometres to the north of the Gangdise Belt, an uplifted granitic batholith forms the northern Kunlun Mountains. This batholith is broadly Permo–Triassic in age (Harris, Xu, Lewis, Hawkesworth & Zhang, this volume) and calcic to calc-alkaline in composition. Trace elements are indicative of formation in a volcanic arc or post-collision setting, but trace element and isotopic constraints require predominantly crustal sources. Magmagenesis can be modelled firstly from anatexis of a garnet-bearing crustal source of intermediate composition, such as a garnet-amphibolite, and secondly by reworking of the earlier-formed plutonic suite. It is postulated that the batholith represents magmagenesis at intermediate crustal depths above an active continental margin prior to and immediately following collision between the Kunlun and Qiangtang terranes.

A belt of Cretaceous tonalite–granite plutons emplaced into the northern Lhasa Terrane constitutes the third plutonic province of the Tibetan Plateau. These form a bimodal suite in which an earlier tonalite–granodiorite component is intruded by peraluminous granite. The bimodal association characterizes post-collision magmagenesis where calc-alkaline magmas are derived from AFC processes above a hydrated mantle wedge and crustal anatexis results from the tectonically thickened crust.

The authors thank A. G. Tindle for reconnaissance microprobe data on accessory phases, N. W. Rogers and J. S. Watson for analytical assistance, J. Taylor for drafting the diagrams and M. Leggett for typing the manuscript.

References

Brown, G. C. 1982 Calc-alkaline intrusive rocks: their diversity, evolution and relation to volcanic arcs. In *Andesites* (ed. R. S. Thorpe), pp. 437–461. New York and London: John Wiley and Sons.

Brown, G. C., Thorpe, R. S. & Webb, P. C. 1984 The geochemical characteristics of granitoids in contrasting arcs and comments on magma sources. *J. geol. Soc.* **141**, 411–426.

Chang Chengfa *et al.* 1986 Preliminary conclusions of the Royal Society and Academia Sinica 1985 geotraverse of Tibet. *Nature Lond.* **323**, 501–507.

Debon, F., Le Fort, P., Sheppard, S. M. F. & Sonet, J. 1986 The four plutonic belts of the Transhimalaya-Himalaya: a chemical, mineralogical, isotopic and chronological synthesis along a Tibet-Nepal section. *J. Petrol.* **27**, 219–250.

Debon, F., Le Fort, P., Dantel, D., Sonet, J. & Zimmermann, J. L. 1987 Granites of western Karakorum and northern Kohistan (Pakistan): A composite Mid-Cretaceous to Upper Cenozoic magmatism. *Lithos* **20**, 19–40.

Dietrich, V. & Gansser, A. 1981 The leucogranites of the Bhutan Himalaya. *Schweiz mineral. petrog. Mitt.* **61**, 177–202.

Fourcade, S. & Allègre, C. J. 1981 Trace element behaviour in granite genesis: a case study. The calc-alkaline plutonic association from the Querigut Complex (Pyrenees, France). *Contr. Miner. Petr.* **76**, 177–195.

Harris, N. B. W., Pearce, J. A. & Tindle, A. G. 1986 Geochemical characteristics of collision zone magmatism. In *Collision tectonics* (ed. A. C. Ries & M. P. Coward), *Geol. Soc. Spec. Publ.* **19**, pp. 67–81.

Honnegar, K., Dietrich, V., Frank, W., Gansser, A., Thoni, M. & Trommsdorff, V. 1982 Magmatism and metamorphism in the Ladakh Himalayas (the Indus-Tsangpo suture zone). *Earth planet. Sci. Lett.* **60**, 253–293.

Jin Chengwei & Xu Ronghua 1980 Les Granitoides de la partie centrale de l'Himalaya et du Gangdise au Xizang (Tibet) meridonal. In *Résultats de la co-operation franco-chinoise au Tibet* (ed. J. L. Mercier & Li Guangquin), pp. 289–308.

Peacock, M. A. 1931 Classification of igneous rock series. *J. Geol.* **39**, 54–67.

Pearce, J. A. 1982 Trace element characteristics of lavas from destructive plate boundaries. In *Andesites* (ed. R. S. Thorpe), pp. 525–548. New York and London: J. Wiley and Sons.

Pearce, J. A., Harris, N. B. W. & Tindle, A. G. 1984 Trace element discrimination diagrams for the tectonic interpretation of granitic rocks. *J. Petrol.* **25**, 956–983.

Petterson, M. G. & Windley, B. F. 1985 Rb-Sr dating of the Kohistan arc batholith in the Trans-Himalaya of north Pakistan and tectonic implications. *Earth planet. Sci. Lett.* **74**, 45–57.

Potts, P. J., Thorpe, O. W. & Watson, J. S. 1981 Determination of the REE abundances in 29 international rock standards by Instrumental Neutron Activation Analysis: a critical appraisal of calibration errors. *Chem. Geol.* **34**, 331–352.

Rapp, R. P. & Watson, E. B. 1986 Monazite solubility and dissolution kinetics: implications for the thorium and light rare earth chemistry. *Contr. Miner. Petr.* **94**, 304–316.

Sawka, W. N., Banfield, J. F. & Chappell, B. W. 1986 A weather-related origin of widespread monazite in S-type granites. *Geochim. Cosmochim. Acta* **50**, 171–175.

Streckeisen, A. 1976 To each plutonic rock its proper name. *Earth Sci. Rev.* **12**, 1–33.

Tindle, A. G. & Pearce, J. A. 1983 Assimilation and partial melting of continental crust: evidence from the mineralogy and geochemistry of autoliths and xenoliths. *Lithos* **12**, 185–202.

Vidal, P., Cocherie, A. & Le Fort, P. 1982 Geochemical investigations of the origin of the Manaslu leucogranite (Nepal). *Geochim. cosmochim. Acta* **46**, 2279–2292.

Wickam, S. M. & Oxburgh, E. R. 1986 A rift tectonic setting for Hercynian high-thermal gradient metamorphism in the Pyrenees. *Tectonophysics* **129**, 53–69.

Xu Ronghua, Scharer, U. & Allègre, C. J. 1985 Magmatism and metamorphism in the Lhasa Block (Tibet): a geochronological study. *J. Geol.* **93**, 41–57.

Phil. Trans. R. Soc. Lond. A **327**, 169–201 (1988) [169]
Printed in Great Britain

Volcanic rocks of the 1985 Tibet Geotraverse: Lhasa to Golmud

By Julian A. Pearce[1] and Mei Houjun[2]

[1] *Department of Geology, The University, Newcastle-upon-Tyne, U.K.*
[2] *Institute of Geochemistry, Chinese Academy of Sciences, Guiyang, People's Republic of China*

[Microfiche in pocket]

Volcanic rocks encountered during the Tibet Geotraverse have been studied in the field, in thin section and by major and trace element geochemistry in order to determine their most probable original eruptive environment. Rocks from a total of eleven distinct volcanic provinces were studied in this way. They provide evidence for: an active continental margin or post-collision province of probable Devonian/early Carboniferous age in the northern Kunlun mountains; an active continental margin of late Carboniferous age in the southern Lhasa Terrane; Permian continental rifts in the central Qiangtang and central Kunlun Terranes; Triassic volcanic arcs in the southern Lhasa and northern Qiangtang Terranes; a Triassic active continental margin dyke swarm in the northern Kunlun mountains; a Jurassic post-collision or back-arc rifting province in the southern Qiangtang Terrane; a Jurassic island arc in the northern Lhasa Terrane; a Cretaceous post-collision province in the northern Lhasa Terrane possibly extending into the southern Qiangtang Terrane; and a Palaeogene active continental margin in the southern Lhasa Terrane. An Oligocene trachyte plug in the northern Qiangtang Terrane was the only evidence encountered during the Geotraverse of volcanism post-dating the Palaeogene India–Eurasia collision. However, the composition of this plug, coupled with new and published analyses from Miocene volcanics in the southern Lhasa terrane and from the Pliocene-Recent volcanic province of northwest Tibet, places important constraints on models for post-collision underplating of Tibet by continental lithosphere: any underplating is likely to have been (*a*) much later than the start of collision, (*b*) directed beneath Tibet from the north as well as the south, and (*c*) limited in extent.

1. Introduction

Volcanic rocks can contribute to our understanding of the Tibetan Plateau in two ways: they can provide information on past tectonic environments as an aid to the palaeo-tectonic reconstruction of the plateau and, in the case of the more recent eruptions, they can place constraints on tectonic models for the India–Eurasia continent-continent collision event. Use of a sequence of volcanic rocks to interpret a past tectonic environment can best be achieved by the systems approach, whereby geochemical fingerprinting techniques are integrated with information on primary and secondary mineralogy, the facies of the intercalated sediment, the types of eruption, the proportions of rock types erupted and a variety of geological criteria such as the nature of associated rock types and of the basement to the volcanic sequence. Use of volcanic rocks to understand continent collision is based on the time–space relationships of syn- and post-collision magmatism, on geochemical and petrologic evidence for the nature of the magma source region and on the type and degree of subsequent crustal interaction. Because few post-(Palaeogene) collision volcanics were collected on this Geotraverse, the principal aim

of this paper is to provide new information on the past tectonic environments of the Geotraverse region; however, an attempt has also been made to compile new and published data relevant to the neotectonics of the Tibetan Plateau.

Eleven volcanic provinces were identified during the Geotraverse (figure 1). For each province, the geological setting and volcanic stratigraphy were studied in as much detail as time permitted for one or more volcanic sequences and a representative suite of samples was collected. In general, 'G' numbers were collected and analysed by the Royal Society group and sample locations are given in Kidd *et al.*, this volume (field slip, microfiche 2, in pocket); 'Qy' numbers were collected and analysed by the Chinese group, and sample locations are

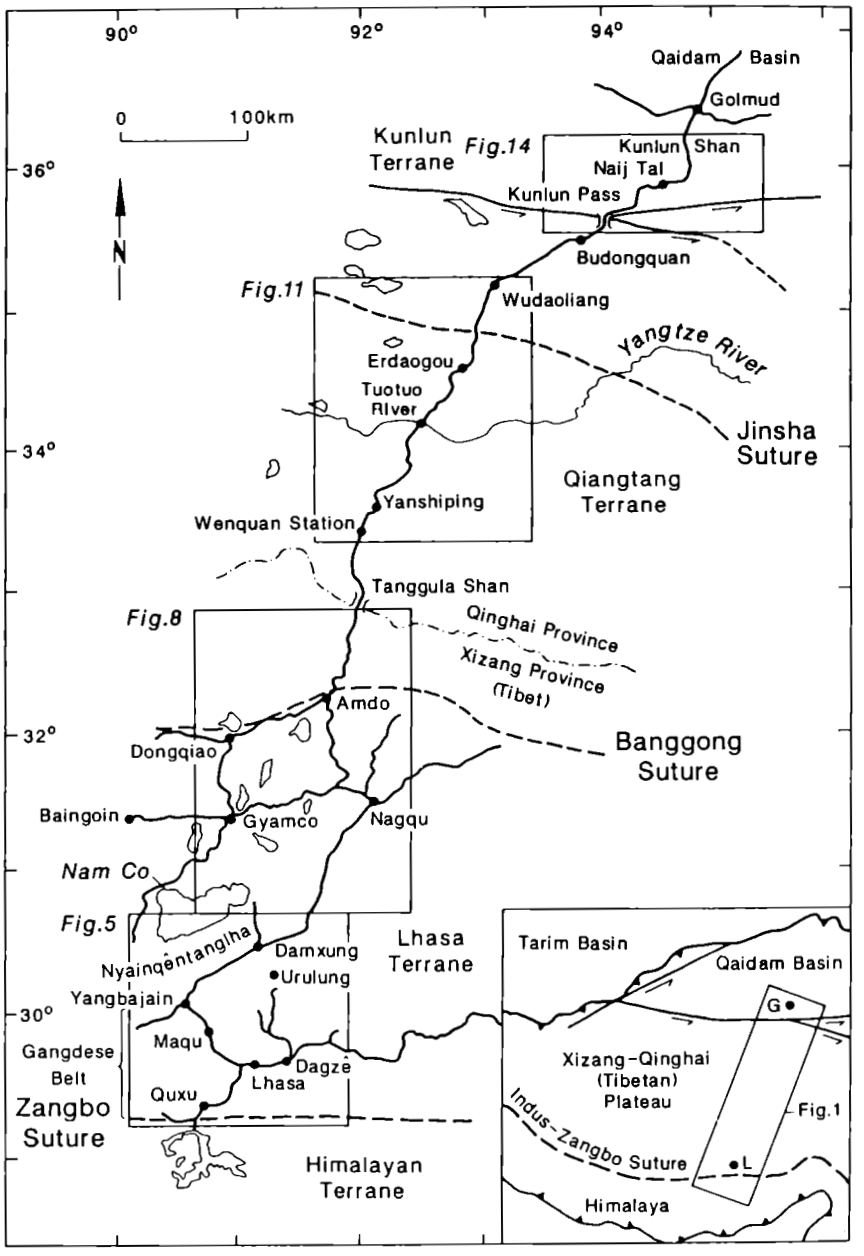

FIGURE 1. Route taken by Geotraverse also showing the location of the larger scale maps in figures 5, 8, 11 and 14.

available from Mei Houjun on request. Subsequently, about 150 samples were examined in thin section and analysed for major elements and a range of trace elements. In this paper, we start by explaining the methodology used; we then report the geological, petrological and geochemical characteristics of each of the provinces studied and discuss the tectonic implications of the data; finally we summarize our results in the context of the evolution of the Tibetan Plateau. This paper concentrates on the non-ophiolitic volcanic rocks and related hypabyssal intrusions, whereas Pearce & Deng (this volume) examine in more detail the ophiolite environments.

2. Methodology

Our main basis for the interpretation of past eruptive environments is geochemical. All samples have been analysed by atomic absorption spectroscopy (AAS) for the major elements, either in Newcastle or in Guiyang. Samples analysed at Newcastle were also analysed for the trace elements Zr, Y, Nb, Rb, Sr and Th by X-ray fluorescence (XRF) and for Cr, Ni, V, Cu, Zn, and Sc by AAS. A representative subset of about 40 samples was also analysed for the rare earth elements (REE), Th, Ta, Hf, Sc and Co by instrumental neutron activation analysis (INAA) at the Open University, at the Institut Laue-Langevin, Grenoble and at the Third Institute of the Department of Nuclear Industry in Beijing. Some additional data on REE and some other elements were obtained by inductively-coupled plasma emission spectrometry (ICP-AES) at the Central Laboratory of Geology in Hebei. Analyses of comparable rocks were analysed in several laboratories to confirm inter-laboratory compatibility. A table of representative data is presented as table 1 and the full data set is published in the Appendix (microfiche 1, in pocket).

Since most of the rocks studied during the traverse were affected by alteration/metamorphism, tectonic classification has in general been restricted to those elements that have been demonstrably immobile since eruption. Classification of rock type has, however, been carried out for orogenic series using the K_2O–SiO_2 diagram of Peccerillo & Taylor (1976), although care was taken not to plot analyses when covariation diagrams of K_2O against immobile elements indicated that potassium had been significantly mobile. The classification of rock type for non-orogenic series was carried out using the Ti/Zr–Nb/Y diagram of Winchester & Floyd (1977), since all available samples of this type were too altered for conventional diagrams such as total alkalis–silica to be used reliably. Classification of tectonic setting has been carried out using MORB-normalized multi-element patterns (Pearce 1984) coupled with the two discrimination diagrams, Ti–Zr–Y (Pearce & Cann 1973) and Th–Ta–Hf (Wood *et al.* 1979). Additional diagrams, such as REE patterns, have been used to examine petrogenetic relationships between rocks, where this is relevant to the tectonic interpretation.

The rationale behind the geochemical techniques is illustrated in figures 2 and 3. The MORB-normalized patterns shown in figure 2 are based on single analyses of basalts, in which the elements Th–Yb are arranged from right to left in order of increasing incompatibility during mantle melting; these patterns resemble those shown in Pearce (1984) except that the mobile elements have been removed from consideration. Figures 2*a–d* show some typical patterns from the various eruptive environments for comparison with the patterns to be presented for the Tibetan samples. Figure 2*a* shows the range of patterns characteristic of oceanic and continental intraplate basalts: they exhibit an enrichment relative to normal MORB for all elements except Y and Yb, a feature that can be explained by derivation from enriched mantle sources (e.g.

TABLE 1. GEOCHEMICAL ANALYSES FOR REPRESENTATIVE SAMPLES OF VOLCANIC ROCKS FROM THE GEOTRAVERSE

(Elements Zr, Y, Nb, Sr and Rb have been analysed by X-ray fluorescence, elements Hf to Lu by instrumental neutron activation analysis, and the remaining elements by atomic absorption. Zr and Nb in Qy numbers are estimated from Hf (Zr = Hf × 37.5) and Ta (Nb = Ta × 16) respectively. Unanalysed elements are given as 0. Key to rock sequences: L = Lhasa Terrane; Q = Qiangtang Terrane; K = Kunlun terrane; T = Tibet; Cb = Carboniferous ; P = Permian; T = Triassic; J = Jurassic; C = Cretaceous; Pg = Palaeogene; Q = Quaternary; U = Upper; L = Lower. Key to rock types: bas. = basalt; and. = andesite; b/a. = basaltic andesite; sho. = shoshonite; p/b. = picrite basalt; rhy. = rhyolite; tra. = trachyte; bsn. = basanite; phn. = phonolite; L = lava; D = dyke; P = plug; S = sill; PL = pillow lava. See figures 5, 8, 11 and 14 for province locations and Kidd *et al.*, this volume (field slips, Microfiche 2, in pocket) and Deng 1978 for precise locations and phenocryst mineralogies).

Samp.	G16E	G32G	G36C	G46C	G106D	G130E	G55G	G99B	OPH474
Seq.	LCb1	LT1	LPg1	LPg2	LJ1	LJ2	LC1	LC2	LC3
Rock	bas.	bas.	b/a.	sho.	bas.	bas.	b/a.	b/a.	bas.
Type	L	L	L	L	PL	L	L	L	L
SiO_2	52.00	48.70	53.20	53.50	47.60	49.50	53.50	53.60	51.83
TiO_2	1.03	0.92	0.83	0.84	0.56	0.52	0.87	0.94	1.56
Al_2O_3	17.00	14.60	21.00	19.70	11.20	14.30	15.20	15.80	16.21
Fe_2O_3	9.06	7.94	6.52	6.22	6.20	8.83	8.35	8.09	8.77
MnO	0.17	0.17	0.07	0.13	0.15	0.15	0.13	0.13	0.21
MgO	5.74	4.39	3.33	1.75	5.04	7.44	7.85	3.93	4.68
CaO	9.61	10.80	7.34	4.27	15.90	12.60	8.92	7.01	5.38
Na_2O	3.95	2.14	4.99	4.12	3.51	1.23	2.35	2.79	4.05
K_2O	0.10	1.05	0.42	6.00	0.68	0.18	1.67	2.13	2.80
P_2O_5	0.23	0.25	0.16	0.42	0.09	0.07	0.19	0.17	0.04
LOI	1.41	9.31	2.69	3.60	9.98	3.77	1.68	5.65	3.75
Total	100.30	100.27	100.55	100.55	100.91	98.59	100.71	100.24	99.28
Zr	88	125	146	401	32	33	109	158	142
Y	22	23	17	35	11	13	20	26	28
Nb	5.8	3.9	5.0	24.0	2.4	2.2	6.6	10.0	10.0
Rb	2.8	49.0	8.5	142.0	13.0	0.0	71.0	91.0	66.0
Sr	502	914	603	99	157	324	309	434	830
Cr	150	83	35	2	480	220	460	57	110
Ni	39	16	21	8	217	58	83	16	37
V	290	210	190	88	180	0	220	0	355
Cu	21	15	30	42	35	118	17	32	42
Zn	83	82	100	93	51	68	76	94	0
Hf	2.09	3.33	3.16	7.57	0.91	1.01	2.49	4.00	3.78
Ta	0.37	0.24	0.41	1.82	0.11	0.14	0.53	0.93	0.65
Th	2.00	17.00	5.52	42.40	0.69	0.54	11.40	15.60	13.20
Sc	35.0	0.0	21.0	7.1	27.1	40.8	29.0	22.1	0.0
Co	32.7	28.0	25.8	34.0	34.8	44.0	37.1	32.5	0.0
La	12.2	0.0	15.2	83.1	3.6	3.7	23.7	30.2	41.5
Ce	26.9	0.0	28.4	171.0	9.5	11.0	46.2	66.1	66.3
Nd	16.9	0.0	15.6	69.0	5.8	10.3	23.2	33.0	28.3
Sm	4.05	0.00	3.52	12.50	1.50	2.17	4.97	5.95	5.57
Eu	1.25	0.00	1.10	2.93	0.52	0.75	1.25	1.35	1.47
Tb	0.67	0.00	0.59	1.67	0.36	0.40	0.73	0.89	0.80
Ho	0.00	0.00	0.00	2.07	1.00	0.59	0.00	1.18	0.00
Tm	0.00	0.00	0.00	0.59	0.16	0.19	0.00	0.44	0.00
Yb	2.22	0.00	1.70	3.39	1.33	1.56	1.93	2.70	1.87
Lu	0.38	0.00	0.28	0.46	0.23	0.27	0.32	0.41	0.29

TABLE 1. (*cont.*)

Samp.	OPH585	G133H	G138H	G151D	Qy61	Qy59	Qy71	Qy78B	Qy77B
Seq.	LC3	LC4	QJ1	QP1	QP1	QP1	QP1	QP2	QP2
Rock	and.	b/a.	b/a.	bas.	bas.	and.	p/b.	b/a.	and.
Type	L	L	L	L	S	L	L	L	L
SiO_2	61.15	54.40	53.10	50.10	47.53	62.86	45.91	53.39	59.38
TiO_2	0.84	2.12	1.64	1.60	2.24	0.54	1.12	0.94	0.66
Al_2O_3	15.73	15.70	16.80	17.30	14.48	16.76	17.68	18.29	18.28
Fe_2O_3	7.01	8.76	11.10	9.53	12.77	5.19	8.99	6.70	4.95
MnO	0.10	0.18	0.06	0.16	0.46	0.20	0.16	0.18	0.12
MgO	3.86	3.39	5.36	5.42	5.10	5.00	7.17	4.80	1.70
CaO	1.09	8.25	2.00	7.78	11.20	3.70	9.82	5.00	2.30
Na_2O	4.63	3.71	5.83	4.83	1.85	4.54	4.03	5.44	8.70
K_2O	2.25	1.03	0.48	0.38	0.68	0.19	0.03	1.30	0.75
P_2O_5	0.08	0.35	0.49	0.43	0.22	0.12	0.30	0.52	0.38
LOI	2.98	3.04	3.93	3.22	2.94	1.00	2.00	3.55	1.82
Total	99.72	100.93	100.79	100.75	99.47	100.10	97.98	100.11	99.04
Zr	180	307	187	149	136	109	112	191	129
Y	23	36	25	25	44	11	26	24	17
Nb	16.0	11.0	11.0	15.0	15.0	11.0	14.0	35.0	8.0
Rb	130.0	29.0	21.0	8.6	7.0	4.0	1.0	33.0	0.0
Sr	450	334	131	613	475	498	160	1133	0
Cr	0	45	200	124	0	0	0	0	0
Ni	80	12	59	94	0	0	0	0	0
V	0	210	280	230	0	0	0	0	0
Cu	41	17	8	9	0	0	0	0	0
Zn	0	140	83	90	0	0	0	0	0
Hf	4.80	6.14	3.63	3.21	3.62	2.91	3.00	5.10	3.46
Ta	0.99	0.88	0.70	0.89	0.95	0.74	0.83	2.17	0.49
Th	19.60	8.40	3.89	2.12	1.00	4.10	1.90	7.30	6.00
Sc	0.0	26.3	18.8	26.5	58.2	23.9	30.0	22.4	13.6
Co	0.1	29.1	30.5	37.5	0.0	0.0	0.0	0.0	0.0
La	30.4	23.7	14.0	22.2	10.5	14.0	19.5	45.3	42.0
Ce	66.9	58.2	37.7	52.4	27.3	25.5	36.0	95.3	69.2
Nd	25.2	32.6	21.5	27.3	19.5	12.9	18.2	39.9	27.0
Sm	5.59	7.08	4.72	5.19	6.60	2.80	5.10	8.10	5.00
Eu	1.25	2.15	1.47	1.79	2.05	0.79	1.26	1.54	1.37
Tb	0.70	1.20	0.80	0.83	1.10	0.45	0.91	0.82	0.60
Ho	0.00	1.85	0.00	1.30	0.00	0.00	0.00	0.00	0.00
Tm	0.00	0.48	0.37	0.32	0.00	0.00	0.00	0.00	0.00
Yb	2.18	4.09	2.42	2.53	4.80	1.00	2.40	1.10	1.00
Lu	0.38	0.57	0.35	0.41	0.62	0.15	0.27	0.30	0.17

Samp.	G154F	G154L	Qy80	Qy85	G216I	Qy171	Qy154	Qy181	Qy206
Seq.	QT1U	QT1L	QT2	QT2	KP1	KD1	KD1	KD1	KD1
Rock	bas.	bas.	bas.	and.	bas.	dac.	latite	rhy.	rhy.
Type	L	L	L	L	L	L	L	L	L
SiO_2	51.30	51.50	51.75	56.91	47.20	63.28	68.48	70.28	77.11
TiO_2	1.00	0.78	0.76	0.66	3.54	0.66	0.36	0.40	0.14
Al_2O_3	18.80	21.40	19.35	18.44	14.40	17.38	15.61	16.01	11.43
Fe_2O_3	9.07	7.99	8.67	10.79	14.90	5.33	4.81	2.55	1.87
MnO	0.23	0.12	0.19	0.08	0.19	0.07	0.08	0.07	0.09
MgO	3.58	2.60	2.87	0.40	5.46	3.30	0.60	0.20	0.10
CaO	8.72	9.94	6.55	1.80	10.10	2.60	1.80	1.00	0.30
Na_2O	3.14	3.62	5.20	9.50	2.58	2.70	1.31	7.70	2.76

TABLE 1. (*cont.*)

Samp.	G154F	G154L	Qy80	Qy85	G216I	Qy171	Qy154	Qy181	Qy206
Seq.	QT1U	QT1L	QT2	QT2	KP1	KD1	KD1	KD1	KD1
Rock	bas.	bas.	bas.	and.	bas.	dac.	latite	rhy.	rhy.
Type	L	L	L	L	L	L	L	L	L
K_2O	2.63	0.46	0.81	0.11	0.73	2.45	4.81	1.15	4.26
P_2O_5	0.45	0.09	0.14	0.10	0.34	0.22	0.24	0.14	0.08
LOI	2.20	1.81	2.73	1.09	0.78	1.67	0.97	0.63	1.93
Total	101.12	100.31	99.02	99.88	100.22	99.66	99.07	100.13	100.07
Zr	207	108	42	59	257	276	402	123	299
Y	25	26	18	13	36	46	37	16	74
Nb	25.0	4.1	4.0	5.0	23.0	16.0	21.0	19.0	20.0
Rb	101.0	6.1	18.0	3.0	18.0	132.0	283.0	43.0	178.0
Sr	526	141	279	174	152	131	39	72	18
Cr	6	7	0	0	240	0	0	0	0
Ni	12	7	0	0	125	0	0	0	0
V	240	280	0	0	430	0	0	0	0
Cu	38	17	0	0	198	0	0	0	0
Zn	103	87	0	0	133	0	0	0	0
Hf	3.05	1.11	1.13	1.50	6.50	7.37	10.72	3.28	7.97
Ta	1.04	0.12	0.00	0.33	1.66	0.75	1.30	1.21	1.60
Th	11.80	1.42	1.60	1.58	2.37	16.60	25.20	4.10	24.30
Sc	19.8	29.2	21.7	16.8	37.9	12.1	13.6	5.6	0.4
Co	29.7	20.9	0.0	0.0	54.0	0.0	0.0	0.0	0.0
La	43.5	4.6	4.3	5.3	19.5	45.9	52.4	14.3	61.4
Ce	86.1	10.7	9.5	14.3	54.1	89.5	109.8	28.8	133.7
Nd	38.4	7.1	7.9	7.2	37.7	38.3	49.6	16.4	53.0
Sm	6.95	2.00	2.30	2.00	8.68	10.10	13.50	3.80	12.00
Eu	1.84	0.81	0.80	0.68	2.82	1.75	1.49	0.74	0.37
Tb	0.93	0.49	0.50	0.41	1.58	1.24	1.60	0.55	1.97
Ho	0.00	0.67	0.00	0.00	2.38	0.00	0.00	0.00	0.00
Tm	0.32	0.19	0.00	0.00	0.78	0.00	0.00	0.00	0.00
Yb	2.64	1.74	2.00	0.90	3.90	2.60	4.40	1.90	4.20
Lu	0.00	0.28	0.26	0.13	0.57	0.28	0.52	0.22	0.57

Samp.	G250C	Qy175	Qy166	G253L	Qy174	Qy87	Bb107	Bb95	Bb124
Seq.	KD2	KD2	KD2	KT1	KT1	QPg1	TQ2	TQ1	TQ3
Rock	b/a.	b/a.	rhy.	bas.	bas.	tra.	bsn.	phn.	and.
Type	L	L	L	D	D	P	L	L	L
SiO_2	53.60	54.25	72.30	50.40	45.67	59.37	44.90	56.90	57.60
TiO_2	1.03	0.94	0.26	0.98	1.00	0.40	1.24	0.93	1.26
Al_2O_3	18.60	19.20	14.63	15.30	19.81	15.39	12.40	17.40	14.20
Fe_2O_3	9.34	8.10	1.93	9.50	9.11	3.53	8.92	5.68	5.68
MnO	0.17	0.25	0.13	0.19	0.20	0.07	0.16	0.09	0.09
MgO	3.64	4.00	0.40	10.10	6.76	1.60	10.30	1.64	2.82
CaO	7.68	8.80	1.80	10.60	11.31	5.68	12.10	3.38	7.28
Na_2O	2.60	2.23	2.38	1.48	1.93	4.06	3.31	2.58	3.18
K_2O	1.14	0.28	3.62	1.28	1.66	5.33	3.89	7.71	3.68
P_2O_5	0.19	0.22	0.08	0.12	0.22	0.40	1.53	0.83	0.65
LOI	2.62	1.74	5.05	1.06	2.09	2.65	1.91	1.98	1.89
Total	100.61	100.01	102.58	101.01	99.76	98.48	100.66	98.92	98.33
Zr	198	170	158	79	93	203	443	587	516
Y	31	31	9	19	23	10	41	37	20
Nb	9.7	12.0	11.0	6.6	8.0	13.0	27.0	40.0	33.0
Rb	60.0	11.0	163. 0	68.0	113.0	169.0	213.0	217.0	130.0

TABLE 1. (*cont.*)

Samp.	G250C	Qy175	Qy166	G253L	Qy174	Qy87	Bb107	Bb95	Bb124
Seq.	KD2	KD2	KD2	KT1	KT1	QPg1	TQ2	TQ1	TQ3
Rock	b/a.	b/a.	rhy.	bas.	bas.	tra.	bsn.	phn.	and.
Type	L	L	L	D	D	P	L	L	L
Sr	259	241	142	208	259	2607	2941	4040	1096
Cr	30	0	0	640	0	0	520	70	61
Ni	9	0	0	125	0	0	148	37	33
V	150	0	0	260	0	0	186	63	75
Cu	17	0	0	40	0	0	47	28	18
Zn	106	0	0	89	0	0	99	101	154
Hf	5.00	4.54	4.20	1.94	2.49	5.40	9.05	12.46	9.65
Ta	0.76	0.29	0.33	0.33	0.84	0.76	1.25	1.82	1.43
Th	8.26	7.40	17.10	1.80	7.00	24.20	89.27	114.16	35.93
Sc	25.7	31.0	5.7	37.6	37.1	7.3	23.3	8.4	8.1
Co	26.3	0.0	0.0	40.7	0.0	0.0	37.9	6.6	8.7
La	21.6	23.7	36.3	8.3	8.3	75.4	325.9	328.4	137.7
Ce	52.3	41.2	57.8	18.6	22.8	139.0	657.8	571.5	275.3
Nd	27.7	21.3	20.0	10.3	12.6	51.3	250.0	204.4	100.5
Sm	5.71	5.60	3.30	2.78	3.80	10.10	33.41	26.01	12.29
Eu	1.59	1.53	0.96	0.83	1.27	1.85	8.38	6.56	2.79
Tb	1.01	0.82	0.37	0.49	0.70	0.57	2.49	1.94	0.93
Ho	1.63	0.00	0.00	0.85	0.00	0.00	0.00	0.00	0.00
Tm	0.42	0.00	0.00	0.19	0.00	0.00	0.00	0.00	0.00
Yb	3.77	1.90	1.00	1.80	2.10	0.90	2.28	2.53	1.35
Lu	0.53	0.28	0.11	0.30	0.30	0.12	0.30	0.34	0.14

Pearce 1984). The patterns drawn depict the range from tholeiitic (OWP1) through alkalic (OWP2 and OWP3) to ultra-alkalic (CWP1). Figure 2*b* shows patterns for four typical continental transitional-to-tholeiitic basalts. Of these, AWP1 and AWP2 also show small and variable degrees of intraplate enrichment: AWP1 is transitional between the oceanic tholeiite pattern (OWP1) and the flat N-MORB pattern; and AWP2 resembles the oceanic tholeiite pattern. By contrast, AWP3 and AWP4 show a small degree of intraplate enrichment on which is superimposed a selective enrichment in large ion lithophile (LIL) elements (Th, La and Ce) which can usually be attributed to crustal assimilation (Thompson *et al.* 1982). The patterns for volcanic arc basalts in figure 2*c* also show selective enrichments in some or all of the LIL elements, in this case due primarily to the metasomatism of the mantle wedge source by aqueous-to-siliceous fluids derived from the subduction zone (see e.g. Pearce 1984). However, it should be noted that subduction and assimilation components cannot be simply distinguished on these plots, and that assimilation can sometimes also be important in these settings: the LIL-enrichment component is therefore termed a subduction/assimilation component in the following text. The degree of LIL element enrichment increases from tholeiitic (OVA1) through calc-alkaline (OVA2 and CVA2) to shoshonitic (CVA1) basalts; basalts erupted in active continental margins (CVA1 and CVA2) and alkaline basalts in island arcs (not shown) can be distinguished from island arc tholeiitic (OVA1) and calc-alkaline (OVA2) basalts by negative slopes of the high field strength (HFS) elements (Nb, Ta, Hf, Zr, Ti, Y and Yb), indicating intraplate as well as subduction/assimilation components. Figure 2*d* illustrates patterns for some post-collision basalts ranging from calc-alkaline (PCL1) through alkalic and shoshonitic (PCL2 and PCL3) to ultrapotassic (PCL4): these most closely resemble patterns from active

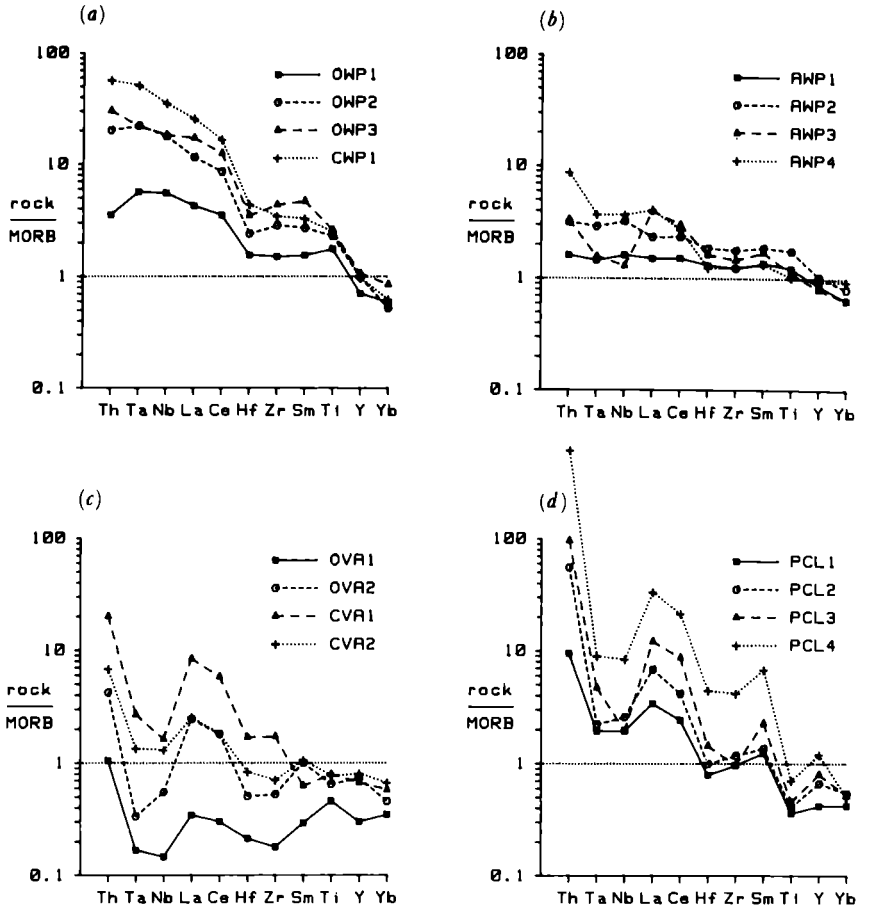

FIGURE 2. Reference MORB-normalized geochemical patterns for basalts of known eruptive environment for comparison with Geotraverse samples in figures 7, 10, 13, 16 and 19. Figure 2*a* shows basalt patterns from oceanic and continental within-plate (OWP and CWP) settings from Loihi, Hawaii (OWP1: Frey & Clague 1983), Ascension and Gough Is. (OWP2 and OWP3: Weaver *et al.* 1987), and Uganda (CWP1: Mitchell & Bell 1976). Figure 2*b* shows basalt patterns from attenuated continental within-plate (AWP) settings from Mull (AWP1: Morrison *et al.* 1980), Skye (AWP2 and AWP3: Thompson *et al.* 1982) and Columbia River (AWP4: Hooper *et al.* 1984). Figure 2*c* shows basalt patterns from oceanic and continental volcanic arc (OVA and CVA) settings from Tonga (OVA1: Ewart *et al.* 1977), New Hebrides (OVA2: Gorton 1977), Chile (CVA1: JAP, unpublished data) and Colombia (CVA2: Marriner & Millward 1984). Figure 2*d* shows basalt patterns from post-collision (PCL) settings from Iran (PCL1: Riou *et al.* 1981), the Alps (PCL2 and PCL4: Venturelli *et al.* 1984), and the Roman province (PCL3: Rogers *et al.* 1985).

continental margin basalts but can occupy all parts of the spectrum from intraplate to continental arc compositions.

The discrimination diagrams utilize the geochemical enrichment patterns shown in the MORB-normalized patterns, but define the boundaries between the various magma types better: thus the Ti–Zr–Y diagram (figure 3*a*) generally indicates the degree of intraplate enrichment, basalts from such sources plotting in the within-plate field on the diagram; and the Th–Ta–Hf diagram (figure 3*b*) generally indicates the degree of subduction zone enrichment, basalts from these sources plotting in the volcanic arc field on this diagram. Since these diagrams were originally published, it has become clear that some ambiguities can occur. Notably: some continental tholeiites may not be derived from sufficiently enriched sources to

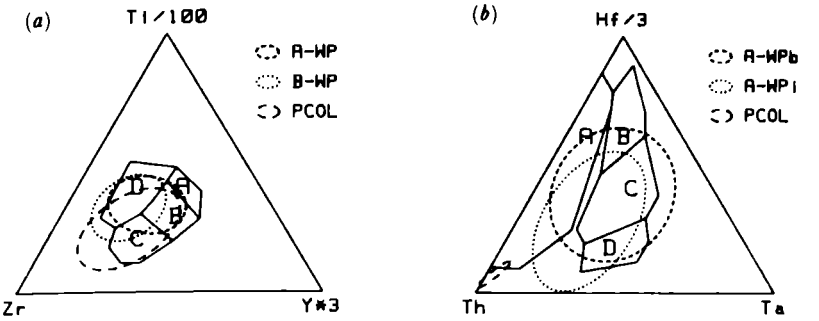

FIGURE 3. Ti–Zr–Y and Th–Ta–Hf discriminant diagrams used to classify Geotraverse basalts, also showing 90% probability ellipses for transitional magma types not considered in original publications. Figure 3*a* shows fields for within-plate basalts (D), mid-ocean ridge basalts (B), island arc tholeiites (A and B) and calc-alkaline basalts (B and C) with additional fields for basalts from normal and back-arc attenuated continental lithosphere (A- and B-WP) and post-collision settings. Figure 3*b* shows fields for volcanic arc basalts (A), mid-ocean ridge basalts (B and C) and within-plate basalts (C and D) with additional fields for basic and intermediate rocks from attenuated continental lithosphere (A-WPb and A-WPi) and for post-collision basalts.

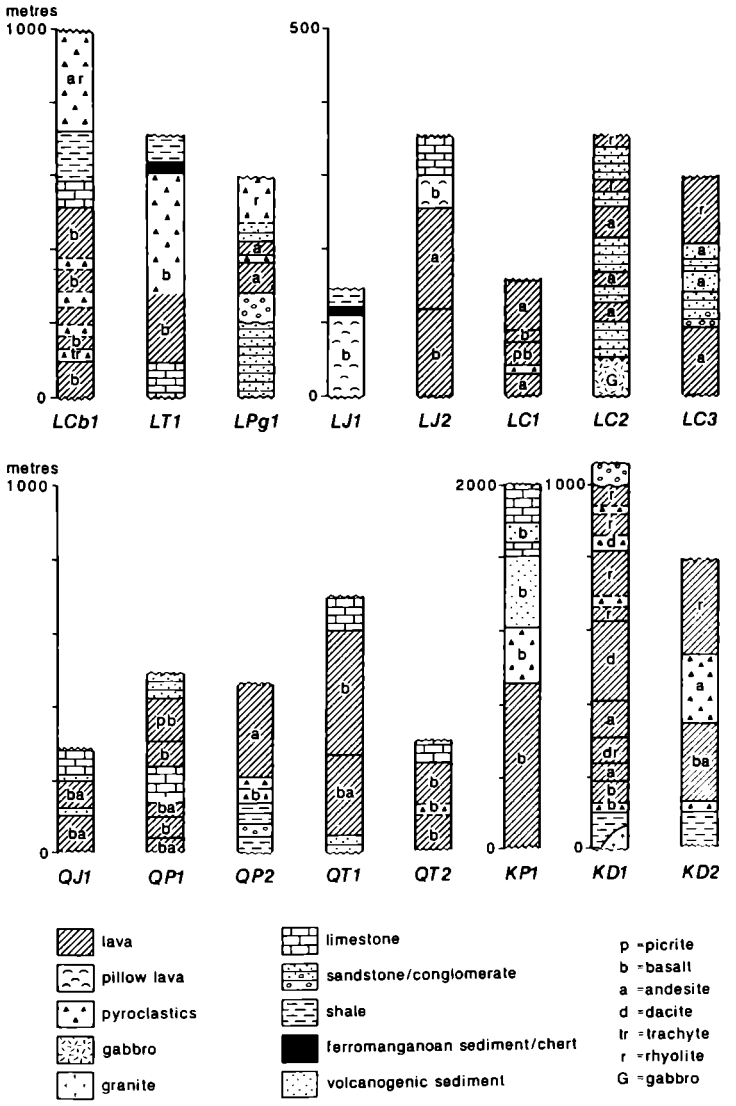

FIGURE 4. Sketch sections showing the volcanic sequences studied during the Geotraverse. For locations, see figures 5, 8, 11 and 14.

plot in the within-plate fields on these diagrams (e.g. Holm 1982); crustal contamination of continental tholeiites may cause them to plot in the volcanic arc field of the Th–Ta–Hf diagram (e.g. Thompson *et al.* 1980); post-collision basalts and some active continental margin basalts may cross from the calc-alkaline basalt to the within-plate field on the Ti–Zr–Y diagram due to the intraplate component in their mantle source; and some basalts, such as ensialic back arc basin volcanics, may be genuinely transitional between the main magma types highlighted in these diagrams. Some additional fields have therefore been superimposed on the two diagrams in figure 3 to take these points into account. Where ambiguities occur, due to basalts plotting in an overlap field, geological and other criteria will be used to try to resolve the ambiguity.

The text that follows considers the geological, petrological and geochemical evidence for the eruptive environments of the various palaeovolcanic provinces encountered during the Geotraverse taken in order from south to north, concluding with a separate discussion of the Tertiary post-collision volcanism and its implications. The volcanic stratigraphy of each sequence studied is recorded in figure 4, although it should be stressed that these were generally mapped at reconnaissance speed. The location of each sequence is given in sketch maps in figures 5, 8, 11, 14 and 18. The sequences are represented in figures and tables by three characters (e.g. LT1), the first representing the terrane, the second the age and the third the location.

3. South Lhasa Terrane (Carboniferous and Triassic) Provinces

Thick sequences of volcanic rocks are exposed east and north-east of Lhasa (figure 5). In their best-exposed area around Dagze they comprise a *ca.* 1500 m-thick sequence of basalt-andesite sheet flows and tuffs (interbedded with mudrocks and limestones) overlain by a thick sequence of ignimbrites and rhyolite flows (figures 4 and 5, section LCb1). In the other area studied, north-east of Maqu, a sequence of basic lavas and tuffs is overlain by ferromanganoan sediments and cherts (figures 4 and 5, section LT1). The lavas overlie and/or are interbedded with platform carbonates in both areas. The carbonates in the north have been dated as late Anisian (Smith & Xu, this volume), and the associated lavas have therefore been taken to be mid-Triassic in age, belonging to the Yeba Formation of southern Tibet (Yin *et al.*, this volume). The southern sequence (LCb1) was originally thought also to be of Triassic age but palynomorphs of late Carboniferous age have recently been identified in shales intercalated within the volcanics (Smith & Xu, this volume).

The basic rocks in both provinces are metamorphosed in greenschist facies to chlorite–epidote–albite–calcite–magnetite assemblages. Phenocrysts, commonly pseudomorphed, are mainly plagioclase with some olivine and clinopyroxene and may comprise up to 50% of the rock. Intermediate and acid rocks are most common in the Carboniferous sequence: the former sometimes also contain phenocrysts of hornblende and the latter typically contain phenocrysts of biotite, feldspar and quartz.

The lavas are strongly altered and so have been classified using the Zr/Ti–Nb/Y diagram (figure 6*a*), both suites plotting within the sub-alkaline basalt and andesite fields (Carboniferous rhyolites are also present but have not been analysed). The Carboniferous basalts exhibit a very slight and variable intraplate component and a major subduction/assimilation component on a MORB-normalized plot (figure 7*a*). They plot within fields B and C

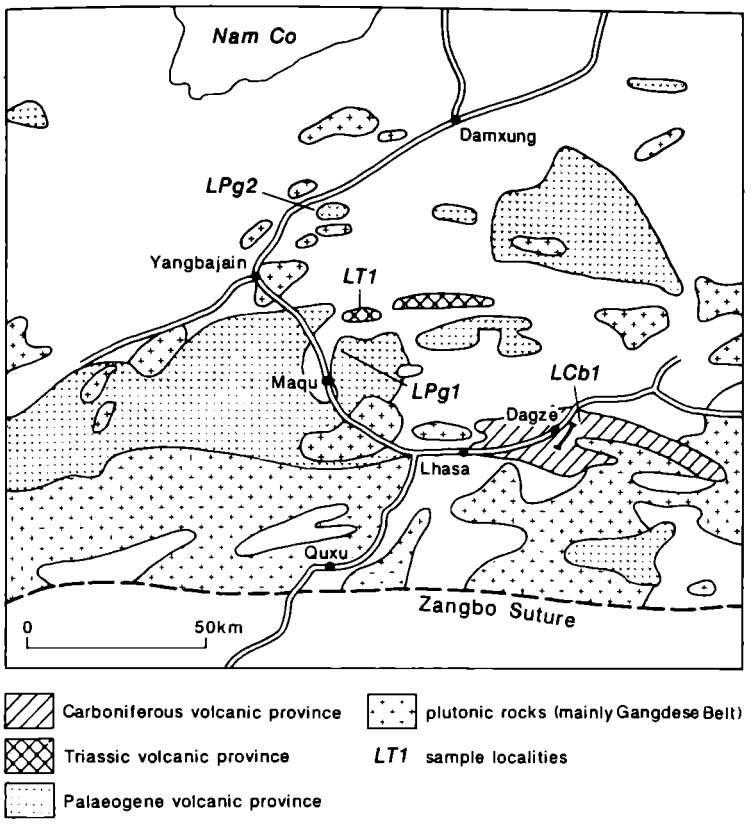

FIGURE 5. Sketch map of the southern part of the Lhasa terrane (see figure 1) showing the approximate known distribution of the volcanic provinces and the locations of the sequences studied.

(calc-alkaline volcanic arc) on the Ti–Zr–Y diagram (figure 7*c*) and in the volcanic arc field on the Th–Ta–Hf diagram (figure 7*d*). The basalts from the Triassic sequence (LT1) have not been fully analysed at the time of writing. However, existing data show that they have similar concentrations of Zr, Y and Nb to the Carboniferous basalts but significantly higher Th concentrations, indicating a similar MORB-normalized pattern shape but with a greater subduction/assimilation component. The two analysed basalts from this sequence plot in the calc-alkaline volcanic arc fields on the Ti–Zr–Y diagram (figure 7*c*) and in the volcanic arc field of the Th–Ta–Hf diagram (figure 7*d*).

Comparison between figure 7*a* and figure 2 shows that the Carboniferous basalts are transitional between the Colombian active continental margin pattern (CVA2) and the New Hebrides pattern (OVA2), but also have some features in common with post-collision basalts; comparison between figures 7*c*, *d* and figure 3 confirms that a volcanic arc origin is most likely but that a post-collision setting is possible. Since the geological evidence indicates a shallow-water submarine environment, possibly associated with carbonate platform break-up (Leeder *et al.*, this volume), an intracontinental post-collision setting can be rejected on geological grounds. However, post-collision rifting to produce an ocean basin, as in the present-day Tyrhennian Sea, remains a possibility. The best interpretation is still, however, that the Carboniferous lavas were erupted in a volcanic arc on transitional crust.

The setting of the Triassic province was probably similar to that of the Carboniferous province: its trace element concentrations are similar, apart from its greater subduction com-

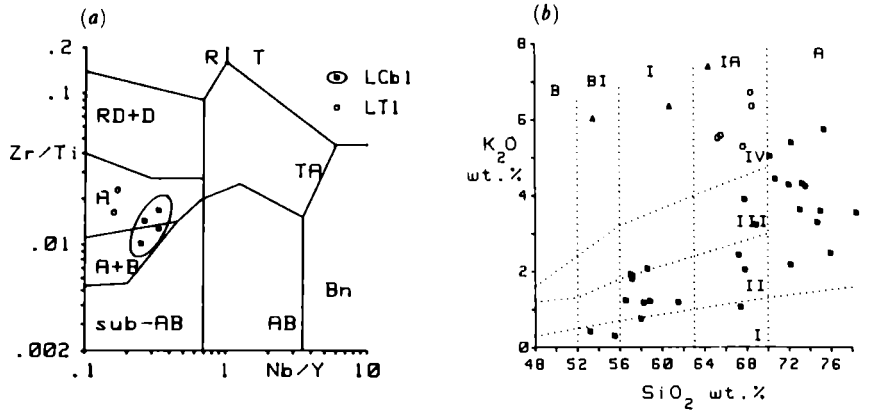

FIGURE 6. (*a*) Zr/Ti–Nb/Y immobile classification diagram and (*b*) K_2O–SiO_2 orogenic rock type classification diagram from South Lhasa Terrane volcanic rocks. In figure 6*a*, the fields shown are for sub-alkaline and alkaline basalts (sub-AB and AB), basalts (B), andesites (A), dacites (D), rhyodacites (RD), rhyolites (R), trachytes (T), trachyandesites (TA) and basanites (Bn). In figure 6*b* vertical boundaries mark the fields for basic (B), basic-intermediate (BI), intermediate (I), intermediate-acid (IA) and acid (A) rocks; boundaries with small positive slopes mark the fields for tholeiitic (I), calc-alkaline (II), high-K calc-alkaline (III) and shoshonitic (IV) series. Also in figure 6*b*, closed squares represent rocks from cycle 1 of the Palaeogene Linzizong Formation (LPg1); open circles represent rocks from cycle 3 of the Linzizong Formation (LPg1); and closed triangles represent rocks from the Yangbajain Basin section of the Linzizong Formation (LPg2).

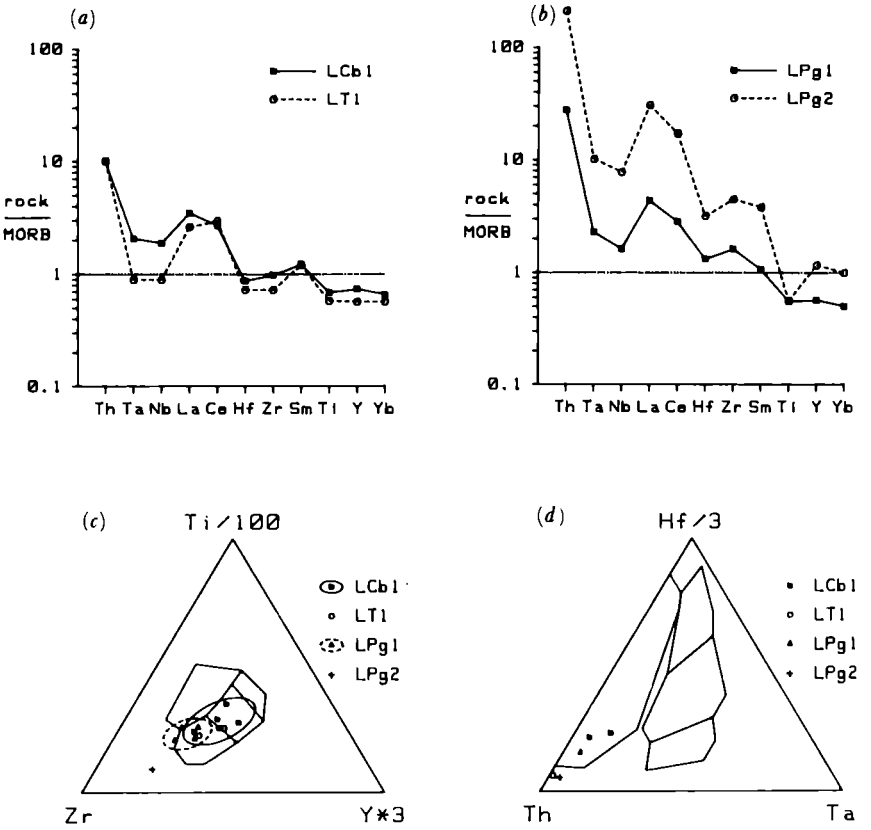

FIGURE 7. (*a*, *b*) MORB-normalized patterns for representative basalts from the Carboniferous (LCb), Triassic (LT) and Palaeogene (LPg) South Lhasa Terrane provinces, and (*c*, *d*) tetonic discrimination diagrams for all basalt samples. Equivalent diagrams for rocks of known setting are given in figures 2 and 3.

ponent; and its geologic setting, notably its relationship to carbonate break-up, is comparable. This interpretation is supported by the volcanic arc characteristics indicated by the Ti–Zr–Y and Th–Ta–Hf plots.

4. South Lhasa Terrane (Palaeogene) Province

Palaeogene volcanism is represented in the Geotraverse area by a 1500–2500 m thick sequence known as the Linzizong Formation, which unconformably overlies folded Upper Cretaceous Takena red-beds between Lhasa and Yangbajain and (locally) further north. This sequence has already been studied in some detail (Wang 1980; Coulon *et al.* 1986) and our work was thus confined to a small, confirmatory study.

Wang (1980) described three cycles of volcanism in the Linzizong formation in the area of north of Lhasa. His first cycle consists of a lowermost unit of andesite lavas and pyroclastic rocks and an upper unit of dacitic and rhyolitic pyroclastics, both interbedded with terrestrial clastic sediments and exceeding 1000 m in cumulative thickness. His second cycle is at least 500 m thick and is made up of thick andesite flows. His third cycle is at least 1000 m thick (top not seen) and consists of tuffaceous sandstone overlain by rhyolitic pyroclastics interbedded with tuffaceous sediment and capped by trachydacitic lavas and pyroclastics. Wang also noted a pause in volcanic activity between the second and third cycles. Our own samples were collected from the Maqu region about 40 km north of Lhasa on the east side of the Lhasa-Yangbajain highway in the area of exposure of Wang's first cycle of volcanics (figures 4 and 5, section LPg1). The Linzizong volcanics in this area have given isotopic ages ranging from 60–50 Ma and are locally intruded by the Lhasa granite, which has been dated at about 53 Ma (Xu *et al.* 1985; Coulon *et al.* 1986). A second set of samples was taken a short distance east of the highway some 30 km NE of Yangbajain on the SE flank of the Yangbajain basin, a narrow NE–SW trending graben structure on the SE margin of the Nyainqentanglha range (figure 4, section LPg2). This locality contains a thin sequence of interbedded trachytes and feldspathoid-bearing basalts and was described in some detail by Coulon *et al.* (1986) who dated the sequence as *ca.* 50 Ma by the ^{40}Ar–^{39}Ar technique.

Petrographically the Maqu sequence is strongly porphyritic, containing up to 40% of phenocrysts of plagioclase and some hornblende and clinopyroxene in a cryptocrystalline groundmass. The rocks contain a small number of vesicles and show incipient alteration, notably of hornblende phenocrysts which are pseudomorphed by chlorite and sphene. The rocks north of Yangbajain are quite distinct: the basic rocks contain large euhedral crystals of leucite (pseudomorphed by analcime), plagioclase, titanaugite and olivine in a groundmass of sanidine, aegirine augite and analcime; the trachytes contain large phenocrysts of sanidine and kaersutite in a fine-grained groundmass.

Of the geochemical diagrams, the K_2O–SiO_2 classification plot (figure 6*b*) illustrates Wang's (1980) observation that the rocks become more potassic for a given degree of evolution from bottom to top of the Linzizong sequence, and further emphasizes the ultrapotassic compositions in the Yangbajain Rift. This plot also indicates that crustal assimilation is important in the trend from basic to acid compositions, since the trend is too steep to be accounted for solely by fractional crystallisation. The MORB-normalized plots (figure 7*b*) show strong intraplate and subduction/assimilation components in the basic rocks from both Maqu and, more noticeably, from the Yangbajain rift and resemble the patterns from Chile (CVA1) and the post-collision

localities in figure 2. The Ti–Zr–Y and Th–Ta–Hf diagrams (figures 7*c* and *d*) show characteristics of active continental margin or post-collision basalts for both groups.

Both the geochemistry and the geology of the Linzizong Formation are therefore consistent with the consensus model of an origin above a northward-dipping subduction zone at an active continental margin (e.g. Coulon *et al.* 1986). The strong increase in potassium from cycle 1 to 3 in the lava sequence may indicate the increasing subduction of sediment that accompanied the arrival of a continental margin (in this case the Indian margin), as can be seen at the present-day in Mediterranean arcs and in the Banda arc; alternatively, it could indicate an intra-arc compressional event of the type that has marked the Neogene history of the Central Andes (Bourgois & Janjou 1981). The ultrapotassic compositions in the Yangbajain Rift may also be explained in terms of either an increase in potassium with depth to the Benioff Zone or an origin related to rifting following intra-arc collision.

5. North Lhasa Terrane (Jurassic) Province

Jurassic volcanic rocks have been reported from two major formations within the Lhasa Terrane: the Sangri Group comprising volcanic rocks interbedded with flysch of latest Jurassic to early Cretaceous age from the south of the Terrane; and the Jienong Group, also comprising volcanic rocks interbedded with flysch but of early-to-mid-Jurassic age and from the north of the Terrane around Gyanco (Yin *et al.*, this volume) Neither of these Groups was identified during the Geotraverse, but two sequences of lavas of probable Jurassic age were recognized these are represented as LJ1 and LJ2 in figure 8. Some of these were clearly part of ophiolite complexes and have been discussed in more detail by Pearce & Deng (this volume). Two sequences showed no definite relationship to ophiolites, however, and these are considered here: they are the Loubochong and South Amdo sequences.

The Loubochong sequence (figures 4 and 8, section LJ1) is a 100 m-thick, inverted section of vesicular pillow lavas. The topmost lavas are veined by cherts and these are overlain by cherts and siliceous mudrocks with thin tuff horizons interbedded with cherts. These sediments have been interpreted by Leeder *et al.* (this volume) as representing an oceanic volcano slope. The section south of Amdo (figures 4 and 8, Section LJ2) comprises massive vesicular basalt flows overlain by porphyritic dacite and rhyolite flows, the uppermost of which are pillowed and veined by calcite; these are then overlain by limestone. Geologically this sequence most resembles the upper part of an island arc seamount. To the south and in uncertain relationship with this sequence is a ridge of massive, homogeneous rhyolite.

Petrographically, the Loubochong lavas are strongly metamorphosed to a greenschist facies (chlorite–epidote–calcite–albite) assemblage, are vesicular and either aphyric or clinopyroxene–phyric. The lavas south of Amdo are strongly porphyritic, containing up to 40% by volume of phenocrysts in a cryptocrystalline matrix. The main phenocryst is plagioclase, but clinopyroxene and (in the more basic rocks) olivine are also present. These rocks are also metamorphosed in greenschist facies (albite–chlorite–epidote–calcite) and most phenocrysts are partly or wholly pseudomorphed by alteration phases.

The geochemistry of both sequences is characteristic of island arc tholeiite transitional to island arc calc-alkaline compositions. This is seen, though unreliably due to alteration, in the K_2O–SiO_2 diagram in figure 9. The MORB-normalized patterns in figure 10*a* show low concentrations of the high field-strength (HFS) elements coupled with relative enrichments in the

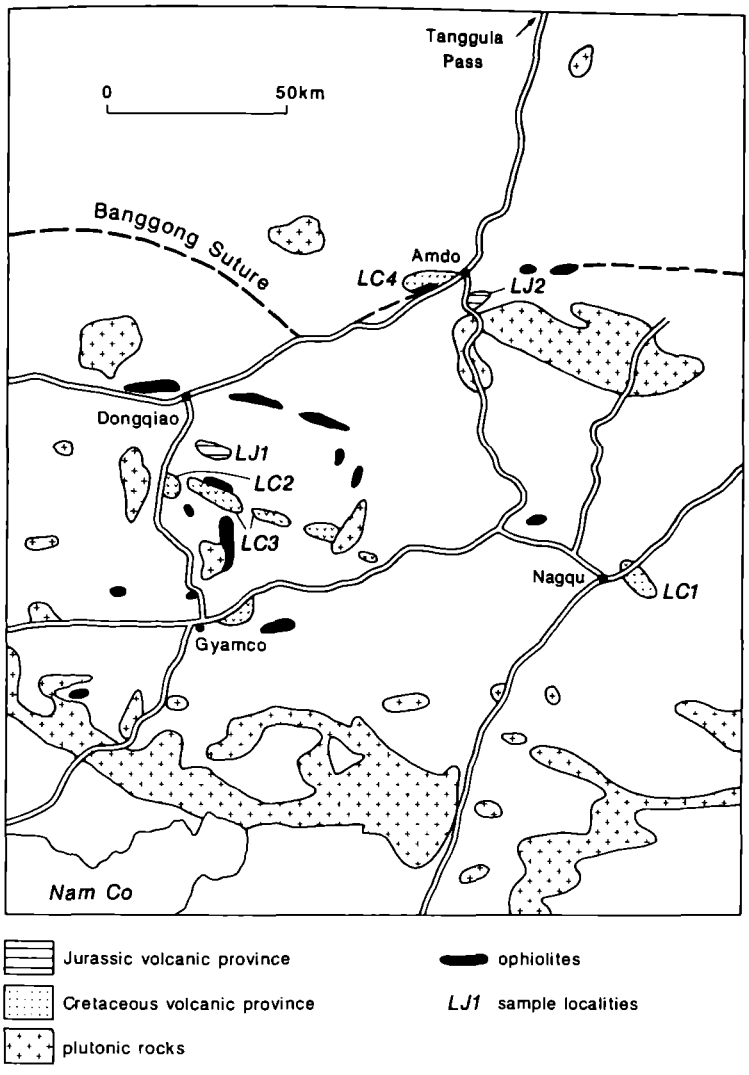

FIGURE 8. Sketch map of the northern part of the Lhasa Terrane showing the approximate known distribution of the volcanic provinces and the locations of the sequences studied.

LIL elements (Th, LREE) and, where not depleted by apatite crystallization, P. Comparison with the 'standard patterns' in figure 2*c* shows strong similarities between both patterns and the patterns for the volcanic arc basalts (OVA1, OVA2 and CVA2). The basic rocks also plot clearly in the volcanic arc fields on the Ti–Zr–Y and Th–Ta–Hf diagrams in figures 10*c* and *d*. A further point of note is that the rhyolite from the ridge south of the South Amdo section is compositionally part of this same province (see data on microfiche 1, in pocket).

Geochemically, therefore, these lavas are of tholeiitic to calc-alkaline island arc composition. Geologically, the lavas south of Amdo probably represent a seamount that approached sea level and accumulated a limestone cover on isostatic subsidence. The rhyolite ridge may also represent some positive submarine topographic feature of the type seen in many recent arc-basin complexes. The Loubochong pillow lavas may represent the flanks of a submarine arc volcano, although they could also have formed at a supra-subduction zone spreading centre: their vesicularity favours the former hypothesis, though not unambiguously. It is probable,

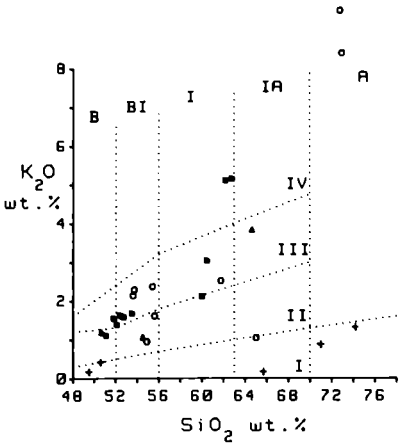

FIGURE 9. K_2O–SiO_2 orogenic rock type classification diagram for North Lhasa Terrane volcanic rocks. Fields are as given in the caption to figure 6. Crosses represent Jurassic volcanics (LJ1 and LJ2 in figure 8); closed squares, open circles and closed triangles represent Cretaceous volcanics from localities LC1, LC2 and LC4 (see figure 8) respectively.

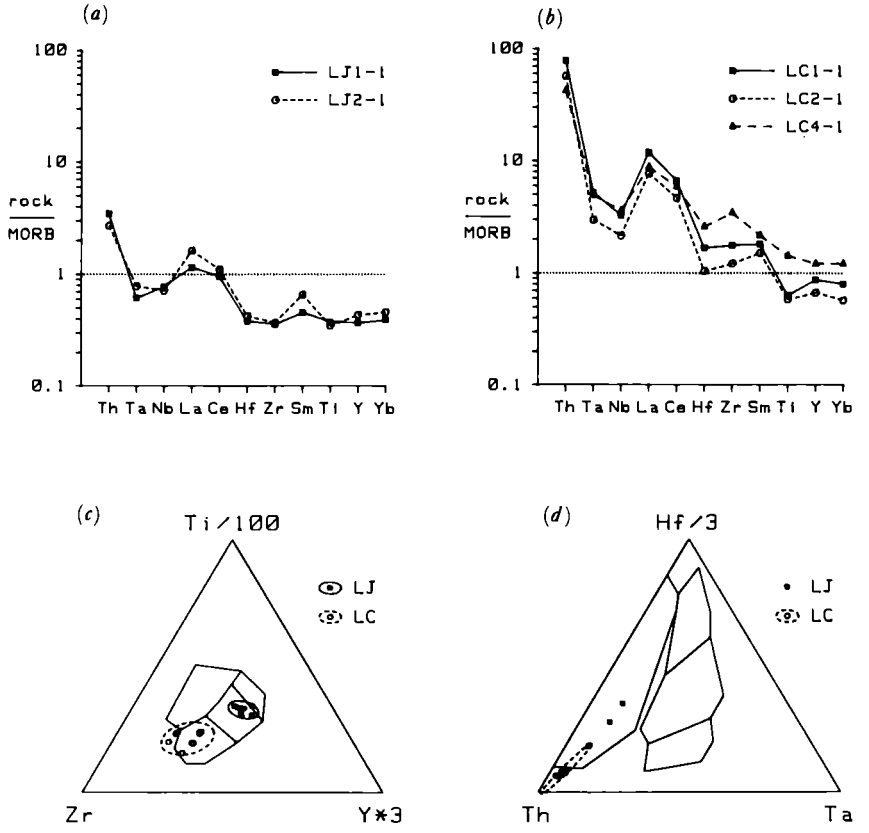

FIGURE 10. (*a*, *b*) MORB-normalized patterns for representative basalts from the Jurassic (LJ) and Cretaceous (LC) North Lhasa Terrane provinces, and (*c*, *d*) tectonic discrimination diagrams for all basalt samples. Equivalent diagrams for rocks of known setting are given in figures 2 and 3.

therefore, that the Jurassic volcanics, together with the ophiolite complexes discussed by Pearce & Deng (this volume), formed in various parts of an arc-basin complex. Although more outcrops need to be examined to reach a definite conclusion, the volcanics studied here could represent an island arc separating a fore-arc terrane in the south from a back-arc terrane in the north-dipping subduction zone.

6. North Lhasa and South Qiangtang (Mid-Cretaceous) Province

As noted by other authors, notably Coulon *et al.* (1986), a major calc-alkaline province was active during the period *ca.* 110–75 Ma over a wide region of the Geotraverse area from Nam Co lake in the South to Amdo and perhaps as far as the Tanggula pass in the north (figure 1). Several sections were studied. The *Nagqu section* (figures 4 and 8, section LC1) is primarily made up of columnar-jointed, vesicular, plagioclase-phyric andesites interbedded with basalts, rare volcanic breccias and red-beds which unconformably overlie Middle–Upper Jurassic mudrocks and flysch. A similar sequence from the Nagqu area has been dated tentatively by the ^{40}Ar–^{39}Ar technique as between 100 and 95 Ma (Coulon *et al.* 1986). The *Norbuzhong and Pung Co sections* (figures 4 and 8, sections LC2 and LC3) north of Gyanco comprise a series of andesite and rhyolite flows interbedded with tuffs and red-beds, in the former case unconformably overlying a fragment of the Dongqiao ophiolite. Parts of this sequence have been dated by Coulon *et al.* (1986) as 95–85 Ma. The *Amdo section* (figure 8, section LC4) is an inverted sequence of ophiolitic gabbro overlain unconformably by basaltic andesite to andesite flows and pyroclastic rocks and overthrust by Cretaceous red-beds. This section has been dated by Coulon *et al.* (1986) as between 80 and 76 Ma. In addition to these sections, lavas, flows, pyroclastic rocks and hypabyssal intrusions of andesite to rhyolite composition are found throughout this area and, by virtue of their similar geological setting are assumed to be of similar age. The northernmost occurrence found during the Geotraverse may be a porphyritic rhyolite stock which intrudes Jurassic shales on the south slope of the Tanggula pass; the southernmost may be a series of rhyolite dykes that cut Carboniferous sediments south of Damxung. High-level plutonic equivalents of many of these volcanic sequences also occur, particularly north of Gyanco.

The petrology of the analysed rocks is broadly similar across the province. Virtually all rocks are porphyritic, containing up to 50% by volume of phenocrysts. Plagioclase is the most common phenocryst throughout the fractionation sequence, but mafic phases are also abundant in the more basic rocks. Olivine, clinopyroxene and magnetite are the most common of these, but hornblende and orthopyroxene are present in some samples. Biotite occurs, together with sanidine, in the more evolved rocks. Some intermediate lavas have trachytic textures. Alteration is variable and generally of sericite–chlorite hydrothermal facies: some sericitization of plagioclase is common; hornblende and orthopyroxene have usually experienced partial or total replacement by chlorite and/or calcite and oxides; clinopyroxene can be carbonated; and biotite is commonly oxidized.

The rocks analysed typically plot in the high-K calc-alkaline series fields of the K_2O–SiO_2 diagram (figure 9). MORB-normalized plots (figure 10*b*) show small intraplate and large subduction/assimilation components for basic rocks from all four sections, resembling the patterns from Chile (CVA1) and the post-collision settings in figure 2. The rocks plot on the volcanic arc (calc-alkaline) - within-plate boundary on the Ti–Zr–Y diagram (figure 10*c*) and

within the volcanic arc field of the Th–Ta–Hf diagram (figure 10*d*), indicating an active continental margin or post-collision setting (see figures 2 and 3).

The combination of geochemistry and geology does not totally resolve the ambiguity between an active continental margin and a post-collision origin. Coulon *et al.* (1986) favoured an origin above a shallow N-dipping subduction zone. They considered a post-collision origin, but argued against it, largely on the grounds that the time interval between the collision in the Banggong Suture Zone was too great for collision and volcanism to have been related. We, however, prefer the post-collision hypothesis on the following grounds: the final collision event could have been as late as the age of intrusion of the Baingoin granitoid belt (*ca.* 130–120 Ma: Harris, Xu, Lewis, Hawkesworth & Zhang, this volume), in which case the time interval between collision and the start of postulated post-collision volcanism would lie between 40 and 30 Ma which is roughly the same period as in Tibet and the Alps; the distance from a trench at the southern margin of the Lhasa Terrane would mean an arc-trench gap of 2–500 km, which is unrealistically large by present-day analogies; there is no major difference in composition between the lavas north of Amdo and those near Nagqu, some 150 km to the south, whereas most active continental margins show major space-time geochemical variations. Clearly, however, the closure of the Banggong Suture was such a complex and poorly-understood event that neither possibility can entirely be ruled out.

7. Qiangtang (Jurassic) Province

A sequence of mainly basic Jurassic volcanic rocks at or near the base of the predominantly sedimentary Yanshiping Group was briefly studied north of Wenquan Station (figures 4 and 11, section QJ1). The sequence comprises reddish-brown massive flows intercalated with and overlain by ferromanganoan sediments and is overlain by a yellow limestone and finally by a thick fluviatile sequence which contains marine incursions dated as mid-Jurassic (Smith & Xu, this volume). The volcanics are therefore considered to be of early mid-Jurassic age.

The lavas mainly contain up to 20% of olivine or olivine and plagioclase phenocrysts in a groundmass of plagioclase, clinopyroxene and magnetite. The samples studied have experienced pervasive oxidative alteration in which olivine phenocrysts were altered to mixtures of iddingsite, smectite and calcite, plagioclase phenocrysts were partially altered to clay minerals and the groundmass has been partly replaced by calcite and clay minerals.

The geochemistry of the rocks is also marked by erratic variations in the abundances of alkali elements due to mobility during alteration. On the Ti/Zr–Nb/Y diagram (figure 12*b*), the rocks classify as sub-alkaline andesites. The MORB-normalized patterns (figure 13*a*) show a strong intraplate component and an additional subduction/assimilation component most resembling the Columbia River basalt pattern (AWP4) in figure 2. The analysed samples plot from the volcanic arc/within-plate boundary into the within-plate field of the Ti–Zr–Y diagram (figure 13*d*) and in the volcanic arc field of the Th–Ta–Hf diagram (figure 13*e*). These results indicate an intraplate origin on attenuated lithosphere, either at a passive margin or in a back-arc ensialic setting: a post-collision setting or active continental margin is a possible, but less likely, interpretation.

The apparently minor extent and geologic setting of this sequence argue against an origin at an active continental margin and for an origin on attenuated continental lithosphere, but

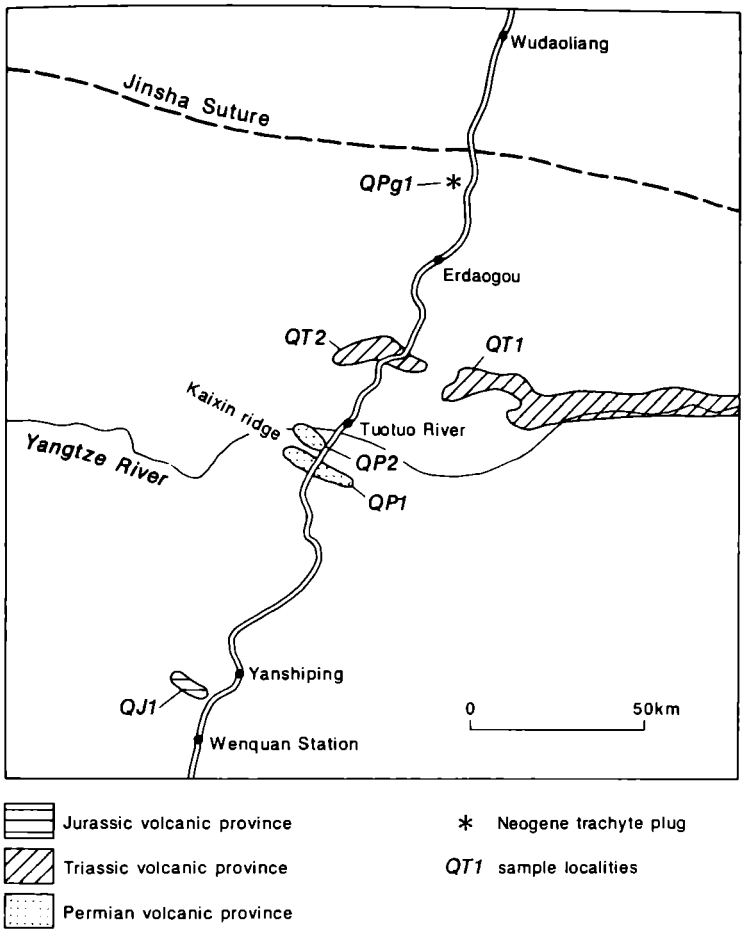

FIGURE 11. Sketch map of the Qiangtang Terrane showing the approximate known distribution of the volcanic provinces and the locations of the sequences studied.

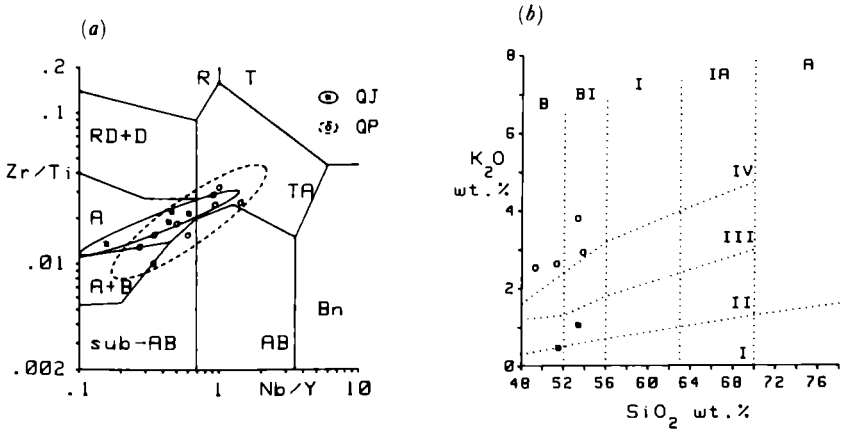

FIGURE 12. (*a*) Zr/Ti–Nb/Y immobile element classification diagram and (*b*) K_2O–SiO_2 orogenic classification diagram for Qiangtang Terrane volcanic rocks. The fields are as given in the caption to figure 6. In figure 12*b*, the closed squares and open circles represent the lower and upper lavas respectively from locality QT1 (figure 11).

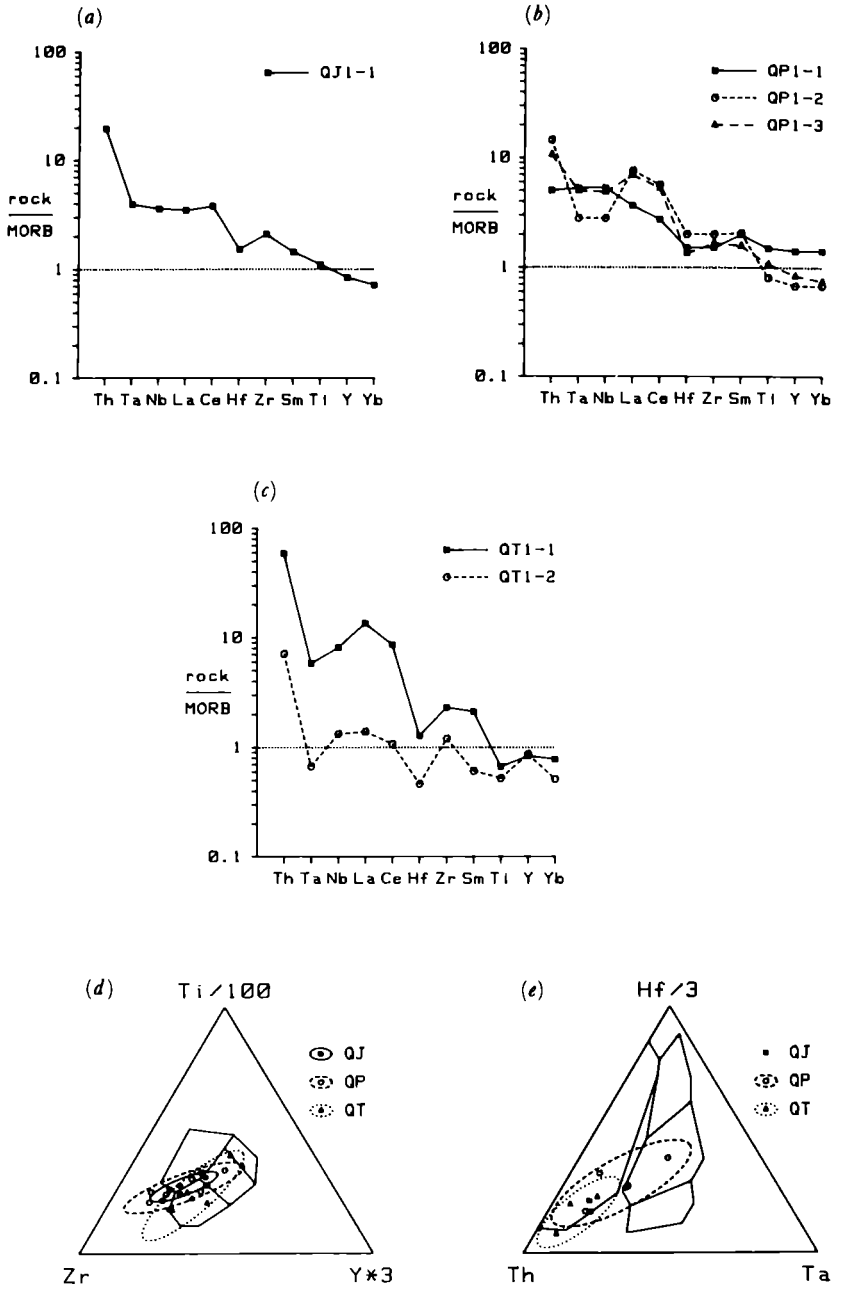

FIGURE 13. (*a–c*) MORB-normalized patterns for representative basalts from the Jurassic (QJ), Permian (QP) and Triassic (QT) provinces, in the Qiangtang Terrane and (*d*, *e*) tectonic discrimination diagrams for all basalt samples. Equivalent diagrams for rocks of known setting are given in figures 2 and 3.

it is not entirely clear whether the eruptive event is best thought of as having taken place in a post-collision rift in a foreland basin related to a Triassic collision event in the north, or at the edge of a marginal basin related to a Jurassic subduction event to the south. Some of the best analogues of both the geology and the geochemistry are found in the trap basalts of Eastern China, on the margin of the Japan and South China Seas (Zhou & Armstrong 1982).

8. Qiangtang (Permian) Province

Lavas from this province were studied during the Geotraverse on and around the Kaixin Ridge, a short distance south of Tuotuohe (figure 11). As explained by Smith & Xu (this volume), the volcanic sequence conformably overlies limestones of early late Permian age and is thus assumed itself to be of late Permian age, correlating with volcanics of the Qamdo region further to the east.

Two sequences were studied, one on the south slope of the Kaixin Ridge (figures 4 and 11, section QP1), the other on the Banacomu Ridge (figures 4 and 11, section QP2). The former is divided into two units separated by a limestone bed. The lower unit is at least 100 m in thickness and comprises (from bottom to top) a basaltic andesite, a dolerite and an andesite unit. The upper unit is about 165 m in thickness and can be divided into a dolerite, a basalt and a picrite basalt unit. The sequence on the Banacomu Ridge begins with variegated red-green mudrocks of assumed continental derivation overlain by about 350 m of volcanic rocks, comprising agglomerate with basalt clasts and a flow-banded andesite. These are overlain by 40 m of coal-bearing clastics with marine bands dated as late Permian (Leeder *et al.*, this volume).

The volcanic rocks are slightly vesicular and generally contain $< 5\%$ of microphenocrysts of plagioclase, and sometimes also olivine and clinopyroxene, in a groundmass of plagioclase, clinopyroxene and magnetite. The picrite, however, contains about 25 % of olivine phenocrysts. The rocks have experienced a variable degree of carbonation and clay mineral alteration of phenocrysts and groundmass, and vesicles have been filled with chlorite and calcite. On the immobile element classification diagram, Ti/Zr–Nb/Y (figure 12*a*), the rocks can be seen to be transitional between tholeiitic and alkalic in composition and to range from basalts to andesites and trachyandesites. On the MORB-normalized plots (figure 13*b*), the lavas show a range of patterns. One sample (QP1-1) shows a typical intraplate pattern with no subduction/assimilation component; the others exhibit both an intraplate component and a subduction/assimilation component. On the Ti–Zr–Y diagram (figure 13*d*), the samples plot in the within-plate field, but on the Th–Ta–Hf diagram (figure 13*e*) they form a field spanning the ocean ridge/within-plate and the volcanic arc field. This spectrum of compositions is not seen in volcanic arcs, but is common in lavas erupted in intracontinental rifts on attenuated continental lithosphere where variable crustal assimilation has taken place; samples contaminated by the crust show selective enrichment in LIL elements on a MORB-normalized plot (cf. patterns AWP3 and AWP4 in figure 2*b*) and plot in the arc field on the Th–Ta–Hf diagram, whereas uncontaminated samples have intraplate-MORB patterns (cf. patterns AWP1 and AWP2 in figure 2*b*) and plot in the intraplate-MORB fields on discrimination diagrams (see also Thompson *et al.* 1982). The strong degree of iron-enrichment in some samples from this province (see Appendix, microfiche 1, in pocket) also supports this interpretation.

The geochemical interpretation of an origin within attenuated continental lithosphere during rifting can be put forward with confidence since no other environment shows this type of intrasequence variation. Moreover, the shallow-water geological setting and the abundance of sheet-flows are both consistent with this interpretation.

9. North Qiangtang (Triassic) Province

A major volcanic formation, the Batang Group, crops out mainly to the east of the traverse area in the Qiangtang Terrane. Although not of the thickness described for the Batang Group in its type area, lavas assumed to belong to this group were identified east and west of the highway between Tuotuohe and Erdaogou (figure 11). In the eastern section, at Zhakongjian (figures 4 and 11, section QT1), a *ca.* 500 m thick sequence of basalt–andesite lavas flows overlies a fluvial sequence of conglomerates and sandstones and is directly overlain by marine carbonates and clastics (Leeder *et al.*, this volume). The limestones have been given a Norian age by Smith

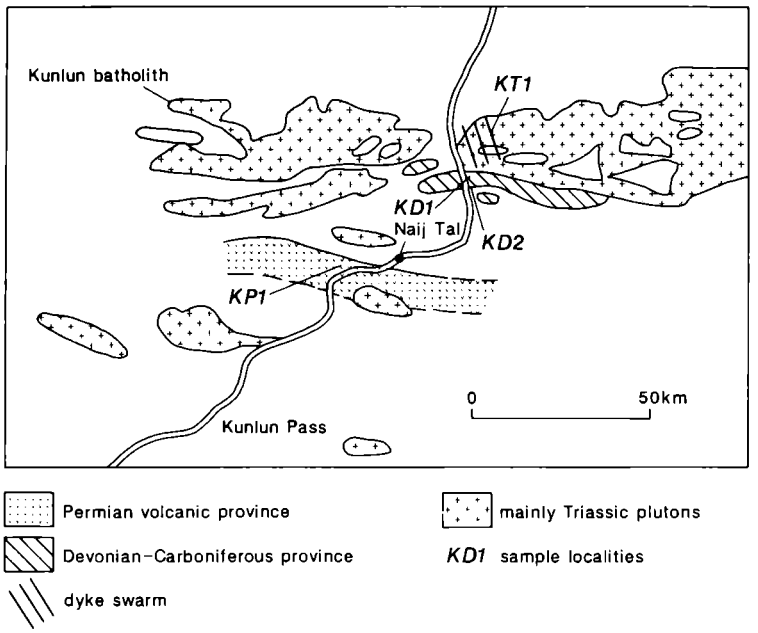

Figure 14. Sketch map of the Kunlun Terrane showing the approximate known distribution of the volcanic provinces and the locations of the sequences studied.

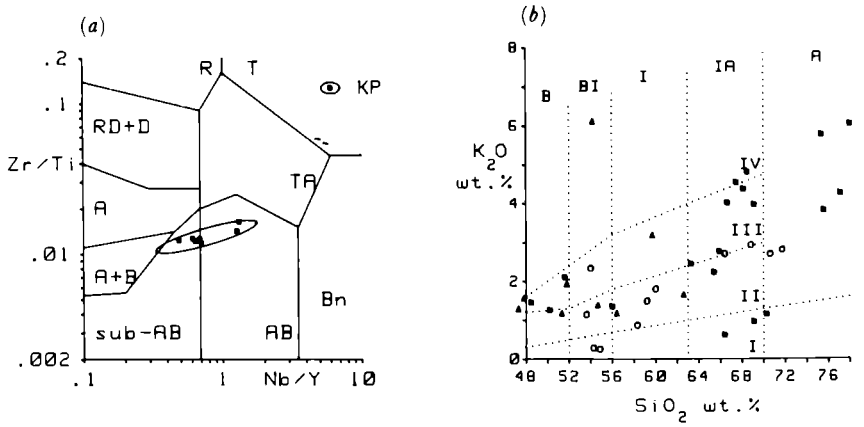

Figure 15. (*a*) Zr/Ti–Nb/Y immobile element classification diagram and (*b*) K_2O–SiO_2 orogenic classification diagram for Kunlun Terrane volcanic rocks. Fields are as given in the caption to figure 6. The closed squares and open circles represent localities KD1 and KD2 (see figure 14) respectively; the closed triangles represent locality KT1.

& Xu (this volume), suggesting that the volcanics are early late Triassic in age. This sequence has been divided into a lower and an upper lava unit on the basis of geochemistry as explained below. The lava flows have a general E–W strike and dip steeply south. In the western section (figures 4 and 11, section QT2), near the 85th Highway Maintenance Squad on the Golmud highway, a *ca.* 130 m sequence of basalt–andesite lava flows and agglomerates (base not seen) is also overlain by a limestone of probable Norian age (Smith & Xu, this volume) and is thus assumed to belong to the same volcanic province. These lavas also strike approximately E–W but dip north at about 45°.

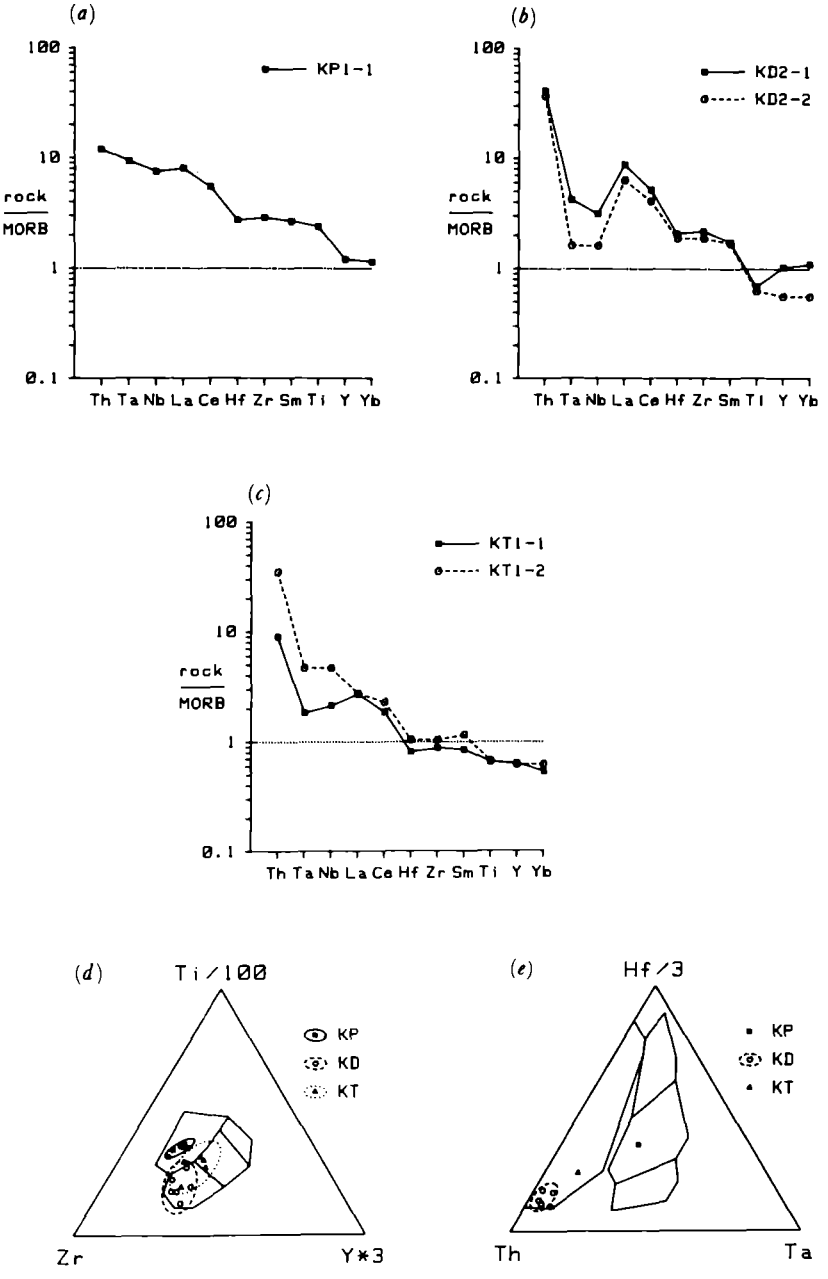

FIGURE 16. (*a–c*) MORB-normalized patterns for representative basalts from the Permian (KP), Devonian/Lower Carboniferous (KD) and Triassic (KT) provinces in the Kunlun Terrane and (*d*, *e*) tectonic discrimination diagrams for all basalt samples. Equivalent diagrams for rocks of known setting are given in figures 2 and 3.

Petrographically, the lavas are all strongly porphyritic, typically containing 30–50% of phenocrysts of olivine, plagioclase and clinopyroxene in a cryptocrystalline matrix. The dominant phenocryst is plagioclase, except in the upper unit from QT1 where the three minerals are in approximately equal proportions. The lavas all exhibit evidence of a moderate degree of low-temperature alteration: olivine is usually partly altered to combinations of iddingsite, serpentine, green and brown smectite and calcite, plagioclase to clay minerals and pyroxene to calcite; brown smectite and calcite are abundant in the groundmass.

Geochemically, the lavas fall into two groups. On the K_2O–SiO_2 diagram (figure 12*b*), the western lavas and the basal group of the eastern lavas plot as members of the calc-alkaline series; whereas the upper group of the eastern lavas plot as members of the shoshonitic series, having very high primary contents of the alkali elements. This distinction is also seen in the MORB-normalized plots (figure 13*c*). Whereas the calc-alkaline basalt of the former group has a pattern characteristic of an oceanic calc-alkaline arc, namely a flat pattern on which a subduction/assimilation component is superimposed (cf. the New Hebrides pattern, OVA2, in figure 2*c*), the shoshonitic basalt shows a large intraplate component as well as the subduction/assimilation component. In view of the close association of these two lavas, the shoshonitic pattern must represent an oceanic alkali arc pattern similar to that of Grenada in the Lesser Antilles (not shown in figure 2), rather than a continental shoshonite. Both groups of lava plot in the volcanic arc fields of the Ti–Zr–Y and Th–Ta–Hf diagrams (figures 13*d* and *e*), thus confirming their volcanic arc characteristics.

The rocks analysed are characteristic of volcanic arc lavas erupted on oceanic or thinned continental lithosphere in terms of both their mineralogy and geochemistry. Their local geological environment, notably their limestone cover, also suggests submarine edifices that have isostatically subsided. The presence of alkali arc lavas in the upper part of the eastern lava sequence may, by analogy with similar compositions elsewhere, such as in Grenada and some of the Aleutian Islands (Delong *et al.* 1975) indicate an origin above a subducted transform fault or close to an arc-transform intersection.

10. Central Kunlun (Permian) Province

This province is known to extend for some distance in an E–W orientation within the Central Kunlun mountains (figure 14). It was studied during the Geotraverse within and to the south of the Wanbaogou valley east of Naij Tal. Despite intense folding and thrusting, it was possible to recognize some stratigraphy (figures 4 and 14, section KP1). The lower unit comprises at least 1.5 km of massive basalts; these are overlain by basic tuffs, then by redeposited tuffs. Thin limestone (marble) bands are intercalated within the upper part of the sequence, which appears to be overlain conformably by limestones of late Permian age (Smith & Xu, this volume); the age of the volcanic episode is tentatively placed at early-mid Permian. Sills within Lower Palaeozoic strata south of the area studied are also thought to have been emplaced during this magmatic episode.

The original petrology of the lavas is largely masked by regional metamorphism: most rocks exhibit a greenschist facies assemblage (chlorite–albite–epidote–calcite), but this rises to amphibolite facies (hornblende–plagioclase–magnetite ± epidote ± zoisite ± calcite) in thrust zones.

The immobile Ti/Zr–Nb/Y classification diagram (figure 15*a*) shows the lavas to be

predominantly basaltic and to be transitional between tholeiitic and alkalic in composition. The MORB-normalized pattern (figure 16*a*) is typical of a transitional intraplate basalt lacking any subduction/assimilation component (c.f. OWP1 in figure 2*a*). This interpretation is supported by the Ti–Zr–Y (figure 16*c*) and Th–Ta–Hf (figure 16*d*) diagrams, both of which show all the analysed samples to have typical intraplate character.

Geochemical evidence is equally consistent with an origin in a continental rift during moderate lithospheric attentuation or in a major oceanic plateau or island chain. Geological evidence, notably the presence of sills within continental basement and the absence of any pillowed flows in the lower part of the sequence favours the continental rift hypothesis.

11. North Kunlun (Devonian/Carboniferous) Province

Volcanic rocks outcrop along the Dagangou valley for about 10 km south of the Kunlun batholith (figure 14); these are thought to be part of a major linear province that extends E–W for thousands of kilometres along the northern part of the Kunlun range. The area studied contains two volcanic formations, one to the north and one to the south, separated by an E–W valley in which there is no exposure. The northern formation (figures 4 and 14, section KD1) strikes consistently at 060° and has a constant 40° SE dip; the southern formation (figures 4 and 14, section KD2) has a similar strike but is gently folded. The 1982 reconnaissance map (Academia Sinica, unpublished data) shows the northern outcrop as 'Devonian' and the southern outcrop as 'Carboniferous'. However, the age of neither formation is completely certain. Both formations are underlain by mudrocks and siltstones of unknown age. The northern formation is intruded and contact metamorphosed by the Triassic Kunlun batholith (Harris, Xu, Lewis & Jin, this volume) and both formations are cut by minor intrusions that are assumed to be of similar age to the batholith. The northern formation is overlain by a thick sequence of conglomerates and arkosic sandstones, a similar sequence to that overlain elsewhere by a fossiliferous sequence of late Visean/early Namurian fluvio-deltaic sediments (Smith & Xu, this volume) and is therefore probably of pre-mid-Carboniferous age. The southern formation was always observed to be in fault contact with these sediments and is therefore of uncertain age. For the purposes of this paper, a Devonian/early Carboniferous age will be assumed for both formations.

Interpretation of the volcanic stratigraphy is complicated by the presence of late Triassic dykes and sills (described in the next section) which cut the volcanic rocks, the Kunlun batholith and the Carboniferous sediments and which have a similar mineralogy and chemical signature to the lavas. Our tentative stratigraphic interpretation shows the northern formation to have an agglomerate at its base, overlain by several units of basalts, andesites and rhyolites; it has a total thickness of *ca.* 900 m. The southern formation also has an andesitic agglomerate at its base overlain by an andesitic and a rhyolitic unit reaching a total thickness (top not seen) *ca.* 700 m.

The mineralogy of the lavas is typically orogenic. The basic-intermediate rocks are porphyritic, containing up to 50 % phenocrysts, mainly of plagioclase, and also of hornblende and magnetite. The acid rocks are also highly porphyritic, containing phenocrysts of K-feldspar, plagioclase, hornblende, biotite and, sometimes, resorbed quartz. All rocks have been strongly altered by hydrothermal processes which were probably associated with the intrusion of the Kunlun batholith. Close to the batholith itself, the lavas have experienced a K-silicate

alteration in which hornblende was pseudomorphed by clusters of biotite and the groundmass largely replaced by tiny biotite grains and secondary quartz. Further from the intrusion, alteration was of propylitic type, in which hornblende was pseudomorphed by clusters of chlorite and magnetite, plagioclase phenocrysts sometimes partly pseudomorphed by epidote and the groundmass converted to an assemblage of sericite, chlorite and secondary quartz. Superimposed sericitic and argillic alteration has altered most feldspar phenocrysts to a mixture of sericite and kaolinite.

Geochemical classification by the K_2O–SiO_2 diagram (figure 15*b*) is not reliable owing to metasomatic effects, by which potassium has been introduced during K-silicate, and removed during propylitic, alteration. However, taking these effects into account, the diagram does indicate that the lavas all belong to the calc-alkaline or high-K calc-alkaline series. The MORB-normalized plots (figure 16*b*) for the most basic lavas reveal a combination of intraplate and subduction/assimilation components typical of active continental margins, some ensialic back-arc rifts and post-collision settings. The Ti–Zr–Y (figure 16*d*) and Th–Ta–Hf (figure 16*e*) discrimination diagrams also show distributions of data points characteristic of these environments. The relationship between the low- and high-K calc-alkaline series can best be represented on plots of more petrogenetic significance. The chondrite-normalized REE plot (figure 17*a*), shows how a parent basalt (Qy175) evolves towards acid compositions. Evolution of the low-K calc-alkaline series towards rhyolites (e.g. Qy166) is accompanied by a slight enrichment in light REE and depletion in heavy REE , a characteristic of significant amphibole fractionation. By contrast, evolution of the high-K calc-alkaline series towards andesites (e.g. Qy171) and rhyolites (e.g. Qy206) is marked by enrichment in both light and heavy REE, giving a somewhat flatter pattern, a feature characteristic of crystallization of anhydrous phases (olivine, plagioclase, pyroxenes and magnetite) throughout. Such a contrast in crystallization behaviour may indicate a change in source region. It can happen during the evolution of active continental margins, but, perhaps significantly, is also characteristic of a change from subduction to collision environment, as for example during Neogene volcanism in Eastern Anatolia (Yilmaz *et al.*, 1987).

Geochemically and geologically, the lavas from this province could have an active continental margin or a post-collision origin, or both. The geochemical argument presented above

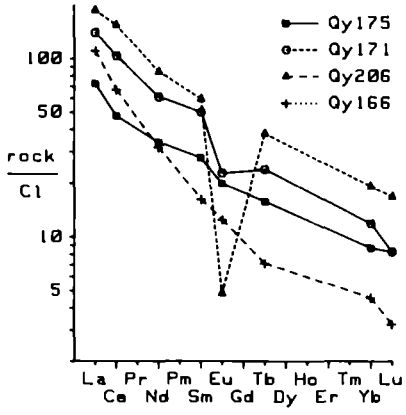

FIGURE 17. Chondrite-normalized REE plot for lavas from the Devonian/Lower Carboniferous province in the Kunlun Terrane: for full analyses see table 1.

gives the lower lava units a greater probability of an origin in an active continental margin, and the upper unit a greater probability of an origin in a post-collision setting, but a final interpretation must await further work on the geology and volcanic evolution of the province.

12. North Kunlun (Permo–Triassic) Province

There are no obvious eruptive products of this province, which is represented in the traverse area by swarms of basalt–andesite dykes which cut the Kunlun batholith and adjacent terrain and by sills of similar composition which cut the Carboniferous sedimentary strata and, as indicated above, the Devonian/Lower Carboniferous volcanic sequences (figure 14, locality KT1). Given the likely age of between 260 and 240 Ma for the Kunlun batholith (Harris, Xu, Lewis, Hawkesworth & Zhang, this volume), the dykes can be assigned an age of post-late Permian. The nature of dyke alteration (discussed below) further indicates that the dykes were intruded before the batholith had cooled; if so, the dykes can be assigned a probable late Permian to early Triassic age. The dyke swarm varies in intensity within the study area, reaching a maximum 10 % of the outcrop in the area shown in figure 14. A brief study indicated two major dyke orientations, the dominant trend being NW–SE with a dip of 75° NE, the subsidiary trend being N–S and vertical.

Texturally, the dykes and sills have equigranular, ophitic textures, and this serves to distinguish them from the porphyritic lavas within the Devonian/Lower Carboniferous terrain. Typically, feldspar laths have been sericitized and poikilitic clinopyroxenes altered to actinolite and biotite. This similarity in hydrothermal alteration assemblages between the Triassic dykes and the Palaeozoic lavas suggests that both were altered at the same time; the zonation of alteration around the batholith in both dykes and lavas suggests that the batholith was the heat source for the hydrothermal alteration: the net conclusion is, therefore, that the dykes were intruded into the batholith while it was still hot enough to set up hydrothermal circulation.

Geochemically, the dykes analysed are dominantly calc-alkaline basaltic andesites and andesites, plotting in the same fields as the Devonian/Lower Carboniferous rocks of similar silica content in the discrimination diagrams of figures 16*c* and *d*. They could also be interpreted equally as active continental margin or post-collision intrusions. The major exception is sample G253Y, which is characterized by high concentrations of HFS elements, most notably Zr, which exceeds 1500 p.p.m. This composition is characteristic only of post-collision settings, but its age is not well-defined since it cuts sediment near the granite contact rather than the granite itself.

Despite the ambiguity in the tectonic interpretation of the dyke geochemistry, geological and isotopic evidence from the Kunlun granitoids (Harris, Xu, Lewis, Hawkesworth & Zhang, this volume) suggests that the 260–240 Ma Kunlun batholith pre-dated collision and that the belt of granitoids south of Naij Tal, dated at 200–190 Ma, post-dated collision. If the dykes are broadly contemporaneous with the Kunlun batholith, they must therefore also pre-date collision and be of active continental margin origin.

13. Oligocene–Recent post-collision volcanism

Although little is known about the timing and distribution of magmatism following the start of India–Eurasia collision in the Palaeogene, three distinct post-collision volcanic provinces can be identified (figure 18). The earliest of these, evidence of which was encountered during the

traverse, is of Oligocene age and runs in an E–W direction between the Tanggula and Kunlun mountains. The second was identified by Coulon *et al.* (1986) in the Maquiang area SW of Yangbajain who dated the rocks by the ^{40}Ar–^{39}Ar technique as 15–10 Ma. The extent of this province is unknown. The third, which lies at its closest some 200 km west of the traverse (and which we attempted, but failed, to reach) was identified by early explorers (e.g. Norin 1946) and later by Landsat imagery (e.g. Sengör & Kidd 1979) and first described in detail by Deng (1978). Limited data suggest that this province became active about 5 Ma ago and remains active, the last recorded eruption being in 1951.

The Oligocene province was represented on the traverse by a trachytic volcanic neck about 200 m in diameter, which is exposed at Zangmaxikong, in the Fenghuoshan (north of Erdaogou), where it penetrates Palaeocene or early Eocene red-beds of the Qiangtang Terrane (figure 18, QPg1), and has been dated at 32 Ma (Harris, Xu, Lewis, Hawkesworth & Zhang, this volume). The rock consists of about 80% sanidine, 9% carbonated clinopyroxene, 8% biotite and accessory magnetite, apatite and zircon. Its composition is marked by moderate concentrations of incompatible HFS elements and extremely high values of the LIL elements, including potassium which exceeds 5 mass% in the analysed samples. Chondrite-normalized REE patterns are very steep (figure 19*b*). The undersaturated composition indicates a mantle source, the very low heavy REE content indicate low-degrees of melting with residual garnet, and the high LIL element content coupled with high $\delta^{18}O$ values indicate significant crustal assimilation.

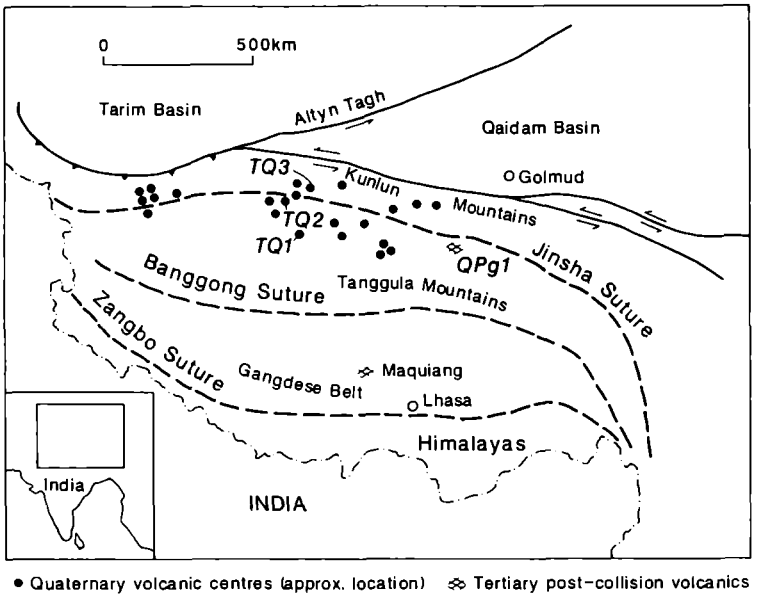

FIGURE 18. Distribution of recognized Tertiary post-collision volcanics on the Tibetan Plateau and locations of areas sampled.

The province, of which this trachyte is thought to be a part, extends from Zadoi county in Southern Qinghai through Muli and Yanbian counties in Western Sichuan to Yaoan county in Northern Yunnan. In all these areas, ages of around 30 Ma have been obtained and leucite lamproite-trachyte volcanic suites, often accompanied by syenite and alkali syenite intrusions, have been described.

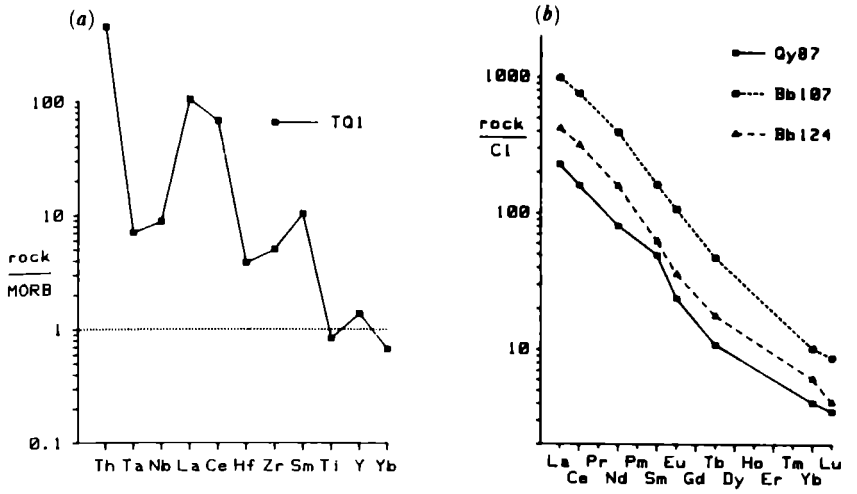

FIGURE 19. (*a*) MORB-normalized pattern and (*b*) chondrite-normalized REE plot for representative samples of Tertiary post-collision volcanics from the Tibetan plateau.

The Miocene volcanism at Maquiang described by Coulon *et al.* (1986) comprises a sequence of andesite–rhyolite flows and pyroclastic rocks. They are described as members of the high-K calc-alkaline series and have a composition which lies within the range of lavas from active continental margins: without an age it would be difficult to distinguish these rocks from their Linzizong precursors.

The NW Tibet Pliocene–Recent Province is, however, quite distinct geochemically. Trace element analyses of three of the samples described by Deng (1978) are given in table 1 and show extremely high concentrations of all incompatible elements, especially Sr, which exceeds 0.5% SrO_2 in some samples, and Zr. Samples from three areas were analysed by Deng (1978). The southernmost of these, in the Qiangtang Terrane, is the Bamaoqiongzong volcanic rock area (figure 18, TQ1) which contains potassic, ultra-alkaline rocks. The MORB-normalized pattern for one of the leucite foidites (figure 19*a*) is a typical post-collision type, closely resembling the ultrapotassic Alpine basalt (PCL4) in figure 2*d*. Its chondrite-normalized pattern shows extreme LREE enrichment, similar to that of the trachyte from Zangmaxikong. The central area (TQ2), also in the Qiangtang Terrane, is the Yongbocuo volcanic area, which contains both pyroxene dacites and trachyandesites. The northernmost area (TQ3), in the Kunlun Terrane, is the Qiangbaqian volcanic area, which contains mainly pyroxene andesites. The chondrite-normalized REE pattern for one of the andesites has been plotted in figure 19*b* and gives a steep pattern similar in shape to the two other samples plotted. These lavas do, however, contain significantly lower concentrations of the LIL elements (e.g. K, Rb, Sr, Th) than the lavas erupted further south (table 1).

The compositions of all the Oligocene–Recent volcanic rocks are characteristic of a highly enriched mantle source that contains major intraplate and subduction/assimilation components. The extremely high values of Sr indicate that the enrichment in LIL elements is due to subduction, rather than assimilation, since the latter would be expected to reduce, or have little effect on, Sr concentrations. This enrichment could have taken place by incorporation of a sialic melt into the sub-Tibetan lithosphere either during the Palaeogene collision event or during earlier subduction or collision events.

Although the precise implications of these observations for our understanding of the collision

event are not clear, the ages, compositions and distributions of these post-collision provinces may still place some constraints on the dynamics of the India–Eurasia collision. The Oligocene trachyte is far from any Palaeogene plate boundary so any mantle enrichment would either have to be inherited from the Triassic subduction-collision event or be the result of some 1000 km of northward underthrusting of the Indian lithosphere or relate to a hitherto unrecognized subduction event. There are insufficient data to resolve these three possibilities, although the first has by far the fewest geological constraints.

The Miocene Maquiang volcanics are less potassic (more calc-alkaline) in character and may simply have resulted from reactivation of the mantle wedge above the Palaeogene active continental margin. It may, however, be significant that this volcanic event occurs during the period of generation of leucogranites along the Main Central Thrust of the Himalayas (Debon *et al.* 1986): it could therefore also be explained by underthrusting of the Indian lithosphere northwards beneath the Gangdise belt.

The Pliocene–Recent volcanism in the NW of the Tibetan Plateau postdates by about 5 Ma the formation of leucogranites in the Kunlun (Molnar *et al.* 1987). The ultrapotassic composition of the volcanics could be explained by an inherited subduction component from the Triassic subduction–collision event, by subduction of the Indian lithosphere northwards, or by subduction of the Tarim basin lithosphere southwards. Of these possibilities, extensive Tibetan underplating by the Indian lithosphere, as proposed, for example by Powell (1986), is much the least likely. According to this model, we would expect extensive volcanic activity over much of the Tibetan Plateau for much of the past 40 Ma. The apparent absence of such activity suggests that any subduction of continental lithosphere was relatively recent. Moreover, the distribution of volcanic centres (figure 18) suggests that, if subduction did take place, it was directed from the north rather than the south. The geochemical polarity, particularly the increase in potassium towards the south, is also consistent with this model.

14. Summary and conclusions

The palaeotectonic information provided by the volcanic rocks of the Tibetan plateau can be summarized as follows.

1. *Devonian/Early Carboniferous active continental margin and/or post collision volcanism in the Northern Kunlun.* The interpretation of this extensive volcanic event is limited by poor age control and the superimposition of a major Triassic collision event. There is good geochemical evidence to suggest that these K-rich calc-alkaline volcanic rocks formed at an active continental margin or post-collision setting, or the transition from one to the other, but there is insufficient geological control to resolve these possibilities.

2. *Carboniferous arc volcanism in the southern Lhasa Terrane.* The sequence of basaltic to rhyolitic calc-alkaline volcanic rocks in the Dagze area east of Lhasa has the geological and geochemical characteristics of an arc volcano built up on transitional crust.

3. *Permian continental rift volcanism in the Qiangtang and Kunlun Terranes.* Permian rift volcanism is a characteristic of many terranes in China and SE Asia and is considered to represent a period of splitting of continental fragments from Eurasia by formation of new spreading centres. It is represented in the traverse area by extensive, mainly basaltic, volcanism south of Tuotuohe and around Naij Tal. The former exhibits geochemical characteristics of greater lithospheric attenuation (e.g. significant, and variable, crustal contamination and a less-enriched mantle

source) and may have been closer to a continental margin. Examples of still greater attenuation are, however, represented in the southern Kunlun Terrane east of the traverse area by a series of Permian submarine lavas, sill complexes and basic intrusions that, though not strictly ophiolitic, may represent incipient spreading.

4. *Triassic arc volcanism in the South Lhasa and Qiangtang Terranes.* Apparent active continental margin volcanism of Triassic age was identified north of Lhasa, although, as in the case of the Palaeozoic Kunlun volcanics, subsequent magmatic and tectonic events have masked any confirmatory geological evidence. Triassic volcanism is common throughout the Tethyan region where it may be either alkalic or, as in this area, calc-alkaline to shoshonitic (e.g. Pamič 1984): there is still much debate over whether the calc-alkaline volcanics owe their geochemical character to post-collision rifting of Hercynian terrain or whether they do represent a volcanic arc. The Batang Group north of Tuotuohe is, however, better constrained geologically and geochemically as an island arc developed on thin continental lithosphere. The presence of alkaline, as well as calc-alkaline, arc lavas further suggests the influence of a transform fault in the origin of the magmas, but the precise geometry cannot be determined without a more regional perspective. Southward subduction is consistent with the known distribution of sutures in the area.

5. *Permo–Triassic active continental margin volcanism in the Northern Kunlun.* Although no volcanic rocks of this age appear to be present, swarms of dykes cutting the Kunlun batholith probably fed now-eroded volcanoes. The composition of these calc-alkaline rocks could fit active continental margin or post-collision settings, but the evidence of a close temporal relationship with the pre-tectonic batholith makes the former much more probable.

6. *A Jurassic arc-basin complex in the North Lhasa Terrane.* The presence of volcanic rocks of clear island arc affinities south of Amdo and Dongqiao, coupled with the ophiolite evidence for marginal basin lithosphere discussed by Pearce & Deng (this volume), suggest that Jurassic northward intraoceanic subduction took place in the northern part of the Lhasa terrane, generating at a fore-arc/arc/back-arc complex which was emplaced as allochthonous slices during the formation of the Banggong Suture.

7. *A Jurassic back-arc or post-collision rift in the Qiangtang Terrane.* A minor basaltic volcanic event is recorded in Jurassic strata just north of Wenquan Station. Its setting and composition are equally consistent with an ensialic rifting event in a back-arc setting related to the Jurassic southward-directed subduction or in a post-collision setting related to the Triassic collision in the north.

8. *A Cretaceous post-collision volcanic event within and around the Banggong Suture.* The closure of the Banggong Suture was followed, after a time interval of 20 Ma or more, by a major outpouring of calc-alkaline to shoshonitic lavas and pyroclastic rocks across 200 km or more of the Geotraverse section for a period of some 30 Ma. Although the hypothesis of a subduction-related origin cannot be ruled out, the absence of any consistent time-space-composition relationships suggests to us that some, and perhaps all, of these lavas may be of post-collision origin. According to this model, the Takena Formation would have formed within a foreland basin related to the crustal thickening event that gave rise to this volcanic province.

9. *A Palaeogene active continental margin in the South Lhasa Terrane.* There is already a consensus that the calc-alkaline to shoshonitic Linzizong volcanics (and the Gangdise batholith) formed at an active continental margin related to the northward subduction of Tethyan lithosphere beneath Tibet. This work supports that consensus, but does note that the lavas at the top of

the sequence north of Lhasa and in the Yangbajain Rift may have more in common with volcanics in regions of intra-arc collision, than with arc volcanics *sensu stricto*.

10. *Oligocene–Recent post-collision volcanism on the Tibet Plateau.* The time-space distribution of post-collision volcanic activity on the Tibetan Plateau begins with the eruption of strongly undersaturated lavas in Central Tibet in Oligocene times, followed by 'typical' calc-alkaline volcanism in the southern part of the plateau in Miocene times and highly incompatible element enriched ultrapotassic volcanism in the NW of the plateau in Pliocene–Recent times. This sequence does not support wholesale underplating of the Tibetan plateau by continental lithosphere but is consistent with a limited amount of crust–mantle interaction by attempted subduction of continental lithosphere of India northwards and of the Tarim basin southwards as part of the crustal thickening event.

We are grateful to all the members of the Geotraverse team for their company and for geological discussions and to Dr P. J. Oakley and Mr P. Murray (Newcastle), Dr N. Rogers (Open University), R. Oliver (Grenoble), Li Sun-Rong and Bao Hui-Lan (Guiyang) and Zhao Yun-Long and Liang Yu-Tang (Beijing) for analytical work.

References

Bourgois, J. & Janjou, D. 1981 Subduction océanique, subduction continentale et surrection andine: l'example de Pérou septentrional. *C.R. Acad. Sci., Paris* **293**, 859–864.

Coulon, C., Maluski, H., Bollinger, C. & Wang, S. 1986 Mesozoic and Cenozoic volcanic rocks from central and southern Tibet: $^{40}Ar/^{39}Ar$ dating, petrological characteristics and geodynamical significance. *Earth planet. Sci. Lett.* **79**, 281–302.

Debon, F., Le Fort, P., Sheppard, S. M. F. & Sonet, J. 1986 The four plutonic belts of the Transhimalaya-Himalaya: a chemical, mineralogical, isotopic and chronological synthesis along a Tibet-Nepal section. *J. Petrol.* **27**, 219–250.

DeLong, S. E., Hodges, F. N. & Arculus, R. J. 1975 Ultramafic and mafic inclusions, Kanaga Island, Alaska and the occurrence of alkaline rocks in island arcs. *J. Geol.* **83**, 721–736.

Deng Wanming 1978 A preliminary study on the petrology and petrochemistry of the Quaternary volcanic rocks of northern Tibet autonomous region. *Acta. geol. Sinica* **52**, 148–162.

Ewart, A., Brothers, R. N. & Mateen, A. 1977 An outline of the geology and geochemistry, and the possible petrogenetic evolution of the volcanic rocks of the Tonga-Kermadec-New Zealand island arc. *J. Volcanol. geotherm. Res.* **2**, 205–250.

Frey, F. A. & Clague, D. A. 1983 Geochemistry of diverse basalt types from Loihi seamount: petrogenetic implications. *Earth planet. Sci. Lett.* **66**, 337–355.

Gorton, M. P. 1977 The geochemistry and origin of Quaternary volcanism in the New Hebrides. *Geochim. cosmochim. Acta* **41**, 1257–1270.

Holm, P. E. 1982 Non-recognition of continental tholeiites using the Ti–Zr–Y diagram. *Contr. Miner. Petr.* **79**, 308–310.

Hooper, P. R., Kleck, W. D., Knowles, C. R., Riedel, S. P. & Thiessen, R. L. 1984 Imaha basalt, Columbia River Basalt group. *J. Petrol.* **25**, 473–500.

Marriner, G. F. & Millward, D. 1984 The petrology and geochemistry of Cretaceous to Recent volcanism in Colombia: the magmatic history of an accretionary plate margin. *J. geol. Soc. Lond.* **141**, 473–486.

Mitchell, R. H. & Bell, K. 1976 Rare-earth geochemistry of potassic lavas from Birunga and Toro-Ankole regions of Uganda, Africa. *Contrib. Miner. Petr.* **58**, 293–303.

Molnar, P., Burchfiel, B. C., Zhao Ziyin, Liang K'uangyi, Wang Shuji & Huang Minmin 1987 Geological evolution of Northern Tibet: results of an expedition to Ulugh Muztagh. *Science, Wash.* **235**, 299–305.

Morrison, M. A., Thompson, R. N., Gibson, I. L. & Marriner, G. F. 1980 Lateral chemical heterogeneity in the Palaeocene upper mantle beneath the Scottish Hebrides. *Phil. Trans. R. Soc. Lond.* A **297**, 229–244.

Norin, E. 1946 Geological explorations in Western Tibet. In *Reports from the scientific expedition to the Northwestern provinces of China under the leadership of Dr. Sven Hedin.*, Publ. 29 (III), Geology 7. Tryckeri Aktiebolaget, Thule, Stockholm.

Pamič, J. J. 1984 Triassic magmatism of the Dinarides in Yugoslavia. *Tectonophysics* **109**, 273–307.

Pearce, J. A. 1984 The role of sub-continental lithosphere in magma genesis at active continental margins. In *Continental basalts and mantle xenoliths* (ed. C. J. Hawkesworth & M. J. Norry).

Pearce, J. A. & Cann, J. R. 1973 Tectonic setting of basic volcanic rocks determined using trace element analysis. *Earth planet. Sci. Lett.* **19**, 290–300.

Peccerillo, A. & Taylor, S. R. 1976 Geochemistry of Eocene calc-alkaline rocks from the Kastamonu area, northern Turkey. *Contr. Miner. Petr.* **58**, 63–81.

Powell, C. McA. 1986 Continental underplating model for the rise of the Tibetan Plateau. *Earth planet. Sci. Lett.* **81**, 79–94.

Riou, R., Dupuy, C. & Dostal, J. 1981 Geochemistry of coexisting alkaline and calk-alkaline volcanic rocks from Northern Azerbaijan (N.W. Iran). *J. Volcanol. geotherm. Res.* **11**, 253–275.

Rogers, N. W., Parker, R. J., Hawkesworth, C. J. & Marsh, J. S. 1985 The geochemistry of potassic lavas from Vulsini, central Italy and implications for mantle enrichment processes beneath the Roman region. *Contr. Miner. Petr.* **88**, 244–257.

Sengör, A. M. C. & Kidd, W. S. F. 1979 Post-collisional tectonics of the Turkish-Iranian Plateau and a comparison with Tibet. *Tectonophysics* **55**, 361–376.

Thompson, R. N., Morrison, M. A., Mattey, D. P., Dickin, A. P. & Moorbath, S. 1980 An assessment of the Th–Ta–Hf diagram as a discriminant for tectonomagmatic classifications and in the detection of crustal contamination of magmas. *Earth planet. Sci. Lett.* **50**, 1–10.

Thompson, R. N., Dickin, A. P., Gibson, I. L. & Morrison, M. A. 1982 Elemental fingerprints of isotopic contamination of Hebridean Palaeocene mantle-derived magmas by Archaean sial. *Contr. Miner. Petr.* **79**, 159–168.

Venturelli, G., Thorpe, R. S., Dal Piaz, G. V., Del Moro, A. & Potts, P. J. 1984 Petrogenesis of calc-alkaline, shoshonitic and associated ultrapotassic Oligocene volcanic rocks from the Northwestern Alps, Italy. *Contr. Miner. Petr.* **86**, 209–220.

Wang, S. 1980 Caracteristiques de la serie volcanique de Linzizong dans le secteur oriental de l'arc volcanique du Gangdese. In *Mission franco-chinois au Tibet 1980 (C.N.R.S)*, pp. 319–333.

Weaver, B. L. Wood, D. A., Tarney, J. & Joron, J. L. 1987 Geochemistry of ocean island basalts from the South Atlantic: Ascension, Bouvet, St. Helena, Gough and Tristan da Cunha. *Geol. Soc. Lond. spec. Paper.* no. 30, pp. 253–267.

Winchester, J. A. & Floyd, P. A. 1977 Geochemical discrimination of different magma series and their differentiation products using immobile elements. *Chem. Geol.* **20**, 325–343.

Wood, D. A., Joron, J.-L. & Treuil, M. 1979 A re-appraisal of the use of trace elements to classify and discriminate between magma series erupted in different tectonic settings. *Earth planet. Sci. Lett.* **45**, 326–336.

Yilmaz, Y., Saroglu, F. & Guner, Y. 1987 Initiation of the neomagmastism in East Anatolia. *Tectonophysics* **134**, 177–199.

Xu Ronghua, Sharer, U. & Allègre, C. J. 1985 Magmatism and metamorphism in the Lhasa Block (Tibet): an U-Pb geochronological study. *J. Geol.* **93**, 41–57.

Zhou Xinghua & Armstrong, R. L. 1982 Cenozoic volcanic rocks of eastern China-secular and geographic trends in chemistry and strontium isotopic composition. *Earth planet. Sci. Lett.* **58**, 301–329.

Phil. Trans. R. Soc. Lond. A **327**, 203–213 (1988) [203]
Printed in Great Britain

Metamorphic rocks of the 1985 Tibet Geotraverse, Lhasa to Golmud

BY N. B. W. HARRIS[1], T. J. B. HOLLAND[2] AND A. G. TINDLE[1]

[1] *Department of Earth Sciences, The Open University, Walton Hall, Milton Keynes MK7 6AA, U.K.*
[2] *Department of Earth Sciences, University of Cambridge, Cambridge CB2 3EQ, U.K.*

Two examples of uplifted basement have been studied in the Lhasa Terrane of the Tibetan Plateau. The Nyainqentanglha orthogneisses are bounded by staurolite–garnet schists to the north which record prograde metamorphism at 5.0 ± 1.3 kbar, 610 ± 70 °C. Garnet–sillimanite xenoliths within the orthogneiss suggest that peak temperatures reached at least 700 ± 70 °C at 5.1 ± 2.5 kbar. These P/T fields reflect high T/low P metamorphism during Eocene subduction, and indicate that the syn-tectonic Nyainqentanglha orthogneiss was emplaced at depths greater than 10 km.

Sillimanite-bearing assemblages from the Amdo gneisses in the northern Lhasa Terrane provide evidence of crustal anatexis at temperatures > 680 °C. This event is poorly constrained in time but is probably Cambrian or earlier.

Within the Kunlun Terrane, biotite and garnet isograds north of the Xidatan Fault indicate an increase in metamorphic grade from north to south, reaching peak metamorphism at 470 ± 30 °C, 4.3 ± 1.5 kbar synchronous with the emplacement of the Triassic batholith. Regional metamorphism was followed by uplift of at least 2 km before emplacement of post-tectonic, early Jurassic granites.

1. INTRODUCTION

The Tibetan Plateau results from the collision of at least three continental fragments; the Lhasa, Qiangtang and Kunlun Terranes (Chang *et al.* 1986). The Zangbo Suture, which marks the site of ocean closure to the south of the Lhasa Terrane, also marks the boundary between metamorphic facies. South of the suture, high grade metamorphic basement is exposed with garnet-, kyanite- or sillimanite-bearing pelites defining a series of reverse metamorphic zones (Bordet *et al.* 1981; Burg *et al.* 1984). Metamorphic grade reaches a peak around the Main Central Thrust of the Himalayas, where assemblages indicate an eroded cover of at least 20 km. North of the Zangbo Suture in the southern Lhasa Terrane, assemblages in the sedimentary cover are indicative of low pressure greenschist metamorphism, and phases such as cordierite and andalusite are generally controlled by the thermal effects of granitoid emplacement (Burg *et al.* 1987). Throughout much of the Lhasa Terrane, cover rocks are generally unmetamorphosed except at the base of thrust sheets, as occurs east of Nagqu. However, in two regions, north of the Nyainqentanglha Mountains and south of Amdo (figure 1) uplifted blocks of basement have exposed deeper levels of the crust which provide medium-high grade metamorphic assemblages. No such basement is exposed in the Qiangtang Terrane along the line of the Geotraverse route. Further north in the Kunlun Terrane, low grade phyllonites are common in the region of the Xidatan Fault, and to the north of the fault biotite and garnet isograds have been located.

2. Techniques

All minerals were analysed on the wavelength dispersive electron microprobe at the Open University. Metamorphic conditions have been estimated by calculations based on extensions to the data-set of Holland & Powell (1985). These extensions involve addition of the phases almandine, annite and celadonite white mica, which have been made consistent with several experimental phase equilibria including Ferry & Spear (1978) and Bohlen *et al.* (1983). Celadonite data has been incorporated following Powell & Evans (1983). Activities for solid phase components in minerals were calculated by assuming ideal mixing on sites (phlogopite, clinochlore, annite), the Newton–Haselton (1981) formulation for garnet activities (pyrope, almandine, grossular), and the Price (1985) and Newton–Haselton (1981) activities for sanidine and anorthite; for muscovite and celadonite ideal mixing on site activities were used but a non-ideal Na–K contribution to the alkali ion site was introduced using the mixing parameters from Chatterjee & Flux (1986). The advantage of using the Holland & Powell (1985) data-set (including extensions described above) is that not only are the equilibria self-consistent but, more importantly, the uncertainties can be realistically assessed (see Powell & Holland, in press).

3. Metamorphism in the Lhasa Terrane

(*a*) *Carboniferous metasediments at Nagqu*

Ten kilometres east of Nagqu, Carboniferous phyllites are overthrust onto Cretaceous red beds (X40, figure 1). The phyllitic assemblages comprise sericite–chlorite–quartz–plagioclase–magnetite, and contain both a penetrative fabric (S_1) and crenulations of that fabric (S_2). Syn-D_2 euhedral chloritoid and andalusite overgrow S_1. The chloritoid (85% Fe, 12% Mg, 3% Mn) is a low-Mn phase, indicative of low-medium grade metamorphism. In the presence of andalusite, $T < 540$ °C, $P < 3$ kbar conditions are suggested (Hoschek 1967; Richardson 1968; Holdaway 1971) and the assemblage andalusite-quartz in the absence of pyrophyllite implies $T > 420$ °C (Kerrich 1968).

(*b*) *Metapelites from the Nyainqentanglha Range*

A 1 km wide band of staurolite-bearing phyllites is exposed within the metasedimentary sequence of carbonates and conglomerates in the northern section of the Nyainqentanglha Range. This is a distinctive horizon (X7, figure 1) containing large porphyroblasts of staurolite (1 cm), and locally andalusite (10 cm); it can be traced 15 km along strike to the south-west. The assemblage throughout this horizon is quartz–plagioclase–biotite–muscovite–staurolite–garnet–ilmenite. Staurolite forms syn-D_2 coarse porphyroblasts with rotated inclusion trails. Garnet grew somewhat earlier (late D_1) and is frequently included in staurolite. In one sample fibrolite, preserved as inclusions in plagioclase, coexists with coarse post-tectonic andalusite.

Further south in the Nyainqentanglha, schistose pelitic xenoliths within the granitic gneisses contain the assemblage quartz–plagioclase–muscovite–biotite–garnet–sillimanite (X12). Sillimanite is strongly aligned with biotite which defines the primary foliation (S_1), but muscovite appears to be post-tectonic and retrogressive. Since the fabric of the Nyainqentanglha orthogneiss implies syn-D_1 emplacement, the P/T conditions of the schist provides valuable evidence for the emplacement conditions of the granite gneiss.

The location of these assemblages in the Thompson A-F-M projection (figure 2) clearly show

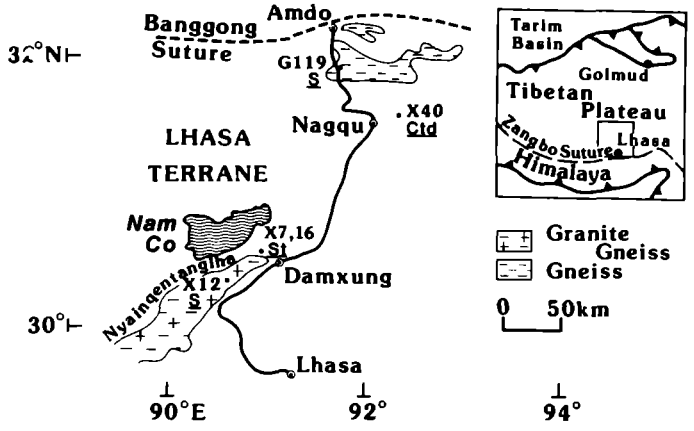

FIGURE 1. Sketch location map showing distribution of metamorphic samples from Lhasa Terrane. Index minerals given by St = staurolite, S = sillimanite, Ctd = chloritoid.

that staurolite from the phyllites lies within the garnet–sillimanite–biotite three phase triangle, indicating its instability within the P/T conditions of the sillimanite-schists.

This relationship can be represented by the equilibrium

$$\text{Staurolite} + \text{Quartz} = \text{Garnet} + \text{Sillimanite} + H_2O \qquad (1)$$

the staurolite in the phyllites forming at lower temperatures than the garnet and sillimanite in the schist.

To determine peak metamorphic conditions of the phyllite, temperatures can be constrained by the equilibrium

$$\text{Fe-Biotite} + \text{Pyrope} = \text{Almandine} + \text{Mg-Biotite}. \qquad (2)$$

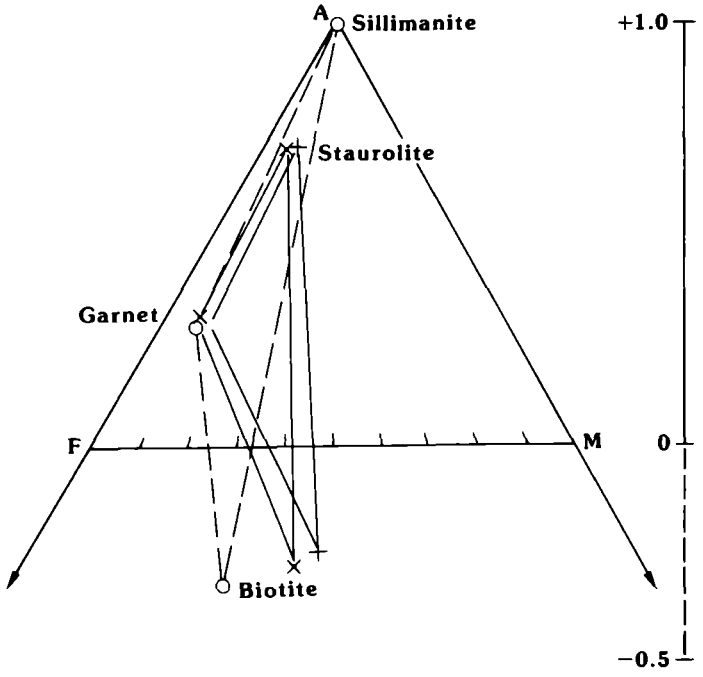

FIGURE 2. A((Al$_2$O$_3$–3K$_2$O)/(Al$_2$O$_3$–3K$_2$O+FeO+MgO)), F(FeO), M(MgO) diagram projected through muscovite (Thompson projection) for Nyainqentanglha samples. + = X7, O = X12, X = X16.

Analyses of non-contiguous biotite–garnet pairs indicate that the garnet grew during increasing temperature since the rims give temperatures about 40 °C above these determined from the cores (tables 1 & 2). Average peak temperatures lie in the range 610±70 °C, based on the experimental study of Ferry & Spear (1978).

A second equilibrium which can be used as a thermometer is given by

$$\text{Alkali feldspar} + \text{Paragonite} = \text{Albite} + \text{Muscovite}. \quad (3)$$

This has been calibrated over a wide range of P/T conditions by Green & Usdansky (1986). Temperatures of ~ 600 °C have been determined from the staurolite-bearing phyllites, in agreement with biotite–garnet thermometry, but the free energy uncertainty in the reaction implies a large uncertainty in this thermometer.

To determine pressures of equilibration, the water-free equilibrium

$$\text{Pyrope} + \text{Grossular} + \text{Muscovite} = \text{Anorthite} + \text{Phlogopite} \quad (4)$$

has been calibrated using the self-consistent data set of Holland & Powell (1985). The addition of annite and almandine to the data-set provides the Fe end-member reaction

$$\text{Almandine} + \text{Grossular} + \text{Muscovite} = \text{Anorthite} + \text{Annite}. \quad (5)$$

At 610 °C, these give pressures of 4.6±1.6 kbar and 4.9±1.2 kbar respectively. Reactions 2, 4 and 5 computed from garnet core compositions intersect at 5.0 kbar, 630 °C. The absence of sillimanite, except as occasional fibrolite inclusions in plagioclase, indicates that reaction (1) has not occurred. Based on the experimental data of Dutrow & Holdaway (1986), $a_{H_2O} > 0.6$ is required for staurolite + quartz to be stable without sillimanite at about 630 °C (figure 3).

Application of these equilibria to the observed assemblages indicates that they formed under conditions of increasing temperature and lie on a prograde P-T-t loop which passes through 5±1 kbar, 610±30 °C. The occurrence of post-tectonic andalusite indicates that metamorphic growth continued below 3.5 kbar, possibly during post-collisional uplift.

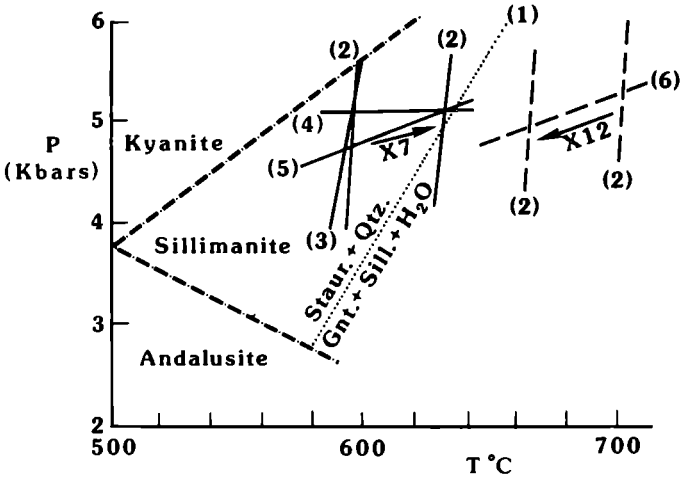

FIGURE 3. Pressure–temperature stability fields for staurolite–garnet–muscovite phyllite (X7, solid lines) and sillimanite-garnet schist (X12, dashed lines) from Nyainqentanglha Mts. Arrows give change of temperature during garnet growth. Numbers in parentheses refer to equilibria in text. (Equilibrium 1 computed for $a_{H_2O} = 0.6$).

Application of biotite–garnet equilibria to the sillimanite schists suggests that garnet grew during decreasing temperatures from 700–660 °C. Temperatures of ~ 600 °C determined from plagioclase–muscovite thermometry (3) confirm the retrograde nature of muscovite. Pressures in the absence of primary muscovite, can be estimated from the equilibrium

$$\text{Grossular} = \text{Anorthite} + \text{Sillimanite} + \text{Quartz}. \quad (6)$$

Using the data-set of Holland & Powell (1985) pressures at 700 °C are 5.1 ± 2.5 kbar (the large uncertainty resulting from low grossular activity in garnet and poorly constrained γ_{an}). Conditions of D_1 metamorphism are given by 700 ± 70 °C, 5.1 ± 2.5 kbar, which places a minimum depth of emplacement for the Nyainqentanglha granite of around 10 km. Since the granite gneisses have been dated by zircon studies at about 50 Ma (Xu *et al.* 1985), it can be concluded that the penetrative fabric of S_1 occurred during a compressive regime at an active continental margin. The high geothermal gradient implied by the sillimanite schists is consistent with such a setting. Subsequent collision resulted in uplift recorded by post-tectonic growth of andalusite in some phyllites.

(*c*) *The Amdo gneisses*

Ten kilometres south of Amdo, an uplifted block (50×50 km^2) of granitic and amphibolite gneiss is exposed bounded by vertical faults to the north and east, and thrust south over Permo–Triassic limestone. Zircon ages of 530 Ma, and model Nd ages of 1240 Ma bracket the time of emplacement of these gneisses. (Harris, Xu, Lewis, Hawkesworth & Zhang, this volume). Schlieren of pelitic paragneiss within the basement contain the assemblage quartz–plagioclase–perthite–biotite–muscovite–sillimanite. The sillimanite forms prograde epitaxial sheaths within or around biotite crystals which define the penetrative schistosity, D_1. The gneisses contain granitic augen (probably anatectic leucosomes), enveloped by restite phases, biotite and sillimanite.

Muscovite appears to be post-D_1 formed by solid state reaction between sillimanite and alkali feldspar. This is confirmed by muscovite–plagioclase equilibria ~ 570 °C (reaction 3), considerably lower than granite melting temperatures. Since muscovite was not apparently stable on the solidus, maximum pressures and temperatures can be obtained from the intersection between the granite melting curve and the equilibrium

$$\text{Muscovite} + \text{Quartz} = \text{Alkali feldspar} + \text{Sillimanite} + H_2O. \quad (7)$$

Applying microprobe analyses to the internally consistent data-set of Holland & Powell (1985), this intersection for $a_{H_2O} = 1$ is located at $T = 650 \pm 15$ °C, $P = 4.0 \pm 0.5$ kbar (table 3). Unfortunately conditions of $a_{H_2O} < 1$ will significantly increase the pressure of this intersection and consequently the assemblage does not provide a useful pressure constraint. A minimum temperature of 570 °C is obtained from the muscovite–plagioclase thermometer. It is assumed muscovite formed from reaction (7), $a_{H_2O} = 0.5$ for reactions (3) and (7) to intersect in the sillimanite stability field (figure 4), although the large uncertainty in the muscovite–plagioclase thermometer poorly constrains this intersection. Melting under such conditions requires $T > 680$ °C (Kerrich 1972) which places a probable minimum peak temperature constraint on anatexis in the gneisses.

Two-feldspar thermometry records a rather approximate temperature of about 530 °C (using the calibration of Price 1985), reflecting retrograde perthite exsolution in the alkali feldspar.

TABLE 1. MICROPROBE ANALYSES FROM GARNET (G) – STAUROLITE (S) – BIOTITE (B) – MUSCOVITE (M) – PLAGIOCLASE (P) – QUARTZ ASSEMBLAGE (X7, NYAINQENTANGLHA)

	G1 core	G1 rim		S1	S2		B1	B2	M1	M2		P1	P2
SiO_2	39.93	37.91	SiO_2	28.33	28.76	SiO_2	34.93	34.95	44.79	45.55	SiO_2	59.67	60.40
TiO_2	0.07	0.05	TiO_2	0.59	0.68	TiO_2	1.65	1.54	0.69	0.45	Al_2O_3	25.82	25.42
Al_2O_3	20.74	21.29	Al_2O_3	55.10	54.97	Al_2O_3	18.99	19.28	33.70	35.31	FeO	0.06	0.14
FeO	30.69	31.74	FeO	12.85	13.04	FeO	19.75	19.82	2.73	1.30	CaO	7.56	7.04
MnO	4.85	4.53	MnO	0.28	0.31	MnO	0.11	0.11	0.02	0.02	Na_2O	7.33	7.49
MgO	2.56	2.94	MgO	1.35	1.27	MgO	9.74	9.70	1.00	0.50	K_2O	0.06	0.19
CaO	2.46	2.61	Na_2O	0.02	0.02	CaO	0.04	0.01	0.22	0.01	Total	100.50	100.68
Total	101.30	101.07	ZnO	0.25	0.29	Na_2O	0.16	0.25	1.18	1.17			
			Total	98.77	99.34	K_2O	8.92	9.57	9.64	9.89			
						Total	94.29	95.23	93.97	94.20			
	Atoms to 12(O)		Atoms to 44(O)			Atoms to 22(O)					Atoms to 8(O)		
Si	3.13	3.01	Si	7.75	7.82	Si	5.38	5.35	6.10	6.13	Si	2.65	2.67
Al	1.92	1.99	Al	17.77	17.63	Al	3.44	3.47	5.41	5.60	Al	1.35	1.33
Fe	2.01	2.11	Ti	0.12	0.14	Ti	0.19	0.18	0.07	0.05	Ca	0.36	0.33
Mn	0.32	0.30	Fe	2.94	2.97	Fe	2.54	2.54	0.31	0.15	Na	0.63	0.64
Mg	0.30	0.35	Mn	0.06	0.07	Mn	0.01	0.01	0.00	0.00	K	0.00	0.01
Ca	0.21	0.22	Mg	0.55	0.52	Mg	2.23	2.21	0.20	0.10			
			Zn	0.05	0.06	Na	0.05	0.07	0.31	0.30			
						K	1.75	1.87	1.67	1.70			

All iron calculated as FeO.

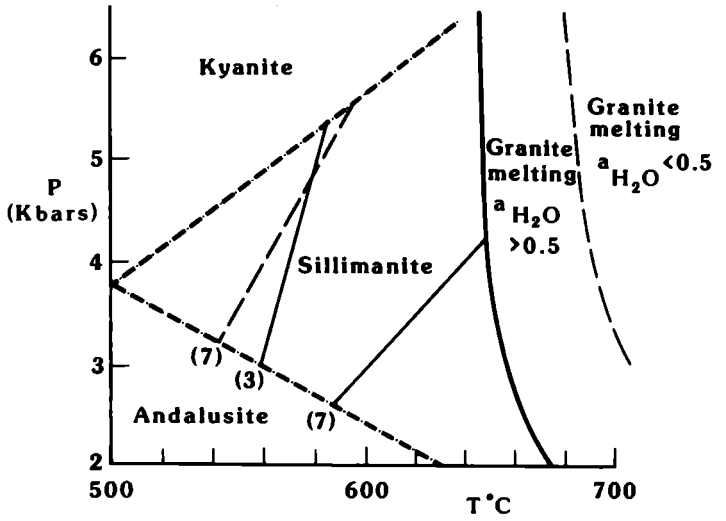

FIGURE 4. Pressure–temperature stability field for sample G119 (sillimanite gneiss) from Amdo basement. Dashed lines indicate $a_{H_2O} = 0.5$; Solid lines $a_{H_2O} = 1$.

TABLE 2. MICROPROBE ANALYSES FROM GARNET (G) – BIOTITE (B) – MUSCOVITE (M) – PLAGIOCLASE (P) – SILLIMANITE – QUARTZ ASSEMBLAGE (X12, NYAINQENTANGLHA)

	G1 core	G1 rim		B1	B2	M1	M2		P1	P2
SiO_2	37.16	37.15	SiO_2	34.54	34.31	44.93	45.07	SiO_2	62.56	62.51
TiO_2	0.02	0.03	TiO_2	2.86	2.78	0.71	0.75	Al_2O_3	22.64	22.91
Al_2O_3	20.92	21.01	Al_2O_3	18.92	19.04	34.67	34.29	FeO	0.03	0.04
FeO	31.39	31.08	FeO	23.30	22.60	1.81	2.07	CaO	4.25	4.50
MnO	8.75	9.06	MnO	0.38	0.31	0.03	0.05	Na_2O	9.36	9.22
MgO	1.87	1.77	MgO	5.99	6.05	0.48	0.54	K_2O	0.17	0.14
CaO	0.87	0.96	CaO	0.01	0.03	0.01	0.00	Total	99.01	99.32
Total	100.98	101.06	Na_2O	0.26	0.19	0.74	0.80			
			K_2O	9.37	9.39	10.27	10.36			
			Total	95.63	94.70	93.65	93.93			
Atoms to 12(O)			Atoms to 22(O)					Atoms to 8(O)		
Si	3.00	3.00	Si	5.36	5.36	6.11	6.13	Si	2.80	2.79
Al	1.99	2.00	Al	3.46	3.51	5.56	5.49	Al	1.19	1.20
Fe	2.12	2.10	Ti	0.33	0.33	0.07	0.08	Ca	0.20	0.21
Mn	0.60	0.62	Fe	3.02	2.95	0.21	0.24	Na	0.81	0.80
Mg	0.23	0.21	Mn	0.05	0.04	0.00	0.00	K	0.01	0.01
Ca	0.08	0.08	Mg	1.38	1.41	0.10	0.11			
			Na	0.08	0.04	0.19	0.21			
			K	1.85	1.87	1.78	1.80			

All iron calculated as FeO.

Tonalitic orthogneisses from the Amdo basement record a Jurassic age for sphene growth and a Cambrian age for zircon growth (Xu *et al.* 1985). The most likely interpretation of the limited data available is that the sphene age records only a low grade event, and that the high grade anatexis observed in the gneisses records an earlier, possibly Cambian event.

TABLE 3. MICROPROBE ANALYSES FROM BIOTITE (B) – MUSCOVITE (M) – PLAGIOCLASE (P) – PERTHITE (K) – SILLIMANITE – QUARTZ ASSEMBLAGE (G119B, AMDO BASEMENT)

	B1	B2	M1	M2		P1	P2	K1	K2
SiO_2	35.22	35.49	45.78	46.14	SiO_2	62.53	63.18	65.24	64.85
TiO_2	2.98	1.86	0.17	0.24	Al_2O_3	22.69	22.28	18.01	18.16
Al_2O_3	18.81	19.66	34.52	35.03	FeO	0.06	0.04	0.03	0.03
FeO	21.27	19.89	1.11	1.02	CaO	4.72	4.21	0.04	0.01
MnO	0.40	0.32	0.02	0.03	Na_2O	9.11	9.35	1.98	1.29
MgO	7.43	7.79	0.55	0.49	K_2O	0.20	0.16	13.64	14.70
CaO	0.01	0.03	0.01	0.00	Total	99.31	99.22	98.94	99.04
Na_2O	0.20	0.20	0.70	0.69					
K_2O	9.52	9.47	10.37	10.50					
Total	95.84	94.71	93.23	94.14					
Atoms to 22(O)					Atoms to 8(O)				
Si	5.39	5.45	6.22	6.20	Si	2.79	2.82	3.02	3.01
Al	3.40	3.56	5.53	5.55	Al	1.19	1.17	0.98	0.99
Ti	0.34	0.22	0.02	0.02	Ca	0.23	0.20	0.00	0.00
Fe	2.72	2.55	0.13	0.12	Na	0.79	0.80	0.18	0.12
Mn	0.05	0.04	0.00	0.00	K	0.01	0.01	0.80	0.87
Mg	1.70	1.78	0.11	0.10					
Na	0.06	0.06	0.19	0.18					
K	1.86	1.86	1.80	1.80					

All iron calculated as FeO.

4. METAMORPHISM IN THE KUNLUN TERRANE

The development of metamorphic minerals in the supracrustal rocks of the Kunlun terrane is restricted to phyllitic and phyllonitic outcrops within 15 km of the Xidatan Fault. Approaching the fault from the north, pelites contain the greenschist assemblage chlorite–quartz ± sericite ± biotite ± magnetite (G200C). Within 10 km of the fault, a garnet-in isograd strikes north-east (figure 5). This results in the assemblage biotite–chlorite–muscovite–garnet–quartz ± ilmenite (X63). The garnet is skeletal and deformed by the penetrative foliation (D_1). The appearance of garnet within this zone is sporadic and composition controlled. Sediments adjacent to post-tectonic granites show thermal metamorphism superimposed on the regional facies. Fe-rich post-kinematic cordierite is developed along the eastern contact of the Xiaonanchuan granite (G213D) in a biotite–muscovite–cordierite–quartz ± tourmaline hornfels in which chlorite has been replaced by post-kinematic biotite. The post-S_2 fabric and high Fe content (42% Mg end-member) of the cordierite argue for its contact metamorphic origin. West of the Xidatan granite post-D_1 andalusite (pseudomorphed by sericite) occurs in a biotite–chlorite–muscovite–quartz phyllite (X68C). The andalusite pseudomorphs predate the east–west fabric recorded in the granite parallel to the Xidatan fault. It is likely that andalusite growth and granite emplacement were concurrent, and both deformed by subsequent movement along the Xidatan fault zone. South of the fault, neither garnet nor contact phenomena have been recorded and pelitic phyllonites contain the assemblage chlorite–sericite–quartz similar to those observed 15 km north of the fault.

The garnet-bearing assemblage (X63) provides biotite–garnet pairs for thermometry (equilibrium 2), but the high Mn content of garnet results in a large uncertainty on the

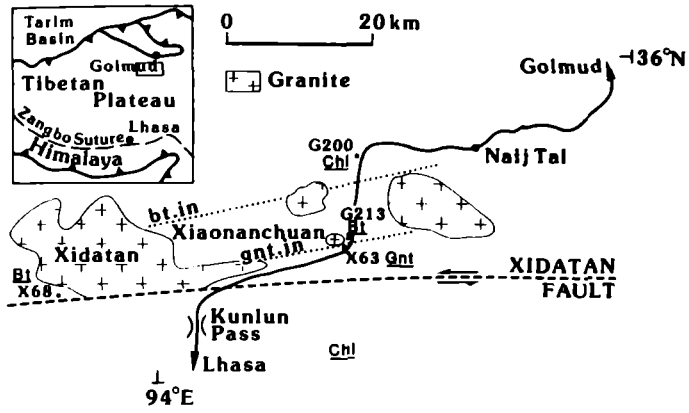

FIGURE 5. Sketch location map showing distribution of metamorphic samples from Kunlun Terrane. Index minerals given by Chl (chlorite), Bt (biotite), Gnt (garnet).

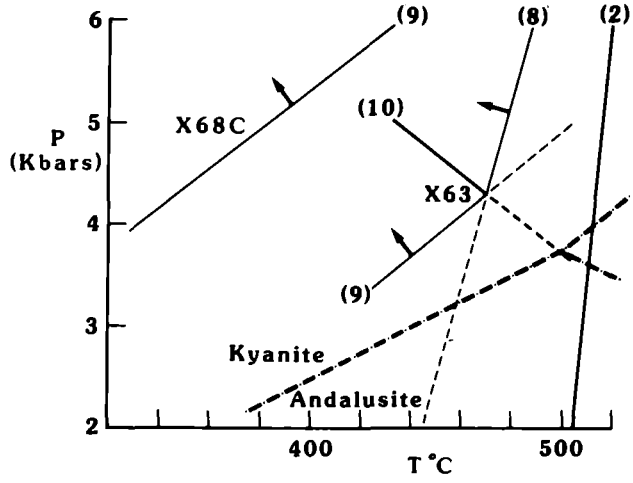

FIGURE 6. Pressure–temperature stability field for samples X63 (garnet–biotite–muscovite–chlorite) and X68C (biotite–muscovite–chlorite) from Kunlun Mts., north of Xidatan Fault. Numbers in parentheses refer to equilibria in text. Arrows indicate limiting constraints provided by solid phase equilibria, assuming $a_{H_2O} = 1$.

calculated temperature 500–520 °C (table 4). A dehydration reaction with steep slope in P/T space is provided by the equilibrium

$$\text{Celadonite} + \text{Clinochlore} = \text{Pyrope} + \text{Phlogopite} + \text{Quartz} + H_2O. \quad (8)$$

Using the data-set of Holland & Powell (1985), extended to include celadonite, a maximum temperature of 470 ± 30 °C is obtained at 5 kbar for garnet-bearing samples.

Minimum pressures (or maximum temperatures) for Kunlun samples north of the fault can be computed for muscovite–biotite–chlorite assemblages through the equilibrium

$$\text{Celadonite} + \text{Clinochlore} = \text{Muscovite} + \text{Phlogopite} + \text{Quartz} + H_2O \quad (9)$$

as calibrated by Powell & Evans (1983). For samples containing the additional phase garnet the vapour-absent equilibrium

$$\text{Celadonite} + \text{Pyrope} = \text{Muscovite} + \text{Phlogopite} + \text{Quartz} \quad (10)$$

may be written. Using the extended data-set of Holland & Powell (1985) reactions (9) and (10) provide pressures at 470 °C of 4.3 ± 1.5 and 4.3 ± 2.1 kbar respectively (figure 6). This defines a model invariant point (for fixed Fe/Mg ratio and a_{H_2O}) at 4.3 kbar, 470 °C for sample X63. Sample X68C (a garnet-absent assemblage) records somewhat lower peak temperatures but with a large uncertainty (340 ± 70 °C at 4.0 kbar based on reaction 9).

TABLE 4. MICROPROBE ANALYSES FROM GARNET (G) – BIOTITE (B) – MUSCOVITE (M) – CHLORITE (C) – QUARTZ ASSEMBLAGES (X63, X68C, KUNLUN)

	G1 (X63)	G2 (X63)		B1 (X63)	B1 (X68C)	M1 (X63)	M1 (X68C)	C1 (X63)	C1 (X68C)
SiO_2	41.01	39.73	SiO_2	36.05	32.08	42.02	47.09	24.88	24.89
TiO_2	0.23	0.14	TiO_2	0.26	0.66	0.24	0.39	0.09	0.09
Al_2O_3	20.08	20.14	Al_2O_3	18.16	22.22	36.19	33.71	21.99	23.41
FeO	20.04	20.20	FeO	18.83	18.81	1.58	2.51	24.07	22.25
MnO	12.38	13.22	MnO	0.26	0.32	0.02	0.03	0.46	0.46
MgO	1.18	1.17	MgO	10.11	13.06	0.83	0.88	14.75	16.19
CaO	6.13	6.33	CaO	0.01	0.01	0.03	0.09	0.03	0.01
Total	101.05	100.93	Na_2O	0.14	0.09	0.72	1.37	0.02	0.02
			K_2O	9.52	4.13	10.19	9.12	0.01	0.01
			Total	94.71	91.38	97.82	95.19	86.30	87.33
	Atoms to 12(O)		Atoms to 22(O)					Atoms to 28(O)	
Si	3.20	3.14	Si	5.51	4.95	6.21	6.28	5.30	5.18
Al	1.85	1.88	Al	3.28	4.04	5.51	5.30	5.53	5.75
Ti	0.01	0.01	Ti	0.18	0.08	0.02	0.04	0.01	0.01
Fe	1.31	1.33	Fe	2.41	2.43	0.17	0.28	4.29	3.87
Mn	0.82	0.88	Mn	0.03	0.04	0.00	0.00	0.08	0.08
Mg	0.14	0.14	Mg	2.30	3.00	0.16	0.17	4.69	5.02
Ca	0.51	0.54	Na	0.04	0.03	0.18	0.35	0.01	0.01
			K	1.86	0.81	1.68	1.55	0.00	0.00

All iron calculated as FeO.

The post-D_1 andalusite in the thermal aureole of the Xidatan granite, and the cordierite hornfels of the Xiaonanchuan granite both suggest emplacement at $P < 3.5$ kbar. This implies that at least 2 km uplift occurred between regional greenschist metamorphism observed in the country rock and intrusion of the Kunlun granites at depths no greater than 10 km. The syn-tectonic granite emplacement ages of 240–260 Ma (Harris, Xu, Lewis, Hawkesworth & Zhang, this volume) indicate a Triassic age for regional greenschist metamorphism.

5. CONCLUSIONS

Throughout the Lhasa and Qiangtang Terranes, supracrustal rocks are generally unmetamorphosed although temperatures of $490 + 70$ °C are recorded at the base of some thrust sheets. Basement gneisses exposed south of Amdo comprise the oldest known rocks from the terranes and granitic leucosomes within sillimanite-bearing pelites indicate temperatures in excess of 680 °C. A second uplifted region exposed north of the Eocene Nyainqentanglha orthogneisses is characterized by staurolite-andalusite pelites which equilibrated under prograde conditions at 5.0 ± 1.3 kbar, 610 ± 70 °C. Xenoliths within the orthogneisses provide garnet–sillimanite assemblages which have equilibrated at 700 ± 70 °C, 5.1 ± 2.5 kbar. The implied steep geothermal gradient probably resulted from thermal convection associated with voluminous granite emplacement at an active continental margin. More than 10 km of cover is indicated during emplacement of the gneisses.

Pelites from the Kunlun Terrane are characterized by low grade chlorite-sericite assemblages. However north of the Xidatan Fault both biotite-in and garnet-in isograds have been identified from a regional metamorphic event which is synchronous with the Triassic emplacement of the syn-tectonic Kunlun batholith. Maximum metamorphic grade has been determined from garnet-bearing metasediments at 4.3 ± 1.5 kbar, 470 ± 30 °C. Post-kinematic cordierite and andalusite from post-tectonic granite aureoles suggest > 2 km of uplift occurred between regional metamorphism and post-collision granite emplacement.

The authors gratefully acknowledge Marilyn Leggett for typing the manuscript and John Taylor for drafting the diagrams.

References

Bohlen, S. R., Wall, V. J. & Boettcher, A. L. 1983 Experimental investigations and geological applications of equilibria in the system FeO–TiO_2–Al_2O_3–SiO_2–H_2O. *Am. Mineral.* **68**, 1049–1058.

Bordet, P., Colchen, M. & Le Fort, P. 1981 The geodynamic evolution of the Himalaya – Ten years of research in Central Nepal Himalaya and some other regions. *Geodynamic Ser.* **3**, *Am. geophys. Un.*, pp. 149–168.

Burg, J.-P., Giraud, M., Chen, G. M. & Li, G. C. 1984 Himalayan metamorphism and deformations in the North Himalayan Belt (southern Tibet, China). *Earth planet. Sci. Lett.* **63**, 391–400.

Burg, J.-P., Leyreloup, A., Girardeau, J. & Chen Guo-Ming 1987 Structure and metamorphism of a tectonically thickened continental crust: the Yalu-Tsangpo suture zone (Tibet). *Phil. Trans. R. Soc. Lond.* A **321**, 67–86.

Chang Chengfa *et al.* 1986 Preliminary conclusions of the Royal Society and Academia Sinica 1985 geotraverse of Tibet. *Nature Lond.* **323**, 501–507.

Chatterjee, N. D. & Flux, S. 1986 Thermodynamic mixing properties of muscovite–paragonite crystalline solutions at high temperatures and pressures, and their geological applications. *J. Petrol.* **27**, 677–693.

Dutrow, B. L. & Holdaway, M. J. 1986 Upper thermal stability of Staurolite + Quartz at medium pressures: a reinvestigation. *Terra Cogn.* **6**, 24 (abstr.).

Ferry, J. H. & Spear, F. S. 1978 Experimental calibration of the partitioning of Fe and Mg between biotite and garnet. *Contr. Mineral. Petrol.* **66**, 113–117.

Green, N. L. & Usdansky, S. I. 1986 Toward a practical plagioclase–muscovite thermometer. *Am. Mineral.* **71**, 1109–1117.

Hoschek, G. 1967 Untersuchungen zum stabilitats bereich von chloritoid und staurolith. *Contr. Mineral. Petrol.* **14**, 123–162.

Holdaway, M. J. 1971 Stability of andalusite and the aluminium silicate phase diagram. *Amer. J. Sci.* **271**, 97–131.

Holland, T. J. B. & Powell, R. 1985 An internally consistent thermodynamic data-set with uncertainties and correlations: 2: Data and results. *J. metamorph. Geol.* **3**, 343–370.

Kerrich, D. M. 1968 Experiments on the upper stability limit of pyrophyllite at 1.8 Kbars and 3.9 Kbars water pressure. *Am. J. Sci.* **266**, 204–214.

Kerrich, D. M. 1972 Experimental determination of muscovite + quartz stability with $P_{H_2O} < P_{total}$. *Am. J. Sci.* **272**, 946–958.

Newton, R. C. & Haselton, H. T. 1981 Thermodynamics of the Garnet–Plagioclase–Al_2SiO_5–Quartz geobarometer. In *Thermodynamics of minerals and melts* (ed. R. C. Newton, A. Narrotsky and B. J. Wood), pp. 129–145. New York: Springer-Verlag.

Powell, R. & Evans, J. 1983 A new geobarometer for the assemblage biotite–muscovite–chlorite–quartz. *J. metamorph. Geol.* **1**, 331–336.

Powell, R. & Holland, T. J. B. 1987 An internally consistent dataset with uncertainties and correlations. 3: application methods, worked examples and a computer program. *J. Mm. Geol.* (In press.)

Price, J. G. 1985 Ideal site mixing in solid solutions with an application to two-feldspar geothermometry. *Am. Mineral.* **70**, 696–701.

Richardson, S. W. 1968 Staurolite stability in a part of the system Fe–Al–Si–O–H. *J. Petrol.* **9**, 467–488.

Xu Ronghua, Scharer, U. & Allègre, C. J. 1985 Magmatism and metamorphism in the Lhasa Block (Tibet): a geochronological study. *J. Geol.* **93**, 41–57.

Phil. Trans. R. Soc. Lond. A **327**, 215–238 (1988) [215]
Printed in Great Britain

The ophiolites of the Tibetan Geotraverses, Lhasa to Golmud (1985) and Lhasa to Kathmandu (1986)

BY JULIAN A. PEARCE[1] AND DENG WANMING[2]

[1] *Department of Geology, University of Newcastle-upon-Tyne, Newcastle-upon-Tyne, U.K.*
[2] *Institute of Geology, Academia Sinica, Beijing, People's Republic of China*

Ophiolite belts are found in Tibet along the Zangbo, Banggong and Jinsha River Sutures and in the Anyemaqen mountains, the eastern extension of the Kunlun mountains. Where studied, the Zangbo Suture ophiolites are characterized by: apparently thin crustal sequences (3–3.5 km); an abundance of sills and dykes throughout the crustal and uppermost mantle sequences; common intraoceanic melanges and unconformities; and an N-MORB petrological and geochemical composition. The ophiolites probably formed within the main neo-Tethyan ocean and the unusual features may be due to proximity to ridge-transform intersections, rather than to genesis at very slow-spreading ridges as the current consensus suggests. The Banggong Suture ophiolites have a supra-subduction zone petrological and geochemical composition – although at least one locality in the Ado Massif shows MORB characteristics. However, it is also apparent that the dykes and lavas show a regional chemical zonation, from boninites and primitive island arc tholeiites in the south of the ophiolite belt, through normal island arc tholeiites in the central belt to island arc tholeiites transitional to N-MORB in the north. The ophiolites could represent fragments of a fore-arc, island arc, back-arc complex developed above a Jurassic, northward-dipping subduction zone and emplaced in several stages during convergence of the Lhasa and Qiangtang terranes. The ophiolites of the Jinsha River Suture have a N-MORB composition where analysed, but more information is needed for a proper characterization. The Anyemaqen ophiolites, where studied, have a within-plate tholeiite composition and may have originated at a passive margin: it is not, however, certain whether true oceanic lithosphere, as opposed to strongly attenuated continental lithosphere, existed in this region.

1. INTRODUCTION

Ophiolites in Tibet are found in association with each of the three sutures: the Palaeogene Zangbo Suture between the Himalayan and Lhasa Terranes; the Cretaceous Banggong Suture between the Lhasa and Qiangtang Terranes; and the Triassic Jinsha River Suture between the Qiangtang and Kunlun terranes (figure 1). A fourth ophiolite belt, in the Anyemaqen mountains of northeast Tibet, has been used to invoke a possible Triassic Suture within the Kunlun Terrane, a hypothesis rejected by the Geotraverse team (Chang *et al.* 1986) owing to the absence of ophiolites within the Kunlun mountains themselves. The ophiolites of the Banggong Suture were studied and sampled at a reconnaissance level during the 1985 Geotraverse from Lhasa to Golmud; during the same Geotraverse we attempted, but failed, to reach on horseback the nearest ophiolite exposure on the Jinsha River Suture (about 100 km from the Lhasa–Golmud highway); geological observations and sample collection were subsequently carried out for us by the Geological Team of Qinghai Province. The ophiolites of the Zangbo Suture were briefly

examined during the short 1986 Geotraverse, from Lhasa to Kathmandu, although one of us (Deng) had previously worked in the area as part of a Chinese Academy of Sciences research team and provided additional material for this study. To complete the study we examined geological maps and analysed samples collected by the Chinese Academy of Sciences from the Anyemaqen ophiolite belt.

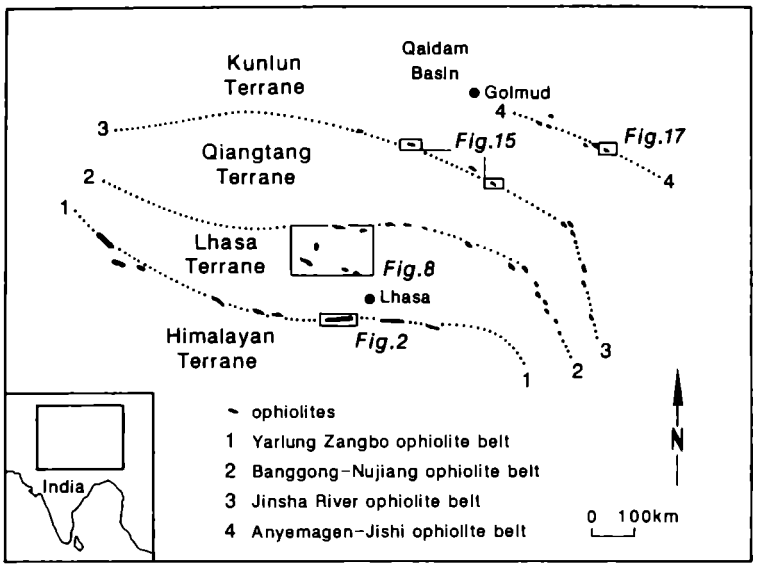

FIGURE 1. Map of Tibet showing the Geotraverse route, the main Suture zones and ophiolite belts and the location of figures 2, 8, 15 and 17.

A considerable quantity of information on the ophiolites of the Zangbo and Banggong sutures has already been published by the Chinese Academy of Sciences (e.g. Wu & Deng 1980; Deng & Zhou 1982; Deng *et al.* 1984, 1985) and the Chinese–French collaborative project (e.g. Girardeau *et al.* 1984, 1985*a*, *b*, *c*; Göpel *et al.* 1984). The aim of this chapter is briefly to summarize existing work on the ophiolite belts and to present new observations and data on this geology and geochemistry. The results will then be used to evaluate the nature of the oceanic lithosphere that separated Tibetan continental terranes prior to the Triassic, Cretaceous and Tertiary continent collision events. Emplacement mechanisms are discussed separately by Coward *et al.*, Kidd *et al.* and Dewey *et al.* (this volume).

2. METHODOLOGY

In order fully to interpret the fragments of oceanic lithosphere found within ophiolite terranes, it is necessary to determine whether that lithosphere formed at a major ridge, at a plume-related ridge, in an incipient ocean or in one of the various types of marginal basin; it is also important to recognize lithosphere that formed at or near ridge-transform intersections and whether off-axis, as well as on-axis, magmatic products are present. To carry out such an interpretation, it is necessary to combine geological, petrological and geochemical evidence to distinguish the various alternative hypotheses. The petrological and geochemical approaches used in this paper are as follows.

(1) The data on lavas, dykes and sills have been plotted on two types of diagram. The first includes MORB-normalized trace element diagrams, chondrite-normalized rare-earth patterns and Th–Ta–Hf (Wood *et al.* 1979) and Ti–Zr–Y (Pearce & Cann 1973) discrimination diagrams. These diagrams have been used to identify the nature of the magma source region and thus to distinguish between a supra-subduction zone (ssz) origin, in which Th has been selectively enriched with respect to Ta, a plume-related mid-ocean ridge basalt (P-MORB) origin, in which all incompatible elements have been enriched, and a normal mid-ocean ridge basalt (N-MORB) origin, which shows no trace element enrichment; the same diagrams can also be used to identify island arc and within-plate seamounts and aseismic ridges which may also be present in ophiolite terranes (cf. Pearce & Mei, this volume). The second type of diagram is based on plots of compatible versus incompatible elements and includes Y–Cr (Pearce 1982), Ti–Cr (Pearce 1975) and $FeO/MgO–TiO_2$ (Glassley 1974). These diagrams can be interpreted in terms of partial melting and crystallization histories, and thus also to distinguish MORB from ssz compositions, the former having higher concentrations of the incompatible element for a given compatible element concentration (Pearce *et al.* 1984).

(2) Of all the plutonic rocks, plagiogranites and any isotropic gabbros were analysed and interpreted as indicated above to determine intrusive setting. Cumulate rocks cannot be treated in this way because crystal cumulation distorts trace element ratios. However, order of crystallization gives some indication of tectonic setting: MORB compositions typically give an order of crystallization olivine, plagioclase, clinopyroxene, whereas ssz compositons give olivine, clinopyroxene, plagioclase (if tholeiitic) and olivine, orthopyroxene, clinopyroxene or olivine, clinopyroxene, orthopyroxene if boninitic (Pearce *et al.* 1984). In addition, microprobe analyses of clinopyroxenes can be used to identify the tectonic setting of cumulate rocks as well as clinopyroxene–phyric dykes and lavas (e.g. Nisbet & Pearce 1977; Leterrier *et al.* 1982).

(3) For the tectonized ultramafic rocks, chrome spinels are the best indicators of tectonic environment, ssz compositions showing higher Cr#(100 . Cr/(Cr + Al) ratios) than MORB compositions due to their higher degree of melting or melting of a more depleted mantle source (Dick & Bullen 1984).

Of the samples chosen for whole rock analysis some (the 'G' numbers in tables 1 and 2) have been analysed in Newcastle for major elements by atomic absorption, for the trace elements, Cr, V, Ni, Cu and Zn also by atomic absorption and for the trace elements Zr, Y, Nb, Rb and Sr by X-ray fluorescence; a subset of these samples has also been analysed for rare-earth elements (REE), Th, Ta, Hf, Sc and Co by instrumental neutron activation analysis (INAA) at the Open University. The precise location of these samples is given in Kidd *et al.*, this volume (field maps, Microfiche 2, in pocket). A second set of samples ('NI' numbers) was provided by Cao Ronglong (Guiyang) and has been analysed by the same procedures. The remaining samples have been analysed at the Institute of Geology in Beijing for the major elements and for the trace elements Zr, Y, Sr, Ba, Cr, V, Ni, Co, Cu, Zn by plasma emission spectroscopy; a subset of these samples has been analysed for REE, Th, Ta and Hf by INAA at the Institute of High Energy Physics in Beijing. The location of these samples is available from Deng Wanming on request. Microprobe analyses of clinopyroxenes and spinels in the basic and ultrabasic rocks from the Banggong Suture were carried out at the Institute of Geology in Beijing.

The four ophiolite belts are now considered in turn.

3. Yarlung–Zangbo ophiolite belt

(*a*) *Geology*

The Yarlung–Zangbo ophiolite belt extends from Ladakh in the west, where it connects with the Indus ophiolite belt, to the bend in the Zangbo river in the east and then extends discontinuously southwards along the Naga hills (figures 1 and 2). It is bordered in the north by the Ladakh and Gangdese granitoid belt and in the south by the low-grade metamorphics of the Himalayan Series over which the ophiolite fragments have been thrust southwards. The age of formation of the ophiolite has been dated as Albian (approximately 110 Ma) from radiolaria in interbedded cherts (Marcoux *et al.* 1982), and at 120 ± 10 Ma using Pb isotopes in clinopyroxenes from peridotites and dolerites (Göpel *et al.* 1984). The ophiolite is unconformably overlain by Xigaze Group flysch, the base of which has been dated using orbitolines as Aptian–Albian (Cherchi & Schroeder 1980), and was probably obducted during the Eocene (e.g. Molnar & Tapponnier 1975).

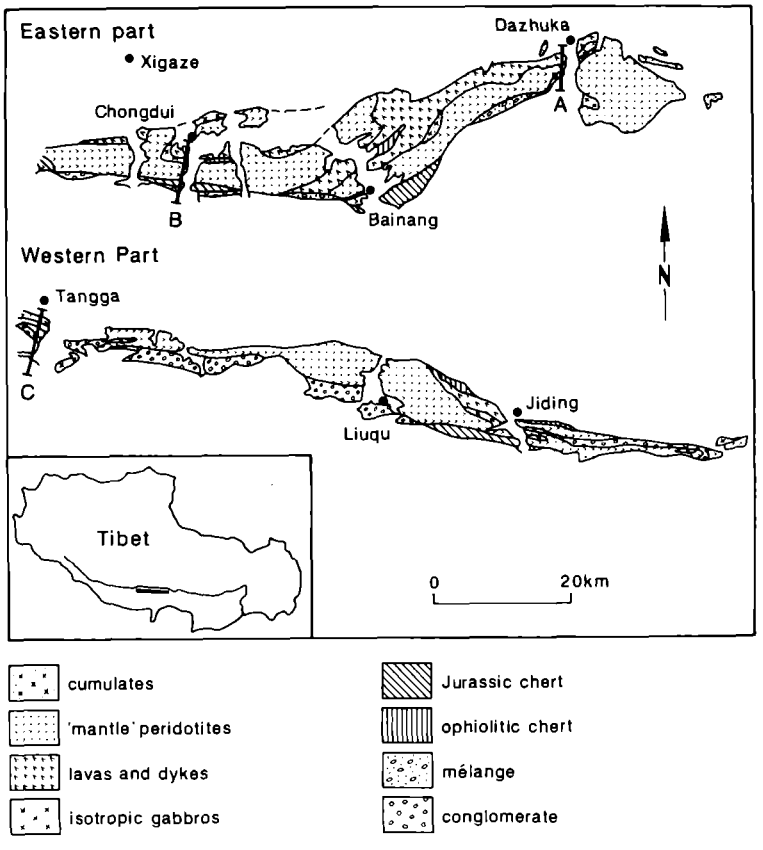

FIGURE 2. Map of the Yarlung–Zangbo ophiolite in the region studied during the Lhasa–Kathmandu 1986 traverse.

The part of the ophiolite belt studied briefly by us during the 1986 traverse from Lhasa to Kathmandu is shown in figure 2. It can be considered in two parts: an eastern part south of Xigaze between Chongdui and Dazhuka; and a western part north of Lhaze between Tangga and Liuqu. Sections through the ophiolite at Dazhuka, Chongdui and Tangga are shown in figure 3 and schematic reconstructions of the ophiolite in these areas, and at Jiding, are shown in figure 4.

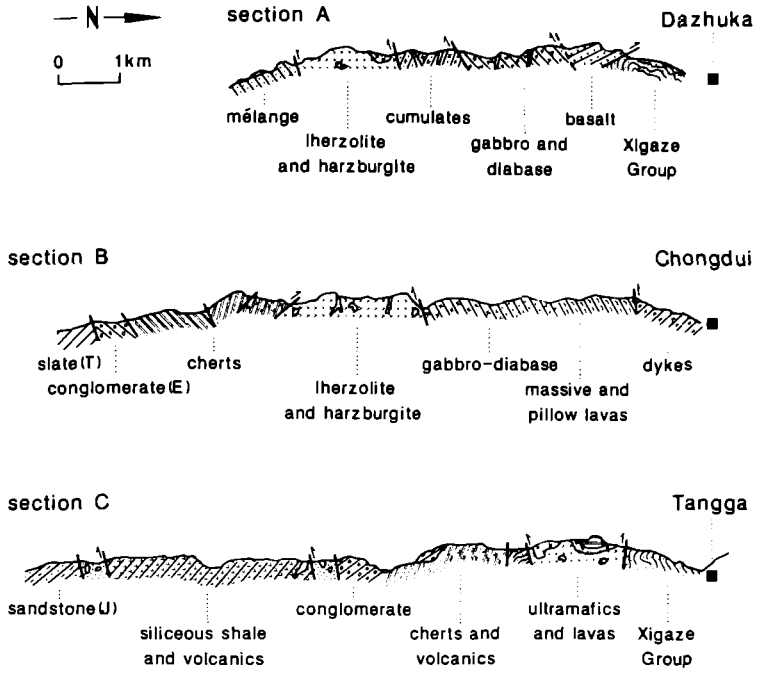

FIGURE 3. Geological sections through the Yarlung–Zangbo ophiolite. Locations of sections are shown in figure 2.

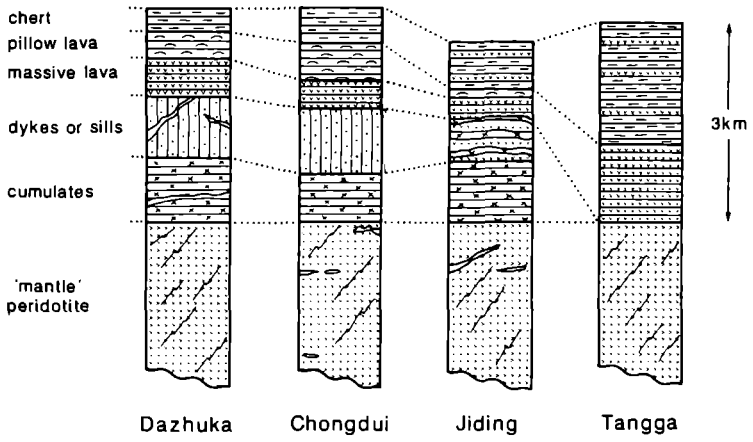

FIGURE 4. Schematic reconstructions of the Yarlung–Zangbo ophiolite for the sections shown in figure 3 and for a section just west of Jiding.

The tectonized ultramafic unit typically comprises about 1 km of serpentinized dunites and harzburgites which grade downwards into a further kilometre of fresh harzburgite with dunite patches and then into a maximum 4 km of exposure of fresh harzburgite containing 1–3% chrome diopside (e.g. Deng 1981, 1982, 1983, 1984; Girardeau *et al.* 1985*b*). Lherzolites are locally present, especially at the base of the unit, and also form the strongly serpentinized Liuqu Massif. The uppermost part is usually invaded by a variable but often large (up to 50% by volume) proportion of dykes and inclined sheets of doleritic to microgabbroic texture; a small number of these intrusions is also found in the lower part of the ultrabasic unit. Structural and petrologic analyses of the tectonite unit has indicated relatively low temperatures of equilibration and deformation (*ca.* 1150 °C) (Nicolas *et al.* 1981; Girardeau *et al.* 1985*a*). It is also apparent that some dykes were intruded before deformation, some after deformation and serpentinization.

Of the sections studied, the cumulate mafic–ultramafic sequence is best exposed south of Dazhuka as an approximately 500 m-thick body of rhythmically-layered dunites, rare wehrlites, troctolites, anorthosites and gabbros; here as elsewhere the layered sequence grades into isotropic gabbros, at the top of which are metre-sized pockets of plagiogranite. These gabbros are also cut by numerous dykes and inclined sheets. The thickest layered sequence reported from the area (2.5 km of continuous section) is at Angren, northwest of Lhaze (Prinzhofer *et al.* 1984). The total thickness of the plutonic unit appears to be on average about 3 km.

Sheeted dyke swarms are rare in the Xigaze–Lhaze area, but occur locally, for example at Baining, where dykes of average width 1.7 m strike E/W–ENE/WNW and dip south at a steep angle. More commonly, isotropic gabbros are overlain by massive and pillowed lavas and the whole sequence is subsequently intruded by dykes and inclined sheets. In the Dazhuka and Chongdui sections, mafic massive lavas or sills are overlain by mafic pillow lavas. The diameter of individual pillows is on average about 1 m and the lavas are often vesicular. In the Lhaze–Tangga sections sheeted lavas or sills are found intercalated with, or intruding, siliceous sediment.

A number of authors (e.g. Nicolas *et al.* 1981; Girardeau *et al.* 1985*a*, *b*) have reconstructed the Xigaze ophiolite and noted that, even taking into account the lack of continuity of exposure, the crustal section appears to be thin (approximately 3–3.5 km) compared with an off-axis oceanic crustal average of 7 km and compared with many other well-preserved ophiolites. Furthermore, the general absence of a sheeted dyke complex between the gabbros and pillow lavas, together with an abundance of dykes, sills and sill swarms throughout the section indicates an unusual type of crust, related, the above authors suggest, to a very slow-spreading ridge axis.

(*b*) *Petrology and geochemistry*

The bulk of our work on the geochemistry of the Xigaze ophiolite is applied to the dykes, sills and pillow lavas. Representative analyses are given in table 1.

Some typical analyses have been plotted as MORB-normalized multi-element patterns and chondrite-normalized rare earth patterns in figure 5. The MORB-normalized patterns are flat for the pillow lavas, massive lavas and dykes, indicating a N-type MORB composition and this is confirmed by the LREE-depleted rare earth patterns. The sills within the siliceous sediments, by contrast, have MORB-normalized patterns characterized by selective enrichment in the more incompatible elements, and REE-patterns that show LREE enrichment. The Ti–Zr–Y diagram (figure 6*a*) shows that this enrichment is sufficient to place the two analysed samples of sills on the boundary between the ocean ridge and within-plate basalt fields (c.f. figure 3 of Pearce & Mei, this volume). It is also apparent from table 1 that these enriched rocks also contain high concentrations of Ti and Fe and could be classed as FeTi basalts. The latter feature is commonly associated with high level magma chambers in propagating rifts. Other samples form a very tight cluster on the Ti–Zr–Y diagram indicative of a uniform magma type of MORB or volcanic arc basalt character: the Cr–Y discriminant diagram (figure 6*b*) then demonstrates that they are of MORB composition.

(*c*) *Tectonic interpretation*

The data presented here thus confirm the general consensus that the Yarlung–Zangbo ophiolite in the Xigaze region is predominantly of N-MORB composition. Although such compositions can be found in incipient oceans or back-arc basins, an absence of clastic sediments

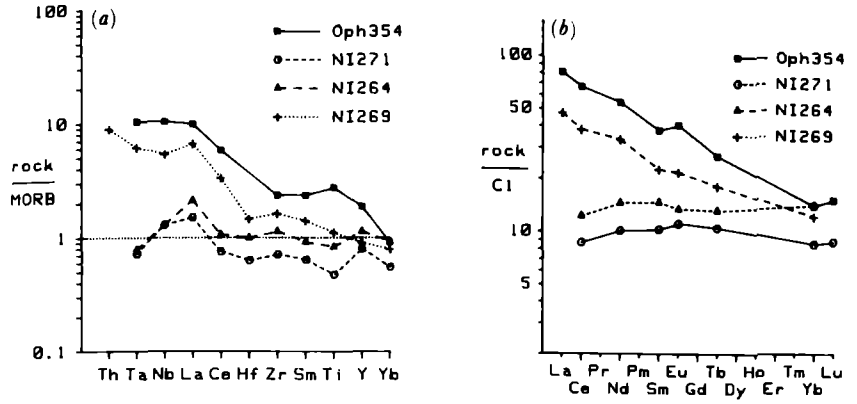

FIGURE 5. (*a*) MORB-normalized trace element patterns and (*b*) chondrite-normalized rare-earth patterns for lavas and dykes from the Yarlung–Zangbo ophiolite. For full analyses and sample localities, see table 1.

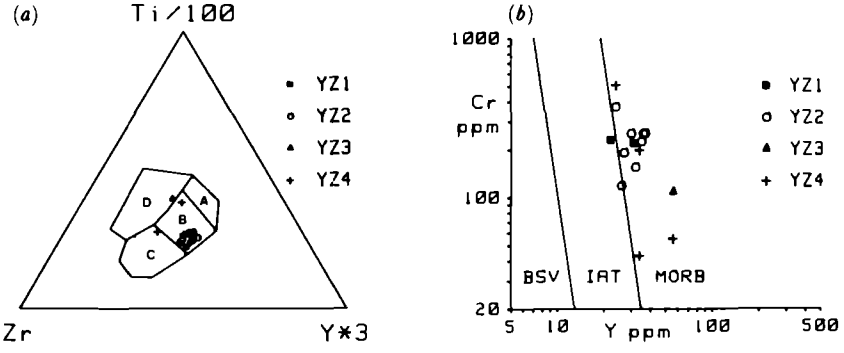

FIGURE 6. (*a*) Ti–Zr–Y and (*b*) Cr–Y discriminant diagrams for lavas and dykes from the Yarlung–Zangbo ophiolite. In figure 6*a*, within-plate field basalts plot in field D, calc-alkaline basalts in fields B and C, mid-ocean ridge basalts in field B and island arc tholeiites in fields A and B. In figure 6*b*, mid-ocean ridge basalts, island arc tholeiites and boninite series volcanics plot in the MORB, IAT and BSV fields respectively. Key to localities: YZ1 = Dazhuka; YZ2 = Chongdui; YZ3 = Jiding; YZ4 = Tangga. The two points plotting on the field B–D boundary in figure 6*a* and towards higher Y values in figure 6*b* are sills.

and, in the latter case also an absence of lavas of arc composition, suggests that the setting was genuinely intraoceanic. The composition of the sills within the overlying siliceous sediment also supports this interpretation, their intraplate composition being consistent with off-axis magmatism in a major ocean.

Nicolas *et al.* (1981) and Girardeau *et al.* (1985*a*, *b*) argue that the thin crustal structure and complex intrusive patterns, as shown by the sill complexes, are indications that the ophiolite formed at a very slow spreading ridge. Pozzi *et al.* (1984) demonstrated that this ridge was oriented approximately north–south and suggested that the ophiolite fragments represented small spreading segments offset by major transforms. They rejected, however, the hypothesis of Sengör (1981) that the transforms had a major part to play in the origin of the ophiolite.

The view of the Lhasa–Kathmandu Geotraverse team, notably Kidd, Abbate and Xenophontos (pers. comms), and supported by ourselves, is that the ophiolites do show major evidence of generation at or near ridge-transform intersections. The main lines of evidence are as follows.

(1) Evidence from extant ocean basins suggests that the degree of partial melting of the

TABLE 1. REPRESENTATIVE GEOCHEMICAL ANALYSES FOR SELECTED SAMPLES OF LAVAS AND DYKES FROM THE YARLUNG-ZANGBO OPHIOLITE BELT

sample	Oph302	Oph303	Oph163	NI475	NI462	NI463	NI319	NI458	NI324
location	YZ1	YZ1	YZ1	YZ2	YZ2	YZ2	YZ2	YZ2	YZ2
rock	bas.	bas.	bas.	bas.	bas.	bas.	bas.	bas.	bas.
type	PL	ML	D	PL/C	PL/C	PL/C	PL	PL	PL
SiO_2	47.61	52.99	51.93	47.30	54.30	54.00	44.60	48.20	55.10
TiO_2	.98	.61	.71	.93	.98	1.15	1.30	1.10	1.18
Al_2O_3	17.89	17.08	15.26	15.90	16.30	16.40	12.90	14.70	14.20
Fe_2O_3	9.76	7.02	8.97	9.70	8.33	10.50	9.20	9.31	9.63
MnO	.18	.14	.14	.11	.12	.09	.30	.16	.14
MgO	5.25	6.10	7.42	5.80	4.43	4.67	9.24	5.51	5.99
CaO	9.51	6.58	6.70	12.20	6.68	4.09	14.70	11.00	7.09
Na_2O	3.65	4.80	5.16	4.04	5.21	7.15	1.20	3.70	4.34
K_2O	.55	.30	.16	.12	1.25	.50	.02	.80	.46
P_2O_5	.15	.06	.16	0.00	0.00	0.00	0.00	0.00	0.00
LOI	4.96	4.64	3.46	3.73	1.47	1.93	2.97	5.78	2.63
Total	100.49	100.07	100.07	99.83	99.07	100.48	96.43	100.26	100.76
Zr	98	63	0	60	67	82	93	94	107
Y	31	22	0	24	25	24	30	29	28
Nb	0.0	0.0	0.0	1.5	2.0	2.2	3.2	2.2	2.3
Rb	0.0	0.0	0.0	1.7	19.1	4.9	.5	15.1	6.0
Sr	180	165	0	92	288	122	29	120	128
Cr	220	230	0	252	191	155	253	253	225
Ni	81	130	0	65	55	56	76	81	77
V	230	140	0	224	166	181	273	224	206
Cu	68	13	0	35	20	15	59	31	21
Zn	0	0	0	72	74	70	93	84	83
Hf	0.00	0.00	0.00	1.54	1.79	1.97	2.36	2.50	2.42
Ta	0.00	0.00	0.00	0.00	.06	.09	.10	.09	.12
Th	0.00	0.00	0.00	0.00	0.00	0.00	0.00	0.00	0.00
Sc	0.0	0.0	0.0	32.8	30.9	31.4	32.9	27.8	28.7
Co	0.0	0.0	0.0	30.0	28.1	28.4	36.7	32.0	31.3
La	0.0	0.0	1.4	0.0	0.0	0.0	0.0	0.0	0.0
Ce	0.0	0.0	5.6	7.5	7.7	8.7	7.6	9.4	9.4
Nd	0.0	0.0	0.0	0.0	7.3	11.5	12.0	10.9	10.2
Sm	0.00	0.00	1.53	2.40	2.40	2.50	3.10	3.10	3.20
Eu	0.00	0.00	.66	.93	.93	.93	1.40	1.10	1.12
Tb	0.00	0.00	.45	.58	.62	.55	.80	.83	.73
Ho	0.00	0.00	0.00	0.00	0.00	0.00	0.00	0.00	0.00
Tm	0.00	0.00	.33	.41	.41	.45	.51	.48	.47
Yb	0.00	0.00	1.72	2.55	2.40	2.30	3.30	2.81	2.98
Lu	0.00	0.00	.26	.45	0.00	0.00	.50	.50	0.00

mantle, and hence the oceanic crustal thickness, decreases within ridge segments towards ridge-transform intersections; this would thus explain the thin crustal section (Fox & Straup 1981).

(2) Intraoceanic melanges with serpentinite matrices are important in oceanic fracture zones and are common in the Xigaze ophiolite, notably at Xiatu, where rodingitized gabbro and diabase blocks are found within a serpentinite matrix.

(3) Intraoceanic unconformities, in which coarse-grained clastic and pelagic sediments ovelie peridotites, are important in oceanic transform faults. They are also found in the Xigaze

TABLE 1. (*cont.*)

sample	Oph174	Oph171	Oph351	Oph93	Oph354	NI271	NI264	NI269	L-20
location	YZ2	YZ2	YZ2	YZ3	YZ3	YZ4	YZ4	YZ4	YZ4
rock	bas.	bas.	bas.	bas.	bas.	bas.	bas.	bas.	bas.
type	PL	ML	D	ML	S	ML?	ML?	S?	S
SiO_2	49.32	47.93	55.02	47.95	46.99	51.80	50.50	42.20	49.03
TiO_2	.84	.90	.76	.74	4.08	.71	1.24	1.66	3.52
Al_2O_3	15.26	15.05	14.77	14.23	12.86	12.90	15.90	15.20	12.63
Fe_2O_3	8.99	8.32	8.98	9.44	16.83	9.20	10.40	9.87	15.87
MnO	.15	.16	.20	.22	.29	.17	.15	.17	.32
MgO	7.94	6.60	7.11	8.04	4.98	8.45	5.86	5.75	3.81
CaO	6.99	5.68	4.87	11.80	7.80	11.10	7.80	20.20	8.03
Na_2O	5.13	5.00	3.70	.40	3.65	2.95	4.04	4.02	4.40
K_2O	.23	.10	.55	.10	.40	.84	.12	.76	.16
P_2O_5	.16	.19	.06	.09	.21	0.00	0.00	0.00	.32
LOI	5.42	10.51	4.35	7.37	2.45	1.14	3.73	3.73	2.85
Total	100.43	100.44	100.37	100.38	100.54	99.26	99.74	103.56	100.94
Zr	61	66	0	0	210	64	102	146	173
Y	24	26	0	0	56	24	34	27	56
Nb	0.0	0.0	0.0	0.0	0.0	4.0	4.0	16.5	0.0
Rb	0.0	0.0	0.0	0.0	0.0	4.0	12.0	2.7	0.0
Sr	128	54	0	0	42	229	139	928	180
Cr	372	118	0	0	108	511	43	199	55
Ni	84	52	0	0	90	136	47	142	60
V	170	200	0	0	420	193	249	245	419
Cu	36	19	0	0	254	12	38	37	170
Zn	0	0	0	0	0	81	87	83	0
Hf	0.00	0.00	0.00	0.00	0.00	1.51	2.38	3.48	0.00
Ta	0.00	0.00	0.00	0.00	0.00	.13	.14	1.10	0.00
Th	0.00	0.00	0.00	0.00	0.00	0.00	0.00	1.79	0.00
Sc	0.0	0.0	0.0	0.0	0.0	36.8	27.8	25.7	0.0
Co	0.0	0.0	0.0	0.0	0.0	38.8	33.7	35.9	0.0
La	1.1	1.4	2.3	0.0	26.4	0.0	0.0	15.5	0.0
Ce	4.3	4.7	7.8	0.0	57.7	7.5	10.6	32.9	0.0
Nd	0.0	0.0	0.0	0.0	34.3	6.4	9.2	21.1	0.0
Sm	1.56	1.79	1.88	0.00	7.69	2.10	3.00	4.60	0.00
Eu	.76	.65	1.04	0.00	3.13	.86	1.04	1.68	0.00
Tb	.54	.58	.55	0.00	1.41	.55	.69	.95	0.00
Ho	0.00	0.00	0.00	0.00	0.00	0.00	0.00	0.00	0.00
Tm	.37	.38	.39	0.00	0.00	0.00	.54	.48	0.00
Yb	1.87	2.29	2.45	0.00	3.11	1.88	3.14	2.70	0.00
Lu	.28	.38	.41	0.00	.52	.30	0.00	0.00	0.00

Elements Si to Zn were analysed by XRF and AA, elements Hf to Lu by INAA. Non-detected/unanalysed elements given as 0. Key to locations: YZ1 = Dazhuka; YZ2 = Chongdui; YZ3 = Jiding; YZ4 = Tangga. Key to rock types: bas. = basalt; PL = pillow lava; ML = massive lava; C = conglomerate; D = dyke.

ophiolite, for example between Gyangze and Xigaze (2907N 8900E) where sheared harzburgite was seen to be overlain by some 2.5 m of ophicalcite breccia, then 30 m of chert-rich clastics and finally > 50 m of red cherts.

(4) Intrusion of dykes into 'cold' oceanic lithosphere, common in the Xigaze ophiolite, is likely to be restricted to ridge-transform intersections where lateral propagation of dykes can take place from the active ridge segment into newly formed lithosphere. Moreover the intrusion of dykes into serpentinized peridotite requires an environment for serpentinization soon after formation that is best provided by a transform zone.

(5) Transform faults are likely sites of the off-axis volcanism seen as sills or flows within overlying sediments.

(6) The lower degree of partial melting in transform zones means that the residual peridotites will be less depleted than beneath the central parts of ridge segments (Ishiwatari 1985); lherzolites such as those from the Liuqu massif are thus likely to be typical of intrusions within transform zones.

Thus, although we agree with the general setting of the ophiolite as proposed by Pozzi *et al.* (1984) and illustrated in figure 7, we consider the character of the ophiolite to relate as much or more to transform faults than to a slow spreading environment.

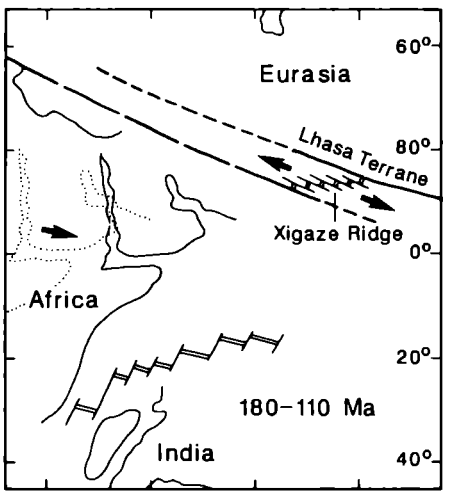

FIGURE 7. Model of Pozzi *et al.* (1984) for the tectonic environment of formation of the Yarlung–Zangbo ophiolite.

4. BANGGONG LAKE–NUJIANG RIVER OPHIOLITE BELT

(*a*) *Geology*

The ophiolite belt associated with the Banggong Suture zone is well exposed in the geotraverse section between the villages of Nagqu, Amdo, Dongqiao and Gyanco (figures 1 and 8), where it has been termed the Dongqiao ophiolite by Girardeau *et al.* (1985*c*). The ophiolite belt is dispersed over a north–south distance of some 200 km and can be divided into several subzones which are roughly parallel to one another (figure 8). This study involved the field examination and sampling of a number of localities within these zones; these localities are shown in figure 8 and the ophiolitic units exposed shown in schematic section in figure 9.

The southernmost subzone (Zone IV), which contains the Xainxa ultramafic rocks described by Girardeau *et al.* (1985*c*), was not visited during the geotraverse, although one of us (Deng) has worked in the area. The Zone contains thin slices dominantly of harzburgite with minor dunite bodies and rare podiform chromites (e.g. at Yangzhong); mafic rocks in the form of isotropic gabbro clasts in serpentinite have been reported from one locality in the Nychang area. These slices are thought to represent southward-thrust klippen from a suture to the north.

The next zone (Zone III) includes the ophiotitic bodies at Baila and Ado west of Gyanco, Nalong east of Gyanco and the Yila Massif northwest of Nagqu. Tectonized ultramafics were

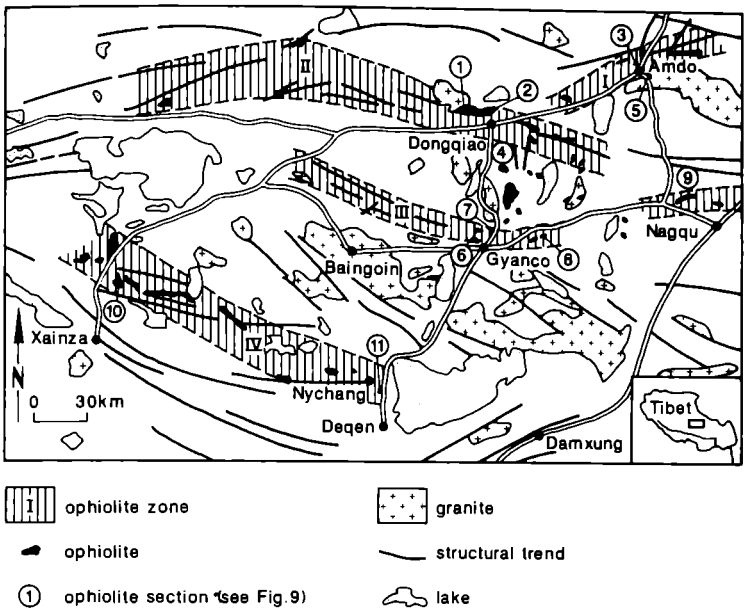

FIGURE 8. Geological setting of the Banggong Lake–Nujiang River ophiolite belt and locations of the areas discussed in the text and represented in figure 9.

studied in the Ado, Nalung and Yila Massifs where they mostly occur as harzburgites with minor dunites, although lherzolites have been sampled in the Ado Massif; they are cut in the Ado Massif west of Pung Co by rodingitised microgabbro dykes. Layered plutonic sections, examined in the Baila and Yila Massifs, comprise dunite–wehrlite sections overlain by layered gabbros. The Ado massif does, however, contain a small troctolite–gabbro body. A small dyke complex cut by dioritic dykes, previously described in detail by Girardeau *et al.* (1984), was studied and sampled in the Baila massif. Lavas are represented mainly in a section some 100 m thick at Nalung, where generally massive flows are overlain by pillowed flows, all cut at a high angle by a series of thin, isolated diabase dykes.

Zone II was studied around Dongqiao, where the major exposures are of harzburgites with minor dunite–chromite bodies and including one significant podiform chromite deposit. Northwest of Donqiao, the harzburgite is in thrust contact with an overturned amphibolitized sequence comprising pillow lavas overlain by pelagic sediments. South of Donqiao, at Loubochong, is an inverted pillow lava sequence described by Pearce & Mei (this volume). As stated in that paper, it is not clear whether or not these lavas belonged to an ophiolite complex or to some non-ophiolitic submarine volcanic edifice.

Zone I was studied south of Amdo village where ophiolites crop out east and west of the main highway. The rock types here range from a sheeted dyke complex comprising 100% dykes through an area of mainly dykes with pillow screens into 100% pillow lavas. In fault contact with this complex is the sequence of lavas of island arc composition described by Pearce & Mei (this volume).

The age of formation of the ophiolite has been identified as Jurassic from isotopic dating of late-magmatic amphiboles (Maluski, Girardeau & Tang, pers. comm. 1986) and by bio-stratigraphic dating of radiolaria in interbedded cherts (Tang & Wang 1984). Obduction of the ophiolite had taken place by the end of the Jurassic, as indicated by shallow water to

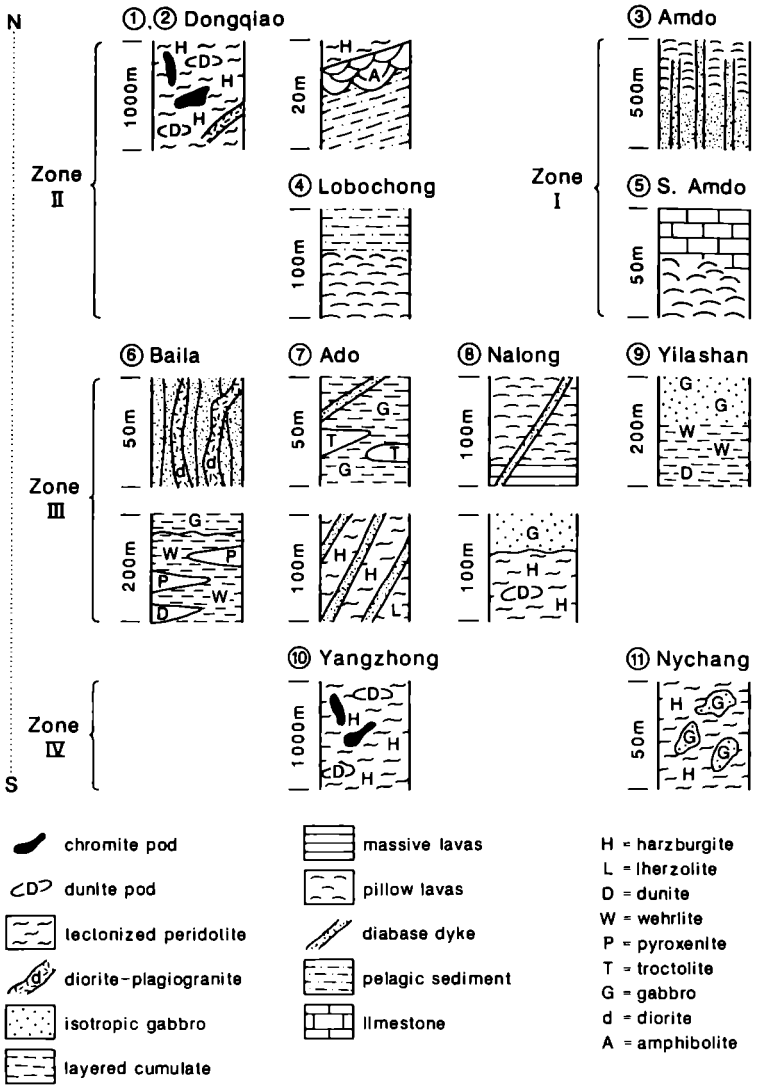

FIGURE 9. Schematic geological sections from some of the studied areas from the Banggong Lake–Nujiang River ophiolite belt. For locations, see figure 8.

continental deposits of the overlying Zigetang formation which have a latest Jurassic to earliest Cretaceous age (Girardeau *et al.* 1985*c*). Mid-Cretaceous redbeds and volcanics unconformably overlie the ophiolite and its sedimentary cover and are thought to post-date the final collision.

Because of the highly fragmentary nature of the ophiolite, the structure has been pieced together from outcrops that expose different levels of the complex (Girardeau 1985*c*). While necessary to obtain a stratigraphy, this approach does assume that (*a*) all fragments belonged to the *same* oceanic lithosphere and (*b*) all fragments belonged to oceanic lithosphere rather than other intraoceanic features. This study aims to use geochemical characterization techniques to evaluate these hypotheses and to consider in further detail the original environment of formation.

(*b*) *Petrology and geochemistry*

Evidence relating to the original tectonic setting of the ophiolite has been obtained from all parts of the complex. Spinel analyses from the tectonized ultramafic units have been plotted on the diagram of Dick & Bullen (1984) in figure 10, and some representative data are given in table 3. It is apparent from figure 10 that the data fall into two groups: the main-group is characterized by the harzburgite-hosted spinels which have high Cr# (Cr/(Cr+Al) ratios) and plot in the boninite and island arc basalt fields on the diagram; a second group, restricted to the Ado locality, is characterized by lherzolite-hosted spinels which have low Cr# and plot in the abyssal peridotite field. Spinels from cumulate dunites have also been plotted on this diagram and reinforce the bimodality of composition. Following the petrogenetic arguments of Dick & Bullen (1984), the harzburgite-hosted high-Cr# spinels are likely to represent residua from a high degree of melting (or re-melting) of the mantle, an interpretation supported by the refractory clinopyroxene-free (15–25 % opx, 70–85 % ol, < 1 % sp) and low Al_2O_3 (0.2–1.5 %) character of their host rocks and indicative of a supra-subduction zone origin. The lherzolite-hosted spinels from the Ado Massif are likely to have been derived by the lower degrees of melting or less depleted sources that characterize MORB genesis.

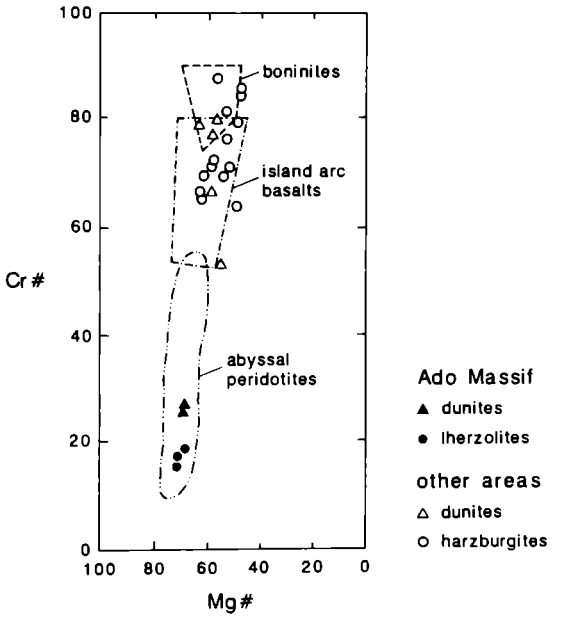

FIGURE 10. Chrome spinel compositions from dunites and tectonized ultramafic rocks from the Banggong Lake–Nujiang River ophiolite belt plotted on the Cr#–Mg# diagram of Dick & Bullen (1984). For representative full analyses, see table 3.

The crystallization sequence of the cumulates also supports a supra-subduction zone origin for almost all the plutonic sequences studied, showing an olivine–clinopyroxene–plagioclase order of crystallization resulting in dunite–wehrlite sequences. Parts of the Ado Massif again present an exception, indicating an olivine–plagioclase–clinopyroxene order of crystallization resulting in a dunite–troctolite sequence. Although crystal cumulation generally prevents the use of whole-rock geochemistry for characterization of these rocks, the Baila diorite is sufficiently

TABLE 2. REPRESENTATIVE GEOCHEMICAL ANALYSES FOR SELECTED SAMPLES OF LAVAS AND DYKES FROM THE BANGGONG SUTURE ZONE OPHIOLITE BELT

sample	G95C	G95B	G95D	G95F	Oph404	1-8	1-8	G92F	Lang-2
location	BG1	BG1	BG1	BG1	BG2	BG2	BG2	BG2	BG2
rock	bon.	bon.	bon.	bas.	b/a.	b/a.	b/a.	bas.	b/a.
type	D	D	D	D	PL	PL	PL	D	D
SiO_2	61.20	51.00	49.10	45.30	53.13	54.20	53.44	51.80	52.59
TiO_2	.41	.50	.32	.40	.58	.51	.52	.59	.81
Al_2O_3	10.60	12.70	16.40	18.40	13.58	13.40	13.68	15.20	14.90
Fe_2O_3	6.23	8.48	9.28	11.28	9.65	9.48	9.44	7.76	9.60
MnO	.12	.14	.12	.11	.18	.19	.18	.14	.18
MgO	10.50	14.60	7.50	6.58	6.89	9.56	9.53	6.52	6.84
CaO	5.69	6.48	10.64	11.10	8.32	7.19	7.89	15.00	6.98
Na_2O	3.49	3.42	1.86	1.22	4.55	4.14	3.95	.98	4.49
K_2O	.06	.06	1.14	1.54	.60	.17	.33	.12	.66
P_2O_5	.11	.15	.02	.04	.08	.06	.04	.05	.08
LOI	1.76	2.47	3.80	3.72	2.26	1.58	1.52	1.70	3.65
Total	100.17	100.00	100.18	99.69	99.82	100.48	100.52	99.86	100.78
Zr	56	67	15	54	0	0	0	34	0
Y	8	10	9	28	0	0	0	14	0
Nb	2.8	3.6	3.3	5.1	0.0	0.0	0.0	1.8	0.0
Rb	1.0	0.0	16.3	8.0	0.0	0.0	0.0	1.5	0.0
Sr	90	150	228	532	0	0	0	214	0
Cr	540	634	56	103	220	404	385	360	198
Ni	203	258	41	49	85	157	141	87	94
V	130	200	338	573	200	0	0	250	325
Cu	108	25	348	478	0	0	0	20	0
Zn	60	85	57	57	0	0	0	54	0
Hf	0.00	0.00	0.00	0.00	1.04	0.00	0.00	1.00	0.00
Ta	0.00	0.00	0.00	0.00	.14	0.00	0.00	.13	0.00
Th	0.00	0.00	0.00	0.00	.37	0.00	0.00	.30	0.00
Sc	0.0	0.0	0.0	0.0	0.0	0.0	0.0	36.8	0.0
Co	0.0	0.0	0.0	0.0	0.0	0.0	0.0	35.4	0.0
La	0.0	0.0	0.0	0.0	2.0	2.1	2.1	1.6	3.9
Ce	0.0	0.0	0.0	0.0	5.3	4.8	5.1	5.6	9.1
Nd	0.0	0.0	0.0	0.0	0.0	3.8	0.0	3.9	9.3
Sm	0.00	0.00	0.00	0.00	1.37	1.25	1.32	1.41	2.18
Eu	0.00	0.00	0.00	0.00	.50	.55	.59	.69	.63
Tb	0.00	0.00	0.00	0.00	.42	.40	.39	.39	.74
Ho	0.00	0.00	0.00	0.00	0.00	0.00	0.00	0.00	0.00
Tm	0.00	0.00	0.00	0.00	0.00	0.00	0.00	.20	0.00
Yb	0.00	0.00	0.00	0.00	1.68	1.70	1.84	1.53	2.53
Lu	0.00	0.00	0.00	0.00	.27	.28	.31	.26	.38

homogeneous to be used in this way: its composition, shown in table 2, shows low incompatible element content and a slight LREE enrichment (figure 11) typical of intermediate rocks of the island arc tholeiite series.

Geochemical discriminants applied to the lavas and dykes further support these broad conclusions, but also provide more detail on the type of supra-subduction zone environment. The diagrams used, MORB-normalized trace element patterns, rare-earth element patterns and Th–Ta–Hf+Cr–Y discriminant plots are shown in figures 12 and 13 respectively. Data representative of those on which these diagrams are based are listed in table 2.

Figure 12 shows patterns representative of Nalong (G92F), Loubochong (G106D), Dongqiao amphibolite (G103C) and Amdo (G127C) pillow lavas. It will be noted that all patterns show

TABLE 2. (*cont.*)

sample	Oph450	G106D	G103C	G127C	Amdo-1	Amdo-5	Oph622	Amdo10	G106D
location	BG3	BG3	BG4	BG5	BG5	BG5	BG5	BG5	BG6
rock	bas.	bas.	bas.	bas.	bas.	bas.	bas.	b/a.	bas.
type	PL	PL	PL	D?	D	D	D?	D?	PL
SiO_2	51.35	47.60	49.80	50.30	48.75	49.59	48.99	53.28	47.60
TiO_2	0.64	0.56	1.22	1.24	.69	1.43	1.22	1.42	.56
Al_2O_3	13.32	11.20	12.80	14.20	13.94	12.90	13.75	12.02	11.20
Fe_2O_3	9.84	6.20	9.36	12.20	10.85	14.98	13.33	13.08	6.20
MnO	0.38	0.15	.17	.19	.15	.29	.21	.20	.15
MgO	3.78	5.04	7.78	7.30	8.24	6.60	7.53	6.37	5.04
CaO	7.35	15.90	13.50	9.95	11.60	7.91	8.42	7.47	15.90
Na_2O	4.90	3.51	3.34	2.71	2.06	3.20	3.34	3.93	3.51
K_2O	0.25	0.68	.28	.22	.11	.10	.05	.05	.68
P_2O_5	0.12	0.09	.10	.08	.05	.09	.07	.12	.09
LOI	7.06	9.98	2.22	1.43	3.80	3.51	4.10	3.20	9.98
Total	98.99	100.91	100.57	99.82	100.24	100.60	101.01	101.14	100.91
Zr	0	32	68	60	0	0	0	0	32
Y	0	11	23	30	0	0	0	0	11
Nb	0.0	2.4	4.0	2.0	0.0	0.0	0.0	0.0	2.4
Rb	0.0	13.0	6.4	3.5	0.0	0.0	0.0	0.0	13.0
Sr	0	157	199	96	0	0	0	0	157
Cr	0	480	200	107	278	59	250	51	480
Ni	0	217	65	47	90	46	130	56	217
V	0	180	290	340	316	456	320	420	180
Cu	0	35	122	55	0	0	0	0	35
Zn	0	51	132	99	0	0	0	0	51
Hf	1.38	.91	1.80	1.75	0.00	0.00	0.00	0.00	.91
Ta	.14	.11	.26	.12	0.00	0.00	0.00	0.00	.11
Th	.72	.69	.73	.30	0.00	0.00	0.00	0.00	.69
Sc	0.0	27.1	37.5	29.4	0.0	0.0	0.0	0.0	27.1
Co	0.0	34.8	38.0	48.9	0.0	0.0	0.0	0.0	34.8
La	6.6	3.6	3.4	1.5	1.7	2.9	3.1	3.2	3.6
Ce	11.2	9.5	10.0	6.8	5.1	9.4	8.3	7.7	9.5
Nd	6.4	5.8	7.8	7.7	0.0	11.9	0.0	8.6	5.8
Sm	1.86	1.50	2.61	3.00	1.89	3.75	2.68	3.64	1.50
Eu	.70	.52	.97	1.00	.85	1.42	1.10	1.41	.52
Tb	.44	.36	.73	.87	.42	1.21	.74	1.10	.36
Ho	0.00	1.00	1.80	0.00	0.00	0.00	0.00	0.00	1.00
Tm	0.00	.16	.25	0.00	0.00	0.00	0.00	0.00	.16
Yb	1.65	1.33	2.76	3.61	2.57	4.41	3.21	4.90	1.33
Lu	.26	.23	.42	.59	.36	.69	.53	.67	.23

Elements Si to Zn were analysed by XRF and AA, elements Hf to Lu by INAA. Non-detected/unanalysed elements given as 0. Key to locations; BG1 = Baila; BG2 = Nalong; BG3 = Loubochong; BG4 = Dongqiao; BG5 = Amdo; BG6 = Amdo (S). Key to rock types: bas. = basalt; b./a. = basaltic andesite; PL = pillow lava; D = dyke; bon. = boninite; dior. = diorite; L = massive lava.

an enrichment in Th relative to Ta indicative of a supra-subduction zone environment, although the twofold enrichment at Nalong is relatively small. In addition, the Loubochong sample shows the greatest subduction component with enrichment of LREE and P as well as Th and hence a more calc-alkaline composition. Variations are also apparent in figure 13: only the Loubochong pattern shows LREE enrichment; the Amdo sample exhibits strong LREE depletion; and the other two samples show slight depletion.

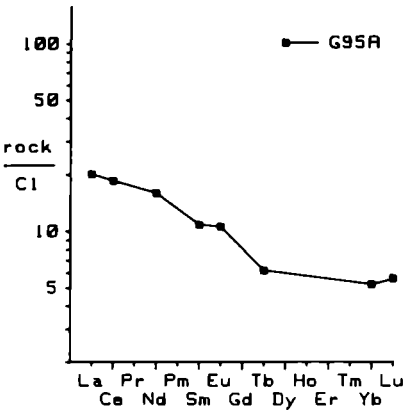

FIGURE 11. Chondrite-normalized rare-earth pattern for the diorite at Baila.

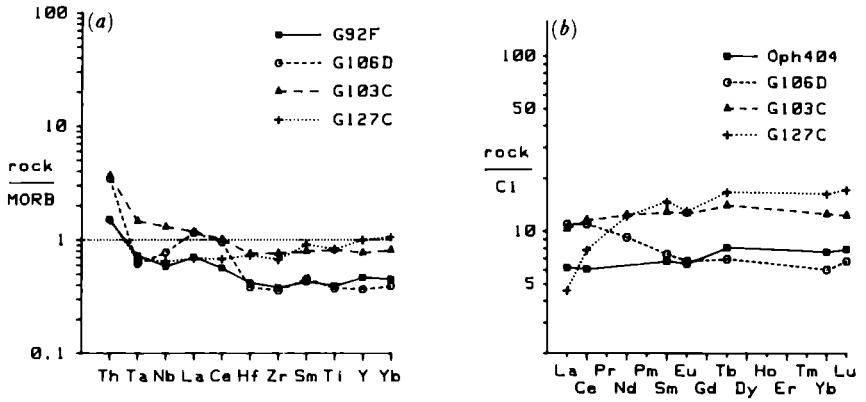

FIGURE 12. (*a*) MORB-normalized trace element patterns and (*b*) chondrite-normalized rare earth patterns for representative samples from the Banggong Lake–Nujiang River ophiolite belt. For full analyses and sample localities, see table 2.

TABLE 3. REPRESENTATIVE MINERAL ANALYSES FROM ULTRABASIC AND BASALTIC ROCKS FROM THE BANGGONG–NUJIANG OPHIOLITE BELT

sample	Nych.	Dong.	Nych.	Ado	Ado	Ado	Ado	Amdo	Nalong
location	OPH546	OPH459	OPH546	Ado-1	Ado-1	Ado-1	Ado-1	Amdo9	OPH403
rock	harz.	harz.	harz.	lherz.	lherz.	lherz.	lherz.	dol.	bas.
min.	ol.	opx.	sp.	ol.	opx.	cpx.	sp.	cpx.	cpx.
SiO_2	39.48	58.14	.06	41.16	54.90	50.54	.03	48.46	51.37
TiO_2	.05	0.00	.39	.05	.11	.31	0.00	.15	.31
Al_2O_3	0.00	.98	7.22	0.00	4.74	7.04	53.34	4.80	4.55
FeO	7.31	4.83	19.16	8.26	6.51	2.60	12.96	17.29	5.82
MnO	.12	.03	.33	.03	.12	.03	.21	.30	.18
MgO	51.67	34.72	9.46	47.21	32.27	15.16	18.55	13.06	17.92
CaO	.02	.73	.02	.04	.76	21.45	0.00	11.02	19.20
Na_2O	.02	.04	.02	.02	.05	.89	.02	.42	.17
Cr_2O_3	0.00	.39	59.31	.04	.50	.99	15.46	.07	.21
Total	98.67	99.86	95.97	96.81	99.96	99.01	100.57	95.57	99.73
Mg#	.93	.93	.47	.91	.90	.91	.71	.57	.84
Cr#	0.00	0.00	.85	0.00	0.00	0.00	.16	0.00	0.00

Key to locations: Nych. = Nychang; Dong. = Dongqiao. Key to rock types: harz. = harzburgite; lherz. = lherzolite, dol. = dolerite; bas. = basalt. Key to minerals: ol. = olivine; opx. = orthopyroxene; cpx. = clinopyroxene; sp. = spinel.

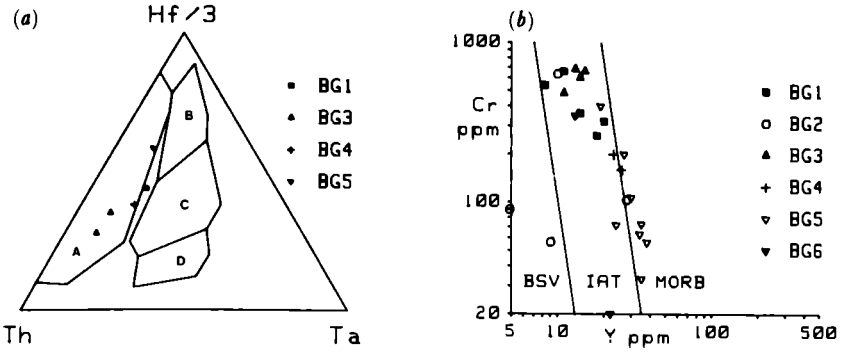

FIGURE 13. (*a*) Th–Ta–Hf and (*b*) Cr–Y discriminant diagrams for basic lavas from the Banggong Lake–Nujiang River ophiolite belt. In figure 13*a*, volcanic arc basalts plot in field A, mid-ocean ridge basalts in fields B and C and within plate basalts in fields C and D. The fields in figure 13*b* are given in the caption to figure 5*b*. Key to localities: BG1 = Baila dykes; BG2 = Nalong lavas and dykes; BG3 = Loubochong pillow lavas; BG4 = Dongqiao amphibolite; BG5 = Amdo pillow lavas/dykes; BG6 = S. Amdo lavas.

Figure 13*a* further demonstrates the selective enrichment of Th over Ta in these rocks which cause the compositions to be displaced away from the MORB field towards the field of volcanic arc basalts. Figure 13*b* shows a greater number of analyses and permits a more detailed discrimination between boninite series volcanics (BSV), island arc tholeiites (IAT) and mid-ocean ridge basalt (MORB) compositions. It is apparent that two of the dykes from Baila have very low Y and high Cr values and plot within the BSV field. This interpretation is supported by inspection of the major element compositions of these rocks in table 3 which, despite alteration, show the combination of high SiO_2 and high MgO that characterizes the BSV series. These compositions, and particularly the variable enrichment in Zr relative to Y, resemble those of the Arakapas area of the Troodos Massif of Cyprus (Rogers *et al*, in press). However it should also be noted that other dykes from this complex show more tholeiitic compositions. Also on this diagram, the lavas and dykes from Nalong span the IAT field, the lavas from Loubochong and South Amdo plot in the centre of the IAT field, and the Dongqiao amphibolite and the lavas and dykes from Amdo plot on the boundary between the MORB and IAT fields.

The primary mineralogy of the lavas and dykes also varies from south to north, although greenschist, sometimes zeolite or amphibolite, facies alteration has affected all rocks. The lavas and dykes in the southern and central zones are noticeably richer in clinopyroxene, sometimes containing clinopyroxene phenocrysts, than the more feldspar-rich lavas and dykes in the Amdo region. Microprobe analyses of clinopyroxenes (table 3) show a distinction between the more chrome-diopsidic compositions at Nalung and the more augitic compositions at Amdo; both groups of pyroxenes plot in orogenic, or island arc fields on pyroxene discrimination diagrams. The boninites are too altered for primary Ca-poor pyroxenes to be identified.

(*c*) *Tectonic interpretation*

The data presented here thus in general support the previous interpretations (Wang *et al.* 1984; Yang & Deng 1986; Girardeau *et al.* 1984) that the Dongqiao ophiolite formed in a supra-subduction zone setting. However, they also suggest that it may be too simplistic to construct a single ophiolite section from the isolated outcrops (Girardeau *et al.* 1984) since they have different compositions and therefore represent different types of oceanic lithosphere. It

may also be too simplistic to assume that all fragments represent klippen from a single suture since the compositional variety is equally, perhaps more, consistent with their emplacement during closure of an arc-basin complex rather than of a single basin. Finally, the lherzolites, troctolites and gabbros in the Ado Massif are of typical MORB composition and may represent incorporated fragments of normal oceanic lithosphere.

In the authors' opinion, the most significant observation is that of the regional zonation in the composition of the dykes and lavas. In their southernmost outcrops (Zone III), genuine boninitic high MgO, high SiO_2 compositions are found in the Baila dyke swarm and have also been reported from the Dengqen ophiolite in the same belt to the east (Zhang & Yang 1986); elsewhere in this belt (and also within the Baila dyke swarm) primitive island arc tholeiites are the normal magmatic product. Between this zone and the northern zones (I and II), typical island arc tholeiite series are present, some (those south of Amdo) clearly representing volcanic edifices rather than oceanic lithosphere (Pearce & Mei, this volume.) In the northern zones, transitional MORB–IAT compositions are found. This type of spatial zonation is common in Western Pacific island arcs, as for example from the Tonga fore-arc, through the Tofua arc to the Lau Basin and from the Mariana fore-arc through the Mariana arc to the Mariana trough (e.g. Hawkins & Melchior 1985; Dietrich *et al.* 1978). According to this analogy, the ophiolites from Zones III and IV would represent fore-arc lithosphere, the lavas from Loubochong and South Amdo would represent island arc and arc seamount edifices and the amphibolites of Zone II and lava-dyke complexes of Zone I would represent back-arc lithosphere, all formed above a Jurassic, northward-dipping subduction zone (figure 14). Because there are such complex variations, however, a final interpretation will require detailed tectonic and petrological study of all the ophiolite fragments within the belt.

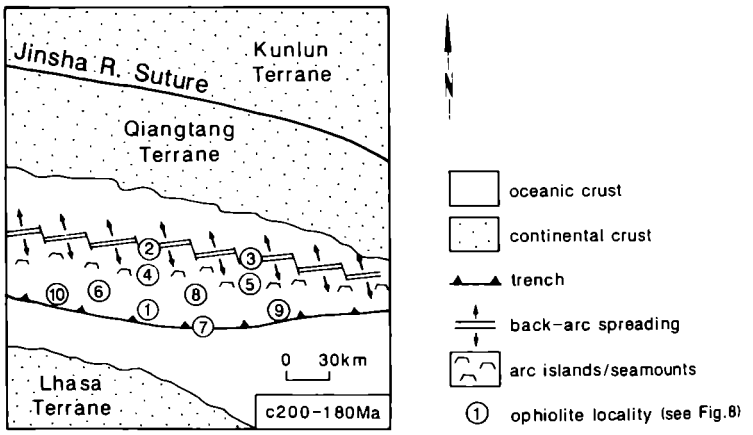

FIGURE 14. Schematic simplified reconstruction of the Jurassic tectonic setting of the Banggong–Nujiang ophiolite belt showing possible environments of formation of the various ophiolite fragments.

5. JINSHA RIVER OPHIOLITE BELT

(*a*) *Geology*

The Jinsha River (also known as the Hoh Xil-Yushu) ophiolite belt is the third ophiolite belt and lies on the Jinsha River Suture between the Qiangtang and Kunlun Terranes. Preliminary data from two ophiolites are reported here: at Bayinchawuma located about 100 km west of

the geotraverse road at Erdaogou; and at Yushu to the east near the Tongtian River on the Qinghai–Sichuan border (figure 1).

The map of the Bayinchawuma ophiolite made by the Geological Team of Qinghai Province is shown in figure 15. Two ophiolite outcrops were recognized, both comprising totally serpentinized harzburgites containing antigorite, bastite and magnetite as alteration minerals and primary chrome spinel, and forming klippen within the Triassic Batang Group.

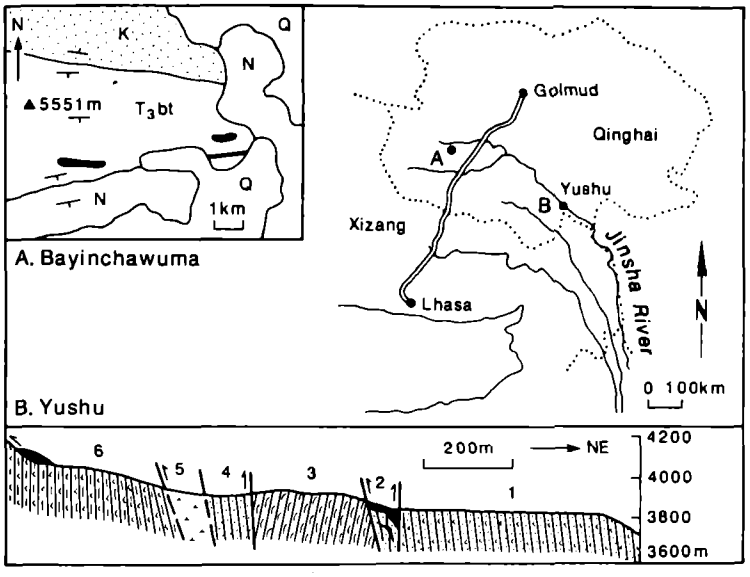

FIGURE 15. Geological maps and sections of the Bayinchawuma and Yushu ophiolite localities in the Jinsha River ophiolite belt. In map A, ophiolite outcrops are shown in black, T_3bt is the Triassic Batang group (sandstone, phyllites, tuffs and bioclastic limestone), K is the Cretaceous Fenguoshan Group (redbeds) and N and Q are Neogene and Quaternary deposits respectively. In section B (taken from Pan 1984), 1 = Batang Group, 2 = peridotites, 3 = pillow basalts and picrites, 4 = siliceous rocks, 5 = gabbros and 6 = tuff slates.

The Yushu ophiolite, discovered by Pan (1984) near the Tongtian River and not visited on the Geotraverse, consists of a disrupted sequence of ultramafic rocks (not showing tectonic fabrics; Pan, pers. comm.), gabbros, pillow basalts and picrites, and associated tuffs and cherts distributed as blocks within the Batang group (figure 15). All rocks are strongly altered, the pillow lavas to greenschists and amphibolites.

(*b*) *Petrology and geochemistry*

Few data exist from this ophiolite belt: spinels from the Bayinchawuma ophiolite are being analysed at the time of writing while only major element data are available for the Yushu ophiolite. Despite limited immobile element data, the Yushu ophiolite can be seen probably to have a MORB chemistry: lava compositions fall consistently within the MORB field of both the Ti–Cr and $FeO/MgO–TiO_2$ discrimination diagrams (figure 16) and the apparent crystallization history is olivine, plagioclase, clinopyroxene.

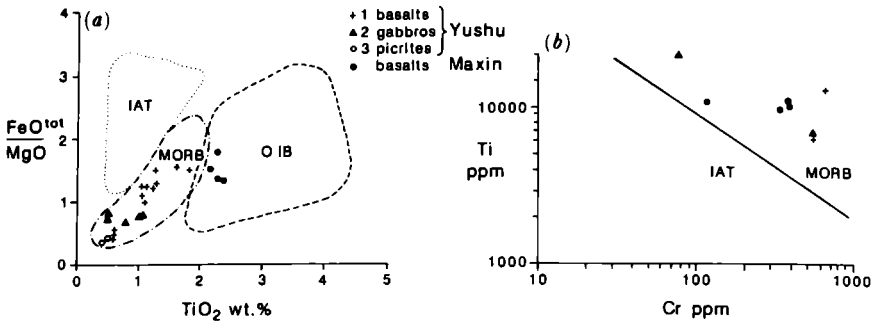

FIGURE 16. (*a*) FeO/MgO–TiO_2 and (*b*) Cr–Ti discriminant diagrams for lavas from the Yushu and Maxin ophiolites. MORB = mid-ocean ridge basalts; IAT = island arc tholeiites; and OIB = ocean island basalts. For full analyses see table 4.

(*c*) *Tectonic interpretation*

The MORB composition of the Yushu ophiolite points to an origin either in a major (incipient or evolved) ocean basin or in a back-arc basin distant from its related subduction zone. More data are clearly required, however, before any concrete conclusions can be drawn for the belt as a whole.

6. ANYEMAQEN-JISHISHAN OPHIOLITE BELT

(*a*) *Geology*

This ophiolite belt was not studied during the Geotraverse. It is, however, important to understand its origin because of the question of whether an additional Suture should be drawn within the Kunlun Terrane. The best-studied ophiolite of this belt is the Maxin ophiolite in eastern Qinghai province (figure 17). The complex occurs in a 30 km-wide NW–SE trending belt within lower Permian bioclastic limestone and associated silty slates, tuffs and basalts. The ophiolite is mainly composed of highly serpentinized and tectonized peridotites, mostly harzburgites but with some lherzolites, which crop out as lenses of varying sizes. Other members of the ophiolite series have not yet been found, although pillow lavas are found possibly interbedded with lower Permian marble.

(*b*) *Petrology and geochemistry*

The peridotites are characterized by 'fertile' compositions, notably high Al_2O_3 and residual clinopyroxene, which indicate that a supra-subduction zone origin is unlikely. The lavas contain some microphenocrysts of clinopyroxene in a groundmass of volcanic glass, plagioclase microlites and clinopyroxene, variably altered to a chlorite, calcite, sericite assemblage; some typical analyses are given in table 4. These data confirm the non-subduction related character, plotting in the MORB field of the immobile element discrimination diagram, Ti–Cr (figure 16*b*). The FeO/MgO–TiO_2 diagram (figure 16*a*) further indicates that the analyses may be of within-plate tholeiite or plume-related (P-type) MORB composition and this interpretation is supported by rare-earth analyses, which show LREE enrichment (figure 18). Comparable compositions are found at the present day in some oceanic islands, or seamounts (e.g. Hawaii, Iceland) and in areas of strongly attenuated continental lithosphere (e.g. Afar).

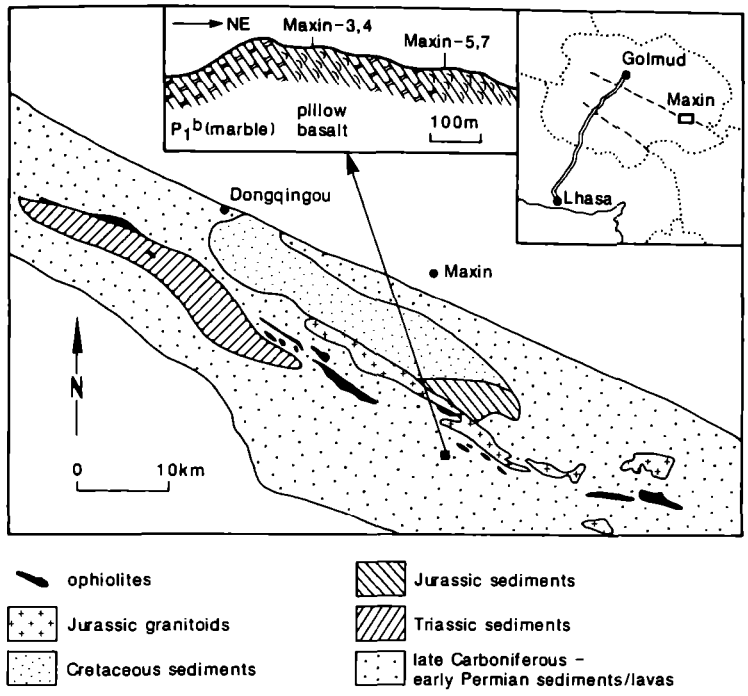

FIGURE 17. Geological map of the Anyemaqen–Jishi mountain ophiolite belt.

TABLE 4. REPRESENTATIVE MAJOR ELEMENT ANALYSES OF BASIC ROCKS FROM THE JINSHA RIVER (YUSHU) AND ANYEMAQEN–JISHI (MAXIN) MOUNTAIN OPHIOLITE BELTS

sample	Yushu	Yushu	Yushu	Yushu	Yushu	Maxin	Maxin	Maxin	Maxin
location	Y-71	Y-79	Y-123	Y-81	Y-107	Maxin3	Maxin4	Maxin5	Maxin7
rock	pic.	gab.	gab.	bas.	bas.	bas.	bas.	bas.	bas.
type	L	Int.	Int.	PL	PL	PL	PL	PL	PL
SiO_2	43.17	48.43	48.35	48.41	44.24	47.25	46.14	46.18	47.05
TiO_2	.25	1.14	3.94	1.20	1.96	2.34	2.19	2.40	2.28
Al_2O_3	6.44	13.47	14.13	14.14	11.37	13.96	13.60	13.15	14.53
Fe_2O_3	13.55	9.22	11.55	8.98	12.90	10.02	10.61	9.71	10.51
MnO	.18	.24	.16	.18	.17	.14	.16	.16	.18
MgO	31.82	7.93	4.44	7.90	12.01	7.77	7.80	7.78	6.39
CaO	2.80	12.93	6.50	11.60	8.18	8.94	10.76	9.59	8.35
Na_2O	.07	2.87	3.56	2.57	.83	3.07	2.84	3.01	3.61
K_2O	.09	.30	1.98	.37	.19	.36	.51	1.06	.80
P_2O_5	.01	.13	.48	.11	.26	.33	.32	.44	.38
LOI	0.00	2.84	3.04	3.05	5.22	4.12	3.94	4.66	3.97
Total	98.38	99.50	98.13	98.51	97.33	98.30	98.87	98.14	98.05
Cr	3600	600	90	500	610	370	351	371	185

Key to rock types: pic. = picrite; gab. = gabbro; bas. = basalt ; L = massive lava; Int. = intrusion; PL = pillow lava.

(*c*) *Interpretation*

The geochemical evidence that the lavas are not of typical ocean ridge type is consistent with the field evidence of possible interbedding with limestone which supports the seamount or attenuated continental lithosphere hypotheses. Possible analogues have been found at the margins of the Red Sea (Coleman 1984) and on the Red Sea island of Zabargad, where

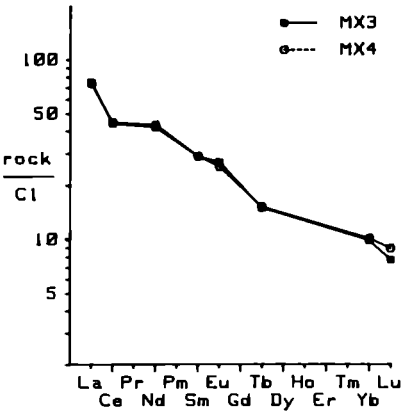

FIGURE 18. Chondrite-normalized rare-earth patterns of two lavas from the Anyemaqen-Jishi mountain ophiolite belt.

peridotites are exposed (Bonatti *et al.* 1981). If such analogies do hold, the ophiolites could represent transitional or immature oceanic lithosphere formed during Permian rifting and emplaced during Triassic closure. There is, as yet, however, no evidence that true oceanic lithosphere existed in the area. In relation to the Geotraverse, it is possible that some of the cumulate igneous rocks found in clasts in glacial moraine along the Kunlun fault formed in a similar setting and are of similar age to the Maxin ophiolite, although their most probable origin is intrusive, related to the post-kinematic Kunlun plutonic complexes (Kidd & Molnar, this volume). Even if this is the case, however, we consider it valid to treat the Kunlun Terrane as a single Terrane (Chang *et al.* 1986), at least until evidence for true oceanic lithosphere is found.

7. Summary and conclusions

The principal conclusions of this study can be summarized as follows.

1. Our data confirm previous interpretations that the ophiolites of the Yarlung–Zangbo Suture are of MORB composition and that they represent anomalous Cretaceous oceanic lithosphere formed within the neo-Tethyan ocean. The lower-than-normal crustal thickness, presence of intra-oceanic unconformities and melanges, presence of 'fertile' peridotites, and late intrusion of dykes and sills of MORB composition into already-formed lithosphere may indicate the importance of ridge-transform intersections in the origin of the ophiolite, an interpretation in line with reconstructions requiring short north–south ridge segments offset by major transform faults.

2. Our data also confirm previous interpretations that the ophiolites associated with the Banggong Suture formed in supra-subduction zone environments. The chemical zonation of lavas and dykes is used further to suggest that the ophiolitic fragments are derived from an arc-basin complex developed above a Jurassic northward-dipping subduction zone, those in the south representing fore-arc lithosphere, those in the central zone representing island arc or arc seamount lithosphere and those in the north representing back-arc lithosphere. MORB-lithosphere appears to be present in one locality, in the Ado Massif. Ophiolite emplacement may have taken place in at least two stages: a continent-arc or continent-fore-arc collision event in the Jurassic; and a continent-continent collision event in the Cretaceous.

3. There is insufficient evidence to make a full interpretation of the tectonic setting of

formation of the ophiolites of the Jinsha River Suture zone. One of the best-studied ophiolites in the zone, the Yushu ophiolite east of the Geotraverse, is of MORB composition, while the Bayinchawuma ophiolite just west of the Geotraverse route comprises strongly depleted harzburgites and may be of supra-subduction zone character.

4. The Anyemaqen–Jishi mountain ophiolite belt east of the Kunlun mountains contains, at Maxin, tectonised peridotites and pillow lavas with within-plate tholeiite character which may have belonged to transitional or immature oceanic lithosphere, but which do not constitute sufficient evidence for placing an additional Suture within the Kunlun Terrane.

We should like to thank: Ernesto Abbate, Costas Xenophontos and members of the Geotraverse team for helpful discussions; Zhang Kiuwu, Zhang Qi and the Geological Team of Qinghai Province for mapping and sampling the Bayinchawuma ophiolite after our own attempt failed; and Peter Oakley, Peter Murray, Nick Rogers, Yang Ruiyang and Liu Jialin for analytical work.

References

Bonatti, E., Hamlyn, P. R. & Ottonello, G. 1981 The upper mantle beneath a young oceanic rift: peridotites from the island of Zabargad (Red Sea). *Geology* **9**, 474–479.

Chang Chengfa *et al.* 1986 Preliminary conclusions of the Royal Society and Academia Sinica 1985 geotraverse of Tibet. *Nature, Lond.* **323**, 501–507.

Cherchi, A. & Schroeder, R. 1980 *Palorbitolinoides hedini* n. gen. n. sp. grand foraminifère du Crétacé inf. du Tibet meridional. *C.r. Acad. Sci., Paris* **291**, 385–388.

Coleman, R. G. 1984 The Tahama Asia igneous complex, a passive margin ophiolite. *27th Internat. Geol. Congress, Moscow* **23**, 93–121.

Deng Wanming 1981 A preliminary study of the petrology and genesis of the Yarlung Zangbo ophiolite belt. In *Proceedings of Symposium on Qinghae-Xizang (Tibet) Plateau (Beijing, China)*, pp. 529–538. New York Science Press; Gordon & Breach.

Deng Wanming 1982 Studies on the igneous petrology of the Yarlung-Zangbo ophiolite, Xizang. In *Proceedings of geological research or Qinghai-Xizang*, pp. 36–52. Beijing Geological Publishing House. (In Chinese.)

Deng Wanming 1983 Geological comparison between the ultrabasic rock belts in Northern and Southern Xizang. *Petr. Res.* **3**, 1–16. (In Chinese.)

Deng Wanming 1984 Petrogenesis of the basic-ultrabasic rock belt along Dongqiao-Nujiang in Northern Xizang (Tibet). *Himalayan Geology* **II**, 81–98. (In Chinese.)

Deng Wanming & Zhou Yusheng 1982 Geological evolution of oceanic crust in Mesozoic eastern Tethys as exemplified by the Yarlung-Zangbo ophiolite zone. *IGAS Research on Geology*, pp 42–48. (In Chinese.)

Deng Wanming, Yang Ruiyang, Huang Zhongxiang, Jiang Yong, Guo Yinghun, Luo Shihua, Zhao Zhenlan & Feng Xizhang 1984 Trace element geochemistry of the ophiolite complex in the Xigaze district, Xizang. In *Sino-French co-operative investigation in Himalayas*, pp. 221–237. Beijing Geological Publishing House. (In Chinese.)

Deng Wanming, Yang Ruiyang & Huang Zhongxiang 1985 Trace element characteristics of the mafic-ultramafic plutons in Northern Xizang. *Petr. Res.* **6**, 47–58.

Dick, H. J. B. & Bullen, T. 1984 Chromium spinel as petrogenetic indicator in abyssal and Alpine type peridotites and spatially associated lavas. *Contr. Miner. Petr.* **86**, 54–76.

Dietrich, V., Emmermann, R., Oberhansli, R. & Puchelt, H. 1978 Geochemistry of basaltic and gabbroic rocks from the West Mariana Basin and the Mariana Trench. *Earth planet. Sci. Lett.* **39**, 127–144.

Fox, P. J. & Straup, J. B. 1981 The plutonic foundation of the oceanic crust. In *The Oceanic lithosphere. The Sea*, VIII (ed. C. Emiliani), pp. 119–218.

Girardeau, J., Marcoux, J., Allègre, C. J., Bassoullet, J. P., Tang Youking, Xiao Xuchang, Zao Yougong & Wang Xibin 1984 Tectonic environment and geodynamic significance of the Neo-Cimmerian Dongqiao ophiolite, Banggong-Nujiang Suture zone, Tibet. *Nature, Lond.* **307**, 27–31.

Girardeau, J., Mercier, J.-C. C. & Zao Yougong 1985*a* Origin of the Xigaze ophiolite, Yarlung Zangbo Suture zone, Southern Tibet. *Tectonophysics* **119**, 407–433.

Girardeau, J., Mercier, J.-C. C. & Wang Xibin 1985*b* Petrology of the mafic rocks of the Xigaze ophiolite, Tibet. *Contr. Miner. Petr.* **90**, 309–321.

Girardeau, J., Marcoux, J, Fourcade, E., Bassoullet, J. P. & Tang Youking 1985*c* Xainxa ultramafic rocks, central Tibet, China; tectonic environment and geodynamic significance. *Geology* **13**, 330–333.

Glassley, W. 1974 Geochemistry and tectonics of the Crescent Volcanic rocks, Olympia Peninsula, Washington. *Bull. geol. Soc. Am.* **85**, 785–794.

Göpel, C., Allègre, C. J. & Xu Ronghua 1984 Lead isotope study of the Xigaze ophiolite (Tibet): the problem of the relationship between magmatites (gabbros, dolerites, lavas) and tectonites (harzburgites). *Earth planet. Sci. Lett.* **69**, 301–310.

Hawkins, J. W. & Melchior, J. T. 1985 Petrology of the Mariana Trough and Lau Basin basalts. *J. geophys. Res.* **90**, 11431–11468.

Ishiwatari, K. 1985 Alpine ophiolite: product of low-degree mantle melting in a Mesozoic transcurrent rift zone. *Earth planet. Sci. Lett.* **76**, 93–108.

Leterrier, J., Maury, R. C., Thonon, P., Girard, D. & Marchal, M. 1982 Clinopyroxene composition as a method of identification of the magmatic affinities of palaeo-volcanic series. *Earth planet. Sci. Lett* **59**, 139–154.

Marcoux, J., De Wever, P., Nicolas, A., Girardeau, J., Xiao Xuchang, Chang Chengfa, Wang Naiwen, Zao Yougong, Bassoullet, J. P., Colchen, M. & Mascle, G. 1982 Preliminary report on depositional sediments on top of the volcanic member: the Xigaze ophiolite (Yarlung-Zangbo suture zone). *Ofioliti* **2/3**, 395–396.

Molnar, P. & Tapponnier, P. 1975 Cenozoic tectonics of Asia: effects of a continental collision. *Science, Wash.* **189**, 419–426.

Nicolas, A., Girardeau, J., Dupré, B., Wang Xibin, Zheng Haixiang, Zao Yougong & Xiao Xuchang 1981 The Xigaze ophiolite: a peculiar oceanic lithosphere. *Nature, Lond* **294**, 414–417.

Nisbet, E. G. & Pearce, J. A. 1977 Clinopyroxene composition in mafic lavas from different tectonic settings. *Contr. Miner. Petr.* **63**, 149–180.

Pan Yusheng 1984 Ophiolite suite was discovered in Tongtian River, Qinghai Province. *Seismol. Geol.* **6**, 44–58.

Pearce, J. A. 1975 Basalt geochemistry used to investigate past tectonic environments on Cyprus. *Tectonophysics* **25**, 41–67.

Pearce, J. A. 1982 Trace element characteristics of lavas from destructive plate boundaries. In *Andesites* (ed. R. S. Thorpe), pp. 525–547. Chichester: J. Wiley and Sons.

Pearce, J. A. & Cann, J. R. 1973 Tectonic setting of basic volcanic rocks determined using trace element analysis. *Earth planet. Sci. Lett.* **19**, 290–300.

Pearce, J. A., Lippard, S. J. & Roberts, S. 1984 Characteristics and tectonic significance of supra-subduction zone ophiolites. In *Marginal Basin. Geology* (ed. B. P. Kokelaar & M. F. Howells), *Geol. Soc. Lond. Spec. Publ.* 16, pp. 77–93.

Pozzi, J. P., Westphal, M., Girardeau, J., Besse, J. & Zhou Yaoxiu 1984 Palaeomagnetism of the Xigaze ophiolite and flysch: latitude and direction of spreading. *Earth planet. Sci. Lett* **70**, 383–394.

Prinzhofer, A., Allègre, C. J., Bao Peisheng & Wang Xibin 1984 Magmatism in southern Tibet: trace element constraints. In *Himalayan Geology. Chengdu Int. Symp. 1984.* Beijing Academia Sinica (abstr.).

Rogers, N., MacLeod, C. J. & Murton, B. J. (in press). Petrogenesis of boninitic lavas from the Limassol Forest Complex, Cyprus.

Sengör, A. M. C. 1981 The geological exploration of Tibet. *Nature, Lond.* **294**, 403–404.

Tang Youking & Wang Fangguo 1984 Primary analysis of the tectonic environment of the ophiolite in Northern Xizang. *Himalayan Geology* **II**, 99–113. (In Chinese.)

Wang Xibin, Bao Beishang & Zheng Haixiang 1984 A structurally disrupted ophiolite in the Lake area of Northern Xizang (Tibet) and its geochemistry. *Himalayan Geology* **II**, 112–141. (In Chinese.)

Wood, D. A., Joron, J.-L. & Treuil, M. 1979 A re-appraisal of the use of trace elements to classify and discriminate between magma series erupted in different tectonic settings. *Earth planet. Sci. Lett.* **45**, 326–336.

Wu Huarao & Deng Wanming 1980 Basic geological features of the Yarlung Zangbo ophiolite belt, Xizang, China. In *Ophiolites* (ed. A. Panayiotou), pp. 462–472. Nicosia Cyprus Geological Survey.

Yang Ruiyang & Deng Wanming 1986 Trace element characteristics of the volcanics in the North Xizang. *Nuclear Techniques* **2**, 17–20. (In Chinese.)

Zhang Qi & Yang Ruiyang 1986 The boninite-like pluton in ophiolite from Dengqen, Xizang, and its geological significance. *Kexue Tongbao* **31**, 405–408.

Phil. Trans. R. Soc. Lond. A **327**, 239–262 (1988) [239]
Printed in Great Britain

Palaeomagnetic results from the Tibetan Plateau

By Lin Jinlu[1] and D. R. Watts[2]

[1] *Institute of Geology, Academia Sinica, Beijing, People's Republic of China*
[2] *Department of Geology, University of Glasgow, Glasgow G12 8QQ, U.K.*

Palaeomagnetic measurements were carried out on 1325 oriented samples collected from 246 sites on a traverse of the Tibetan Plateau from Lhasa to Golmud in 1985, crossing the Lhasa Terrane, Qiangtang Terrane, and Kunlun Terrane. High blocking temperature, high coercivity, statistically grouped magnetizations were isolated from the following units: Lhasa Terrane – Cretaceous Takena Formation, mid-Cretaceous Nagqu volcanics, mid-Cretaceous Qelico volcanics; Qiangtang Terrane – Norian Batang Group volcanics, Kimmeridgian Yanshiping Group, Paleocene to Eocene Fenghuoshan Group; Kunlun Terrane – Visean to Namurian Dagangou Formation, dykes of the Triassic igneous province. The Triassic data from the Kunlun Terrane, Triassic and Lower Tertiary data from the Qiangtang Terrane and the Cretaceous data from the Lhasa Terrane indicate palaeolatitudes *ca.* 20° S of their present position within the Eurasian frame of reference. A possible interpretation is that the terranes successively accreted to Eurasia and remained in the southern position until the convergence of India drove them northward via a process of tectonic shortening and/or displacement of continental crust. The Carboniferous data from the Kunlun Terrane are consistent with moderate Southern Hemisphere latitude, well separated from Eurasia which was in the Northern Hemisphere at this time, implying the existence of ocean crust between these blocks during the Carboniferous.

1. Introduction

Palaeomagnetic data are potentially useful for resolving tectonic problems posed by the geodynamic evolution of Asia. The Phanerozoic geological history of southeast Asia has involved lateral translation of continental crust by thousands of kilometres. Although the present process is perhaps better modelled as deformation of a continuum, the past evolution must be described using discrete terranes as this is the only tractable approach, given the decrease of information with the passage of geological time. Palaeomagnetism provides the only quantitative means of determining palaeolatitude and palaeoazimuth of crustal blocks as a function of time in the absence of a marine magnetic anomaly record. Rotations between and within blocks may be detected; but with a small data set it may be difficult to distinguish local rotations from terrane-scale displacements.

For these reasons, palaeomagnetic study was included as a part of the Tibetan Geotraverse. It has been suggested that the plateau is crossed by at least three sutures, separating four terranes (Chang *et al.* 1986), including India, the Lhasa Terrane, the Qiangtang Terrane, and the Kunlun Terrane. It is not yet possible to construct polar wander paths for the last three Tibetan terranes. Local rotations obscure the palaeoazimuth determination. Remagnetization and the rather small stratigraphic range of suitable rock types on each terrane limit the amount of useful palaeomagnetic data that can be gathered. Even without polar wander paths,

measurement of the palaeomagnetic inclination with respect to bedding allows the construction of a time sequence of movement in palaeolatitude, and affinity with one or another of the major continental units can be tested.

2. Method

Table 1 lists the sampling localities, letter designations of samples, age of units, and numbers of samples and sites of the palaeomagnetic collections from the Tibetan Plateau. Figure 1 is a map of the traverse area showing the palaeomagnetic sampling localities labelled with the locality designations given in table 1.

With the exception of twentyfour block samples collected from the Dagze volcanics near Quesongsi, orientated drill cores were taken using a portable petrol-driven drill. Magnetic remanence and susceptibility were measured in the field to evaluate the potential of each lithological unit as a suitable recorder of the palaeomagnetic field. Rocks with konigsberger ratios greater than unity were regarded as especially promising. Orientations were measured with a clinometer, magnetic compass and, when possible, a solar compass.

Table 1. Palaeomagnetic sampling localities

(Listed are the locality designations, place names, latitudes, and longitudes of the sampling localities, geological unit, age, number of samples and number of sites.)

locality	place name	lat.	long.	unit	age	samples	sites
P1	Linzhou	29° 54′	91° 14′	Takena Formation	uK	42	7
P2	Linzhou	29° 57′	91° 09′	Takena Formation	uK	13	2
P3	Maqu	29° 50′	90° 44′	Takena (dolomite)	uK	23	3
P4	Quesongsi	30° 00′	90° 44′	Dagze volcanics	Tr	24	8
P5	Damxung	30° 32′	91° 03′	limestone	uC	25	2
P6	Damxung	30° 32′	91° 03′	mixtite	uC	8	1
P7	Nagqu	31° 29′	91° 49′	Diorite	?	6	1
P8	Nagqu	31° 29′	92° 02′	andesites	(96 Ma)	61	9
P9–10	Qelico	31° 42′	90° 57′	andesites	(90 Ma)	42	7
P11	Jang Co	31° 30′	90° 54′	gabbro	?	36	6
P12	Jang Co	31° 28′	90° 40′	mixtite	uC	46	9
P13	Dongqiao	31° 55′	90° 51′	Jienong Formation	mJ	11	2
P14	Tojiu Pass	32° 33′	91° 51′	Yanshiping Group	mJ	41	7
P15	114 station	32° 26′	91° 48′	flysch	mJ	33	6
P16–18	Amdo	32° 13′	91° 29′	Takena Formation	uK	62	10
P19	Yanshiping	33° 36′	92° 04′	Yanshiping Group	mJ	104	17
P20	Yanshiping	33° 34′	92° 03′	Yanshiping Group	mJ	31	6
P21	Kaixinling	34° 08′	92° 23′	Kaixinling Group	uP	51	8
P22	Kaixinling	34° 06′	92° 23′	Kaixinling Group	uP	43	7
P23	Erdaogou	34° 34′	92° 42′	Fenghuoshan Group	Pal-Eo	87	20
P24	Erdaogou	34° 37′	92° 47′	Fenghuoshan Group	Pal-Eo	72	20
P25	Yaxico	34° 19′	93° 28′	Batang Group	uTr	39	6
P26	Xiaonamchuan	35° 51′	94° 21′	volcanics	uTr	29	5
P27	Xiaonamchuan	35° 48′	94° 21′	volcanics	uTr	14	2
P28	Kunlun pass	35° 38′	94° 04′	lake varves	Q	1	1
P29	Yeniuqou	35° 52′	94° 20′	volcanics	P?	26	4
P30–31	Xidatan	35° 46′	94° 20′	Xidatan granite	?	49	8
P32	816 station	36° 10′	94° 47′	andesite dykes	240 Ma	80	22
P33	Dongdatan	35° 47′	94° 58′	redbeds	?	21	3
P34	823 station	36° 05′	94° 49′	volcanics	D	29	5
P35–36	823 station	36° 03′	94° 51′	volcanics	C?	49	9
P37–38	823 station	36° 05′	94° 49′	volcanics	D	33	6
P39–40	Dagangou	36° 02′	95° 00′	Dagangou Formation	C	48	9
P41	Dagangou	36° 02′	95° 00′	Dagangou Formation	C	24	4
P42–43	Golmud	36° 13′	94° 43′	andesite dykes	240 Ma	22	4

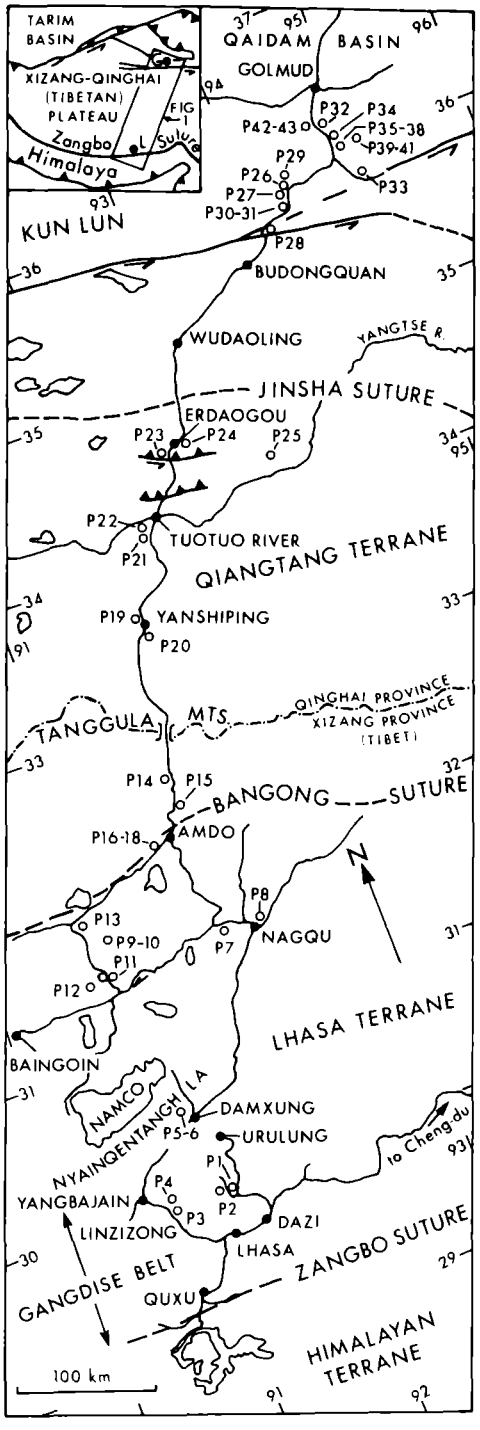

FIGURE 1. Map of Geotraverse area of Tibet showing palaeomagnetic sampling localities, P1–P43.

Samples were cut into cylindrical specimens 2.5 cm in diameter and 2.3 cm high. Magnetic measurements were carried out at the University of Leeds (L.J.L.) using a cryogenic magnetometer and fluxgate spinner magnetometer, and at the University of Glasgow (D.R.W.) with a fluxgate spinner magnetometer. The error of individual measurements was determined at each stage. Alternating field demagnetizations were carried out with a tumbler device

(McElhinny 1966) at Leeds, and a three axis, static, microcomputer-controlled demagnetizer working at 186 Hz at Glasgow. Thermal demagnetizations were carried out with a Helmholtz coil nulled oven (McElhinny *et al.* 1971) at Leeds and a microcomputer-controlled bench type, mu-metal shielded oven at Glasgow. Selected redbed samples were chemically demagnetized by cutting slices in the specimens and immersing them in 8 N HCl with the earth's field nulled by mu-metal boxes. Each specimen was demagnetized in detail. The behaviour of the magnetization was continuously monitored using orthogonal projections (Zijderveld 1967), displayed after each step. In some cases, alternating field demagnetization failed to remove a significant percent of the magnetization after a maximum field treatment. The investigation of such samples was continued using thermal demagnetization.

The final evaluation of the component structure of each specimen was done using orthogonal projections interactively with the principal component analysis algorithm of Kent *et al.* (1983) which utilizes the individual errors of measurement. Data were exchanged between Leeds and Glasgow via computer tape and the JANET network. Principal component directions and intensities were written into computer files which were edited, isolating magnetizations with similar directions and physical properties. Mean site directions and statistics were computed from these files.

Analysis analogous to the great circle method of Halls (1978) was also employed. The Kent *et al.* algorithm fits planes as well as lines to distributions of points in a demagnetization sequence. For each data set, the poles to the best-fitting planes were written into a computer file, plotted on an equal area projection and examined for great circle distributions. The pole of this great circle is the direction of magnetization that is common to all of the planes and is identical to the direction that would be identified by converging demagnetization circles.

The properties of the magnetization, mean site directions and associated statistics for those lithological units which have a palaeomagnetic signal are discussed in turn, according to the terrane in which they are found. A number of units listed in table 1 were found to have magnetizations with the following properties and are not representative of the palaeomagnetic field:

1. magnetizations which displayed random walk trajectories on orthogonal projections without linear or planar distribution of points;

2. magnetizations with low blocking temperature (generally less than 200 °C and/or low blocking fields (generally less than 100 oersted);

3. magnetizations with a random distribution (estimate of Fisher's precision parameter, k, less than 4).

3. Properties and directions of magnetization

(*a*) *Lhasa Terrane*

(i) *Takena Formation* (P1, P2)

Fine-grained sandstone and siltstone were sampled from two localities, P1 and P2, near Linzhou. The two sections have different attitudes and therefore allow a fold test. A heavy mineral seam 10 cm thick was collected from section P1, site T7.

The problem of the age of this unit is discussed by Smith & Xu (this volume) and is typical of the difficulty posed by continental redbeds. Following Smith & Xu, the age of the redbed member of the Takena Formation is taken to be early Upper Cretaceous.

Figure 2 illustrates the behaviour of the magnetization characteristic of these sections.

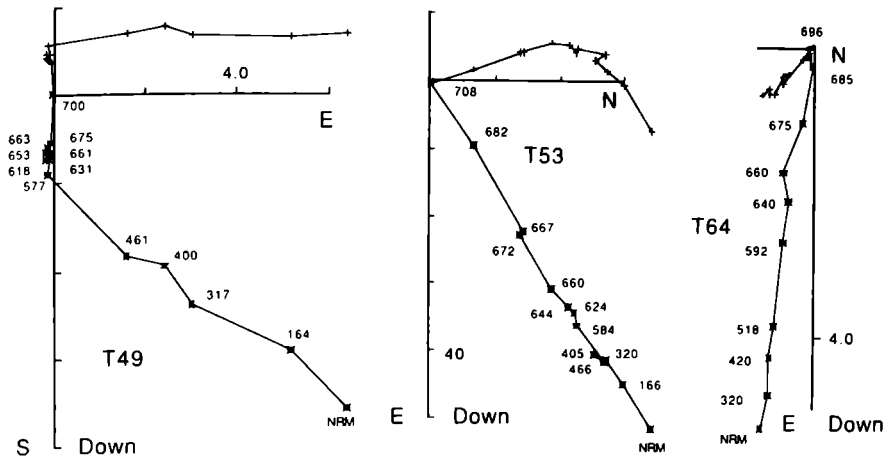

FIGURE 2. Orthogonal projections of thermal demagnetization results from the Takena Formation redbeds. Asterisks denote the intersection of the magnetization vector with the vertical plane, crosses denote the intersection with the horizontal plane. Units of the axes are amp/metre $\times 10^{-3}$.

Specimens T49 and T64 are typical fine-grained red sandstones. Specimen T53 was collected from the heavy mineral seam. The magnetization deemed representative of the palaeomagnetic field is the high blocking temperature component revealed between demagnetization temperatures of 630–660 °C at the lower end of the range and up to 696–708 °C. In many specimens this component was revealed between a narrow range of temperatures near the Neel temperature of hematite as illustrated by T53 and T64. The heavy mineral seam has the same palaeomagnetic signature as the fine sandstone but the NRM (natural remanent magnetization) intensities are 40 mamp/metre, about an order of magnitude greater than the sandstone at 4 mamp/metre.

The mean site directions, associated statistics, pole positions and palaeolatitudes derived from the Takena Formation, before and after structural correction, are summarized in table 2.

TABLE 2. TAKENA FORMATION: MEAN SITE DIRECTIONS, STATISTICS, POLE POSITIONS AND PALAEOLATITUDES

(The parameters are given before (left columns) and after (right columns) structural correction. *N* is the number of samples/sites from which a determination is made; *Dec* is the mean declination; *Inc* is the mean inclination; *k* is the estimate of Fisher's precision parameter; alpha95 is the apical half angle of the cone of 95 % confidence; dp is the estimate of the error of the palaeolatitude; dm is the estimate of the error of palaeoazimuth.)

Unit: Takena Formation (P1, P2)
Age: uK
Location: Linzhou (29° 54′, 91° 14′; 29° 57′, 91° 09′)

site	*N*	*Dec*	*Inc*	*k*	alpha95	*Dec*	*Inc*	*k*	alpha95
T01	4	19	48	58	12.1	6	15	59	12.1
T02	4	17	48	52	12.9	5	15	52	12.9
T03	7	19	45	47	8.9	7	12	47	8.9
T04	6	358	53	42	10.5	351	17	42	10.5
T05	10	6	49	19	11.5	357	14	19	11.5
T06	6	343	54	375	3.5	338	11	375	3.5
T07	6	28	85	9	23.0	355	17	9	23.0
T08	8	13	87	32	10.0	355	15	32	10.0
Mean	8	8	59	19	13.0	357	15	70	6.7

Pole: lat = 78, long = 123,
dp = 14.5, dm = 22.5
Palaeolatitude: = 39.8 ± 14.5°

Pole: lat = 68°, long = 279°
dp = 3.5, dm = 6.9
Palaeolatitude: = 7.6 ± 3.5°

The directions of magnetization have the smallest dispersion after structural correction, passing the fold test at the 99% level of confidence. Secondary magnetizations are present and are thermally distributed but do not define a meaningful population. This reproduces the results of Achache *et al.* (1984) for this formation.

(ii) *Nagqu mid-Cretaceous volcanics* (P8)

This section, P8, comprises andesites interbedded with basalts of the mid-Cretaceous volcanic province (see Pearce & Mei, this volume). In the Nagqu area, these rocks have $^{40}Ar/^{39}Ar$ ages between 100 and 95 Ma.

Typical response to demagnetization is shown by the orthogonal projections in figure 3. Specimen ZN15a is subjected only to thermal demagnetization. The orthogonal projection reveals a high blocking temperature, thermally discrete magnetization removed between 532 and 641 °C. Specimens ZN27a and ZN45a were treated by alternating field demagnetization, followed by thermal demagnetization. The characteristic magnetization is only partially removed by alternating fields up to 1000 oersted. No persistent, statistically viable secondary magnetizations were found.

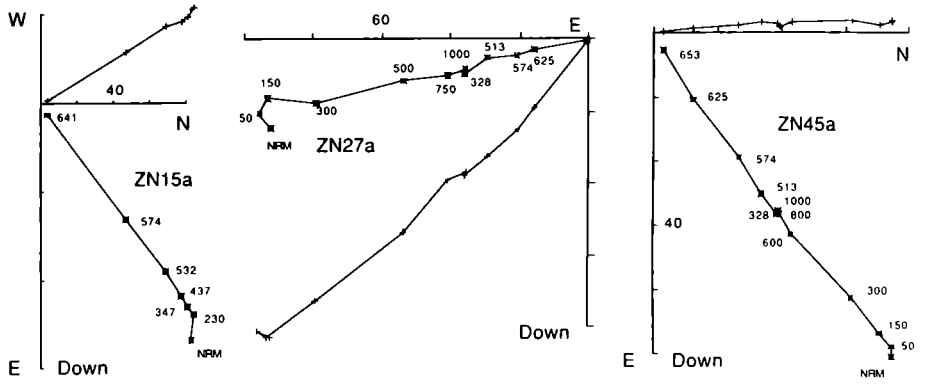

FIGURE 3. Orthogonal projections of thermal and alternating field demagnetization results from the Nagqu mid-Cretaceous volcanics. Convention of plotting is as in figure 2.

Table 3 summarizes the mean site directions, statistics, pole positions and palaeolatitude estimates, before and after structural correction. The estimate of Fisher's (1953) precision parameter, k, drops from 74 to 54 after structural correction. This may either reflect a remagnetization or an imprecise attitude determination of the individual sites. The measurement of the strike and dip of this section is difficult as the indicators of bedding are vague and equivocal. The structurally corrected mean direction reproduces the result of Achache *et al.* (1984), who noted that the mean direction of magnetization seems anomalously steep compared to other units with the same age. This may be related to the difficulty of determining a precise structural attitude from this locality.

(iii) *Qelico section, mid-Cretaceous volcanics* (P9, P10)

Oriented core samples were collected from the andesites of the north Lhasa Terrane mid-Cretaceous volcanic province (Pearce & Mei, this volume) from localities P9 and P10. At P9 the andesites underlie redbeds of probable Cretaceous age. $^{40}Ar/^{39}Ar$ ages are between 95 and 85 Ma near these localities (Coulon *et al.* 1986).

Specimens from this unit showed two types of response to demagnetization as shown in figure 4. The response which reveals the palaeomagnetic signal is illustrated by projections of demagnetizations of specimens QL01a and QL03. Thermal demagnetization removes a thermally distributed secondary magnetization to reveal a high blocking temperature magnetization which is taken to be a record of the palaeomagnetic field. This magnetization has

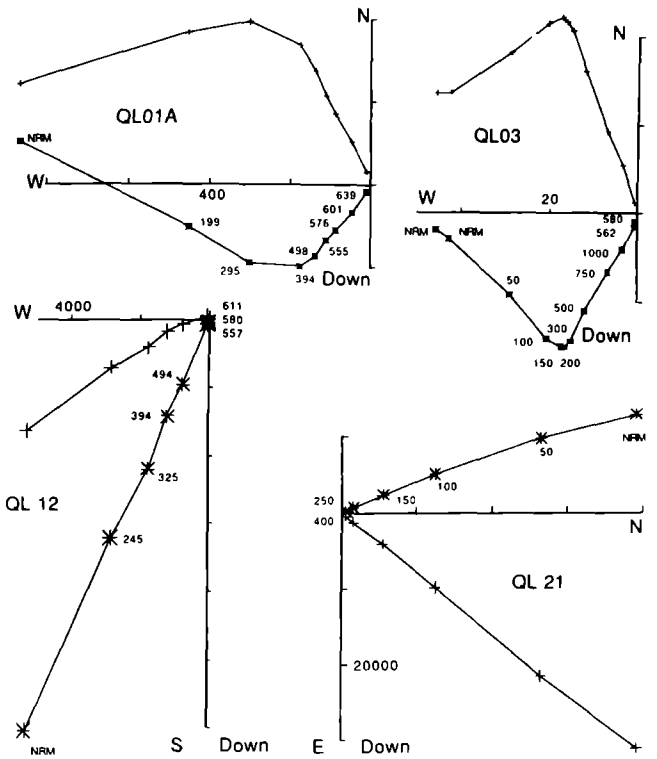

FIGURE 4. Orthogonal projections of thermal and alternating field demagnetization results from the Qelico mid-Cretaceous volcanics. Convention of plotting is as in figure 2.

TABLE 3. NAGQU SECTION OF MID-CRETACEOUS VOLCANICS: MEAN SITE DIRECTIONS, STATISTICS, POLE POSITIONS AND PALAEOLATITUDES

(The arrangement and parameters are as in table 2.)

Unit: Nagqu Cretaceous Andesites (P8)
Age: Cretaceous 96 Ma
Location: Nagqu (31° 29′, 92° 02′)

site	*N*	*Dec*	*Inc*	*k*	alpha95	*Dec*	*Inc*	*k*	alpha95
ZN01	4	314	54	354	4.9	354	38	352	4.9
ZN02	4	321	59	573	3.8	2	38	584	3.8
ZN03	5	323	52	344	4.1	357	33	345	4.1
ZN04	5	325	52	930	2.5	358	32	929	2.5
ZN06	3	314	50	713	4.6	350	36	724	4.6
ZN07	4	353	57	128	8.1	16	26	128	8.1
ZN08	2	338	57	1020	7.8	8	31	1062	7.7
ZN09	3	307	47	350	6.6	344	38	346	6.6
ZN10	3	310	50	509	5.5	348	38	506	5.5
Mean	9	322	54	74.3	6.0	358	35	54	6.0

Pole: lat = 58, long = 18
dp = 5.9, dm = 8.4
Palaeolatitude: 35 ± 5.9°

Pole: lat = 78, long = 282
dp = 4.0, dm = 6.9
Palaeolatitude: 19 ± 4.0°

blocking temperatures between 498 and 639 °C. Alternating field demagnetization removes the secondary magnetization at about 200 oersted, and a part of the characteristic magnetization is removed at higher fields, up to 1000 oersted. Thermal demagnetization completes the removal of the characteristic magnetization as illustrated by QL03.

The second type of behaviour is illustrated by thermal demagnetization of QL12 and alternating demagnetization of QL21. Such samples are strongly magnetized with NRMs at least an order of magnitude greater than samples with the previous type of magnetization. This second behaviour is characterized by a univector appearance on the orthogonal projection and thermally distributed response as shown by QL12. This type of magnetization is also quickly removed by alternating field demagnetization with 99% of the NRM removed at 400 oersted.

The thermally distributed, low blocking temperature magnetization has a high between-site dispersion. This population of magnetizations may be due to lightning strikes or to large multi-domain carriers of magnetization. The mean directions in table 4 for this unit are calculated

TABLE 4. QELICO SECTION OF MID-CRETACEOUS VOLCANICS: MEAN SITE DIRECTIONS, STATISTICS, POLE POSITIONS AND PALAEOLATITUDES

(The arrangement and parameters are as in table 2.)

Unit: Andesite Volcanics (P9–10)
Qelico, near Jang Co (31° 42′, 90° 57′)
Age: 90 Ma

site	*N*	*Dec*	*Inc*	*k*	alpha95	*Dec*	*Inc*	*k*	alpha95
QL01	5	337	30	825	2.7	350	24	835	2.6
QL02	4	343	36	35	15.8	358	28	35	15.8
QL03	3	16	−49	3	84.9	343	−62	3	84.9
QL04	5	32	−20	21	17.1	24	−41	21	17.1
QL05	5	212	73	716	2.9	97	77	711	2.9
QL06	4	319	49	36	15.5	348	47	35	15.7
QL07	7	327	59	360	3.2	331	42	366	3.2
Mean	4	333	44	29.4	17.2	347	36	32	16.5
		Pole: lat = 65, long = 354				Pole: lat = 74, long = 318			
		dp = 13.5, dm = 21.6				dp = 11.1, dm = 19.1			
		Palaeolatitude: 25.8 ± 13.5°				Palaeolatitude: 19.8 ± 11.1°			

exclusively from the high blocking temperature thermally discrete magnetizations first described. The two localities have different attitudes; structural correction increases the k of the population of the discrete magnetizations, but the increase is not statistically significant.

(*b*) *Qiangtang Terrane*

(i) *Batang Group volcanics* (P25)

This section of andesite–basalt lavas is described by Pearce & Mei (this volume). The age is determined by the Norian marine carbonates that conformably overlie these rocks (Smith & Xu, this volume).

Figure 5 shows orthogonal projections that summarize the response to thermal and alternating field treatment. Specimens QT2 and QT4 illustrate nearly univector magnetizations with blocking fields up to 1800 oersted and blocking temperatures between 529 and 572 °C. As illustrated by QT16 and QT38, a number of specimens have significant secondary magnetizations that dominate the NRM. These secondary magnetizations are removed at 600 oersted

and 434 °C to reveal the characteristic magnetization with the same direction as the high blocking field, thermally discrete univector magnetizations.

The mean site directions, statistics, pole positions, and estimates of palaeolatitude are summarized in table 5, before and after structural correction. The section has a substantial dip, but the attitude of the volcanics is well-determined by the overlying bedded marine carbonates. Unfortunately only the one limb of the structure could be sampled so a fold test is not possible.

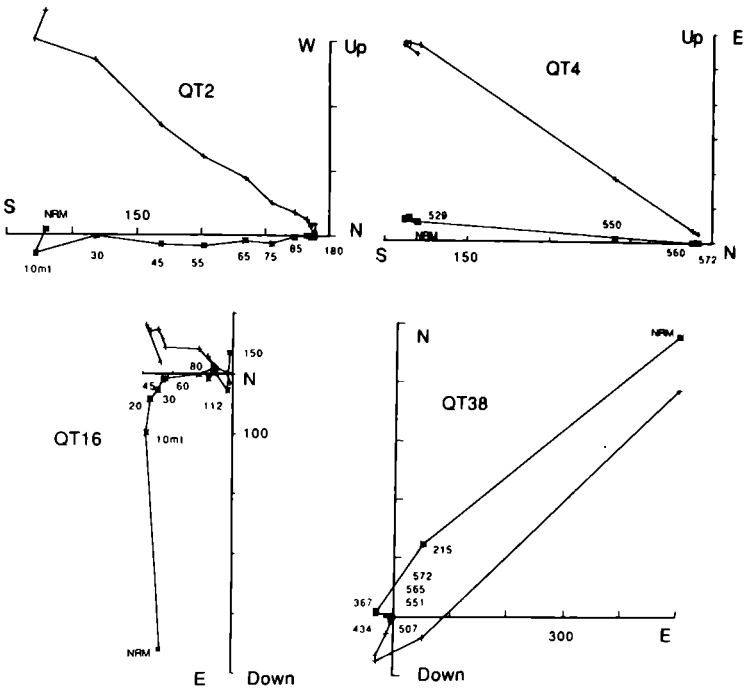

FIGURE 5. Orthogonal projections of thermal and alternating field demagnetization results from the Batang Group volcanics. Convention of plotting is as in figure 2.

TABLE 5. BATANG GROUP VOLCANICS: MEAN SITE DIRECTIONS, STATISTICS, POLE POSITIONS AND PALAEOLATITUDES

(The arrangement and parameters are as in table 2.)

Unit: Batang Group volcanics (P25)
Location: Yaxico (34° 19′, 93° 28′)
Age: Norian (205 Ma)

site	*N*	*Dec*	*Inc*	*k*	alpha95	*Dec*	*Inc*	*k*	alpha95
QT01	6	215	−2	281	4.0	234	−58	282	4.0
QT02	6	223	18	23	14.2	228	−36	23	14.2
QT03	6	204	13	53	9.3	207	−47	53	9.3
QT04–05	7	192	27	4	35.0	192	−34	4	35.0
QT06	9	210	−2	90	5.5	224	−60	90	5.5
Mean	5	209	11	23	16.2	215	−48	23	16.2
		Pole: lat = 42°, long = 234°				Pole: lat = 59°, long = 184°			
		$dp = 8.3°$, $dm = 16.4°$				$dp = 13.8°$, $dm = 21.2°$			
		Palaeolatitude: $-6 \pm 8.6°$				Palaeolatitude: $29 \pm 13.8°$			

(ii) *Yanshiping Group* (P19, P20)

The Yanshiping Group is an extensive sequence of redbeds 2 kilometres thick with occasional marine incursions of Bathonian to Kimmeridgian age (Smith & Xu, this volume). Two localities, P19 and P20, were sampled. P19 is a vertical sequence of redbeds along the road in and just north of Yanshiping. P20 is a moderately dipping section of limestones interbedded with red sandstones about 3 kilometres south of Yanshiping.

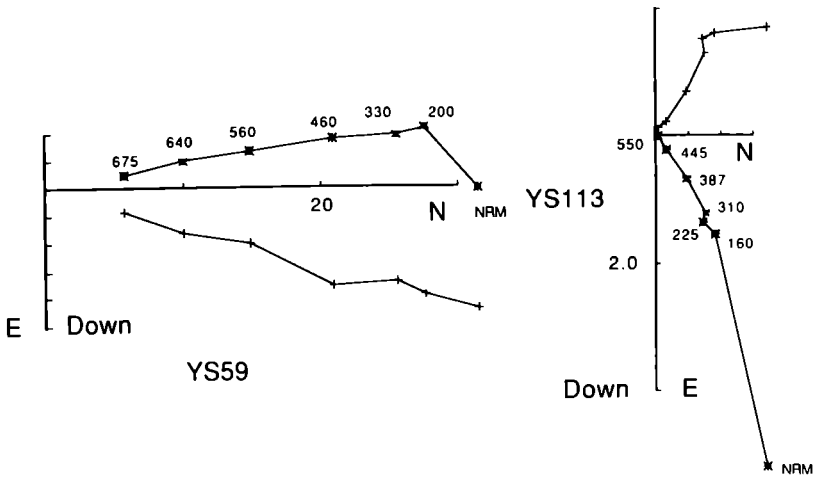

FIGURE 6. Orthogonal projections of thermal and alternating field demagnetization results from the Yanshiping Group redbeds (YS59) and carbonates (YS113). Convention of plotting is as in figure 2.

Figure 6 shows the response to thermal demagnetization typified by the redbed specimen, YS59, and the limestone YS113. The magnetization of the redbeds was nearly univector with low intensity, randomly oriented secondary magnetizations. Blocking temperatures of the redbed magnetization are distributed from 200 to 675 °C. The NRM of the limestone is typically about 4 mamp/metre, about an order of magnitude less than the redbeds. Thermal demagnetization of the limestone revealed a distributed magnetization with maximum blocking temperatures up to 550 °C. The carrier of the magnetization in the redbeds is likely to be hematite and in the limestone, magnetite.

The mean site directions of these magnetizations from the Yanshiping Group are given in table 6. Figure 7 shows two equal area projections of the total population of magnetization directions. Although there is a significantly lower dispersion after structural correction, the lowest dispersion actually occurs at an intermediate state. Figure 8 is a plot of the estimate k, of Fisher's precision parameter of the total distribution as a function of the percentage of the total structural correction. The maximum k at an intermediate stage in the structural correction indicates that the magnetization in either or both localities was acquired during the folding of this sequence. This demonstration shows that the palaeomagnetic record from these rocks is useless as an indicator of palaeolatitude. If the magnetization was acquired during the folding, bedding is no longer representative of palaeohorizontal.

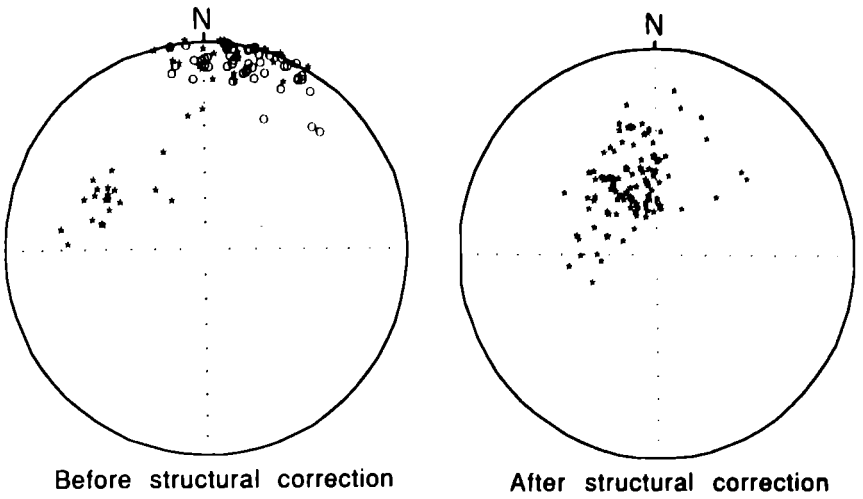

FIGURE 7. Equal area projections of Yanshiping Group characteristic directions of magnetization before (left) and after (right) structural correction. Asterisks denote intersection with the lower hemisphere. Circles denote intersection with the upper hemisphere.

TABLE 6. YANSHIPING GROUP: MEAN DIRECTION, STATISTICS, POLE POSITIONS AND PALAEOLATITUDES

(The arrangement and parameters are as in table 2. Sites YS01–YS15 were collected from locality P19. Sites YS16–YS23 were collected from locality P20.)

Unit: Yanshiping Group (P19, P20)
Age: Bathonian to Kimmeridgian (145–166 Ma)
Location: (33° 36′, 92° 04′)

site	*N*	*Dec*	*Inc*	*k*	alpha95	*Dec*	*Inc*	*k*	alpha95
YS01	7	4	14	148	4.9	275	61	148	4.9
YS02	8	358	−5	81	6.2	313	56	81	6.2
YS03	5	356	4	46	11.4	315	57	36	12.9
YS04	8	17	0	81	6.2	352	66	79	6.3
YS05	6	15	−7	125	6.0	356	62	125	6.0
YS06	7	10	0	206	4.2	325	69	206	4.2
YS07	6	15	−3	43	10.4	329	64	43	10.4
YS08	8	23	−6	123	5.0	346	69	123	5.0
YS09	9	16	−4	48	7.5	328	61	48	7.5
YS10–11	3	359	0	38	20.3	325	56	38	20.2
YS12	4	357	7	13	26.2	308	61	14	25.6
YS13	5	30	−22	27	14.9	35	49	27	14.9
YS14	3	357	−15	72	14.6	344	50	72	14.6
YS15	4	5	11	24	19.1	297	72	24	19.1
YS16	3	295	45	13	35.6	348	39	13	35.6
YS17–18	4	299	48	30	16.9	352	37	30	16.9
YS19–20	3	301	43	11	39.0	345	38	12	36.5
YS21	5	294	44	161	6.0	352	43	161	6.0
YS22	3	292	40	96	12.7	349	45	101	12.3
YS23	3	287	45	161	9.7	355	48	161	9.8
Mean	20	353	14	4.5	17.4	339	58	21.3	7.2
		Pole: lat = 63, long = 287 $dp = 9.1$, $dm = 17.8$ Palaeolatitude:				Pole: lat = 72, long = 25 $dp = 7.8$, $dm = 10.6$ Palaeolatitude: = 39 ± 7.8°			

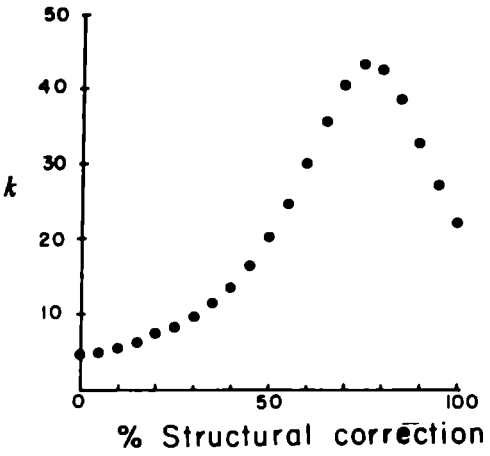

FIGURE 8. Plot of the estimate of Fisher's precision parameter, k, against percent of structural correction for the Yanshiping Group characteristic directions of magnetization.

(iii) *Fenghuoshan Group* (P23, P24)

The Fenghuoshan Group is a thick sequence of continental redbeds with thin lacustrine limestones yielding a fauna of Palaeocene to early Eocene age. These sediments form monotonously dipping sequences riding on thrust faults. Two sections were sampled from this Group at localities P23 and P24.

Figure 9 illustrates the typical response to demagnetization experiments of the samples collected from locality P23. The sister specimens FH15a and FH15b, from the same sample, were treated by chemical and thermal demagnetization methods respectively. Comparison of

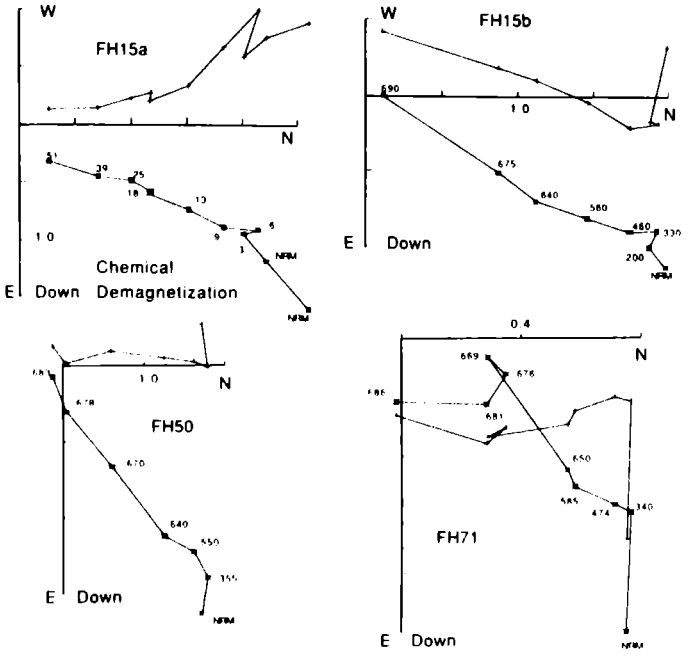

FIGURE 9. Orthogonal projections of chemical and thermal demagnetization results from the Fenghuoshan Group redbeds, locality P23. Convention of plotting is as in figure 2.

the response using orthogonal projections shows that chemical leaching simultaneously removes a secondary magnetization and a more stable magnetization. Thermal demagnetization quickly removes the secondary component to reveal a high blocking temperature thermally discrete magnetization that has a linear trajectory but does not move directly toward the origin of the diagram. At the last stages of treatment the magnetizations were very weak, near the sensitivity of the cryogenic magnetometer, and the errors of the individual measurements were greater than 10°. It was not possible to isolate a component of magnetization near the origin of the orthogonal projections. In the case of FH71 the characteristic magnetization is revealed between steps of 585 and 669 °C.

TABLE 7. FENGHUOSHAN GROUP: LOCALITY P23, MEAN SITE DIRECTIONS, STATISTICS, POLE POSITIONS AND PALAEOLATITUDES

(The arrangement and parameters are as in table 2.)

Unit: Fenghuoshan Group (P23)
Age: Palaeocene–Eocene
Location: Erdaogou (34° 34′, 92° 23′)

site	*N*	*Dec*	*Inc*	*k*	alpha95	*Dec*	*Inc*	*k*	alpha95
FH01	7	352	64	12	18.2	351	17	12	18.2
FH02	6	18	59	17	16.8	5	15	17	16.8
FH03	8	359	33	14	15.0	1	−10	14	15.0
FH04	9	20	52	39	8.3	15	8	37	8.6
FH05	5	69	64	69	9.3	33	31	69	9.3
FH06	6	38	57	8	25.5	15	20	8	25.5
FH07	6	38	39	96	6.9	25	4	96	6.9
FH08	5	30	62	71	9.2	16	24	70	9.2
FH09	6	15	51	79	7.6	10	12	79	7.6
FH10–11	3	15	64	35	21.1	0	20	35	21.1
FH12	3	20	49	61	15.9	9	8	61	15.9
FH13–14	7	41	58	10	19.9	21	20	10	19.6
FH15	5	12	55	24	15.9	6	13	2	16.0
FH18	4	347	52	118	8.5	352	5	117	8.5
FH19	4	28	63	104	9.1	2	24	103	9.1
Mean	15	20	56	31	6.9	9	14	29	7.2
		Pole: lat = 73, long = 169				Pole: lat = 61, long = 253			
		$dp = 7.2$, $dm = 10.0$				$dp = 3.8$, $dm = 7.4$			
		Palaeolatitude: = $36.9 \pm 7.2°$				Palaeolatitude: = $7.3 \pm 3.8°$			

Table 7 summarizes the mean site directions, associated statistics and pole positions, before and after structural correction. All of the high blocking temperature magnetizations are of normal polarity and the mean direction, computed from all of the sites, is near the present-day field direction for this site, before structural correction is applied. The structural correction takes the mean direction of magnetization to a shallow inclination.

Figure 10 shows the results of thermal demagnetizations of specimens from locality P24, near Erdaogou. Chemical demagnetization was not successful because of the high carbonate content of these sandstones. Typical responses to thermal demagnetization are shown in specimens FE03, FE04, FE06 and FE28. The demagnetization trajectory does not move toward the origin of the orthogonal projections, and in some cases, moves past the origin, into another quadrant. Repeated, closely-stepped, thermal treatment usually failed to reveal the direction of the higher blocking temperature magnetization. However, a component is shown in most specimens from this section, isolated between 350 °C to, generally, 580 °C. The upper limit of the temperature

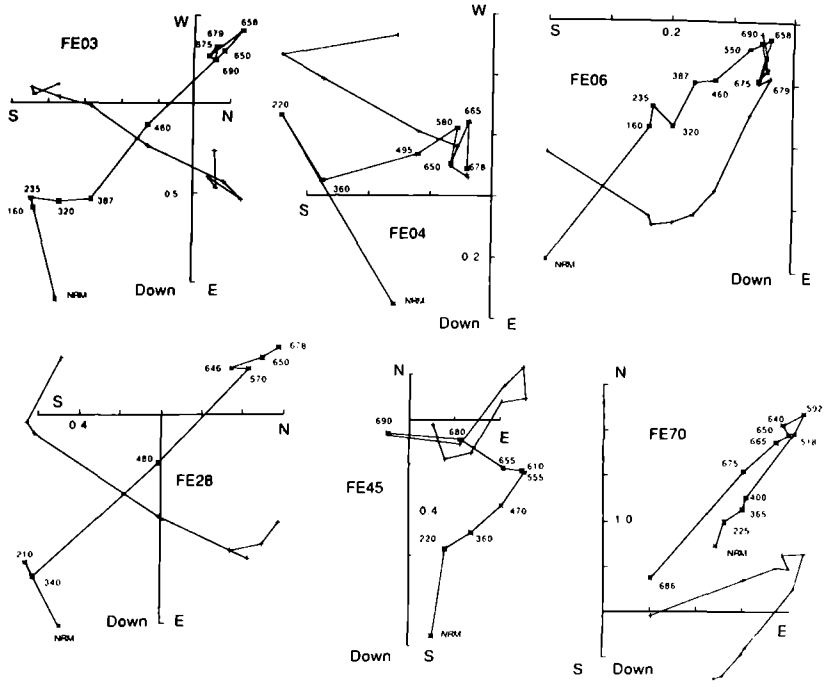

FIGURE 10. Orthogonal projections of thermal demagnetization results from the Fenghuoshan Group redbeds, locality P24. Convention of plotting is as in figure 2.

does vary, sometimes persisting up to 660 °C. Examination of each result depicted in figure 10 shows a component of magnetization with blocking temperatures in a range consistent with magnetite or titantomagnetite as a carrier. FE45 shows this magnetite-carried component superimposed on complex behaviour at temperatures higher than 555 °C. Only rarely is the highest blocking temperature magnetization revealed as illustrated by FE70. The magnetite-carried remanence is shown in this specimen as the lower blocking temperature component between treatments of 365 and 592 °C.

Table 8 lists the mean site directions, statistics and pole positions and palaeolatitudes of the lower-blocking temperature magnetization which is all that can be isolated by detailed demagnetisation experiments on specimens from this section. The population of the high-blocking temperature magnetization such as exhibited by specimen FE70, is too sparse for a meaningful average to be calculated.

The mean direction of the lower-blocking temperature magnetization is southwest and down before structural correction. The tilt correction of the uniformly dipping section takes the mean to a southeast and up direction which could be representative of a Tertiary reversed palaeomagnetic field. In neither case, before or after the structural correction, is this a present day field direction.

The lower-blocking temperature magnetization may not necessarily be an overprint. It could be an early magnetization carried either by detrital or early diagentic magnetite with an overprint carried by later developed hematite.

Figure 11 is an equal area projection of the directions of magnetization from the two sections of the Fenghuoshan Group that were collected, before and after structural correction. Structural correction carries the distribution of magnetizations into a somewhat normal and

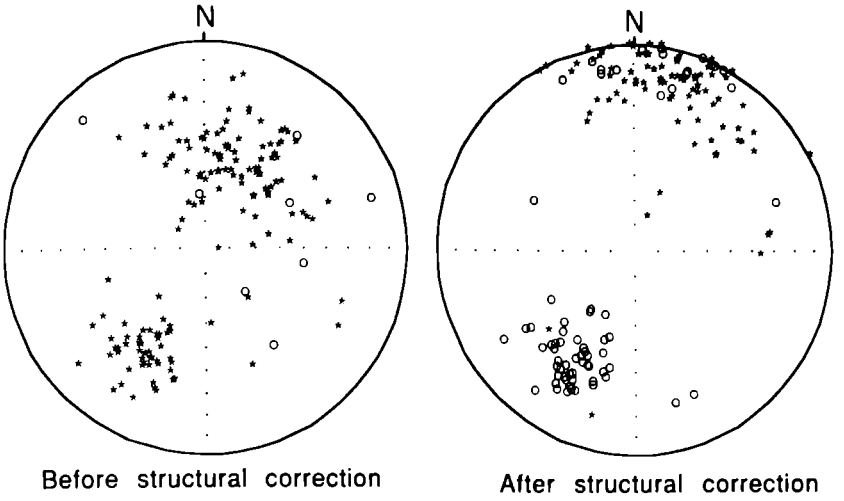

FIGURE 11. Equal area projection of Fenghuoshan Group characteristic magnetization directions before (left) and after (right) structural correction. Convention of plotting is as in figure 7.

TABLE 8. FENGHUOSHAN GROUP: LOCALITY P24, MEAN SITE DIRECTIONS, STATISTICS, POLE POSITIONS AND PALAEOLATITUDES

(The arrangement and parameters are as in table 2.)

Unit: Fenghuoshan Group (P24)
Age: Palaeocene–Eocene
Location: Erdaogou (34° 34′, 92° 47′)

site	*N*	*Dec*	*Inc*	*k*	alpha95	*Dec*	*Inc*	*k*	alpha95
FE01	3	226	58	15	32.9	217	−23	15	32.9
FE02	6	215	29	20	15.3	218	−50	20	15.3
FE03	3	232	43	8	46.3	227	−31	8	46.3
FE04–07	6	224	35	9	24.5	225	−38	9	23.4
FE08–09	6	210	38	50	9.6	210	−35	37	11.2
FE10–12	8	203	36	25	11.4	203	−38	25	11.4
FE13–14	4	223	35	46	13.6	223	−36	50	13.1
FE16	3	213	47	96	12.6	213	−30	97	12.6
FE17	8	214	46	54	7.6	214	−31	54	7.6
FE18	3	210	50	65	15.4	211	−30	86	13.4
FE19	3	207	42	124	11.1	207	−30	124	11.1
FE20	4	209	40	70	11.0	209	−32	71	11.0
Mean	12	215	42	64	5.5	215	−34	79	4.9
		Pole: lat = −22, long = 58				Pole: lat = 55, long = 201			
		$dp = 4.1$, $dm = 6.8$				$dp = 3.2$, $dm = 5.6$			
		Palaeolatitude: = $-24 \pm 4.1°$				Palaeolatitude: = $18.4 \pm 3.2°$			

reversed distribution, but the mean directions of the two populations are not antipodal. The mean of the normal magnetizations has a distinguishably shallower inclination than the mean of the reversed population. Because the two populations of magnetization are distinct, in terms of their polarity, physical properties and mean directions, they are treated separately for the purpose of calculating the pole positions and estimating palaeolatitudes.

(c) *Kunlun Terrane*

(i) *Dagangou Formation* (P39–40, P41)

The Dagangou Formation is found in the northern Kunlun Mountains, comprising several kilometres of red siltstones, sandstones and arkoses conformably overlain by a marine limestone/shale sequence of latest Visean or early Namurian age (Smith & Xu, this volume).

The siltstone members of this unit were collected at two localities (P39–40 and P41). Typical demagnetization results from P41 are shown in figure 12 and from locality P39–40 in

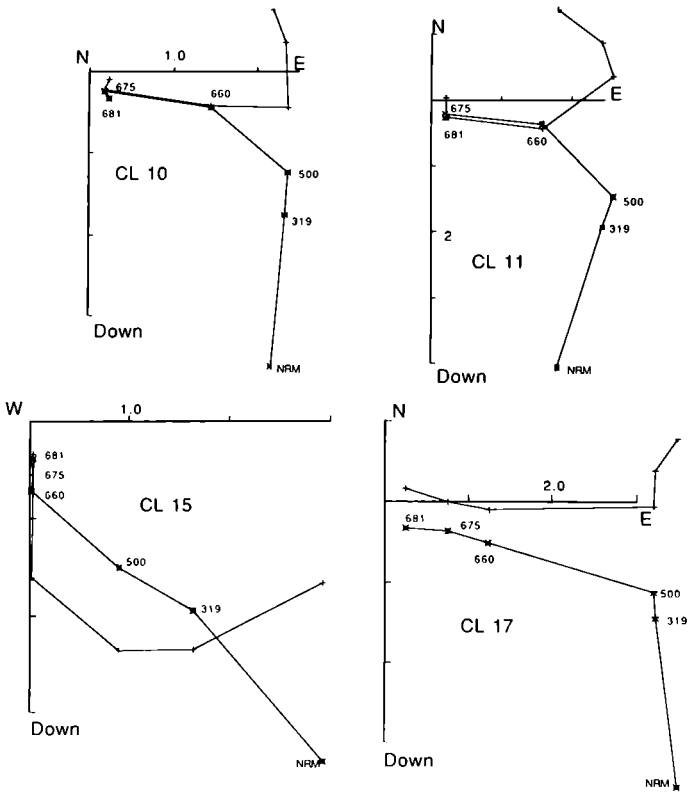

FIGURE 12. Orthogonal projections of thermal demagnetization results from the Dagangou Formation, locality P41. Convention of plotting is as in figure 2.

figure 13. The characteristic magnetization from P41 is thermally discrete and revealed between demagnetization steps of approximately 660 to 681 °C. The behaviour was rather more variable in samples from locality P39–40. Secondary magnetizations are common and sometimes dominate the NRM as illustrated by the behaviour of CS48. Even in such samples it was possible to isolate a high blocking temperature magnetization which is characteristic of the Dagangou Formation at this locality. In all samples, the characteristic magnetization has blocking temperatures between 580 and 678 °C.

The mean directions, statistics, pole positions and estimated palaeolatitudes for section P41 are given in table 9, and those derived from P39 40 in table 10. The localities are dealt with separately because the declination of the characteristic magnetization found in section P39–40 is distinguishable from that found in section P41. The inclinations, after structural correction, are the same.

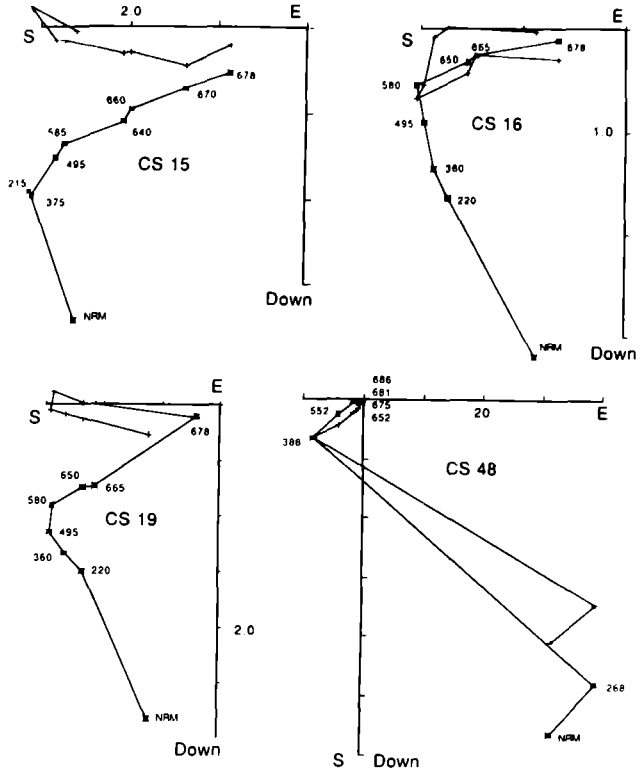

FIGURE 13. Orthogonal projections of thermal demagnetization results from the Dagangou Formation, locality P39–40. Convention of plotting is as in figure 2.

TABLE 9. DAGANGOU FORMATION: LOCALITY P41, MEAN SITE DIRECTIONS, STATISTICS, POLE POSITIONS AND PALAEOLATITUDES

(The arrangement and parameters are as in table 2. The mean direction after correction for a 70° plunge to the west is also given.)

Unit: Dagangou Formation (P41)
Age: Visean to Namurian (325 Ma)
Location: (36° 02′, 95° 00′)

site	*n*	*Dec*	*Inc*	*k*	alpha95	*Dec*	*Inc*	*k*	alpha95
CL01	4	79	29	56	12.3	123	40	56	12.3
CL02	2	89	63	20	59.9	168	44	20	59.9
CL03	6	90	23	15	18.1	119	32	15	18.1
CL04	5	76	23	8	28.8	99	29	8	28.2
Mean	4	83	35	16	23.4	125	39	12	27.8
		Pole: lat = 17, long = 173				Pole: lat = −12°, long = 146°			
		dp = 15.5°, dm = 27.0°				dp = 19.8, dm = 33.2			
		Palaeolatitude: = 19 ± 198°				Palaeolatitude: = −22 ± 19.2°			
		Mean corrected for plunge 70° west:				164	39	12	27.8

Structural evidence suggests that locality P39–40 is on the limb of a fold which is plunging westwards at 70°. No information on a possible plunge of locality P41 is available, but it is interesting to note that if both localities are corrected for a steep plunge to the west, the mean declinations swing around to the south, converging towards each other (see tables 9 and 10).

Other possible explanations for the difference in declination may be local rotations or

TABLE 10. DAGANGOU FORMATION: LOCALITY P39–40, MEAN SITE DIRECTIONS, STATISTICS, POLE POSITIONS AND PALAEOLATITUDES

(The arrangement and parameters are as in table 2. The mean direction after correction for a 70° plunge to the west is also given.)

Unit: Dagangou Formation (P39–40)
Age: Viscan to Namurian (325 Ma)
Location: (36° 02′, 95° 00′)

site	*N*	*Dec*	*Inc*	*k*	alpha95	*Dec*	*Inc*	*k*	alpha95
CS01	6	150	26	11	21.1	265	64	11	21.2
CS02	4	189	45	7	36.4	267	28	7	36.4
CS03	6	167	31	13	19.5	258	48	13	19.4
CS04	7	152	39	10	20.1	281	54	10	20.1
CS05	4	196	11	62	11.7	222	23	62	11.7
CS06	5	186	17	41	12.1	227	34	41	12.1
CS07–08–09	8	201	−4	10	18.7	209	14	10	18.7
Mean	7	178	25	10	19.6	243	41	9	21.7
		Pole: lat = −40, long = 97.6				Pole: lat = −6, long = 40			
		$dp = 11.3$, $dm = 21.1$				$dp = 16.0$, $dm = 26.4$			
		Palaeolatitude: = −13 ± 11.3°				Palaeolatitude: = −23 ± 16.0°			
		Mean corrected for plunge 70° west:				215	41	9	21.7

different ages of magnetization. If the declination difference is due to local rotation, the inclination is still a valid indicator of palaeolatitude. The mean direction of magnetization from locality P39–40 is indicative of a Southern Hemisphere, reversed palaeomagnetic field. The mean direction from locality P41 is also in the appropriate quadrant for a Southern Hemisphere reversed magnetization. The correction for plunge causes the magnetization directions to converge toward a direction which is also consistent with a Southern Hemisphere magnetization. The high blocking temperatures of the characteristic magnetizations and the fact that the inclinations are identical after structural correction leads to the hypothesis that the Kunlun Terrane was in moderate southern latitudes during the Carboniferous.

(ii) *Dykes of the Triassic igneous province* (P32, P42, P43)

In the northern Kunlun a swarm of basalt–andesite dykes cuts the Kunlun batholith. Although the dykes are not directly dated, the petrology indicates they intruded the batholith while the body was still hot (Pearce & Mei, this volume). The Kunlun batholith is dated isotopically at 260–240 Ma (Harris, Xu, Lewis, & Jin, this volume) and the dykes are likely to be in this age range.

Figure 14 illustrates typical thermal demagnetization responses of specimens from these dykes. As illustrated by the behaviour of DK15, DK42 and DK55, a high-temperature component is isolated between temperatures of 500 and 590 °C. This component generally has the same direction as a thermally-distributed magnetization removed at temperatures below 500 °C. Some specimens, like DK20, have only a thermally distributed magnetization which is the same direction as the high blocking temperature magnetizations in other specimens.

Mean site directions, statistics, pole positions and palaeolatitude are summarized in table 11. It is not possible to apply a structural correction to dykes.

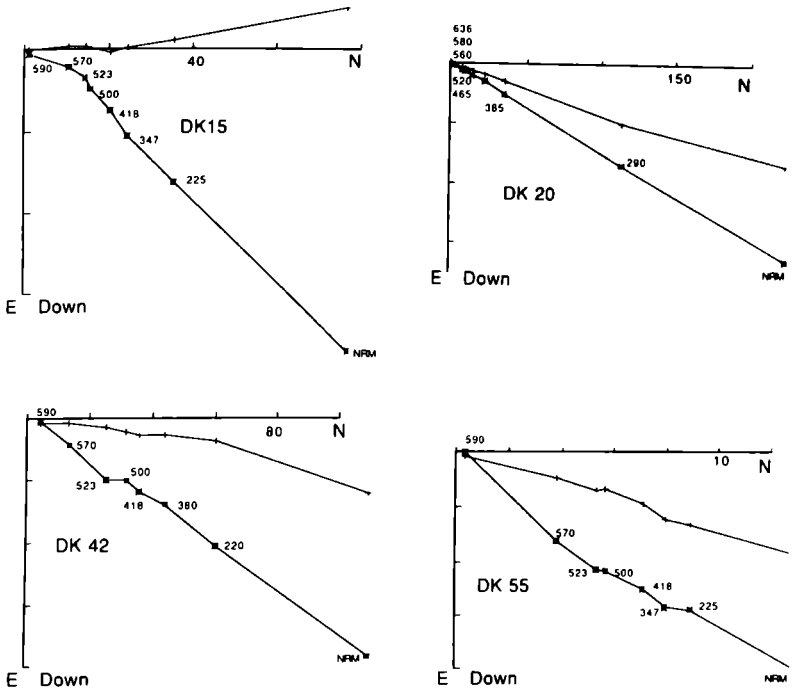

FIGURE 14. Orthogonal projections of thermal demagnetization results from the dykes intruding the Kunlun Batholith. Convention of plotting is as in figure 2.

TABLE 11. DYKES INTRUDING KUNLUN BATHOLITH, MEAN SITE DIRECTIONS, STATISTICS, POLE POSITIONS AND PALAEOLATITUDES

(The arrangement and parameters are as in table 2.)

Unit: Triassic dykes (P32, P42-43)
Location: South of Golmud (36° 10′, 94° 47′)
Age: 240 Ma

site	*N*	*Dec*	*Inc*	*k*	alpha95
DK01	6	18	37	85	7.3
DK02	6	15	36	67	8.2
DK03	3	2	38	40	19.8
DK04	3	3	39	49	17.7
DK05–6	4	5	39	14	26.0
DK07–8	5	12	40	57	10.2
DK10–11	4	17	45	62	11.7
DK12	5	13	41	126	6.9
DK13	4	349	69	5	45.1
DK14–15	4	23	48	63	11.7
DK16	4	17	53	61	11.8
DK17–19	5	8	43	43	11.8
DK20–21	6	4	46	17	16.9
AK01	4	2	37	128	8.1
AK02–3	5	356	34	278	4.6
AK04	5	14	41	160	6.1
Mean	16	9	43	60	4.8

Pole: lat = 76°, long = 237°, dp = 3.7°, dm = 5.9°
Palaeolatitude: = 25 ± 3.7°

4. Discussion and conclusions

The present data set from the Tibetan Plateau is too sparse to draw apparent polar wander paths for individual terranes. Even with a much larger set of results, it may prove impossible to do this as local rotations within deformed terranes will obscure palaeoazimuths. Palaeolatitude may be determined from a valid palaeomagnetic mean direction and the analysis of terrane configuration can be done using latitude anomalies, much as Irving (1977) investigated the arrangement of the elements of Pangea. Achache *et al.* (1984) also used a similar approach to examine the position of the Lhasa Terrane relative to Eurasia and India.

Latitude anomalies are calculated using various reference apparent polar wander paths for Eurasia. A palaeolatitude is calculated for a given palaeomagnetic locality using the present latitude and longitude of the site and the pole position with the appropriate age from the reference compilation. From this is subtracted the observed palaeolatitude calculated from the mean palaeomagnetic direction to form the latitude anomaly. Southern latitudes are considered negative so if the latitude anomaly is positive, the terrane is determined to have been south of the calculated latitude. If the site is found to have been north of the calculated position, the latitude anomaly is negative. If the site is determined to have been at the same relative latitude within the Eurasian frame of reference, the latitude anomaly is zero.

The calculation of latitude anomalies is carried out using four separate compilations of the reference apparent polar wander path for Eurasia including those of Irving (1977), Jowett *et al.* (1987) and Westphal *et al.* (1986). Both the 20 Ma and the 30 Ma running average computations of Jowett *et al.* (1987) are used. The Westphal *et al.* (1986) compilation does not include Palaeozoic pole positions. Although results differ somewhat in the value of the latitude anomaly and in the error associated with each result, the latitude anomalies all remain positive.

Table 12 summarizes the results of this calculation for the data from the Tibetan Plateau for each of the reference apparent polar wander paths. Latitude anomaly is plotted as a function of the estimated age of acquisition of the mean direction of magnetization in figure 15 for each of the polar wander paths. The choice of apparent polar wander path does not seem to affect the overall result. The errors of the latitude anomaly are found by adding the error of the relevant pole position to the estimated error, dp, of the palaeolatitude. Results from each terrane are identified with the appropriate symbols.

The estimate of the latitude anomaly from the Dagangou Formation palaeomagnetic determination for the Carboniferous Kunlun Terrane does have an error of the order of $\pm 25°$, which is a combination of the error of the relevant pole position and the estimate of the error in the palaeolatitude. Even with this error, the latitude anomaly does indicate a position of the Kunlun Terrane well south of its present position relative to Eurasia. The large error in the estimate of the palaeolatitude arises from the small number of sites used for the computation of the mean directions. The difference in the mean declination between the two localities in the Dagangou Formation adds a degree of uncertainty to this result. A correction for a plunge of the folds 70° west brings the declinations closer together to the extent that the cones of 95% confidence for the two localities overlap. The resulting palaeomagnetic directions are definitely of Southern Hemisphere affinity. In view of the uncertainty of the appropriate structural correction, emphasis is placed on the palaeomagnetic inclinations from the Carboniferous results. The magnitude of the latitude anomaly for the Kunlun does indicate that an ocean existed between the Kunlun Terrane and Eurasia with the suture somewhere north of the palaeomagnetic localities investigated in this study.

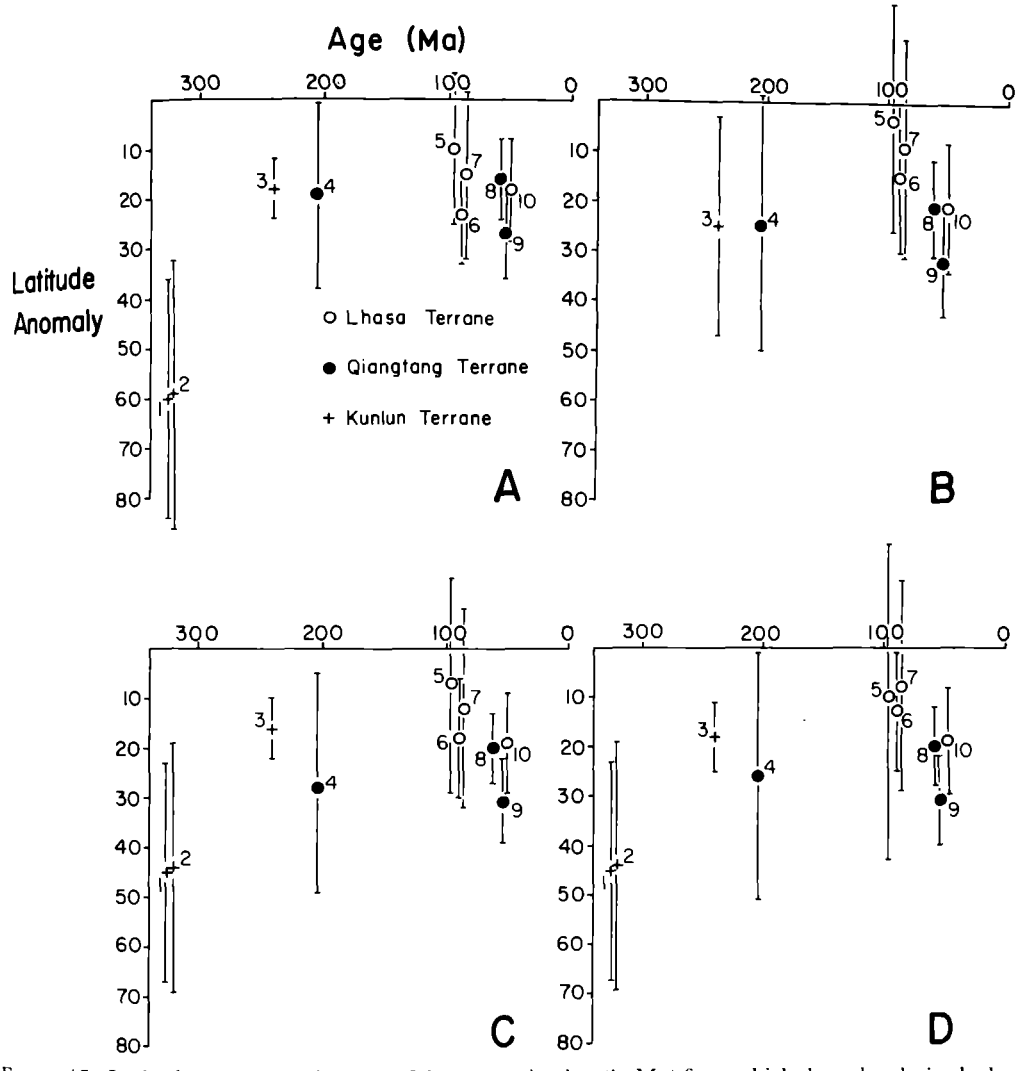

FIGURE 15. Latitude anomalies. The age of the magnetization (in Ma) from which the palaeolatitude determination is made is plotted against the latitude anomaly. The latitude anomalies are calculated from various reference apparent polar wander paths for Eurasia including: Irving (1977); B, Westphal *et al.* (1986); Jowett *et al.* (1987), 30 Ma running average; D, Jowett *et al.* (1987), 20 Ma running average. The individual points are: 1, Dagangou Formation, locality P41; 2, Dangangou Formation, locality P39–40; 3, Dykes intruding Kunlun Batholith; 4, Batang Group volcanics; 5, Nagqu mid-Cretaceous volcanics; 6, Takena Formation redbeds (this study & Achache *et al.* 1984); 7, Qelico mid-Cretaceous volcanics; 8, Fenghuoshan Group, locality P24; 9, Fenghuoshan Group locality P23; 10, Linzizong Group volcanics (Achache *et al.* 1984).

The latitude anomaly for the Kunlun Terrane is reduced to about 20° by the Triassic, if this is indeed the age of magnetization of the basaltic and andesite dykes which cut the Kunlun batholith.

The data from the Batang Group volcanics of Norian age (205 Ma) also indicate a latitude anomaly of about 20°. A direct comparison of the results from this unit with the basalt and andesite dykes cutting the Kunlun batholith is difficult, given the probable difference of 35 Ma between the ages of magnetization. Both determinations show the Kunlun Terrane and the Qiangtang Terrane in the same latitude belt during the Triassic. It is unfortunate that no pre-Triassic magnetizations could be found in the Qiangtang Terrane to test for separation across the Jinsha Suture.

TABLE 12. LATITUDE ANOMALIES

(The measured palaeolatitude is determined from the appropriate palaeomagnetic result. The predicted palaeolatitudes (pred) are calculated from the Eurasian apparent polar wander paths of: A, Irving (1977); B, Westphal *et al.* (1986); Jowett *et al.* (1987) 30 Ma running average; D, Jowett *et al.* (1987) 20 Ma running average. The latitude anomaly (anomaly) is determined by subtracting the measured latitude from the predicted latitude. The error is determined by adding the error, dp, of the measured latitude to the error in the appropriate reference palaeomagnetic pole.)

geological unit	terrane	age/Ma	measured latitude	Irving (A) Pred	Irving (A) Anomaly	Westphal (B) Pred	Westphal (B) Anomaly
Dagangou Formation (P39–40)	Kunlun	325	-23 ± 16	37 ± 8	60 ± 24	*****	*****
Dagangou Formation (P41)	Kunlun	325	-22 ± 19	37 ± 8	59 ± 27	*****	*****
Kunlun dykes	Kunlun	240	25 ± 4	43 ± 3	18 ± 7	*****	*****
Batang Group	Qiangtang	205	29 ± 14	47 ± 4	19 ± 18	54 ± 13	25 ± 27
Fenghuoshan Group (P23)	Qiangtang	50	7 ± 4	34 ± 5	27 ± 9	39 ± 7	32 ± 11
Fenghuoshan Group (P24)	Qiangtang	50	18 ± 3	34 ± 5	16 ± 8	39 ± 7	21 ± 10
Nagqu Cretaceous volcanics	Lhasa	96	19 ± 4	36 ± 6	17 ± 10	29 ± 14	10 ± 18
Qelico Cretaceous volcanics	Lhasa	90	20 ± 11	35 ± 6	15 ± 17	29 ± 12	9 ± 22
Takena formation	Lhasa	90	11 ± 4	34 ± 6	22 ± 8	28 ± 12	15 ± 15
Linzizong Formation	Lhasa	50	13 ± 6	31 ± 4	18 ± 10	34 ± 7	21 ± 13

geological unit	terrane	age/Ma	measured latitude	Jowett (C) Pred	Jowett (C) Anomaly	Jowett (D) Pred	Jowett (D) Anomaly
Dagangou Formation (P39–40)	Kunlun	325	-23 ± 16	22 ± 6	45 ± 22	22 ± 6	45 ± 22
Dagangou Formation (P41)	Kunlun	325	-22 ± 19	22 ± 6	44 ± 25	22 ± 6	44 ± 25
Kunlun dykes	Kunlun	240	25 ± 4	41 ± 2	16 ± 6	43 ± 3	18 ± 7
Batang Group	Qiangtang	205	29 ± 14	54 ± 9	28 ± 23	52 ± 11	26 ± 25
Fenghuoshan Group (P23)	Qiangtang	50	7 ± 4	38 ± 4	31 ± 8	38 ± 5	31 ± 9
Fenghuoshan Group (P24)	Qiangtang	50	18 ± 3	38 ± 4	20 ± 7	38 ± 5	20 ± 8
Nagqu Cretaceous volcanics	Lhasa	96	19 ± 4	33 ± 12	14 ± 26	36 ± 24	17 ± 28
Qelico Cretaceous volcanics	Lhasa	90	20 ± 11	32 ± 9	12 ± 20	28 ± 10	8 ± 21
Takena formation	Lhasa	90	11 ± 4	30 ± 9	18 ± 12	26 ± 10	13 ± 12
Linzizong Formation	Lhasa	50	13 ± 6	32 ± 4	19 ± 10	32 ± 5	19 ± 11

The 20° latitude anomaly appears to persist for the Qiangtang Terrane until Palaeocene–Eocene time, or the time of magnetization of the Fenghuoshan Group. The P23 section shows a rather more southerly latitude anomaly than the P24 section. As noted previously, the P23 mean direction of magnetization, before structural correction, is near the present-day field for the central Tibetan Plateau. The mean direction derived from the P23 section is not present field, either before or after structural correction. For this reason, the estimate of the latitude anomaly from the P24 section is probably the more reliable.

The results of Achache *et al.* (1984) showing the Lhasa Terrane about 20° south of its present position within the Eurasian frame of reference are reproduced for the Takena Formation and further supported by the data from the mid-Cretaceous andesites near Qelico.

The contemporaneous magnetizations from the Linzizong volcanics in the southern Lhasa Terrane and the Fenghuoshan Group in the Qiangtang Terrane are directly comparable. Such an exercise shows no resolvable separation in latitude other than what presently exists. Certainly no separation over the Banggong Suture is expected as it was closed by late Jurassic time. More importantly, no north–south crustal shortening is resolved between these two points on the Tibetan Plateau. The early Tertiary estimate of the latitude of Erdaogou is $18\pm3°$ and the early Tertiary southern Lhasa Terrane is $13\pm6°$. The difference is close to the present separation of 4° of latitude. The total error on this estimate is 9° or ±1000 kilometres.

Figure 15 shows a persistent 20° southern latitude anomaly for the Tibetan Plateau from the Triassic thorough the Eocene. One interpretation is that each terrane successively accreted to

Eurasia about 20° south of their present locations within the Eurasian frame of reference. They remained at such a position until the Eocene, after which a converging India drove them northward. In the absence of evidence for Eocene ocean crust between the Kunlun Terrane and Eurasia, this process must have involved either shortening of continental crust and/or pushing it out of the way via a Tapponier *et al.* (1982) mechanism. No post-Eocene crustal shortening between the southern Lhasa Terrane and the central Qiangtang Terrane (Erdaogou) is resolved, but the uncertainty is ±9° of latitude or about ±1000 kilometres. An outstanding question that can be addressed by future work in this part of the world is how far northward does the latitude anomaly persist in Asia for rocks of early Tertiary age? Is there an abrupt boundary over which this anomaly disappears or does it vanish gradually as the northward distance from Erdaogou increases?

The Carboniferous Southern Hemisphere, moderate latitude of the Kunlun Terrane is shared by a number of other blocks now incorporated in Asia. These include the South China block (Lin 1984), Iran (Soffel & Forster 1980) and Turkey (Lauer 1984). Palaeomagnetic data do indicate that a considerable amount of continental crust, now incorporated in Eurasia, was in moderate southern latitudes during the Carboniferous. Although it is not possible to use the palaeomagnetic data to constrain the relative positions of these blocks because of the ambiguity in the longitude, a possible reconstruction of these blocks is shown in figure 16, illustrating relative latitude with respect to major continental blocks. The blocks are arranged in longitude according to the minimum movement criteria of Irving (1977). Afghanistan is included in this assemblage of continental crust in moderate southern hemisphere latitudes as the limited data available for only the Permian (Krumsiek 1976) suggest that it was in moderate Southern Hemisphere latitudes during the Upper Palaeozoic. No data for the Palaeozoic are available for the Qiangtang Terrane or the Lhasa Terrane. The Qiangtang Terrane is positioned near the Kunlun Terrane as the palaeontological data (Smith & Xu, this volume) do

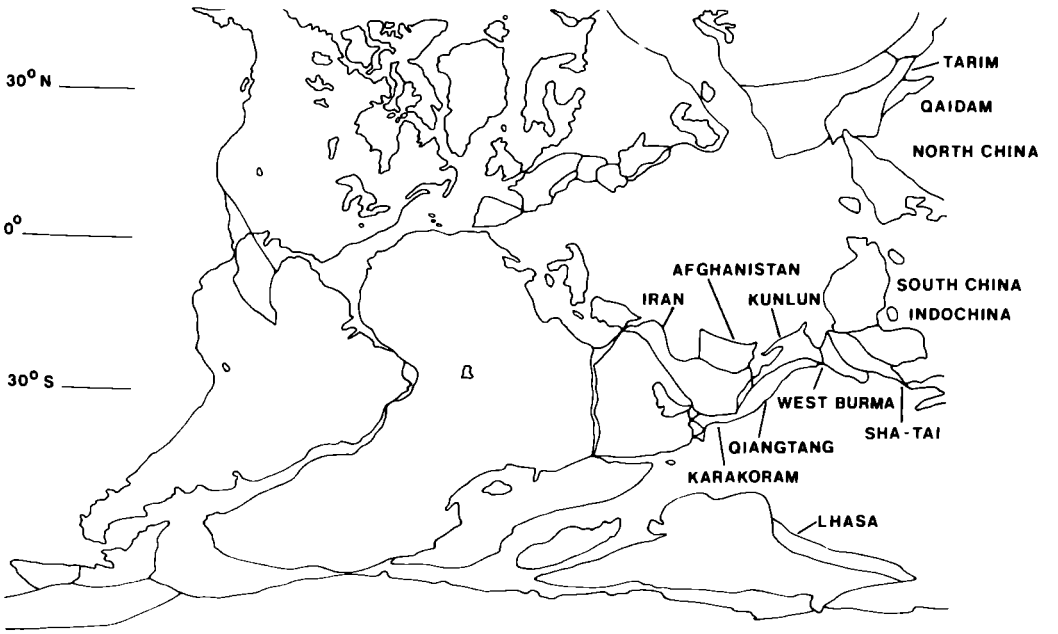

FIGURE 16. Upper Palaeozoic (Carboniferous) palaeogeographic reconstruction showing location of various southern Asian blocks with respect to major continents.

not suggest a substantial difference in palaeolatitude. The Lhasa Terrane is shown in a high southern latitude as suggested by the occurrence of the Carboniferous mixtites. As only the latitudes of these blocks are constrained, and a considerable difference in longitude could exist, the continuity implied by figure 16 must be tested by palaeontological methods.

We thank Professor J. C. Briden for making the laboratory facility at the University of Leeds available for the measurements of the samples. Sample preparation and measurement were supported by the Natural Environmental Research Council. K. Roberts assisted in the measurement of the samples. R. Cumberland helped with the transfer of computer files. A. G. Smith kindly provided computer facilities.

References

Achache, J., Courtillot, V. & Xu, Z. Y. 1984 Paleogeographic and tectonic evolution of southern Tibet since Middle Cretaceous time: New paleomagnetic data and synthesis. *J. geophys. Res.* **89**, 10311–10339.

Chang Chengfa and 26 others 1986 Preliminary conclusions of the Royal Society and Academia Sinica 1985 geotraverse of Tibet. *Nature, Lond.* **323**, 501–507.

Coulon, C., Maluski, H., Bollinger, C. & Wang, S. 1986 Mesozoic and Cenozoic volcanic rocks from central and southern Tibet: $^{40}Ar/^{39}Ar$ dating, petrological characteristics and geodynamical significance. *Earth planet. Sci. Lett.* **79**, 281–302.

Halls, H. 1978 The use of converging remagnetization circles in paleomagnetism. *Phys. Earth Planet Int.* **16**, 1–11.

Irving, E. 1977 Drift of the major continental blocks since the Devonian. *Nature, Lond.* **270**, 304–309.

Jowett, E. C., Pearce, G. W. & Rydzewski, A. 1987 A mid-Triassic paleomagnetic age of the Kupferschiefer mineralization in Poland based on a revised apparent polar wander path for Europe and Russia. *J. geophys. Res.* **92**, 581–598.

Kent, J. T., Briden, J. C. & Mardia, K. V. 1983 Linear and planar structure in ordered multivariate data as applied to progressive demagnetization of palaeomagnetic remanence. *Geophys. Jl R. astr. Soc.* **75**, 593–620.

Krumsiek, K. 1976 Zur Bewegung der Iranish-Afghanischen Platte. *Geol. Rundsch.* **65**, 908–929.

Lauer, J. P. 1984 The geodynamic evolution of Turkey and Cyprus in the light of recent palaeomagnetic data. In *The geological evolution of the Eastern Mediterranean* (ed. J. E. Dixon & A. H. F. Robertson). *Spec. Publ. Geol. Soc. London* **17**, 483–491.

Lin, J. L. 1984 The apparent polar wander paths for the North and South China blocks. Ph.D. thesis, University of California, Santa Barbara.

McElhinny, M. W. 1966 An improved method for demagnetizing rocks in alternating magnetic fields. *Geophys. Jl R. astr. Soc.* **10**, 369–374.

McElhinny, M. W., Luck, G. G. & Edwards, D. 1971 A large volume magnetic field-free space for thermal demagnetization and other experiments. *Pure appl. Geophys.* **80**, 127–130.

Soffel, H. C. & Forster, H. G. 1980 Apparent polar wander path of central Iran and its geotectonic interpretation. *J. Geomagn. Geoelect.* **32** (suppl. III), 117–135.

Tapponnier, P., Peltzer, G., Le Dain, A. Y., Armijo, R. & Cobbold, P. 1982 Propagating extrusion tectonics in Asia: new insights from simple experiments with plasticine. *Geology* **10**, 611–616.

Westphal, M., Bazhenov, M. L., Lauer, J. P., Pechersky, D. M. & Sibuet, J. C. 1986 Paleomagnetic implications on the evolution of the Tethys Belt from the Atlantic Ocean to the Pamirs since the Triassic. *Tectonophysics* **123**, 37–82.

Zijderveld, J. D. A. 1967 A. C. demagnetization of rocks: Analysis of results. In *Methods in palaeomagnetism* (ed. D. W. Collinson, K. Creer & S. K. Runcorn), pp. 254–286. Elsevier: Amsterdam.

Phil. Trans. R. Soc. Lond. A **327**, 263–285 (1988) [263]
Printed in Great Britain

Isotope geochemistry of the 1985 Tibet Geotraverse, Lhasa to Golmud

By N. B. W. Harris[1], Xu Ronghua[2], C. L. Lewis[1], C. J. Hawkesworth[1] and Zhang Yuquan[3]

[1] *Department of Earth Sciences, The Open University, Walton Hall, Milton Keynes, MK7 6AA, U.K.*
[2] *Institute of Geology, Academia Sinica, P.O. Box* 634, *Beijing, People's Republic of China*
[3] *Institute of Geochemistry, Academia Sinica, Guizang, Guizhou, People's Republic of China*

Geochronological data from the Golmud–Lhasa section across the Tibetan Plateau indicate progressively younger periods of magmatism from north to south associated with successively younger ocean closures.

Pre-collision Eocene magmatism (50–40 Ma) exposed along the southern margin of the Lhasa Terrane in the Gangdise Belt resulted from anatexis of mid-Proterozoic crust (~ 1000 Ma) at depths greater than 10 km, but at higher crustal levels subduction-related intrusions were predominantly mantle-derived with ~ 30% crustal assimilation.

Intrusions from the northern Lhasa Terrane are early Cretaceous in age (130–110 Ma). These form a bimodal suite comprised of two-mica granites derived from anatexis of Mid-Proterozoic crust and of biotite-hornblende granodiorites from about 60% crustal assimilation by mantle magmas above a post-collision subduction zone. They place a minimum constraint on collision between the Lhasa and Qiangtang Terranes of 130 Ma.

Granite magmatism from the Kunlun Mountains is late Permian–early Jurassic in age (260–190 Ma). The Kunlun batholith represents reworked mid-Proterozoic crust (1400–1000 Ma) at an active continental margin from 260–240 Ma. Post-tectonic granites were emplaced in a post-collision setting (200–190 Ma). Collision between the Qiangtang and Kunlun Terranes is dated as end-Triassic.

Nd model ages of sediments from across the plateau record uplift and erosion of young source regions throughout the Phanerozoic confirming that the Tibetan Plateau is the site of multiple continental collision through time. Phanerozoic magmagenesis throughout the plateau requires considerable crustal reworking and limited crustal growth which suggests thickened continental crust in the region may predate the most recent Eocene collision.

1. Introduction

The Sino–British Geotraverse of Tibet identified at least three continental fragments which now comprise the Tibetan Plateau; the Lhasa, Qiangtang and Kunlun Terranes (Chang *et al.* 1986). The distribution of plutonic rocks throughout these terranes is described in detail in Harris, Xu, Lewis & Jin (this volume). They are concentrated in a Palaeogene belt from the southern Lhasa Terrane, a Cretaceous belt from the northern Lhasa Terrane and a late Permian–early Jurassic belt from the Kunlun Terrane. Isotopic studies from the geotraverse have concentrated firstly on the geochronology and petrogenesis of granitoids in these three belts, and secondly on the Nd isotope compositions of sediments from across the plateau in order to constrain periods of new crust formation and of crustal accretion (collision) from the Tibetan Plateau. This paper describes the geochronology and isotopic constraints on source characteristics of the three granitoid belts, in order of increasing age (from south to north).

Reconnaissance oxygen isotope data from the intrusions are also described. Nd isotopic data from clastic sediments are presented and integrated into a synthesis of the isotopic evolution of the Tibetan Plateau.

2. Paleogene magmatism of the southern Lhasa Terrane

(*a*) *Introduction*

The calc-alkaline magmatic province exposed along the southern margin of the Lhasa Terrane is part of the 3000 km Gangdise Belt within which four regions have been the subject of isotopic studies (figure 1): Kohistan, Ladakh, Kailas and the Lhasa–Zangbo traverse (see table 1 for references). The major and trace element geochemistry of granitic rocks from the belt support magmagenesis at an active continental margin above a northward-dipping subduction zone now represented by the Zangbo Suture. Published isotopic data (table 1) indicate that calc-alkaline magmatism occurred throughout the belt during the Paleogene (61–39 Ma), continuing at least with minor intrusions until 29 Ma. An earlier Cretaceous pulse (111–94 Ma) has been recorded in Kohistan, Ladakh and Dazhuka (150 km WSW of Lhasa). There is no indication that magmatism was diachronous along strike of the belt. Isotopic studies on the main Paleogene period of magmatism indicate a predominantly low Rb/Sr source (initial $^{87}Sr/^{86}Sr < 0.707$) in contrast to the initial $^{87}Sr/^{86}Sr$ of the crustally derived High Himalayan granites (> 0.74). Inherited lead from zircon studies of the Gangdise Belt (Scharer *et al.* 1984; Xu *et al.* 1985) indicates that a Precambrian crustal component was present in magmagenesis for intrusions from the Lhasa–Zangbo traverse. A crustal component is also indicated by both Pb–Pb systematics (Gariepy *et al.* 1985) and stable isotope studies of the belt (Blattner *et al.* 1983).

An important problem posed by the Lhasa–Yangbajain section sampled on the geotraverse is the present northern limit of Paleogene magmatism. Xu *et al.* (1985) noted the similarity of lead isotope characteristics between zircons from the Linzizong Formation, the Yangbajain granite and Nyainqentanglha orthogneisses, all of which indicate formation at 60–50 Ma with a much older (> 1000 Ma) inherited component. The geochemical similarities between the Quxu–Lhasa, Yangbajain and Nyainqentanglha intrusions have also been noted (Harris, Xu & Jin, this volume) and they are therefore considered together in this chapter.

A period of Neogene vulcanism (16–10 Ma) has been recorded from a $^{39}Ar/^{40}Ar$ study of ignimbrites west of Yangbajain (Coulon *et al.* 1986). This coincides with a period of aplites and subalkaline granites (15–9 Ma) recorded in the Karakoram (Debon *et al.* 1987). The Yangbajain pyroclastics are high K calc-alkaline in composition and are geochemically quite distinct from the Paleogene intrusives. Whereas Cretaceous and Eocene magmatism is interpreted as related to subduction processes, the Neogene phase is post-collisional and extensional in nature (Coulon *et al.* 1986).

(*b*) Sr–Nd *systematics*

For granite rocks the initial $^{87}Sr/^{86}Sr$ of a whole rock isochron is that of the emplaced magmas, which may in turn be used to infer the age or the Rb/Sr ratio of the source from which the granites were derived. Similarly the initial $^{143}Nd/^{144}Nd$ values are the Nd-isotope ratios of the granites at the time of emplacement, and they may be used to estimate the age or Sm/Nd ratios of their source regions. Crustal-derived granites and sediments appear to have Sm/Nd

TABLE 1. PUBLISHED ISOTOPE DATA FROM THE GANGDISE BELT

	U–Pb zircon (Ma)	Rb–Sr (Ma)	Isochron	$^{39}Ar/^{40}Ar$ (Ma)	Ref
Karakorum					
Granite	—	111 ± 6	0.7044 ± 1		Debon *et al.* 1987
		59 ± 2	0.7042 ± 3		—
		43 ± 3	0.7056 ± 3		—
Granodiorite	95 ± 6	97 ± 17	0.7097 ± 1		—
Granite	—	54 ± 4	0.7041 ± 1		Petterson & Windley
Granodiorite	—	40 ± 6	0.7044 ± 1		1985
Tonalite	—	102 ± 12	0.7039 ± 1		—
Aplite	—	34 ± 16	0.7045 ± 1		—
		29 ± 8	0.7052 ± 1		—
Granite	—	—	—	19–56	Casnedi *et al.* 1978
Ladakh					
Granite	60.7 ± 0.4	—	—		Scharer *et al.* 1983
Granodiorite	101 ± 2	—	—		—
Granite	—	60 ± 10	0.7048 ± 5		Honnegar *et al.* 1982
Granodiorite	—	~ 51	~ 0.7050		Allègre & Ben Othman 1980
Kailas					
Granite	—	39 ± 1	0.7061 ± 2		Honnegar *et al.* 1982
Dazhuka					
Diorite	93.4 ± 1.0	—	—		Scharer *et al.* 1984
	94.2 ± 1.0	—	—		—
	—	—	—	90–110	Maluski *et al.* 1982
Quxu					
Granite	41.4 ± 0.4	—	—		Scharer *et al.* 1984
	41.7 ± 0.4	—	—		—
	—	44 ± 14	0.7067 ± 4		Debon *et al.* 1982
	—	46 ± 8	0.7065 ± 2		—
Lhasa					
Granite	~ 53	—	—		Scharer *et al.* 1984
		56 ± 10	~ 0.7057		Xu & Jin 1984
Linzizong					
Ignimbrite	56 ± 1	—	—		Xu *et al.* 1985
—				60	Maluski *et al.* 1982
Andesite	—	—	—	49–51	Coulon *et al.* 1986
Yangbajain					
Granite	—	47 ± 3	0.7071 ± 1		Debon *et al.* 1982
Migmatite	~ 50	—	—		Xu *et al.* 1985
Maquiang					
Ignimbrites	—	—	—	10–16	Coulon *et al.* 1986
Nyainqentanglha					
Gneiss	~ 50	—	—		Xu *et al.* 1985

ratios broadly similar to those of their crustal source regions, so that Sm–Nd isotope data can be used to estimate the age of crustal source rocks, which in turn allows the Rb/Sr ratio of the source to be calculated. It must be emphasized, however, that both granites and sediments are often mixtures of material from more than one source, whereupon the inferred source ages and trace element ratios will be just weighted averages of those different sources.

Initial Sr- and Nd-isotope results may be plotted together on an $\varepsilon_{Nd}(T)$–$\varepsilon_{Sr}(T)$ diagram, in which those data are expressed relative to the isotope ratios of the bulk earth at the same time. In general igneous rocks derived directly from the upper mantle, or from very young crust, tend

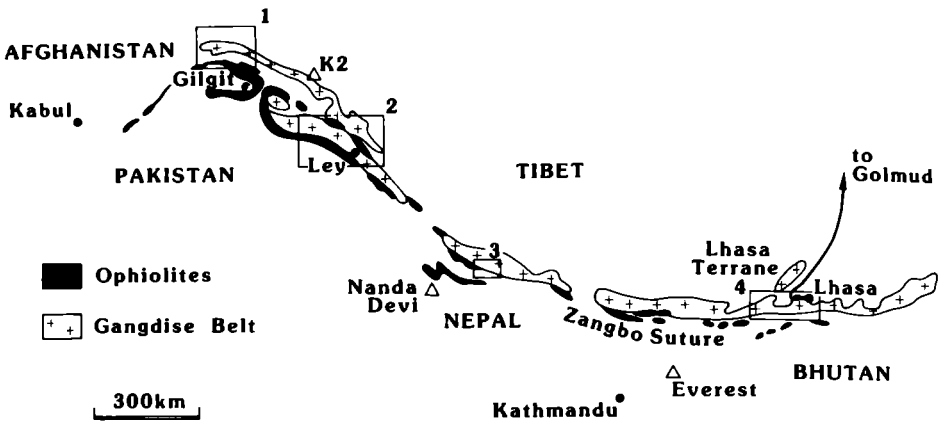

FIGURE 1. Sketch map of distribution of granitoids from the Gangdise Belt intruded north of the Zangbo Suture. Localities of published isotopic data (see table 1); 1 Karakoram and northern Kohistan, 2 Ladakh, 3 Kailas, 4 Lhasa-Zangbo traverse.

to plot in the upper quadrants (positive ε_{Nd}), sometimes slightly to the right of the so-called mantle array as seen in the field for Pan-African granites from Arabia (figure 2). Older crust plots in the lower (negative ε_{Nd}) quadrants, and so granites derived from, or simply containing more older crustal material will be displaced to lower ε_{Nd}. Moreover, since the upper crust is characterized by relatively high Rb/Sr, with time it also has relatively high $^{87}Sr/^{86}Sr$, so that S-type granites, for example, have low ε_{Nd} and relatively high ε_{Sr} (figure 2). Thus, a Himalayan leucogranite with $\varepsilon_{Sr} = +480$ and $\varepsilon_{Nd} = -16$ (Allègre & Ben Othman 1980), was probably

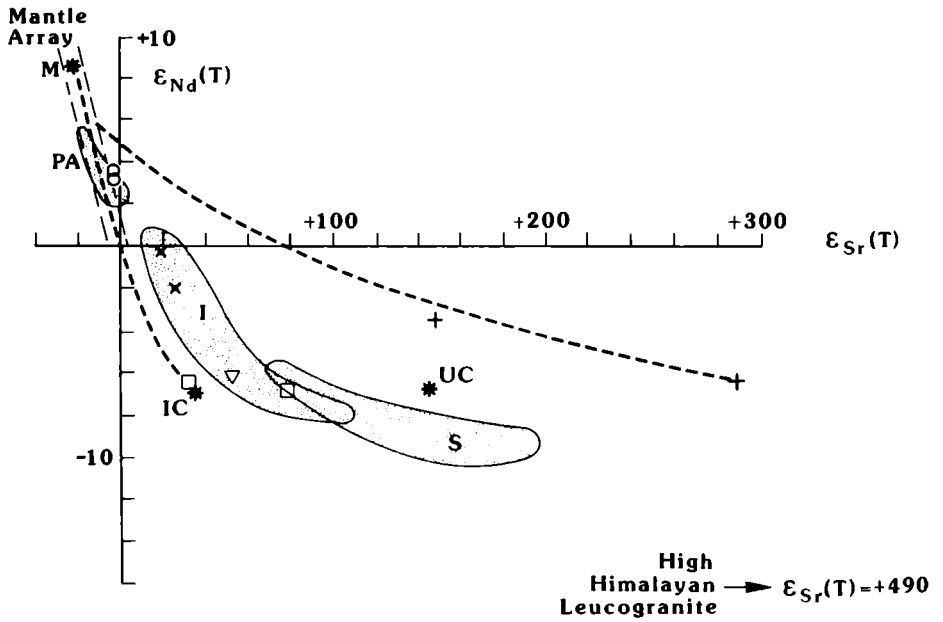

FIGURE 2. $\varepsilon_{Sr}(T)$–$\varepsilon_{Nd}(T)$ plot for samples from Lhasa Terrane; Gangdise Belt (○), Nyainqentanglha (□), Baingoin (▽), Mo Tian Ling (×) and Amdo Basement (+). PA = Pan-African Arabian granites (Duyverman *et al.* 1982), I = I-type Palaeozoic granites, S = S-type Palaeozoic granites (McCulloch & Chappell 1982). Dashed line indicates mixing curve between sample and depleted mantle. UC, IC, M indicate upper crust, intermediate crust, depleted mantle at 50 Ma, crustal extraction at 1040 Ma. Crustal parameters from Weaver & Tarney 1980. ε values calculated assuming $(^{143}Nd/^{144}Nd)_{CHUR}$(present day) 0.512 64; $(^{147}Sm/^{144}Nd)_{CHUR} = 0.1967$; $(^{87}Sr/^{86}Sr)_{UR}$(present day) = 0.7047; $(^{87}Rb/^{86}Sr)_{UR} = 0.0847$.

derived from an upper crustal Precambrian source. Granites falling in the I-type field of figure 2 can be interpreted either as melts from mixed mantle and crustal sources, or as crustal melts from low Rb/Sr source regions as in basic to intermediate igneous rocks.

For Nd, because Sm/Nd in a granite or sediment is believed to be similar to that in their source, the age of the source may also be inferred from the present day $^{143}Nd/^{144}Nd$ and $^{147}Sm/^{144}Nd$. Such ages are called model Nd ages and they represent the time when material (be it granite, sediment or their source regions) with the measured present day $^{143}Nd/^{144}Nd$ and $^{147}Sm/^{144}Nd$ was extracted from the upper mantle. There is some choice as to the preferred isotope characteristics of the upper mantle, but the model Nd ages discussed here are calculated relative to the depleted mantle of De Paolo (1981). Finally, these model ages must be treated with some caution, because they are sensitive both to the assumption that Sm/Nd in the granite or sediment *is* the same as that in its source region, and to the problem that several source regions may be involved, whereupon the significance of the calculated (average) model Nd age may be difficult to evaluate. In the simplest case granite derived by fractional crystallization from a mantle-derived melt will have a model Nd age equal to its emplacement age.

Two samples of Gangdise Belt intrusives from near Lhasa (sample G10 is a 41.4 ± 0.4 Ma biotite granite from Quxu and sample G15A is a 56 ± 10 Ma tonalite from Dagze, see figure 3 and table 1), provide $\varepsilon_{Sr}(T)$ close to depleted mantle. Both give positive $\varepsilon_{Nd}(T)$ $(+3.1, +3.5)$

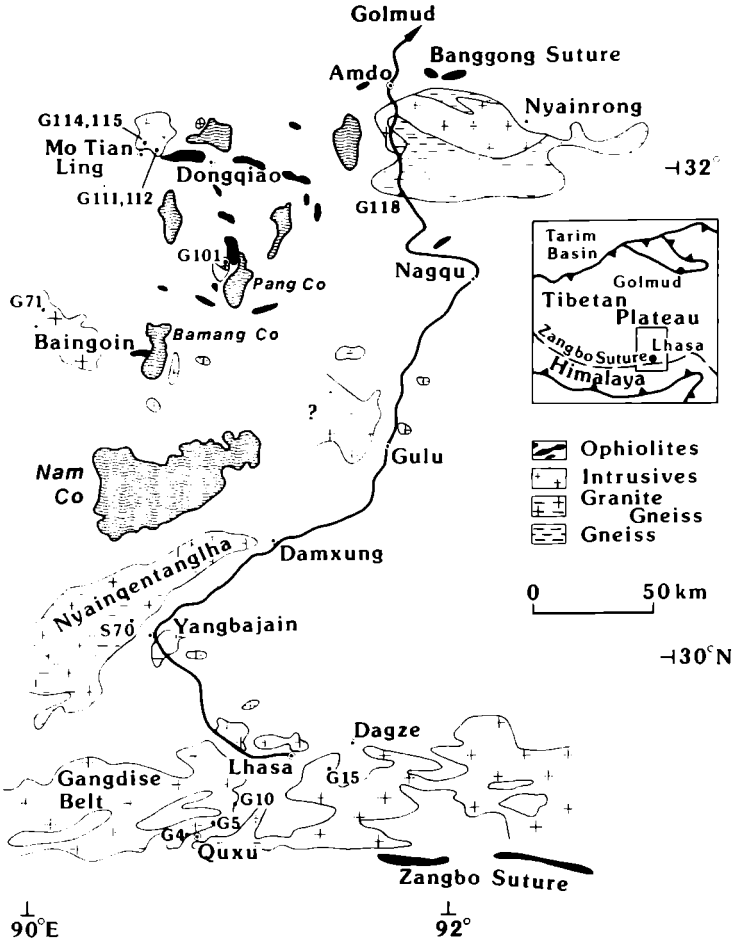

FIGURE 3. Sample location map for igneous samples selected for isotopic analysis from the Lhasa Terrane.

TABLE 2. SR–ND DATA FROM INTRUSIVES, LHASA TERRANE

Locality	Sample	Age (Ma)	$^{87}Sr/^{86}Sr$	$^{87}Rb/^{86}Sr$	$\varepsilon_{Sr}(T)$	$^{143}Nd/^{144}Nd$	Sm	Nd	$^{147}Sm/^{144}Nd$	$\varepsilon_{Nd}(T)$	T_{DM}
Gangdese											
Granite (Quxu)	G10	41.4±0.4[1]	0.70536	1.64	−3.5	0.51279±1	1.68	13.8	0.073	+3.5	305
Tonalite (Dagze)	G15A	56±10[2]	0.70464	0.35	−3.8	0.51278±1	4.16	20.2	0.124	+3.1	481
Nyainqentanglha											
Granite gneiss	S70C	50[3]	0.71581	7.73	+81	0.51226±1	8.11	38.5	0.127	−6.9	(1382)
Fol. granite	S70D	50[3]	0.70915	3.24	+31	0.51229±1	6.29	37.1	0.103	−6.2	1040
Baingoin											
Granite	G71	121±2[3]	0.72571	10.12	+53	0.51228±1	5.18	24.0	0.130	−6.0	(1402)
Mo Tian Ling											
Diorite	G112A	129±26[4]	0.70765	0.96	+19	0.51258±2	4.08	19.8	0.125	0.0	815
Granodiorite	G115B	129±26[4]	0.71011	2.03	+26	0.51247±1	5.22	28.5	0.111	−1.9	858
Amdo											
Orthogneiss	G118A	531±14[3]	0.73263	2.41	+147	0.51214±2	5.68	33.7	0.102	−3.4	1242
	G118D	531±14[3]	0.74505	2.73	+289	0.51206±1	4.48	22.2	0.122	−6.3	1646

[1] Scharer *et al.* 1984 [2] Xu and Jin 1984 [3] Xu *et al.* 1985 [4] Table 3.

$\varepsilon_{Nd}(T)$ is the deviation from the value expected in chondritic reservoir (CHUR) at time T where $^{143}Nd/^{144}Nd_{CHUR}(T) = 0.51264–0.1967$ $((\exp \lambda_{Sm} T)-1)$. T_{DM} calculated from De Paolo 1981 (values in parentheses indicates possible Sm/Nd fractionation in sample). Analyst Xu Ronghua.

and model Nd ages of 300–500 Ma (table 2, figure 4). Although the youngest model Nd ages obtained in this study, these are significantly older than the age of intrusion and so suggest that some crustal material is present in the granites. On the isotope data alone they could represent crustal melts of a 300–500 Ma source or, and perhaps more likely, some mixture of mantle with older crustal material. It is not possible to constrain the proportion of mantle/crust in the source without defining the composition and age of the crustal end-member.

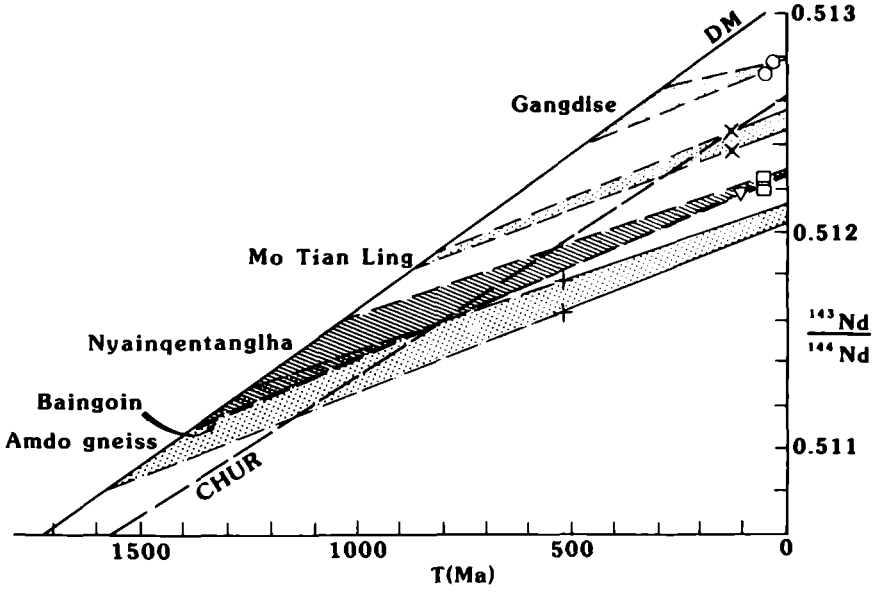

FIGURE 4. Nd evolution diagram of samples from the Lhasa Terrane. Symbols as for figure 2. DM = Depleted mantle, calculated from De Paolo (1981). Data from table 2.

Two granites from the Nyainqentanglha (S70C, S70D, figure 2) are isotopically quite distinct from the Gangdise samples; they have high positive $\varepsilon_{Sr}(T)$, negative $\varepsilon_{Nd}(T)$ and mid-Proterozoic model Nd ages (1040–1382 Ma), all indicating a greater crustal component and/or assimilation of older crust compared with the petrogenesis of the southern Gangdise Belt. Trace elements indicate elevated Rb/Zr ratios relative to the Gangdise Belt which, taken with the high SiO_2 and Rb contents of the granites are indicative of an origin by crustal anatexis. Mineral equilibria from pelitic xenoliths place a minimum depth for emplacement of 10 km (Harris, Holland & Tindle, this volume). The two Nyainqentanglha granites have very similar initial ε_{Nd} but different model Nd ages which suggests that at least one of the model Nd ages reflects Sm/Nd fractionation during magmagenesis. Of the two model Nd ages, the older value (1382 Ma) has a higher Sm/Nd and represents a highly siliceous gneiss (SiO_2 > 76 wt %). Small volume crustal melts appear to be characterized by higher Sm/Nd than their inferred source rocks (Hawkesworth *et al.* 1981) and such fractionation, due to residual LREE-rich accessory phases, will result in anomalously high model Nd ages. Thus the lower age of 1040 Ma provides a closer estimate of the age of the crustal progenitor.

ε values of a 1040 Ma crust at 50 Ma are plotted on figure 2 for both average upper crust (UC) and intermediate crust (IC). The Nyainqentanglha gneiss (S70C) lies close to the intermediate crust value indicating a source Rb/Sr somewhat lower than that of average upper

crust. Samples from the southern Gangdise Belt lie close to a mixing line between such a crustal source and upper mantle, and can be modelled as mantle melts with ~ 30% assimilation of a mid-Proterozoic crust.

3. Cretaceous magmatism of the northern Lhasa Terrane

(*a*) *Introduction*

North of Nam Co to the Banggong Suture, which marks the northern limit of the Lhasa Terrane, numerous discrete granitic plutons intrude both sedimentary cover and gneissic basement. Published data on these intrusives are restricted to a monazite age of 121 ± 2 and 130 ± 10 Ma from two-mica granites at Baingoin and Amdo respectively (Xu *et al.* 1985). The orthogneiss basement intruded by the Amdo granite gives an upper intercept zircon age of 531 ± 14 Ma and a sphene lower intercept age of 171 ± 6 Ma (Xu *et al.* 1985). $^{39}Ar/^{40}Ar$ ages from volcanics in the northern Lhasa Terrane also indicate Cretaceous magmatism (74–112 Ma, Coulon *et al.* 1986).

Radiometric constraints on the closure and ophiolite obduction between the Qiangtang and Lhasa Terranes are unclear. The sphene age from the crystalline basement at Amdo (171 ± 6 Ma) dates a low grade metamorphic event which could indicate a mid-Jurassic age for collision or ophiolite obduction. Final emplacement of the Dongqiao ophiolite appears from published $^{39}Ar/^{40}Ar$ constraints to be considerably younger. An upper age for emplacement would appear to be 85 ± 2 Ma, which was obtained by $^{39}Ar/^{40}Ar$ on a dacite clast extracted from a conglomerate overthrust by an ophiolite klippe east of Gyanco (Coulon *et al.* 1986) even though the same publication quotes a minimum emplacement age of 90 ± 2 Ma from plagioclase extracted from andesite lava unconformably overlying the ophiolite north of Pung Co.

(*b*) Rb–Sr *whole rock data*

Five whole granodiorite–granite samples from the Mo Tian Ling intrusion fall on an errorchron corresponding to an age of 129 ± 26 Ma (MSWD 45), $^{87}Sr/^{86}Sr = 0.7065 \pm 5$, within error of a biotite K/Ar age of 117 Ma (table 3). The intrusion is therefore coeval with the Baingoin–Amdo granites to the south and together they identify an early Cretaceous magmatic province in the northern Lhasa Terrane which has geochemical characteristics of a post-collision environment; this inference is supported by evidence for rapid uplift of the Baingoin granite (Harris, Xu, Lewis & Jin, this volume). These data imply that collision occurred during the early Cretaceous or end-Jurassic along the Banggong Suture. Palaeontological constraints require a pre-late Jurassic obduction age for the Dongqiao ophiolite (Smith & Xu, this volume). The mid-Cretaceous emplacement ages determined from $^{39}Ar/^{40}Ar$ studies (Coulon *et al.* 1986) therefore record post-collision imbrication of the ophiolite nappe, which was obducted in early or mid Jurassic times prior to collision in the early Cretaceous or end-Jurassic.

Six whole rock samples of the Pung Co granodiorite (G101, figure 3) provide an errorchron age of 44 ± 20 Ma (MSWD 6) and initial $^{87}Sr/^{86}Sr$ of 0.7102 ± 5. This age is not easy to interpret. The geochemistry of the granodiorite shows an enrichment of LIL elements similar to that of other tonalites and granodiorites in the northern Lhasa Terrane which predate the Cretaceous Baingoin granite (Harris, Xu, Lewis & Jin, this volume) and indicates an origin from an active or recently active, continental margin. Either the Pung Co granodiorite is a

TABLE 3. GEOCHRONOLOGICAL AND STABLE ISOTOPE DATA FROM THE TIBETAN PLATEAU

	U–Pb[1] zircon (Ma)	Rb–Sr age (Ma)	isochron $^{87}Sr/^{86}Sr$	Rb–Sr[1] biotite (Ma)	K–Ar[2] biotite (Ma)	$^{18}\delta O^{2}_{smow}$ whole rock (‰)
Lhasa Terrane						
Pung Co	—	—	—	—	—	—
G101 (granodiorite)	—	44±20	0.7102±5[2]	—	—	7.2
G100 (granite)	—	—	—	—	123±1	—
Mo Tian Ling	—	—	—	—	—	—
G111–115 (granodiorite)	—	126±26	0.7065±5[1]	—	117±2	7.6
Qiangtang Terrane						
Fenghuoshan	—	—	—	—	—	—
G141 (syenite)	—	—	—	—	31±1	11.2
Kunlun Terrane						
Wudaoliang	—	—	—	—	—	—
G142 (tonalite)	—	—	—	—	228±4	9.3
Xidatan	—	—	—	—	—	—
G206 (granite gneiss)	—	194±17	0.7083±2[1]	120	130±2	10.0
Naij Tal	—	—	—	—	—	—
G236 (granite)	—	198±56	0.7097±4[1]	140	168±3	—
Wanbaugou	—	—	—	—	—	—
G222 (granite)	—	—	—	—	431±7	10.4
Golmud Hydro	—	—	—	—	—	—
G244,245 (granite)	—	257±21	0.7098±20[1]	252	270±5	8.8
G248 (granodiorite)	—	—	—	—	251±4	9.9
G247 (tonalite)	—	—	—	—	246±4	10.2
Golmud East	—	—	—	—	—	—
G273 (granodiorite)	240±6	—	—	226	—	8.7
Duo Ya He	—	—	—	—	—	—
G266 (granodiorite)	—	—	—	241	—	6.5

[1] data from Department of Earth Sciences, Open University.
[2] data from Academia Sinica, Beijing.

Paleogene intrusion or it is a Cretaceous post-collision body related to the Banggong Suture, coeval with the Baingoin and Mo Tian Ling plutons. In the first case the isochron age is primary and in the second it has undergone post-magmatic isotopic re-equilibration reducing its apparent age. The large distance from an active Eocene plate margin (250 km north of the Zangbo Suture), the large proportional error on its age, its high initial $^{87}Sr/^{86}Sr$ and the geochemical similarity between this and known Cretaceous bodies all support the latter interpretation. A K–Ar age of 91 Ma from the peraluminous granite which intrudes the granodiorite supports a Cretaceous age of emplacement. The Rb/Sr isotopic system may have been partially reset during late Cretaceous tectonism resulting in a spurious errorchron 'age'.

(*c*) Sr–Nd *systematics*

The Mo Tian Ling intrusion (G111–G115, figure 3) is a Cretaceous granodiorite with slightly negative $\varepsilon_{Nd}(T)$ lying within the field of I-type granites (figure 2). Model Nd ages of ~ 850 Ma confirm a crustal component in the petrogenesis of the intrusion. These data could be interpreted either as a crustal melt of ~ 850 Ma crust, or a mantle melt with assimilation of crust older than 850 Ma.

The Cretaceous two-mica granite from Baingoin (G71, figure 3) has a higher $\varepsilon_{Sr}(T)$, lower $\varepsilon_{Nd}(T)$ and older model Nd age (1402 Ma) than the coeval Mo Tian Ling intrusion. The very

high Rb/Zr ratio of this sample indicates an origin from crustal melting and its high Sm/Nd may therefore reflect fractionation during anatexis which leads to an anomalously high model Nd age. The similarity in initial $^{143}Nd/^{144}Nd$ of the Nyainqentanglha and the Baingoin granites suggests that both result from anatexis of a mid-Proterozoic crust ($\sim$ 1000 Ma). Assuming the Mo Tian Ling intrusion results from assimilation of crust of this age, it requires about 60% of such crustal material, somewhat higher than that inferred from Gangdise samples. Like many post-collision intrusions, the granodiorite has a geochemistry indicative of a source in a hydrated mantle wedge above a subduction zone, but it presumably ascended through tectonically thickened crust. The high crustal component compared with magmas formed at an active continental margin, such as the Gangdise Belt, is therefore to be expected.

The oldest known basement from the Lhasa Terrane, the Amdo gneisses, was analysed (G118, figure 3) to evaluate its contribution to the Cretaceous magmatic event. The range of model Nd ages for the Amdo orthogneisses (1242–1646 Ma) is older than that of other analysed samples from the Lhasa Terrane (figure 4), and the $\varepsilon_{Sr}(T)$–$\varepsilon_{Nd}(T)$ plot rules out the gneisses as possible sources for more recent magmatism. Assuming a Cambrian age of gneiss emplacement from zircon data (Xu *et al.* 1985) it provides Sr and Nd isotope ratios strongly indicative of a crustal source for the orthogneisses (figure 2) with an estimated $^{87}Rb/^{86}Sr$ in the source of 1.3.

4. Late Permian–Early Jurassic magmatism in the Kunlun Terrane

(*a*) *Introduction*

The northern margin of the Kunlun Terrane is marked by the uplifted syn-tectonic granitic batholith of the Kunlun Mountains. South of the batholith several post-tectonic granites are intruded and an orthogneiss is emplaced north of the Xidatan Fault. Geochemically the granites are calc-alkaline to calcic with trace elements indicative of formation either at an active continental margin, or in a post-collision setting. The southern limit of the Kunlun Terrane is marked by the Jinsha Suture, poorly represented in the Geotraverse region by an inlier of ultramafics and gabbros. Evidence for northward underthrusting along this possible plate margin comes from the southward-facing recumbancy of the structures in the south of the terrane, and Jurassic molasse, derived from the north, deposited south of the suture. There are no published geochronological data from this terrane, but previous stratigraphic studies favour a Permo-Triassic age for closure along the Jinsha suture (Chang & Pan 1981). The batholith intrudes Permian sediment.

(*b*) *Geochronology*

Five whole rock suites were selected for Rb–Sr whole-rock isochron studies. Of these, the Golmud East granodiorite and the Duo Ya He granodiorite from the syn-tectonic batholith have too little variation in Rb/Sr to yield useful whole rock ages. Seven samples from the Xidatan orthogneiss (G206 figure 5) fall on an errorchron with an 'age' of 189 ± 7 Ma (MSWD 19), and an initial $^{87}Sr/^{86}Sr$ of 0.7083 ± 2. Since this suite of gneisses includes two rock-types (biotite granite gneiss and leucogneiss) which have different geochemical characteristics and distinct model ages (see next section) it may be more realistic to estimate the age from the four biotite granite gneiss samples which have similar trace element signatures and similar model Nd ages. This results in an age of 194 ± 17 Ma (MSWD 25), $^{87}Sr/^{86}Sr$ of

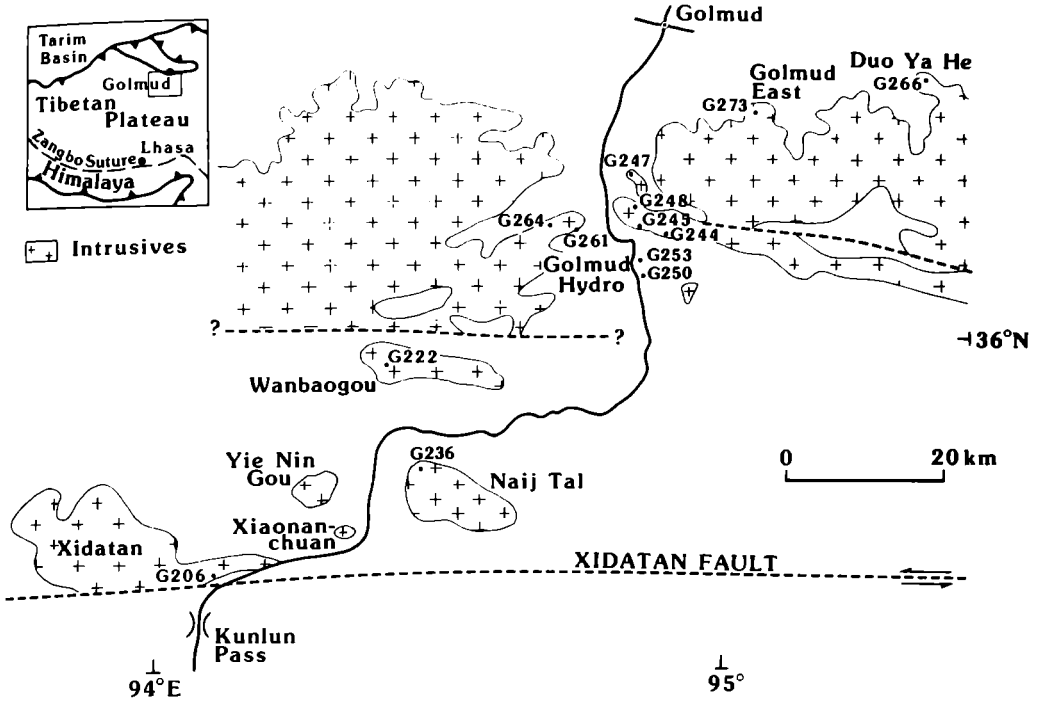

FIGURE 5. Sample location map for igneous samples selected for isotopic analysis from the Kunlun Terrane.

0.7083 ± 2, and the similarity of these data with the age and initial ratio derived from all Xidatan samples implies the same, or geochemically similar, sources for both gneisses. A similar but poorly constrained age of 198 ± 56 Ma (MSWD 140) and an initial $^{87}Sr/^{86}Sr$ of 0.7097 ± 4 has been obtained for five samples of the post-tectonic Naij Tal granite (G236, figure 5), the large uncertainty resulting from a small spread in Rb/Sr ratios. The syn-tectonic Golmud Hydro granite has also proved difficult to date by whole rock isochron. A total of 6 samples from G244–G245 (figure 5) give an age of 257 ± 26 Ma (MSWD 44), initial $^{87}Sr/^{86}Sr$ 0.710 ± 2. To determine the age of the Golmud East granodiorite, three populations of zircons were analysed and found to give a virtually concordant age of 240 ± 6 Ma (table 4). The syn-tectonic batholith was therefore emplaced from 270–240 Ma (this range is supported by K–Ar ages from the Golmud Hydro complex) and the post tectonic intrusions to the south from 200–190 Ma. K–Ar data from the Wanbaogou granite, which lies south of the Kunlun batholith, indicate an early Palaeozoic age (431 Ma), and this result is supported by preliminary Rb–Sr data. A post-tectonic tonalite plug, emplaced into the Triassic accretionary prism 100 km south of the Kunlun Pass near Wudaoliang, is dated at 213 Ma by the K/Ar method and clearly post-dates collisional deformation in the southern Kunlun Terrane.

In an attempt to constrain further the timing of events in the Kunlun Shan, biotite separates from five suites were analysed for Rb–Sr isotopes. Since the closure temperature of biotites is 300–350 °C (Dodson 1979), the data obtained by the method record the last time the rock cooled through this temperature. The Golmud Hydro and Golmud East intrusions have indistinguishable emplacement and mica ages (table 3). However, the Naij Tal and Xidatan suites give considerably younger biotite-whole rock ages of 140 Ma and 120 Ma respectively despite their early Jurassic intrusion ages. The Xidatan gneisses are strongly foliated parallel

TABLE 4. U–Pb ISOTOPIC DATA FROM ZIRCONS FROM GOLMUD EAST GRANODIORITE (G273)

Sample	Grain characteristics	Uranium 10^{-12}M	Radiogenic Pb[1] 10^{-12}M	Common Pb 10^{-12}M	$^{206}Pb/^{238}U$	$^{207}Pb/^{235}U$	$^{207}Pb/^{206}Pb$	$^{206}Pb/^{238}U$ Apparent ages (Ma)	$^{207}Pb/^{208}U$ Apparent ages (Ma)
G273–4	0.125–0.063 mm Non-mag at 3–10° Length/width = 4/1	268.5	12.738	0.902	0.03832	0.26753	0.05029	242.4	239.3
G273–5	0.125–0.063 mm Non-mag at 3–10° Length/width = 2.5/1	243.3	11.409	0.456	0.03852	0.26537	0.04996	243.6	239.0
G273–6	0.125–0.063 mm Non-mag at 3–10° Length/width = 2.0/1	546.8	24.585	1.466	0.03771	0.25952	0.04991	238.6	234.3

[1] corrected for common Pb. 206/204 = 17.48, 207/204 = 15.50, 206/204 = 37.21.
Analyst Xu Ronghua.

to the east-trending Xidatan Fault with a recrystallized mica fabric and it is likely the mica age dates the penetrative fabric in this rock. Since the fabric and the fault are parallel, it raises the intriguing possibility that the micas record the time of early movement on this fault zone. The Naij Tal pluton is some 15 km north of the fault, does not have a strong fabric, and perhaps the isotopes are only partially reset giving a somewhat older age (140 Ma). K–Ar mica ages for these two bodies lie in the range 130–170 Ma. Since this range of mineral ages from two isotopic systems overlaps with the inferred end-Jurassic collision along the Banggong Suture it is possible that the fault was initiated, or at least reactivated, by collision between the Lhasa and Qiangtang terranes.

(*c*) Sr–Nd *systematics*

Model Nd ages of fifteen samples from the Kunlun granites have been determined (table 5). Model ages vary from 920–1880 Ma, with wide variations being recorded from those plutons which have a distinctive crustal melt geochemistry. For example, within the Xidatan gneisses the biotite granite gneisses have younger model Nd ages ($\sim$ 1000 Ma) than the leucogneisses (1600–1900 Ma). The high model Nd ages are again associated, not with low $^{143}Nd/^{144}Nd$, but with high Sm/Nd, with silica contents $>$ 76wt % and with elevated Rb/Zr indicative of small volume partial melts. The implication is that for crustally-derived granitic samples with $^{147}Sm/^{144}Nd > 0.14$, model ages may be too high due to Sm/Nd fractionation (see section 2*b*). In the case of the Xidatan gneisses, the best estimate of the source age is probably $\sim$ 1000 Ma, indicated by the biotite gneisses. The Golmud Hydro granite also has high model ages associated with high $^{147}Sm/^{144}Nd$ samples with elevated Rb/Zr. In this case, best estimate of source model age lies in the range 1100–1250 Ma.

The $\varepsilon_{Nd}(T)$–$\varepsilon_{Sr}(T)$ plot (figure 6) indicates that all Kunlun intrusions have negative $\varepsilon_{Nd}(T)$ and strongly positive $\varepsilon_{Sr}(T)$ indicating a high crustal component. The data are also displaced to higher values of $\varepsilon_{Sr}(T)$ compared with Lhasa Terrane samples which indicates a higher

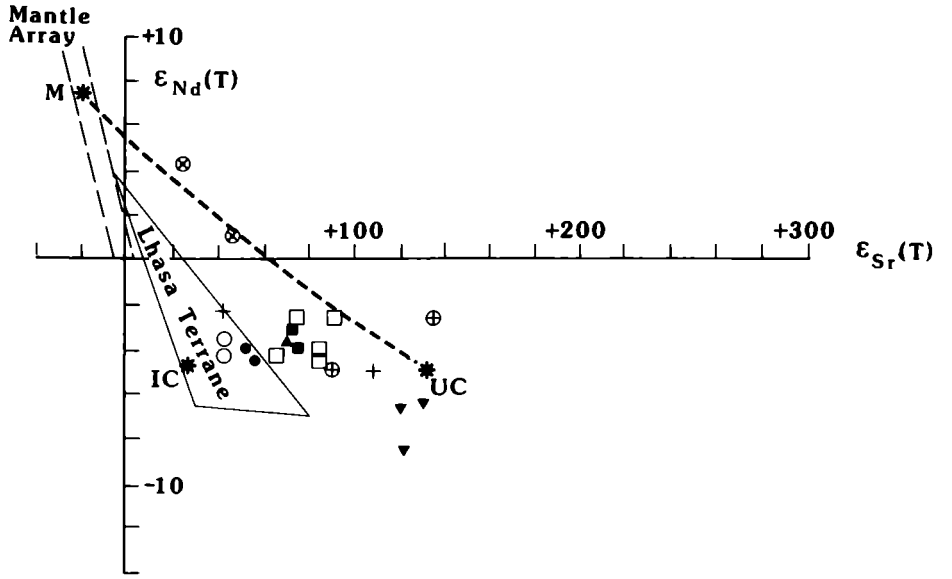

FIGURE 6. $\varepsilon_{Sr}(T)$–$\varepsilon_{Nd}(T)$ plot for samples from Kunlun Terrane. ● = Xidatan (biotite gneiss), ○ = Xidatan (leucogneiss), ■ = Naij Tal, □ = Golmud Hydro, ▲ = Golmud East, ▼ = Duo Ya He, + = Triassic (?) Volcanics, ⊕ = Triassic (?) Dyke, ⊗ = dykes intruding Devonian Volcanics. UC, IC, M indicate upper crust, intermediate crust and upper mantle at 240 Ma, crustal extraction at 1100 Ma. Dashed-line shows mixing curve between average upper crust and depleted mantle. Crustal parameters from Weaver & Tarney 1980.

TABLE 5. SR–ND DATA FROM IGNEOUS SAMPLES, KUNLUN TERRANE

Locality		Sample	Age (Ma)	$^{87}Sr/^{86}Sr$	$^{87}Rb/^{86}Sr$	$\varepsilon_{Sr}(T)$	$^{143}Nd/^{144}Nd$	Sm ppm	Nd ppm	$^{147}Sm/^{144}$ Nd	$\varepsilon_{Nd}(T)$	T_{DM} Ma
Xidatan	Biotite gneiss	G206A	194±17	0.70989	0.58	+54	0.51230±1	7.10	47.6	0.090	−3.9	921
	—	G206B		0.71185	1.22	+57	0.51229±1	6.60	40.3	0.099	−4.5	1016
	Leucogneiss	G206C		0.72625	6.78	+44	0.51239±2	3.00	11.4	0.160	−4.1	(1880)
	—	G206D		0.72747	7.25	+43	0.51240±2	2.80	11.2	0.151	−3.6	(1586)
Naij Tal	Granite	G236D	198±56	0.71130	0.55	+75	0.51231±1	4.22	26.0	0.098	−3.9	1020
	—	G236E		0.71248	1.04	+72	0.51233±1	3.44	20.0	0.104	−3.0	970
Golmud Hydro	Granite	G244A	257±26	0.72384	3.71	+83	0.51224±2	3.90	21.6	0.109	−4.9	1181
	—	G245A		0.74425	9.73	+61	0.51231±7	3.07	12.9	0.144	−4.7	(1610)
	—	G245C		0.74576	9.76	+82	0.51230±4	2.72	12.0	0.140	−4.8	(1470)
	—	G245F		0.72786	5.04	+71	0.51239±3	2.60	12.7	0.130	−2.7	1244
	—	G261B		0.71858	2.08	+93	0.51238±1	5.20	25.7	0.122	−2.6	1108
Golmud East	Granodiorite	G273C	240±6	0.71181	0.68	+72	0.51229±1	3.80	26.1	0.089	−3.6	940
North Kunlun	Granodiorite	G266A	240[1]	0.71727	1.22	+124	0.51208±1	5.50	34.8	0.096	−8.4	1250
	—	G266C		0.71744	1.19	+132	0.51215±1	5.00	25.8	0.117	−6.4	1420
	—	G266E		0.71678	1.10	+122	0.51215±2	4.90	29.0	0.102	−6.6	1230
Dacite flow	—	G250A	240[1]	0.71710	1.52	+108	0.51223±2	7.90	35.8	0.133	−6.0	1546
Andesite dyke	—	G250C		0.71305	0.71	+90	0.51230±1	6.10	25.1	0.147	−5.1	1700
Andesite flow	—	G250F		0.70887	0.50	+40	0.51245±2	6.40	26.5	0.147	−2.1	1345
Basalt dyke		G253Y		0.72666	3.63	+141	0.51241±1	12.00	51.2	0.142	−2.8	1341
Rhyolite dyke	—	G253H	384[2]	0.70938	0.31	+49	0.51251±2	3.10	15.3	0.123	+1.2	899
Basalt dyke	—	G253I		0.71506	1.65	+26	0.51275±1	5.10	19.9	0.155	+4.3	775

[1] Assumed from Golmud East zircon age

[2] Assumed from stratigraphic evidence

T_{DM} values in parentheses indicate possible Sm/Nd fractionation of sample

Analyst C. L. Lewis

Rb/Sr in the source. If it is assumed that the crustal source has a model age of 1100 Ma (taken as an average from Kunlun samples with $^{147}Sm/^{144}Nd < 0.14$), and anatexis occurred at 240 Ma, then the isotopic ratios of crust with average Rb/Sr and Sm/Nd for upper and intermediate crust are given by UC and IC respectively in figure 6. Naij Tal, Golmud Hydro, Golmud East and Xidatan intrusives have somewhat lower Rb/Sr sources than average upper crust. Some samples lie close to a mixing curve between upper crust and depleted mantle, and this could either indicate a shorter period of crustal residency in the source or up to 20% mantle component in the granite petrogenesis. The Duo Ya He granodiorites are displaced from the array of other Kunlun data to lower $\varepsilon_{Nd}(T)$ values suggesting a slightly older crustal source.

Six volcanic and hypabyssal samples have been analysed for Sr Nd isotopes from the Dagangou Formation south of the syn-tectonic Kunlun batholith. Interpretation of these results is uncertain, both because distinction between flows and dykes is unclear, and because it is not known whether the formation comprises two distinct suites. Dykes and flows from a fault-bounded block (G250) have isotopic characteristics similar to those of the Permo-Triassic batholith and may be the extrusive equivalent (figure 6). Dykes intruding a suite with known Devonian age (G253) have younger model Nd ages and a large mantle component.

5. Oxygen isotope data

A reconnaissance study of oxygen isotopes from 15 granitoid whole rock samples has been undertaken (table 3) and compared with published data from the Gangdise Belt and High Himalayan leucogranites (Blattner *et al.* 1983; Debon *et al.* 1986). There is a general small increase in $\delta^{18}O$ with silica content for the Gangdise Belt (figure 7) which is consistent with assimilation and fractional crystallization processes. The leucogranites show high $\delta^{18}O$ which together with high initial $^{87}Sr/^{86}Sr$, indicate crustal melting. Data presented in this study show that samples from Pung Co and Mo Tian Ling in the northern Lhasa Terrane lie within the

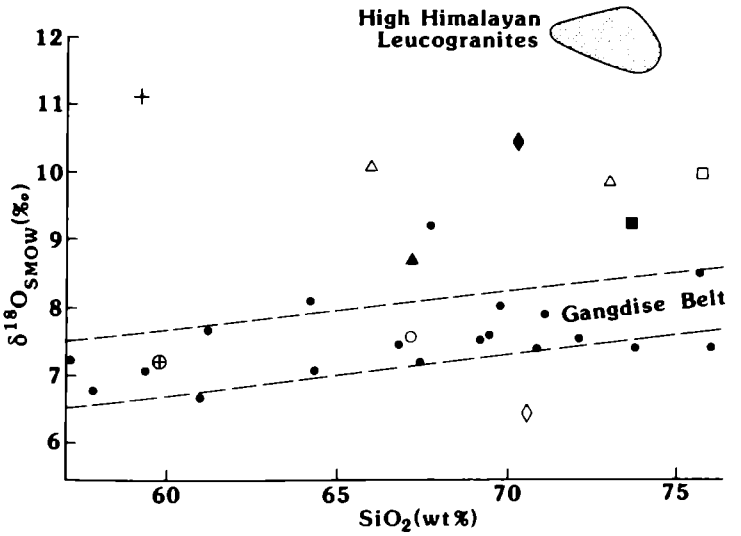

Figure 7. Variation of $\delta^{18}O_{SMOW}$ with silica content. ● = Gangdese Belt, ○ = Mo Tian Ling, ⊕ = Pung Co, + = Fenguoshan syenite, □ = Xidatan, ■ = Naij Tal, △ = Golmud Hydro, ▲ = Golmud East, ◇ = Duo Ya He, ◆ = Wanbaogou. Data from table 3. Blattner *et al.* 1983, Debon *et al.* 1986.

Gangdise trend. Strong evidence either for a crustal contribution or extensive fluid/rock interaction comes from the high $\delta^{18}O$ values of the Fenghuoshan microsyenite from the Qiangtang terrane, and the granitic intrusions of the Kunlun (with the exception of the Duo Ya He granodiorite).

Samples from the Gangdise Belt show reasonable correlation between $\delta^{18}O$ and initial $^{87}Sr/^{86}Sr$ (coefficient of 0.83 for seven samples) (figure 8) which implies that these data record primary genetic processes and is consistent with crustal assimilation and fractional crystallization. Assimilation or reworking of continental crust causes an increase in both parameters as observed in the Xidatan, Naij Tal, Wanbaogou and Golmud intrusions from the Kunlun. The Pung Co granodiorite (G101) from the northern Lhasa Terrane has mantle oxygen values but elevated strontium ratios and this supports the evidence (section 3*b*) for post-magmatic re-equilibration which not only reduces the apparent age, but also elevates the initial ratio. Interestingly the Duo Ya He granodiorite records even higher strontium ratios at low $\delta^{18}O$. It is possible that this facies within the Kunlun batholith represents a much older granitic inlier. Supporting evidence comes from its strong foliation and low $^{143}Nd/^{144}Nd$ indicative of an older source region than other analysed intrusions from the Kunlun batholith. In order to reduce the initial $^{87}Sr/^{86}Sr$ to 0.707, a value within the range typical of mantle-derived magmas, an intrusion age of $\sim$ 600 Ma is required. It therefore remains equivocal that the Duo Ya He granodiorite is part of the Triassic magmatic event.

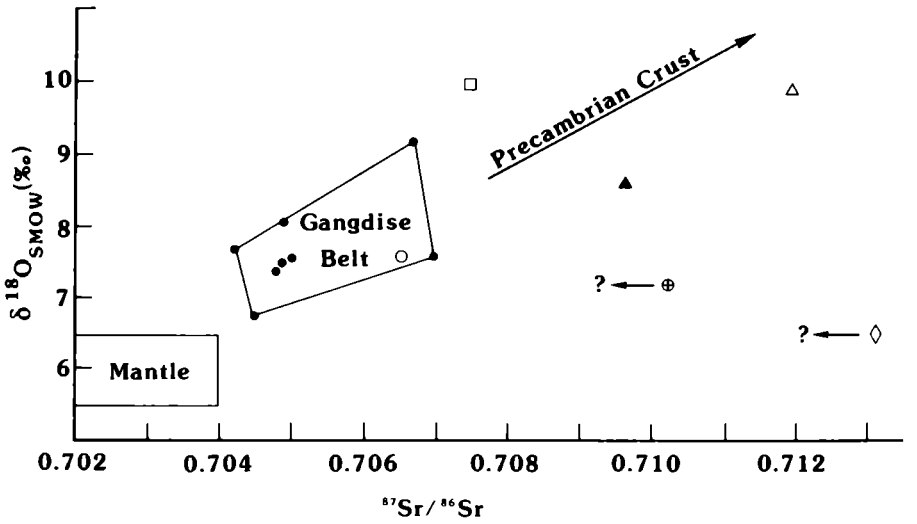

FIGURE 8. Variation of $\delta^{18}O_{SMOW}$ with initial $^{87}Sr/^{86}Sr$. Symbols as for figure 7. Data from table 3.

6. Model Nd ages of sediments

Nd model ages of fine-grained clastic sediments provide an indication of average age of their source regions, provided Sm/Nd has not fractionated since the sediment progenitors were extracted from the mantle. This technique has been successfully applied to Phanerozoic sediments to identify periods of crustal growth and orogenesis (Michard *et al.* 1985) and periods of ocean closure (Davies *et al.* 1985). In this study Sm/Nd data from sediments from critical horizons within the Lhasa, Qiangtang and Kunlun terranes (figure 9) have been analysed to

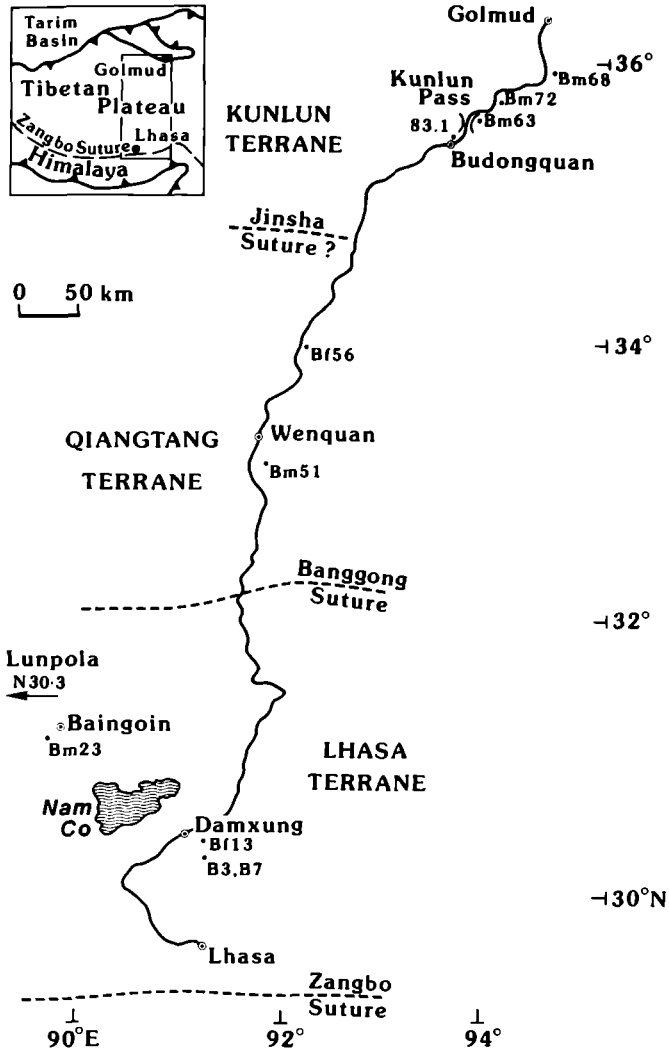

FIGURE 9. Sample location map for samples of sediment selected for Nd isotope analysis.

determine variations of source region age with time and hence possible periods of ocean closure which allow new source regions to become available for erosion. Such a technique will only be successful if the colliding plates have uplifted regions of contrasting average ages.

Of the eleven analysed samples, nine define a trend indicating a general increase in ε_{Nd} with decreasing age of sedimentation (figure 10). This means that source region ages become younger, relative to bulk earth, in the younger sediments.

Within the Lhasa Terrane the Late Carboniferous drop-stone glacial deposits (B7) require significantly older Precambrian sources regions than the overlying siltstones (B3) which identifies the availability of older regions in Gondwanaland for erosion during Carboniferous glaciation. The significantly older model age is consistent with the drop-stones being transported from an Archean land-mass to the south and deposited in relatively young terrane.

Two Lower Cretaceous to mid-Jurassic sediments from either side of the Banggong Suture indicate similar model ages. In this case it is not possible to confirm the time of collision since both plates apparently provided source regions of similar age prior to collision.

In the north of the Qiangtang terrane, the Upper Permian shale (Bf56) has a significantly younger model age than either the mid Carboniferous shale (Bm72) or the Upper Jurassic silt (83.1) of the southern Kunlun. Transport directions in Upper Permian strata are from the north, but adjacent strata contain numerous tuffaceous horizons and the shales are overlain by Permian volcanics. The young model age of the Permian shale is therefore attributed to magmatism within the Qiangtang plate and not to an influx of material from a pre-Upper Permian collision with younger source regions to the north. Since juvenile volcano-sedimentary detritus was apparently derived within the Qiangtang Terrane, these data do not help identify the time of collision with a rising younger source region to the north. In any event the bulk of Kunlun magmatism probably occurred around 240 Ma and could not affect pre-Triassic sediments.

The general trend of model age with sedimentation age seen in the Tibetan Plateau (figure 10) is contrary to trends observed in studies from Australia and from Britain. The trend of Australian shales, representative of at least part of Gondwana, is of a slight decrease in ε_{Nd} in young sediments during the Phanerozoic (Allègre & Rousseau 1984). In British sediments the relatively sharp decrease in ε_{Nd} with decreasing sedimentation age is accredited to detritus from the Precambrian terrane to the north after closure of the Iapetus Ocean (Davies *et al.* 1985). The reverse trend shown by the Tibetan sediments has been recorded in late Proterozoic sediments from the Damara Belt of Namibia (McDermott 1987). Such a trend is remarkable since continuous reworking of crust with no introduction of younger material by either magmatic or tectonic processes will always lead to a decrease in ε_{Nd} in younger sediments as shown by the crustal reworking vector of figure 10. The reverse trend can be explained in one of two ways.

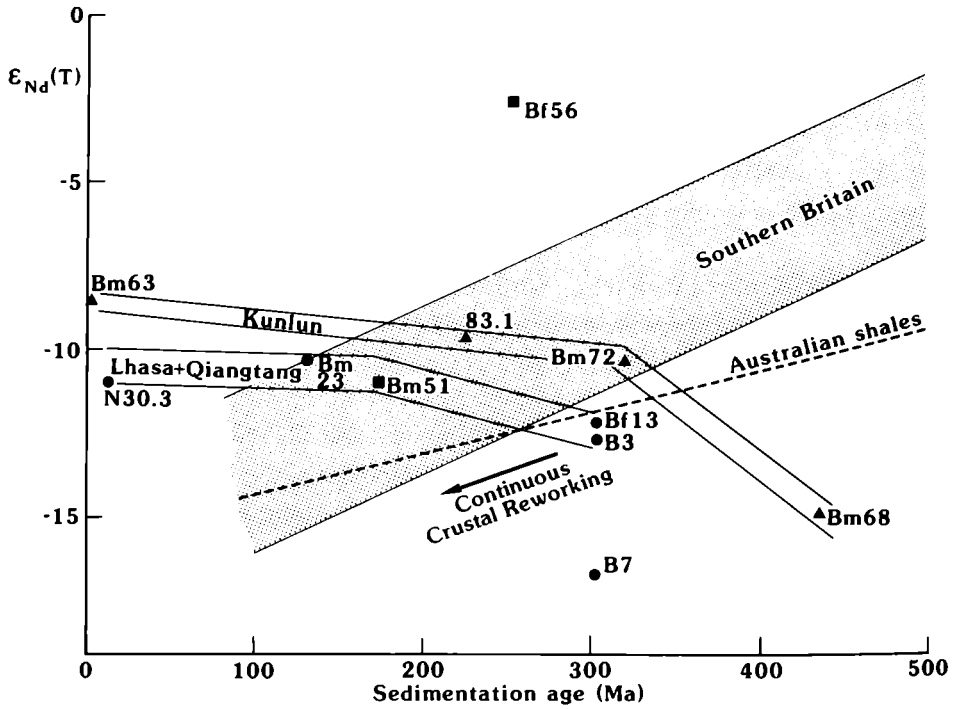

FIGURE 10. Variation of $\varepsilon_{Nd}(T)$ with sedimentation age for sediments from the Tibetan Plateau. ● = Lhasa, ■ = Qiangtang, ▲ = Kunlun Terranes. Shaded region marks evolution of sediments from southern Britain (Davies *et al.* 1985), dashed line indicates shale data from Australia (Allègre & Rousseau 1984).

TABLE 6. ND ISOTOPIC DATA FROM SEDIMENTS

Locality		Sample	Sedimentation Age		$^{143}Nd/^{144}Nd$	Sm ppm	Nd ppm	$^{147}Sm/^{144}Nd$	$\epsilon_{Nd}(T)$	T_{DM} Ma
Lhasa Terrane										
Lhasa	Laminated siltstone	B3	Late Carb.	303±17	0.51183±1	6.32	33.3	0.115	−12.6	1873
	Glacial (Drop-stone)	B7	Late Carb.	303±17	0.51161±1	2.09	11.6	0.109	−16.7	2099
Damxung	Siltstone	Bf13	Late Carb.	303±17	0.51185±1	5.75	30.2	0.115	−12.2	1855
Baingoin	Estuarine siltstone	Bm23	Lower Cret.	131±7	0.51206±1	5.58	25.8	0.131	−10.3	1823
Lunpola	Lacustrine siltstone	N30.3	Neogene	13±11	0.51207±1	6.11	31.1	0.119	−10.9	1558
Qiangtang Terrane										
Kaixingling	Shale	Bf56	Upper Perm.	258±5	0.51241±1	6.14	27.3	0.136	−2.5	1257
Wenquan	Plant shale	Bm51	Mid. Jur.	175±12	0.51199±2	5.63	29.8	0.114	−10.8	1613
Kunlun Terrane										
N. Kunlun	Silty limestone	Bm68	Ord./Sil.	435±25	0.51169±2	2.36	10.8	0.132	−14.9	2546
Xidatan	Shale	Bm72	Mid. Carb.	320±15	0.51198±1	11.29	50.6	0.135	−10.3	2067
Budongquan	Siltstone	83.1	Triassic	226±17	0.51204±1	5.92	29.3	0.122	−9.6	1681
Kunlun Pass	Lacustrine Siltstone	Bm63	Quaternary	0.8±0.8	0.51220±1	3.19	15.8	0.122	−8.5	1402

Analyst Xu Ronghua

(1) The terranes which constitute the plateau are sites of rapid crustal growth during the Phanerozoic providing juvenile magmatic material to the sediment. About 25% crustal growth is required in Tibet during the Phanerozoic assuming an initial crust of 2000 Ma average age from the average age of upper crust (Goldstein *et al.* 1984).

(2) A relatively young source region (late Proterozoic) was progressively uplifted and eroded more rapidly than older source regions during most of the Phanerozoic.

There is no evidence in the preserved fragments of crust now exposed for significant new crust during the last 500 Ma. The magmatic rocks which are exposed have a strong crustal component and the major opportunity for crustal growth came only in the last 40 Ma with the evolution of the Gangdise Belt. The decrease in age of sedimentary source regions from the Carboniferous to the Jurassic would seem to result from preferentially-uplifted juvenile material. Certainly, in the Lhasa Terrane, uplift of a young source region is required which predates not only the Himalayan orogeny, but also closure of the Banggong Suture. After closure of the Banggong Suture, the uplifted Kunlun Mountains, which represent sites of voluminous magmatism during Triassic times and possibly earlier, provide a relatively young northerly source from the southern Kunlun to the Qiangtang and Lhasa terranes.

The two samples of recent sedimentation (Neogene silts from the Lhasa Terrane and Quaternary silts from the Kunlun) give ε_{Nd} values of -10.9 and -8.5. The slightly younger model age for the northern deposits may reflect the proximity of the uplifted Kunlun batholith. These values are similar to that of sediment from the Yangtze River (-10.9) which has its source in Tibet (Goldstein *et al.* 1984). They are in strong contrast to sediments derived from either juvenile continental crust (such as Nile sediments $\varepsilon_{Nd} = -3.3$) or to those derived from predominantly Archaean continental crust (such as Congo sediments $\varepsilon_{Nd} = +16.1$). Uplifted regions of the Tibetan Plateau therefore have average model Nd ages of 1400–1600 Ma, somewhat younger than those of average continental crust (2000 Ma). This can be accounted for either by widespread mantle-derived magmatism in Tibet not hitherto sampled or by tectonic processes which have selectively uplifted younger terranes.

7. Discussion and conclusions

A compilation of available geochronological data from the Lhasa to Golmud section across the Tibetan Plateau (figure 11) indicates progressively younger periods of intrusive magmatism from north to south, associated with successively younger ocean closures. In the north of the plateau the Kunlun batholith was emplaced at a continental margin during active subduction in late Permian–mid Triassic times (260–240 Ma) and south of the batholith granites were emplaced in a post-collision environment in the early Jurassic (200–190 Ma). Micas from intrusions near the Xidatan Fault record distinctly younger ages (140–120 Ma) possibly due to tectonism associated with closure of the Banggong Suture. South of the Banggong Suture in the northern Lhasa Terrane, Cretaceous post-collision intrusions (130–110 Ma) slightly pre-date post-collision volcanism (110–70 Ma). In the southern Lhasa Terrane magmatism is predominantly Eocene (60–40 Ma), pre-dating collision between the Himalayan and Lhasa terranes, although Cretaceous plutonism ($\sim$ 90 Ma) WSW of Lhasa records an earlier period of subduction.

Nd model ages from sediments exposed in all three crustal fragments define a trend of increasing ε_{Nd} with decreasing age of sedimentation. The samples define a band which repre-

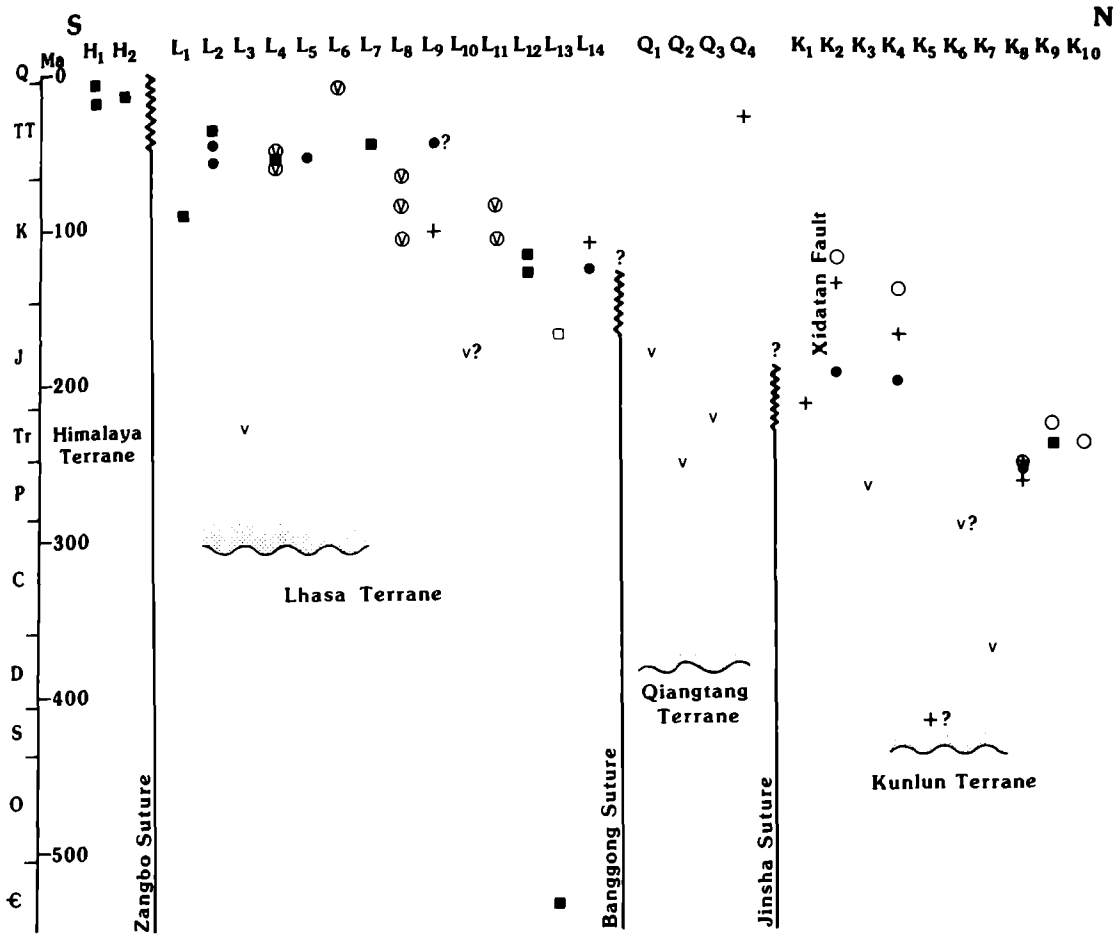

FIGURE 11. Compilation of geochronological data in geographic sequence from south to north along geotraverse route (extended south of the Zangbo suture). ■ = U–Pb monazite or zircon age, □ = U–Pb sphene age, ● = Rb–Sr isochron age, ○ = Rb–Sr biotite age, + = K–Ar biotite age, Ⓥ= $^{39}Ar/^{40}Ar$ age on volcanics, v = undated volcanics. Shading indicates oldest fossiliferous strata for each terrane. H_1 = High Himalaya, H_2 = North Himalaya, L1 = Dazhuka, L2 = Quxu–Lhasa, L3 = Dagze, L4 = Linzizong Formation, L5 = Yangbajain, L6 = Macquiang, L7 = Nyainqentanglha, L8 = Nam Co, L9 = Pung Co, L10 = Nagqu, L11 = Dongqiao, L12 = Baingoin-Amdo, L13 = Amdo (basement), L14 = Mo Tian Ling, Q1 = Yanshiping Group, Q2 = Kaixingling Group, Q3 = Batang Group, Q4 = Fenghuoshan, K1 = Wudaoliang, K2 = Xidatan, K3 = Wanbaogou Group, K4 = Naij Tal, K5 = Wanbaogou, K6, K7 = Dagangou Formation, K8 = Golmud Hydro, K9 = Golmud East, K10 = Duo Ya He.

sents Nd data for average Tibetan crust exposed during the Phanerozoic (figure 12). $\varepsilon_{Nd}(T)$ from igneous samples lie in an envelope constrained by a depleted mantle reservoir and the sediment data. Hence on the basis of Nd data alone, magmagenesis can be modelled from mixing upper crustal and mantle end-members. Considerations of Sr–Nd systematics however, indicate that the Kunlun granites result predominantly from anatexis of upper–intermediate mid-Proterozoic crust whereas peraluminous Cretaceous plutons from the northern Lhasa terrane and Eocene plutons from the Nyainqentanglha Shan result from melting crustal sources of similar age and intermediate compositions. Calc-alkaline intrusions from the northern Lhasa Terrane and from the Gangdise Belt have a mantle signature, but require 30–60 % assimilation of crustal material.

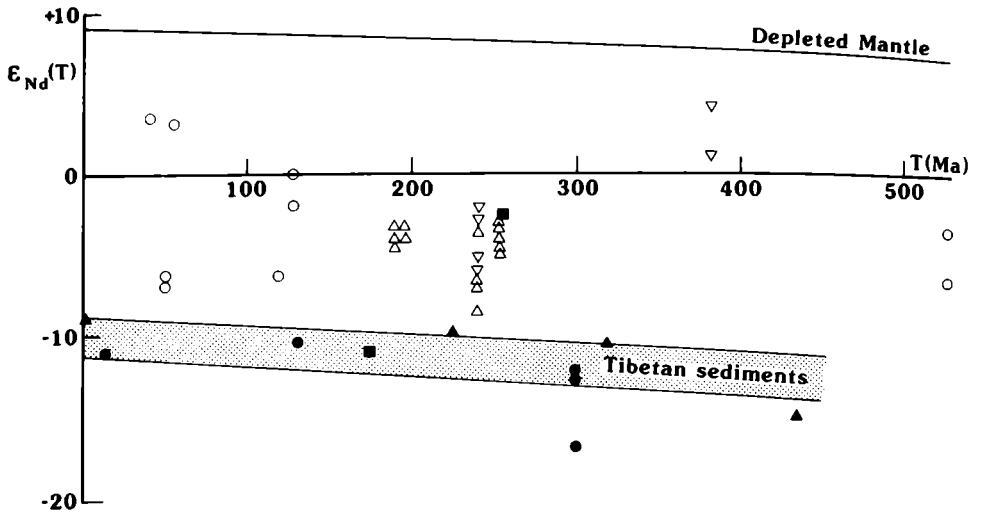

FIGURE 12. Variation of $\varepsilon_{Nd}(T)$ with time for samples from Tibetan Plateau. Open symbols indicate igneous samples and filled symbols sediment data (see figure 10 for legend). ▽ = volcanics from Kunlun Terrane. Depleted mantle from De Paolo 1981.

From the analysed samples, there is no evidence that crustal growth occurred on a large-scale during the Phanerozoic in any of the three terranes, and all intrusions result from partial or total crustal reworking. Indeed a distinctive feature of intrusions from the Tibetan Plateau is that, irrespective of age, they have a substantial crustal component in their petrogenesis. This raises the intriguing possibility that anomalously thickened continental crust is a characteristic which considerably predates the most recent (Eocene) collision recorded in the rocks from the plateau.

Peter van Calsteren and Andy Gledhill were responsible for the smooth running of the mass spectrometer and for chemical separation. Isotopic analytical facilities at the Open University are supported by NERC. We thank John Taylor for drafting the figures and Marilyn Leggett for typing the manuscript.

REFERENCES

Allègre, C. J. & Ben Othman, D. 1980 Nd and Sr isotopic relationship in granitoid rocks and continental crust development: a chemical approach to orogenesis. *Nature, Lond.* **286**, 335–342.

Allègre, C. J. & Rousseau, D. 1984 The growth of continent through geological time studied by Nd and isotope analysis of shales. *Earth planet. Sci. Lett.* **67**, 19–34.

Blattner, P., Dietrich, V. & Gansser, A. 1983 Contrasting ^{18}O enrichment and origin of High Himalayan and Transhimalayan intrusives. *Earth planet. Sci. Lett.* **65**, 276–286.

Casnedi, R., Desio, A., Forcelle, F., Nicoletti, M. & Petrucciani, C. 1978 Absolute age of some granitoid rocks between Hindu Raj and Gilgit River. *Rend. Sci. fis. mat. e nat.* **64**, 204–210.

Chang Chengfa & Pan Yushen 1981 A brief discussion on the tectonic evolution of the Qinghai-Xizang plateau. *Proceedings on Qinghai-Xizang (Tibet) Plateau*, **1**, 1–18. Beijing.

Chang Chengfa *et al.* 1986 Preliminary conclusions of the Royal Society and Academia Sinica 1985 geotraverse of Tibet. *Nature, Lond.* **323**, 501–507.

Coulon, C., Maluski, H., Bollinger, C. & Wang, S. 1986 Mesozoic and Cenozoic volcanic rocks from central and southern Tibet: ^{39}Ar-^{40}Ar dating, petrological characteristics and geodynamical significance. *Earth planet. Sci. Lett.* **80**, 281–302.

Davies, G., Gledhill, A. & Hawkesworth, C. 1985 Upper crustal recycling in southern Britain: evidence from Nd and Sr isotopes. *Earth planet. Sci. Lett.* **75**, 1–12.

Debon, F., Sonet, J., Lin Guohue, Jin Chengwei & Xu Ronghua 1982 Caractères chimico-mineralogiques et datations par Rb–Sr des trois ceintures plutoniques du Tibet meridional. *C. R. Acad Sci Paris* **295**, 213–218.

Debon, F., Le Fort, P., Sheppard, S. M. F. & Sonet J. 1986 The four plutonic belts of the Transhimalaya-Himalaya: a chemical, mineralogical, isotopic and chronological synthesis along a Tibet-Nepal section. *J. Petrol.* **27**, 219–250.

Debon, F., Le Fort, P., Dantel, D., Sonet, J. & Zimmermann, J. L. 1987 Granites of western Karakorum and northern Kohistan (Pakistan): A composite Mid-Cretaceous to Upper Cenozoic magmatism. *Lithos* **20**, 19–40.

De Paolo, D. J. 1981 Nd isotopes in the Colorado Front Range and crust-mantle evolution in the Proterozoic. *Nature, Lond.* **291**, 193–196.

Dodson, M. H. 1979 The theory of cooling ages. In *Lectures in isotope geology* (ed. E. Jager and J. C. Hunziker), pp. 194–202. Heidelberg: Springer-Verlag.

Duyverman, H. J., Harris, N. B. W. & Hawkesworth, C. J. 1982 Crustal accretion in the Pan African: Nd and Sr isotope evidence from that Arabian Shield. *Earth planet. Sci. Lett.* **59**, 315–326.

Gariepy, C., Allègre, C. J. & Xu Ronghua 1985 The Pb isotope geochemistry of granitoids from the Himalaya-Tibet collision zone: implications for crustal evolution. *Earth planet. Sci. Lett.* **74**, 220–234.

Goldstein, S. L., O'Nions, R. K. & Hamilton, P. J. 1984 A Sm-Nd isotopic study of atmospheric dusts and particulates from major river systems. *Earth planet. Sci. Lett.* **70**, 221–236.

Hawkesworth, C. J., Kramers, J. D. & Miller, R. McG. 1981 Old model Nd ages in Namibian Pan-African rocks. *Nature, Lond.* **289**, 278–282.

Honneger, K., Dietrich, V., Frank, W., Gansser, A., Thoni, M. & Trommsdorff, W. 1982 Magmatism and metamorphism in the Ladakh Himalayas (the Indus-Tsangpo suture zone). *Earth planet. Sci. Lett.* **60**, 253–292.

Maluski, H., Proust, F. & Xiao, X. C. 1982 $^{39}Ar/^{40}Ar$ dating of the Trans-Himalayan calc-alkaline magmatism of southern Tibet. *Nature, Lond.* **298**, 152–154.

McCulloch, M. T. & Chappell, B. W. 1982 Nd isotopic characteristics of S and I-type granites. *Earth planet. Sci. Lett.* **58**, 51–64.

McDermott, F. 1987 Granite petrogenetic crustal evolution studies in the Damara Pan-African orogenic belt, Namibia. Unpubl. Ph.D. thesis, Open University.

Michard, A., Gurnet, P., Soudant, M. & Albarede, F. 1985 Nd isotopes in French Phanerozoic shales: external vs. internal aspects of crustal evolution. *Geochim. cosmochim. Acta.* **49**, 101–610.

Petterson, M. G. & Windley, B. F. 1985 Rb–Sr dating of the Kohistan arc batholith in the Trans-Himalaya of north Pakistan and tectonic implications. *Earth planet. Sci. Lett.* **74**, 45–57.

Scharer, U., Hamet, J. & Allègre, C. J. 1983 The Transhimalaya (Gangdese) plutonism in the Ladakh region: an U–Pb and Rb/Sr study. *Earth planet. Sci. Lett.* **67**, 327–339.

Scharer, U., Xu Ronghua & Allègre, C. J. 1984 U–Pb geochronology of the Gangdese (Transhimalaya) plutonism in the Lhasa-Xigaze region, Tibet. *Earth planet. Sci. Lett.* **67**, 311–320.

Weaver, B. L. & Tarney, J. 1980 Continental crust composition and nature of the lower crust: constraints from mantle Nd–Sr isotope correlation. *Nature, Lond.* **286**, 342–346.

Xu Ronghua & Jin Chengwei 1984 A geochronological study of the Quxu batholith, Xizang. *Sci. Geol. Sinica*, 414–422.

Xu Ronghua, Scharer, U. & Allègre, C. J. 1985 Magmatism and metamorphism in the Lhasa Block (Tibet): a geochronological study. *J. Geol.* **93**, 41–57.

Phil. Trans. R. Soc. Lond. A **327**, 287–305 (1988) [287]
Printed in Great Britain

Geological mapping of the 1985 Chinese–British Tibetan (Xizang–Qinghai) Plateau Geotraverse route

By W. S. F. Kidd[1], Pan Yusheng[2], Chang Chengfa[2], M. P. Coward[3], J. F. Dewey[4], F.R.S., A. Gansser[5], P. Molnar[6], R. M. Shackleton[7], F.R.S., and Sun Yiyin[2]

[1] *Department of Geological Sciences, State University of New York, Albany, New York* 12222, *U.S.A.*
[2] *Institute of Geology, Academia Sinica, Box* 634, *Beijing, People's Republic of China*
[3] *Department of Geology, Imperial College, Prince Consort Road, London SW*7 2*BP, U.K.*
[4] *Department of Earth Sciences, University of Oxford, Parks Road, Oxford OX*1 3*PR, U.K.*
[5] *Geologisches Institut, Eidgenossische Technische Hochschule, CH-*8092, *Zürich, Switzerland*
[6] *Department of Earth, Atmospheric, and Planetary Sciences, Massachusetts Institute of Technology, Cambridge, Massachusetts* 02139, *U.S.A.*
[7] *Department of Earth Sciences, The Open University, Walton Hall, Milton Keynes, MK*7 6*AA, U.K.*

[Map and microfiche in pockets]

The 1:500,000 coloured geological map of the traverse route combines observations from the Geotraverse, previous mapping, and interpretation of orbital images. The position of all localities visited by Geotraverse participants and basic geological data collected by them along the traverse route are shown on a set of maps originally drawn at 1:100,000 scale, reproduced on microfiche for this publication. More detailed mapping, beyond a single line of section, was achieved in five separate areas. The relationships between major rock units in these areas, and their significance, are outlined in this paper. Near Gyanco, (Lhasa Terrane) an ophiolite nappe, apparently connected with outcrops of ophiolites in the Banggong Suture about 100 km to the north, was underthrust by a discontinuous slice of Carboniferous–Permian clastic rocks and limestone, contrary to a previous report of the opposite sequence. At Amdo, a compressional left-lateral strike-slip fault zone has modified relationships along the Banggong Suture. Near Wuli, (northern Qiangtang Terrane) limited truncation of Triassic strata at the angular unconformity below Eocene redbeds demonstrates that most of the folding here is of Tertiary age. The map of the nearby Erdaogou region displays strong fold and thrust-shortening of the Eocene redbeds, evidence of significant crustal shortening after the India–Asia collision began. In the Xidatan–Kunlun Pass area, blocks of contrasting Permo–Triassic rocks are separated by east-trending faults. Some of these faults are ductile and of late Triassic – early Jurassic age, others are brittle and part of the Neogene–Quaternary Kunlun left-lateral strike-slip fault system. Some more significant remaining problems that geological mapping might help to solve are discussed briefly, including evidence for a possible additional ophiolitic suture within the Qiangtang Terrane.

1. Introduction

The purposes of this chapter are to document the sources used to compile the 1:500,000 scale geological map of the Geotraverse route and its surroundings (map 1, in pocket) and to discuss briefly the detailed geological maps, originally drawn on the 1:100,000 scale topographic map

sheets provided by Academia Sinica, that record localities and basic data collected by all working groups during the traverse (microfiche 2).

Fifty-five days were spent on the traverse route, from June 4th to July 28th, 1985, covering a distance of about 1300 km along the main paved road from Lhasa to Golmud, with additional distances of several hundred kilometres on subsidiary traverses along less travelled dirt roads and tracks leading away from the main road. This required an average of about 30 km of section completed each day. Consequently, *detailed* geological mapping, in the strict sense of areally extensive and well-distributed observations, was not possible (nor was it originally intended) at most places along the traverse route. Where detailed observation of more than a narrow section line (i.e., mapping) was achieved, the results are discussed below. The immense scope for further investigations in many sections of the traverse route is well-illustrated by the current lack of detailed geological maps along most of its length, not to mention the vast remainder of the rest of the Qinghai–Xizang (Tibetan) Plateau. Some of the more critical geological problems remaining from the Geotraverse route whose solution would likely be provided or assisted by detailed mapping are also briefly discussed.

2. Geological map of the Geotraverse route

The coloured map (map 1, in pocket) is partly based on the field observations and subsequent laboratory results of the participants of the 1985 Academia Sinica – Royal Society Geotraverse, documented in the papers in this volume, on earlier work from various Chinese sources, and on the 1981–83 Franco-Chinese collaboration. Information from both the 1985 Geotraverse and the earlier sources has been extrapolated using interpretations of orbital imagery, which have also been used to modify previous map patterns in some places.

(*a*) *Previous work*

The principal maps used for compilation of map 1 are:

a) Geological map of the Southern Tethys of the Qinghai–Xizang Plateau [1:1 million scale]. (Yin Jixiang *et al.*, in press.)

b) Geological map of Qinghai Province [1:million scale] (Qinghai Bureau of Geology and Mineral Resources 1981).

c) Geological map of the Qinghai–Xizang (Tibet) Plateau [1:1.5 million scale]. (Ministry of Geology and Mineral Resources, Beijing, 1980).

d) Geological map of Lhasa Sheet [1:1 million scale] (Xizang Bureau of Geology and Mineral Resources 1979).

e) Geological map of Golmud Sheet, and Geological map of Naij Tal Sheet [1:200,000 scale] (Qinghai Bureau of Geology and Mineral Resources 1984).

f) Carte géologique du sud du Tibet [1:500,000 scale] (J. P. Burg 1983).

Stratigraphic units, defined by previous work, to which reference is made in this chapter or in the map legend are discussed, with citations, by Yin *et al.* (this volume).

(*b*) *Orbital imagery*

For most of the Qinghai–Xizang Plateau, the only orbital imagery at the time of the geotraverse consisted of multispectral scanner (MSS) images from the older series of LANDSAT platforms. Other imagery available to us consisted of a line of Metric Camera (colour film

original) images obtained from a Shuttle–Spacelab mission that closely follows much of the line of the Geotraverse. The large-format Camera (9 × 18 inch negative, black and white) flown on another Shuttle mission provides a few spectacularly high-resolution images from two paths crossing the northern end of the Geotraverse route.

The LANDSAT imagery was obtained in false colour composite prints at a scale of 1 : 250,000. Because these images are from the older 4-spectral-band MSS instrument, they have a limited capability to discriminate bedrock lithologies (and lithologic units), especially when compared with the more recent Thematic Mapper (TM) 7-band instrument. Because of certain operating constraints on the LANDSAT 4 and 5 platforms, and a lack of a suitable data-relay satellite, TM images are not available for most of the Qinghai–Xizang (Tibetan) Plateau. Unlike the TM data, MSS images do not generally yield significant additional geologic information over the standard false colour print when various computer-generated enhancements are applied to the original digital image data. It may be possible to make certain features more obvious but, in most cases, they are easily seen on the original "unenhanced" images.

The Metric Camera images (obtained as prints at a scale of about 1 : 240,000), being visible light products, have an even more limited capability to discriminate lithologies. Lithologic boundaries and units can be clearly seen *locally* on these two kinds of images, especially the LANDSAT images, but it is not possible in most places to distinguish bedrock units with any confidence, or to follow contacts precisely, over more than a few kilometres. For this reason alone, it would be inappropriate to use the imagery to extrapolate from the detailed traverse observations to fill each sheet of the 1 : 100,000 scale maps. There are two reasons why it is difficult to distinguish most lithologic units and/or their boundaries on the images; the rocks along the traverse route are with minor exceptions not structurally simple, and the rock exposures are quite extensively veneered with *felsenmeer* or solifluction materials in the less rugged areas, it being hard to trace structurally complex units in any area of rugged relief no matter how good the exposure. However, reliably distinguishable lithologic contrasts do occur in some local areas, usually where the contrast is very striking on the ground, and these can be used to check or modify previous maps for the compilation of the 1 : 500,000 traverse route map. For example, the contacts between granites and darker and/or more fractured rocks can be seen in several, but not all places, near Gyanco and Dongqiao, and in the southern Kunlun Shan. Contacts of limestones with darker sedimentary rocks also stand out in some places, for instance between Ordovician carbonates and Triassic arenites in the Golmud River valley, and between volcanics and carbonates near Yaxi Co. Where topography is modest, a fairly general lithologic distinction can be seen on the LANDSAT images between redbeds (of several ages) and other rocks, for example near Gyanco, Amdo, Yanshiping, and near Erdaogou. This can be done because the redbeds have, in many places, a distinctive yellow–orange tone on the false-colour images. However, where the topography becomes rugged, and where soil or solifluction cover is developed, this feature becomes less prominent, and it is clear that it does not show reliably all areas of redbed occurrence.

Although lithologies and their contacts are generally difficult to distinguish, stratification expressed by topographic features is more easily identified and followed on these images. It is not always possible to show the full amount of stratification detail available from the images on the 1 : 500,000 scale map, but the general trends and the major folds are included. Because of the poor expression of the stratification in most places, it is not possible to identify easily old, inactive faults subparallel with strike. The assumption must be that most of these fault structures are not detected reliably from the images.

The structures that are most prominent on the images are the active (Quaternary) faults, as has been known for some time (Molnar & Tapponnier 1978). These are distinguished from the older faults on the 1:500,000 map. The observations made during the geotraverse on these structures are discussed by Kidd & Molnar, this volume). Most concern the major east-trending left-lateral strike-slip fault system in the southern Kunlun Shan, of which two major fault strands, the Xidatan and Kunlun Pass Faults, are crossed by the traverse route. The north-trending normal faults, and related NE- and NW-trending strike-slip faults, seen in several places along the southern half of the route, have been recently described in detail by Armijo *et al.* (1986).

The orbital imagery, therefore, is extremely helpful in providing a general overview of the topography and geology, and for mapping some more detailed aspects of the geology, particularly neotectonic structures. It has limitations, however, in extrapolation of lithologic map units and older (inactive) structures. The speculative nature of most of these extrapolations means that the 1:500,000 map will probably need revision when ground investigation is done of areas not covered by our traverse or previous Chinese field work. Several of the Chinese maps, particularly the 1:1.5 million scale geological map of the Qinghai–Xizang plateau, have incorporated substantial input from interpretation of LANDSAT images. The areas in which this has been done are not readily separable from those in which there is ground-based map data. Therefore caution is needed in using particular map patterns or relations on the 1:500,000 scale traverse map for far-reaching conclusions, particularly for geology far from that known on the ground.

3. Detailed traverse maps

(*a*) *Introduction*

Base maps used during the traverse were provided by the Academy of Sciences and consisted of a set of 69 topographic maps at 1:100,000 scale (figure 1) of excellent detail and quality. Most have a contour interval of 20 metres; some, in areas of rugged topography, have an interval of 40 metres. These maps proved ideal for the purposes of recording locations and basic geology throughout the traverse. In a few places, some Geotraverse groups locally went beyond the coverage of these maps; in these areas we used 1:100,000 scale black-and-white prints of the LANDSAT images as base maps, although it was clearly easier and preferable to use the topographic maps for location in the field rather than the images. A set of the topographic maps is lodged with the British Museum (Natural History).

Localities and basic geological information, such as observed lithologies, lithologic unit boundaries, faults, fold hinges, attitudes of bedding, foliation, lineation, etc., were recorded on a master set of maps during the traverse. These data were checked and supplemented from participants' field notes after the end of the traverse. The master set of geotraverse geologic maps is lodged in the collections of the British Museum (Natural History). The localities and all the geological information have been abstracted by redrafting from the 48 topographic map sheets that were used, for reproduction on microfiche (in pocket). The intention is that these maps show only data observed in the field, and modest extrapolations ("field glasses geology") made in the field at the time by those who visited the particular localities. Because all the localities visited by all participants are shown on these maps, each with its locality number, it will be clear which information is from outcrop observations and which consists of extrapolation

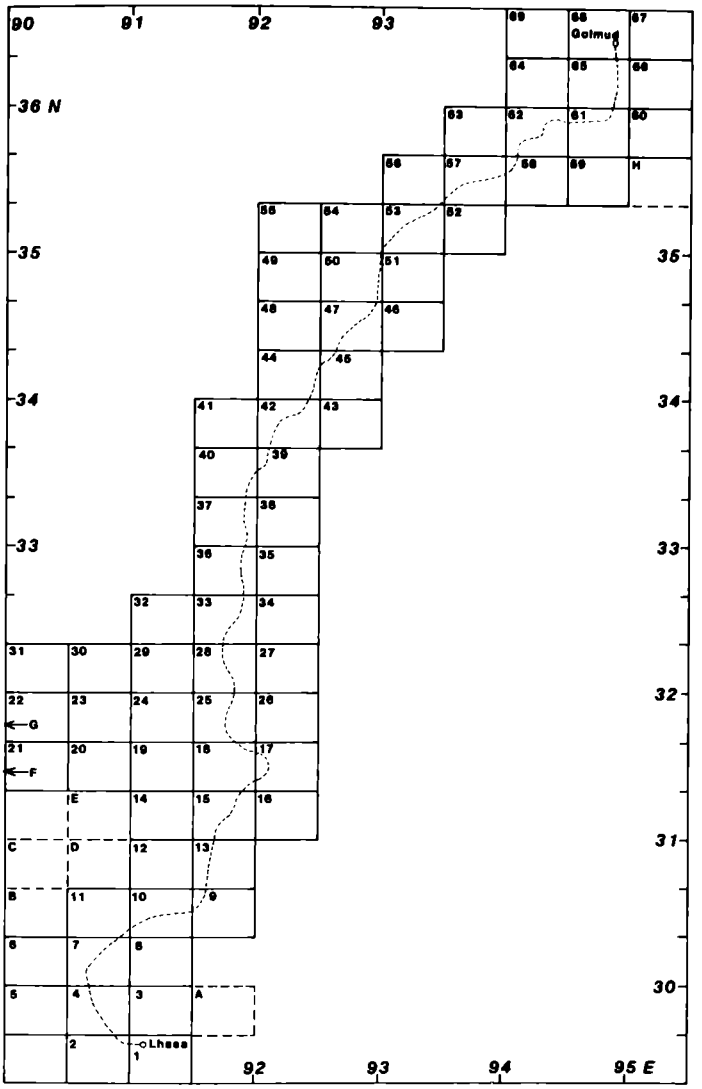

FIGURE 1. Index map to topographic map sheets (1:100,000 scale) provided for the Geotraverse. Lhasa–Golmud highway shown by dashed line. Numbers are keyed to map sheet names in the list below. Detailed geological maps drawn on this base (microfiche, in pocket) use these sheet numbers and names for identification. Not all map sheets were used and in cases where only a small proportion of a map sheet was used, it may be combined with an adjacent sheet in the microfiche geological maps. Areas labelled with letters A–H refer to geological observations made on LANDSAT image base maps; these areas are included with the other maps on microfiche.

1. Lhasa City
2. Quxu
3. Lhunzhub
4. Maqu
5. Jidaguo
6. Junmaching
7. Yangbajian
8. Pangduo
9. Baga
10. Damxung
11. Ningzhong
12. Nam Lake
13. Gulu
14. Bengcuo
15. Sangxiong
16. Dareng
17. Nagqu
18. Gajia
19. Baerda
20. Jiangcuo
21. Baingoin
22. Dongkacuo
23. Dongqiao
24. Jibuxiang
25. Erdaohe Station
26. Nyimaqu
27. Nyainrong County
28. Amdo
29. Zhashuqu
30. Cigetangcuo
31. Yatucuo
32. Chaqu
33. 112th Station
34. Maisairi
35. Dengka
36. Tanggula Pass
37. Wenquan
38. Longyala
39. Yanshiping
40. Wenquan Station
41. Jiri
42. Tongtian Bank
43. Cuojiangqin
44. Tuotuo River
45. Yaxicuo
46. Bayingzangtuoma
47. Erdaogou
48. Tangrijiapang
49. Gelushankecuo
50. Fenghuoshan
51. Lemacuo
52. Duoqun
53. Wudaoliang
54. Gongmaorima
55. Cuorendejia
56. Haidingluoer
57. Budongquan
58. 63rd Station
59. Zheseke
60. Reshui
61. Naij Tal
62. Qingbanshan
63. Diayingshan
64. Tuotuolalin
65. Dishantou
66. Duoyahe
67. Golmud East Farm
68. Comm. of Golmud
69. Dazaohuo

from them. The locality numbers can be used to relocate precisely the sampling and fossil localities to which reference is made in other papers in this volume and in any subsequent publications on the material collected.

The locations of the cross-sections of Coward *et al.* (this volume) are given on each map; in most cases, one section crosses several sheets and the continuation is indicated by subscript letters in sequence. In a few places along the Geotraverse route, some detailed mapping beyond a single line of section was achieved. Results from those areas are now discussed briefly. The location of each of the detailed maps (figures 3, 4, 6, 7, and 8) are given with respect to the traverse route on figure 2.

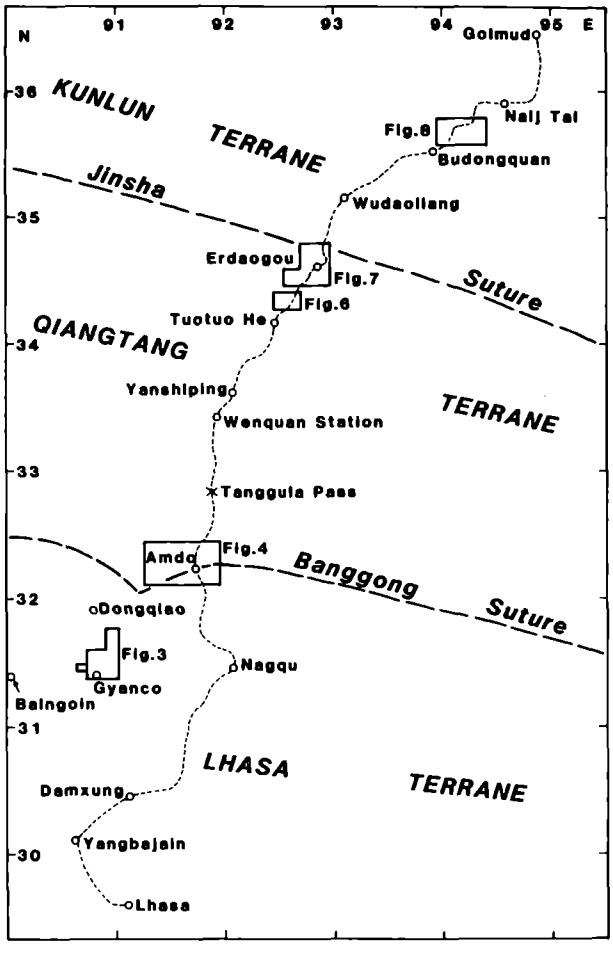

FIGURE 2. Sketch map showing location along the traverse route of detailed geological maps (figures 3, 4, 6, 7, and 8).

(*b*) *Gyanco–Pung Co*

In this area (figure 3), stratigraphic and structural relationships are exposed between the Banggong Suture-derived ophiolite nappe, Carboniferous–Permian clastics, limestones of uncertain age (?Permian or ?Jurassic), and Jurassic flysch. Mid-Cretaceous red clastics and andesite–rhyolite volcanics are also present, and mid-Cretaceous granitoid rocks and NNW-trending andesite dykes were observed to intrude all lithologies except the Cretaceous clastics

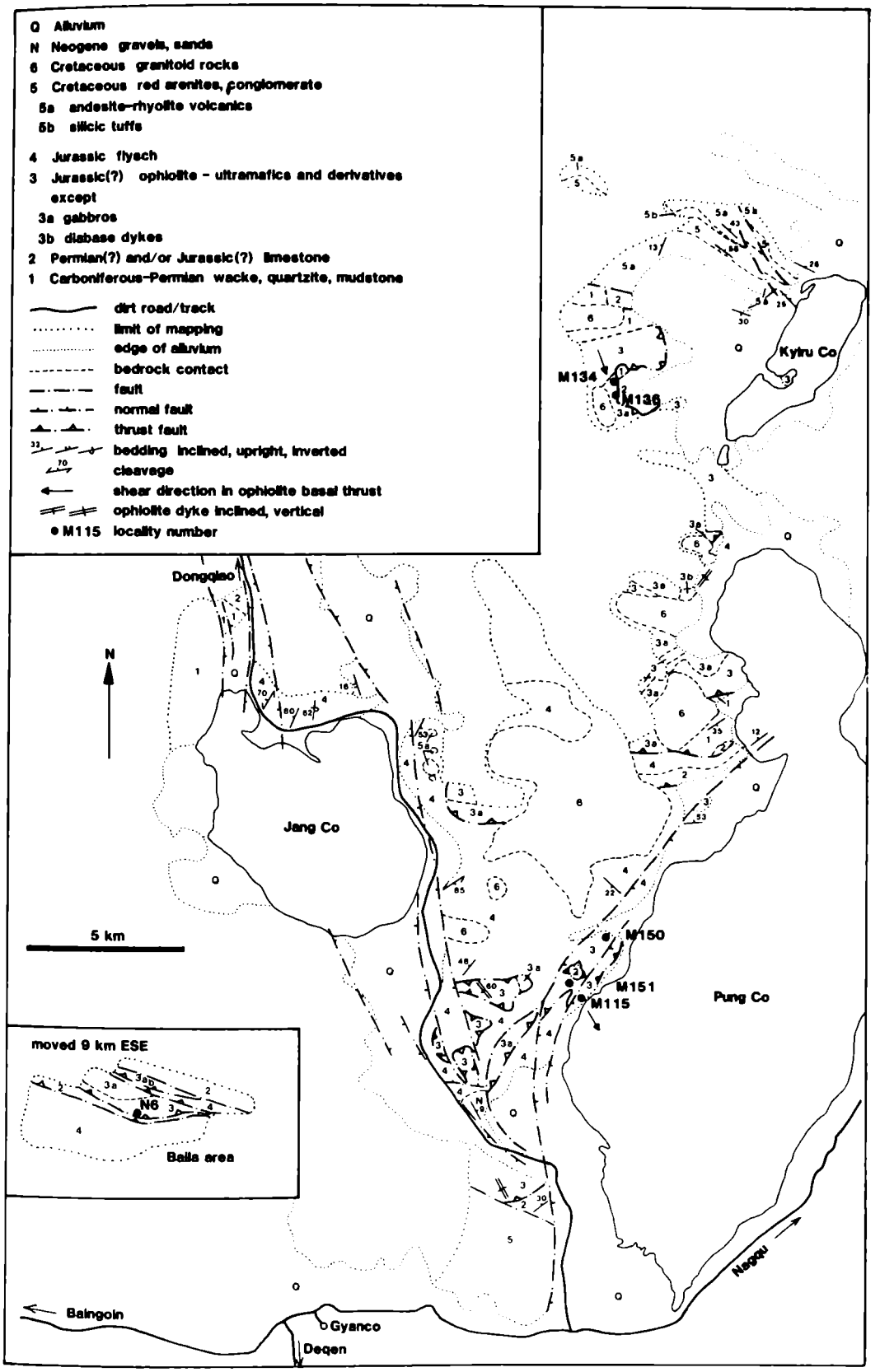

FIGURE 3. Geology in the vicinity of Gyanco and Pung Co. For location, see figure 2. This figure, and the other detailed maps, may be found easier to interpret if some or all of the units are coloured. The inset of the Baila area has been moved 9 km ESE from the true position with respect to the main area of the map.

and volcanics. A previous report on a larger area that encloses this one (Girardeau *et al.* 1984) maintains that the carbonates and the Carbo–Permian clastics form a nappe on top of the ophiolite. Our mapping in this area, and observations to the west near Baila (figure 3), demonstrates that this is not so, and that the Carboniferous–Permian clastics and the carbonates all lie in an imbricate zone (or duplex) at the base of the ophiolite nappe. The mapping also suggests why the confusion arose: if the normal faults near to and subparallel with the west shore of Pung Co are not recognised, it appears as if the ophiolite ultramafic rocks exposed near the lake shore are structurally below these sediments (and also Jurassic flysch) exposed to the west in the hillside. Our mapping was not extensive enough, given the less-than-perfect exposure, to determine whether any original large-scale relationships are preserved among the various ophiolite lithologies, nor did we determine whether the mid-Cretaceous volcanics and clastics were deposited unconformably above a severely folded or a basically flat-lying nappe pile. Structures at the basal contact of the ophiolite nappe, where serpentinite and carbonated derivatives of ultramafics are in original fault contact with Jurassic flysch, or with the Carboniferous–Permian clastics, or limestone, show clear SSE-directed sense-of-shear and shear direction indicators at localities M115, M134, M136, M150 and M151, on the west side of the Pung Co valley. These include S-C-type oblique foliations, oblique vein and fracture sets, steps in fibrous vein slickensides, and asymmetric folds. Oblique S-C-type foliation was also seen in the same position, and giving the same shear sense, at locality N6, near Baila, about 20 km west of Gyanco.

(*c*) *Amdo region*

The mapping in this area covered the ENE-trending range straddling the town of Amdo. Ophiolite lithologies occur on the south side of this range (figure 4). They mark the present location of the suture between the Lhasa and Qiangtang Terranes.

In the southwest, red clastic rocks of uncertain, Cretaceous or Tertiary age define a large asymmetrical syncline with a steeply N-dipping axial surface, which is cut by two prominent NNW-trending tear faults. Nearer Amdo, ophiolite lithologies (serpentinite and gabbro) are imbricated in south-directed thrusts with redbeds that contain andesitic volcanics, which are probably of mid-Cretaceous age. This imbricate zone projects westward above the large syncline of redbeds. The northern contact of ophiolite serpentinite in the section along the river valley about 10 km west of Amdo is a steep S-dipping fault, probably with a N-directed thrust component. Other steep faults and a moderately S-dipping, N-directed thrust cut folded redbeds and andesitic volcanics north of this point. East of Amdo, the extension of these redbeds is truncated by a steep fault with a S-side down component of displacement against mid and late Jurassic shale, limestone and arenites; west of Amdo it is not clear whether the equivalent contact is faulted or is unconformable. The Jurassic strata belong to the Qiangtang Terrane. They form a large, west-plunging anticline north and east of Amdo, and they are thrust north over redbeds of uncertain age (Cretaceous or Tertiary). In the same area (figure 4), some of these redbeds are themselves thrust northward over similar but finer-grained and softer red strata, which may be of Tertiary age. It is suspected that some of the redbeds west of Amdo unconformably cover the overthrust Jurassic strata, but a lack of good exposure prevented a firm conclusion. The northern redbeds are inferred to rest with angular unconformity on folded Jurassic strata of the Qiangtang Terrane, because a prominent erosion surface with reddening below it (figure 4) is seen about 20 km NNE of Amdo.

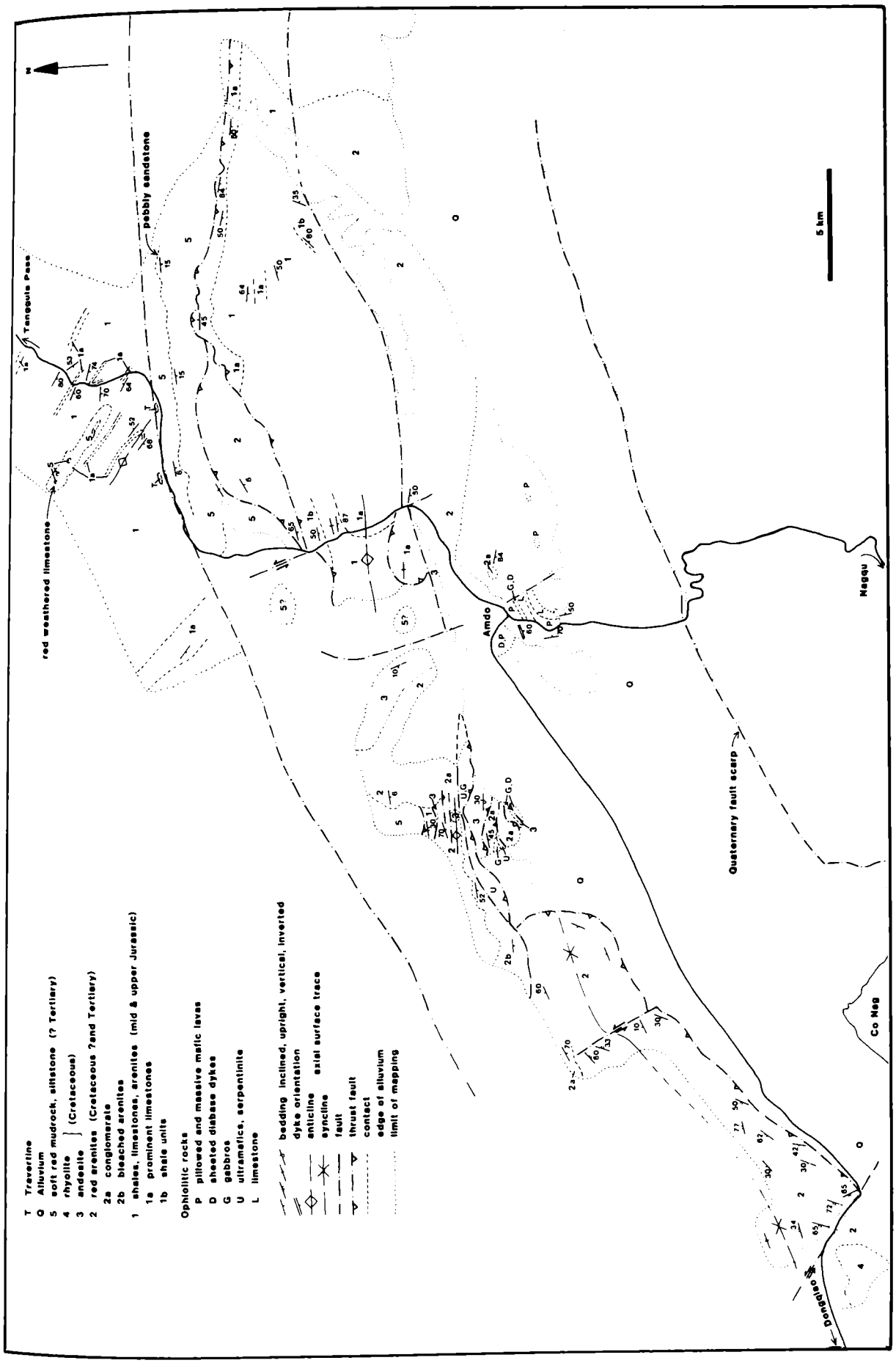

FIGURE 4. Geological map of the Amdo area. For location, see figure 2.

The fold trends (ESE) in these Jurassic rocks of this part of the Qiangtang Terrane are strongly oblique to and truncated by the ENE-trending fold and fault trends of the Amdo range. Furthermore, oblique slickensides and offset markers in outcrop imply that at least some of the faults in the Amdo range have a significant left-lateral strike-slip component of displacement. The overall structure of the narrow range, with outward-directed thrusts and steep faults with strike-slip components is identical to the "flower-structure" described from well-documented strike-slip fault zones with oblique compressional motion. This compressional displacement explains both the truncation of folded strata of the Qiangtang Terrane in this area, and the strong modification of the original relationships of the ophiolite in the suture zone. The structures seen in the Amdo region are thus largely the product of tectonic events younger than the initial suturing of the Qiangtang and Lhasa Terranes, even though these ophiolite occurrences now mark the position of the (modified) suture in this transect. At least a small amount of the compressional strike-slip tectonism affecting this area is probably Quaternary; several rivers crossing the Amdo range have a sharply antecedent relationship to it (see Kidd & Molnar, this volume), and the fault scarp on the south side of the Co Nag valley (figure 4) is also clearly an active tectonic feature.

The truncation of folds in the Qiangtang Terrane (figure 5) is more or less restricted to the length of the area mapped in figure 4. The trend of the Banggong Suture, inferred from ophiolite

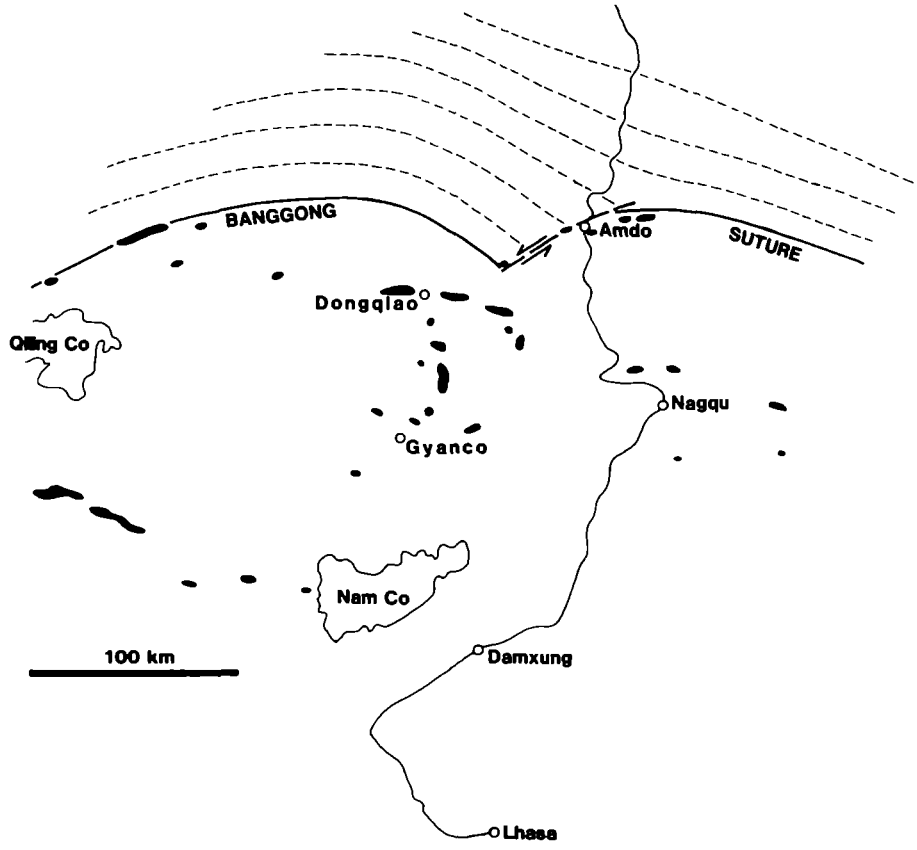

FIGURE 5. Sketch map of ophiolite occurrences in the Lhasa Terrane near the line of the geotraverse. Position of Banggong Suture and its concordance with the trend of folds in the southern Qiangtang Terrane (dashed lines) is indicated. Left-lateral strike-slip offset of the suture occurs near Amdo, coincident with truncation of the Qiangtang fold trends.

occurrences shown on the Geologic map of the Qinghai–Xizang Plateau, become parallel with these folds farther east and west (figure 5). The Amdo strike-slip zone, however, does not appear (from LANDSAT image interpretation) to extend obliquely into either the Qiangtang or Lhasa Terranes and its strike-slip displacement is therefore likely to have been accommodated by additional thrusting in the general vicinity of the suture beyond the ends of the Amdo range.

(*d*) *Tuotuo River–Wuli area*

Mapping in this area (figure 6) was aimed at understanding the relationship between the Eocene red clastics of the Fenghuoshan Group and the underlying Triassic Batang Group carbonates, andesitic volcanics, and clastics, and Jurassic Yanshiping Group clastics. The map shows that an angular unconformity occurs at the base of the Fenghuoshan redbeds but, from measured dips, and from the limited truncation of the underlying Batang Group (figure 6) it is concluded that the latter was only gently folded, at least in this area, prior to redbed deposition. The relations of the Yanshiping Group to this unconformity were not determined conclusively. However, if the extremely pure pale quartzite seen along part of the northern outcrop of the Batang Group is at the base of the Jurassic sequence, its occurrence at two places below redbeds to the north near Erdaogou (figure 7) suggests little discordance between the redbeds and the Jurassic sequence, as long as the latter is of modest thickness in this area. Previous maps show the volcanics and carbonates below the redbeds near the main road as of Permian age, correlative with the Wuli Group, (see Yin *et al.*, this volume). The lithologic types and sequence, and the fossils of Norian age in the limestones at locality M225 (Smith & Xu, this volume) show that these strata belong to the Triassic Batang Group.

Structures observed (vein and fracture sets, slickensides) in the well-lithified redbeds of the Fenghuoshan Group on the southern edge of this range indicate southward overthrusting over adjacent poorly-lithified marls and sands (presumed Neogene in age). Unlike the Erdaogou area (see below), no strong evidence for Quaternary thrusting was seen here, but most of the folding of the strata in this area is of Tertiary age. The implications of this observation for the age of folding in the Qiangtang Terrane as a whole are discussed below.

(*e*) *Erdaogou area*

Upright folds and mostly northward-dipping thrust faults in the Eocene Fenghuoshan Group redbeds must be related to crustal shortening during the India–Asia collision. The map of this area (figure 7) and the cross-section derived from it (see Coward *et al.*, this volume) yield substantial shortening values, a minimum of about 40% by folding alone. The LANDSAT image and the topographic maps give a fairly clear idea, from well-developed stratification trends, where the major folds and thrusts are located. With the distributed ground observations, including abundant younging indicators in the redbed arenites, most of the structures shown are identified with confidence.

A prominent thrust outcrops in the southernmost range of hills placing the well-lithified Eocene red arenites over soft red marls and pale sands that are presumed from their state of lithification to be younger than the Eocene strata. A well-exposed small thrust duplex of the lithified red arenites occurs in the flank of the hill on the east bank of the river Qu Ma Liu (Moron Us; Leeder *et al.*, this volume) adjacent to the main road (locality M191), and a similar imbrication, in this case involving the young marls, is seen about 7 km west of this point. Evidence for very young (Quaternary) thrust tectonics is suggested by the presence of an

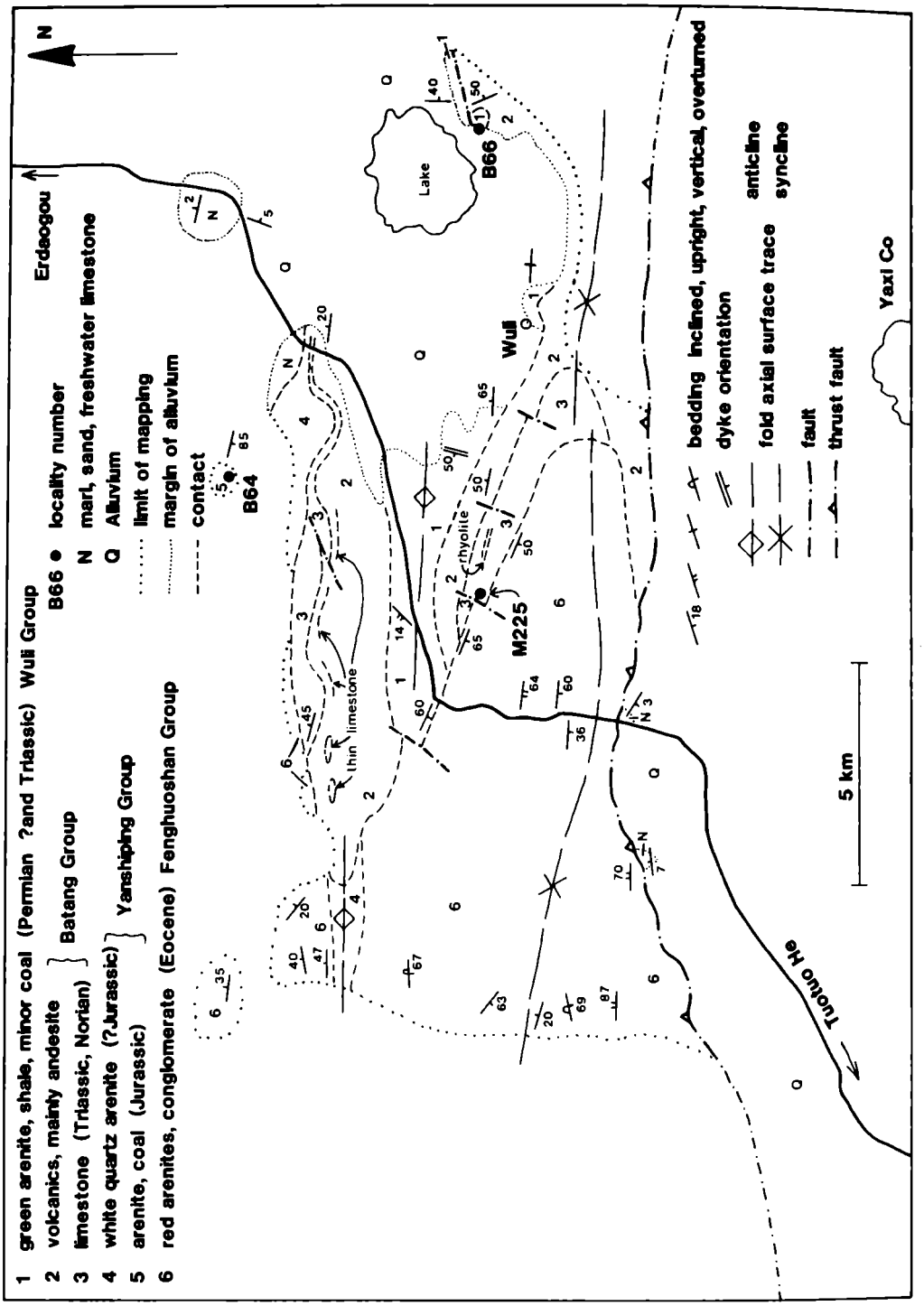

FIGURE 6. Geological map of an area near Wuli. For location, see figure 2.

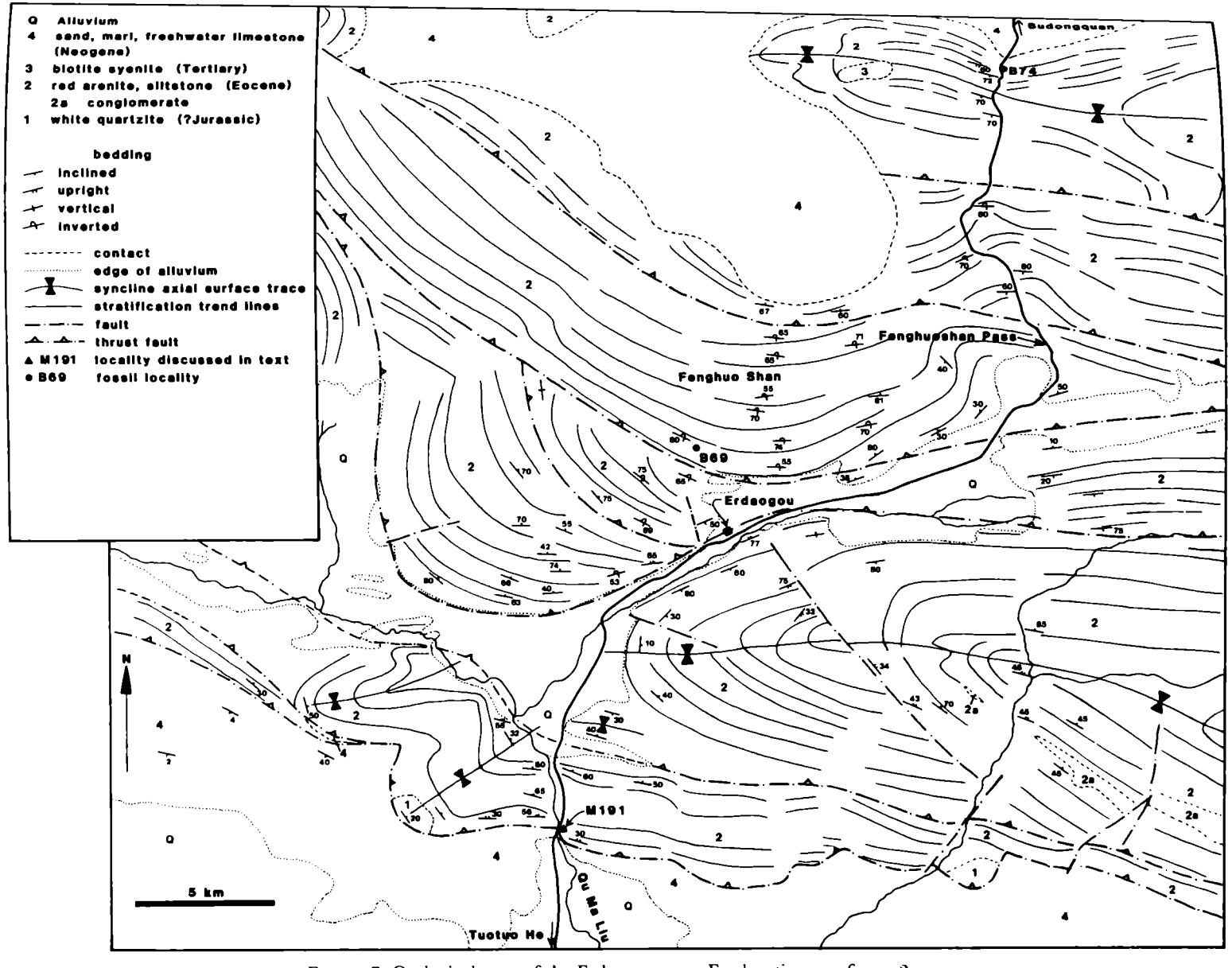

FIGURE 7. Geological map of the Erdaogou area. For location, see figure 2.

incised meander in a small side valley joining the east side of the valley of the Qu Ma Liu (Moron Us), where the thrust outcrops by the main road (locality M191). The local antecedent relationship that this river, and others like it farther east, has with this southernmost range of the Fenghuoshan also suggests late Neogene-Quaternary uplift, most likely by movement on this thrust (see Kidd & Molnar, this volume and Leeder *et al.*, this volume).

(*f*) *Xidatan Valley–Burhan Budai Mountains*

The Burhan Budai mountains form the southern side of the Xidatan valley, which marks the location of the main strand of the Kunlun Fault system, a major left-lateral strike-slip zone (see Kidd & Molnar, this volume). The bedrock on the southern side of this valley was mapped (figure 8) to try to determine the nature and age of the contacts between the several contrasting rock units that occur there, and to see whether any of the faults related to the Kunlun Fault.

A prominent ductile high strain zone in the form of a grey-black phyllonite unit several hundred metres thick occurs at lower elevations on the southern margin of the valley. The thickness suggests that it must be a zone of major displacement. The phyllonite contains a single strong phyllitic foliation dipping on average moderately to steeply north. Boudinaged quartz veins are common in this foliation. It is affected by a pervasive set of outcrop-scale open to tight folds with gently-dipping axial surfaces and gently east- or west-plunging hinge lines. Both these later folds, and a less intense to phyllitic cleavage are seen in the two major structural blocks to the south of the phyllonite; that is, all the bedrock south of the Xidatan in this map area shares the same outcrop-scale structural sequence, which is thought from regional evidence to have been formed in late Triassic – early Jurassic times.

In one locality (M306), north of the phyllonite, dark grey highly-strained limestone and pale-coloured pure limestone in variably disrupted thick beds occur in a melange-like disrupted grey slaty matrix. Evidence in outcrop of south-directed thrusting (offset layers, asymmetric folds) suggests that this material perhaps formed part of the hanging wall to the phyllonite, in which evidence of south-directed thrust-sense shear (asymmetric boudins of veins, shear-band cleavage) was also seen locally.

However, at the eastern end of the mapped area, green phyllitic rocks, partly arenaceous and feldspathic, resembling those seen structurally below the carbonates farther east in the Dongdatan area, occur to the north of the phyllonite. Either a large lateral ramp structure, or (perhaps more likely) the original occurrence of the carbonates in an imbricate slice adjacent to the phyllonite, are needed to explain this change, unless the carbonates form part of a slice bounded by a younger strike-slip fault and have been displaced many kilometres from the nearest source to the east. As the contact between the carbonates and the phyllonite is not exposed, this problem cannot be resolved without further mapping.

The southern boundary of the phyllonite is, in most places, a brittle subvertical fault that truncates the phyllonite foliation. In one locality (M244), by contrast, a short section of strongly-foliated green phyllites with thin arenite layers occur under a contact with very dark phyllonites, the contact dipping north concordant with the cleavage. Because this occurrence is so restricted, it is unclear whether this represents the footwall of the phyllonite zone or just a lens of somewhat less-strained rock within it. The brittle fault that truncates the phyllonite elsewhere was found exposed in only one locality (M284), where layering and foliation is locally folded on both sides within about 5 metres of the fault. The fault itself consists of gouge about

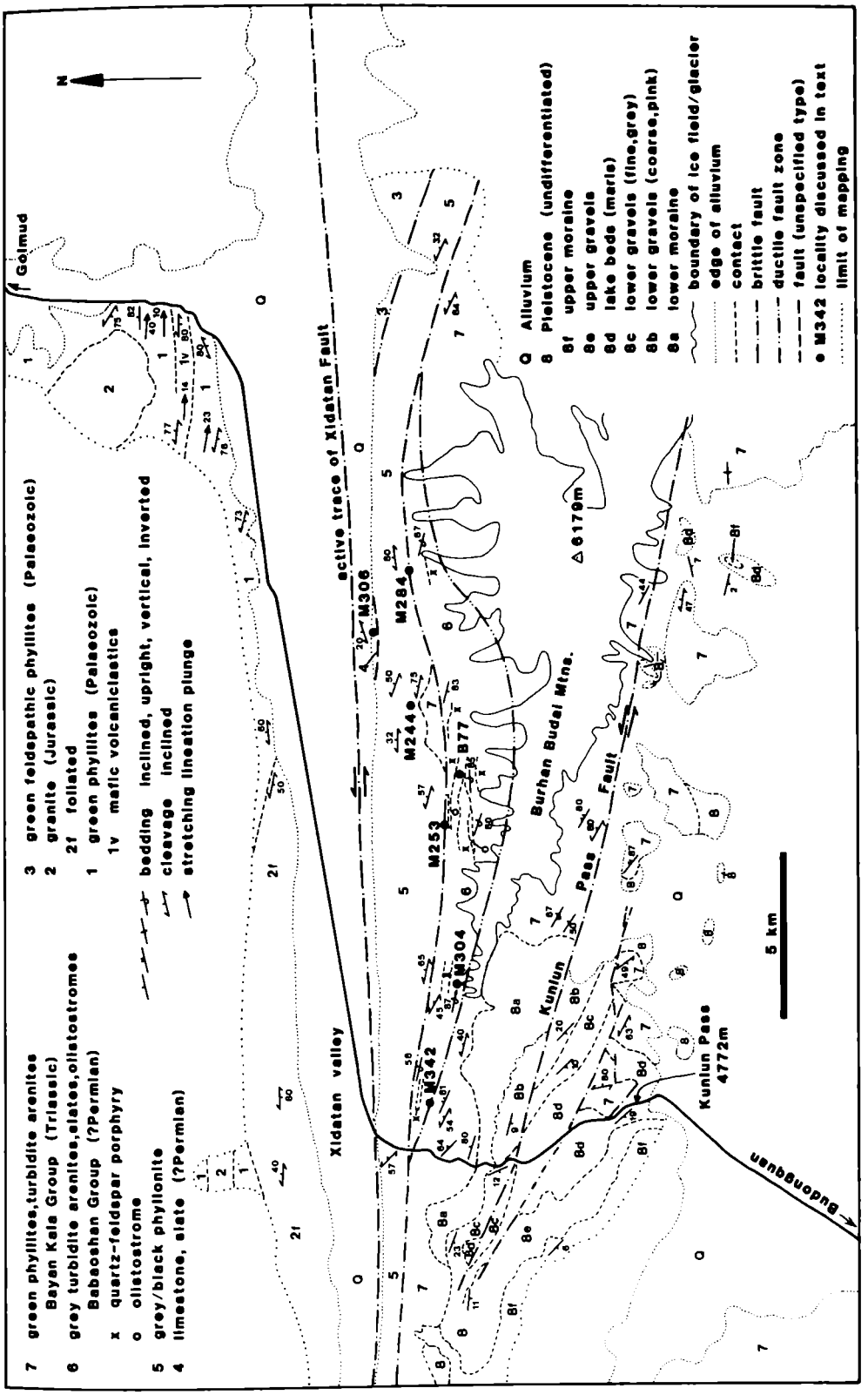

FIGURE 8. Geological map of the Xidatan–Kunlun Pass – Burhan Budai Mountains area. For location, see figure 2.

1 metre wide largely derived from the phyllonite. Vertically-plunging asymmetric minor folds of foliation adjacent to the gouge and in larger intact wall-rock lenses within the gouge, oblique S-C foliation in some of these lenses, and horizontal groove slickensides all suggest left-lateral strike-slip displacement on this fault. The displacement sense and the dominantly brittle character imply that it is related to the present Kunlun Fault system but there is no geomorphological evidence for Quaternary activity on this fault.

West of the main road, and eastward from near the east end of the Xidatan valley, this fault places phyllonite against steeply north-dipping well-foliated green phyllites and thin quartzose turbidite arenites of the Bayan Kala Group (figure 8). Along much of the length of the Xidatan valley, however, a lens up to about 2 km wide intervenes, which consists dominantly of steeply north-dipping, south-younging (and upward-facing) grey quartzose turbidite arenites and slates (Babaoshan Group). These seem not as strongly deformed or metamorphosed as the green phyllitic turbidites to their south, based on the intensity and appearance of foliation development in the pelites in each unit. Well-preserved flute and groove marks are seen on bed bases in a number of localities. Thick olistostromal deposits are exposed in two sections (localities M253 and M304). At the first locality, limestone, quartzose arenite, and calcareous quartz arenite clasts, most 10 cm or less across, but with a few up to 5 m across, occur in a dark grey shaly (slaty) matrix. At the other locality, a single fossiliferous limestone boulder 10 m long is exposed in shale. Because these submarine mudflow deposits only appear locally within the turbidite sections it is inferred that they are confined to channels. A few silicic tuff beds up to 10 cm thick are seen in the turbidites in at least one section (near M284). In every section examined in these rocks, there are somewhat irregular sills, typically 100–300 metres thick, of badly-altered, epidotised quartz-feldspar porphyry that occupy about 20–30 % of the section. These are clearly intrusive into both the olistostrome and the turbidites and were intruded prior to development of the single cleavage.

The southern contact of the tectonic lens containing this assemblage of lithologies was seen in one valley (locality M342); elsewhere it is mostly covered by the icefield on the higher parts of the Burhan Budai, or (at the main road) cut by the younger strike-slip fault on the northern side of the lens. At M342 a zone about 150 m wide appeared to be a syn-cleavage fault with mixing of lithologies from both sides. Rather poor shear sense indicators (oblique S-C type cleavage) suggest north-over-south thrusting on the now subvertical zone. Abundant float presumed to be derived from this zone, consisting of highly transposed quartz veins in a dark pelitic matrix, was seen in the valley of locality M284; the source, somewhere above the snout of the glacier, could not be reached.

One other narrow section of rocks has been reported to be within the Babaoshan Group. This occurs at locality B77 where a small section (about 25 m) of arenites, shales, tuff, and a coal bed with Mesozoic plant fragments is exposed (Yin *et al.*, this volume). The coal and the associated fluvial sediments seem unlikely lithological associates of the turbidites and olistostromes that make up most of the Babaoshan Group. Perhaps this occurrence is a block in the olistostrome that occurs in the adjacent valley. Alternatively, it may perhaps occur in a separate tectonic lens ("horse") along the northern boundary fault. In the latter case it could be related to the clastics with local red beds and coaly beds seen about 50 km east in the Dongdatan, and which overlie folded Permo-Triassic rocks with angular unconformity.

The Pleistocene sequence near the Kunlun Pass (figure 8) is regionally tilted to the SSW, and locally dips as much as 23°. This deformation is connected, but not in a precisely understood

way, with the interaction of the Kunlun Pass Fault and the Xidatan Fault, because the area of maximum tilting is in the zone where the faults approach one another. The apparently irregular distribution of outcrop of the Triassic Bayan Kala Group south of the Kunlun Pass Fault (figure 8) is largely due to palaeotopography. South- to southwest-trending valleys filled by the Pleistocene sequence alternate with ridges of the Triassic arenites and phyllites; the ridges terminate to the south because of the southerly tilting.

4. Problems needing further mapping

Some geological problems can be solved by examining a single good exposure or section, but others require well-distributed information (in other words, mapping) for their solution. It is, in many cases, only by looking systematically and in detail through an area that some of the key localities and sections are found, and the variability assessed in stratigraphic and structural sequences and other features. We contest vigorously the idea that all, or everything of significance, is solved by one geotraverse. This is particularly true where outcrop is discontinuous and the structure complex, as along most of the traverse route. In the interest of brevity, only a few questions are raised here; in other words, the discussion below is not comprehensive.

The timing of the beginning of the collision between the Lhasa and Qiangtang Terranes is poorly known, and it is not known whether the late Jurassic uplift of the Dongqiao ophiolite is indicative of thrusting of ophiolite onto continental lithosphere of the Lhasa block ("obduction") or reflects some other intra-oceanic event. This is so because the relations between the Triassic platform carbonates of the Lhasa Terrane and the Jurassic flysch are ill-defined. Was the flysch deposited over carbonates and continental basement and, if so, when did it start? Conversely, was it tectonically transported from an oceanic environment significantly later than its depositional age? The significance of the isolated occurrences of Triassic carbonate turbidites could be related; do they represent a response to platform rifting or are they an early response to thrust loading of the Lhasa Terrane? The basic relationships and ages of these strata will have to be established by mapping to answer these questions.

Also in the Lhasa Terrane, only extensive accurate mapping of the mid Cretaceous and younger rocks will yield useful estimates of the crustal shortening that there has been prior to and subsequent to mid-Cretaceous times, essential information for testing crustal thickening models for the India–Asia collision. Similar comments are applicable to Tertiary rocks elsewhere on the plateau, although our mapping near Erdaogou (see above) illustrates that modest efforts can quickly improve understanding.

There is still a large question to be answered about the age of folding in the Qiangtang Terrane. In the north, around Wuli, most of the shortening is younger than Eocene (see paragraph 3*d* above). In the southernmost part, just north of Amdo, the folding of the mid and late Jurassic strata predates some of the redbeds (paragraph 3*c* above). The problem rests on the age of those redbeds; are they Cretaceous, or are they Tertiary, and could the folding be Tertiary as it is in the north? If the folding in the south is Cretaceous, where in the Qiangtang Terrane does the change occur to the younger deformation seen in the north?

Besides the obvious need to define what lies below the Jurassic covering the southern two-thirds of the Qiangtang Terrane along the traverse line, the relationship of the Triassic Batang Group arc volcanics to Permian rocks is ill-defined. Could the arc volcanics be allochthonous, overthrust from the Jinsha Suture?

For the Kunlun Terrane, systematic mapping will reveal the large-scale structural relations of the Permo-Triassic sections north of the Xidatan Fault to older rocks (cf. Coward *et al.*, this volume) – essential information in understanding the tectonic significance of these Permo-Triassic rocks (were they deposited in extensional basins?). Although isotopic ages may help to solve the problem of whether there are one or two sequences of volcanics in the northern Kunlun, and whether they are Devonian, Carboniferous, or Permo–Triassic, mapping would contribute greatly to the confidence placed in the ages, if it revealed the original relationship(s) of the volcanics to the Carboniferous strata, for example.

As a final and more general problem, the location of sutures and the occurrence of ophiolites are critical to the interpretation of the assembly of the crust of the Qinghai–Xizang Plateau.

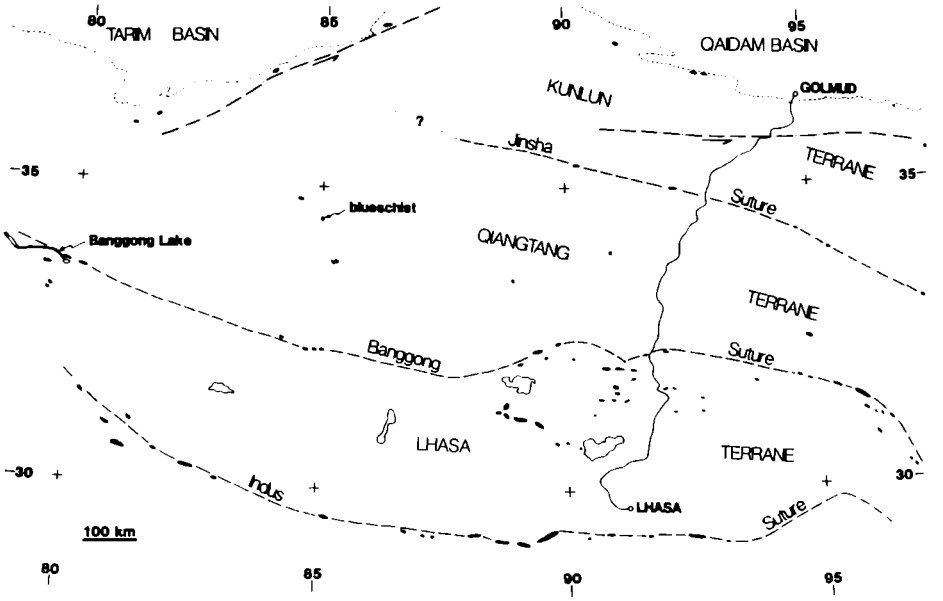

FIGURE 9. Sketch map of ophiolite occurrences in the central and western parts of the Qinghai–Xizang Plateau, with the known sutures indicated. Ophiolite and blueschist occurrences within the Qiangtang Terrane may indicate the presence of one (or perhaps more) additional sutures.)

Figure 9 shows the occurrence of ophiolites from the 1 : 1.5 million scale Geological Map of the Plateau, with the addition of two localities from the samples and detailed topographic maps of Hedin (Hennig 1915). The ophiolites scattered across the Lhasa Terrane south of the Banggong Suture are thought, from mapping, to be remnants of a large nappe (Girardeau *et al.* 1984, 1985, Chang Chengfa *et al.* 1986). However, the nature of the ophiolite and blueschist occurrences within what is currently identified as the Qiangtang Terrane are unknown. This possible suture within the Qiangtang Terrane is as well if not better defined, at least by ophiolites, than much of the length of the Jinsha Suture. Whether this is an additional suture, and whether it might help explain the odd distribution of Gondwana-type Carboniferous–Permian at the western end versus Cathaysian-type at the eastern end of the Qiangtang Terrane, are questions that could be answered by detailed mapping of these purported ophiolites and their surroundings. Similar comments apply to the possible occurrence of small arc-type terranes and an additional suture within the southern Kunlun and Songpan–Ganzi area east and southeast of the northern part of the geotraverse route.

We thank David Rothery for his work in selecting and producing the LANDSAT imagery used for the geotraverse. Kevin Burke and the Lunar and Planetary Institute are thanked for access to image processing facilities and for loan of enlargements of Large Format Camera images.

We also thank Susan L. Anderson for design and much of the drafting of the 82 detailed geological data maps reproduced here on microfiche, the Department of Geological Sciences, State University of New York at Albany, for providing essential equipment and material supplies for the drafting of these maps, and Diane Paton for typing the microfiche-reproduced tables. Pan Yun and Wang Ping are thanked for translating Chinese geographic names from the topographic maps.

References

Armijo, R., Tapponnier, P., Mercier, J. L. & Han Tonglin 1986 Quaternary extension in southern Tibet: field observations and tectonic implications. *J. geophy. Res.* **91**, 13803–13872.

Burg, J. P. (compiler) 1983 *Carte géologique du sud du Tibet (1:500,000 scale)*. C.N.R.S., Paris, and Ministry of Geology, Beijing.

Chang Chengfa & 26 others 1986 Preliminary conclusions of the Royal Society and Academia Sinica 1985 geotraverse of Tibet. *Nature, Lond.* **323**, 501–507.

Girardeau, J., Marcoux, J., Allègre, C. J., Bassoullet, J. P., Tang Youking, Xiao Xuchang, Zao Yougong & Wang Xibin. 1984 Tectonic environment and geodynamic significance of the Neo-Cimmerian Donqiao ophiolite, Bangong-Nujiang suture zone, Tibet. *Nature, Lond.* **307**, 27–31.

Girardeau, J., Marcoux, J., Fourcade, E., Bassoullet, J. P. & Tang Youking 1985 Xainxa ultramafic rocks, central Tibet, China: tectonic environment and geodynamic significance. *Geology* **13**, 330–333.

Hennig, A. 1915 Zur petrographie und geologie von sudwest-Tibet. Vol. 5 *in Southern Tibet* (ed. S. Hedin), 220 pp., Norstedt, Stockholm.

Ministry of Geology and Natural Resources 1980 *Geological map of the Qinghai-Xizang (Tibet) Plateau (1:1.5 million scale)*. Ministry of Geology and Natural Resources, Beijing.

Molnar, P. & Tapponnier, P. 1978 Active tectonics of Tibet. *J. geophys Res.* **83**, 5361–5375.

Qinghai Bureau of Geology and Mineral Resources 1981 *Geological map of Qinghai Province (1:1 million scale)*. Qinghai Bureau of Geology and Mineral Resources, Xining.

Qinghai Bureau of Geology and Mineral Resources 1984 *Geological maps of Golmud and Naij Tal sheets (1:200,000 scale)*. Qinghai Bureau of Geology and Mineral Resources, Xining.

Xizang Bureau of Geology and Mineral Resources 1979 *Geological map of Lhasa sheet (1:1 million scale)*. Xizang Bureau of Geology and Mineral Resources, Lhasa.

Yin Jixiang, *et al.* (in press) *Geological map of the southern Tethys of the Qinghai-Xizang Plateau (1:1 million scale)*. Institute of Geology, Academy of Sciences, Beijing.

Phil. Trans. R. Soc. Lond. A **327**, 307–336 (1988) [307]
Printed in Great Britain

The structure of the 1985 Tibet Geotraverse, Lhasa to Golmud

By M. P. Coward[1], W. S. F. Kidd[2], Pan Yun[3], R. M. Shackleton[4], F.R.S., and Zhang Hu[3]

[1] *Geology Department, Imperial College, London SW7 2BP, U.K.*
[2] *Geology Department, S.U.N.Y., Albany, New York, U.S.A.*
[3] *Institute of Geochemistry, Academia Sinica, Guiyang, People's Republic of China*
[4] *Department of Earth Sciences, Open University, Milton Keynes MK7 6AA, U.K.*

With an appendix by Zhang Hu

The structures of Tibet were generated during the accretion on to the Asian plate, firstly of the Qiangtang Terrane during the Triassic, then the Lhasa Terrane during the Jurassic–Cretaceous and finally the Indian continent during the Palaeogene. The southern Kunlun mountains show intense deformation associated with the accretion of deep water sediments on to an active plate margin. The deformation was essentially by footwall propagation of thrusts, though there was pronounced out-of-sequence thrusting with the deformation of basins above the main thrust zone, and the back steepening and backthrusting of earlier structures. The Jinsha Suture probably represents the southern edge of this zone.

The Banggong Suture between the Qiangtang and Lhasa Terranes is characterized by pre-collisional ophiolite obduction for over 100 km to the south across the Lhasa Terrane, plus local intense intracratonic deformation of parts of the Lhasa Terrane. However, for this collision there is now very little evidence for intense deformation along the line of the suture and the Qiangtang Terrane itself remained only weakly deformed throughout.

Post–Middle Cretaceous, pre-Tertiary deformation of the Lhasa region produced upright- to north-verging folds which decrease in intensity northwards. They may have been formed at the margin of the Gangdise batholith, or they may have originated from early collisional phases along the line of the Indus–Zangbo Suture. However this deformation is approximately synchronous with the more intense deformation of the Xigatse flysch on the accretionary prism and is therefore probably subduction-related, predating collision.

Tertiary deformation is relatively widespread across Tibet, producing SSE-directed thrusts across the Fenghuo Shan region of the Qiangtang Terrane and across the northern part of the Lhasa Terrane. Several hundred kilometres shortening can be estimated to have occurred during this deformation, probably reworking older Mesozoic structures. However this shortening is insufficient to provide all of that estimated from palaeomagnetic work or from a study of displacement rates of the Indian plate, and much of the displacement of India into Asia during the Tertiary must be taken up on strike-slip faults in Tibet or on thrusts and strike-slip faults in central Asia north of the Tibetan Plateau. The Tertiary shortening cannot account for all the thickening of the Tibetan crust.

1. Introduction

The structural history of Tibet involves the accretion of several crustal blocks on to the Asian continent (Li *et al.*, 1979; Bally *et al.* 1980; Chang & Pan 1981; Sengör 1984; Zhang 1984; Chang *et al.* 1986). The earliest sutures formed in the region of the Tien Shan–Junggar Basin

during the late Palaeozoic (Zhang 1984; Watson *et al.* in press), accreting what is here termed the Kunlun Terrane on to the Asian Plate. On the section line covered by the 1985 Geotraverse, however (figure 1), only the sutures south of the Kunlun Terrane were examined; these developed in sequence from north to south (see Chang *et al.* 1986). The Jinsha Suture joins the Qiangtang and Kunlun Terranes and formed in the Triassic. The Banggong Suture joins the Lhasa and Qiangtang Terranes and formed in Jurassic–Cretaceous times. The Indus–Zangbo Suture between the Indian and Lhasa Terranes was the last to form in the early Eocene.

Structures were produced during each phase of accretion. Sometimes they represent pre-collisional deformation; elsewhere they may reflect terrane collision or the late to post-collisional shortening of rocks on either side of the suture. Sometimes accretion formed only narrow zones of deformation, but in the collision which produced the Indus–Zangbo Suture, during the accretion of the major Indian continent, there was late to post-collisional deformation for a large distance across the Indian sub-continent to the south, and across much of central Asia to the north. Apart from these structures which can be tentatively related to continental or microcontinental collision, there are also several enigmatic phases of deformation whose origin is uncertain.

To attempt to unravel this complex history, the structures will be described from north to south, in approximately their sequence of development. The descriptions rely on cross sections, which have been produced from the geological maps made on the Geotraverse (Kidd *et al.*, this volume), stratigraphic information produced by Yin *et al.*, Leeder *et al.* and Smith & Xu. (all this volume) and detailed field observations by the authors. As the traverse strip was narrow and essentially two-dimensional, these cross-sections cannot always be supported by parallel sections, as should be done in any detailed tectonic study of a fold-thrust belt. The cross-sections also have to rely on limited surface data, as generally it was impossible to map sufficient area to produce downplunge projections. Because of the line of traverse, it was often impossible to draw the sections parallel to the thrust transport directions and so material must have moved in or out of the planes of section and they cannot be considered as having undergone plane strain. Furthermore, the fault transport direction was not constant during the deformation. Many regions show a history of deformation involving more than one thrust phase and many of the later thrusts breach earlier thrusts or are cut by later normal or strike-slip faults. Thus it is impossible to produce any truly balanced cross sections through the region (c.f. Dahlstrom 1969; Hossack 1979) and any conclusions concerning the deep structure or the amounts of displacement must be viewed in this light. The conclusions must be considered as educated guesses and hence interpretations will probably change when more detailed and more regionally extensive work is done.

The distribution of terranes and sutures is shown on figure 1, as are the lines of cross-section. The positions of the terrane boundaries follow Chang *et al.* (1986) and rely heavily on the full tectonic interpretation, including stratigraphic, petrological and geochemical data, not just the structural geology.

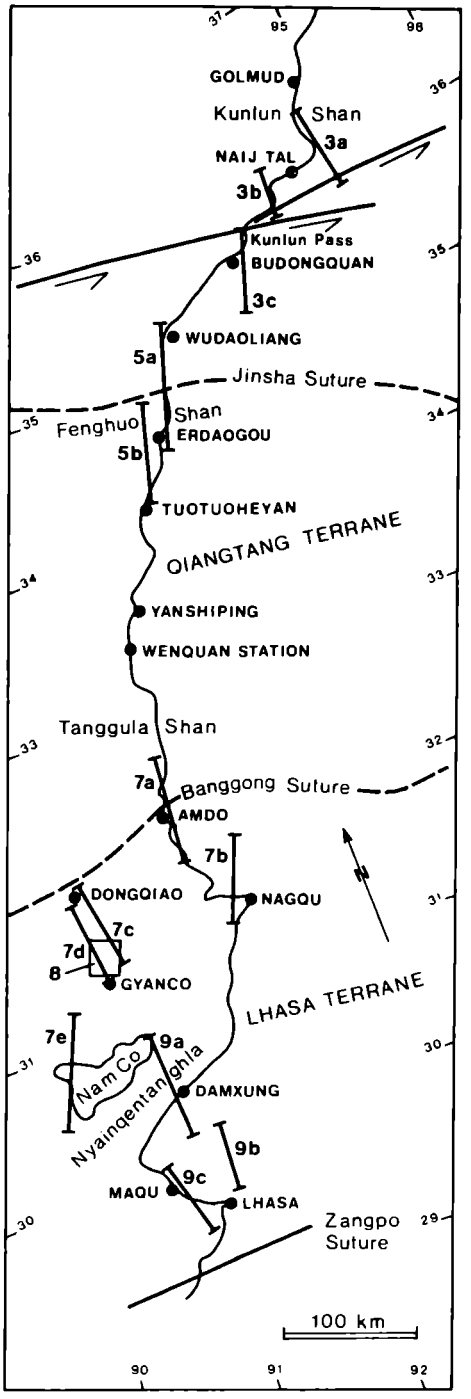

FIGURE 1. Map of the Geotraverse route, showing the terranes and terrane boundaries (after Chang *et al.* 1986) and the section lines described in this paper.

2. Structure of the Kunlun Terrane and the northern (Jinsha) Suture

(a) *General*

In this discussion, the area north of the Jinsha Suture is treated as a single tectonic unit, with structural and stratigraphic continuity across the terrane. Here the stratigraphic sequence is divided into very broad structural-stratigraphic units; details of the stratigraphy are published elsewhere (Yin *et al.*, this volume). In the parts of the main Kunlun ranges traversed there are two older Palaeozoic successions, dated by fossil evidence: one is Ordovician, the other Devonian, Carboniferous and Permian. The sequence consists largely of shales and limestones, though basic volcanics predominate in the Devonian and Carboniferous. To the west of Naij Tal, in the Wanbaogou valley, there is a thick succession of brown-weathering massive limestones which is considered to be Permian in age.

This Palaeozoic succession is overlain by a thick sequence of turbidites, which, especially at the base, are coarse and conglomeratic. The boulders consist of Palaeozoic sediments and also granite rocks which we interpret as probably derived from the Kunlun magmatic arc, dated as end Permian–early Triassic (Harris, Xu, Lewis, Hawkesworth & Zhang, this volume). Hence we consider these turbidites to be of Triassic age and possibly as young as Norian (Leeder *et al.*, this volume). Nowhere was their original stratigraphic contact with the older Palaeozoic rocks seen; the contacts are all faulted or intensely sheared and hence the magnitude of the unconformity between the two successions is conjectural. The turbidites were probably deposited in local basins on the Palaeozoic sediments, but whether the basins were of extensional or flexural origin is uncertain.

Red beds and associated coals were deposited in local basins, probably after much of the deformation. They are dated as Triassic or Jurassic in age by fossil material in the coals. (South of the Kunlun Shan there is a fourth structural-stratigraphic succession, the Bayan Har Group, mainly fine-grained turbidites. No fossil evidence for their age was found from the Geotraverse section, but Triassic faunas have been reported from this zone elsewhere (Yin *et al.*, this volume).)

The distribution of these successions is shown in simplified form in figure 2, as are the lines of section used to describe the Kunlun structure. The sections are (i) in the eastern part of the traverse area, starting north of the area shown in figure 2 along the main valley south of Golmud to Shuinichang (on figure 2) and then up Tuolungou south along the old drovers' road to the Dongdatan valley, and (ii) through the western part of the traverse area from Wanbaogou to the Xidatan valley. Sections through the Bayan Har Group turbidites in the southern part of the Kunlun Ranges are given in figure 3*c*.

The major deformation was Triassic, post-dating the Triassic sediments and predating some early Jurassic granites in the southern Kunlun, which have been dated at about 195 Ma (Harris, Xu, Lewis, Hawkesworth & Zhang, this volume).

(b) *The eastern section line*

The eastern section, from about 20 km south of Golmud to the Dongdatan valley, is given in figure 3*a*. In the north, part of the Kunlun batholith, dated as 257 ± 21 Ma (mid Permian) (Harris, Xu, Lewis, Hawkesworth & Zhang, this volume) intrudes openly folded but sometimes steeply dipping Palaeozoic volcanics. Dykes, intruded soon after granite intrusion (Pearce & Mei, this volume), also cross-cut the folded volcanics, indicating that tilting occurred prior to the late Permian–early Triassic.

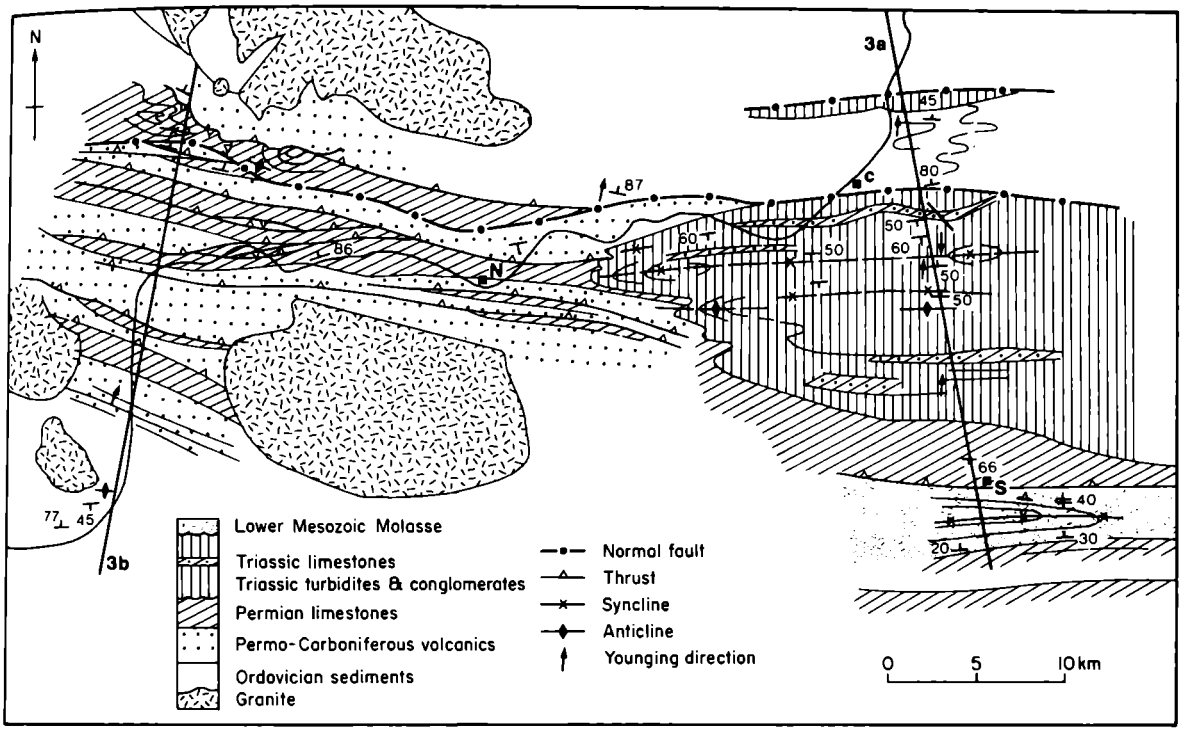

FIGURE 2. Simplified geological map of the Kunlun Shan, north of the Kunlun Pass, to show the possible correlations between structures shown on the eastern and western cross-sections. Section lines 3*a* and 3*b* are given in figure 4. N = Naij Tal, C = Shuinichang, S = Locality S471.

South of the volcanics and their overlying Carboniferous sediments, there is a series of Upper Palaeozoic fluvial red sandstones, with a weak cleavage and moderately tight upward to northward-facing folds plunging steeply north. The northern boundary of this group of rocks may be a faulted or a normal contact. To the south, most of the rocks carry a penetrative cleavage; the contact marks the northern boundary of the more intense Kunlun deformation. As shown on the section (figure 3*a*), Ordovician shales and limestones are thrust over these Upper Palaeozoic rocks and show tight to isoclinal folding, with axial surfaces which dip steeply to the south, a pronounced cleavage, generally high finite strains and a mineral and stretching lineation with a steep plunge to the south. Triassic conglomerates are downfaulted into this section of Ordovician rocks, in the form of a small wedge, whose master fault occurs on the north side, with a steep southerly dip, similar to that of the thrusts and fold axial planes in the Ordovician rocks. The southern contact of the conglomerates is also tectonic, but is probably close to the deformed unconformity. The finer beds within this Triassic sequence are locally strongly deformed with a strain of similar orientation to that in the Ordovician rocks. Though the contacts between Permo–Triassic beds and older rocks are always tectonic, both groups have a similar deformation history; we saw no evidence within the traverse area for any major phase of folding or cleavage production which affected the Lower Palaeozoic rocks before the Permian, but some of the Permo–Triassic boulder conglomerates contain boulders of limestone of unknown age, which had been deformed before erosion (M. Leeder, pers. comm. 1985).

The map and sections show the fault contacts as essentially thrust or normal faults, however some of the faults crossing this northernmost portion of the traverse route in the Golmud river

valley may have Neogene strike-slip components in their overall displacement (see figure 9 of Kidd & Molnar, this volume).

The dominant structure in the central part of the section is a large syncline affecting Triassic rocks, which consist of turbidites with coarse conglomerates, overlain by sandstones in the northern part of the structure. The northern boundary is again a normal fault, downthrowing to the south. The age of this fault is uncertain; it is possible that the fault developed synchronously with the deposition of the turbidites, but it could be a late tectonic structure, post-dating the folding. As the turbidites appear to thicken towards the fault on the section (figure 3*a*), it has some of the characteristics of a growth fault. However, the conglomerates contain boulders of material presumably derived from the Kunlun batholith, over 20 km to the north, that is, they are not locally derived from the fault scarp, as would be expected from a syn-sedimentary fault environment.

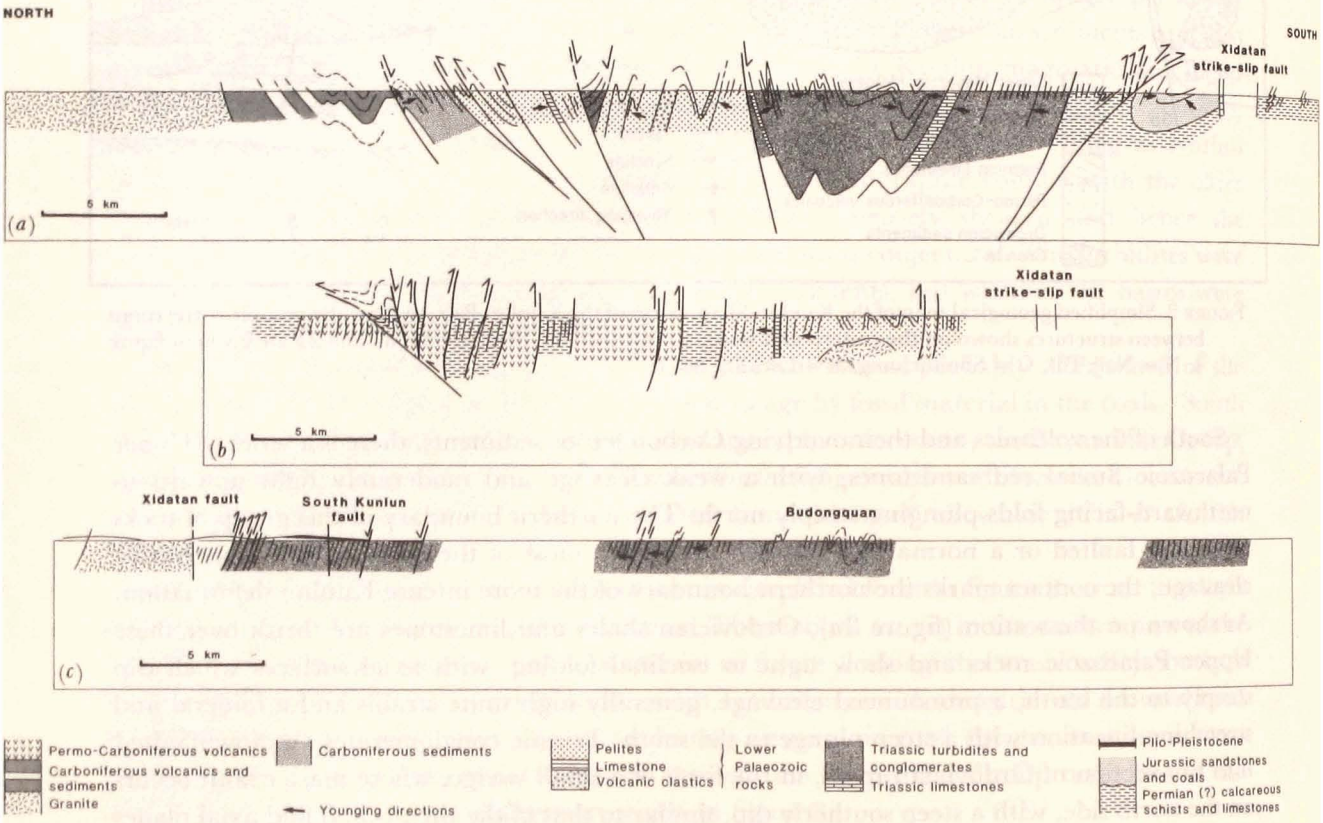

FIGURE 3. Cross-sections through the Kunlun Terrane. Section (*a*) refers to the eastern section of figure 2, Section (*b*) the western section. The location of Section (*c*) is shown in figure 1.

The folds are upright and locally tight, with subhorizontal axes trending east to eastnortheast. Cleavage is well-developed in the medium- to fine-grained rocks, though the pebbles and boulders show variable strains due to the ductility contrast with the matrix. The cleavage is upright, parallel to the fold axial planes and the mineral lineations, where observed, plunge steeply down dip.

To the south, the folds are tighter. The positions of fold axial planes can be determined from changes in bedding-cleavage relations and younging directions, though the exact positions of fold traces are difficult to see as the structures are often isoclinal. A zone, at least 200 m thick,

with pebbly horizons (loc. S476), younging north, overlies a zone of intensely deformed shales to the south, with grading indicating that they generally young towards the north. A second-phase crenulation cleavage affects the shales; it dips to the north and is associated with medium-scale south-verging folds and minor shear zones. These folds face downwards to the north or upwards to the south, depending on their position on a first-phase fold. South of the deformed shales there is a zone of intensely deformed slates and limestones, throughout which the bedding and cleavage are parallel, and no clear younging directions were obtained. Mineral lineations plunge to the northnorthwest. The limestone often occurs as discontinuous layers within the shale matrix and appears to be a tectonic melange. Figure 4 shows a sketch map of the structure east of the main track along the Xidatan drovers' trail, (loc. S471, S on figure 2) where the limestone blocks are clearly truncated by a southward-verging F2 shear, which intensifies and locally crenulates the main F1 cleavage. On a larger scale the limestone-shale sequence may be considered as a southerly-directed imbricate zone.

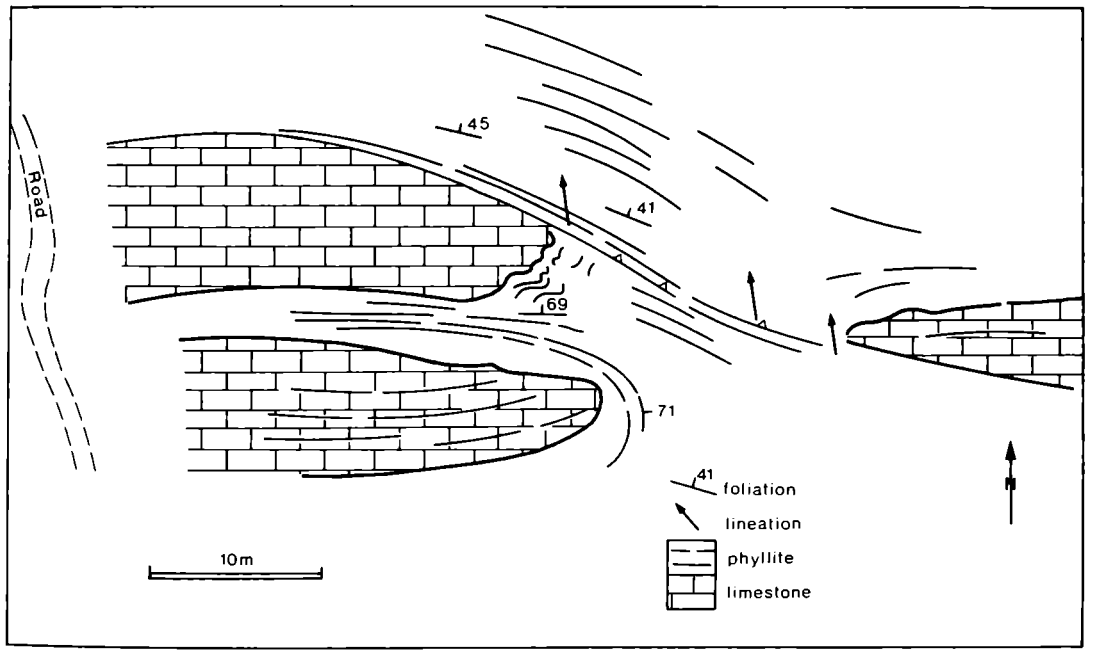

FIGURE 4. Sketch map of locality S471 on the eastern Kunlun section, to show the shear deformation breaking the structure to give a tectonic melange.

This tectonic melange has been thrust over mudstones, sandstones and conglomerates which are locally red. The deformation intensity and metamorphism are far less in these red molassic rocks than in the slates and limestones to the north, and the basal breccia of this sequence was seen lying unconformably on Permo–Triassic carbonates. Thin shaly coal seams are preserved in places and may be of similar age to thin coals in red beds of late Triassic age in the Xidatan valley farther west, or to Jurassic clastics with coal in the same region (Yin *et al.*, this volume). The dominant structure consists of an inclined south-verging syncline, with an overturned northern limb beneath the footwall of a major thrust, which carries the tectonic melange on its hanging-wall (figure 3*a*).

Beneath the red beds is a series of limestones with a gently dipping tectonic fabric. The limestones are heavily fractured, probably due to the proximity of the Xidatan fault, a major

Neogene to Recent strike-slip fault described fully by Kidd & Molnar (this volume). It disrupts the structural sequence and it is not possible to continue any large-scale structure across the main Dongdatan valley. To the south, the deformation is intense and a main-phase cleavage has been intensely crenulated into south-verging medium-scale folds in limestones and phyllitic sediments.

The overall structure is therefore one of northward-verging folds in the north and upright folds in the central part of the Kunlun, near the Naij Tal valley. These overlie a zone of intensely deformed southward-verging structures in shales and molasse-like red beds which are themselves deformed into a footwall syncline, though they lack the intense cleavage of the rocks on the hanging-wall. The dominant thrusting direction in this southern part of the Kunlun was probably towards the south, as determined from the north-plunging mineral lineations, though there is a slight swing of the lineations to northwest near the Xidatan fault, suggesting a sinistral shear couple. Intense brecciation affects the rocks near this fault, though no small scale kinematic indicators were observed in bedrock.

(*c*) *The western section from the Wanbaogou valley to the Xidatan*

The western section, from the Wanbaogou valley to the Xidatan fault, is given in figure 3*b*. Structures and rock types are clearly different from those of the eastern section. There are no coarse conglomerates or turbidites; these die out in a fold closure east of Naij Tal. The sequence in the north is dominated by brown-weathering limestones, of probable Permian age. They show upright folds and a spaced cleavage; to the south the deformation is more intense, the dip is often close to vertical and the limestones show a strong cleavage with a down-dip mineral lineation. The limestones are generally in tectonic contact with adjacent rocks. In the northern part of the section the massive limestones are locally flat-lying but overlie alternations of steeply dipping greenschist and calcareous schist. This contact is clearly tectonic, with an intense schistosity parallel to the contact in its footwall and hanging-wall. Small-scale north-verging crenulations of this cleavage and well-developed shear bands indicate that the upper limestones have been sheared northwards over the steeper-dipping volcanics and calcareous rocks of the footwall.

The southern contact of these limestones with the underlying schists is tectonized, but it is not known if this contact is a thrust, a normal fault, or a sheared stratigraphic contact. The fabric adjacent to the contact has a steep northerly dip and a down-dip mineral elongation.

To the south, in the Naij Tal valley, there are several alternations of mylonitic limestones and metabasic volcanics. Lithological layering and cleavage are steep and small-scale folds and mineral lineations show a steep plunge to the northnorthwest. The younging directions of these rocks are not known. It is clear that the rocks have been repeated, presumably by thrust imbrication associated with the intense deformation, but it is uncertain which rock has been thrust over which. These lithological repetitions are considered to represent the lateral equivalents of the imbricated tectonic melange zone which occurs in the south of the eastern section (figures 2 and 3*a*, loc. S471).

In the central part of the western section, phyllitic volcaniclastic rocks overlie intensely deformed siliceous pelites and conglomeratic limestones. They have been intruded by sills or dykes of greenstone material, probably related to the overlying volcanic rocks. The conglomeratic limestones are similar to Ordovician conglomeratic limestones which occur near Shuinichang, along the eastern section, and they may be of a similar age. Grading in the

overlying volcaniclastics indicates that they young to the north, away from the supposedly Ordovician conglomeratic limestones.

South of the limestones, there is a sequence of arenites and phyllites with locally well-preserved younging directions and angular relationships between bedding and cleavage that enable a structure of upright folds to be discerned, as shown in figure 3*b*. These rocks show a slightly higher metamorphic grade than the others in the Kunlun, possibly up to low amphibolite facies (Harris, Holland & Tindle, this volume).

Though the detailed structure is uncertain, due to the lack of good stratigraphy, the favoured interpretation is one of a sequence of Ordovician limestones and schists, overlain by volcanics and volcaniclastics, possibly of late Palaeozoic age, overlain by brown Permian limestones. These were deformed into a series of upright to south-verging folds and thrusts in this western section, but in the north, later north-verging thrusts carried the Permian limestones over steeply dipping older rocks. The less intensely deformed Triassic turbidites of the eastern section (figure 3*a*) presumably originally overlay the Palaeozoic limestones, shales and volcanics, but disappear to the west, due to easterly fold plunge (figure 2) or, possibly, the edge of the conglomerate–turbidite basin.

The suggested structural correlations are shown on the map of the Kunlun Shan in figure 2, with the major thrust sheets outlined as discussed above. The intense deformation in the Palaeozoic limestones and volcaniclastics of the western section is considered to link with the intense deformation in the tectonic melange in the southern part of the eastern section. The Permo–Triassic turbidites show a less intense deformation and lack the fault repetition. The conglomerates may either (i) predate the intense deformation in the Palaeozoic rocks, but overlie a roof thrust to the intensely deformed structures beneath, or (ii) post-date the intense deformation and hence have formed in a fault-controlled hanging-wall basin above the overthrust Palaeozoic rocks. This latter alternative argues for several phases of superposed co-axial deformation in the Kunlun.

Almost all the deformation predates the intrusion of early Jurassic granites (see Harris, Xu, Lewis & Jin, this volume), which have clearly discordant contacts with the country rock sediments. Along the north side of the Xidatan valley, however, there is an intensely deformed gneissic granite with kinematic indicators suggesting overthrusting to the south. This gneissic granite gives the same radiometric age as the undeformed granites near Naij Tal, supporting the argument for either diachronous or locally superposed deformations.

(*d*) *Kunlun Pass to Budongquan*

South of the Xidatan fault (see figure 3*c*) there is a thick zone of dark grey-black phyllonites which, along much of the Xidatan, adjoin the north side of a tectonically-bounded lens of grey quartzose arenites, slates and olistostromes, with rare silicic tuffs, all intruded pre-kinematically by thick sills and more irregular bodies of altered feldspar and quartz–feldspar porphyry. The arenites are turbidites, which young consistently to the south in steeply north-dipping beds. In one valley, an occurrence of coal yielding a possible Triassic flora occurs near the northern fault boundary. It is unclear if this coal belongs stratigraphically with the turbidites, or is in a structurally isolated sliver along the fault. The coal may be a relict of a basin like that seen farther to the east in the Dongdatan. The fault on the north side of the lens was observed in one locality, where a narrow zone of vertical brittle fault rocks with sinistral strike-slip kinematic indicators was seen. On the south side of the lens, a subvertical fault zone about

150 m wide contains no unequivocal kinematic indicators where seen, although there were questionable structures suggesting south-directed thrusting. This lens is of limited lateral extent, ending eastward before the eastern end of the Xidatan, and to the west where the main road crosses the mountains to the Kunlun pass south of the Xidatan. Beyond these points, the phyllonite is juxtaposed along a steep contact with green phyllitic turbidite arenites and slates (the Bayan Har Group) that extended far to the south.

In the phyllonites, a single strong foliation contains small-scale structures indicating thrusting towards the south, but we have not been able to identify how much shearing and thrust displacement took place on this zone before it was cut by later strike-slip faults. A phyllitic cleavage very nearly parallel, or parallel, to bedding is seen in the grey slate-arenite succession of the tectonic lens and in the green arenites and slates of the Bayan Har Group to the south. In the region less than about 10 km south of the Xidatan and Dongdatan valleys, the foliation in all these rocks, including the phyllonite, is strongly crenulated by folds with gently-dipping axial surfaces and sub-horizontal hinges. These do not have a well-developed axial surface foliation.

The green phyllonitic turbidites are steeply dipping to vertical, young to the north and show phyllonitic zones of intense deformation and thrusts which are parallel to bedding. At least seven zones of intense deformation, considered to be bedding-parallel shear zones, were recognized along the excellent exposures near the Kunlun Pass. Some folds can be identified, but most of the beds dip steeply to the north or south and with few exceptions show cleavage relationships and younging directions which indicate anticlinal closures to the south.

Immediately south of the Kunlun Pass, the structures are masked by Pleistocene glacial deposits, gravels and lake beds and are cut by the Kunlun Pass Fault (see Kidd & Molnar, this volume). However, to the south, there are flags and siltstones with similar structures to those of the Kunlun Pass. The beds are steep, with a cleavage dipping less steeply to the south, indicating anticlinal closure to the south. Local graded bedding shows that the rocks young to the north and occasional cleavage-bearing folds face upwards.

Immediately south of Budongquan, the grey flags and turbidites show a series of tight folds whose axial planes are upright or dip steeply southwards. South of these, there is a region of poor exposure, with local outcrops of well-cleaved slates, but no sign of bedding.

The whole succession of graded flags and shales to phyllonites appears to be over 15 km thick, probably far too thick to be interpreted as an unfaulted sequence. It is interpreted as an imbricated sequence of deep-water sediments, where the beds and the bedding-parallel shear zones and thrusts have been rotated to the vertical by subsequent thrust accretion. From the lineations and folds, the accretion direction was normal to strike, that is north to south; there is no indication of strike-slip deformation before the much younger movements on the Kunlun Pass fault. The amount of shortening is unknown, as there is no undeformed template with which to compare stratigraphic thicknesses. From comparison with other accretionary thrust wedges, the shortening should be at least 50% and from the steepness of the faults and the bedding, and the intensity of the cleavage, it is unlikely to be in excess of 75%.

(*e*) *Budongquan to the Jinsha Suture*

South of Budongquan, the exposure is very poor; most of the deformed rocks are covered by Pliocene to Recent deposits. However, near Wudaoliang there is a set of graded mudstones and siltstones similar to those north of Budongquan. Their structures are shown on the section in figure 5*a*. Three phases of deformation affect the fine-grained turbidites. The prominent folds

have axial planes which dip steeply- to moderately-southwards, being folded by a late-phase deformation. There is a main-phase cleavage which is strongly convergent or divergent depending on the competence of the beds and this is deformed by the later-phase crenulation cleavage which dips to the north at a moderate angle; where well developed, it produces a finite pencil cleavage by its intersection with the earlier main cleavage. The main-phase folds show a variation in facing direction. In the northern part of the section they face upwards or northwards, but in the southern part they face downwards, though the main cleavage consistently dips southwards.

The structures, therefore, can be considered in terms of three deformation phases. The first produced a tight to isoclinal fold, with a north-dipping axial plane but no detectable cleavage. The facing direction of this fold is uncertain, but the simplest explanation would be that it faced south. The second, or locally main, phase produced many folds and a well-developed southerly-dipping slaty cleavage, where the folds face upwards on the northern limb of the F1 antiform and downwards on the southern overturned limb. This cleavage was subsequently deformed by north-dipping crenulations.

The age of these structures and their correlation with the structures in the graded siltstones and flags of the Budongquan region is unknown. Immediately south of Wudaoliang, purple sands rest unconformably on the deformed graded mudstones, but are folded into a large open syncline which may be of similar age to the F3 deformation phase in the underlying rocks.

To the south, most of the structure is obscured by Neogene deposits or by Palaeocene red beds, and the nature of the Jinsha Suture is unknown. Outcrops of supposedly ophiolitic rocks are reported from 60 km west of the main road, and other ophiolites associated with radiolarites have been recognized far to the west and eastsoutheast (Chang & Pan 1981). How much deformation was related to this suture and what structures are associated with obduction of the ophiolite are completely unknown.

(*f*) *Summary and interpretation of the structure of the Kunlun Terrane*

The structures can be considered in terms of the accretion of deep water sediments on to a magmatic arc, which punched through a terrane with a cover of Palaeozoic rocks. There is no structural evidence from the present traverse of any basement older than the Palaeozoic rocks, though isotope studies on the Kunlun granites suggest reworking of an older Mid-Proterozoic crust (Harris, Xu, Lewis, Hawkesworth & Zhang, this volume). The Palaeozoic sediments consist of Ordovician volcanic rocks, shales and limestones, which are often conglomeratic and underlie Upper Palaeozoic basic volcanics. Apart from possible minor unconformities, there is no evidence of any deformation affecting these rocks before the deposition of the Permo–Carboniferous sequence. There must have been some pre-Triassic uplift, however, as the Triassic boulder conglomerates were derived from Ordovician rocks and hence the Upper Palaeozoic rocks must have been removed.

The turbidites, coarse conglomerates and boulder beds, east of Naij Tal, presumably represent the proximal phase of Triassic turbiditic sediments deposited on the older Palaeozoic sediments, though all the observed steep contacts are tectonic. The Ordovician sediments are themselves intensely sheared in the region between Naij Tal and the Xidatan, where they are inferred to have been originally thrust over the phyllonites. These phyllonites probably mark the southern edge of the Kunlun Terrane proper and form the zone of most intense deformation. Their lithologic origin is unknown; they may be intensely deformed Palaeozoic sediments or, more likely, Triassic sediments derived from the magmatic arc. The phyllonites

were originally thrust over deep water, more distal turbiditic sediments of the Kunlun Pass to Budongquan section. No basement rocks occur in the thrust wedges south of the Kunlun Pass and hence the thrusts probably decoupled above the basement. The original basement under these deep water sediments must have been subducted, presumably to the north beneath the Kunlun. The total section covered by these intensely-deformed sediments is over 100 km across strike. If they originally lay on a continental basement, then, assuming a minimum of 50% shortening, 100 km of that basement would have been subducted beneath the Kunlun. We favour the interpretation that these sediments were deposited on continental margin or ocean floor rocks which were then subducted below the Kunlun, generating the later part of the Kunlun granitic magmatism.

Thus the deep water sediments themselves may be considered as part of the suture zone. There may be several individual sutures within the zone, especially if the accretion involved thicker parts of oceanic crust (seamounts), or arcs. The degree of outcrop south of the Kunlun is insufficient clearly to identify any major thrusts or sutures, and the mapped Jinsha Suture is simply the line of scattered ophiolitic outcrops at the southern edge of this zone. That the structure may be more complex than the normal thrust accretion in a foredeep wedge is indicated by the long fold history near Wudaoliang.

Thus much of the repetition in the deep water sediments may be considered as pre-collisional, during the accretion of ocean floor material. The final arrival of the Qiangtang Terrane must have tightened the structures, steepened the thrusts and possibly produced the south-dipping cleavage at Wudaoliang. The upright folds and southward-directed thrusts in the Kunlun may be pre-collisional or may have developed during terrane collision. Certainly back-steepening of thrusts and tightening of folds affected the Kunlun ranges, with the production of north-verging thrusts at Wanbaogou, carrying Permian limestones back over the intensely deformed Palaeozoic rocks. It also produced the north-verging folds and thrusts, north of Shuinichang. The deformation intensity decreases in the north of the Kunlun range, where, near the main Kunlun batholith, the Palaeozoic sediments and volcanics are not cleaved only, openly folded or faulted. The batholith and associated dyke swarm show no evidence of regional tectonic strain.

Molassic sediments were formed in the Kunlun, particularly along the southern margin, near the present Xidatan fault. These must have developed in some form of inter-montane (piggy-back or pull-apart) basin, to be subsequently incorporated into the late phase of thrust tectonics, which itself might have been in a largely strike-slip setting. Locally this late phase of deformation was as intense as in the Xidatan phyllonites. The Triassic turbidites and conglomerates of the eastern section may also have developed in a syn-tectonic basin, above already intensely deformed rocks. From the deformation state of the granites between Naij Tal and the Xidatan, the deformation must have been diachronous, or there must have been superposed co-axial episodes. Thus though the general accretion can be considered in terms of footwall-propagating thrust tectonics, back-steepening the earliest thrusts, there is clear evidence for later hanging-wall deformation, in the form of the northward-directed thrusts and the deformation of the molassic basins.

The dominant overthrust directions were towards the southsoutheast and northnorthwest, suggesting that this was the main plate convergence vector, as well as the accretion direction of ocean floor material. There is a slight swing of the lineations near the Xidatan zone, suggesting a sinistral shear component here. As this shear deformation does not affect the late

granites which punch through the Kunlun, nor are the contact metamorphic minerals deformed by any regional tectonics, we attribute the shearing to Triassic collision.

3. Structure of the Qiangtang Terrane

(*a*) *General*

The Qiangtang Terrane occupies much of the northern part of the Tibet Plateau and extends for over 300 km from the Jinsha Suture south to the Banggong Suture. The stratigraphy is summarized by Chang *et al.* (1986) and by Yin *et al.* (this volume). The oldest exposed rocks are Permian to Triassic in age and include clastic sediments with coals and some limestones, with basaltic and silicic volcanics. However, the sedimentary sequence in the Qiangtang Terrane is dominated by thick (> 2 km) Jurassic molassic deposits, which were presumably derived from the Kunlun Terrane to the north (see Chang *et al.* 1986). No older basement rocks were seen. All show post-Jurassic, pre-Palaeogene deformation, which we interpret as related to the Banggong Suture.

The exposure of the Mesozoic rocks is poor. Most of the Palaeozoic and Mesozoic rocks are covered by Neogene deposits or recent scree and alluvium. In the north, near Erdaogou, there are Palaeogene red beds, which show considerable folding and thrust repetition. This deformation must locally affect the older rocks. Thus the structure of the Qiangtang Terrane will be described in two parts: deformation which affected the Tertiary rocks and that which affected only the older sediments.

(*b*) *The Tertiary deformation of Erdaogou and the Fenghuo Shan*

Cross sections through the Fenghuo Shan and ranges to the south are shown in figures 5*a* and 5*b*. The eastern section (figure 5*a*) displays open folds in the Palaeogene red beds to the north, but tight to isoclinal structures and southward-directed thrusts in the south. The thrusts and folds are upright, having been back-steepened by the development of lower thrusts in a piggy-back propagation sequence. To the west, (figure 5*b*) the red beds have been further thrust over Neogene sediments south of Erdaogou. There are folds in the Palaeogene red beds on the hanging-wall of a thrust in the hills close to the Tuotuo River (figure 5*b*). Figure 6 shows a composite section through these ranges, where all the thrusts and folds are considered to have developed above a sole fault inclined to the north at the base of the red beds at Erdaogou and on a lower fault within the Mesozoic basement near the Tuotuo River.

The thrusts and folds strike ENE and from slickensides the dominant overthrust direction was towards the SSE, though on some faults there are subhorizontal slickensides indicating a component of strike-slip displacement. The shortening can be estimated at about 40%, possibly up to 50 km across the whole zone. This shortening must have occurred since the Palaeogene.

(*c*) *Deformation in the Palaeozoic and Mesozoic sediments*

Between Erdaogou and Wenquan Station the Permian and Jurassic sediments show upright folds which are locally tight and have steep northwest-trending axial surfaces. The folds are slightly asymmetric, generally verging towards the north east. There is a weak cleavage in the steeper-dipping beds and the structures are dismembered by numerous steep faults, generally parallel to the fold axial surfaces. Near Yanshiping the Jurassic red beds are folded and

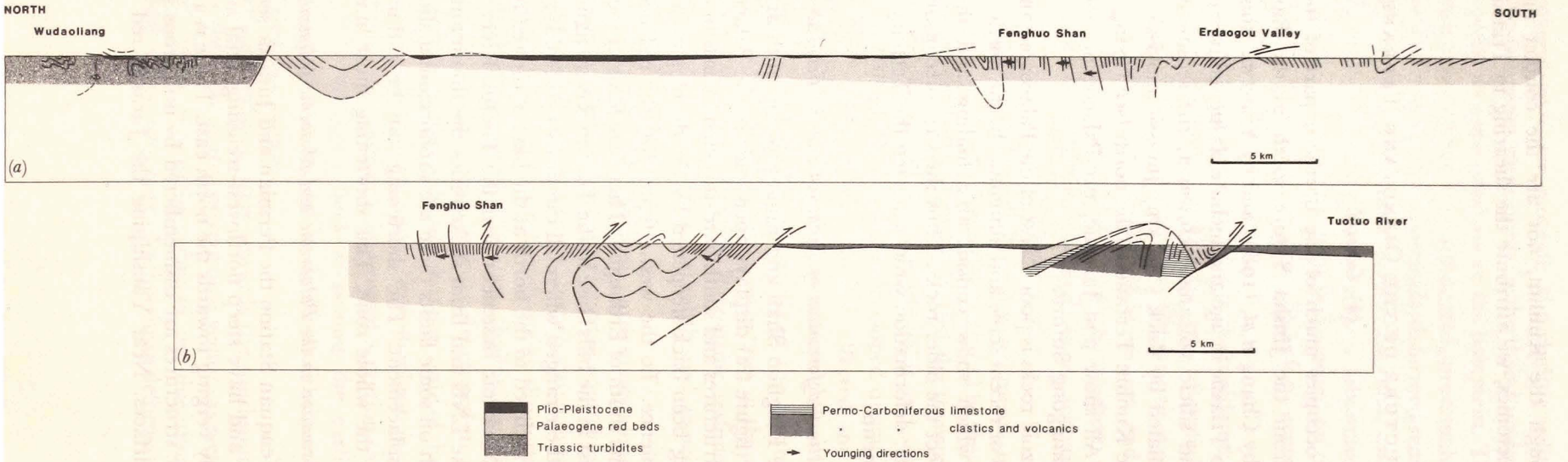

FIGURE 5. Cross sections through the Qiangtang Terrane, section lines shown on figure 1.

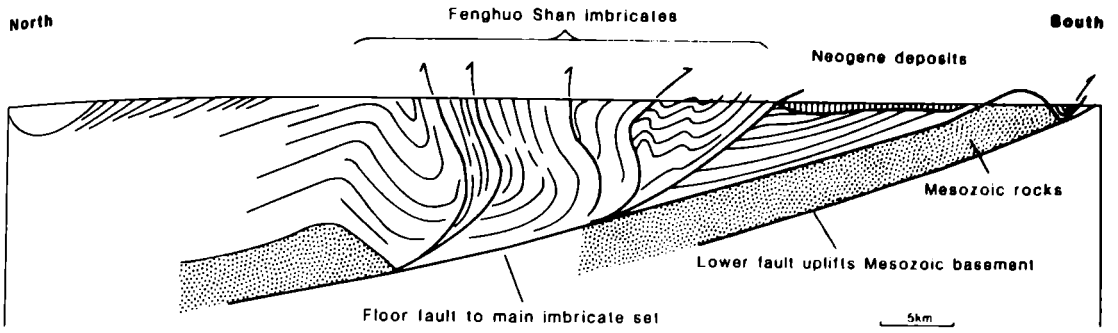

FIGURE 6. Simplified but composite cross sections through the Fenghuo Shan, to show the form of the Tertiary thrust imbrication.

imbricated by low-angle thrusts and cut by later normal faults. The structures probably decoupled on evaporites at depth; a gypsum diapir has risen into the core of an anticline about 10 km south of Yanshiping. The Jurassic red beds show only weak deformation, with steep fractures inclined to the south and generally no cleavage. Where cleavage does occur, it dips steeply either northwards or southwards.

At Wenquan Station there is a WNW-trending zone 5 km wide of strike-slip movement which locally disrupts the red beds. Kinematic indicators, such as slickensides and oblique vein and fracture sets in the zone, give a left-lateral shear sense. Secondary normal and thrust faults are common within this densely faulted zone, and vertically-plunging folds are locally prominent. Indications of left-lateral strike-slip faulting were also seen in the Jurassic strata outside this zone, near Yanshiping. The age of this zone of strike-slip faulting is unconstrained. South of Wenquan Station there are several low-angle thrusts with hanging-wall folds of similar style to those seen farther north. The thrusts and the folds verge towards the north or northeast. Between the Tanggula Pass and the Banggong Suture near Amdo there are open folds which are tighter to the south, where they are unconformably overlain by the Amdo red beds, considered to be Cretaceous or possibly Tertiary in age.

Thus the Qiangtang Terrane is relatively weakly deformed. Southward-directed thrusts of Tertiary age affect the region north of the Tuotuo River, but to the south there is no evidence for Tertiary deformation and Palaeogene red beds within 10 km of Amdo are flat and unconformably overlie northwest-trending open to close folds in the Jurassic sediments. The Mesozoic deformation was of variable intensity; the folds are upright to northeast-verging and often decouple on the lower Mesozoic evaporites. This northwest-trend to the folds is in marked contrast to the eastnortheast-trend of the later Tertiary structures.

4. The Banggong Suture and the Lhasa Terrane

(*a*) *General*

The stratigraphy of the Lhasa Terrane is markedly different from that of the Qiangtang Terrane to the north. The oldest rocks consist of Precambrian to Cambrian basement gneisses which outcrop south of Amdo and give a U–Pb zircon age of about 530 Ma (Xu *et al.* 1985). They show an intense tectonic fabric which was isoclinically folded by structures with

north-trending axial planes, under amphibolite facies conditions. Sillimanite-bearing assemblages suggest crustal anatexis at > 680 °C (Harris, Xu & Jin, this volume). The isoclines were refolded by later east-trending folds and were then carried south on major biotite-grade shear zones and later brittle thrusts. We consider that only these late shear and thrust zones developed in the Mesozoic or Tertiary and that the earlier intense deformation, with associated high-grade metamorphism, developed during late Precambrian tectonic events. All the observed lithological contacts between younger rocks and the gneisses were either tectonic or intrusive.

The oldest Phanerozoic sediments in this Terrane observed on the Geotraverse were Carboniferous in age and consist of sandstones with some glaciomarine deposits, overlain by Permian shelf carbonates and Triassic and Jurassic reef limestones and clastics. North of the Nyainqentanglha Shan, the Mesozoic succession is dominated by a thick sequence of Jurassic (?) flysch (Yin *et al.* this volume).

A change in sedimentation occurred during the Cretaceous, with the deposition of a thick sequence of red sandstones and intermediate volcanic rocks. These were followed by Albian–Aptian Orbitolina limestones and then more red beds and volcanics. A phase of deformation affected these rocks before the deposition of the youngest red beds and volcanics during the early Tertiary. Where interbedded with the Orbitolina limestones, or overlying the end-Cretaceous unconformity, as observed northwest of Lhasa, the red beds are easy to date. Elsewhere however, as near Amdo, the age of the red beds, and hence of their deformation, is uncertain.

The northern boundary of the Lhasa Terrane is taken to lie north of the northernmost outcrops of ophiolite, which extend from Amdo to Dongqiao within the Geotraverse area, but can also be traced approximately eastwards and westwards across most of the central Tibetan Plateau. Scattered outcrops of ophiolite occur south of this line. All of the ophiolites show evidence of having been thrust approximately southwards during the Mesozoic or Tertiary and we consider the scattered outcrops to be parts of a single nappe which was subsequently disrupted by later faulting.

The deformation of the Lhasa Terrane occurred in several phases, as summarized below.

(i) Southward obduction of the ophiolites from the approximate line of the Banggong Suture, for a present distance of 150 km over the Lhasa Terrane. Some deformation of the underlying Mesozoic rocks probably occurred at this time.

(ii) Deformation of the Palaeozoic and Mesozoic rocks, before the intrusion of Lower Cretaceous granites and granodiorites and before the deposition of Lower to Middle Cretaceous red beds and volcanics. This deformation is most prominent in the central part of the Lhasa Terrane.

(iii) Deformation of the Cretaceous red beds together with the older Mesozoic sediments in the Lhasa area, before the deposition of lower Tertiary volcanics and red beds and before the intrusion of the Gangdise granitic batholith.

(iv) Deformation of the Tertiary red beds, particularly in the region south of the Nyainqentanglha Shan. Cretaceous red beds are deformed across much of the Lhasa Terrane, but it is not known how much of this deformation is Cretaceous and how much is Tertiary.

The evidence for these different episodes and the regional structure will be described in a series of cross sections from the Amdo region, from the Dongqiao–Gyanco–Namco region, from Nyainqentangla and from Lhasa.

(*b*) *The Amdo region*

Much of the earlier structure of the Amdo region is unfortunately obscured by late Tertiary faulting. Ophiolites occur south of Amdo and are overlain by red beds of unknown age, which mask the possible site of the suture. The red beds are folded gently and are bounded to the north by a normal fault which drops the red beds down to the south. North of this fault, Jurassic sediments of the Qiangtang Terrane are thrust over the red beds as shown in figure 7*a*. (For a map of the Amdo area, see Kidd *et al.*, this volume, figure 4).

South of the Amdo ophiolite, there is a 6 km wide east–west-trending late Tertiary graben. On the southern side of the graben, Cretaceous (?) granites intrude the Amdo basement gneisses, which are thrust over Carboniferous clastics and Mesozoic limestones to the south (figure 7*b*).

This structural pattern changes slightly west of Amdo, across a northnorthwest-trending tear fault, which presumably acted as a transfer zone during the compressional deformation and the later extension. West of this tear fault, the red beds overlie ophiolitic material, but all show evidence of imbrication on thrusts directed to the south. Some thrusting is possibly young, carrying red beds over (?) Pliocene–Pleistocene deposits.

The red beds in the western part of the range are in a large asymmetric syncline with a steeply north-dipping axial surface, which is offset by two prominent northwest-trending tear faults. The red beds are uncleaved except very locally near the southern margin of the range. Nearer Amdo, the ophiolitic ultramafic and gabbroic rocks are imbricated with the red beds, thrust over them both southward, and, locally northward. In one section near Amdo, altered ultramafics overlie a gently north-dipping inverted section of probable Cretaceous andesites with minor red bed intercalations. Folded and faulted red beds obscure the relation between Jurassic sediments of Qiangtang Terrane affinity, and the ophiolitic rocks. Several steep ENE-trending faults cut this section and limited evidence of a component of left-lateral strike-slip was seen in outcrop, besides the components of vertical displacement. The overall structure seen in this range, west of Amdo, is reminiscent of the 'flower structure' seen in compressional segments of large strike-slip fault zones where outward-directed thrusts mingle with steep faults having oblique displacements.

Thus this region shows evidence of ophiolite uplift, though the base of the ophiolite was not seen, followed by post-Cretaceous, and possibly Tertiary, thrusting. Compressional tectonics continued until Recent times. The thrusts were directed both northwards and and southwards. Restoration of the thrusts north of Amdo indicates that ophiolites with their cover of red beds must have been thrust north, along with the Jurassic limestones; presumably the northward- and southward-directed thrusts interdigitate at depth. However, no accurate cross sections can be constructed until more regional studies are done, as the region has certainly suffered some strike-slip tectonics. At the present level of erosion, there is no indication of any major deformation related to the collision of the Qiangtang and Lhasa Terranes; if the terranes were locally intensely deformed, this deformation zone must be buried by post-Cretaceous over-thrusting, or removed in this transect by strike-slip displacements.

The original obduction direction is difficult to identify from the Amdo structures, but ophiolites occur as thrust slices about 75 km southsoutheast of Amdo, northwest of Nagqu. From the scattered outcrops in this region, the ophiolite stratigraphy can be seen to be repeated by thrusting and the underlying Jurassic and older sediments show moderate to tight south-verging folds and thrusts.

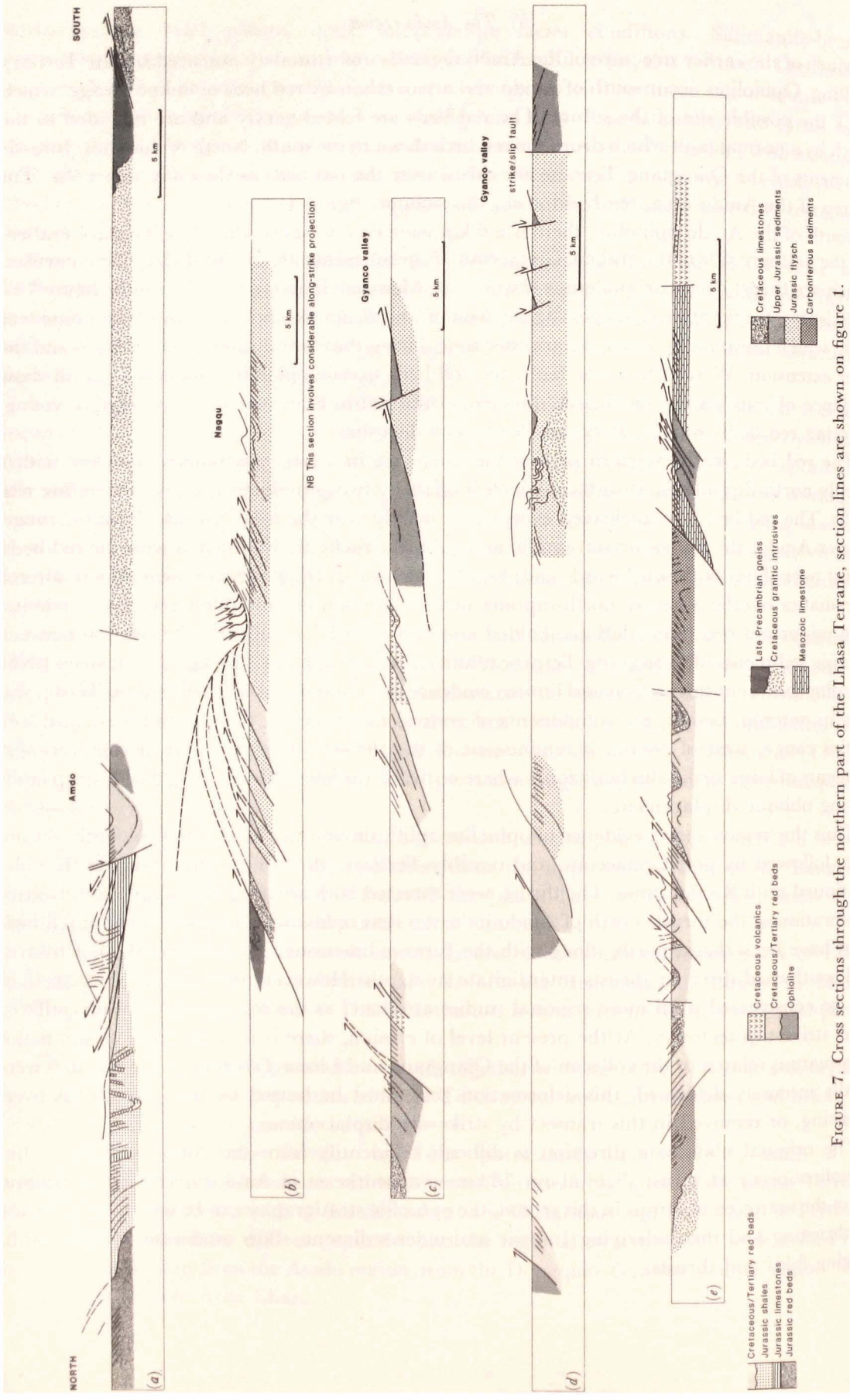

FIGURE 7. Cross sections through the northern part of the Lhasa Terrane, section lines are shown on figure 1.

(*c*) *The Dongqiao–Gyanco region*

Northwest of Dongqiao, ultramafic rocks of the ophiolite suite are unconformably overlain by soil horizons and fluvial sandstones and limestones of Upper Jurassic age, indicating that the ophiolites had been obducted before this time. The ophiolites dip steeply and face to the north. The suture is considered to lie somewhere to the north of these outcrops under Neogene sediments.

South of Dongqiao there are outliers of an originally more extensive thrust sheet of ophiolite. Observations of ductile shear zones at the base of the ophiolitic remnants suggest that the sheet was emplaced towards the southsoutheast. It was thrust over Jurassic flysch, which is deformed into moderately-tight inclined folds with axes trending eastnortheast and axial planes with an associated axial–planar cleavage dipping steeply to the northnorthwest. We consider that much of this folding and the shearing at the base of the ophiolite occurred during obduction. There is no evidence for any higher level thrust sheet of Carboniferous–Permian sediments above the ophiolite, as suggested by Girardeau *et al.* (1984).

In fact, these Carboniferous–Permian clastics and limestones, possibly including some Jurassic limestones as well, underlie the ophiolite thrust sheet, forming slivers at its base. Confusion has arisen because late Tertiary–Recent normal faulting has modified the elevation of the base of the ophiolite sheet; if these faults are not detected, it can appear as if the Carboniferous–Permian rocks locally overlie the ophiolite (see Kidd *et al.*, this volume). Post-mid-Cretaceous thrust imbrication may also locally contribute to reversal of the original tectonic sequence.

Between Dongqiao and Gyanco the ophiolite was probably largely unconformably covered by later Cretaceous volcanics and red beds. There are large Cretaceous granitic bodies which cut the ophiolite and the folded flysch and have generally undeformed zones of contact metamorphism (Harris, Xu, Lewis & Jin, this volume).

As shown in figure 7*c* and *d*, the ophiolite sheet has been dismembered by later faulting. Jurassic flysch sediments have been thrust on to the ophiolite and ophiolite is locally thrust over the Cretaceous succession. This deformation is part of the widespread regional post-Cretaceous deformation which also affects the red beds and the ophiolite at Amdo. All the thrusts are cut by steep normal faults related to Neogene graben formation. Figure 8 shows a map of part of this faulted region, north of Gyanco. For details of the Neogene tectonics in this region, see Armijo *et al.* (1986).

(*d*) *The Gyanco–Dejing section*

At Gyanco there are steep WNW-trending Neogene faults, with dextral strike-slip movement; to the south the rocks are predominantly Carboniferous sandstones and mixtites, cut by Cretaceous granites. Cleavage is only weakly developed in the sediments and the sandstones show little to no cleavage, though there are numerous tension gash arrays indicating a north–south maximum compression direction. In the north these sediments are deformed into large open folds. On the southern margin of the Cretaceous batholith, however, the deformation is more intense and the rocks have an upright to south-dipping cleavage. The Cretaceous granites are undeformed and appear to have been intruded after the deformation of the Carboniferous sediments. About 10 km N of Nam Co, the deformed sediments are unconformably overlain by conglomeratic red beds, which have only a gentle dip to the south, though the pebbles are slightly cracked and stretched with a maximum elongation direction

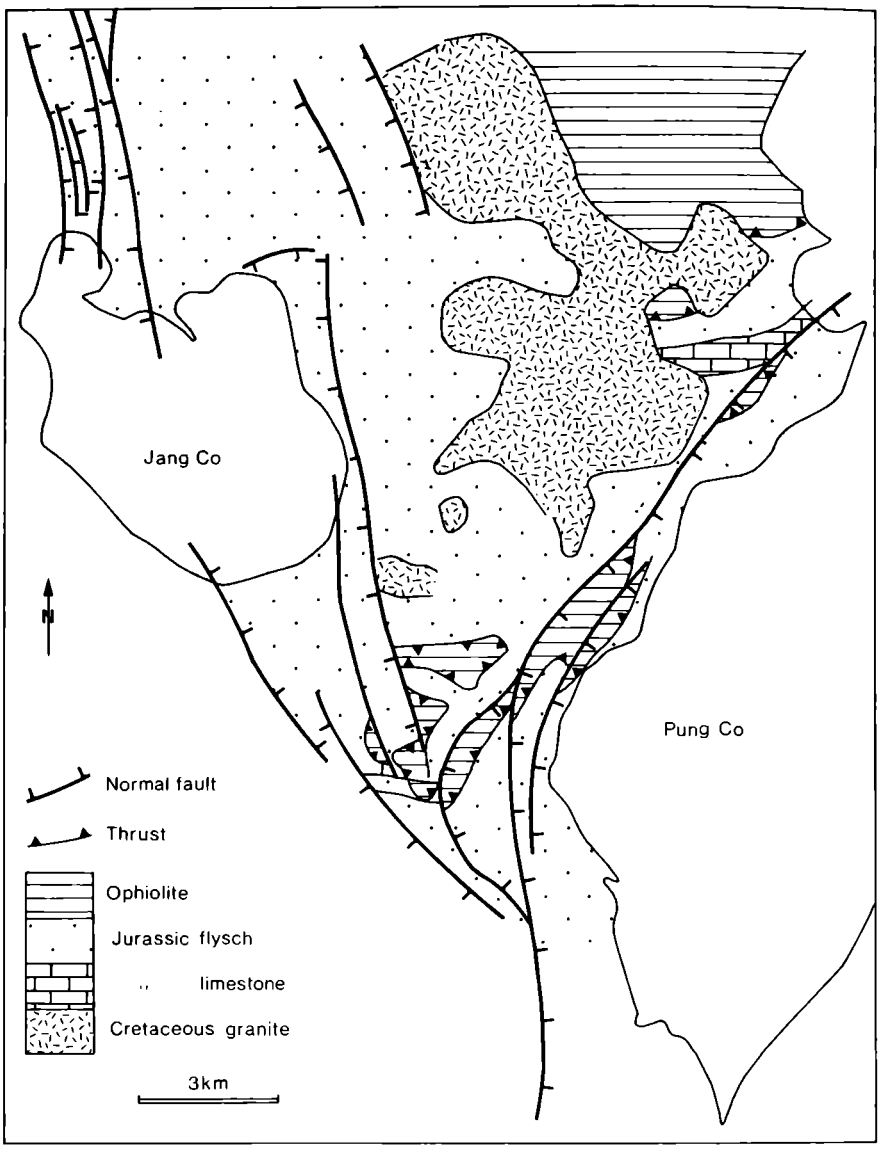

FIGURE 8. Detailed map showing the break up, by thrusts and normal faults, of the once widespread Jurassic ophiolite suite, north of Gyanco (locality shown by box '8' on figure 1).

plunging steeply to the SSE. To the south are Orbitolina limestones, which are deformed by post-Cretaceous folds and thrusts as shown on figure 7*e*. Near the northwest corner of Nam Co, outcrops of Cretaceous rocks end at another zone of probably steep strike-slip Neogene faults. South of this are faulted and folded quartzites, shales and limestones, supposedly Upper Palaeozoic in age (1:1.5 M Geol. Map of Tibet). Limestones extend south to a complex imbricate zone in which slices of limestone and ophiolite alternate. The structurally-lowest ophiolite seen outcrops in a flat dome, where it is overthrust by limestones of Jurassic age (Smith & Xu, this volume), whose steep bedding is cut off against the thrust. A possible interpretation of this zone, involving several breaching thrusts, is shown in Figure 7*e*. This ophiolite zone is known to extend more than 120 km to the WNW (1:1.5 M Geol. Map of Tibet).

How these ophiolites were obducted into their present position is unknown. The original base of the obducted sheet was not seen. Presumably they were thrust over Jurassic and older rocks and the sequence then thoroughly imbricated during subsequent deformation. All the kinematic indicators suggest thrusting to the southsoutheast and we believe that these Namco–Dejing ophiolites were originally part of the same sheet as that north of Gyanco. To the south, this 20 km wide block, comprising Upper Palaeozoic and Jurassic sediments and ophiolite slices, is faulted against gently-dipping Cretaceous limestones and red beds; south of these to a fault zone near Dejing is a sequence apparently several kilometres thick, of Upper Cretaceous volcanics (Coulon *et al.*, 1986) which, away from the Dejing faults, dip gently northwards.

(*e*) *The Nyainqentanglha range*

The Nyainqentanglha Range is an uplifted block trending about N 060°, separated by faults from the Yangbajian Graben to the southeast and the Nam Co depression to the northwest. It widens from about 10 km in the northeast to about 35 km in the southwest.

The eastern part of the range consists mainly of pelitic sediments with some orthoquartzites and calcareous slates with a general east–west strike. The pelitic rocks are weakly to moderately strong cleaved and are mapped as Jurassic (1 : 1.5 M Geol. Map of Tibet). Farther to the west, pelitic sediments are associated with calc-phyllites, phyllitic-matrix conglomerates and an olistostrome with limestone blocks. These rocks, which are more deformed and metamorphosed in the greenschist facies, have been mapped as Carboniferous (1 : 1.5 M Geol. Map of Tibet), but we consider them, at least in part, to be the same as the supposed Jurassic rocks farther east, since both contain a very distinctive marly rock with calcareous concretions. These sediments, where seen near the Damxung to Nam Co track, vary in strike, both of bedding and cleavage, from northeast-trending in the north, through north-trending to east-trending in the southern half of the section. The lineation shown by the metamorphic minerals and strongly elongate conglomerate clasts plunges to the eastsoutheast, suggesting locally an oblique shear component. The cleavage is crenulated by later structures, whose crenulation cleavages and axial planes dip to the northwest. The rocks show syn- to post-tectonic garnet and staurolite growth, which indicate metamorphic conditions of *ca.* 700 °C and 5 ± 2.5 kbar (Harris, Holland & Tindle, this volume).

Still farther west, there are gneissose rocks, mainly orthogneiss but with some metasediments. The foliation in the orthogneiss dips gently. In places the rocks are cataclastic and their strike is approximately northeast, parallel to the range, but between these cataclastic zones, the strike is nearly north–south, transverse to the range. The northeast-trending cataclastic fabric appears to be superimposed on earlier structures.

Isotopic studies indicate that the Nyainqentanglha granitic orthogneiss is about 50 Ma old, not Precambrian as suggested on the 1 : 1.5 M Geological Map, although Precambrian crustal material (1200–2000 Ma) was involved in its generation (Xu *et al.* 1985). Late to post-tectonic metamorphic minerals such as andalusite may be associated with granite intrusion, but much of the intense deformation in the slates and phyllites must be earlier, as the cleaved rocks are clearly unconformably overlain by Cretaceous sediments on the northern side of the range (figure 9*a*). Pebbles in the basal conglomerates, which have been transported northwards off the range, are mostly of quartzite, limestone and quartz, without any boulders of Nyainqentanglha granite. The Cretaceous red beds have been subsequently deformed into north-verging northeast trending folds. They locally show a weak north-verging cleavage.

Thus the tectonic history of the Nyainqentanglha Range includes:

(i) folding and locally intense cleavage development in the slates and phyllites, with some metamorphism;

(ii) uplift and erosion followed by the deposition of Cretaceous red beds;

(iii) intrusion of the Nyainqentanglha granite at about 50 Ma;

(iv) folding of the Cretaceous red beds, uplift and deformation of the granite and probably refolding of the cleavage in the slates and phyllites.

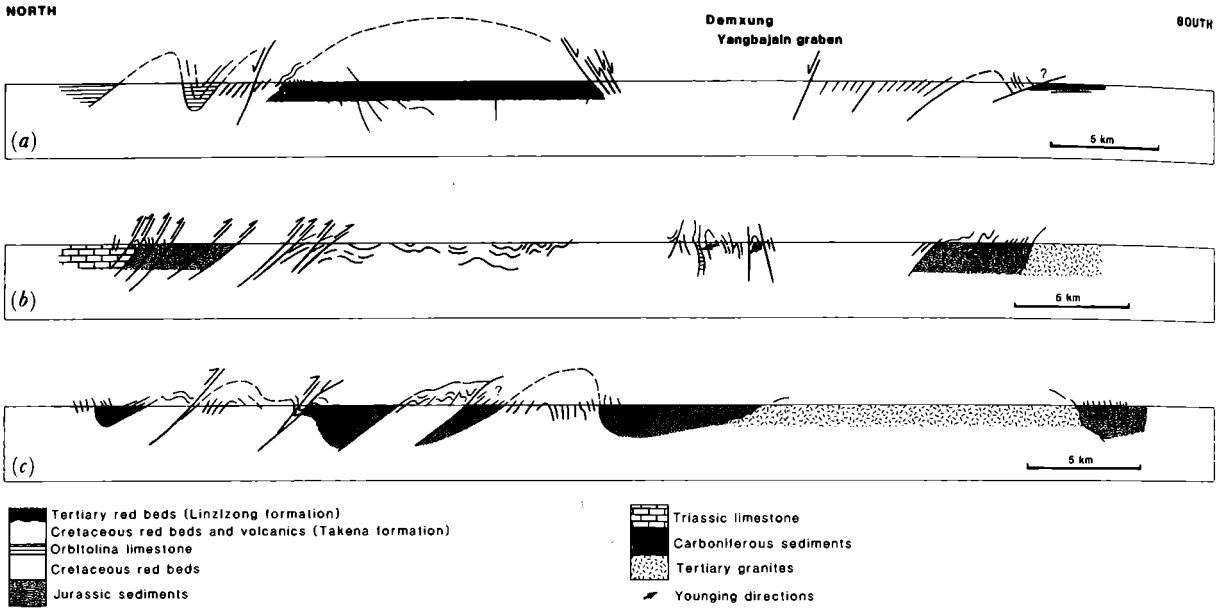

FIGURE 9. Cross sections through the southern part of the Lhasa Terrane, from the Nam Co to north of Lhasa; lines are shown on figure 1. The '?' indicate a degree of uncertainty in the age and/or structure of the red beds.

The Nyainqentanglha granite is itself strongly sheared along its southeastern margin and shows an intense and locally mylonitic fabric with shear bands indicating that the shear direction was analogous to that of a low angle normal fault, with its top side moving down to the southeast. Elongate quartz ribbons define a pronounced southeast-plunging lineation. The origin of this fabric may be due to:

(i) shearing associated with granite emplacement, unrelated to regional tectonics;

(ii) low-angle extensional faulting, producing a detachment along the northwest side of the Yangbajain graben, similar to the ductile detachment zones in the Basin and Range (Davis & Lister, in press); or

(iii) low angle thrust faulting, reoriented by underlying thrust structures.

The ductile thrust model is considered possible, though the thrust would have to be folded along the Nyainqentanglha range, to root on the northwest side. No evidence for this thrust was found on the northwest side of the range, though it could have been disrupted by later normal faults.

There is some support for the low-angle extensional model in that unpublished $^{39}Ar/^{40}Ar$ dates on micas and feldspars from the Nyainqentanglha granite and the high strain zone indicate rapid uplift within the last 10 Ma (W. Kidd, pers. comm. 1987). This zone shows high

ductility related to these possible extensional tectonics. Elsewhere in this region the normal faulting forms only high-level brittle structures, though normal faults, with red beds on the hanging-walls, do detach on the Nyainqentanglha shear zone.

The model of shear related to intrusion is possible, if one believes that granites can be intruded by such a mechanism, involving intense simple shear along the upper margin. The preference of one of the authors (R.M.S.) is that the intrusion of the granites itself produced all the shear deformation. It is possible that the granites were intruded into an active, relatively deep level, shear zone. Similar ductile mylonite-bearing shear zones were observed in the Gangdise batholith south-east of Lhasa, where the shear sense is analogous to low angle normal faulting where the hanging-wall has dropped to the north. If these interpretations, that the granites intruded into a deforming regime, are correct, then the Gangdise batholith can be considered to have been intruded into a region undergoing NNW–SSE extension.

(*f*) *The region between Yangbajain and Lhasa*

The Yangbajain graben is a Pleistocene to Recent structure (Armijo *et al.* 1986) with well-preserved fault scarps in the valley sides and present-day hydrothermal activity. It is part of a system of north–south-trending grabens, linked by westnorthwest dextral tear faults (see Armijo *et al.* 1986).

Southeast of the Yangbajain graben, Carboniferous rocks are folded into large upright to south-verging structures. The age of this deformation is uncertain. To the southeast there are large thrusts which carry Mesozoic rocks to the southeast over Palaeogene sediments and volcanics (figures 9*b* and *c*). These folds and thrusts trend northeast and are associated with NNW-trending tear faults, suggesting a NNW to SSE transport direction.

Where no unconformity is present, it is difficult to separate the deformation affecting the Tertiary rocks, which in the area north-west of Lhasa are essentially volcanics known as the Linzizong Formation, from earlier deformation affecting the Cretaceous Takena Formation. Deformed unconformities between the Linzizong and Takena Formations were studied in the two regions shown by the sections in figure 9*b* and *c*. In these areas the post-Linzizong deformation produced open to close folds verging to the southeast, while the pre-Linzizong deformation produced upright to north-verging folds.

The intensity of deformation in the Takena Formation increases southwards, towards Lhasa, where the structures are obscured by intrusions related to the Gangdise batholith. South of Lhasa, Mesozoic sediments show locally intense deformation, with a steep cleavage cut by a later gently northward-dipping crenulation cleavage. The main-phase folds are upright to northward-verging and the cleavage carries a mineral lineation which plunges steeply down dip. Small shear zones, with a sense of overthrusting from the south, cut the bedding and cleavage. Burg *et al.* (1983) described three phases of deformation from these sediments south of Lhasa, including an early pre-cleavage phase, but no evidence for their earliest deformation phase was found during our work.

(*g*) *Summary of the structure in the Lhasa Terrane*

The Lhasa Terrane appears to have had the structure of a passive margin until mid Jurassic times. During the mid Jurassic, ophiolitic material was obducted at least 150 km southwards onto the Lhasa Terrane. This is the present distance across strike covered sporadically by the dismembered ophiolite sheet. As the zone has been shortened by post-Cretaceous deformation,

the distance covered by the ophiolite obduction may have been much greater, possibly of the order of 200 km.

The obducted sheet was probably originally relatively thin, only a few kilometres thick, as there is no evidence for any thrust cover during obduction. It is difficult to envisage what driving mechanism could thrust such a thin wedge so large a distance, without the sheet being thoroughly broken. It is possible that the ophiolite was not part of one single sheet, but represents several individual obducted slices, but this would imply several sutures. We observed no structural evidence for sutures within the Lhasa Terrane nor did we observe any zones of anomalous deformation or metamorphism which could indicate the presence of a suture: we consider the Mesozoic stratigraphy to be continuous across the Terrane. Rather these ophiolites appear as thrust slices or klippen, probably as an imbricated overthrust sheet.

There was probably some deformation of the footwall of the obducted ophiolite, producing folds in the Jurassic flysch. Some of the ophiolite obduction may have occurred by transport on thrusts within the Mesozoic succession.

Between Gyanco and Yangbajain the Carboniferous to Jurassic sediments were deformed by pre-Cretaceous, upright to approximately northward verging structures. To the northwest of Gyanco the pre-Cretaceous structures have a different vergence; Jurassic flysch shows southeast-verging structures probably associated with ophiolite obduction. The north-verging deformation was obviously localized. It may somehow be related to early collisional events on the Banggong Suture, but probably it is related to localized intracratonic deformation.

There seems to have been little deformation associated with the collision between the Qiangtang and Lhasa Terranes. No zone of locally intense deformation comparable to that of the western Alps or western Himalayas was observed along the line of the suture; indeed, as described above, the most intense Mesozoic deformation and metamorphism occurs to the south, in the Nyainqentanglha range. Any zone of deformation along the Banggong Suture has subsequently been buried by later thrusting or by Tertiary sedimentation. There is little evidence for major crustal thickening of the Qiangtang Terrane during this collision; the Mesozoic sediments are only weakly deformed by northward-verging structures. Similarly across the Lhasa Terrane there is no evidence for a late Mesozoic mountain belt, in that thick molassic deposits are absent and Albian–Aptian limestones extended across the terrane, suggesting shallow water marine conditions.

The Gangdise batholith was generated by northward subduction from the Tethyan ocean to the south. Granite intrusion dates from over 90 Ma, but the main phase occurred from about 60 to 40 Ma (Harris, Xu, Lewis & Jin and Harris, Xu, Lewis, Hawkesworth & Zhang, this volume). Deformation of the Mesozoic sediments around Lhasa occurred after deposition of the Middle to Upper Cretaceous sediments (*ca.* 100 Ma) and before the Linzizong volcanics, dated at 56 Ma (Xu *et al.* 1985). Estimates of the timing of collision between India and the northern collage of micro-continents range from 55 to 40 Ma, based on the movement of India as determined from magnetic anomalies in the Indian Ocean and by the disappearance of the last remnants of the Tethyan ocean. The deformation of the Mesozoic sediments on the Lhasa Terrane may pre-date this closure and relate to the intrusion of parts of the Gangdise batholith (England & Searle 1986). Alternatively it may be related to the first stages of closure along this suture zone, or to the accretion of minor island arc or sea-mount material, similar to the origin of the post Albian–Aptian deformation which affects the Karakoram region to the west, in northern Pakistan (Coward *et al.* 1986). However the deformation appears to be synchronous

with the strong deformation of the Xigatse flysch along the Zangbo Suture to the southwest and may be subduction-related.

The post-Albian–Aptian, but pre-Linzizong deformation in the Lhasa region forms upright to northward-verging structures, which decrease in intensity northwards. Thus the SSE-verging structures which affect the red bed successions throughout the central and northern parts of the Lhasa Terrane, as in the Amdo region and northwest of the Nyainqentanglha Shan, are considered to be part of the Tertiary deformation, similar to the SSE-verging folds and thrusts which affect Palaeogene red beds between Lhasa and Yangbajain (figure 9*b* and *c*). We consider this supposedly Tertiary deformation to be related to the closure of the main Indus–Zangbo Suture. However, on the 1:1.5 M Geological Map of Tibet, Eocene rocks are shown unconformable on Cretaceous, west of Nam Co and west of Baingoin; in the Lunpola Basin, Eocene (?) conglomerates of the Niubao Formation rest unconformably on the Cretaceous (Song & Liu 1981). Without more detailed study of these areas, it is not possible to determine how much of the deformation is late Cretaceous and how much is post-Eocene.

5. Tertiary shortening and crustal thickening across Tibet

Figure 10 shows the regions which have suffered possible Eocene deformation on the SSE-directed thrusts, which are thought to be related to Tertiary collision. There is clear evidence for Tertiary deformation in the Erdaogou region, possibly accounting for about 50 km displacement. There may have been some Tertiary shortening of the Kunlun ranges; indeed some shortening and thickening of northern Tibet is indicated from the growth history of the Tertiary flexural basins of the Tarim and Tsaidam along the northern margin of Tibet. However the nature of this deformation is obscure, as any Tertiary thrusts are covered by Neogene deposits or indistinguishable from earlier Mesozoic structures in the Kunlun. South of the Tuotuo River, however, there was little to no Tertiary shortening; in fact there was relatively little total shortening across this part of the Qiangtang Terrane. Along the traverse line the obvious Tertiary deformation appears to be concentrated near the older (Jinsha) suture and may have involved reworking of earlier Triassic thrusts.

South of the Banggong Suture, some Eocene deformation affects the rocks of the Lhasa Terrane as far south as Lhasa. The amount of shortening is relatively small. Apart from the basement gneisses south of Amdo and the Nyainqentanglha metamorphic rocks, there is no evidence for any intense crustal shortening which brought up metamorphic rocks. The generally low metamorphic grade suggests that the shortening was taken up by small movements on several thrusts. It is impossible to make any accurate estimates of the amount of shortening because of the later strike-slip faulting which offsets structural domains. Estimates of the shortening, based on simple reconstructions of the sections as they stand, ignoring the strike-slip components, gives values between 30 and 40%, that is, there may have been between 75 and 100 km shortening across the Lhasa Terrane.

Thus the total post-Eocene shortening across Tibet can only be estimated in terms of a few hundred kilometres. This contrasts with the estimates of 2000 ± 500 km shortening across the Asian Plate made using the movement pattern of the Indian Plate, as shown by magnetic anomaly stripes in the Indian Ocean (Molnar & Tapponnier 1975; Patriat & Achache 1984). However considerable crustal shortening could be attained by movement on the network of strike-slip faults which cut through Tibet, or by major strike-slip displacements along the

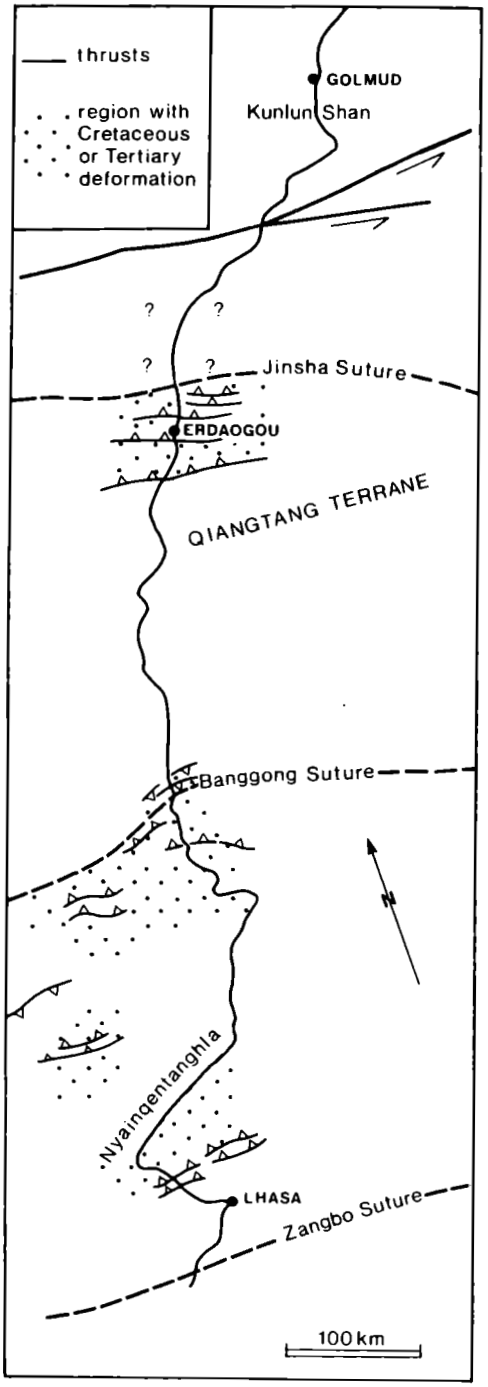

FIGURE 10. Simplified map to show the distribution of Tertiary deformation across Tibet.

Kunlun and Zangbo fault zones as is discussed by Tapponnier *et al.* 1982) and Kidd & Molnar (this volume). Our data do not support the hypothesis put forward by Dewey & Burke (1973) and England & Houseman (1986) that plane strain shortening during the Tertiary collision doubled the crustal thickness, allowing for up to 2000 km displacement across Tibet (England & Houseman 1986). Similarly our data do not support the models of Allègre *et al.* (1984)

involving shortening on several large scale thrusts. We recognize only a small amount of shortening on distributed thrust zones. Some mechanism, other than one involving solely regional pure shear or alternatively crustal-scale thrust-stacking, is needed to explain the thickening of the Tibetan crust. Such mechanisms will be discussed in a later chapter (Dewey *et al.* this volume).

References

Allègre, C. J. and 34 others 1984 Structure and evolution of the Himalayan-Tibet orogenic belt. *Nature, Lond.* **307**, 17–22.

Armijo, R., Tapponnier, P., Mercier, J.-L. & Han Tonglin 1986 Quaternary extension in southern Tibet: Field observations and tectonic implications. *J. geophys. Res.* **91**, 13803–13872.

Bally, A. W., Allen, C. R., Geyer, R. B., Hamilton, W. B., Hopson, C. A., Molnar, P. H., Oliver, J. E., Opdyke, N. D., Plafker, G. & Wu, F. T. 1980 Notes on the geology of Tibet and adjacent areas – report of the American plate tectonics delegation to the Peoples' Republic of China. *Geol. Surv. Amer. Open File Rept* **80–501**.

Burg, J.-P., Proust, F., Tapponnier, P. & Chen, G. M. 1983 Deformation phases and tectonic evolution of the Lhasa block (southern Tibet, China). *Eclog. geol. helv.* **76**, 643–665.

Chang Chengfa & Pan Yusheng 1981 A brief discussion on the tectonic evolution of the Qinghai-Xizang plateau. In *Geological and Ecological Studies of the Qinghai-Xizang (Tibet) Plateau* **1**, 1–18. Beijing, Science Press.

Chang Chengfa and 26 others 1986 Preliminary conclusions of the Royal Society and Academia Sinica 1985 geotraverse of Tibet. *Nature, Lond.* **323**, 501–507.

Coulon, C., Maluski, H., Bollinger, C. & Wang, S. 1986 Mesozoic and Cenozoic volcanic rocks from central and Southern Tibet: $^{40}Ar/^{39}Ar$ dating, petrological characteristics and geodynamical significance. *Earth planet. Sci. Lett.* **79**, 281–302.

Coward, M. P., Windley, B. F., Broughton, R., Luff, I. W., Petterson, M. G., Pudsey, C., Rex, D. & Khan, M. A. 1986 Collision tectonics in the N. W. Himalayas. In *Collision tectonics* (ed. M. P. Coward & A. C. Ries). *Spec. Publ. geol. Soc. Lond.* **19**, 203–219.

Dahlstrom, C. D. A. 1969 Balanced cross-sections. *Can. J. Earth Sci.* **6**, 743–757.

Davis, G. A. & Lister, G. S. (in press) Detachment faulting in continental extension: perspectives from the southwestern U.S. Cordillera. *Mem. geol. Soc. Am.*

Dewey, J. F. & Burke, K. C. A. 1973 Tibetan, Variscan and Precambrian basement reactivation: Product of continental collision. *J. Geol.* **81**, 683–692.

England, P. C. & Houseman, G. A. 1986 Finite strain calculations of continental deformation. 2. Comparison with the India-Asia collision. *J. geophys. Res.* **91**, 3664–3676.

England, P. C. & Searle, M. 1986 The Cretaceous–Tertiary deformation of the Lhasa block and its implications for crustal thickening in Tibet. *Tectonics* **5**, 1–14.

Girardeau, J., Marcoux, J., Allègre, C. J., Bassoullet, J. P., Tang Youking, Xiao Xuchang, Zao Yougong & Wang Xibin. 1984 Tectonic environment and geodynamic significance of the Neo-Cimmerian Dongqiuo ophiolite, Banggong-Nujiang Suture zone, Tibet. *Nature, Lond.* **307**, 27–31.

Hossack, J. R. 1979 The use of balanced cross-sections in the calculation of orogenic contraction, a review. *J. geol. Soc. Lond.* **136**, 705–711.

Li Chunyu, Liu Xueya, Wang Quan & Zhang Zhimeng. 1979 A tentative contribution to plate tectonics of China. *Institute of Geology, Chinese Acad. Geol. Sci.* Mimeographed handout.

Molnar, P. & Tapponnier, P. 1975 Cenozoic tectonics of Asia: effects of a continental collision. *Science, Wash.* **189**, 419–426.

Patriat, P. & Achache, J. 1984 India–Eurasia collision chronology and its implications for crustal shortening and driving mechanisms of plates. *Nature, Lond.* **311**, 615–621.

Sengör, A. M. C. 1984 The Cimmeride orogenic system and the tectonics of Eurasia. *Geol. Soc. Am. Spec. Paper* **195**, 82.

Song Zichen & Liu Gengwu 1981 Palynological assemblages from Xizang with reference to their palaeogeographical significance. In *Geological and Ecological Studies of the Qinghai-Xizang (Tibet) Plateau* **1**, 207–214. Beijing, Science Press.

Tapponnier, P., Pelzer, G., Le Dain, A. Y., Armijo, R. & Cobbold, P. 1982 Propagating extrusion tectonics in Asia: new insights from simple experiments with plasticene. *Geology* **10**, 611–616.

Watson, M. P., Hayward, A. B., Parkinson, D. N. & Zhang, Z. M. (in press). Plate tectonic history, basin development and petroleum source rock deposition onshore China. *J. marine Petrol. Geol.*

Xu Ronghua, Scharer, U. & Allègre, C. J. 1985 Magmatism and metamorphism in the Lhasa block (Tibet): a geochronological study. *J. Geol.* **93**, 41–57.

Zhang, Z. M. 1984 An outline of the plate tectonics of China. *Bull. Geol. Soc. Am.* **95**, 295–312.

Appendix. Structures and fabrics in the Kunlun Shan: evidence for mid-Palaeozoic (pre-Upper Devonian) deformation

By Zhang Hu†

Institute of Geochemistry, Academia Sinica, Guiyang, Guizhou, People's Republic of China

For the purpose of this discussion, three tectonic units referred to as the North Kunlun, South Kunlun and Bayan Har Units, separated by the Middle Kunlun and Xidatan Faults, are distinguished (figure A 1).

1. The North Kunlun Unit

In the North Kunlun Unit, an angular unconformity between pre-Upper Devonian metamorphic rocks (Binggou Group) and unmetamorphosed Upper Devonian is recognized in the Daobangou Valley, about 35 km S 10° E from Golmud (see Yin *et al.*, this volume, figure 2). The underlying series, of quartz mica schists, quartzite and marble, shows a steeply

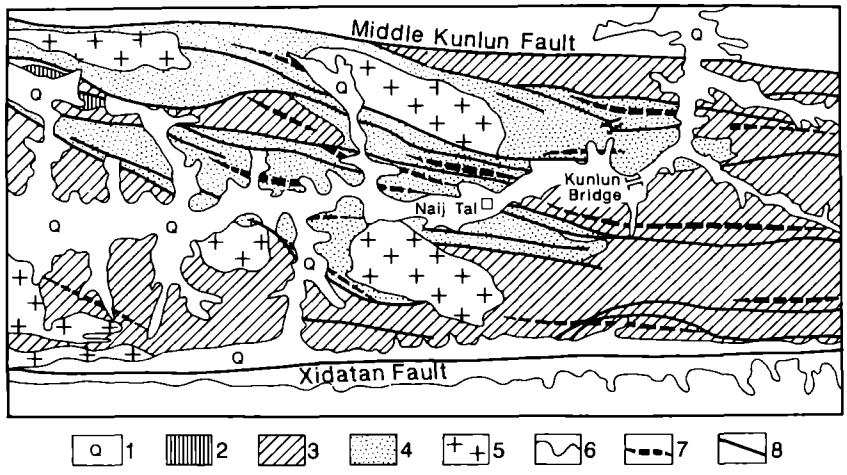

Figure A 1. Structural lines in the South Kunlun Unit. 1 (Q): Quaternary. 2: Neogene. 3: Upper structural stage (Carboniferous to Triassic). 4: Lower structural stage (Precambrian to Ordovician). 5: Granitic rocks. 6: Geological boundary line. 7: Axial trace of fold. 8: Compressional fault. 9: (MKF) Middle Kunlun Fault. 10: (XF) Xidatan Fault. 11: Naij Tal. 12: Kunlun Bridge.

northward-dipping schistosity and complex transposed folds. The overlying sequence, mapped as Upper Devonian but here unfossiliferous, with a basal conglomerate over 100 m thick, dips regularly southwards at a moderate angle. The conglomerate contains well-rounded pebbles of igneous and metamorphic rocks including marble, gneiss, quartzite, granite, sericite schist and amphibolite. The abundant marble pebbles are lithologically similar to the marble in the underlying sequence. According to published information (Wang *et al.* 1983; 1:1.5 M Geological Map of Qinghai–Xizang Plateau 1980), these metamorphic rocks extend at least 700 km in an east–west direction.

† The author was unable, owing to ill health, to participate in the 1985 Geotraverse, but took part in preparatory work before 1985.

2. The Middle Kunlun fault

The Middle Kunlun Fault is taken to separate the North and South Kunlun Units. It dips steeply southwards. A cleavage zone several hundred metres wide on the north side of the fault indicates sinistral displacement, combined with south side up. The fault can be traced far to the east and west of the traverse area; to the east, some ultramafic masses and pillow lavas have been found in this zone.

3. The South Kunlun Unit

In this unit, the Upper Trias Babaoshan Group overlies metamorphosed Middle Triassic and older rocks with an angular unconformity. No definite field evidence of either an end-Permian or a mid-Palaeozoic unconformity has yet been seen: they are inferred on indirect evidence and are thought to have been obscured by the end-Triassic deformation and metamorphism which became increasingly intense southwards.

Fabric elements which have been studied include schistosity, lineations (mineral lineations, intersection lineations, fold axes, quartz lenses). The attitudes of the lineations in the older rocks (Ordovician and Precambrian (?)) differ from those in the Upper Palaeozoic and Triassic: in the older rocks, they plunge steeply, in the younger, gently (figure A 2). A few steeply-plunging minor folds are seen in the Ordovician (Naij Tal Group), whereas in the Carboniferous and Triassic, the fold axes plunge gently [but note steep westerly plunge of Carboniferous Red Beds immediately south of the Middle Kunlun Fault – Ed.)].

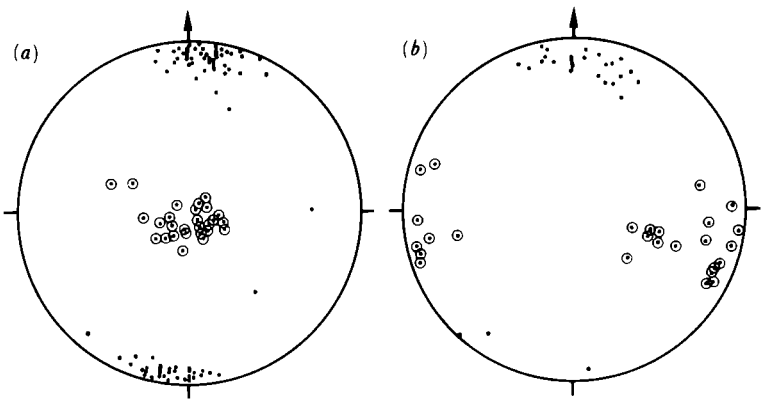

Figure A 2. Projections (equal area net) of poles to schistosities (dots) and lineations (circles round dots). (*a*) Lower structural stage (Precambrian to Ordovician; (*b*) Middle structural stage (Carboniferous to Triassic). South Kunlun Unit.

The schistosities in the older (Lower Palaeozoic) and younger (Carboniferous to Triassic) rocks are superficially similar but detailed microscopic study shows two schistosities in the older rocks but only one in the younger. In thin sections, in some of the older rocks (e.g. a schistose greywacke from west of Kunlun Bridge) it appears that an early schistosity is defined by shape-orientation of classic grains and by a penetrative mica fabric, while a later fabric, at an angle to the first one, is defined by mica in discrete planes. In such cases, it is only the later schistosity that is seen in the field. These two schistosities have not been seen in the younger rocks. The earlier one is inferred to be pre-Carboniferous. Oriented thin sections show that the early schistosity tends to strike WNW, with a steep southward dip, while the later one strikes

east–west, also dipping steeply. The intersection between them, in the older rocks, plunges steeply.

4. The Xidatan Fault

This separates the South Kunlun and Bayan Har Units. It extends for over 1000 km east–west. Numerous microscopic features show that the sinistral shear was combined with a north-side up displacement. The fault dips northwards. (See Kidd & Molnar, this volume, for more details.)

5. The Bayan Har Unit

In this unit, the prevailing rocks are assigned to the Triassic Bayan Har Group of slates and turbidites. In them, south of the Xidatan Fault, the schistosity dips northwards and early lineations are subhorizontal, but farther south around Wudaoliang the schistosity dips southwards.

6. Tectonic interpretation

The structural and other evidence is considered to indicate that the North Kunlun, South Kunlun and Bayan Har Units represent separate terranes or microplates, separated by the Middle Kunlun and Xidatan Faults which are thought to represent or conceal sutures. These are believed, from attitude of schistosities, distribution of calk-alkaline volcanics and sedimentation, to follow northward subduction. The northerly of the two supposed sutures is thought to mark the closure of a backarc basin in the late Permian; the southern one, along the Xidatan Fault Zone, is thought to have closed in the late Triassic.

References

Wang Yunshan, Zhang Qinxing & Shi Congyan 1983 The Precambrian feature of Qinghai. *Contr. Geol. Qinghai-Xizang (Tibet) Plateau* **2**, 56–69.

1:1.5 M Geological Map of the Qinghai-Xizang Plateau 1980 *Institute of Plateau Geology, Academia Sinica*. Beijing: Map Press.

Phil. Trans. R. Soc. Lond. A **327**, 337–363 (1988) [337]
Printed in Great Britain

Quaternary and active faulting observed on the 1985 Academia Sinica–Royal Society Geotraverse of Tibet

BY WILLIAM S. F. KIDD[1] AND PETER MOLNAR[2]

[1] *Department of Geological Sciences, State University of New York, Albany, New York* 12222, *U.S.A.*
[2] *Department of Earth, Atmospheric, and Planetary Sciences, Massachusetts Institute of Technology, Cambridge, Massachusetts* 02139, *U.S.A.*

[Plates 1–13]

Active and recent faulting along the main north–south road in Tibet is dominated by normal faulting occurring on northerly-trending planes and by strike-slip faulting, both of which reflect an east–west extension of the plateau. Normal faulting is prevalent in the southern half of the plateau, but we saw no evidence for any major graben in the northern half. Strike-slip faulting on roughly easterly-trending structures is more prevalent in the northern half, but conjugate faulting, with right-lateral slip on northwesterly-trending planes and left-lateral slip on north-easterly-trending planes, is common in the southern half. In two areas, we also observed components of thrust faulting, apparently in association with young strike-slip faulting.

Our most important results are bounds on the rates of slip on the two main strands of the Kunlun strike-slip fault system, which trends east–west through the Kunlun range. Ground moraine containing boulders of pyroxenite is separated by 30 km from the nearest outcrop of such rock, implying that amount of displacement in the last 1.5 to 3 Ma. Therefore the average rate of slip during the Quaternary period has been between 10 and 20 mm/a, with a likely value of 13 mm/a. Abundant fresh tension cracks and mole tracks imply continued slip on the main strand, the Xidatan–Tuosuohu–Maqu fault, and the likely occurrence of a major earthquake in the last few hundred years. Consistent offsets of gullies and dry stream channels of about 10 m may reflect slip of that amount during such an earthquake, and possible multiple offsets at one site suggest that slip may occur by large displacements of 10 m during infrequent great earthquakes. Along the other strand, the Kunlun Pass fault, offsets of roughly 50 to 150 m of, apparently, post-glacial valleys and of one glacier and its terminal moraine suggest a Holocene rate of slip between 5 and 20 mm/a, and most likely about 10 mm/a, on this fault. These rapid rates of displacement imply that Tibet is being extruded rapidly eastward, at a rate comparable to the rate at which India is penetrating into Eurasia, and therefore that, at present, a substantial fraction of this penetration is being absorbed by the eastward extrusion of Tibet.

INTRODUCTION

The study of Quaternary and active faulting of Tibet essentially began in the early 1970s with the study of Landsat imagery, or perhaps a decade earlier with the installation of the World-Wide Standardized Seismograph Network (WWSSN). Most early explorers of Tibet had little or no geologic training and made few useful geologic observations. An exception was Littledale

(1896), whose accurate mapping of young volcanoes was particularly useful to us, among others, in our first studies of Tibet (Burke *et al.* 1974; Kidd 1975; Molnar & Tapponnier 1978; Sengör & Kidd 1979). Nevertheless, even those who took care to gather geologic samples, such as Sven Hedin (see Hennig 1915), were less concerned with geologic structures, particularly with recent ones, than with collecting representative examples of particular rock types. Erik Norin, perhaps the first geologist to carry out serious geologic mapping within Tibet, described folding and thrust faulting of Tertiary sedimentary rock on the northern margin of western Tibet (Norin 1946), but even he wrote little about Quaternary or active deformation on the plateau itself. Thus when the Landsat imagery became available, a wealth of information was suddenly available to be gleaned.

Studies both of the Landsat imagery and of the larger earthquakes ($M \geqslant 5.5$) indicate that the most recent deformation is by normal and strike-slip faulting (Armijo *et al.* 1986, in press; Molnar & Chen 1983; Molnar & Tapponnier 1975, 1978; Ni & York 1978; Rothery & Drury 1984; Tapponnier & Molnar 1977; Tapponnier *et al.* 1981*a*, 1981*b*). Several north–south trending grabens are clear on the satellite imagery of southern Tibet (Armijo *et al.* 1986; Tapponnier *et al.* 1981*b*), and nearly all fault plane solutions of earthquakes in southern Tibet indicate large components of normal faulting (Molnar & Chen 1983; Molnar & Tapponnier 1978; Ni & York 1978). Some grabens in southern Tibet are linked by strike-slip faults (figure 1) (Armijo *et al.* 1986), and several metres of right-lateral slip on a northwest-trending fault can be associated with the largest earthquake (18 November 1951; $M = 8$) to have occurred within the Tibetan plateau in this century (Armijo *et al.* in press). Both fault plane solutions and structures visible on the Landsat imagery indicate a greater significance of strike-slip faulting in central and northern than southern Tibet (Armijo *et al.* in press; Molnar & Chen 1983; Molnar & Tapponnier 1978; Rothery & Drury 1984). Short strike-slip faults seem to link normal faults so as to form a mosaic of blocks that move with respect to one another and to yield an average east–west extensional regional strain (Rothery & Drury 1984). Farther north, near the edge of the plateau, left-lateral slip on the Altyn Tagh and Kunlun fault systems (figure 1) accommodates an eastward displacement of Tibet with respect to the areas to the north, the Tarim and Qaidam basins and the Nan Shan (Molnar & Tapponnier 1975; Tapponnier & Molnar 1977).

The strike-slip faulting within Tibet, on northwest- and northeast-trending planes, reflects some active north–south shortening of the plateau (Rothery & Drury 1984), perhaps as rapidly as half of the rate at which it extends in an east–west direction (Molnar & Chen 1983). Although there is abundant evidence for thrust-faulting and folding of Tertiary rock on the margins of the plateau (figure 1), i.e. in the Himalaya, in the Altyn Tagh (Molnar *et al.* 1987*a*, 1987*b*), or on the northeast edge of the plateau (Burchfiel *et al.* in press), there is little evidence for active or recent north–south crustal shortening by thrust or reverse faulting or by folding *within* the high plateau. No reliable fault plane solution of an earthquake within the high plateau shows a significant reverse or thrust component (Molnar & Chen 1983); and, in general, structures suggestive of folding or reverse faulting that can be recognized from the Landsat imagery are cut by recent normal or strike-slip faults (Armijo *et al.* 1986; Molnar & Tapponnier 1978; Ni & York 1978; Rothery & Drury 1984). Thus the prevalence of normal and strike-slip faulting requires a change in the style of deformation from that which built the plateau; the abundant evidence for Tertiary north–south crustal shortening (Chang *et al.* 1986; Dewey, Shackleton, Chang & Sun, this volume) contrasts markedly with the present style of deformation.

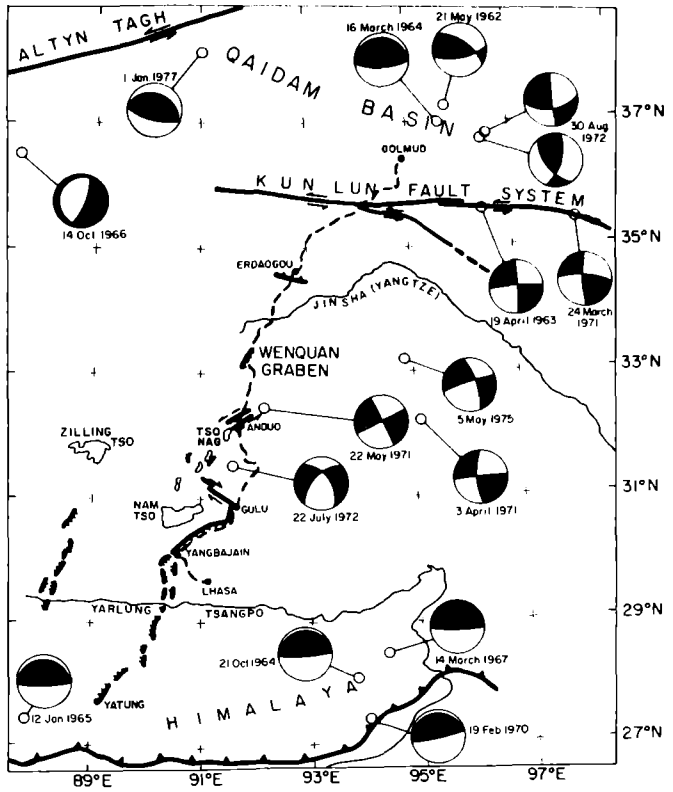

FIGURE 1. Map of the region of Tibet traversed, showing the main road, major towns, rivers, and faults, and lower hemisphere projections of fault plane solutions of earthquakes. The numerous examples of active normal faulting in southern Tibet, shown by dark lines with teeth on the downthrown side, were taken from Armijo *et al.* (1986). Note how the Kunlun Pass fault curves southward to the east, and how the Xidatan–Tuosuohu–Maqu fault continues west for several hundred km. For fault plane solutions, taken from Molnar & Chen (1983), Molnar & Tapponnier (1978), Molnar *et al.* (1977), and Tapponnier & Molnar (1977), the darkened quadrants contain compressional first motions, and therefore the T-axes.

The studies of the Landsat imagery and of seismicity have provided a general, qualitative description of the active and recent deformation of Tibet, but what clearly cannot be learned from them are tight constraints on the amounts, the timing, and the rates of these processes. One of the important questions to be answered surely is: When did the change from folding and thrust faulting to normal faulting and east–west extension occur? It is likely that this change took place at different times at different places. The folding of Pliocene sedimentary rock in the Lunpola basin [east of Zilling Tso (figure 1)] (Burke & Lucas in press; Lee 1984), and the overthrusting of (possibly late) Neogene sedimentary rock 15 km south of Erdaogou (figure 1) (Chang *et al.* 1986; Dewey, Shackleton, Chang & Sun, this volume) imply that crustal shortening must have occurred, at least in some parts of Tibet, in late Tertiary time and perhaps during the Quaternary period. Correspondingly, from the distribution and the disruption of moraines presumed to be of Quaternary age, Armijo *et al.* (1986) inferred that the normal faulting in southern Tibet did not begin until Quaternary time. Unfortunately, however, as discussed by Smith & Xu (this volume), the ages of Tertiary and Quaternary rocks are not well constrained, so that precise dating of late Cenozoic folding and faulting is difficult. Nevertheless, taken together the evidence suggests that the initiation of the present style of deformation began relatively recently in geologic time.

An important goal of many geologists studying the late Cenozoic tectonics of Asia is the determination of how much Tibet has been extruded eastward out of the way of India's path toward the rest of Asia (e.g. Armijo *et al.* in press; Molnar & Deng 1984; Molnar & Tapponnier 1975; Tapponnier *et al.* 1982, 1986). Accordingly, we seek answers to: How much displacement has occurred on the strike-slip and normal faults? How far has Tibet slid eastward with respect to the Tarim Basin, and how much extension has occurred within Tibet? Related to these questions is: What is the average rate of slip on individual faults?

In the first attempt to address any of these questions with geologic data, Armijo *et al.* (1986) studied two of seven prominent graben systems in southern Tibet, and from their inferred rate of extension in one, the Yatung–Yangbajain–Gulu 'rift' (figure 1), they made a seven-fold extrapolation to estimate an overall rate of extension across the plateau of 10 ± 5 mm/a. Armijo *et al.* (in press) estimated rates of slip of 10 to 20 mm/a on short, WNW-trending right-lateral strike-slip faults that lie north of the rifts. Presuming these strike-slip faults to be linked to a major right-lateral shear zone in south central Tibet, they inferred a rapid eastward extrusion of Tibet at a rate of tens of mm/a. Despite the care with which their studies were made, however, much more field work will be needed before their extrapolated and inferred rates can be tested and before most of these questions can be given quantitatively meaningful answers.

It should be noted that the study of active and recent deformation was not one of the major objectives of the Academia Sinica/Royal Society Geotraverse, for there was rarely time to carry out the detailed investigations needed to make quantitative measurements of amounts, ages, or rates of deformation. Moreover, we were both familiar with the preliminary work on the active tectonics of southern Tibet (Tapponnier *et al.* 1981*a*, 1981*b*) and aware that Armijo *et al.* (1986, in press) had already carried out a more detailed study than we would be able to make in the portion of southern Tibet that we traversed. Thus, our focus was on the area north of where Armijo, Tapponnier and their colleagues had worked, and specifically on the Kunlun strike-slip fault system (figure 1), by far the most significant fault system that we crossed. Consequently we addressed, in essence, only one of the basic questions noted above; we sought constraints on the rates of slip on the two main segments of the Kunlun strike-slip fault system.

Although the bulk of this chapter addresses the evidence for Quaternary to recent activity on the Kunlun fault system, we report a few observations made in areas not studied by Armijo *et al.* (1986, in press) or Tapponnier *et al.* (1981*a*, 1981*b*). Before describing these, however, it is worth noting that in our brief reconnaissance of the Yangbajain–Gulu areas (figure 1), where we saw many of the spectacular examples of recent faulting described by Armijo *et al.* (1986), we saw no evidence of any process inconsistent with those inferred to have operated by Armijo *et al.* (1986, in press), from their more extensive observations.

Active faulting in the central part of the traverse

Armijo *et al.* (1986) described in detail a graben system that extends north from south of the Yarlung Zangbo through Yangbajain and Gulu and possibly northeast as far as the lake Tso Nag (figure 1). Tso Nag seems to lie in a northerly-trending graben or half-graben; a metric camera satellite photograph shows a clear scarp on its east side (A in figure 2). Northeast of Tso Nag, northeast-trending linear escarpments are also clear on the satellite photo (B and C

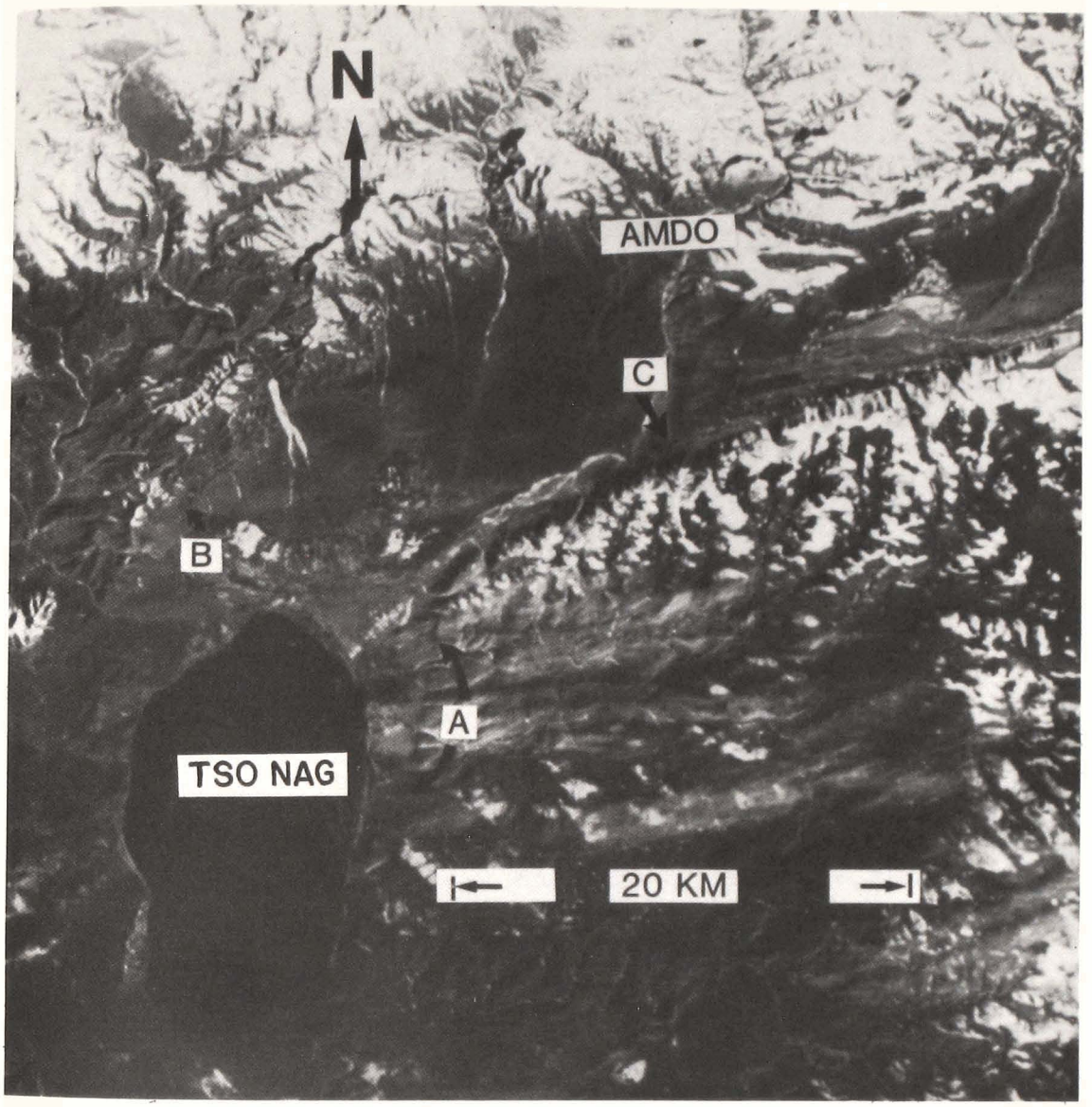

FIGURE 2. Portion of a shuttle metric camera photograph showing the area near Amdo and the lake Tso Nag (figure 1). Note the clear scarp on the east side of Tso Nag (A), which we presume to mark an active or recently active normal fault. To the northeast, the valley containing the town of Amdo is bounded by linear scarps, along which we think there is a large strike-slip component. At C, recent sand and gravel is disrupted (figure 3). At B, there is a component of thrust or reverse faulting, but the linearity of the scarp suggests that there is a significant strike-slip component.

(*Facing p.* 340)

FIGURE 3. Photograph, taken at C in figure 2, showing folded and faulted layers of sand and gravel along a zone where oblique normal and left-lateral strike-slip faulting seems to have occurred. The view is to the south.

FIGURE 4. Photograph of young scarp near hot springs on the west side of a graben (or half-graben) near Wenquan (figure 1). View is to the west-southwest.

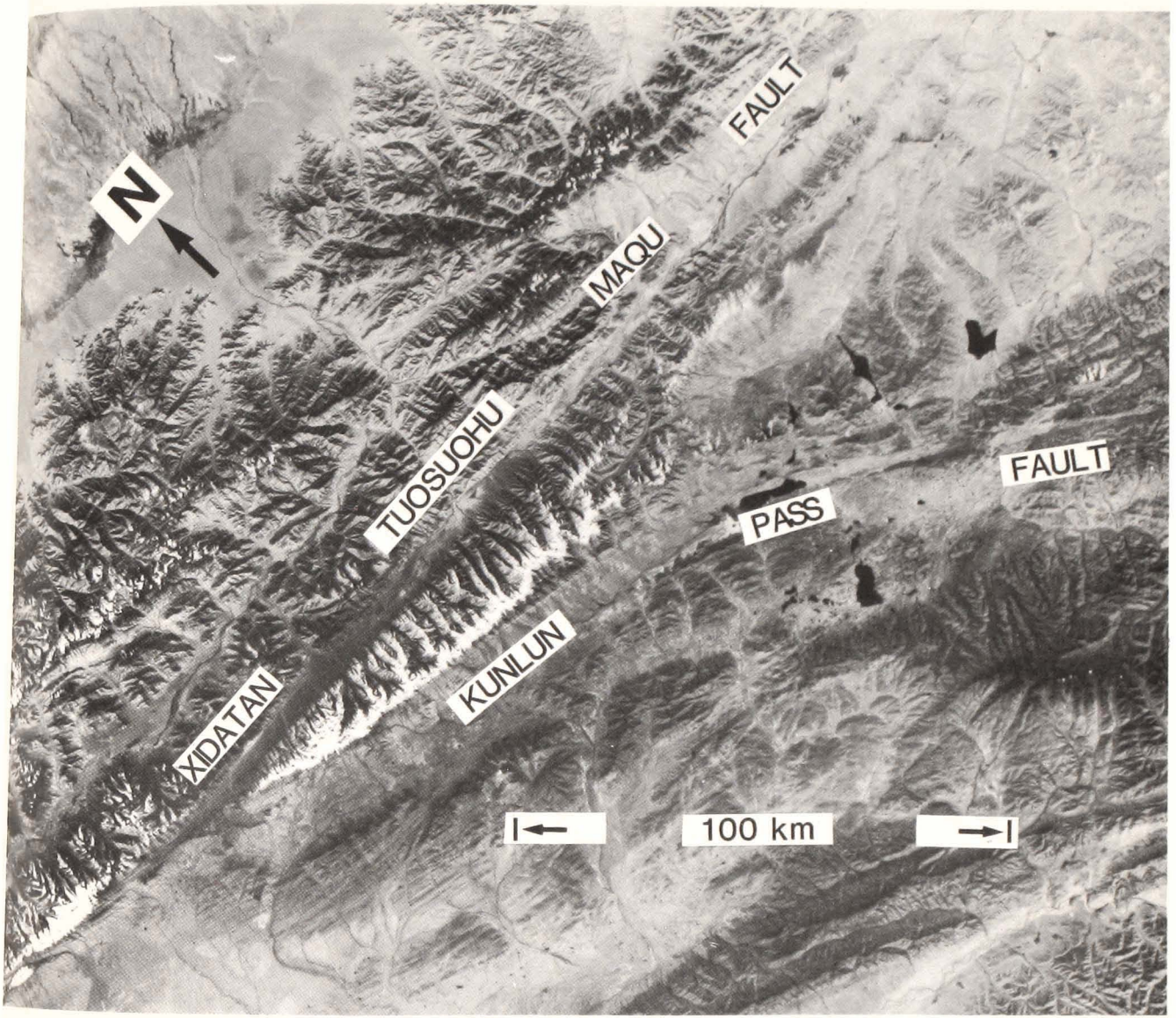

FIGURE 5. Large format camera photograph of the area including the Xidatan, Burhan Budai, and Kunlun Pass region. The Burhan Budai is the easterly-trending snow-capped range in the west-central part of the image between the Xidatan–Tuosuohu–Maqu and Kunlun Pass faults. The Xidatan–Tuosuohu–Maqu fault passes north of the Burhan Budai through the easterly-trending valleys, the Xidatan (figures 7 and 8) and Dongdatan (figures 23 and 31), and continues into a large pull-apart structure (figure 31). South of the Burhan Budai the Kunlun Pass fault is visible at the break in slope at the foot of the range (figure 14). Toward the west the Kunlun Pass fault approaches the Xidatan–Tuosuohu–Maqu fault but does not appear to intersect it (see figure 8).

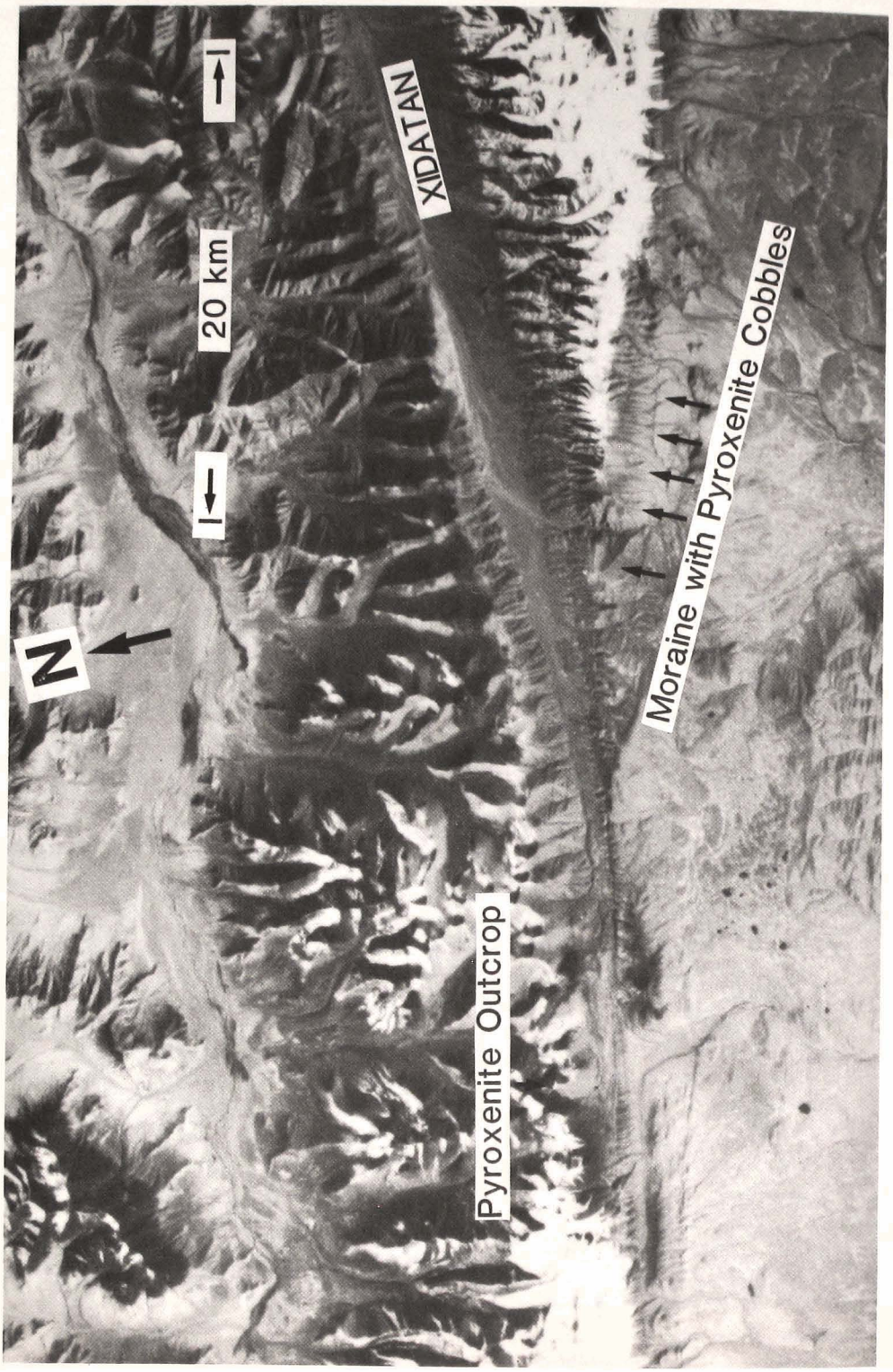

FIGURE 8. Large format camera photograph of the area where the Xidatan–Tuosuohu–Maqu and Kunlun Pass faults approach one another showing the locations of the outcrop of pyroxenite and the moraines containing pyroxenite cobbles.

in figure 2). They bound a northeast-trending valley, which appears to be a graben. Bedrock crops out in places in the valley, but most of its floor is covered by recent fluvial gravel, deposited by southwesterly-flowing rivers. Although there is an obvious vertical component of displacement on the edges of the valley, with the flanks of the valley standing several hundred metres above the valley floor, the relative importance of normal and strike-slip faulting cannot be evaluated easily from the satellite imagery. The fault plane solution of one earthquake, which occurred on 22 May 1971 east of Amdo (figure 1), indicates essentially pure strike-slip displacement with a left-lateral sense on the northeast-trending nodal plane (Molnar & Chen 1983).

We examined evidence for recent faulting at localities on both sides of this northeast-trending valley. On the south side of the valley, we saw no clear evidence of a recent fault scarp, but we examined only a short segment where the main road crosses the southern edge of the valley (C in figure 2). The unconsolidated cobbles and gravel exposed in the roadcut have been folded and thrust over one another (figure 3), similar to those observed in cross-sections across mole tracks and shutter ridges along the Xidatan–Tuosuohu–Maqu fault in the Kunlun, described below. Thus we infer that the deformation of these unconsolidated sediments is due to a large component of strike-slip, and not just normal, or reverse, faulting.

We examined the northern side of the valley near its western end (B in figure 2), where the north–south graben containing Tso Nag ends, and where Tertiary or Cretaceous redbeds crop out. In the mountains on the northern side of the valley, the redbeds dip steeply and are thrust southward over less consolidated conglomerates. Minor thrust faults are present in these poorly indurated sediments. In addition, the antecedent drainage of several rivers crossing this range and the incision of young alluvial fans on its south side suggest recent uplift of the range. Although we saw no clear recent scarp, the southern edge of the mountain range forms a relatively linear topographic front (B in figure 2), similar to but less impressive than that at the northern edge of the range on the south side of the valley. Moreover, an alignment of springs parallel to the front of the range suggests that a buried fault constitutes a groundwater barrier or a conduit for groundwater. These lines of evidence suggest that this deformation is very young.

The evidence for a component of thrust or reverse faulting is unequivocal, but we lack evidence constraining the proportion of strike-slip displacement. From the fault plane solution of the earthquake on 22 May 1971, from the linearity of the mountain front, and from small- and large-scale features seen in the range, we suspect that the strike-slip component is at least as large as the thrust component. In particular, small faults and slickensides almost subparallel to the southern margin commonly show a component of strike-slip displacement, dominantly of left-lateral sense. Also, the overall structure of the narrow range, with thrust faults dipping beneath both margins, is characteristic of compressional strike-slip zones ('flower structure').

North of the Tanggula, the pass where the road crosses from the province of Xizang to Qinghai, our route passed through a north–south valley a few km southwest of Wenquan (figure 1). At the southern end and on the west side of the part of the valley that we visited, hot springs emanate from an area with young, apparently Holocene, scarps with heights of several metres (figure 4). Beginning farther north on the west side of the valley, a recent scarp with about 1 m of displacement was clear along most of the part of the valley that we saw. The scarp is similar to, but smaller than, those on the west edges of the Gulu and Yangbajain grabens (see photos in Armijo *et al.* 1986 and Tapponnier *et al.* 1981*b*), and it probably reflects the

occurrence of an earthquake in the last few hundred years. In map view the scarp is not straight; it crosses small ridges and valleys on the east flank of the mountains that bound the valley in such a manner that if the fault is roughly planar, it dips eastward beneath the valley. Thus it is a normal fault, and the valley is a half-graben, or perhaps a graben, but we could see no evidence from the ground for young faulting on the east side of the valley.

This graben, north of the Tanggula, might be considered an extension of the Yangbajain–Gulu rift, mapped by Armijo *et al.* (1986). If the grabens are connected, however, the link between the northern end of the Yangbajain–Gulu system and the southern end of the Wenquan graben is not prominent on the satellite imagery of this regioin. Thus it seems possible that this graben, like most in northern Tibet, is more isolated from the others than the relatively continuous rift systems in southern Tibet.

We observed no other unequivocal evidence for recent faulting north of the Yangbajain graben and south of the Kunlun strike-slip fault system, over a distance of 250 km. A pair of nearly linear scarps in alluvial deposits can be seen on the Landsat imagery bounding a segment of the Tongtian River (a branch of the Jinsha or Yangtze) northeast of Wenquan, but we were unable to visit these scarps. The topographic maps show that their heights are about 10–20 m. They do not closely resemble the river terraces elsewhere along the river, and we suspect that they are young fault scarps. If so, they are the northernmost examples of normal faulting visible on the Landsat imagery near our route. Thus these features and the Wenquan graben mark a diminishing in importance of normal faulting northward.

South of Erdaogou, a prominent thrust fault (figure 1) was seen in outcrop carrying well-lithified Eocene red arenites southward over less consolidated marls and lake deposits of younger Tertiary age. Most of the displacement on this fault may be older than Quaternary, but some of it, at least, is probably very young. Southerly-flowing rivers from the interior of the Erdaogou ranges cut across the topographic barrier of the frontal range, and a small-scale incised meander was observed in a minor side stream in this frontal range, very close to the outcrop of the fault at the Lhasa–Golmud highway. The uplift implied by these drainage features is probably due to continued or renewed movement on the thrust fault. Moreover, obliquely-oriented slickensides in the Eocene arenites, like those in the redbed range near Amdo, indicate a component of strike-slip displacement.

This area and that near Amdo are among the few localities in the high plateau where a component of young reverse or thrust faulting can be reasonably inferred. Armijo *et al.* (in press) report another example several hundred km southwest, in clear association with strike-slip faulting. Although some workers might seize on these observations of reverse faulting as proof that crustal thickening is an important active process in Tibet, we consider it likely that the strike-slip components in these areas are comparable with the reverse components and unlikely that thrust faulting is widespread. Readers might recall that although the crust of the Basin and Range province in the western United States is undergoing horizontal extension by normal and strike-slip faulting, localized active thrust or reverse faulting also occurs within the province, such as at the east end of the Garlock strike-slip fault.

Major recent strike-slip faulting in the Kunlun

It is evident from the Landsat imagery and from satellite based photographs using the large format camera that, near the Lhasa–Golmud road, two major strike-slip faults, part of the Kunlun fault system, trend roughly east–west through the Kunlun Shan (figures 5, 9 and 10).

The northern of these faults, called the Xidatan fault by Chinese scientists, can be traced from several hundred km west of our traverse through the Xidatan ('western valley') and Dongdatan ('eastern valley'), where we worked extensively (figures 5, 9 and 10), and eastward several hundred kilometres through the lake Tuosuohu and the town of Maqu, where it is called the Maqu–Tuosuohu fault by Chinese scientists (e.g. Cui & Yang 1979; Li & Jia 1981) (figure 1). Left-lateral slip was inferred from adjacent structures seen on the Landsat imagery and from fault plane solutions of two earthquakes that occurred on it (Molnar & Tapponnier 1975; Tapponnier & Molnar 1977). One of those earthquakes, which occurred on 19 April 1963, was quite large: $M = 7.0$. Recent work by Cui & Yang (1979) showed numerous stream offsets and other features indicative of active left-lateral slip, and Li & Jia (1981) found a fresh rupture zone some 300 km in length with both vertical and left-lateral horizontal components of displacement reaching several metres near Maqu. Thus there is little doubt that the Xidatan–Tuosuohu–Maqu fault is a major, active, left-lateral strike-slip fault.

The second fault, the Kunlun Pass fault, is slightly oblique to the Xidatan–Tuosuohu–Maqu fault and follows the southern margin of the Burhan Budai mountains (figures 5, 6, 7, 8, 9 and 10). This fault can be traced on the satellite imagery east of the highway for about one hundred kilometres where it appears to curve southward (figures 5, 9, and 10) and where a component of thrust faulting should become increasingly significant. The average trend of the Kunlun Pass fault ($\approx 095°$) is slightly different from that ($\approx 090°$) of the Xidatan–Tuosuohu–Maqu fault. If projected west, the Kunlun Pass fault would intersect the Xidatan–Tuosuohu–Maqu fault just west of the west end of the Xidatan, approximately 25 km west of Kunlun Pass (figures 6 and 8). The fault trace disappears on both the Landsat imagery and the large format camera photos (figures 5 and 7) before intersecting the Xidatan–Tuosuohu–Maqu fault; it also proved impossible to trace the Kunlun Pass fault on the ground more than about 4 km west of the road.

The small- and large-scale geomorphology and the Quaternary offsets determined by us suggest that the Xidatan–Tuosuohu–Maqu fault is the major branch of the Kunlun fault system. The Kunlun Pass fault, while apparently having a substantial rate of movement in Holocene time, does not seem to have a large total offset. Landsat MSS images of the area crossed by the traverse and west of this area allow the main strand of the Kunlun fault to be followed as a clearly defined feature for 340 km west of the Xidatan, and it may continue as a less well defined array of splay faults, for about another 100 km to the southern margin of the Ayak Kum Köl basin. To the north of this main fault, another strand (not named) is almost as prominent on the Landsat images from 230 to 370 km west of the Kunlun Pass (figures 9 and 10), well to the west of the traverse line.

On the satellite imagery, this unnamed strand forms part of a zone of otherwise less continuous and/or oblique fault segments and splays and other linear features (figures 9 and 10). The discontinuous nature of this fault zone suggests that the overall displacement on it is small, at least compared with that on the main Xidatan–Tuosuohu–Maqu fault. It is likely, however, that there is some young displacement on these discontinuous faults and splays. Note that this zone lies west of the area where the main Xidatan–Tuosuohu–Maqu fault is transposed through a series of pull-apart basins and west of where the main fault undergoes a regional change in trend (figures 9 and 10). Thus it appears that this zone may have absorbed part of the slip on the eastern segment of the Xidatan–Tuosuohu–Maqu fault, and may continue to do so at the present time.

The traverse route approaches or crosses a few of these discontinuous faults and linear

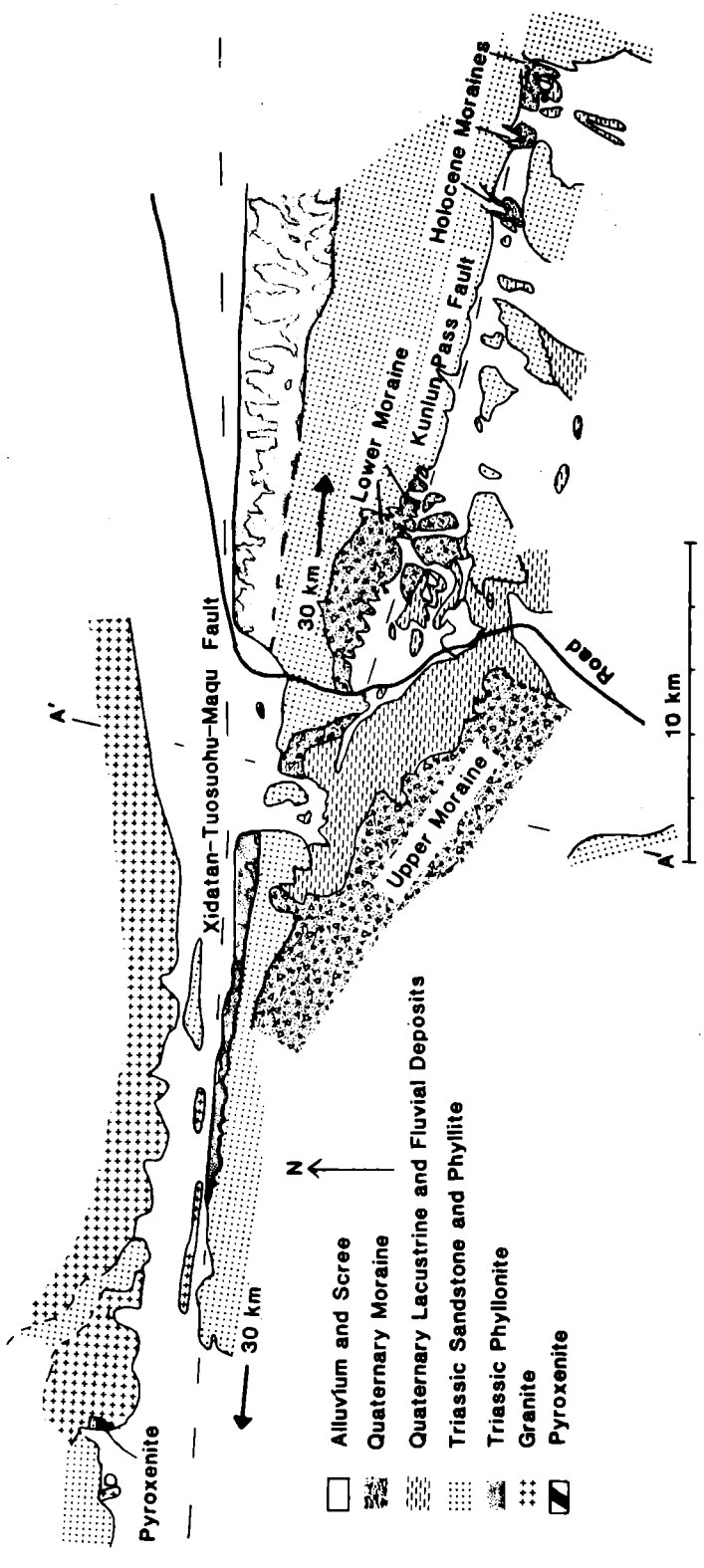

FIGURE 6. Geologic Map of Xidatan, Burhan Budai and Kunlun Pass region. The Burhan Budai consists mostly of Triassic sandstone, phyllite, and phyllonite, but on the ridge north of the Xidatan, granite crops out widely. South and west of the Burhan Budai a sequence of lacustrine deposits overlies alluvial deposits, which in turn overlie an older, lower moraine. This sequence is capped by a second, younger moraine. The lower, older moraine contains boulders of Triassic sandstone and phyllite, hornblende granite, gabbro, and pyroxenite. Pyroxenite was found in outcrop only to the west of the Xidatan, north of the fault. The distance between this outcrop and the easternmost exposure of moraine containing cobbles of pyroxenite is 30 km.

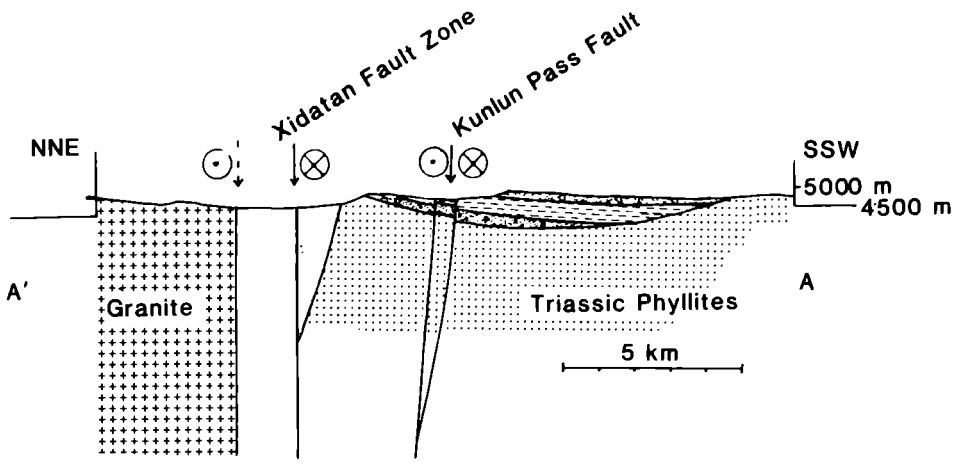

FIGURE 7. Geologic cross section across the Xidatan and lake beds just west of the Kunlun Pass, showing the two main strike-slip faults, the belt of phyllonite, and the lake beds. The extrapolation of rock units at depth is, of course, only tentative, and below the Xidatan no extrapolation of recent alluvial deposits was made. Symbols and location are those shown in figure 6.

features. In particular, the so-called North Kunlun faults (figures 9, 10 and 11), which separate the less deformed Carboniferous and volcanic rocks, lacking a cleavage, from strongly cleaved Ordovician and Permo-Triassic rocks to the south, appear to be part of this zone (see Coward *et al.*, this volume and Kidd *et al.*, this volume). The sense and amount of displacement along this contact zone is unknown, but from the observations noted above, it is possible that some displacement might be young and connected with the overall Kunlun fault system. The lack of prominent geomorphologic expression of the fault trace seen on the ground near the traverse suggests that any young displacement is likely to be small (not more than a few kilometres).

Our work focused on quantifying the rate of slip on the Xidatan–Tuosuohu–Maqu and Kunlun Pass faults and to a lesser extent on placing bounds on when the faults became active and on how recently slip might have occurred. Both because of its greater significance and its greater accessibility, the Xidatan–Tuosuohu–Maqu fault received more of our attention. We obtained an approximate average rate of slip for the Quaternary period and impressions both of when the last major earthquake occurred and how much slip can be associated with it. For the Kunlun Pass fault, we estimated an average slip-rate for Holocene time and a possible bound for the date of initiation of slip. We first discuss constraints on the displacement during Quaternary time and the age of initiation of the faults. Next we discuss Holocene displacements and average rates for the last 10,000 years, and then the evidence for recent offsets.

Quaternary offset and average slip-rate on the Xidatan–Tuosuohu–Maqu fault

As was described by Kidd *et al.*, this volume, and Smith & Xu, this volume, a relatively thick sequence of Quaternary deposits can be seen in the area around the Kunlun Pass and on the south slope of the Burhan Budai mountains (figures 6, 7, and 8). The oldest of these deposits appear to be ground moraine–unsorted, angular fragments, from sand-size to boulders, of Triassic sandstone and phyllite, granite, hornblende gabbro, and pyroxenite. These deposits seem to lie directly on green Triassic sandstone and phyllite. Overlying the moraine is alluvial gravel, in which an imbrication of pebbles implies a southerly direction of flow. This gravel, in turn, is overlain by fine sand, silt and clay deposited in a lake and by interbedded alluvial

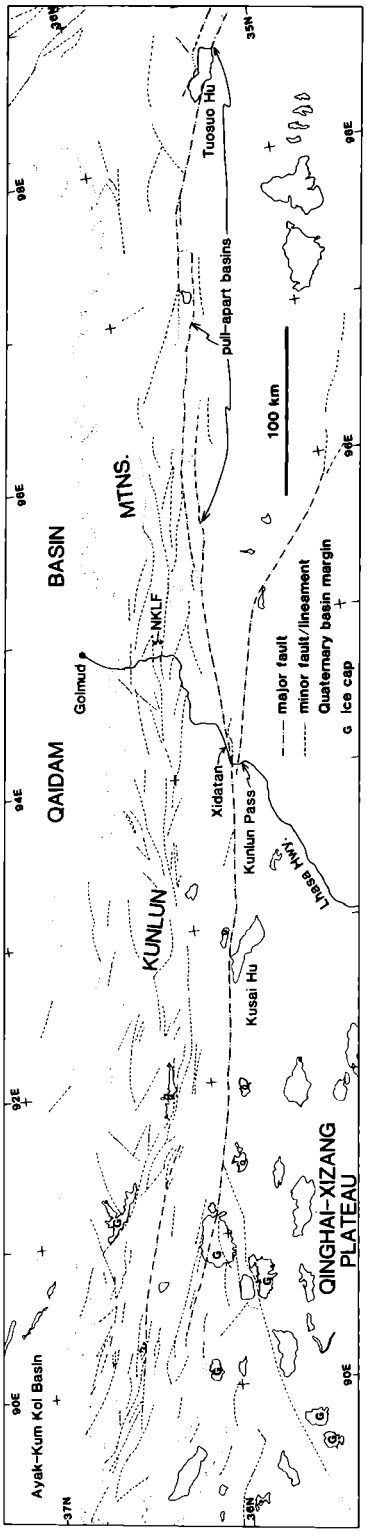

FIGURE 9. Sketch map of the western part of the Kunlun fault system with the main and subsidiary fault strands identified from satellite imagery. The 'North Kunlun Faults' (NKLF) appear to be subsidiary faults. See text for details.

FIGURE 10. Mosaic of three Landsat images covering a portion of the western reaches of the Kunlun fault system. The main Xidatan–Tuosuohu–Maqu fault extends from about 90.5° E to 95° E on this mosaic. The traverse line crosses this fault in the Xidatan, near Kunlun Pass (see figure 9 to locate the mosaic). The minor faults and linear features identified in the area of the mosaic are indicated on figure 9. Locations of possible offset continuations of the phyllonite unit identified on these images are shown on figure 11.

(*Facing p.* 346)

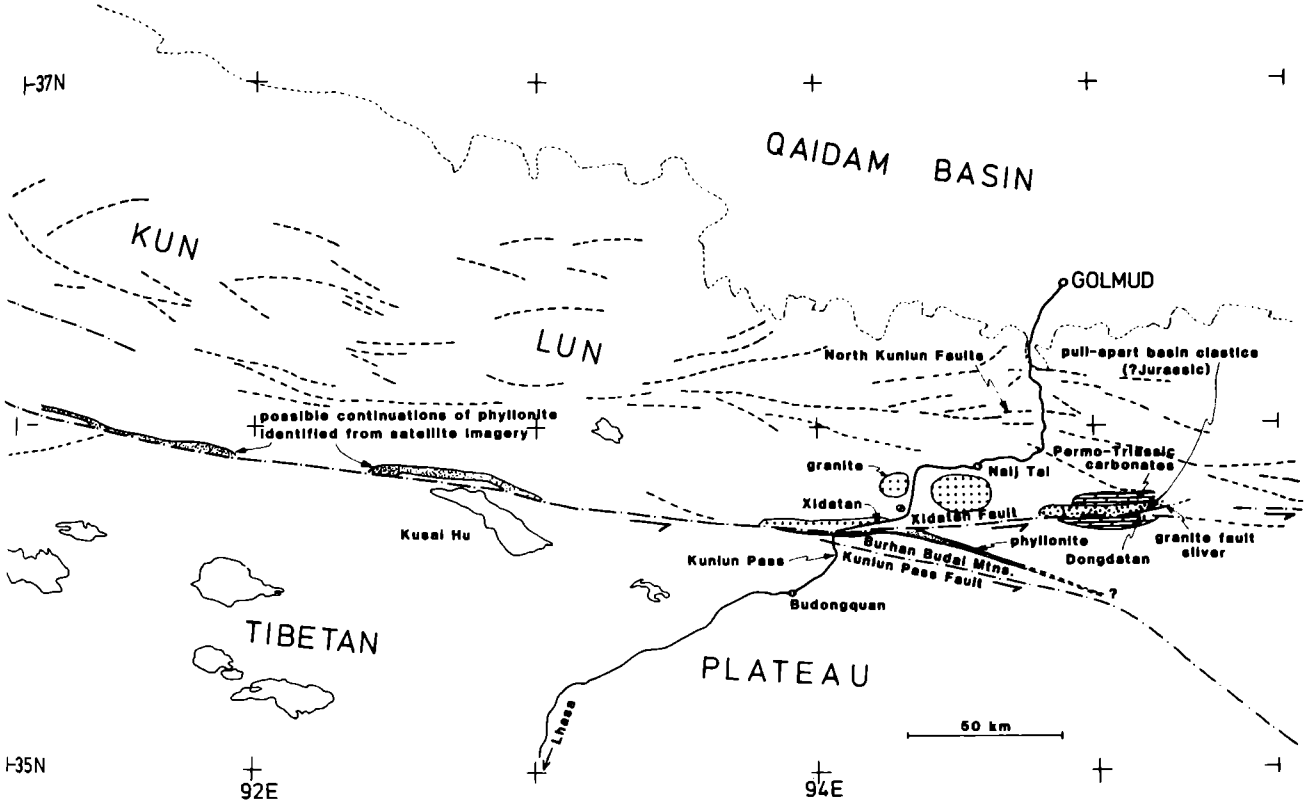

FIGURE 11. Sketch map of a portion of the Kunlun fault system showing possible offset segments of the phyllonite unit that is seen truncated just west of the Kunlun Pass region. The Dongdatan pull-apart sequence (?Jurassic) is shown together with known areas of granite and carbonate rocks adjacent to the Xidatan–Tuosuohu–Maqu fault.

sand. This relatively thick sequence, 100–200 m, is overlain by ground moraine consisting largely of blocks of Triassic(?) sandstone and phyllite with some granite clasts. The entire sequence dips roughly south at 10° to 15° (figure 7).

We, like Wu *et al.* (1982), infer a southward flow of the glaciers that deposited both moraines. This inference derives principally from the imbrication of the pebbles in the intervening layer of alluvial gravel. In addition, however, we saw no granite outcrops in this area except north of the Xidatan, implying that the blocks of granite in the moraines were derived from the north.

As Wu *et al.* (1982) pointed out, a northern source requires that the Xidatan, a valley more than 1000 m deep (figure 6), be younger than the moraines, which are perched on the surrounding mountains. The linear configuration of the Xidatan, parallel to the Xidatan–Tuosuohu–Maqu fault, suggests that its existence is due to slip on that fault, possibly with a small component of extension across it. Although valley glaciers with terminal moraines are present in the valleys high in the Burhan Budai, no clear moraines were seen within the Xidatan. Moreover, hanging valleys, typical of the sides of deep glacially eroded valleys, also were not seen along the Xidatan. Thus we infer that the Xidatan did not form by glacial erosion. Wu *et al.* (1982) inferred that slip on the fault began after the lake beds and the moraine covering them were deposited, an inference with which we do not concur; nevertheless, the formation of the valley probably is quite young (latest Pliocene at the oldest).

Most of the boulders in the older moraine, and all of those in the younger moraine, could have been derived from nearby sources. Triassic green sandstone and phyllite abound throughout the Burhan Budai, and granite crops out widely along the northern edge of the Xidatan. Finding gabbro and especially pyroxenite in the older moraine, however, was a surprise, and with left-lateral strike-slip faulting in mind, we sought a source west of the moraine in which boulders of them had been found. Both gabbro and pyroxenite were found cropping out only in a small area adjacent to Triassic schist at the western end of the granite, which borders the Xidatan (figure 6), as Wu *et al.* (1982) had already found, unbeknownst to us at that time. We infer that the boulders in the moraine near the Kunlun Pass were derived from this small outcrop (or, if not, from another source farther west, too far for us to visit). The distance from this outcrop to the eastern end of the moraine where pyroxenite boulders are present is about 30 km. Thus, 30 km (or more) of left-lateral slip seems to have occurred since the moraine was deposited.

We cannot eliminate completely the possibility that a glacier flowed east from the pyroxenite outcrop to the moraine, but we doubt this strongly. First, we did not see the moraine farther west than that shown on the map (figure 6) and therefore closer than 20 km to the pyroxenite outcrop. Second, the imbrication in the pebbles directly overlying the lower moraine indicates a direction of transport toward the south, not the east. Third, the lack of evidence for glaciation within the Xidatan is consistent with that valley being formed by tectonic, and not by glacial, processes. Thus, although none of these arguments proves that the glaciers that deposited the pyroxenite flowed south a few kilometres instead of east many tens of kilometres, we consider this latter possibility very unlikely.

The age of the older moraine is probably not older than late Pliocene, or approximately 2.4 Ma, when ice-rafted material was first deposited in abundance in the Atlantic Ocean (Shackleton *et al.* 1984) and when glaciation first became widespread in Europe and North America (e.g. Holmes 1965). Qian *et al.* (1982) investigated the magnetostratigraphy of the lake bed sequence and inferred an extrapolated age for the older moraine of 2.8 Ma. The sparse sampling in the lake beds and the imperfect correlation of reversals with the geomagnetic reversal time scale make their inferred ages quite uncertain, and it seems remotely possible to us that the age of the older moraine is as young as 1.5 Ma. Thus we conclude that average rate of slip during the Quaternary period has been at least 10 mm/a, probably closer to 13 mm/a if the age of the moraine is 2.4 Ma, and possibly as much as 20 mm/a.

Total offset and age of displacement on the Xidatan–Tuosuohu–Maqu fault

A large-scale, low-angle truncation of a thick phyllonite unit (discussed by Kidd *et al.*, this volume) was observed on the south side of the Xidatan–Tuosuohu–Maqu fault 20 km WNW of the Kunlun Pass (figures 6, 11, and 12). The phyllonite, because of its prominent phyllitic muscovite foliation, is a very distinctive lithologic unit, and, when seen at a distance in the field, contrasts strongly with adjacent green phyllitic Triassic arenites and slates. This contrast is also clearly distinguishable on the unenhanced Landsat MSS image of the area. The bluish-white tone of the phyllonite unit on the image is also distinct from both of the other light-toned rock units in the vicinity, and in particular from the pinkish-tan tone of granitic rocks, which occur along the western part of the north side of the Xidatan, as well as from the tan tone of Permo-Triassic carbonates seen on the north and south sides of the Dongdatan (figure 11).

Given that substantial left-lateral slip has occurred across the Kunlun fault system, the offset

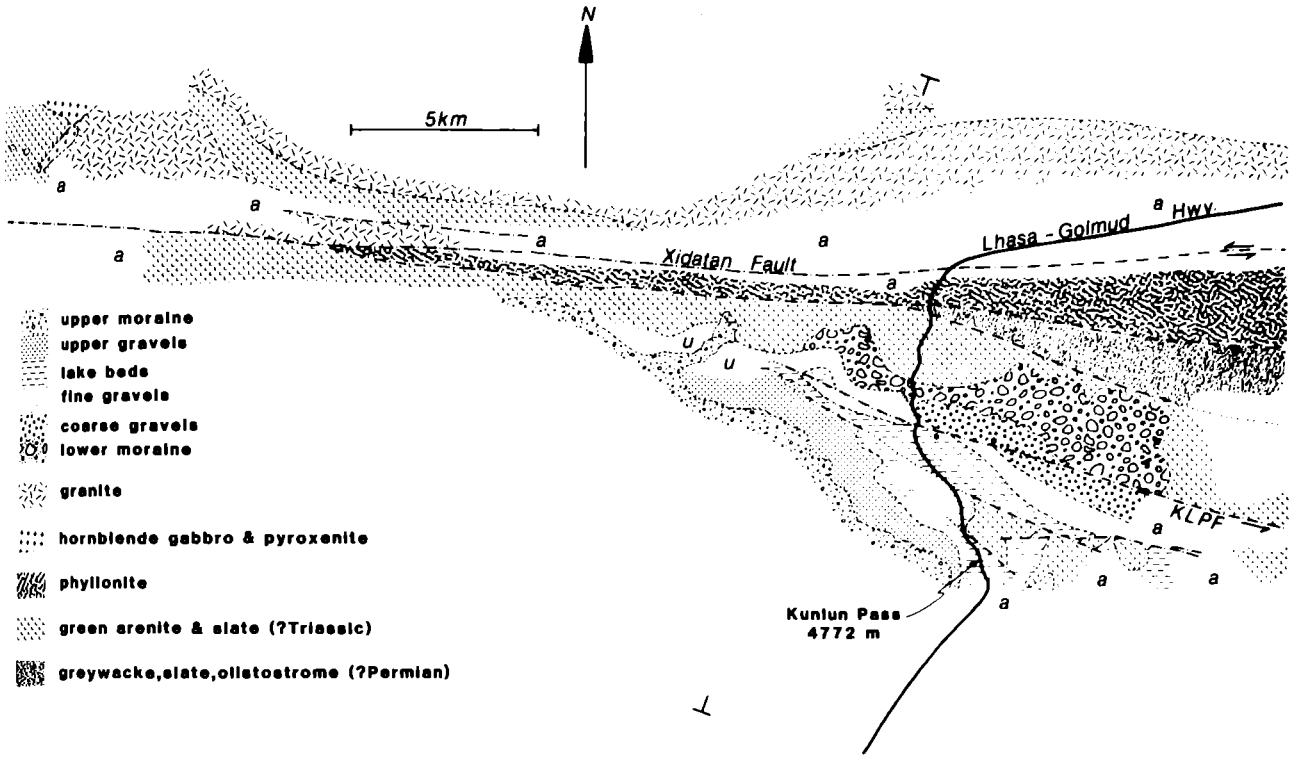

FIGURE 12. Geological map of bedrock in the Kunlun Pass region, showing the possible total offset on the Kunlun Pass fault (KLPF); the contact of lower coarse and fine gravel units is truncated by the fault at points marked with asterisks. Ends of the cross section (figure 7) are marked by Ts; u – undifferentiated Pleistocene sequence; a – Alluvium; blank – unmapped; dash-dot lines – faults, dotted where uncertain or imprecisely located.

continuation of the phyllonite should be found west of the Kunlun Pass region, on the north side of the fault. On the Landsat images, a pale unit, which more closely resembles the phyllonite in tone that it does known granite or limestone, is first seen on the north side of the main strand of the Kunlun fault system (Xidatan–Tuosuohu–Maqu fault) 75 km west of the truncation of the phyllonite observed in the field (figure 11). If this pale unit is the phyllonite, and not limestone or marble, then the minimum total offset of the main (Xidatan) strand of the Kunlun fault system is 75 km. At the rates of displacement deduced by us from Quaternary offsets, this total displacement would have accumulated in no more than about 7 Ma.

The total offset could be more, perhaps by a substantial amount, than the 75 km deduced above. First, south of the Xidatan, the southern side of the phyllonite is in sharp, subvertical fault contact, involving brittle deformation, with either the green Triassic arenites and phyllitic slates or with a sliver of Permian(?) greywackes, slates, and local olistostromes. This fault is also a sinistral strike-slip structure presumed to be related to the present Kunlun fault system, but not a currently active strand and with an unknown total displacement.

Second, the proposed offset continuation of the phyllonite seen on the images is truncated against the north side of the main Kunlun fault strand in three places, not just one (figure 11), making it less certain which should be matched with the truncation on the south side. Given the uncertainties, we suggest that the 75 km offset may be only a minimum total offset for the main strand (Xidatan–Tuosuohu–Maqu fault) of the Kunlun fault system.

In the Dongdatan, a sequence of arenaceous clastics, locally red and including minor coal beds, lies in a narrow, largely fault-bounded belt adjacent to and parallel with the north side of the present fault valley. This well-lithified sequence (not directly dated) lies unconformably on the Permo-Triassic carbonates adjacent to it. Although it is moderately folded, it must have been deposited after the main folding and foliation of the carbonates, an event that we think occurred in late Triassic to mid-Jurassic time. The present geometry, facies, and structural relationships of this sequence suggest that it represents a deformed pull-apart basin on a strike-slip fault. While it could be relatively young (Miocene, for example), it could alternatively be as old as Jurassic; coal containing a possibly Mesozoic plant fossil (Smith & Xu, this volume) occurs in a minuscule fault sliver adjoining the phyllonite on the south side of the Xidatan (figure 11) and perhaps came from this or a related basin. The significance of this sequence of rocks is that it suggests that some of the displacement on the Kunlun fault system could be relatively old (Mesozoic) and unrelated to the present tectonics. The overall geometry of this possible pull-apart structure suggests that the sense of displacement was left-lateral, but confirming evidence for this was not seen in the rocks from that pull-apart basin.

The deformation implied by a prominent change in the orientation of the ductile stretching lineation (Coward *et al.*, this volume), as one approaches the Xidatan from the north along the main Golmud–Llasa highway, does suggest Jurassic strike-slip displacement along the zone now occupied by the Xidatan–Tuosuohu–Maqu fault. North of the present fault valley, the lineation plunges steeply; coming towards the Xidatan, it progressively changes, over a distance of about 2 km, to a sub-horizontal attitude, and the nature of the change implies left-lateral offset. This deformation, unlike the other evidence for strike-slip faulting discussed above, involved ductile strain at depths of at least several kilometres; nevertheless, any offsets of lithic units produced by it will contribute to the total offset and complicate the determination of the offset resulting from the collision of India with Asia.

The southern margin of this probable pull-apart basin sequence, which forms the northern edge of the Dongdatan Valley, has a sliver of chloritised and densely fractured granitic rock faulted against it (figure 11). While no feature was seen in this badly altered rock to connect it conclusively with other granitoid rocks observed to the west, the nearest outcrop of granitic rock that is immediately adjacent to the Xidatan–Tuosuohu–Maqu fault is about 90 km to the west in the Xidatan. At present, we do not attach much significance to this possible offset because the rocks need not be from the same body. If it is a real offset, however, this distance is not likely to be a total offset because both occurrences are on the north side of the main (Xidatan–Tuosuohu–Maqu) fault strand.

Holocene slip on the Kunlun Pass fault

As described above, the Kunlun strike-slip fault system consists of two strands. The Xidatan–Tuosuohu–Maqu fault is the major one of the two. The Kunlun Pass fault lies south of it and strikes at an acute angle to it, and they approach one another just west of the Kunlun Pass (figures 5, 6, 12, and 13). We studied a segment of the Kunlun Pass fault extending east from the main road for about 25 km. West of the road this fault was not very clear, and we could not trace it with confidence. Thus we gained little insight into how the two faults intersect, or interact.

The Kunlun Pass fault is very clearly defined both on the satellite imagery (figures 5 and 14) and on the contour maps provided to us (figures 6 and 13). It follows the foot of the Burhan

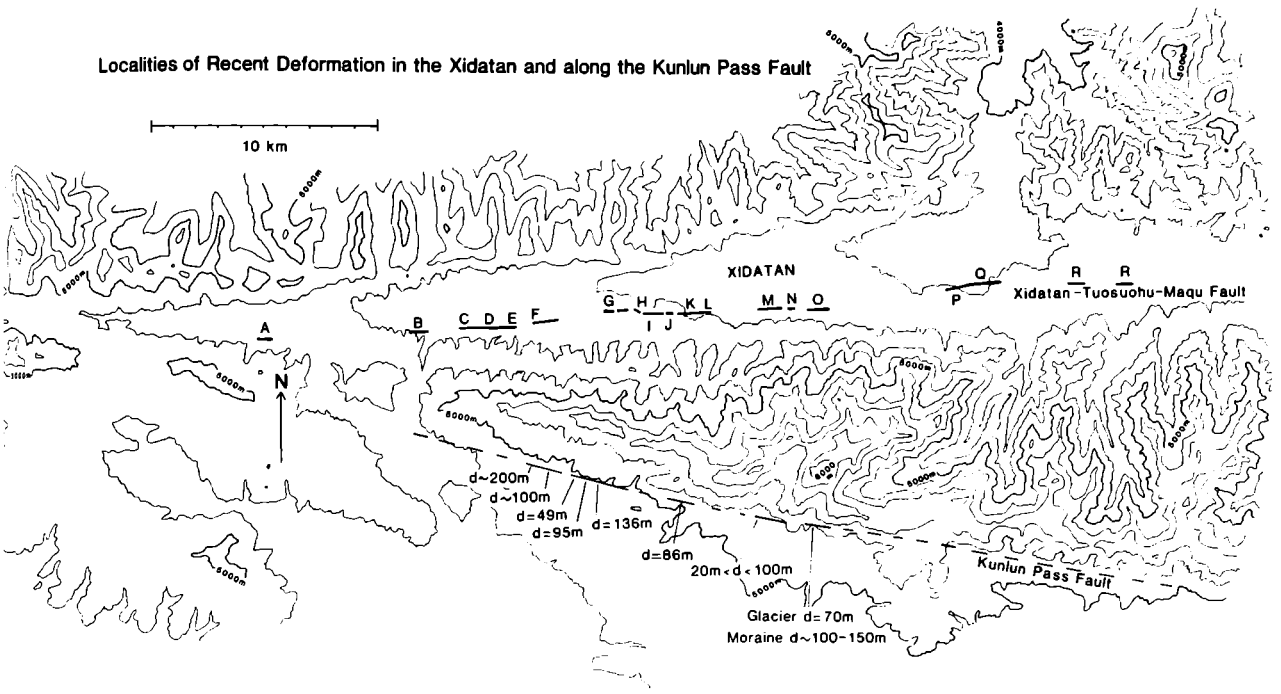

FIGURE 13. Map showing localities of clear offsets (d) on the Kunlun Pass fault (see also table 1) and areas of disruption along the Xidatan–Tuosuohu–Maqu fault in the Xidatan. Letters indicate areas discussed in the text.

Budai mountains on their southern side at the break in slope. The fault is also very clear from the ground, for it displaces most small streams that cross the fault (figures 15 and 16). We did not see, however, features clearly offset only a few metres by slip on the fault or other evidence of recent deformation, such as tension gashes or mole tracks, that might be associated with a recent moderate or large earthquake.

The offset streams demonstrate clear left-lateral slip, which probably has occurred during Holocene time, or at least since the last glaciation. Virtually all streams with length of 1 km or more are displaced. The measured amounts of displacement vary from 49 m to 135 m and possibly to 200 m. In some cases it is difficult to distinguish offset due to faulting from other bends in streams or possible stream capture. In such cases we include large uncertainties in our estimates of the offsets. In other cases, V-shaped valleys are clearly displaced as the streams debouch onto their alluvial fans south of the fault (figures 15 and 16).

The amount of offset is clearly larger for longer streams and for deeper valleys. In all but one case we measured offsets using a tape measure. In that one exception we paced the offset. There was insufficient time to make detailed contour maps. Using the topographic maps we measured the lengths (l) of the V-shaped valleys of the streams with clear offsets and their maximum widths (w) and depths (h), where the streams reached the fault. These quantities, plus estimates of the volume of material eroded ($V \approx 1/6\, l \cdot w \cdot h$) and of the area of the drainage basin ($A \approx 1/2\, l \cdot w$), are listed with the measured offsets in table 1. The locations of the streams are identified on figure 13 by the measured offsets.

The volume of the material eroded divided by the area of the drainage basin ($V/A \approx 1/3\, h$) equals the product of the average erosion rate and the duration of incision. Thus, if both the

TABLE 1. OFFSETS AND DIMENSIONS OF VALLEYS BY THE KUNLUN PASS FAULT

offset/m	maximum depth/m	maximum width/m	length/m	volume/m^3	area of drainage basin/m^2
136 ± 10	120	400	1200	9.6×10^6	2.4×10^5
95 ± 6	100	400	900	6.0×10^6	1.8×10^5
49 ± 4	50	400	600	2.0×10^6	1.2×10^5
86 ± 10	80	600	800	6.4×10^6	2.4×10^5
100^{+100}_{-50}	60	500	1800	9.0×10^6	4.5×10^5
200 ± 50	40	300	1000	2.0×10^6	1.5×10^5

erosion rate and the slip rate were constant when averaged over periods of a thousand years or so, then the amounts of offset should be proportional to the depths of the valleys. A plot of V/A vs. d (displacement) does yield a linear relationship if one ignores one offset of dubious certainty (figure 17). The inferred slip rate would be 3.2 times the erosion rate. Thus, an estimate for the erosion rate would yield an estimate of the slip rate, or conversely a slip rate of 10 mm/a would imply denudation at 3 mm/a.

We are not aware of any attempts to estimate erosion rates in northern Tibet, to say nothing of the small drainage basins in the Burhan Budai. Nevertheless, a rate of 3 mm/a seems reasonable to us in the climatic conditions at an elevation of 5000 m for erosion of relatively thinly bedded sandstone and phyllite in small, steep drainage basins. Plots of denudation rates vs. the areas of drainage basins in the midwestern United States (Brune 1948) indicate an overall tendency for the rates to decrease proportionally to the 0.15 power of the area (Langbein & Schumm 1958). Schumm (1963) concluded that the mean denudation rate for a basin of about 3800 km^2 (1500 sq. mi.) is about 1 mm/a. An extrapolation of this to basins with areas of 0.1 to 0.4 km^2 yields denudation rates of 4.0 to 4.9 mm/a. Although this extrapolation for different climatic conditions and different rock types cannot be used to predict accurate denudation rates, it does indicate that erosion rates of a few mm/a are not unreasonable.

We cannot determine accurate ages of these valleys or the rate of slip, but three observations suggest a Holocene age and hence a slip-rate of about 10 mm/a. First, the valleys are more nearly V-shaped than U-shaped in cross section (figures 15 and 16), and therefore they do not appear to be glacial in origin. Second, there are no terminal moraines in front of these small streams. The existence of active glaciers in neighbouring valleys, however, makes it virtually certain that there was glaciation in the Burhan Budai and probably a glacial maximum in the last 18,000 years, as there was elsewhere in the world. Thus these valleys are probably post-glacial in age. Third, at present one glacier crosses the fault, and indeed the eastern edge of that south-flowing glacier is offset 70 m left-laterally (figures 14 and 18). The glacier is receding, and much of its terminal and lateral moraines are preserved. The eastern edges of these moraines lie 100 to 150 m east of the eastern edge of the glacial valley north of the fault and through which the ice flows. The age of this moraine is probably also Holocene or very late Pleistocene (less than 18,000 years).

The assignment of a Holocene age to features displaced approximately 100 m yields an average slip rate of about 10 mm/a. Clearly this estimate is quite uncertain, and a range from 5 to 20 mm/a is probably allowed by the varying amounts of offset and the uncertainty in the ages for when incision began. Nevertheless, it is important to note that the average Holocene slip rate on the secondary fault in the Kunlun fault system is at least several mm/a. Clearly this fault also is a major one.

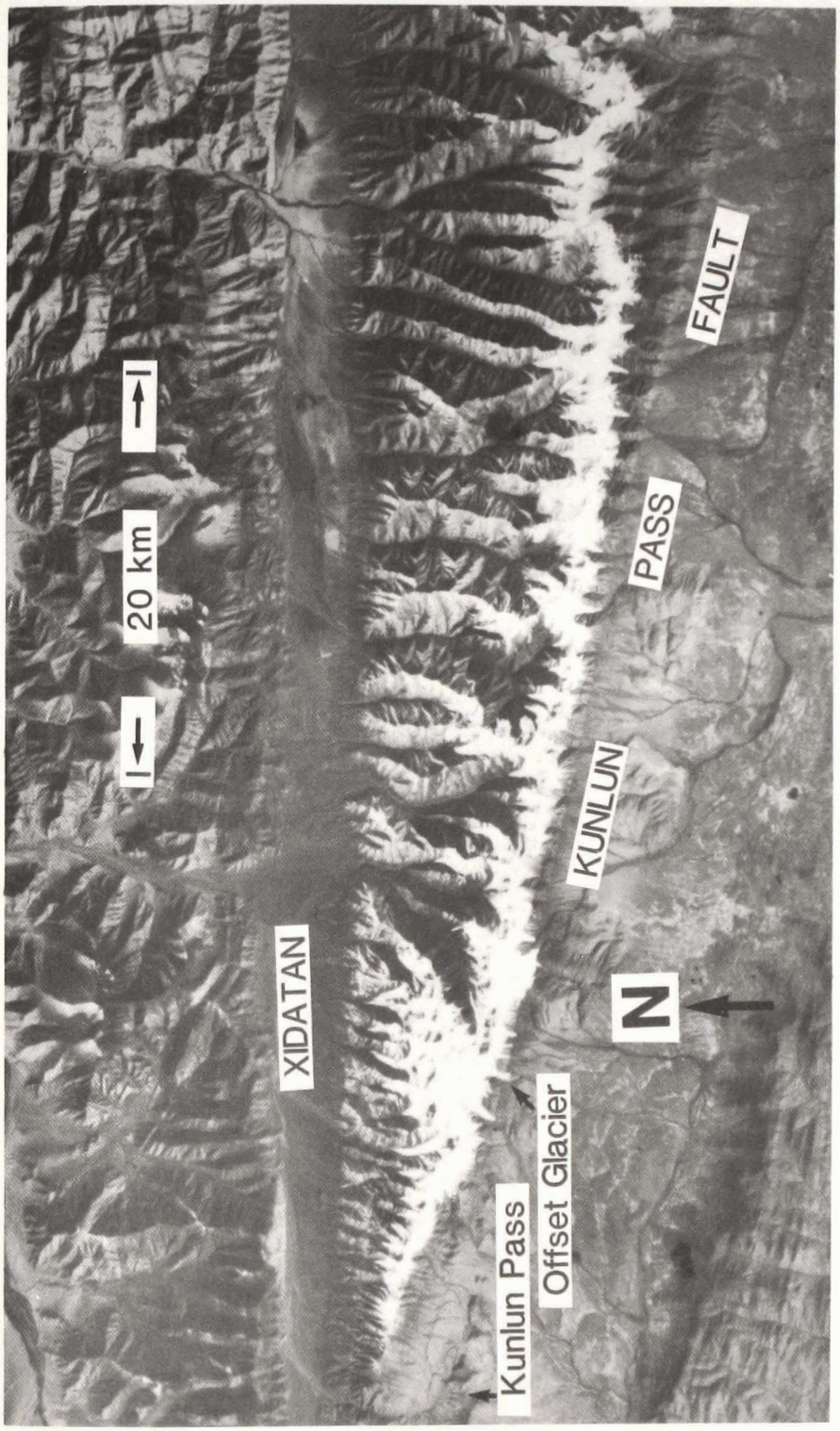

FIGURE 14. Large format camera photograph of the Kunlun Pass fault, showing the clear topographic expression of the fault and the location of the offset glacier (figure 18).

(Facing p. 352)

FIGURE 15. Photo looking north at an offset stream along the Kunlun Pass fault. The stream in the valley in the centre of the photo flows toward the photographer, but at the foot of the nearer hills it is displaced to the right (east) 49 ± 4 m.

FIGURE 16. Photo looking north at a second offset stream along the Kunlun Pass fault. The valley in the centre of the photo is the same one shown on the right edge of the photo in figure 15. Again the stream flows directly toward the photographer but is offset at the Kunlun Pass fault, at the foot of the hills. The amount of offset is 95 ± 6 m.

FIGURE 18. Photo looking north at a major glacier flowing south from the highest peak in the Burhan Budai. Where the glacier reaches the Kunlun Pass fault at the foot of the mountains, it is offset about 70 m (see also figure 14). The terminal moraine of the receding glacier is offset between 100 and 150 m. Since this moraine probably was left by the last glaciation some 10 ka to 18 ka, the average rate of slip during Holocene time probably has been about 10 mm/a.

FIGURE 19. Photo looking west along the Xidatan–Tuosuohu–Maqu fault in its western segment near D in figure 13. The dark linear zone in the middle foreground is a tension gash obliquely crossing a shutter ridge that recedes from the photographer. Sag ponds farther in the distance have formed by segments of shutter ridges blocking the northerly-flowing streams.

FIGURE 20. Photo (taken with a lens with a focal length of 135 mm) looking west along the Xidatan–Tuosuohu–Maqu fault from a hill near the locality I in figure 13. Streams in the foreground and the middle of the photo have obliterated evidence of surface faulting. Between the streams a small man-made hill lies within a zone of large tension gashes that trend northeast–southwest (see figure 21). In the distance, the fault has formed a ground-water barrier that is manifested by dark areas of more lush vegetation than on the neighbouring alluvial fans.

FIGURE 21. Photo taken from the man-made hill shown in figure 20 and looking east along the Xidatan–Tuosuohu–Maqu fault (J in figure 13). Doyle Watts is shown standing in a large tension gash, which trends northeast–southwest. The depth is nearly 2 m. As in figure 20, the fault is defined clearly by the darker vegetation growing on and adjacent to it in the distance.

FIGURE 24. Photo looking north-northwest at a small offset of a small stream gully. The gully entering the photo on the left trends north and is offset about 10 ± 2 m before reaching a wide braided stream. This locality is labelled V in figure 23.

FIGURE 25. Photo looking east along the Xidatan–Tuosuohu–Maqu fault and showing sag ponds and a shutter ridge in the Dongdatan (W in figure 23). Drainage from the south (right) is blocked by the shutter ridge that recedes from the left lower edge of the photo across and away to the middle of the photo. A dry sag pond in the middle of the photo is about 20 m wide. The height of the shutter ridge is as much as 5 m higher than the dry bottom of the sag pond.

FIGURE 26. Photo looking southwest toward a huge tension gash within a high shutter ridge in the Dongdatan (W in figure 23). Michael Ward, standing in the tension gash, stands about 180 cm tall.

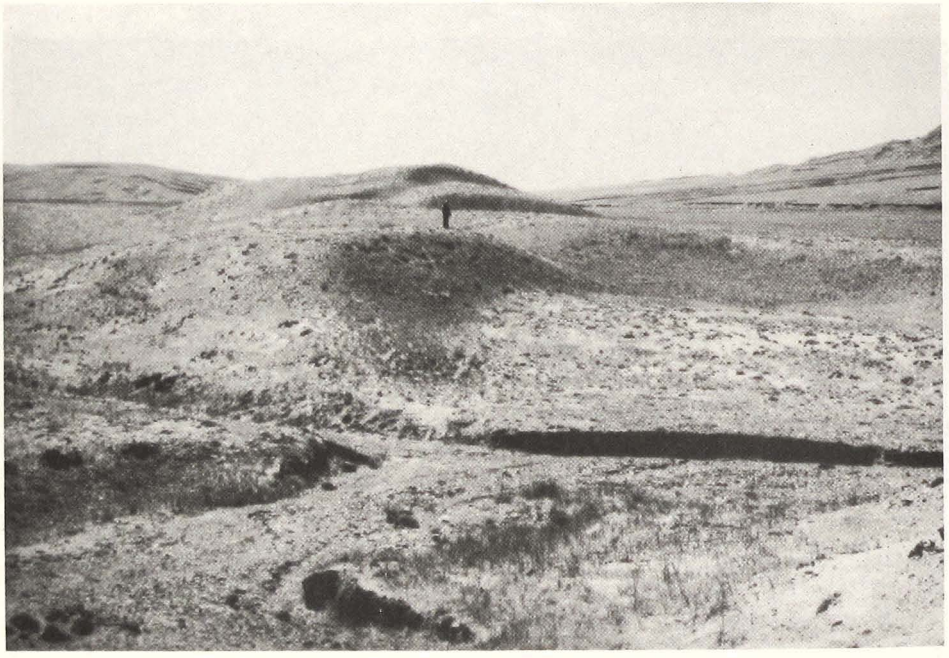

FIGURE 27. Photo looking west along the shutter ridge and the escarpment where the contour map in figure 28 was made. Two north-flowing streams join in the foreground where they cross the fault. Bill Kidd stands just south of (to the left of) a large area in which stream cobbles are exposed in groups. These cobbles apparently were deposited by the stream in the foreground when the flat area once lay closer to the photographer.

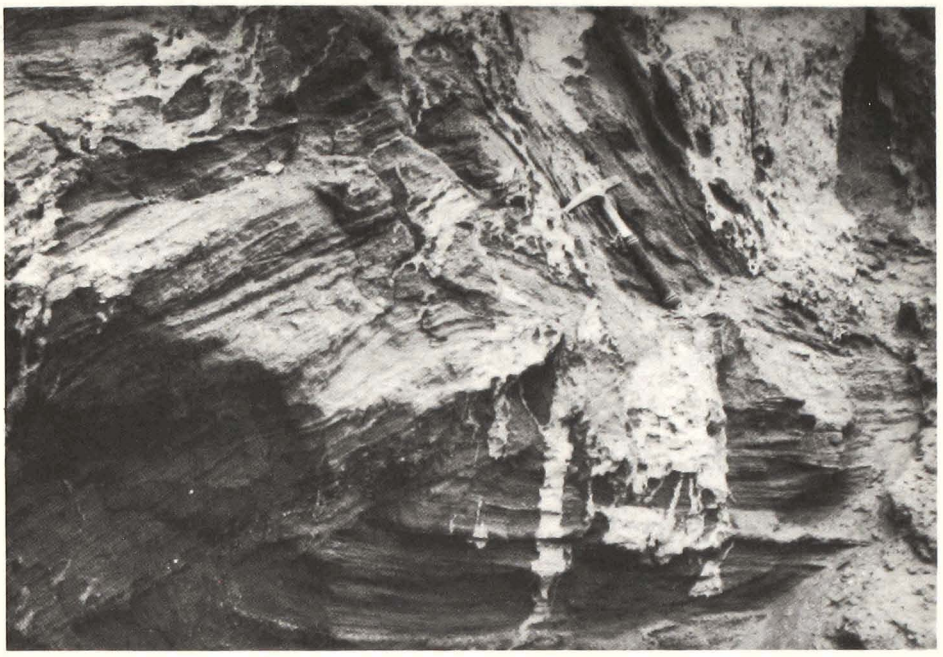

FIGURE 29. Photo, looking east, of a small thrust fault in sand and gravel deposited within the fault zone in the Dongdatan (Y in figure 23) and deformed by the formation of a shutter ridge.

FIGURE 30. Photo, looking east, of a small fold in stream gravels within a shutter ridge in the Dongdatan (Y in figure 23). The hammer in the centre of the photo gives a scale; the gravel is folded into an overturned fold with a steep northern flank. Left of the hammer the gravel beds dip nearly vertically, but to the right they are nearly flat. The overlying sand reveals the same folding but less clearly than the gravel.

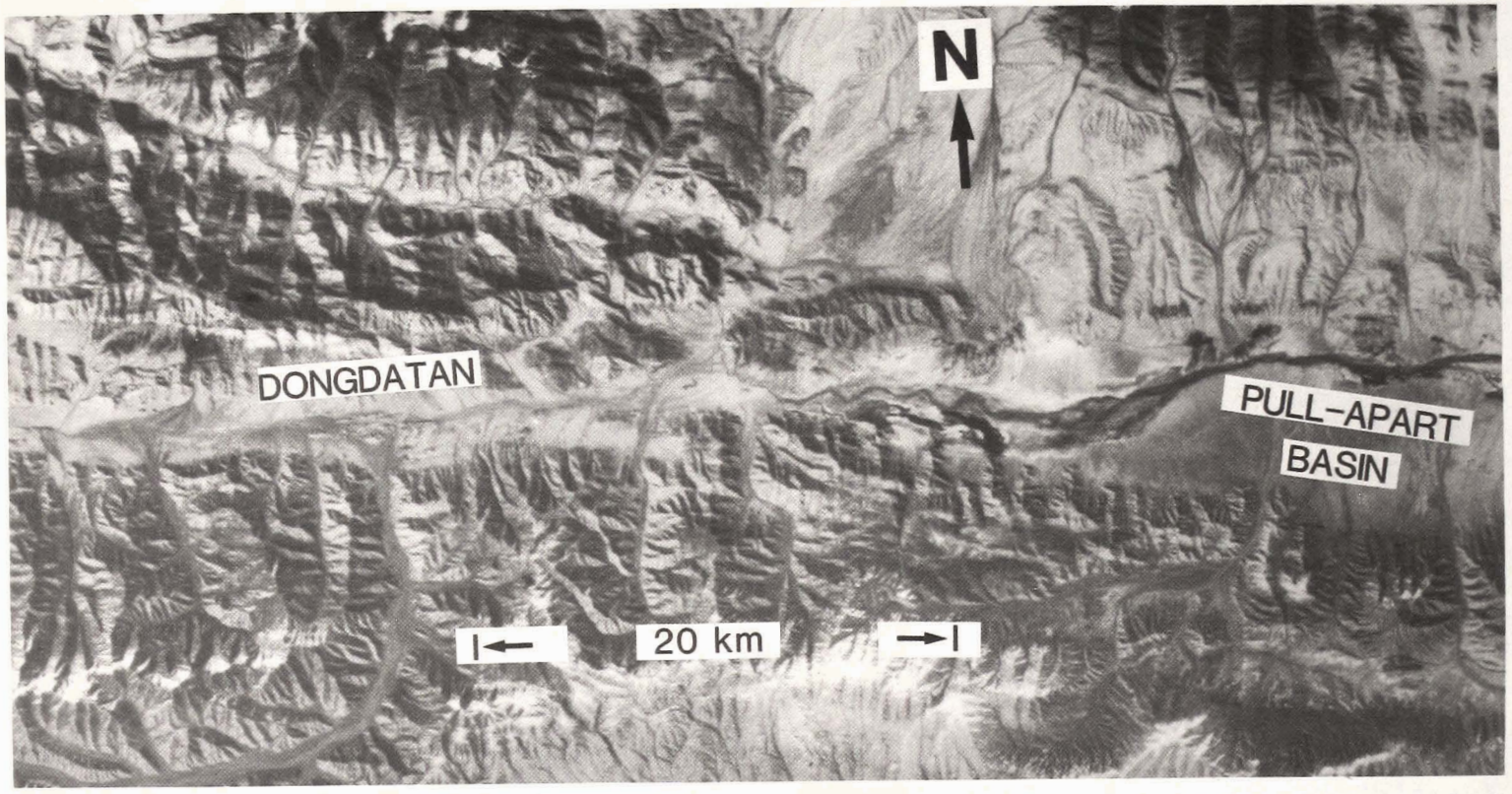

FIGURE 31. Large format camera photograph of the Dongdatan and the pull-apart basin to the east. Although the recent trace lies within the valley, segments of it have a clear topographic expression.

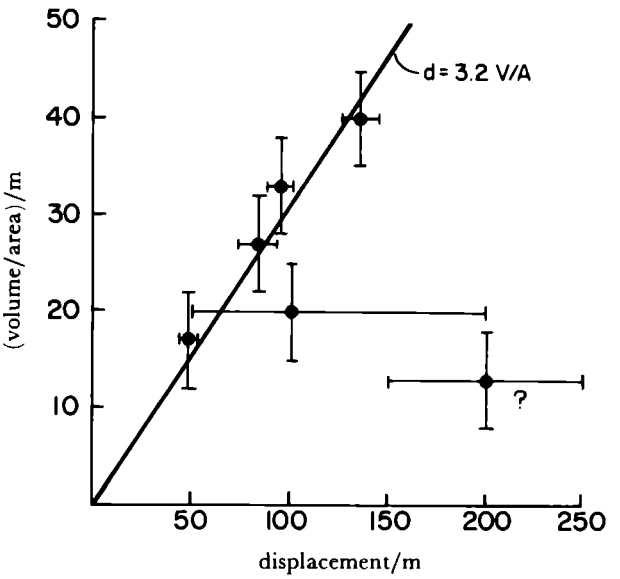

FIGURE 17. Plot of the average thickness of material eroded from the drainage basins (the ratio of the volume of the valley to its area) vs. the measured offsets of the streams. The linear relationship implies that the average erosion rate and the average slip rate on the fault are proportional to one another. Hence, the measurement of one yields an estimate of the other.

Total offset on the Kunlun Pass fault

We constructed a geologic map of the bedrock of the Kunlun Pass area (figure 12) to show the inferred distributions of the Pleistocene sequence of moraines, gravels, and lake beds and of the Triassic arenite and phyllitic slate; the cover of the very young alluvial and solifluction deposits was omitted. This map has interpolated boundaries, but at the scale mapped (1:100,000) we judge it unlikely that their positions would be altered significantly if outcrops were more widely exposed. One boundary defined within the lower part of the Pleistocene sequence, between coarser pinkish gravel below and finer, thinner bedded grey gravel above, appears to be offset 1.7 km horizontally in a left-lateral sense by the trace of the Kunlun Pass fault (asterisks in figure 12). Because the beds dip at a gentle angle (12°–20°) and strike very obliquely to the fault, this offset is a maximum for the strike-slip displacement since the gravel was deposited. Any dip-slip component of displacement (with the south side down) would reduce the real strike-slip offset. It may not be a coincidence that the contact between the lower gravel and the lake bed unit is also separated in a left-lateral sense about 3 km, but the topography in the area of the offset lake beds north of the fault implies that erosion has contributed significantly to the apparent offset in this case.

We observed another fault strand in the field a short distance south of the main fault and within the Pleistocene sequence (see figure 11), but we judge this to be a minor feature, based on its visible effects in outcrop, on its short, intermittent trace on the ground, and on the insignificance of its geomorphological expression on the satellite image compared with the main strand of the Kunlun Pass fault.

The small total strike-slip offset that we deduce contrasts strongly with the prominent geomorphological expression of the Kunlun Pass fault, at least east of the main Lhasa–Golmud highway, and with the non-trivial Holocene offset rate for this fault deduced from stream offsets.

Two features of the geomorphological expression of this fault, however, are perhaps consistent with limited total offset. First, it is difficult to trace the fault west of the Lhasa–Golmud highway, either on the ground or on Landsat MSS images and shuttle large-format camera photos, and even subtle (and somewhat debatable) expressions vanish completely 4 km west of the road. Second, when the prominent fault trace is followed on the space-based imagery to about 100 km east of where the highway crosses it, in a short distance its trend turns from 100° (along the prominent portion) to about 130° (figures 5, 9, and 10), but southeastward the topographic contrast across the fault is abruptly reduced. If the fault had extensive strike-slip displacement, this portion trending 130° should have a larger overthrust component than the portion trending 100°, and there should consequently be a major topographic expression of this thrust slip. The absence of such topographic expression is consistent with the Kunlun Pass fault having a small total strike-slip offset.

The elevation of the highest peaks in the ice-covered Burhan Budai mountains, just to the north of the prominent segment of the Kunlun Pass fault, and of the ground surface south of the fault are about 6100 m and between 4800–5100 m, respectively. If this relief developed entirely by a thrust component across the Kunlun Pass fault, then the vertical and lateral displacements on this fault would be comparable. The lack of topographic contrast across the fault, however, where the thrust component should be even larger (more than 100 km east of the highway), suggests that the relief has not developed as a result of oblique thrust and strike-slip faulting on the Kunlun Pass fault. Nevertheless, it remains the case that the Kunlun Pass fault is most prominent where the high relief occurs adjacent to it. Both to the west (where we observed it) and to the east (seen only from satellite images), the fault either disappears or is much subdued in expression where the topographic contrast lessens or vanishes.

Late Holocene faulting on the Xidatan–Tuosuohu–Maqu (Kunlun) fault

At many localities within the Xidatan and Dongdatan, we saw evidence of very recent, large-scale deformation along the most recent trace of the Xidatan–Tuosuohu–Maqu fault. This deformation includes tension gashes and mole tracks (or pressure ridges: see Richter 1958, p. 179–180 for a general description) oriented obliquely to the overall east–west trend of the fault, and offset fans, terraces, and stream channels. Many tension gashes were as deep as 1 m (in some cases 2 m) and as long as 10–20 m (in rare cases 30 m). Fresh mole tracks were of comparable dimensions. The dimensions and the freshness of these features, which are commonly associated with large earthquakes, suggest that a very large earthquake occurred on this segment of the Xidatan–Tuosuohu–Maqu (Kunlun) fault within the last few hundred years. The heights of some of the mole tracks, which must have formed by slip during several earthquakes, are more than 3 metres. In one area where recent incision by young, now dry streams had exposed cross sections through mole tracks, folds and thrust faults in very young alluvial sand and gravel were exposed. Linear ridges, with mole tracks and tension gashes crossing them, defined a zone of recent disturbance 10 to 30 m in width, and the heights of the ridges allowed this recent strand of the fault to be seen very clearly between alluvial fans where streams were flowing.

The large dimensions of the tension gashes and mole tracks made it difficult to measure reliably offsets smaller than about 10 metres. Offsets of streams and terraces of 10 to 20 m and more, however, are clear in may places. In all cases they attest to left-lateral slip. In general stream gullies shallower than about 0.5 m are not offset, but those deeper than 1 m are offset

10 m or more. In a couple of places multiple offsets could be inferred, and at one in particular, 3 or 4 repeated offsets of 10–15 m each can be inferred. Thus we conclude that movement has occurred by large amounts of slip during earthquakes.

We note that the fault zone is the locus of numerous cold springs, as are major faults throughout the world.

Below we describe and illustrate the deformation observed at individual localities. We hope that these descriptions will provide guidance for future workers on where to pursue further study of recent seismicity and deformation. We present these descriptions also in lieu of numerous, more objective large-scale contour maps. We constructed crude contour maps at two localities using a sightlevel, a compass, and a tape measure, or by pacing distances. We were not equipped with a plane-table and alidade, and we lacked the time to make additional contour maps. Using figure 13, we begin our discussion with features at the western end of the Xidatan.

Xidatan. Although the Xidatan–Tuosuohu–Maqu fault is clear on the satellite photos of the western end of the Xidatan and west of it (figures 5 and 7), and although the fault zone can be seen clearly on the ground in this area, we saw no evidence of recent slip or disruption near the western end of the Xidatan. At the westernmost locality where we did see disruption (A in figure 13), the disruption was among the least impressive of the localities that we visited. At that locality we saw a beheaded fan, low mole tracks (height $\approx$ 100s of mm) trending 130°, and shallow tension gashes trending 050°–055°. Young stream channels, however, complicate the topography.

In the 4 km east of this locality, evidence for recent deformation is not very convincing, but we did not have time to examine the area thoroughly. On the west bank of the main north–south valley and tributary to the Xidatan (B in figure 13), where the Lhasa–Golmud highway passes, fresh tension gashes and mole tracks are present.

One of us (P.M.) walked along nearly all of the segment up to 25 km east of this locality, and evidence for disruption was plentiful and clear. Approximately 1.5 km east of the valley (C in figure 13), the fault is marked by a low shutter (or pressure) ridge with mole tracks on it oriented 125°. The east side of an alluvial fan appears to be offset 10 to 30 m, but the possibility of a small vertical component of slip makes it difficult to define this value more precisely. The shutter ridge blocks a dry sag pond with dimensions of about 7 m × 10 m, and 2 m deeper than the crest of the ridge. Tension gashes 15 m in length and oriented 045° are clear. The fault zone is evident for 3 km, and no major streams or fans cross it. A shutter ridge with a height of a few metres is cut by tension gashes 100s of mm deep, 10–20 m long and oriented 045° (D in figure 13), and another small dry sag pond is clear south of the ridge (figure 19). At the east end of this zone (E in figure 13), the shutter ridge blocks, but is not dissected by, a young stream. The overall trend of the active fault is 090° ($\pm 2°$).

An actively eroding and redepositing fan without vegetation separates this segment from another farther east where the average trend of the recent scarp is 084°. The zone is marked by a prominent shutter ridge, 5 m in height, and is cut by numerous tension gashes 0.5 to 2 m deep, 5–15 m in length and trending 040°–050° (F in figure 13). One dry stream valley is offset 25–30 m left-laterally. Rounded cobbles north of the recent fault trace and now lying 11 ± 1 m west of the present main channel may imply a recent 11 ± 1 m left-lateral offset of this channel.

East of this area, deposition and erosion on large fans apparently has obliterated any recent

scarp for 2 km. Farther east a low (height < 0.4 m) south-facing, eroded scarp marks the recent trace (G in figure 13). Springs are also present. A short, north-facing scarp trends 110°, very differently oriented from the typical trend of 085°–090° (H in figure 13); probably a significant thrust component is present there.

At the west end of a high (≈ 40 m) east–west trending hill, a stream valley approximately 3 m deep is offset 15±5 m (I in figure 13). Farther east there is a sag pond on the south side of the hill. East of the hill, are clear, very large tension gashes with trends of 068°, 068°, 076°, 068°, 055°, and 068°, 0.5–2.0 m deep, 3 to 10 m wide, and up to 30 m long (J in figure 13; figures 20 and 21). An old stream terrace 0.3 m above and west of a younger stream bed has been offset left-laterally 34±5 m. The overall trend of this segment of the fault is 085°.

East of a wide stream channel (visible in figure 20), the fault zone is marked clearly by tension gashes trending 056°, mole tracks trending 145° and 155°, and a spring (K in figure 13). Farther east, the west side of an alluvial fan is offset left-laterally approximately 100 m, and the fault zone is defined by a shutter ridge 1–3 m high (L in figure 13; figure 22). Deposition and erosion are in the process of modifying the east side of the fan (the eastern side of the area shown in the contour map in figure 22). No evidence of recent faulting was seen in the gravel exposed in sections in the banks of channels.

Approximately 2 km farther east, the fault zone is again marked by numerous large tension gashes 1.5–2 m deep and trending 068° (M in figure 13). Two old terraces on the west side of an active stream have been offset 68±5 m and 75±7 m. East of another active stream, more large tension gashes, 0.5 to 1.5 m deep, trend 060° across a broad shutter ridge (width ≈ 40 m) (N in Figure 13). The west bank of a north-flowing, now dry, stream bed has been offset 15±5 m. The eastern end of this segment of the fault zone, in turn, is defined by a high shutter ridge (height ≈ 20 m) with *en echelon* hills and troughs suggestive of both tension gashes (045°) and mole tracks (120°) crossing it (O in figure 13). Prominent breaks in slope on the north side of the ridge may result from a component of thrust or reverse faulting on south-dipping faults.

We did not examine much of the 4 km east of this shutter ridge, but farther east the fault zone is again very clear. Another shutter ridge trending 080°, with relief of 2–2.5 m seems to be cut by both tension cracks and mole tracks (P in figure 13). Both dry sag ponds and springs are present on the south side of the fault trace. Farther east, on the west side of a very large fan, a high (≈ 5 m), south-facing scarp trends 085° for a distance of more than 1 km (Q in figure 13). Small hills can be seen several km farther to the east (R in figure 13) and probably mark an eastward continuation, in the direction 090°, of the active trace.

Dongdatan. We were unable to examine the 50 km of the Xidatan and Dongdatan to the east of this large scarp, but we did examine the active trace along 25 km of the Dongdatan. Springs emanate from an area near a prominent low scarp at the west end of the area studied (S in figure 23). To the east erosion and deposition along active streams and fans has obliterated this low scarp (height ≈ 1 m), but it can be seen again several km farther east (T in figure 23). Its trend is 086±2°. Low mole tracks (height ≈ 0.5 m) with dimensions of 3–4 m by 2–3 m trend northwest–southeast in the eastern part of this segment. Farther east, erosion and deposition again has obliterated any young trace.

A continuous zone of recent disruption is clear where the fault crosses a hilly area in which major streams are absent (U in figure 23). Large tension gashes 2 m deep, 20–40 m long and trending 070° are very prominent. Sag ponds, both dry and wet, are present on the north or south sides of the trace, depending upon the slope of the hilly topography.

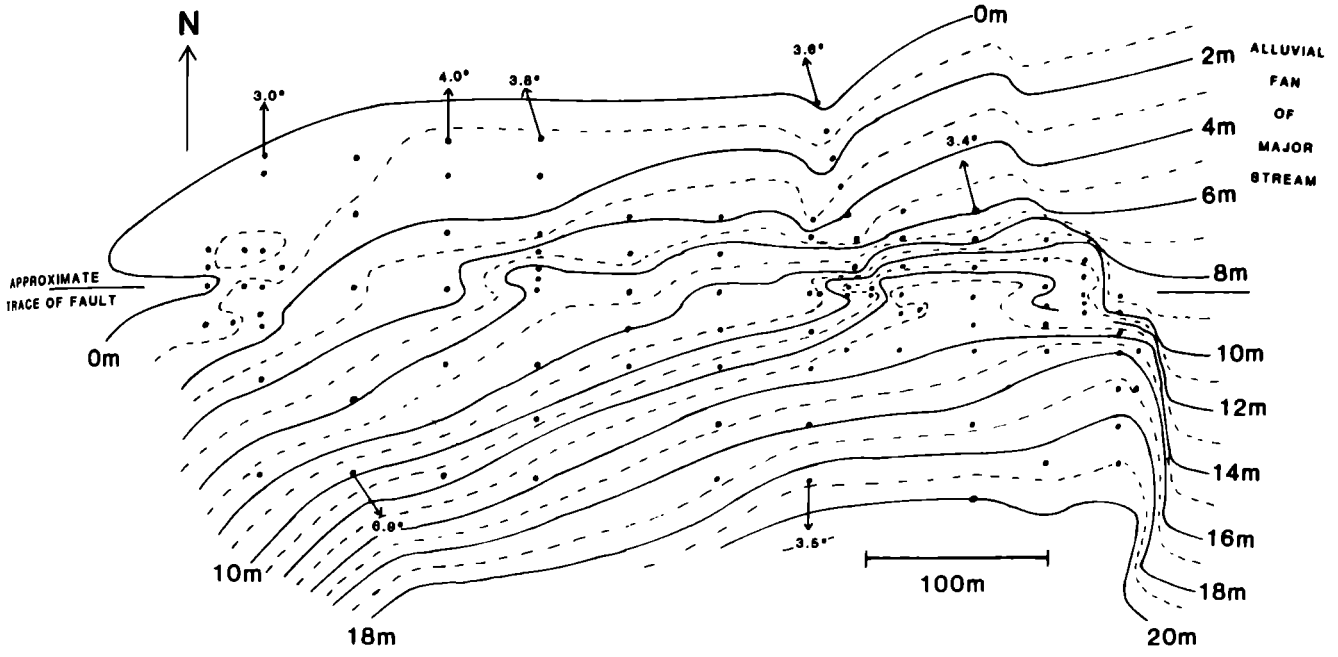

FIGURE 22. Contour map of an offset alluvial fan at locality L in figure 13. This map was made by using a tape measure or by pacing to determine distances between points, shown as dots, and a compass to determine their relative positions. Elevations were determined using a sightlevel to measure angles relative to the horizontal. Arrows give the average slopes of the surface, where it is smooth, in the directions defined by the arrows. Uncertainties in differences in elevations over distances of 100 m are about 1 m. Note the clear shutter ridge along the fault and the apparent left-lateral offset of the fan of about 100 m. At the eastern edge of the map a braided stream is actively eroding the fan and has obliterated evidence of faulting.

A large stream from the south crosses the hills and is incised into bedrock close to the fault in a locally antecedent relationship. North of the fault, the stream flows east parallel to it and has obliterated the surface expression of another 2 km of recent faulting. Farther east the fault zone lies south of the river valley, and a segment some 4 km long contains some of the most impressive evidence for recent faulting that we have ever seen. These include huge shutter ridges, sag ponds, deep tension gashes, cross sections of mole tracks, and offset gullies and stream beds.

At the west end of this segment, a dry stream bed is offset 10 ± 2 m (V in figure 23; figure 24). Farther east a prominent shutter ridge, 5 to 6 m in height bounds dry sag ponds on its south (figure 25) and is cut by huge tension gashes more than 2–3 m deep, 10–20 m in length, and with trends of about 055° (figure 26). One dry stream bed seems to have been multiply offset (W in figure 23). Two northward-flowing streams merge at the scarp, which is marked by a prominent shutter ridge (figure 27). Three or four groups of rounded cobbles on the north side of the fault appear to mark abandoned stream channels that apparently have successively been displaced westward by slip on the fault (figure 28). Spacings between them of 11 m, 11 m, 10 m, and roughly 8 m (or possibly 1 of 15 to 18 m) (figure 28) suggest that slip has occurred by discrete events of comparable magnitude and probably not by continuous fault creep.

The high shutter ridge with heights reaching 6 to 7 m continues east for 2 km (X in figure 23) and is cut by huge tension gashes, more than 3 m deep in one case and trending 030° to 060°. The fault zone is quite wide, up to 50 m, and within that zone gravels have been tilted

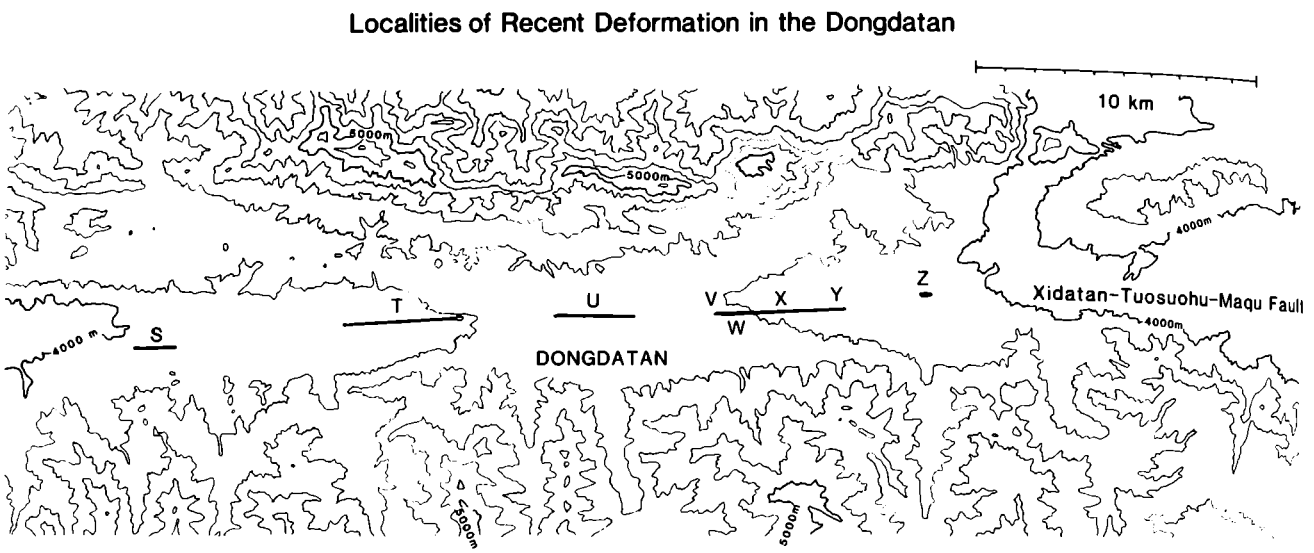

FIGURE 23. Map showing areas of recent disruption along the Xidatan–Tuosuohu–Maqu fault in the Dongdatan. Letters correspond to areas discussed in the text.

from 20°–30° to as much as 55° (Y in figure 23; figure 29). Cross sections exposed by streams through mole tracks and through the main shutter ridge reveal thrust faulting and folding within these young deposits (figure 30). These features are clearly due to localised horizontal compression.

Erosion and deposition seem to have obliterated much of the recent deformation in the 3 km farther east, but an east–west alignment of low mounds (height ≈ 0.5 m) seems to mark the fault zone on a large fan (Z in figure 23). They might be eroded mole tracks. We did not have time to examine features farther east, where the fault enters a large pull-apart basin (figure 31).

Summary of late Holocene deformation along the Xidatan–Tuosuohu–Maqu fault.

The features described above attest to recent strike-slip faulting on this fault, and they suggest that this displacement has occurred by slip during large earthquakes. The last such earthquake probably occurred within the last few hundred years.

Young disruption is clear along at least 110 km of the fault, the distance between the westernmost and the easternmost points of observation. This disruption includes large mole tracks and deep tension cracks, features commonly associated with earthquakes (Richter 1958, pp. 179–180). If all of the disruption occurred during the same event, then by comparison with other events in Asia, a maximum fault length of 110 km would imply that the magnitude of the earthquake was at least $7\frac{1}{2}$ (e.g. Molnar & Deng 1984).

Many of the tension cracks are bounded by free faces; thus they are in a youthful stage of erosion. By analogy with free faces on fault scarps, the existence of free faces implies that the tension cracks are only a few hundred years old, and possibly only 100 years old (Wallace 1977). Permafrost did not seem to be present in this area, and consequently these features probably have not been maintained for unusually long times by frozen ground. They probably are not associated with the 19 April 1963 earthquake with $M = 7.0$, which occurred 210 km east of our westernmost observation. The large scale of the deformation and the required fault

length of 200 km are both greater than what are likely for an event with a magnitude of only 7.0. No other earthquake with a magnitude greater than 7 is listed by Gutenberg & Richter (1954), Duda (1965), or Geller & Kanamori (1977) for this region in this century. Thus, the earthquake responsible for the tension gashes and mole tracks probably occurred before 1900, but almost certainly since 1500 to 1700 A.D.

The dimensions of the tension cracks and mole tracks are unusually large–larger than those of the 1920 Haiyuan earthquake ($M = 8.7$), for which the average displacement was 8 m and for which the displacement in places reached 10–12 m (Deng *et al.* 1984, 1986; Zhang *et al.* 1987). The observations of displaced stream gullies of 10 to 15 m at various localities along the Xidatan–Tuosuohu–Maqu fault are sufficiently numerous to suggest that offset of this amount occurred during the same earthquake responsible for the tension cracks and mole tracks, but the difficulties in measuring smaller offsets allow for this inference to be false. The groups of cobbles that seem to indicate abandoned channels of a successively displaced stream channel in the Dongdatan (figure 28), however, also concur with repeated offsets of 10–15 m. The observations from this one locality also are not, by themselves, enough to prove that slip has occurred in jumps of 10 to 15 m during large earthquakes, but we think that this is the most sensible interpretation of the distribution of cobbles shown in figure 28.

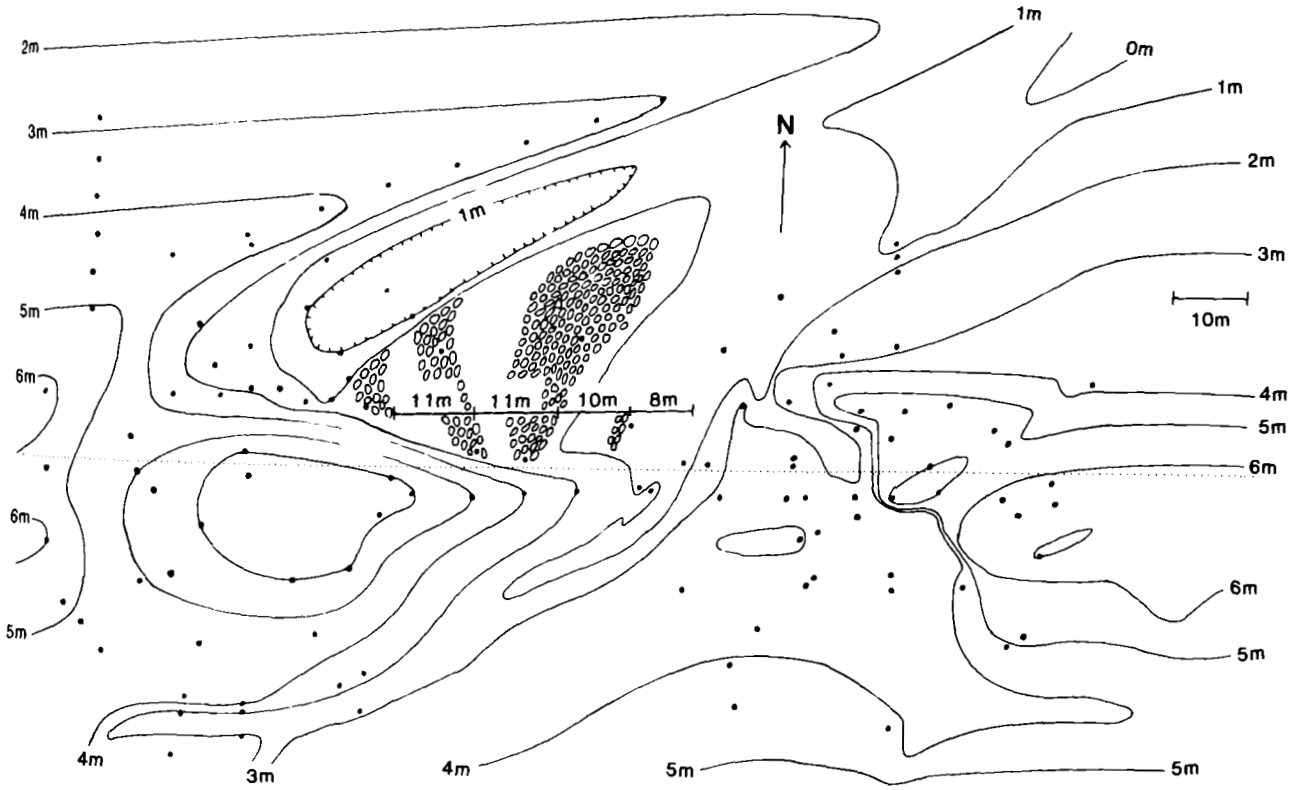

FIGURE 28. Contour map of the area shown in figure 27. Groups of cobbles are shown in areas separated from one another by 11 m, 11 m, and 10 m. We interpret these as having been deposited by the ancestral stream of that shown crossing the fault and presently about 8 m east of the easternmost, small group of cobbles. Thus these observations seem to indicate multiple offsets of the stream. Probably at an earlier stage the stream passed through the area including the closed contour northwest of the groups of cobbles. Note also the subtle northeast trend of topography on the prominent easterly trending shutter ridge, which is apparent in the shape of the 6 m contour; this northeast trend reflects the existence of tension gashes obliquely crossing the shutter ridge.

We have no evidence constraining the recurrence intervals of such large earthquakes. If the slip rate is 10 or 20 mm/a, as discussed above, and if large events can be associated with 10 or 15 m of slip, then recurrence intervals are likely to be between 500 and 1500 years. The steepness of erosional escarpments offset 20 to 40 m, presumably by 2 or more earthquakes, certainly allows them to be only a few thousand years old, but we lack any useful quantitative observations to constrain the recurrence interval.

Unfortuantely we found no clear Holocene or post-glacial features, such as moraines, that were offset and that could be used to estimate a Holocene average slip rate. The offsets of small streams and of fans, of as much as 100 m in one case, could have occurred during late Holocene time, or if the average rate of slip were only 10 mm/a, they could represent slip during the entire Holocene. Unfortunately, we could not date them.

Thus, the recent disruption along the Xidatan–Tuosuohu–Maqu fault attests to its recent activity. The types of features – tension gashes and mole tracks – imply the occurrence of a recent earthquake. The dimensions of these features and the amounts of offsets of gullies and dry stream valleys imply that that earthquake was very large. Finally we suspect that slip has occurred several times in the last few thousand years by displacement of 10 to 15 m during earthquakes.

Conclusions

Our most significant conclusion is that the rate of slip on the Kunlun strike-slip fault system is more than 10 mm/a for the Quaternary period, and possibly more than 20 mm/a for the most recent 10 ka to 20 ka. A moraine, presumably of late Pliocene or early Quaternary age and containing very distinctive blocks of pyroxenite, has been displaced 30 km from the only known outcrop of pyroxenite in the area, an outcrop that lies very near to the Xidatan–Tuosuohu–Maqu fault, the principal active fault in the Kunlun system. If the age of the moraine is 2.4 Ma, then the rate of slip is about 13 mm/a, with minimum and maximum possible values 10 and 20 mm/a. Stream valleys crossing a second fault in the Kunlun fault system, the Kunlun Pass fault, are displaced 50 to 150 m. Several observations suggest that the incision of these valleys began in the latest Pleistocene or Holocene epochs, and if so then the average rate of slip on this fault is also about 10 mm/a (between 5 and 20 mm/a). Detailed mapping of gravel layers beneath the lake beds revealed a small offset of this gravel unit: less than 1.7 km. Thus we suspect that the Kunlun Pass fault may not have been active for the whole of the Quaternary period. Accordingly, it would be unwise to assume that the sum of the Holocene rate for this fault and the Quaternary rate for the Xidatan–Tuosuohu–Maqu fault is applicable to the whole of the Quaternary period.

We found abundant evidence for very recent disruption along the Xidatan–Tuosuohu–Maqu fault in both the Xidatan and the Dongdatan. Very large tension gashes and mole tracks attest to surface deformation, probably associated with a major earthquake, in the last few hundred years. Offsets of several features of about 10 m imply that slip of that amount occurred during such an earthquake, and the distribution of stream cobbles deposited in apparently successively offset stream channels, suggest multiple offsets of this amount. We conclude that the Xidatan–Tuosuohu–Maqu fault is still very active, and that slip on it probably occurs abruptly in rare large earthquakes. Moreover, the apparent recent initiation of slip on the Kunlun Pass fault probably should not be associated with any decline in the rate of slip on the Xidatan–Tuosuohu–Maqu fault.

A correlation of the truncation of a well-defined phyllonitic unit, mapped in the Kunlun Pass area, with a light-coloured unit, seen on the Landsat imagery of the area north of the Xidatan Tuosuohu–Maqu fault and 75 km west of the Kunlun Pass, suggests a minimum total offset of 75 km for that fault.

In addition recent normal faulting was observed in a northerly-trending half-graben near Wenquan, and recent deformation of thrust and probably strike-slip sense was observed in the northeasterly-trending valley containing the town of Amdo and at the southern margin of the Erdaogou range (figure 1). Such observations of reverse or thrust faulting are unusual *within* the high plateau, where the active tectonics are characterized by normal and strike-slip faulting. Nevertheless, from the linearity of the scarps, the fault plane solution of nearby earthquakes, and the orientations of a few slickensides, we infer that the left-lateral strike-slip displacements are comparable with the vertical components, and that these localized examples of thrust faulting probably are not reliable indicators of the regional tectonic strain field.

The prevalence of normal faulting on northerly-trending grabens in southern Tibet (e.g. Armijo *et al.* 1986), and the conjugate strike-slip faulting, with left-lateral slip on northwesterly-striking planes and right-lateral slip on northeasterly-striking planes, reflect an east west extension of the plateau and an eastward extrusion of the crust within Tibet (e.g. Molnar & Tapponnier 1975, 1978). Left-lateral slip on the Kunlun strike-slip fault system of more than 10 mm/a, and possibly at 20 mm/a in the last 10 ka shows that the area south of the Kunlun is being rapidly displaced eastward with respect to the area farther north. This eastward displacement is probably a consequence of the continuing penetration of India into the rest of Eurasia (e.g. Molnar & Tapponnier 1975; Tapponnier & Molnar 1977). The high elevation and thick crust of the Tibetan Plateau make further crustal thickening of Tibet energetically difficult, and eastward extrusion of the plateau allows India's penetration without further increase in the gravitational potential energy stored in Tibet's crust (e.g. England & Houseman 1986; Molnar & Lyon-Caen 1988; Molnar & Tapponnier 1978).

The rapid rate of slip implies a correspondingly rapid rate of extrusion, which manifests itself both by active mountain building on the eastern edge of the plateau and by the eastward expulsion of southeast China over the Pacific and Philippine sea plates. The demonstration of this rapid displacement in a direction perpendicular to the direction of convergence of the Indian and Eurasian plates is a reminder of how difficult it is, in general, to infer the direction of relative plate motion in ancient orogenic belts solely from the strain within those belts, especially in only small fragments of them.

We thank the logistic staff of Academia Sinica, in particular Ma Xuezheng and Wang Zhe, and of the Royal Society, particularly L. U. Mole, for making the Geotraverse efficient and productive, and also the driver, Chen Guozhen, whose bold driving took us to places ordinarily too far to reach. We also thank K. C. A. Burke for the loan of large format camera images and for the use of the image processing facilities of the Lunar and Planetary Institute. He, J. A. Jackson, and K. Sieh made helpful suggestions for the improvement of the manuscript, and S. A. Schumm offered some guidance with erosion rates. This research was supported in part by the National Science Foundation through grant EAR-8417640 and by NASA through grant NAG-G5-524.

Chang Chengfa, J. F. Dewey, A. Gansser and J. A. Pearce participated in the field work and offered helpful suggestions. John Dewey, in particular, pointed out the incised meanders in the Erdaogou region and their implications for recent activity there.

References

Armijo, R., Tapponnier, P., Mercier, J. L. & Han Tonglin 1986 Quaternary extension in southern Tibet: Field observations and tectonic implications. *J. geophys. Res.* **91**, 13,803–13,872.

Armijo, R., Tapponnier, R. & Han Tonglin (in press) Late Cenozoic right-lateral strike-slip faulting across southern Tibet. *J. geophys. Res.* **93**.

Brune, G. 1948 Rates of sediment production in midwestern United States. *Soil Conservation Service Tech. Pub. 65*, 40 pp.

Burchfiel, B. C., Zhang Peizhen, Wang Yipeng, Zhang Weiqi, Jiao Decheng, Song Fangmin, Deng Qidong, Molnar, P., & Royden L. (in press) Geology of the Haiyuan Fault Zone, Ningxia-Hui Autonomous Region, China and its Relation to the Evolution of the Northeastern Margin of the Tibetan Plateau. *Bull. geol. Soc. Am.*

Burke, K. C. A. & Lucas, L. (in press) Lumpola Basin: Thrusting on the Tibetan Plateau within the last 5 Ma. In *Tectonic Evolution of the Tethyan Regions* (ed. A. M. C. Sengör). Nato Advanced Study Institute. Dordrecht: Reidel.

Burke, K. C. A., Dewey, J. F. & Kidd W. S. F. 1974 The Tibetan Plateau, Its significance for tectonics and petrology. *Geol. Soc. Amer. Abstr. Programs* **6**, 1027–1028.

Chang Chengfa, Chen Nansheng, Coward, M. P., Deng Wanming, Dewey, J. F., Gansser, A., Harris, N. B. W., Jin Changwei, Kidd, W. S. F., Leeder, M. R., Li Huan, Lin Jinlu, Liu Changjie, Mei Houjun, Molnar, P., Pan Yun, Pan Yusheng, Pearce, J. A., Shackleton, R. M., Smith, A. B., Sun Yiyin, Ward, M., Watts, D., Xu Juntao, Xu Ronghua, Yin Jixiang & Zhang Yuquan 1986 Preliminary conclusions of the Royal Society and Academia Sinica 1985 Geotraverse of Tibet, *Nature, Lond.* **323**, 501–507.

Cui Zhengyuan & Yang Bin 1979 On the Tuosuohu–Maqu active fault zone (in Chinese). *Northwest. seismol. Jl.* **1**(2), 57–61.

Deng Qidong, Song Fangmin, Zhu Shilong, Li Mengluan, Wang Tielin, Zhang Weiqi, Burchfiel, B. C., Molnar, P. & Zhang Peizhen 1984 Active faulting and tectonics of the southern Ningxia-Hui Autonomous Region, *J. geophys. Res.* **89**, 4427–4445.

Deng Qidong, Chen Shefa, Song Fangmin, Zhu Shilong, Wang Yipeng, Zhang Weiqi, Jiao Decheng, Burchfiel, B. C., Molnar, P., Royden, L. & Zhang Peizhen 1986 Variations in the geometry and amount of slip on the Haiyuan fault zone and the surface rupture of the 1920 Haiyuan earthquake. *Maurice Ewing Series* **6**, Amer. Geophys. Un., Washington, D.C., 160–182.

Duda, S. J. 1965 Secular seismic energy release in the circum-Pacific belt. *Tectonophysics* **2**, 409–452.

England, P. C. & Houseman, G. A. 1986 Finite strain calculations of continental deformation; 2. Comparison with the India–Asia collision. *J. geophys. Res.* **91**, 3664–3676.

Geller, R. J. & Kanamori H. 1977 Magnitude of great shallow earthquakes from 1904 to 1952. *Bull. seismol. Soc. Amer.* **67**, 587–598.

Gutenberg, B. & Richter, C. F. 1954 *The Seismicity of the Earth.* 310 pp. New York: Hafner.

Hennig, A. 1915 *Zur Petrographie und Geologie von Sudwestibet, Southern Tibet*, vol. V. Stockholm: Kung. Boktryekeriet. P. A. Norstedt.

Holmes, A. 1965 *Principles of Physical Geology.* London: Thomas Nelson & Sons Ltd. Chapter XXI.

Kidd, W. S. F. 1975 Widespread late Neogene and Quaternary alkaline volcanism on the Tibetan Plateau. (abstract). *EOS. Trans. Amer. geophys. Un.* **56**, 453.

Langbein, W. B. & Schumm, S. A. 1958 Yield of sediment in relation to mean annual precipitation. *Trans. Amer. geophys. Un.* **39**, 1076–1084.

Lee, K. Y. 1984 Tertiary system and its petroleum potential in the Lunpola Basin, Xizang (Tibet). *Open-File Report 84-420.* U.S. Geologic Survey.

Li Longhai & Jia Yunhong 1981 Characteristics of the deformation band of the 1937 Tuosuohu earthquake ($M = 7.5$) in Qinghai (in Chinese). *Northwest. seismol. Jl.* **3**(3), 61–65.

Littledale, St. G. R. 1896 A journey across Tibet, from north to south, and west to Ladak. *Geogr. Jl.* **7**, 453–483.

Molnar, P. & Chen W.-P. 1983 Focal depths and fault plane solutions of earthquakes under the Tibetan plateau. *J. geophys. Res.* **88**, 1180–1196.

Molnar, P. & Deng Qidong 1984 Faulting associated with large earthquakes and the average rate of deformation in central and eastern Asia. *J. geophys. Res.* **89**, 6203–6227.

Molnar, P. & Lyon-Caen H. 1988 Some simple physical aspects of the structure, support, and evolutions of mountain belts. *Geol. Soc. Am. Spec. Pap.* 218, pp. 179–207.

Molnar, P. & Tapponnier P. 1975 Cenozoic tectonics of Asia: Effects of a continental collision. *Science, Wash.* **189**, 419–425.

Molnar, P. & Tapponnier P. 1978 Active tectonics of Tibet. *J. geophys. Res.* **83**, 5361–5375.

Molnar, P., Chen, W.-P., Fitch, T. J., Tapponnier, P., Warsi, W. E. K. & Wu, F. T. 1977 Structure and tectonics of the Himalaya: A brief summary of relevant geophysical observations. *Colloque Internationaux du CNRS, No. 268, Himalaya: Sciences de la Terre.* Editions du centre National de la Recherche Scientifique, Paris, 269–294.

Molnar, P., Burchfiel, B. C., Zhao Ziyun, Liang K'uangyi, Wang Shuji & Huang Minmin 1987*a* The geologic evolution of northern Tibet: Results from an expedition to Ulugh Muztagh. *Science, Wash.* **235**, 299–305.

Molnar, P., Burchfiel, B. C., Liang K'uangyi & Zhao Ziyun 1987*b* Geomorphic evidence for active faulting in the Altyn Tagh and northern Tibet and qualitative estimates of its contribution to the convergence of India and Eurasia. *Geology* **15**, 249–253.

Ni, J. & York, J. E. 1978 Late Cenozoic extensional tectonics of the Tibetan Plateau. *J. geophys Res.* **83**, 5377–5387.

Norin, E. 1946 Geological Explorations in Western Tibet. *Reports from the Scientific Expedition to the Northwestern Provinces of China under the Leadership of Dr. Sven Hedin, Publ. 29, (III), Geology 7.* Thule, Stockholm: Tryckeri Aktiebolaget.

Qian Fang, Ma Xinghua, Wu Xihao & Pu Qingyu 1982 Study of the magnetic stratigraphy of the Qiangtang and Quguo formations (in Chinese). *Contributions to the Geology of the Qinghai-Xizang (Tibet) Plateau* **4**. Beijing: Geol. Pub. House, 121–130.

Richter, C. F. 1958 *Elementary Seismology*, San Francisco: W. H. Freeman, pp. 179–180.

Rothery, D. A. & Drury S. A. 1984 The neotectonics of the Tibetan Plateau. *Tectonics* **3**, 19–26.

Schumm, S. A. 1963 *The Disparity Between Present Rates of Denudation and Orogeny. U.S. Geol. Surv. Prof. Paper 454-H.* U.S. Govt. Printing Office.

Sengör, A. M. C. & Kidd, W. S. F. 1979 Post-collisional tectonics of the Turkish-Iranian Plateau and a comparison with Tibet. *Tectonophysics* **55**, 361–376.

Shackleton, N. J., Backman, J., Zimmerman, H., Kent, D. V., Hall, M. A., Roberts, D. G., Schnitker, D., Baldauf, J. G., Desprairies, A., Homrighausen, R., Huddlestun, P., Keene, J. B., Kaltenback, A. J., Krumsiek, K. A. O., Morton, A. C., Murray, J. W. & Westberg-Smith J. 1984 Oxygen isotope calibration of the onset of ice-rafting and history of glaciation in the North Atlantic region. *Nature, Lond.* **307**, 620–623.

Tapponnier, P. & Molnar, P. 1977 Active faulting and Cenozoic tectonics of China. *J. geophys. Res.* **82**, 2905–2930.

Tapponnier, P. *et al.* 1981*a* The Tibetan side of the India Eurasia collision. *Nature, Lond.* **294**, 405–410.

Tapponnier, P., Mercier, J. L., Armijo, R., Han T. & Zhou J. 1981*b* Field evidence for active normal faulting in Tibet. *Nature, Lond.* **294**, 410–414.

Tapponnier, P., Peltzer, G., Le Dain, A. Y., Armijo, R. & Cobbold, P. 1982 Propagating extrusion tectonics in Asia: New insights from simple experiments with plasticine. *Geology* **10**, 611–616.

Tapponnier, P., Peltzer, G. & Armijo, R. 1986 On the mechanics of the collision between India and Asia. In *Collision Tectonics* (ed. M. P. Coward & A. C. Ries) Geological Society, London, pp. 115–157.

Wallace, R. E. 1977 Profiles and ages of young fault scarps, north-central Nevada. *Bull. geol. Soc. Am.* **88**, 1267–1281.

Wu Xihao, Qian Fang & Pu Qingyu 1982 Quaternary glaciogeology of the east Kunlun mountains (in Chinese). *Contributions to the Geology of the Qinghai-Xizang (Tibet) Plateau* **4**, 1–18. Beijing: Geol. Pub. House.

Zhang Weiqi, Jiao Decheng, Zhang Peizhen, Molnar, P., Burchfiel, B. C., Deng Qidong & Wang Yipeng 1987 Displacement along the Haiyuan fault associated with the great 1920 Haiyuan, China, earthquake. *Bull. seismol. Soc. Am.* **77**, 117–131.

Phil. Trans. R. Soc. Lond. A **327**, 365–377 (1988) [365]
Printed in Great Britain

Cenozoic uplift and deformation of the Tibetan Plateau: the geomorphological evidence

By R. M. Shackleton[1], F.R.S., and Chang Chengfa[2]

[1] *The Open University, Department of Earth Sciences, Milton Keynes MK7 6AA, U.K.*
[2] *Institute of Geology, Academia Sinica, Beijing, People's Republic of China*

[Plates 1 and 2]

An erosion surface, interpreted as a pediplain, is traced across the Tibetan Plateau. As a result of faulting and warping, its elevation now varies from approximately 4500–6000 m. It was cut across folded and thrust Eocene strata and mid-Miocene granites, but was dislocated by major faults before the Pliocene. Its age is thought to be mid- to late Miocene. Crustal shortening after pediplanation is small. If the crust beneath the Plateau was thickened by deformation during crustal shortening, the thickening must mainly have occurred before the pediplanation.

1. Introduction

The Tibet Plateau is a vast elevated area, about 2000 km from east to west, and up to nearly 800 km from north to south. Much of this area is over 5000 m above sea level. It is, however, by no means a plateau in the literal sense of 'an elevated tract of comparatively flat and level land'. Mountain ranges, among them the Gangdise Shan, Nyainqentanglha Shan, Tanggula Shan and Kunlun Shan, rise to 7000 m. Rivers have cut down to 3000 m.

The 1985 Geotraverse crossed the Plateau from Lhasa to Golmud, near the limit between a western region of lakes and internal drainage and an eastern region where the drainage is towards the east and southeast. Field excursions from Lhasa to Kathmandu in 1981 and 1986, arranged by Academia Sinica, extended the traverse southwestwards through southern Tibet and the Himalaya. During these traverses, it became clear that relics of a widespread former erosion surface could be recognized (figure 1) and that its present form puts constraints on interpretations of the tectonic evolution of the Plateau.

A striking feature of all the mountain ranges crossed by the Geotraverse is the evenness of the summit levels, which at once suggested the existence of a formerly planar, though now deeply eroded, erosion surface. Since many of the ranges are bounded by major fault scarps, it is clear that extensive faulting occurred after the planation; many of these faults are still active (Kidd & Molnar, this volume).

The existence of block mountains surmounted by planar erosion surfaces was recognized by many of the early explorers of Central Asia (Berkey & Morris 1927; Norin 1935; de Terra 1933). More recently, much work on the erosion surfaces in Tibet has been done by Chinese geologists and geographers (Li Jijun *et al.* 1981; Zhang Qingsong *et al.* 1981; Xu Shuying 1981). However, there is no clear agreement about the number, correlation or age of these surfaces, nor about the chronology of the uplift of the Plateau. Evidence obtained during the Geotraverse is described here, in particular that relevant to tectonic interpretation.

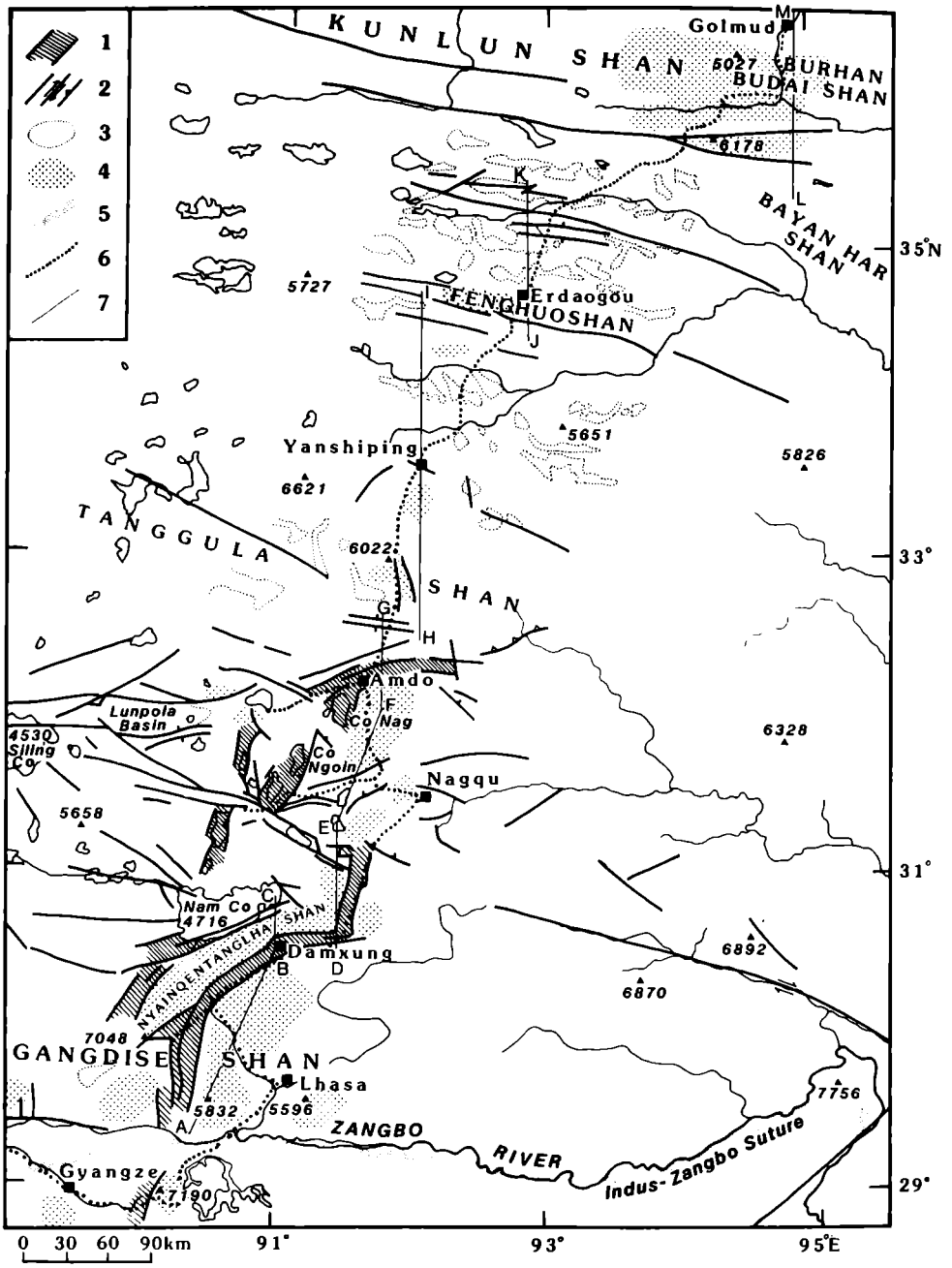

FIGURE 1. Map of Geotraverse route (6) to show observed remnants of the pediplain (4), postpediplain grabens (1) and faults (2), Neogene deposits (3), the Indus–Zangbo Suture (5) and the lines of profiles used in figure 2 (7).

Topographic data, particularly elevations, are taken from the very high quality 1:100000 topographic maps published by the State Bureau of Surveying and Mapping, Beijing, which were made available to us through Academia Sinica. Copies of these maps are deposited in the British Museum (Natural History).

2. The interpretation of accordant summit levels as planation remnants

When seen from a distance (usually only possible from the north or south, at right angles to the prevailing trend of the ranges) most of the ranges, from south of the Zangbo north to the Kunlun, display uniform summit levels (figures 3, 4, 6 and 8, plates 1 and 2) even though the individual summits are mostly sharp peaks separated by deeply eroded valleys. While the uniform summit level along the ranges is clear, the transverse profiles are less easily seen.

The evidence from the different sections of the Geotraverse is here discussed from south to north on the basis of a profile (figure 2) derived from plotting summit elevations from a band 10 km wide across the Plateau, on the lines shown on figure 1.

(*a*) *The southern part of the Lhasa Terrane (Gangdise Shan)*

The Gangdise Shan (Transhimalaya) represents an Andean volcanic and plutonic arc, trending east–west, which extends immediately north of the Indus–Zangbo Suture for some 3000 km. In the Lhasa region, and for at least 300 km westwards, the rocks forming the arc have been eroded down to a remarkably even summit surface (figure 1 and figure 3). This summit surface has been cut, by the erosion of several kilometres of rock, indiscriminately across Cretaceous and lower Tertiary volcanic and plutonic rocks and a variety of sediments, as well as across both complex late Cretaceous structures and less intense post-Eocene structures, including the late thrusts which brought Palaeozoic rocks over Tertiary volcanics 25 km north of Lhasa (Kidd *et al.*, this volume; Map in pocket; Coward *et al.*, this volume). The summit surface is itself deeply incised and dissected; its elevation is now about 5700 m in the south of the Lhasa Terrane, falling gradually to about 5000 m 100 km farther north. The Zangbo River south of Lhasa is below 3700 m.

The fact that the summit surface is cut across a variety of rocks of differing resistance to erosion and across folds, faults and thrusts clearly shows that it represents an originally planar erosion surface. It follows that at least this part of the Gangdise Shan no longer existed as a mountain range by the time planation was completed.

(*b*) *The Yangbajain graben*

The northward limit of the area around Lhasa shown in figures 1 and 3 is formed by the Yangbajain graben, probably a pull-apart basin, about 10 km wide (Armijo *et al.* 1986). Steep faults, along some of which recent gravels are displaced, bound the graben. Its floor is about 700 m below the summit surface immediately to the south and about 1000 m below the main extent of the surface farther south. It is filled with at least 300 m of Pleistocene deposits (Academia Sinica 1980).

On the north side of the graben, the even summit surface is seen again on the Nyainqentanglha Shan; it must underlie the Pleistocene deposits in the graben, having been displaced downwards by at least 1500 m relative to the block to the south.

(*c*) *The Nyainqentanglha Shan*

This range, trending WSW–ENE and varying in width from 10 to 30 km, displays (figure 4, plate 1) the same even summit surface as the block south of the Yangbajain graben, though more deeply dissected by erosion. Its northern limit, less sharply defined than the southern one,

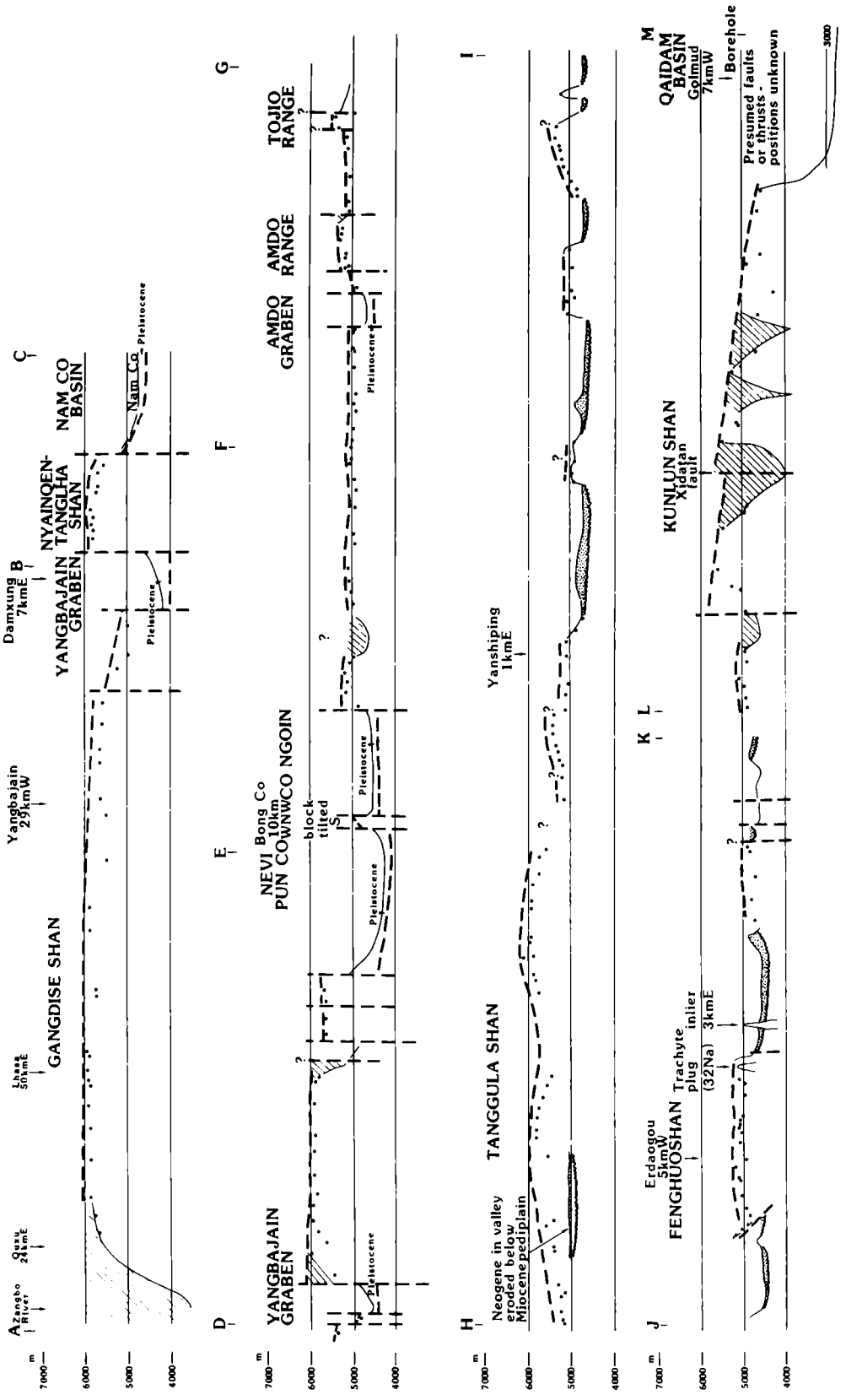

FIGURE 2. Profiles, based on elevations of peaks (dots) within 5 km of the lines shown on figure 1. Estimated position of pediplain shown by heavy broken lines. Post-pediplain faults are shown as vertical since their hade is not known. Diagonal shading indicates major post-pediplain erosion. Neogene deposits stippled. Thin lines indicate topographic surface where relevant.

FIGURE 3. View looking 352° across the Zanbgo River from 5250 m col SW of Lhasa to show peneplain cut across southern part of Lhasa Terrane.

FIGURE 4. View looking SE across Nam Co to Nyainqentanglha Shan to show inselberg (centre, snow-covered) rising above pediplain.

FIGURE 5. Pediplain, folded into gentle syncline, cut across Jurassic and Cretaceous sediments, looking east across the southern part of the Zigetang Co from W of Gyanco.

(*Facing p.* 368)

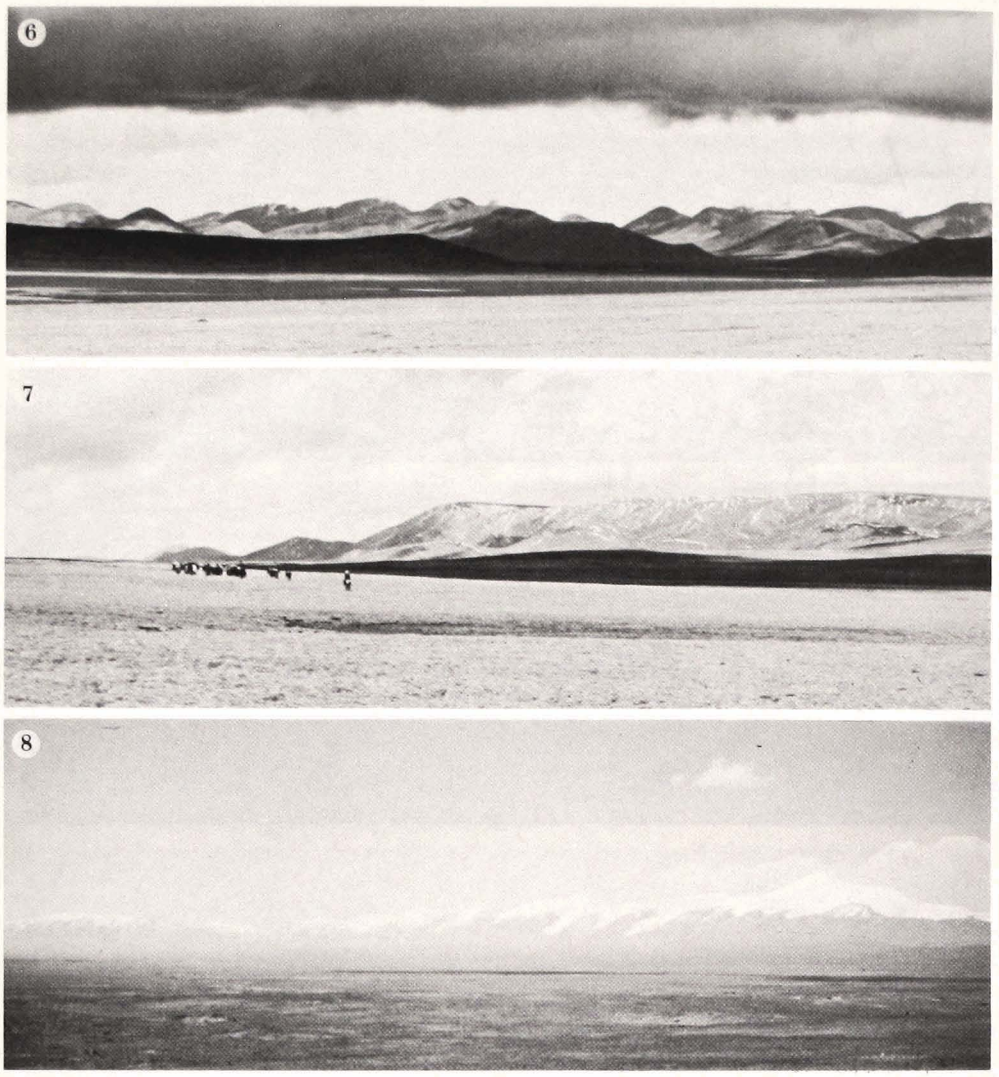

FIGURE 6. View of Tanggula Shan from south showing deeply dissected pediplan.

FIGURE 7. Pediplan cut across folded Eocene red beds. Fenghuo Shan, about 35 km NW of Erdaogou looking WSW.

FIGURE 8. View of Kunlun Shan, looking NW, with inselberg (right-hand side) rising above even summit level which represents pediplain.

is determined by several faults along the south side of Nam Co, a large lake, elevation 4716 m, in a tectonic basin. The profile (figure 2) suggests that the surface itself may be warped as well as faulted down to Nam Co.

The Nyainqentanglha Shan shows a regular longitudinal summit profile when seen from north or south, except for a single conical peak which rises abruptly to 7102 m, some seven or eight hundred metres above the general summit level (figure 4). Like a few others to be mentioned, this has the appearance of an inselberg. Transverse profiles across the section of the range south of Nam Co show that the even summit surface is only preserved, and even there in a deeply dissected state, across the central 15 km or less, beyond which erosion back from the northern fault scarp of the Yangbajain graben to the south and the series of faults to the north has left irregular slopes. The elevation of the remnants of the erosion surface varies from about 5700 m to about 6100 m, considerably higher than the block south of the Yangbajain graben. There is a distinct increase in elevation westwards but 1:100000 maps showing elevations were not available west of 90° 20′ E. Because of its elevation, the range was extensively glaciated and eroded during the Pleistocene. Snowfields and glaciers remain.

The central part of the Nyainqentanglha Shan is formed of granitoid orthogneisses, with metasediments. The orthogneiss is dated about 50 Ma and the rocks now exposed crystallized at depths of about 15 km (Harris, Xu, Lewis & Jin, this volume). Uplift and erosion of that thickness occurred before or during the planation represented by the summit surface. Further uplift raised the summit surface to its present elevation of about 6 km above sea level.

To the east the Nyainqentanglha Shan merges into a NNE-trending range immediately west of the Gulu graben, with which the Yangbajain graben connects (figure 1). In this part of the range the summit surface is tilted westwards. A profile along its eastern side (figure 2D–E) shows that the erosion surface stands at just over 6000 m; an inselberg rises to 6590 m.

(*d*) *The Nam Co Basin*

The profiles (figure 2 B–C & D–E) pass east of Nam Co. The lake forms part of the interior drainage system of the western part of the Plateau. The profiles suggest that the lake occupies a downwarp of the surface trending about 070° and pitching, east of the lake, at about 1 in 50 WSW.

(*e*) *The Bong Co fault complex*

A set of WNW-trending faults defines the Bong Co graben. The profile, passing about 10 km east of the lake, crosses a block on which the summit surface pitches at about 1 in 30 towards the WNW. A 10 km wide strip south of the fault complex cannot be interpreted without field control.

(*f*) *Area SW of Nagqu: Nevi Pun Co and Co Ngoin basins*

Immediately north of the northernmost of the Bong Co faults, there is a WNW-trending 12 km wide block with a regular summit surface at about 5000 m, rising slightly higher at the southern edge. Its northern limit is presumably a fault. North of the Nevi Pun Co the surface rises to another fault, trending nearly E–W, which defines the southern limit of the Co Ngoin trough. The northern limit of this trough is a fault trending ENE.

West of Co Ngoin, two fault strips, each a few kilometres wide, were clearly seen in the field to be tilted southwards. Southwards, the surface is warped into a shallow syncline (figure 5, plate 1).

(*g*) *Area from Co Ngoin to the Amdo graben*

Less than 3 km north of the northern boundary fault of the Co Ngoin basin, the summit elevation is just over 5100 m. For about 70 km northwards to the southern boundary fault of the Amdo graben the summit surface remains at an almost constant level (figure 2) with perhaps very slight undulations and a very slight fall to the north to about 4950 m immediately south of the Amdo graben. This uniform summit surface is cut across folded Jurassic in the southern part, then across the Precambrian Amdo gneisses which are thrust south over the Jurassic. The surface shows no reflection of the change in rock types, nor of the major thrust. It extends west nearly as far as Co Nag (figure 1).

(*h*) *The Amdo graben*

At the profile line, the elevation of the floor of this graben is just over 4600 m. The floor under the Pleistocene fill must be below 4500 m.

(*i*) *The Amdo range*

The topography of this structurally complex zone, between two major WSW-trending sinistral strike-slip faults, is irregular and no clear summit surface was recognized.

(*j*) *From the Amdo Range to the south foot of the Tanggula Shan*

Across this zone the summit surface is regular, dropping very slightly from just over 5100 m in the south to 5000 m in the north, except for the narrow (3 km) ridge of the Tojio Range, which rises to 5364 m. The reason for this narrow range is not clear.

At the northern side of this zone, Neogene deposits have been mapped. Their elevation is about 5000 m (figure 2).

(*k*) *The Tanggula Shan*

The Tanggula Shan has been very intensely eroded during the Pleistocene glaciations and the pre-glacial geomorphology could not be understood during the very short time available there on the Geotraverse, nor does the profile (figure 2) based on the 1:100000 maps show any regular pattern because the strip on which the profile is based is too narrow (*ca.* 10 km) relative to the scale of the glacial erosion. To try to overcome this, a profile was based on a strip 40 km wide, the centre line passing through Tanggula Pass, with a trend N 27.5° E, normal to the trend of the range. The highest points in successive 2 km strips normal to this centre line were plotted. The result still failed to show any convincing regular summit surface. This is surprising because a number of Chinese workers agree in recognizing a peneplain on the Tanggula Shan.

One possible interpretation of the irregular profile is that this part of the Tanggula Shan is an eroded remnant of a mountain range which existed before the planar surface was eroded and which withstood planation. Alternatively, it may be that the surface was irregularly deformed there. More probably, however, the difficulty in recognizing the surface is simply that the Tanggula Shan, like other high ranges such as the Nyainqentanglha Shan and the Kunlun Shan, all strongly glaciated, has been so intensely eroded that the surface is barely recognizable. During the Geotraverse, several small areas with accordant summit levels were seen. In each case they appeared tilted, and the slopes were in different directions. Their interpretation is doubtful. However, the distant view of the Tanggula Shan from the south

(figure 6) strongly suggests that it is carved from a block on which a planar erosion surface existed. The view is essentially similar to those of the Nyainqentanglha Shan and the Kunlun Shan. The reality of the surface on the Tanggula Shan is therefore accepted.

The northern limit of the Tanggula Shan is rather indefinite. The elevation diminishes gradually but irregularly northwards; but even as far north as 25 km east of Wenquan a subcircular plutonic intrusion rises (as an inselberg?) to 5883 m, nearly 700 m above the surrounding area with summit levels at about 5200 m.

Immediately north of Yanshiping the mountainous country ends rather suddenly.

(*l*) *The region between the Tanggula Shan and the Kunlun Shan*

This is a wide region of relatively low relief, the elevation ranging from a maximum of just under 5500 m in the Fenghuo Shan down to about 4400 m. About half of the region is underlain by Neogene fluviatile and lacustrine deposits (figure 1). These areas form the lower ground, occupying irregular tracts roughly elongated sub-parallel to an array of faults, slightly curved but with a general ESE–WNW trend. The elevation of the surface of the Neogene deposits drops gradually eastwards at about 1 in 50. The pre-Neogene rocks form irregular hilly areas separating the Neogene deposits. While some contacts of the Neogene with older rocks are post-Neogene faults, at most of the contacts the Neogene is unconformable on older rocks, and many of the shapes of the Neogene areas are irregular. Their distribution and shapes are essentially the same as those of the hundreds of lakes scattered across the Tibet Plateau farther west. As could be seen in the case of the array of lakes near the Geotraverse, between the Nyainqentanglha Shan and Amdo, the lakes are in tectonic depressions, most of which are bounded by faults. Their irregular shapes are the result of the complexity of the fault patterns (figure 1).

Most of the hills formed by the older rocks between the lower areas of Neogene deposits are not, in the Geotraverse area, extensive enough to give any useful information about any erosion surface. However in the Fenghuo Shan, across a width of about 25 km, a fairly uniform summit surface, at an elevation of about 5200 m, can be seen (figure 7, plate 2) and again just south of Wudaoliang, a range, trending slightly south of east, about 10 km wide and bounded by faults, rises to a regular summit surface whose elevation is about 5000 m.

(*m*) *The Kunlun Shan*

The even summit level of this range is obvious when viewed from the south (figure 8). A single conical peak rises abruptly above the even summit level. The range is deeply eroded especially along the great faults by which it is traversed. The surface slopes down northwards, across a width of nearly 70 km, from about 5900 m to about 5000 m. North of that its elevation drops much more rapidly until, some 40 km east of Golmud in a borehole, it is at about 1580 m. Further out under the Qaidam Basin, the basement surface is much deeper still. It is not clear whether the drop from Kunlun to Qaidam is achieved by faulting, flexure or both but a remarkable planar area about 60 km 225° from Golmud, not accessible during the Geotraverse, may be a remnant of cover on the erosion surface. It appears to slope much more gently north than the general slope down to the Qaidam Basin, suggesting that the slope represents a series of fault steps rather than a flexure.

(n) Summary of evidence from the profile of summit elevations

From just north of the Zangbo River to the southern edge of the Tanggula Shan, the continuity of a well-defined even summit surface is clearly established. Across the Tanggula Shan it is much less clear although Chinese workers who have studied it there in more detail than was possible during the Geotraverse are satisfied that it occurs there. Between the Tanggula Shan and the Kunlun Shan it can be recognized on two of the ranges rising above the mass of Pliocene and Pleistocene deposits which fill an array of tectonic depressions. On the Kunlun Shan a surface identical in its features to the surface traced across the south of the Plateau is clearly visible. The sudden changes in elevation of the surface, for example at the Yangbajain graben and at the south side of the Kunlun Shan, are clearly the result of deformations, usually faults. The remnants of the surface have not been isolated by erosion. The surface must have extended across the whole Plateau.

3. Evidence from the drainage systems

The drainage of the Tibetan Plateau can be separated into several systems: (i) northwards into the Tarim and Qaidam basins; (ii) internal drainage, into lakes in the western half of the Plateau; (iii) eastwards and southwards across the eastern half of the Plateau: the Jinsha, Lancang and Nujiang river systems; (iv) eastwards, then deviously south, along the Zangbo River (mainly following the Indus–Zangbo Suture); (v) southwards through, and from, the Himalayas. The Geotraverse was near the eastern limit of internal drainage.

The complexity of the fault pattern which produced the structural depressions containing the vast number (some 1500) of lakes on the Plateau is apparent in the area between the Nyainqentanglha Shan and Amdo. The drainage pattern is correspondingly complex. The eastward drainage becomes increasingly constricted and structurally controlled southeastwards. The western, dendritic, part of this drainage system is remarkably independent of structures, in particular the array of faults, many with substantial post-Pliocene displacements, which curve across the eastern part of the Plateau. In many places, rivers cut through uplifted blocks, in a manner which clearly shows that they are antecedent in relation to the upfaulting of the blocks. Examples are the river which flows out of the Yangbajain graben, across the Lhasa block (figure 9), and the river which flows through the Kunlun Shan from Kunlun Pass.

The simplicity of the drainage pattern has evidently been modified by capture, erosion along faults and subsidence of basins. Nevertheless, its remarkable independence of young faults and the simplicity of the dendritic pattern inescapably imply that it originated on an extensive relatively flat surface, quite unlike the present 'Plateau' with its diversity of mountain ranges, fault blocks and tectonic depressions.

It is concluded that the drainage originated on a surface of very low relief, before the major dislocations which determine the existing topography.

There are indications that the Gangdise Shan, at least westwards from Lhasa, the Tanggula Shan and the Bayan Har Shan may have been slightly elevated at the time the drainage pattern was initiated since they form watersheds. It is tempting to speculate that the Zangbo is a relic from Tethys, into which the Andean Gangdise arc must have drained, but this cannot be proved.

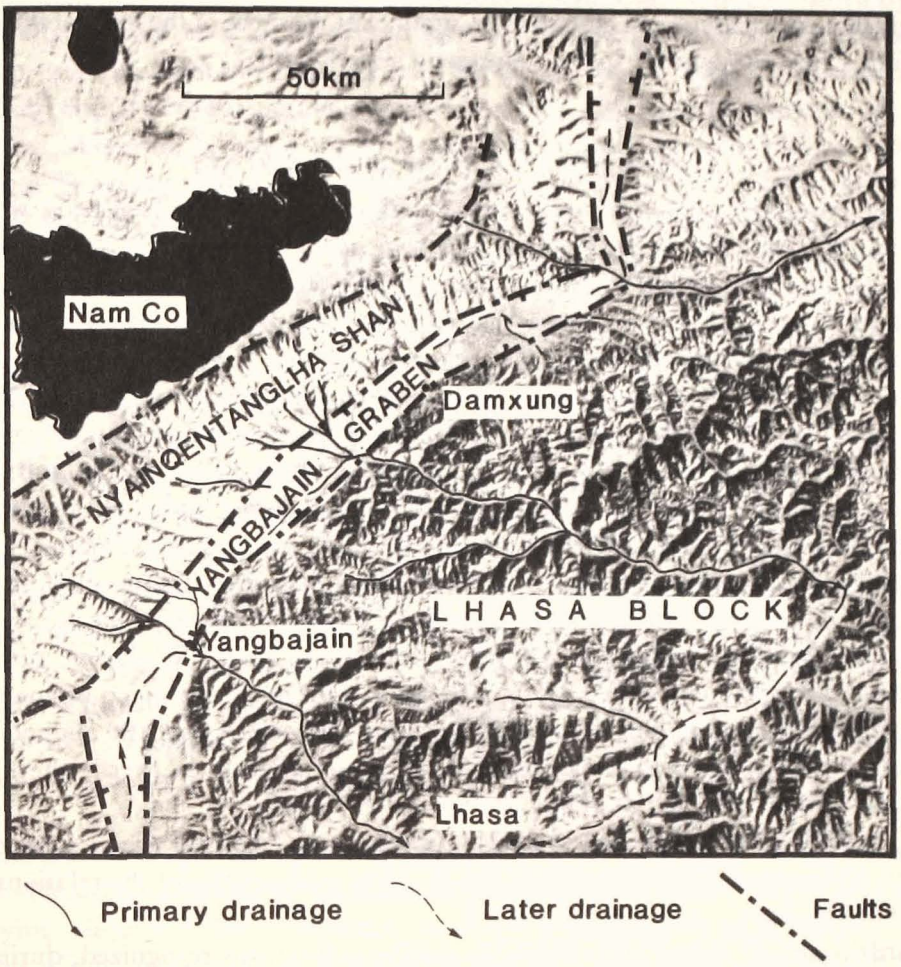

FIGURE 9. Satellite view of Nam Co, Nyainqentanglha Shan, Yangbajain graben and southern part of Lhasa Terrane, showing antecedent primary drainage cutting through fault scarp along SE side of Yangbajain graben.

4. THE PROCESS BY WHICH THE EROSION SURFACE WAS FORMED

The summit erosion surface might be attributed to peneplanation, pediplanation (King 1962) or 'equilibrium' (Selby 1985). The last is rejected because it seems impossible that such a variety of rock types could be so evenly lowered many kilometres by erosion without the control of a base level, yet still leave isolated peaks standing high above the general surface. The reason that pediplanation seems more plausible than peneplanation is that there are, as on the Nyainqentanglha Shan and on the Kunlun Shan, rare but conspicuous isolated peaks which rise abruptly up to 700 m above the general summit surface. Their form suggests that they are inselbergs formed by scarp retreat although without visiting them it remains uncertain why they stand so high. Since, however, it is persuasively argued (Twidale 1976) that peneplanation and pediplanation are not sharply distinct processes characteristic of different climatic regimes (temperate and arid) but can occur together, the distinction may be unimportant. As envisaged by King (1962), however, a pediplain is necessarily diachronous, younger inland

than at the base level (not necessarily the sea) whence it started, and so the distinction may be chronologically, even though not climatically, significant. Because of the form of the inselbergs, it is concluded that the summit surface represents a pediplain.

5. The age of the erosion surface

The surface transects the folded and thrust Fenghuoshan Group of red beds, which range up to Middle Eocene. This relationship is best seen in the Fenghuo Shan. The surface also transects the folded and thrust Linzizong, dated as 60–50 Ma and deformed (as a result of collision) later than 45 Ma. It cannot therefore be older than late Eocene. The upper limit is less certain because no Oligocene beds were seen in the Geotraverse area and the Neogene beds are not well dated. Published data indicate that west of the Geotraverse area, in the Lunpola Basin (about 89° 30′ E, 32° N), there is over 3 km of Tertiary sediments, ranging from mid- and late Eocene and Oligocene clastics to Pliocene lake beds (Song & Liu 1981), or from possible late Eocene to Oligocene (Xia 1983). The latter author indicates an unconformity between the Miocene and the Oligocene within the Deqen (Dengqen) Formation but it is not clear whether it is structurally significant. It seems likely that deposition in the Lunpola Basin was essentially continuous from late Eocene or early Oligocene times to the Miocene. In the Qaidam Basin also deposition was apparently continuous from the Eocene onwards; the Eocene is unconformable on Cretaceous or older rocks. However, since such basins could have existed during the planation, they do not date it. In the Tanggula Shan, 100 and more km west of the Geotraverse, basalts and andesites of Miocene age are said to overlie the (Tanggula) erosion surface, there standing at about 5900 m (Li *et al.* 1981).

Similar, possibly coeval volcanics near Maquiang, at and beyond the western end of the Yangbajain graben, are dated at about 10 Ma (Coulon *et al.* 1986) but the relationship to the surface is not known.

Westwards from the Geotraverse area, the erosion surface was recognized, during a rapid traverse in 1986 from Lhasa to Kathmandu, as far as the northern slopes of the Himalaya. It appears to extend across the area in which strongly folded marine Eocene rocks occur, and across the Lhagoi Kangri granites dated at *ca.* 10 Ma (Maluski 1984). The same conclusion was reached by Armijo *et al.* (1986).

The combination of evidence indicates that the age of the pediplanation is mid- to late Miocene, *ca.* 10 Ma. The erosion which produced the surface must have continued for a long time. The 'age' represents the termination of the process, probably when erosion could no longer keep pace with faulting.

6. A Pliocene peneplain not confirmed

It is thought by some workers that a second, lower and younger (Pliocene) surface can be recognized (Li *et al.* 1981; Zhang *et al.* 1981; Xu Shuying 1981). The older surface 'manifested by peaks and platforms of similar altitudes' is regarded as Oligo-Miocene; the younger 'part of the present Plateau' is thought to be Pliocene (Zhang *et al.* 1981). They seem to imply that the remnants of the higher, older surface are at a uniform elevation and were isolated not by faulting but by erosion, but as can be seen from the profile (figure 2), the remnants are not at a uniform level and it is clear that the straight scarps which bound many of the high ranges are fault scarps. The high ranges cannot have been simply separated by erosion.

Since the high erosion surface seen on the Kunlun Shan must be faulted down by the south Kunlun faults (as well as being displaced laterally), and since it is at least older than late Miocene, it probably underlies many of the Plio-Pleistocene fluviatile and lacustrine deposits which occupy much of the region between the Kunlun and Tanggula ranges. These deposits occupy areas where the Miocene erosion surface was faulted or warped down relative to the Kunlun and Tanggula ranges. The faulted surface was substantially eroded before the Plio-Pleistocene deposits were formed; on the northern flank of the Tanggula Shan they were deposited in a deep valley (figure 2) and immediately north of the Fenghuo Shan, itself truncated by the Miocene surface, there are isolated hills rising through the Plio-Pleistocene deposits (figure 2). These inliers are too irregular to be interpreted as separated by faulting from the main Fenghuo Shan block. The original northern limit of the Fenghuo Shan block may have been a fault, now buried under the Plio-Pleistocene.

The present surfaces of the Plio-Pleistocene deposits are not flat but gently undulating. Their elevation varies greatly from one to another (figure 2). These variations are not systematic in a manner which could be attributed to the deformation of a formerly planar erosion surface. On the contrary, their elevations are simply related to their positions in the antecedent drainage system. Farther west, in the region of interior drainage, many of the existing lakes are within areas of Plio-Pleistocene deposits and are evidently remnants in pre-existing basins. The existing subdued topography of the Plio-Pleistocene deposits cannot be interpreted as a single Plateau-wide Pliocene peneplain. That topography has evolved by erosion adjusted to the elevation of rivers which in the west drain into isolated basins while those to the east form a pattern developed on the Miocene surface before the formation of the Plio-Pleistocene basins.

It is concluded that there is no Pliocene peneplain across the Tibet Plateau. The topography of the Plio-Pleistocene deposits is essentially the result of aggradation and then stream erosion. The varying elevations imply separate areas of deposition in structural and erosional depressions within an antecedent drainage system, not a single unified erosion surface.

7. The uplift history of the plateau

The last remnants of the Tethyan ocean south of the Lhasa Terrane are represented by Lower Eocene limestones near Tingri (87° E, 24° 40′ N). Palaeogene fluviatile red beds deposited in foreland-type and ramp valley basins (Leeder *et al.*, this volume) demonstrate considerable relief at that time. All these were strongly deformed as a result of the India–Asia collision. During Oligocene and early Miocene times, erosion was dominant over the Plateau; deposition was confined to a few mostly E–W trending basins including Lunpola (90° E, 32° N). The thick (*ca.* 2000 m) Oligocene clastic deposits in the Lunpola basin, overlying a basal conglomerate which may be Eocene (Xia 1983), contain a tropical flora; the Plateau was at a low altitude (*ca.* 500 m) (Xu Ren 1981; Li *et al.* 1981; Song & Liu 1981). The floras from the Lower Miocene beds of the Lunpola Basin suggest a complex topography with some parts over 2000 m elevation and valleys below 1000 m (Xu Ren 1981).

A mid- to late Miocene flora from the Wulong Formation in the Namling area, on the southern slopes of the Gangdise Shan, about 150 km west of Lhasa, is thought to imply an elevation of over 1500 m and a humid warm climate (Guo 1981).

The relation of these and other Miocene deposits to the pediplain is not clear. It seems that by mid-Miocene times pediplanation had reduced a vast region to an even surface from which

only a few inselbergs projected. The elevation of the Plateau, even some 1000 km from the ocean, was probably only a few hundred metres. The pediplain extended to the northern flanks of the present Himalaya and, if correctly correlated, to the present Qilian mountains (Li *et al.* 1981), so it is unlikely that it was adjusted to an intracontinental base level (cf. Armijo *et al.* 1986).

By late Miocene times, differential uplift was occurring. On the southern slopes of the Gangdise Range, at Moincer (50° 30′ E, 31° 12′ N), the elevation was more than 1500 m and deciduous broad-leaved forests flourished (Xu Ren 1981; Guo 1981).

By the Pliocene, the Miocene pediplain had been severely dislocated by faults and deeply eroded (Xu Shuying 1981). The Gangdise, Tanggula and Kunlun ranges were relatively uplifted to elevations of 2000 m or more (Zhang *et al.* 1981; Kong & Du 1981). Fluviatile and lacustrine deposits, mainly silts and clays, and also, in the north, evaporites, were laid down in shallow tectonic depressions similar to those which now contain lakes in the western half of the Plateau. Other fluvial deposits accumulated in deep (*ca.* 1000 m) valleys in the Tanggula Shan. The floras varied from tropical forest to subtropical steppe; the *Hipparion* fauna was widespread.

If the Plio-Pleistocene sediments were deposited in many separate tectonic depressions and erosional valleys, related to an antecedent drainage system initiated on a Miocene pediplain, they need not imply a low elevation, as they would if they were related to a Pliocene peneplain.

The geomorphological evidence thus shows that until about 10 Ma ago, erosion across the Plateau and beyond kept pace with uplift, which was slow. Unpublished $^{39}Ar/^{40}Ar$ ages on micas and feldspars from the Nyainqentanglha granite indicate rapid uplift over the last 10 Ma (W. Kidd, pers. comm., 1987). No new evidence was obtained during the present work to confirm or modify the view (e.g. Zhang *et al.* 1981) that the major uplift occurred in the Pleistocene. This view is based partly on the evidence, from floras and faunas, of progressively changing climate, partly from fission track data from the Himalayas which indicates very rapid recent uplift, and partly on the sudden deposition in the Pleistocene, of coarse conglomerates, on top of earlier finer-grained deposits, both in the Siwalik trough to the south and in the Qaidam basin to the north of the Plateau. Pliocene molassic deposits have recently been found along the eastern margins of the Plateau in Darji, Qionglai and Emei (Sichuan province) (Zheng 1986). Episodic post-Pliocene uplift is inferred from three knickpoints recognized on the major rivers – at 4500 m, 3500 m and 2800 m on the Zangbo River (Zhang *et al.* 1981; Yang *et al.* 1983).

The amount of crustal shortening by internal deformation across the Tibet Plateau since the pediplanation cycle was ended some 10 Ma ago cannot be more than a few per cent. Wide stretches of the pediplain are almost flat (figure 3), although Pliocene strata are locally overthrust and folded and dips of 5° are common. Crustal shortening during this period was mainly south of the Main Central Thrust in the Himalayas. However, the geomorphological evidence does not exclude shortening by lateral extrusion of crustal blocks limited by strike-slip faults (Tapponnier *et al.* 1986).

References

Academia Sinica 1980 *A Scientific Guidebook to South Xizang* (Tibet) (ed. Yin Jixiang & 13 others), 104 pp.

Armijo, R., Tapponnier, P., Mercier, J. L. & Han Tonglin 1986 Quaternary extension in southern Tibet: field observations and tectonic implications. *J. geophys. Res.* **91**, 13803–13872.

Berkey, C. & Morris, F. K. 1927 *The Geology of Mongolia*, **2**. Am. Mus. Nat. Hist., 474 pp.

Coulon, C., Maluski, H., Bollinger, C. & Wang, S. 1986 Mesozoic and Cenozoic volcanic rocks from Central and Southern Tibet; ^{39}Ar-^{40}Ar dating, petrological characteristics and geodynamical significance. *Earth planet. Sci. Lett.* **79**, 281–302.

de Terra, H. 1933 Geomorphologische Studien zwischen oberen Industal und sudlichen Tarimbecken. *Zeit. f. Geomorph.* **5**, 79–131.

Guo Shuanxing 1981 On the elevation and climatic changes of the Qinghai-Xizang Plateau based on fossil angiosperms. In *Geological and Ecological Studies of Qinghai-Xizang Plateau* **1**, 201–206.

King, L. C. 1962 *Morphology of the Earth*. Edinburgh: Oliver and Boyd. 726 pp.

Kong Zhaoshen & Du Naiqui 1981 Preliminary study on the vegetation of the Qinghai-Xizang Plateau during Neogene and Quaternary periods. In *Geological and Ecological Studies of Qinghai-Xizang Plateau* **1**, 239–246.

Li Jijun, Li Bingyuan, Wang Fubao, Zhang Qingsong, Wen Shixuan & Zheng Benxing 1981 The process of the uplift of the Qinghai-Xizang Plateau. In *Geological and Ecological Studies of Qinghai-Xizang Plateau* **1**, 111–118.

Maluski, H. 1984 ^{39}Ar-^{40}Ar ages of some granitic bodies and metamorphic series of the north Himalayan belt (Southern Tibet, China). *Paper presented to the International Symposium on Geology of the Himalayas*. Ministry of Geology, Chengdu, People's Republic of China.

Norin, E. 1935 Tertiary of the Tarim basin. *Bull. geol. Soc. China* **14**, 337–347.

Selby, M. J. 1985 *Earth's Changing surface. An Introduction to Geomorphology*. Oxford: Clarendon Press. 607 pp.

Song Zichen & Liu Gengwu 1981 Tertiary palynological assemblages from Xizang with reference to their paleogeographic significance. In *Geological and Ecological Studies of Qinghai-Xizang Plateau* **1**, 207–214.

Tapponnier, P., Peltzer, G. & Armijo, R. 1986 On the mechanics of the collision between India and Asia. In *Collision Tectonics* (ed. M. P. Coward & A. C. Ries) Geol. Soc. Sp. Publ. **19**, 115–157.

Twidale, C. R. 1976 *Analysis of Landforms*. Wiley: New York. 572 pp.

Yang Yichou *et al.* 1983 *Geomorphology of Xizang (Tibet)*. 238 pp. (in Chinese). Beijing: Science Press.

Xia Jinbao 1983 Cenozoic of Bangoin and its bordering Xizang (Tibet) (in Chinese with English Abstract). In *Cont. Geology Qinghai-Xizang (Tibet) Plateau* **3**, 243–154. Beijing: Geological Publishing House.

Xu Ren, 1981 Vegetational changes in the past and the uplift of Qinghai-Xizang Plateau. In *Geological and Ecological Studies of Qinghai-Xizang (Tibet) Plateau* **1**, 139–144.

Xu Shuying 1981 The evolution of the palaeogeographic environments in the Tanggula mountains in the Pliocene-Quaternary. In *Geological and Ecological Studies of Qinghai-Xizang (Tibet) Plateau* **1**, 247–256.

Zhang Qingsong, Li Bingyuan, Yang Yichou, Yin Zeshen & Wang Fubao 1981 Basic characteristics of neotectonic movements of Qinghai-Xizang Plateau. In *Geological and Ecological Studies of Qinghai Xizang Plateau* **1**, 103–110.

Zeng Binghua 1986 Qinghai-Xizang Plateau lineaments and their characteristic activities. *Seismology & Geology* **8**, 25–34 (in Chinese).

Phil. Trans. R. Soc. Lond. A **327**, 379–413 (1988) [379]
Printed in Great Britain

The tectonic evolution of the Tibetan Plateau

By John F. Dewey[1], F.R.S., Robert M. Shackleton[2], F.R.S., Chang Chengfa[3] and Sun Yiyin[3]

[1] *Department of Earth Sciences, Parks Road, Oxford OX1 3PR, U.K.*
[2] *The Croft Barn, Church Street, East Hendred, Oxfordshire OX12 8LA, U.K.*
[3] *Academia Sinica, Beijing, People's Republic of China*

The Tibetan Plateau, between the Kunlun Shan and the Himalayas, consists of terranes accreted successively to Eurasia. The northernmost, the Songban–Ganzi Terrane, was accreted to the Kunlun (Tarim–North China Terrane) along the Kunlun–Qinling Suture during the late Permian. The Qiangtang Terrane accreted to the Songban–Ganzi along the Jinsha Suture during the late Triassic or earliest Jurassic, the Lhasa Terrane to the Qiangtang along the Banggong Suture during the late Jurassic and, finally, Peninsular India to the Lhasa Terrane along the Zangbo Suture during the Middle Eocene. The Kunlun Shan, Qiangtang and Lhasa Terranes are all underlain by Precambrian continental crust at least a billion years old. The Qiangtang and Lhasa Terranes came from Gondwanaland. Substantial southward ophiolite obduction occurred across the Lhasa Terrane from the Banggong Suture in the late Jurassic and from the Zangbo Suture in the latest Cretaceous–earliest Palaeocene. Palaeomagnetic data suggest successive wide Palaeotethyan oceans during the late Palaeozoic and early Mesozoic and a Neotethys which was at least 6000 km wide during the mid-Cretaceous.

Thickening of the Tibetan crust to almost double the normal thickness occurred by northward-migrating north–south shortening and vertical stretching during the mid-Eocene to earliest Miocene indentation of Asia by India; Neogene strata are almost flat-lying and rest unconformably upon Palaeogene or older strata. Since the early Miocene, the northward motion of India has been accommodated principally by north–south shortening both north and south of Tibet. From early Pliocene to the Present, the Tibetan Plateau has risen by about two kilometres and has suffered east–west extension. Little, if any, of the India–Eurasia convergence has been accommodated by eastward lateral extrusion.

1. Introduction

This tectonic synthesis of the work done during and after the 1985 Royal Society–Academia Sinica Tibet Geotraverse has been written by Robert Shackleton (pre-Cretaceous tectonics) and John Dewey (Cretaceous–present). The views expressed are, unavoidably, to some extent theirs but the work on which the synthesis is based was done by all of the team. When discussing regions away from the Geotraverse, we have relied especially on a major synthesis of the tectonics of the whole Tibetan Plateau and beyond by Chang Chengfa and Sun Yiyin, which, it is hoped, will be published in full elsewhere.

It is now generally accepted that the Tibetan Plateau north of the Indus–Zangbo Suture consists of a series of microplates that were accreted to Asia before the India–Asia collision. The basis for this interpretation was the recognition by Chinese geologists (Chang & Zheng 1973; Chang & Pan 1981, 1984) of many ophiolites, some concentrated along zones which were

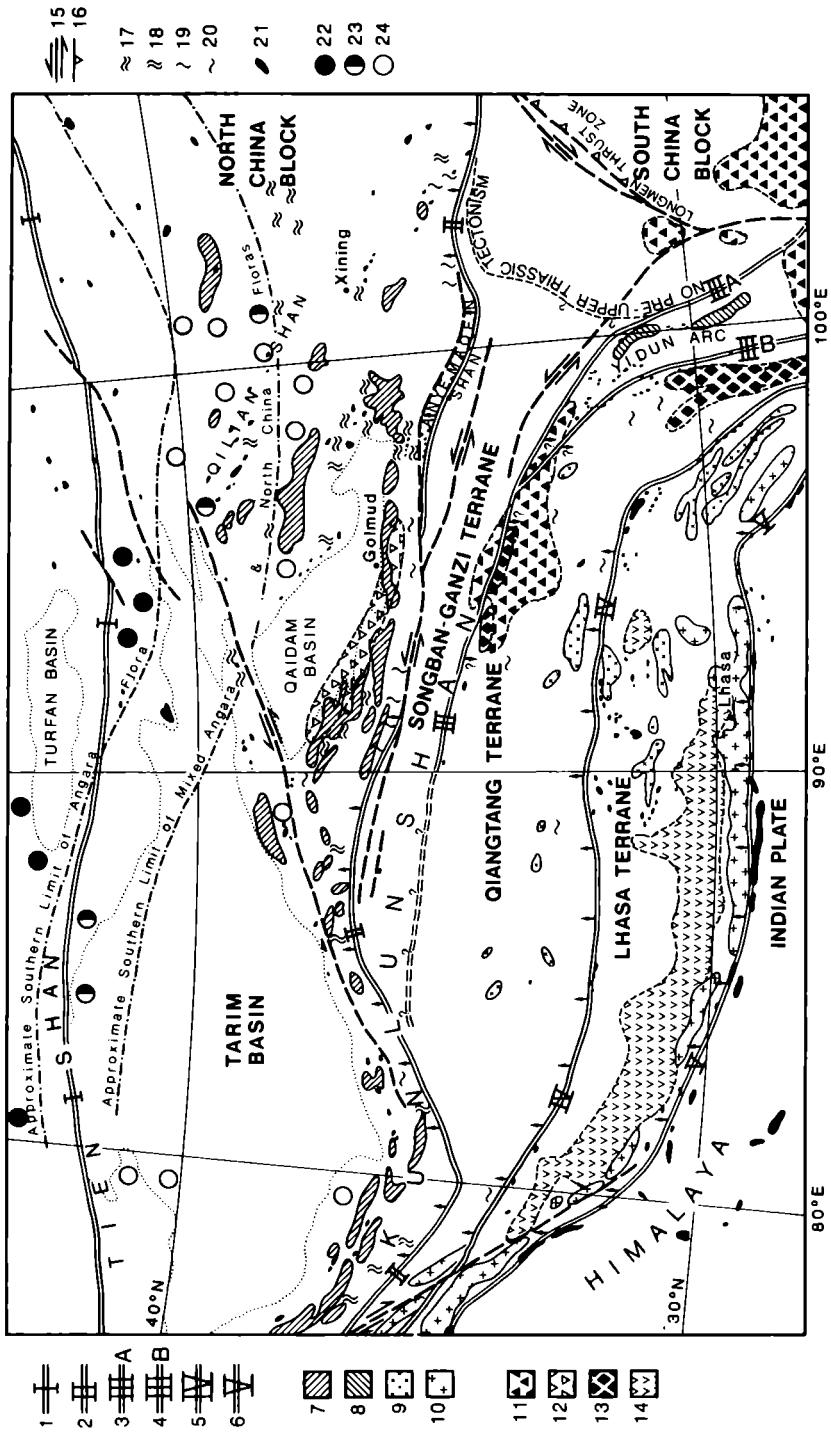

FIGURE 1. Tectonic map of Tibet, based on 1:1.5 M Geological Map, Qinghai–Xizang (Tibet) Plateau (1980); 1:1 M Geological Map, Qinghai Province (1981); 1:8 M Tectonic Map of Asia (1982); Watson *et al.* 1987; Zhang & He 1985 and Geotraverse data. 1: Tien Shan–Hegen Suture, 2: Kunlun–Qilian Suture, 3 & 4: (III) Jinsha Suture (3: Litang Suture, 4: Jinsha Suture, continued), 5: Banggong Suture, 6: Indus–Zangbo Suture, 7: Upper Palaeozoic plutons, 8: Triassic plutons, 9: Cretaceous plutons, 10: Late Cretaceous–Tertiary plutons, 11: Permian rift-related volcanic rocks, 12: Permian subduction-related volcanic rocks, 13: Triassic subduction-related volcanic rocks, 14: Tertiary subduction-related volcanic rocks, 15: strike-slip faults, 16: thrusts, 17: Lower Palaeozoic tectonism, 18: Carboniferous tectonism, 19: Permian tectonism, 20: Late Triassic (or early Jurassic) tectonism, 21: ophiolite, 22: Angaran flora, 23: Mixed Angaran and North Cathaysian flora, 24: North Cathaysian flora. Small arrows on sutures indicate inferred direction of subduction.

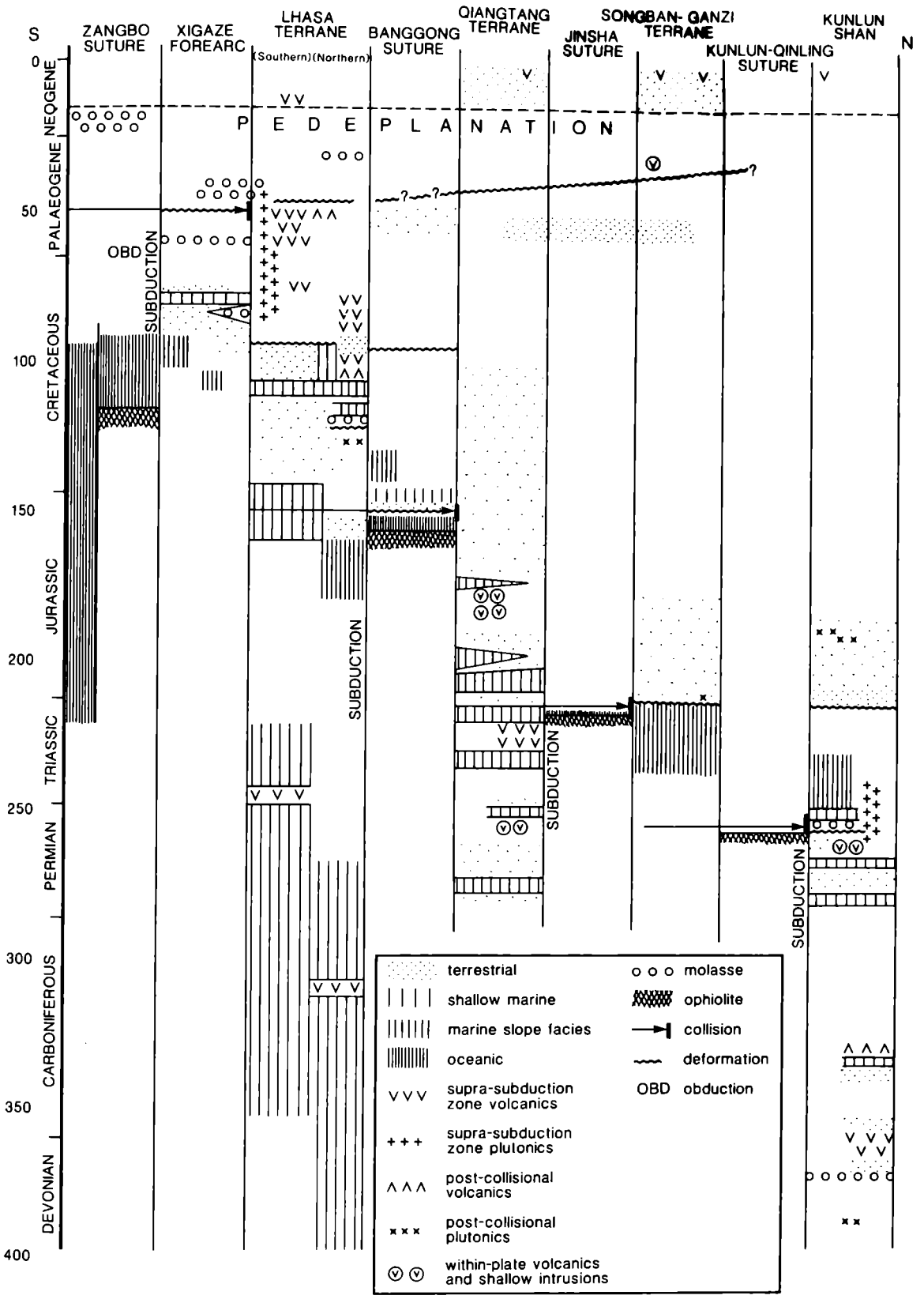

FIGURE 2. Summary of the tectonic chronology of Tibet.

interpreted as sutures, combined with the knowledge that the deformations become younger southwards across the Plateau. One major aim of the 1985 Geotraverse was to define the history of microplate accretion more precisely.

In the previous papers in this volume, the Lhasa, Qiangtang and Kunlun Terranes, separated by the Banggong and Jinsha Sutures, are accepted as established. However, ophiolites are widely scattered across the Plateau, rather than concentrated in distinct linear zones (figure 1); few of them are dated; the criteria for distinguishing the terranes are inconclusive and the supposed ophiolites may not all represent fragments of oceanic crust. Therefore, because we are uncertain whether the ophiolites of the Lhasa Terrane are the klippen of a single sheet obducted from the Banggong Suture, our previous separation into terranes may not be valid. There may be more sutures; those recognized may not have been correctly located or extrapolated. Here, therefore, we do not assume *a priori* that the sutures and terranes have been defined.

The account is arranged chronologically. The supposed sequence of events is shown in figures 2 and 10.

2. Precambrian tectonics

Within the Geotraverse area, only one undoubtedly Precambrian group of rocks, the Amdo Gneisses, was seen. Gneisses in the southwest Nyainqentanglha Shan and a sedimentary series in the Kunlun Shan have been interpreted by some workers as Precambrian.

The gneisses in the Nyainqentanglha Shan include granitoid and migmatitic gneisses. The isotopic data (Harris, Xu, Lewis, Hawkesworth & Zhang, this volume) indicate the emplacement, approximately 50 Ma ago, of granitic melt, of anatectic origin, from a middle crustal source with an age of approximately 1000 Ma. The gneiss contains inherited zircons dating from about 1000 to 2000 Ma ago. These gneisses are not Precambrian. No clear evidence has been published that indicates that any Precambrian rocks are exposed in the Nyainqentanglha Shan. The age of the metasediments, which near to the granitoid gneiss contain staurolite, garnet, andalusite and sillimanite (Harris, Holland & Tindle, this volume) is uncertain but there is nothing to suggest that they are Precambrian.

The Amdo Gneisses comprise pelitic, psammitic and calcareous metasediments, amphibole gneisses and tonalitic gneiss. The latter has given a zircon age of 531 ± 14 (Xu *et al.* 1985) and Nd model ages of 1242 and 1646 Ma. These Nd model ages are taken to indicate a mid-Proterozoic crustal source (Harris, Xu, Lewis, Hawkesworth & Zhang, this volume). The intense D_1 foliation was isoclinally folded on N-striking axial surfaces and then refolded on E–W axes (Coward *et al.*, this volume). These structures are likely to represent continued deformation during cooling. Later biotite grade shear zones and thrusts are thought to be Mesozoic, perhaps at the time of sphene growth, 171 ± 6 Ma ago (Xu *et al.* 1985) or ophiolite obduction (*ca.* end-Jurassic). The whole assemblage was intruded by the Amdo bimodal granite suite dated 130 ± 10 Ma (Xu *et al.* 1985). The anatexis of tonalitic magma from Proterozoic crust and the associated sequence of intense deformations suggest a collisional environment. Considering the time involved, from the start of collision to anatexis in thickened crust and rise of the melt, it seems clear that at least the metasediments in the Amdo Gneisses are late Precambrian. The assemblage invites comparison with the Pan-African of Gondwanaland whence the Lhasa Terrane came, as well as with the array of granites in the Himalayas dated between 550 and 450 Ma.

The sequence in the Kunlun Shan, attributed to the late Precambrian and Cambro-Sinian, comprises marbles, pelites, greywackes and possibly basic volcanics. Stromatolites thought to indicate a Precambrian age have been found in the marbles at several localities (Yin *et al.*, this volume). The extent and precise age of these rocks is uncertain: they include some that are almost certainly Ordovician because, near the top, they include highly characteristic mass flow deposits with limestone clasts (Leeder *et al.*, this volume), and some that are thought to be Permian (Smith & Xu, this volume). Whether or not some of these rocks are Precambrian, there is no evidence that they were affected by any Precambrian tectonism. We conclude that the only exposed rocks in the Geotraverse area that show Precambrian tectonism or metamorphism are the Amdo Gneisses.

As well as the evidence from exposures, there is important isotopic evidence concerning the age of the deeper crust under the Plateau. Inherited zircons in the Nyainqentanglha granite gneiss give upper intercept ages of *ca.* 1000 and 2000 Ma (Xu *et al.* 1985) and Nd model ages also indicate the presence of Precambrian (1000 Ma or older) crust beneath the Lhasa and Kunlun Terranes. Evidence from the Qiangtang Terrane is not available but there can be little doubt that it too is underlain by Proterozoic or older crust. The Nd model ages show significant variations across the Plateau. Some of these differences are attributed to fractionation processes but those from the Amdo Gneisses in the north of the Lhasa Terrane (1242 and 1646 Ma) and from the Golmud Granite in the north of the Kunlun Shan (source model age 1100–1250 Ma) are significantly higher than the others, which are about 1000 Ma (Harris, Xu, Lewis, Hawkesworth & Zhang, this volume). From this evidence, it can be concluded that the whole of the Plateau is underlain at depth by Precambrian crust at least 1000 Ma old. The Amdo Gneisses in the Lhasa Terrane show exposed evidence of an end-Proterozoic ('Pan-African') collision. Neither the extent nor trend of this end-Proterozoic domain is known.

There is no evidence to show the existence of Archaean rocks under the Plateau: an Archaean component in the Carboniferous glaciomarine diamictite in the Lhasa Terrane is presumed to have come from the Indian shield. From the palaeolontological data, it seems that the Lhasa and Qiangtang Terranes were formerly attached, with India, to Gondwanaland, but the Precambrian exposures in Tibet are too limited to suggest any pattern of connections with the Precambrian of India.

3. Lower Palaeozoic tectonism

About 20 km south of Golmud, the basal conglomerate of the Upper Devonian rests unconformably on late Precambrian or Cambro–Sinian beds which include sericite schists and marbles (Zhang, appendix to Coward *et al.* this volume). The Devonian and Carboniferous sediments and volcanics of that area are folded and commonly dip steeply but they are not cleaved and are only metamorphosed near contacts with plutons. Farther south between Naij Tal and the Xidatan, the supposed Cambro-Sinian sequence (Yin *et al.*, this volume) appears to pass up continuously into rocks identified as Lower Ordovician by the presence of distinctive mass-flow deposits with limestone clasts (Leeder *et al.*, this volume). These relationships indicate a post-Ordovician, pre-Upper Devonian, cleavage-producing deformation and low-grade metamorphism. No Silurian is known in the part of the Kunlun Shan reached during the Geotraverse so the timing is imprecise. Another indication of such a deformation event is that

the Ordovician rocks of the central Kunlun consistently show high finite strains. In the mass-flow deposits, the limestone clasts usually show $X:Z = \sim 3:1, X$ (the extension direction) plunging steeply down dip on the cleavage. Fold axes often plunge 70° or more either eastwards or westwards, indicating sheath folds such as are not seen in the Upper Palaeozoic or Triassic rocks of the area. In the Triassic rocks of the middle Kunlun, finite strains are low except in narrow shear zones, and in the northern Kunlun, Triassic dykes are undeformed. Fragments of limestone, probably Lower Palaeozoic (as the largest clasts, up to 5 m long, certainly are) show cleavages in different directions in different clasts in only weakly deformed Triassic boulder conglomerates, where rotation during deformation is unlikely (M. Leeder pers. comm. 1985; RMS, loc. S551). Two cleavages at an acute angle can be seen in some of the Ordovician rocks of the middle Kunlun Shan. These various observations, taken together, show that in the parts of the central and northern Kunlun studied during the Geotraverse, there was a phase of strong deformation in the interval between the Ordovician and the Upper Devonian. Because the attitude of the main cleavage in the Palaeozoic and Triassic in those areas is essentially the same, the pre-Devonian and post-Triassic cleavage and folds must have been virtually coaxial. Southwards through the Kunlun Shan, the later, post-Triassic deformation becomes increasingly intense and the early Palaeozoic deformation, if present, has not been recognised.

Some of the magmatic activity in the northern part of the Kunlun Shan may be related to pre-Upper Devonian collisional tectonism; the Qinbazhan granite has yielded an early Devonian age of 389 ± 10 Ma (C. L. Lewis, pers. comm. 1988) and the supposedly Upper Devonian (?) volcanics are thought, from their chemistry, possibly to indicate an active continental margin while those of supposedly early Carboniferous age are post-collisional (Pearce & Mei, this volume). Such a relationship of this magmatism to the post-Ordovician tectonism suggests that the tectonism occurred not long before the unconformable Upper Devonian was deposited. The volcanism occurred along a belt extending far to the ESE (figure 1). Evidence of mid-Palaeozoic tectonism extends over a large area (figure 1) from the West Kunlun to the Qilian Shan and beyond. Its southern limit is not well defined but is either at the Kunlun–Qilian Suture or slightly further north.

4. Late Carboniferous or early Permian tectonism

No indication of late Carboniferous or early Permian tectonism was seen on the Geotraverse and the Tienshan Suture, of late Carboniferous or early Permian age (Watson *et al.* 1987) lies far to the north of the area covered (figure 1). Nevertheless a collision between a terrane which included the northern Kunlun and a plate to the north seems to be necessitated by the palaeomagnetic data and by the evidence on the geological maps (1:1.5 M Qinghai and 1:1 M Tibet) of widespread deformation at this time (figure 1). The palaeomagnetic data came from the red beds of the Dagangou Formation, which is either late Devonian (Yin *et al.*, this volume) or early Carboniferous (Smith & Xu, this volume). The data are interpreted as showing a palaeolatitude of $-23° \pm 16$ (Lin & Watts, this volume).

The palaeomagnetic evidence from the Tibetan Plateau is presented in a diagrammatic form in figure 3. This is intended to show that the data can be interpreted in terms of the successive accretion to Eurasia of a series of terranes, some certainly derived from the south. The positions suggested for the terranes are drawn schematically, with the control of the palaeomagnetic

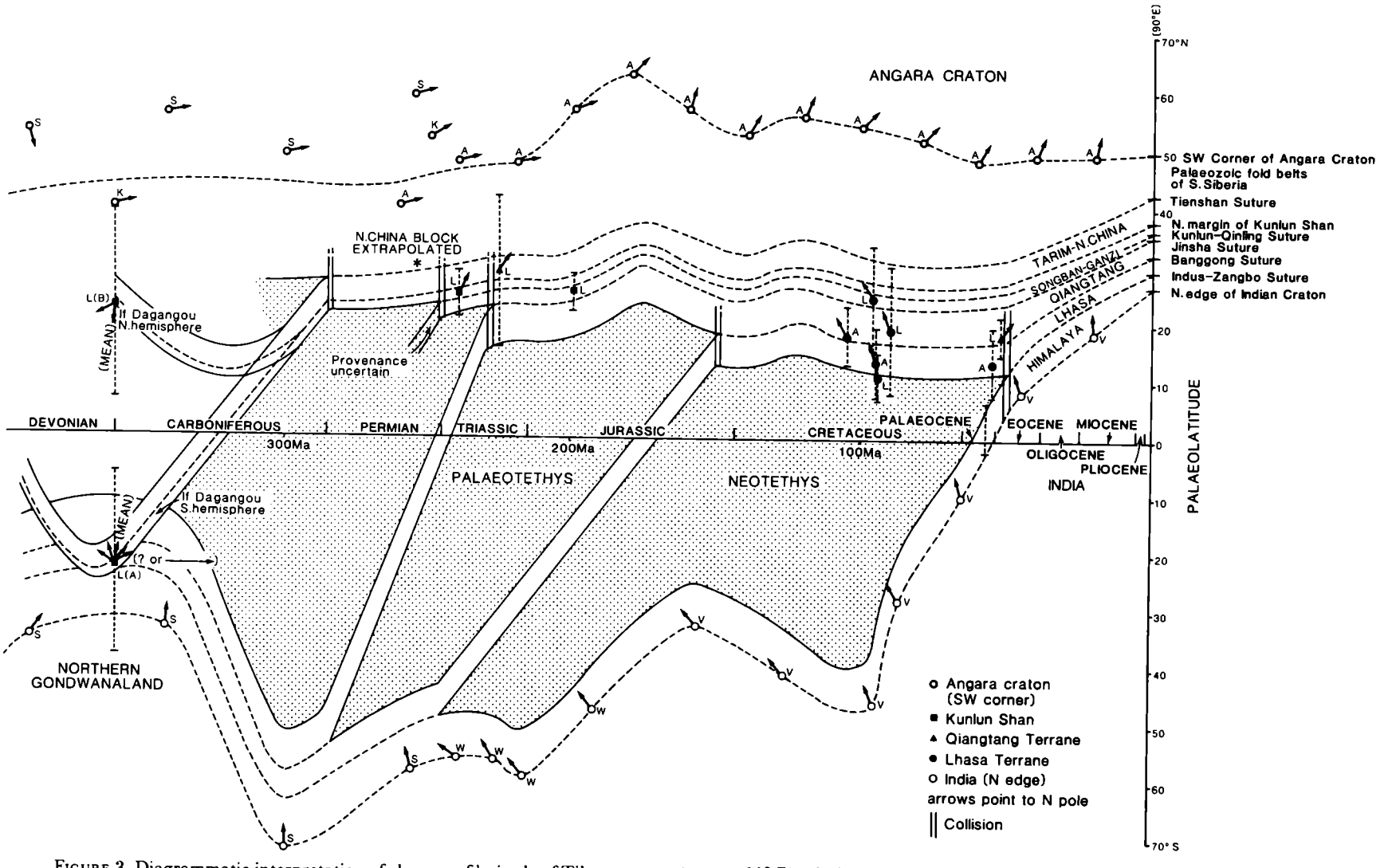

FIGURE 3. Diagrammatic interpretation of changes of latitude of Tibet terranes (now at 90° E) relative to India and the Angara craton. Based on Lin & Watts, this volume (L); Acache *et al.* 1984 (A); Khramov *et al.* 1981 (K); Scotese *et al.* 1979 (S); F. J. Vine (pers. comm. 1983) (V); and Westphal *et al.* 1983 (W). For explanation see text.

data, so as to follow the assumed path of the Eurasian plate when they were supposedly attached to it. Note, however, that only latitudinal differences can be shown. Because of possible rotations, these would not necessarily remain constant as indicated; nor need apparent convergences mean real convergences; two terranes may converge to the same latitude but be far apart longitudinally. Note too that the diagram shows the supposed palaeolatitudes of points that are now on 90°E meridian. There is not reason to suppose that these points preserved this longitudinal relation through time.

Although the inclinations from two sites on the Dagangou Formation are in close agreement, the declinations differ widely. Values from opposite limbs of a major fold, 245° and 125°, are reduced to 215° and 168° (all means) by correcting for a plunge of 70° to the west (Lin & Watts, this volume). However, with a Northern Hemisphere position (B on figure 3) any of these declinations would imply a very large rotation of this part of the Kunlun Shan before the Permian (see figure 3). This is the main reason for interpreting the results as indicating a southern latitude (see Lin & Watts, this volume). If the southern hemisphere position (A on figure 3) for the Dagangou Formation is accepted, that block must have moved 5000 km northwards during the next 100 Ma, with no great rotation. A northern latitude interpretation (B on figure 3) would imply little change in latitude in the same interval but about 180° rotation. Either interpretation would imply motion quite different from the Asian Plate to the north and therefore a suture between the two. Two problems arise, firstly the position of the suture which must bound the Terrane containing the Dagangou Formation to the north and secondly the previous attachment of this part of the Kunlun Shan, whether to Asia, to Gondwanaland or to neither.

There are two possible positions for the suture. It may be the late Carboniferous or early Permian Tianshan Suture, in which case this part of the Kunlun Shan formed part of the Tarim and North China Terrane, or it may be a suture which is suggested by a line of small basic masses, mapped as late Palaeozoic (1:1 M Geological Map, Qinghai; Geotraverse geological map, this volume), through the Qimantage Shan and extending at least 130 km ESE of Golmud. This line is about 70 km north of the Anyemaqen Shan ophiolite zone (see below) from which it is clearly distinct (cf. Zhang *et al.* 1984). The evidence obtained on the Geotraverse does not help to decide between these alternatives but, on balance, it seems more probable that the whole region between the Kunlun–Qinling Suture to the south (see below) and the Tienshan Suture to the north formed a single terrane, the Tarim–North China Terrane (itself possibly composite) during the late Palaeozoic.

The attachment, earlier in the Palaeozoic, of the Kunlun area and the Tarim Terrane, seems likely to have been to the Asian Plate, primarily because there are Lower Palaeozoic ophiolite belts, tectonism and magmatism (figure 1) that seem to be continuous, allowing for some displacement on the Altyn Tagh fault, with similar ophiolite belts, tectonism and magmatism within the Asian Plate, where they encircle the Angara nucleus. It therefore seems that, if the Kunlun block was in the Southern Hemisphere in the early Carboniferous, it had previously been much farther north and part of the Asian plate.

5. End-Permian–early Triassic collision: the Southern Kunlun ophiolite belt

From late Devonian to late Permian times, shallow-marine and terrestrial sedimentation proceeded, though how continuously is uncertain, across the northern part (north of the

Middle Kunlun Fault; figure 1) of the area covered during the Geotraverse. Some of the Lower Carboniferous beds are regarded as molassic, derived from mountains to the north (Leeder *et al.*, this volume).

Two different cycles of magmatic activity can be recognized in the northern Kunlun Shan: the earlier, late Devonian and early Carboniferous, perhaps 370–320 Ma ago, is regarded here as the last phase of the pre-mid-Devonian tectonism (see above). The later cycle is represented by the North Kunlun batholithic intrusions, dated at 260–240 Ma (Harris, Xu, Lewis, Hawkesworth & Zhang, this volume), and the closely related NNW-trending basic dyke swarm which transects the plutons. The chemistry of the plutonic rocks implies an active continental margin; the only slightly younger dykes are regarded as post-collisional (Harris, Xu, Lewis & Jin, this volume). If this is correct, this major phase of magmatism in the northern Kunlun Shan cannot be related to the end-Triassic or earliest Jurassic (Indo–Sinian) collisional tectonism which affected a vast region to the south (see below), but rather to an end-Permian or early Triassic tectonism.

Late Palaeozoic deformation is clearly demonstrated by the folding, strong enough to produce local northward overturning (loc. S549) of the lower Carboniferous sediments and volcanics, though not strong enough to produce a cleavage, before the injection of the undeformed NNW-trending basic dyke swarm, which cuts through the folded rocks, and before the intrusion of the batholith which hornfelsed already vertical beds. Debris from the batholith and from now eroded volcanics is seen in the massive conglomerates at or near the base of the Triassic sequence to the south (loc. S551 etc).

These magmatic and tectonic events appear to be related to the most impressive ophiolite belt on the Tibetan Plateau apart from that on the Indus–Zangbo Suture, namely the Anyemaqen Shan belt. This strikingly linear belt, along which more than a hundred ophiolite bodies have been mapped, extends for about 400 km through the Anyemaqen Shan (figure 1). It reaches to within about 300 km east of the Geotraverse line, where it intersects, and is truncated by, the eastward continuation of the Xidatan fault. Associated with the ophiolite belt is glaucophane schist as well as melanges, one of which has Lower Permian exotics in a Permian flysch matrix; another has Permian limestone exotics in a Triassic matrix. Clearly, this zone represents an important suture, which is known as the Kunlun–Qinling Suture (Watson *et al.* 1987). These ophiolites have not been dated but from published maps (1 : 1 M Geological Map, Qinghai) they appear generally to occur within a continuous band of Permian rocks, although locally in older or younger ones. It seems likely that they are late Permian or early Triassic.

The band of Permian rocks continues about 300 km farther west than the ophiolites, almost to the Geotraverse line, before it too is truncated by the Xidatan fault. On the north side of the fault the ophiolite belt is not clearly identifiable on the published maps. The total displacement on this fault is not known. Kidd & Molnar (this volume) demonstrate a Quaternary left-lateral slip of 30 km and suggest a total offset of *ca.* 75 km, based on the tentative recognition on satellite imagery of the phyllonite belt that has been mapped just south of the Xidatan fault. There is no indication of any extension of the ophiolite zone north of the supposed phyllonite.

In spite of its apparent failure to continue, the suture cannot have stopped at the Xidatan fault. Even if the fault dates back to the Permian, it is at too acute an angle to the suture to be taken for a transform fault, considering that all the indications of transport direction, from stretching lineations, are almost north–south. It is possible that the western continuation of the

suture is represented by the ophiolite (age unknown) immediately north of Ulugh Muztagh (Molnar *et al.* 1987*b*). Alternatively (Watson *et al.* 1987), the continuation of the suture may be towards the WNW through the Qimantagh Shan, along the southwest side of the Qaidam Basin, where several ophiolites of late Palaeozoic age are indicated on the maps (1:1 M Geological Map, Qinghai, 1:1.5 M Geological Map, Tibet). This seems improbable because it would take the suture obliquely across an apparently continuous belt of plutons and across the belt of Devonian volcanics, and also because of evidence both of Lower Palaeozoic and Carboniferous tectonism well to the south of the Qimantagh ophiolites (figure 1).

Indications of Lower Palaeozoic tectonism continue SW along the NW side of the Altyn Tagh and between the Karakoram Fault and the Tarim Basin, where unconformities indicate significant tectonism during the Carboniferous. Because these pre-Permian tectonisms, which affected extensive regions to the north, cannot have affected the terrane south of the suture before it arrived there, the suture must continue south of the Kunlun Shan, approximately as shown in figure 1. If the position of the Kunlun–Qinling Suture has been correctly identified, it is likely that the subduction zone dipped northwards because Upper Palaeozoic I-type plutons lie to the north of the suture.

The late Permian Kunlun–Qinling Suture separates areas with the Northern Cathaysian flora from those with the Southern Cathaysian flora (Watson *et al.* 1987; figure 1). A line can be tentatively drawn to represent the southern limit of mixed Angaran and Northern Cathaysian floras, and about 200 km still farther north, a line at the southern limit of the Angaran floras. The fact that in the late Permian (*ca.* 225 Ma ago) these three zones appear to have been gradational, but separate from the Southern Cathaysian flora of the South China and Qiangtang Terranes (Smith & Xu, this volume) supports the view that the Kunlun–Qinling Suture marks the southern limit of the composite Eurasian plate, before the accretion of the Terrane to the south.

Recognition of the Kunlun–Qinling Suture makes it necessary to separate by name the terranes to the north and south of it, as has previously been done by Chinese geologists (Li *et al.* 1979) but not previously by the Geotraverse team (Chang *et al.* 1986; previous papers in this volume). The Terranes will be referred to as the Tarim–North China (probably composite) and Songban–Ganzi Terranes, north and south of the Kunlun–Qinling Suture (figure 1) respectively.

In the part of the Songban–Ganzi Terrane seen on the Geotraverse, only Triassic and younger rocks are exposed. The Trias is represented by an extensive flysch wedge (Bayan Har Group) presumed to have been transported from the north (Leeder *et al.*, this volume). However, farther east, older rocks appear where maps (1:1 M Geological Map, Qinghai, 1:1.5 M Geological Map, Tibet) show that there is an extensive area west of the Longmen Shan thrust belt which is taken to mark the edge of the South China Block, where there is no sign of any significant deformation in the Palaeozoic, nor below the Upper Trias. It must be suspected that the same is true father west, where there is no exposed evidence. On this view, the Songban–Ganzi Terrane is an extension of the South China block.

From the middle Kunlun Fault to just south of Wudaoliang, a distance of a little over 100 km across strike, the Triassic rocks are strongly deformed. This deformation took place at the end of the Triassic: in the Kunlun Shan, Middle Triassic rocks, and father south, Upper Triassic (Bayan Har Group) are affected by the main deformation, while a post-tectonic

tonalite intrusion is dated at 213±6 Ma (Harris, Xu, Lewis, Hawkesworth & Zhang, this volume), which corresponds to the Triassic–Jurassic boundary. Farther east, and southeast, the region affected by the end-Triassic tectonism is much wider (figure 1).

The southern limit of this strong end-Triassic deformation cannot be seen in the Geotraverse area because of the cover of Neogene and Palaeogene deposits in the Fenghuo Shan. An inlier, which we were not able to reach, northwest of Erdaogou exposes an ophiolite (associated with Triassic sediments), which is taken to mark the approximate position of the Jinsha Suture to which the end-Triassic deformation is related. The area was subsequently mapped by a group led by Colin Stark (pers. comm. 1988). Their work showed that the ophiolite occurs as numerous separate angular masses, in a matrix of Triassic sandstones. The ophiolites appear to be in a melange. South of the Fenghuo Shan, the Triassic rocks which reappear from under the Tertiary cover are quite different from those to the north of it. The end-Triassic deformation is much weaker, the sedimentary facies is different and there are volcanic rocks which are not seen north of the suture. The suture clearly separates two different domains. It is taken to represent a Palaeotethyan ocean, which before collision separated the Eurasian Plate from the Qiangtang Terrane. Indications of weak end-Triassic folding can be recognized from published maps right across the Qiangtang Terrane.

The recognition of the Jinsha Suture zone is based primarily on the occurrence of ophiolites along it. In the region of the Geotraverse these are few and far apart – one 60 km NW of Erdaogou, another 200 km farther WNW, others 200 and 400 km ESE. However, from Yushu southeastwards, there are very many ophiolites. They occur (figure 1), along either side of, and to some extent within, a wedge shaped area known as the Yidun Island Arc Belt. The concentration of ophiolites along the northeast side of the wedge marks the Yushu–Litang Suture zone. Here, a nearly uninterrupted ophiolitic melange with greenschist facies metamorphism has been traced for about a thousand kilometres through Yushu, Garze and Litang to Wuli. At least one fairly complete, though dismembered, ophiolite, is recognized, at Zimenda, with harzburgite, gabbro, pillow lavas and cherts. Exotic blocks include Permian, Carboniferous and even Silurian limestones and radiolarites and basalts. The matrix of this melange consists of Triassic clastics and flysch; a rich microfauna in siliceous rocks overlying the basic lavas is early Triassic. The ophiolites are regarded as late Permian or early Triassic: if so their position is difficult to explain. It would seem to imply that the Yidun Island Arc was accreted to Eurasia in the late Permian or early Triassic, but this cannot be so because the arc, which is thought to be composite, consists of late Triassic arc volcanics and I-type plutons and flysch. The underlying sequence extends down at least to the Ordovician (Yin *et al.*, this volume) suggesting that it was built on continental crust.

The ophiolites along the southwest side of the Yidun Arc define the Jinsha River Suture Zone. This is best seen in a belt about 40 km wide extending more than 700 km SSE. Along the western side of the belt is an ophiolitic melange with Devonian, Carboniferous and Permian limestone exotics in an Upper Triassic matrix. A convincing ophiolite, as well as many ultramafic diapirs, is recognized. Because island arc rocks occur between the two supposed sutures, it has been suggested that Benioff zones, above which the volcanics were erupted, dipped inwards under the arc from both sides. An apparent continuation of the Jinsha River Suture Zone is seen, beyond a gap, in the Ailao Mountains-Tongtian River fracture zone where phyllonites and mylonites are associated with many ultramafic bodies in an ophiolite melange,

which is covered unconformably by late Triassic red beds. Blueschists to the southwest and high-T metamorphism to the northeast suggest a paired metamorphic belt and subduction northeastwards under the Yangzi Block.

This summary of the relationship along the Jinsha River Suture zone far to the southeast of the Geotraverse area is included here because the evidence obtained along the Geotraverse does not show clearly whether Palaeotethys 1 was subducted northwards (Coward *et al.*, this volume), southwards (Pearce & Mei, this volume) or both (Leeder *et al.*, this volume). The argument from structures is based on the recognition, in the southern Kunlun Shan and south of it, of steep north-side up faults and a phyllonite zone with the same displacement sense. It is proposed (Coward *et al.*, this volume) that these structures were initiated as gently dipping thrusts and have been rotated up northwards to their present steep attitude in a forearc prism.

Towards the southern margin of the Triassic flysch wedge, north of Wudaoliang, the early folds are refolded but appear to have been recumbent, and the structures face southwards. The associated cleavage is folded but often dips south. Farther east in Qinghai, the foliation dips about 40 °N or NW in the Bayan Har Group (observations by Chinese members of the team, after the Geotraverse).

The magmatic evidence is that arc-type volcanics occur south of the Jinsha Suture (Pearce & Mei, this volume). They are thought to represent the edge of the Upper Triassic Baitang Group, although not so mapped on the 1:1 M Geological map of Qinghai. They continue along the SW side of the suture for over 1000 km to the southeast (figure 1).

It seems likely that the exotics in the melanges along the sutures southeast of the traverse came from the southwest, where such rocks are known, rather than from the huge area of Bayan Har Group muds and turbidites to the northeast. This suggests that ophiolites were being obducted along the southwest side of the suture zone.

On balance it seems more likely, despite the structural evidence, that subduction on the Jinsha Suture Zone was southwards. If so, the strong deformation was in the downgoing plate and the weaker in the overriding one, as is commonly the case.

6. End Jurassic (Yenshanian) tectonism

The southern limit of the Qiangtang Terrane is marked by the sudden appearance of ophiolites (figure 1). They are not, however, restricted to a narrow linear zone, but are distributed across strike for about 150 km. Those in the north, in the area studied, dip northwards and show a shear-sense towards the SSE (Kidd *et al.* this volume). Especially between Dongqiao and Gyanco, the ophiolite forms a flat thrust sheet. It is thought that the ophiolite was obducted southwards and later re-imbricated (Coward *et al.*, this volume). For these reasons, the suture zone is thought to be along the northern limit of the array of ophiolites. The projection of the suture westwards from just north of Siling Co, to the ophiolites south of Banggong Lake, is based on the occurrence of one ophiolite mapped north of Dong Co., about midway in a stretch of 800 km, and on map indications of late- or post-Triassic deformation nearly as far south as the supposed line (figure 1). The age of the ophiolites and their obduction, in the area studied, is well-established as late Jurassic (Girardeau *et al.* 1984; Smith & Xu, this volume). From the structural evidence, it seems clear that subduction was northwards.

During the Jurassic, much of the Qiangtang Terrane in the areas studied to the north of the suture was a coastal plain over which molassic continental clastics were spread from the north and northeast; while farther south, nearer the oceanic area represented in the Banggong Suture zone, shallow-marine carbonates were deposited (Leeder *et al.*, this volume). In sharp contrast, over much of the Lhasa Terrane south of the Banggong Suture, muds and turbidites, the 'Lake Area Flysch' (Yin *et al.*, this volume) were deposited. The oceanic sediments, seen overlying the ophiolite, include radiolarites. Island arc magmatism was not recognised on either side of the Banggong Suture.

The Banggong Suture is not marked by a zone of strong deformation. To the north, in the Qiangtang Terrane, mapping (1:1 M Geological Map, Qinghai) indicates that widespread moderate folding of the Jurassic beds took place before the deposition of the unconformably overlying Palaeogene. This folding is presumably associated with the collision along the Banggong Suture. South of the suture in the Lhasa Terrane, there seems to be no clear evidence of significant deformation at the time of the collision. It can only be concluded that pre-collisional subduction was so slow, and post-collisional convergence so slight, that no magmatism and very little deformation was produced.

7. Cenozoic tectonism: the India–Asia collision

Since Argand's (1924) recognition that the Cenozoic tectonics of Asia are principally the result of the convergence of Gondwanan continental fragments with Laurasia, there has been general acceptance of the view that the approximate doubling of crustal thickness, uplift, and roughly north–south shortening of the Himalayas and Tibet have been caused by the collision of the Indian subcontinent with the bulk of Asia along the Indus–Zangbo Suture following the subduction of a substantial ocean, the Tethys (Allègre *et al.* 1984; Carey 1955; Dewey & Bird 1970; Dewey & Burke 1973; Holmes 1965; Molnar & Tapponnier 1975), or rather its Mesozoic Neotethyan tract (Sengör 1979).

The Tibetan Plateau, part of a broader zone of deformation from the Himalayan thrust front to Lake Baikal (figure 4), is a remarkably level plateau, with a dissected average elevation just below 5 km, of approximately 7×10^5 km^2, an area about equal to the US Cordillera and Rockies. Relief is somewhat subdued, the plateau consisting mainly of rolling hill terrain with about 1.0 km of relief, local plateaux between 5 and 6 km and local mountain ranges such as the Tanggula Shan rising to above 7 km with permanent snow and ice. Localized consequent drainage systems feed mostly into larger meandering rivers that drain into lakes whose long term evaporation rates exceed fluvial input in the dry Tibetan climate in the precipitation shadow of the Himalayas. Only a few larger rivers meander across the plateau either to plunge off the eastern edge of the plateau through spectacular gorges or to cut through the Himalayas as antecedent rivers. Therefore, the Tibetan landscape is one of low ablative relief as a consequence of which there has been little Tertiary denudation except in the marginal thrust belts. Most of Tibet, except the Gangdese and Kunlun belts, consists of high-level sequences. The plateau, containing 70% of the Chinese permafrost, is about one fifth karstic probably formed at a time when Tibet enjoyed a wetter climate at a lower elevation.

There is general agreement that the Tibetan Plateau is underlain by a continental crust between 60 and 85 km thick with a small free-air gravity anomaly that implies near isostatic equilibrium. Love and Rayleigh wave velocities are much lower beneath Tibet than beneath

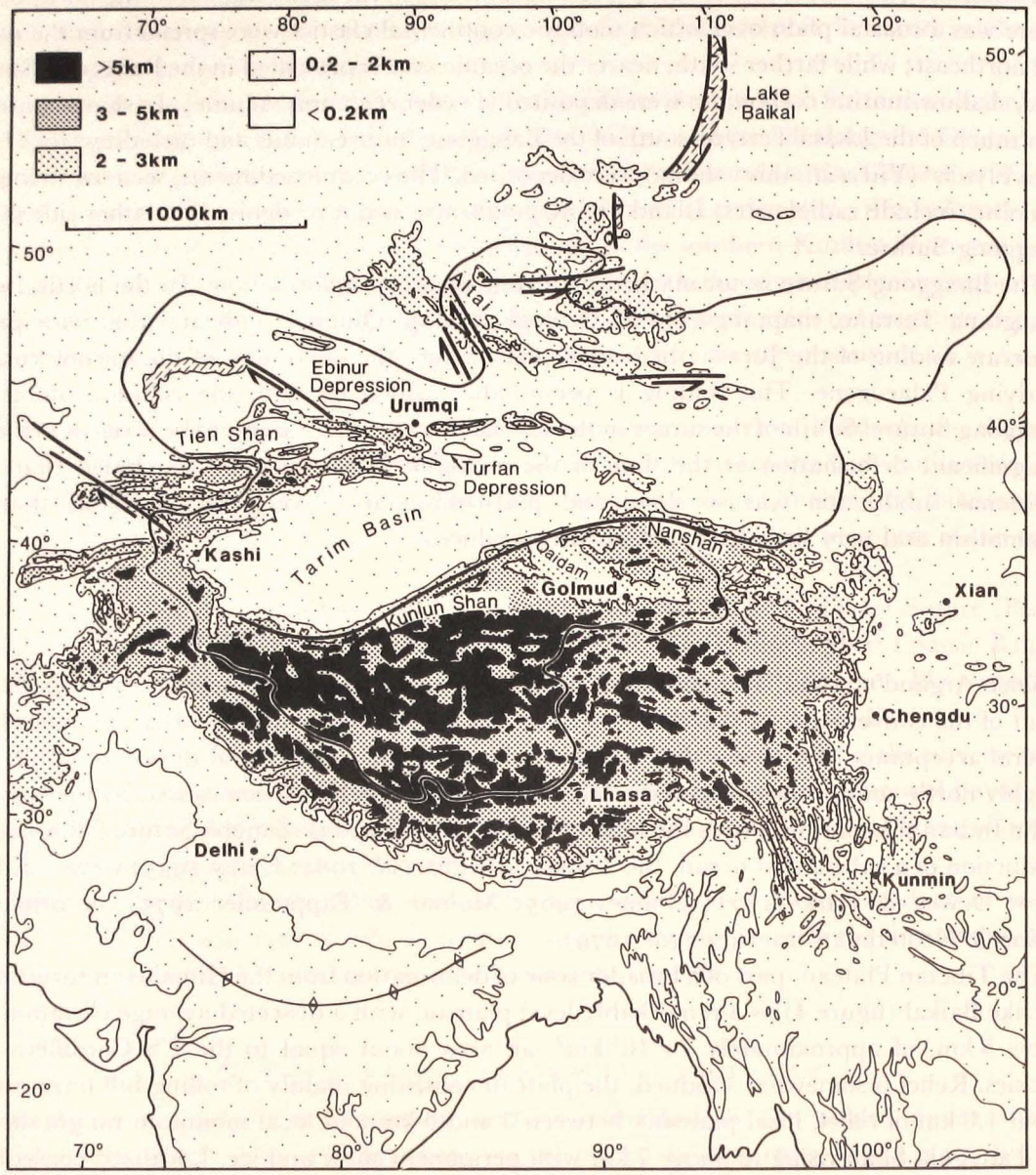

FIGURE 4. Simplified topographic map of the India–Eurasia collision zone. Lakes indicated by oblique ornament; area of internal drainage enclosed by continuous line; line with anticline symbol indicates crest of flexural bulge.

peninsular India and somewhat lower than north of Tibet implying a thinner lithospheric boundary conduction layer and a higher geothermal gradient beneath Tibet (Romanowicz 1982). Furthermore, there is a Magsat crustal negative anomaly field over Tibet (Achache *et al.* 1987), which, in a region where the crust is thick but magnetically thin, suggests a high geothermal gradient. A generalized crust/mantle profile from peninsular India across the Himalayas and the Tibetan Plateau to the Qaidam Basin and the Nan Shan (figure 5) is derived from the data and arguments of Barazangi & Ni (1982), Bird & Toksoz (1975, 1977), Brandon & Romanowicz (1986), Chen & Molnar (1975, 1981), Choudhury (1975), Chun &

McEvilly (1986), Chun & Yoshii (1977), Gupta & Narain (1967), Hirn *et al.* (1984*a*, *b*, *c*), Jobert *et al.* (1985), Lyon-Caen (1986), Lyon-Caen & Molnar (1983, 1984, 1985), Matthews & Hirn (1984), Min & Wu (1987), Molnar *et al.* (1987*b*), Ni & Barazangi (1983), Pines *et al.* (1980), Romanowicz (1982), Ruzaikeri *et al.* (1977), Shaw & Orcutt (1984), Teng (1980), Teng *et al.* (1981, 1983) and Zhou *et al.* (1981). Data on the seismicity of the plateau is from Chen & Molnar (1983), Chen *et al.* (1981), Molnar & Chen (1978), Molnar & Deng (1984) and Ni & Barazangi (1984). Data and views on the heatflow, geothermal structure and recent magmatism of the plateau are from Chen & Molnar (1981), Coulon *et al.* (1986), Deng (1978), Dewey & Burke (1973), Francheteau *et al.* (1984), Hennig (1915), Jaupart *et al.* (1985), Kidd (1975) and Van *et al.* (1986).

The crust thickens from about 33 km beneath the Indian Shield to a maximum of about 75 km beneath the Himalayas and a regional average of 65 km beneath Tibet, with about 20 km denuded from the Himalayas, about 10 km from the Gangdise Belt in Southern Tibet and an average of about 2 km from the Tibetan Plateau between the Gangdise Belt and the Kunlun. The crust and lithospheric mantle are multilayered in six zones (figure 5). A low velocity veneer about 5 km thick, probably consisting mainly of supracrustals (1) is underlain by a higher velocity layer (2) to about 17 km. Crustal earthquakes are concentrated in this layer mostly between 5 and 10 km with normal and strike-slip first motion solutions. A crustal low velocity zone (3) between about 17 km and 30 km with a conductivity anomaly and low Poisson's Ratio may be a partial melt zone or, less likely, a zone of high pore pressure. A higher velocity lower crust (4) between 30 km and a Moho at about 65 km show steep shear wave velocity gradients. The upper mantle has a high velocity lid (5) to about 100 km with two earthquake hypocentres at about 85 km giving normal fault solutions beneath which the lower lithosphere (6) is completed by a 4.4 shear wave velocity (Vs) layer to 150 km. Therefore, the crust of Tibet is about twice the thickness of the Indian crust, whereas the Tibetan lithosphere is about three fifths the thickness of the Indian shield lithosphere. A Tibetan lithosphere of about 150 km is consistent with a convex-up geothermal gradient of about 27 °C km^{-1} in the uppermost crust and 18 °C km^{-1} in the lower crust with a Moho temperature of about 750 °C. The widespread recent volcanism across the plateau supports the idea of a thinner boundary conduction layer beneath Tibet.

There has been less agreement about the timing, mechanism and rates of crustal thickening and uplift during the collisional process although the timing is generally believed to have been during the latest Cretaceous to late Eocene interval with a recent rapid uplift. Three broad classes of hypotheses have been suggested to account for the Tibetan Plateau in its regional Asian tectonic setting, namely crustal underthrusting, crustal shortening and thickening, and lateral eastward crustal extrusion.

Argand (1924) proposed that the Tibetan Plateau is underlain by a double normal thickness crust produced by the underthrusting of the northern margin of peninsular India or 'Greater India' beneath the Asian crust (figure 6A), a view supported by Barazangi & Ni (1982), Holmes (1965), Powell & Conaghan (1973, 1975) and Ni & Barazangi (1984). Bird (1978) introduced the variant of lithospheric delamination and underthrusting. Powell (1986) suggested wholescale subduction of the Indian continental crust followed by its buoyant uprise to underplate the Asian Tibetan continental crust. Cohen & Morgan (1987) and Zhao & Morgan (1987) suggested the further variant of the injection of the Indian crust into a softer Asian Tibetan lower crust.

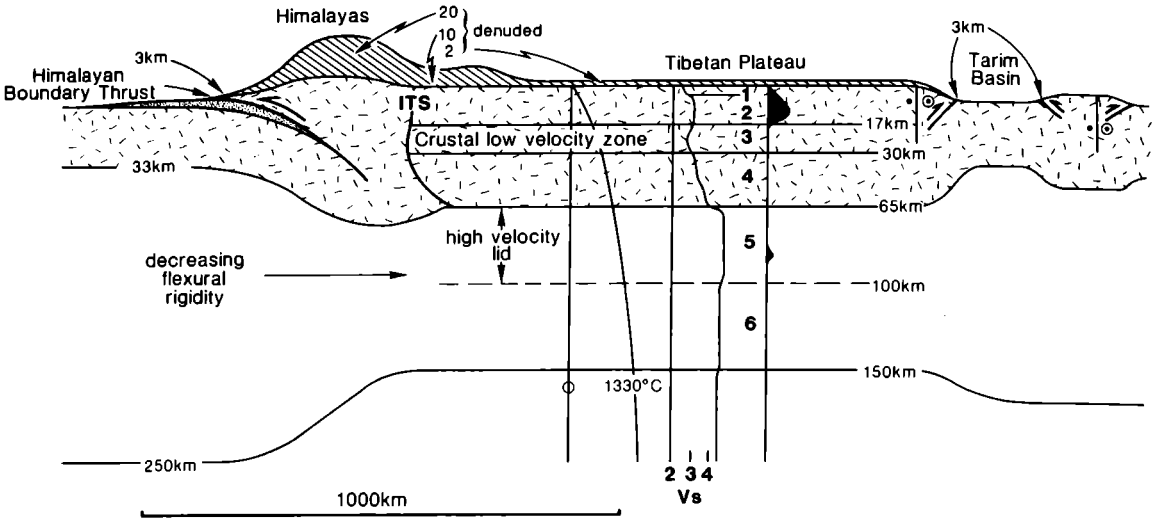

FIGURE 5. Simplified and idealised cross section of the Himalayas, Tibetan Plateau and Tarim Basin showing crustal and lithospheric thickness variations. Vs, shear wave velocity.

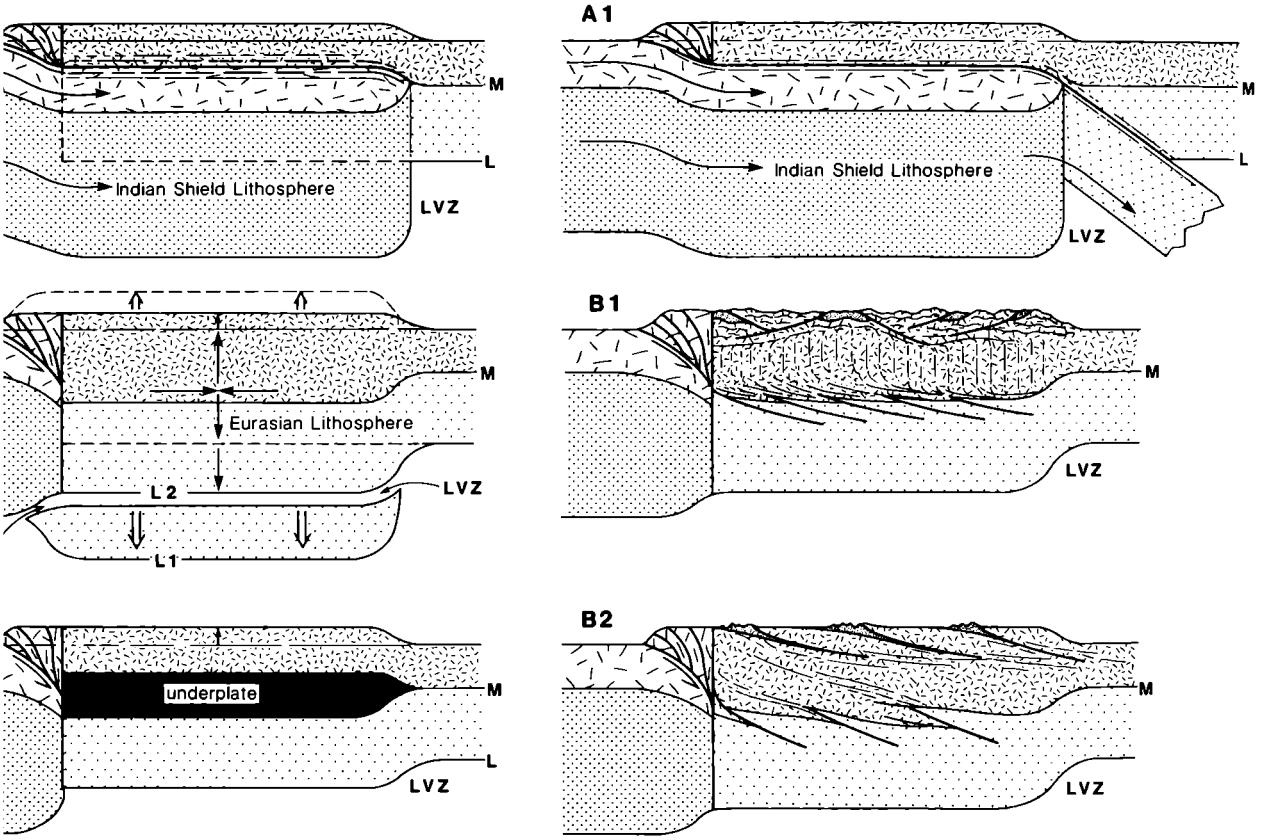

FIGURE 6. Mechanics for crustal and lithospheric thickening and thinning, and uplift. A: Indian lithosphere underthrusts Eurasia following delamination of the Eurasian lithospheric mantle along the Moho. B: Eurasian lithosphere thickens by vertical plane strain north-south shortening. B1 & B2: Structural expressions of B. C: Tibetan crust thickens and rises by magmatic underplating. M – Moho, L – base of thermal lithosphere, L1 – base of thermal lithosphere at end of thickening phase, L2 – base of thermal lithosphere after delamination, LVZ – low velocity zone.

Dewey & Bird (1970) and Dewey & Burke (1973) argued that the thick Tibetan crust was formed by horizontal shortening and vertical stretching of the Asian crust (figure 6B) in advance of the 'bull-dozing' Indian subcontinent. The shortening/thickening hypothesis was further supported by Bird & Toksoz (1975, 1977), Bird, Toksoz & Sleep (1975), Chen & Molnar (1981), Vilotte, Daignières & Madariaga (1982) and Vilotte *et al.* (1984, 1986). The quantitative modelling work of England & McKenzie (1982, 1983), England & Houseman (1985, 1986), Houseman & England (1986), Houseman, McKenzie & Molnar (1981) and England & Houseman (1988) has led to an integrated model of viscous vertical plane strain shortening and thickening of the Asian lithosphere progressively spreading northwards into Asia, with strong inhomogeneities like the Tarim Basin that resist thickening. In this model, the Tibetan Plateau is uplifted by two mechanisms, slow uplift caused by crustal/lithospheric thickening followed by rapid uplift caused by catastrophic lithospheric advective thinning (England & Houseman 1988).

The alternative mode of horizontal plane strain of the Tibetan lithosphere to accommodate the northward motion of India was suggested and developed by Molnar & Tapponnier (1975, 1977), Tapponnier & Molnar (1976, 1977) and Tapponnier *et al.* (1982). This involves the eastward lateral extrusion of Tibet and parts of Asia to the north along an array of giant transforms such as the Kunlun and Altyn Tagh Faults.

There are sufficient consistent palaeomagnetic data to help to constrain our choice of Tibetan models (Achache, Courtillot & Besse 1983; Achache, Courtillot & Zhou 1984; Allègre *et al.* 1984; Besse *et al.* 1984; Bingham & Klootwijk 1980; Klootwijk 1979; Klootwijk, Conaghan & Powell 1985; Klootwijk & Pierce 1979; Klootwijk *et al.* 1979; Pozzi *et al.* 1982; Westphal *et al.* 1983, Lin & Watts, this volume). The palaeomagnetic data are supported by relative motion solutions based upon magnetic anomaly and fracture zone studies in the Atlantic and Indian Oceans (McKenzie & Sclater 1971; Patriat & Achache 1984; S. Cande and W. C. Pitman, pers. comm). Since the late Cretaceous (84 Ma), India has moved northwards with respect to stable Eurasia by some 52° (5720 km) and rotated counterclockwise by about 35°. Since the time of the India–Asia collision (about 45 Ma, argued below) India has moved northwards with respect to 'stable' Eurasia by about 22° (2420 km) and rotated counterclockwise by 21°. Between 84 Ma and 45 Ma, the northward motion of about 3300 km was absorbed principally by northward subduction beneath the Gangdise arc of Neotethyan ocean between India and the Lhasa Block. Since 45 Ma, the northward motion has been absorbed along an intracontinental convergent boundary north of the Himalayan Boundary Fault. The southern edge of the Lhasa Terrane has moved northwards by 18° and rotated counterclockwise by up to 30° during the last 45 Ma and, therefore, little of the northward motion of India can have been absorbed by Greater India underthrusting Tibet. Lin & Watts (this volume) can detect no Tertiary latitudinal separational change between Lhasa and Erdaogou from palaeomagnetic data; however, the errors are large and the present separation is 500 km and the maximum Eocene separation would have been only about 1000 km according to the shortening/thickening model. The 4° (440 km) difference between the northward motion of India and the southern Lhasa Terrane since collision is probably taken up by shortening in the Himalayas. The involvement of basement in the thrust sheets and the preservation of Mesozoic continental margin facies in the Himalayas, south of the Indus–Zangbo Suture suggest, also, that little of the Indian crust has vanished beneath Tibet. Arguments based on balanced sections for the cover stripped from the basement in the outer

Himalayan zones of Pakistan (Coward & Butler 1985) indicate a northward subduction of the Indian crust by about 470 km, very close to the 440 km, indicated from palaeomagnetic and oceanic data. This is likely to have been taken up by crustal thickening in the Himalayas.

Therefore, about 1980 km of intracontinental convergence has been absorbed by the Asian lithosphere north of the Indus–Zangbo Suture. The principal mechanism cannot have been eastward lateral extrusion from Tibet by horizontal plane strain for two main reasons. First, extrusion cannot account for the crustal thickening in Tibet and in areas such as the Tien Shan (Nelson, McCaffrey & Molnar 1987) and the Nan Shan to the north. Second, the high plateau of Tibet is largely immediately north of and opposite the Indian 'indenter'. Only a maximum of about 15% of the plateau can be considered to lie east of the indented margin and, therefore, had extrusion been a major factor, it would have predated crustal thickening and uplift.

Therefore, because most of the northward motion of India relative to Eurasia cannot be accounted for by underthrusting of Greater India or by eastward lateral extrusion from Tibet, vertical plane strain during north–south shortening seems the likely dominant mechanism in that it accommodates the displacement and accounts for crustal thickening. Furthermore, the Tibetan Plateau is only a part, albeit an important and spectacular part of a zone of north–south compressional deformation (figure 4) that extends northwards to Lake Baikal (Molnar & Deng 1984; Molnar & Chen 1978). Clearly the Indian crust cannot underthrust as far as Lake Baikal and it seems unlikely, therefore, that wholly different mechanics thickened the crust of Tibet and the areas north of Tibet. Within this zone of deformation, rigid regions such as the Tarim and possibly the Qaidam Basins, the former probably underlain by Precambrian lithosphere, resisted deformation and it is possible that major strike-slip zones, such as the Altyn Tagh and Kunlun Faults, result not from extrusion *per se*, but from jostling between hard lithospheric zones and from compatibility problems resulting from adjacent deforming and non-deforming zones. If this were the case, the Altyn Tagh and Kunlun Faults would show an increasing eastwards displacement; existing data are insufficient to test this hypothesis.

Lastly, the shortening and thickening of the Eurasian lithosphere by an Indian indenter is supported by the regional form and deformation of Tethyan sutures between India and Eurasia (figure 7). India moved northwards relative to Eurasia between two giant transforms that linked the Indus–Zangbo subduction zone with contemporaneous subduction zones in the Gulf of Oman–Zagros to the west and a zone to the east through the East Indies. If India had advanced mainly by underthrusting Tibet, the Tethyan sutures would have today approximately their pre-collisional form. It is difficult to accept that the suture offsets that coincide with the western and eastern transform boundaries of the Indian protrusion are pre-collisional and that the Indian protrusion slipped precisely into a pre-determined embayment in Eurasia. Furthermore, the underthrust model would imply that displacements on the two bounding transform zones should drop abruptly at each end of the Indus–Zangbo suture; according to the shortening/thickening model the displacements should diminish northwards gradually and terminate on line with the northward limit of Eurasian shortening. On the western edge of India, the Owen Fracture Zone is continued on land as the Chamaun and associated faults, which form a 1500 km sinistral transpressional zone linking the Indus–Zangbo suture with the Gulf of Oman. Allowing for post-45 Ma subduction accretion in the Makhran and some crustal shortening west of the Chamaun Zone, the offset of the Indus–Zsangbo Suture is about 1300 km, that of the Kunlun–Qinling Suture about 700, and that of the

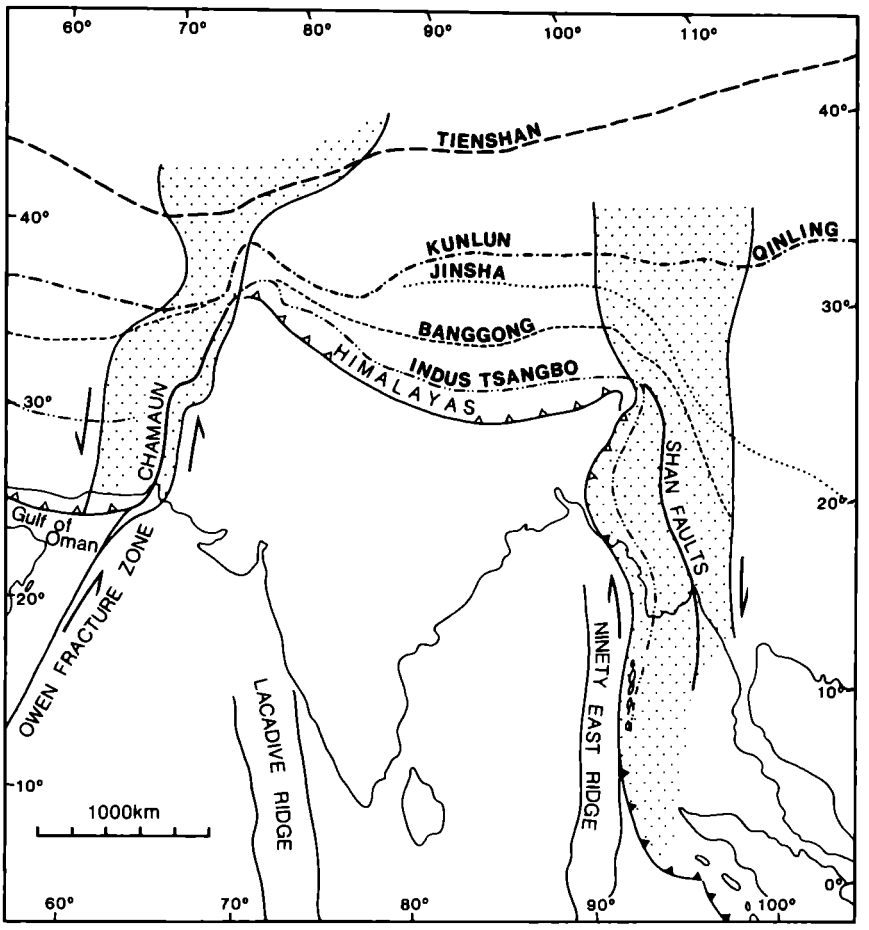

FIGURE 7. Map showing the distribution of the principal sutures from the Indus–Zangbo to the Tien Shan and their deformation by the indentation of Eurasia by India. The dotted ornament indicates the zones of northward-decreasing shear strain that bound the Indian indenter.

Tienshan a maximum of about 500 km. Therefore, we view the western dotted zone of figure 7 as representing a left-lateral transpressional zone of distributed shear bounding the Indian indenter. Similarly, the eastern margin of the Indian indenter is a 400 km wide right-lateral transform complex consisting of the Andaman and Shan Faults approximately on line with the Ninety East Ridge, originally a right-lateral transform between the Indian and Australian Plates. Across this dextral zone of transpressional shear, the Indus–Zangbo Suture is displaced at least 2000 km, the Jinsha Suture by about 1000 km and the Kunlun–Qinling Suture by perhaps 400 km, whereas the Tienshan Suture appears not to be displaced. Thus the eastern dotted zone in figure 7 is believed to represent a zone of distributed right-lateral shear that forms the eastern boundary of the Indian indenter.

The underthrusting and vertical plane strain mechanisms of crustal thickening should produce quite different structural geometries in the Tibetan crust. Underthrusting, in its simplest form (figure 6A), would involve little or no north–south shortening of the upper Tibetan crust and supracrustals, but would generate substantial simple shear deformation of the thrusted interface region of the Indian and Tibetan crust to develop widespread horizontal

or sub-horizontal fabrics at the base of the Asian and top of the Indian crust. In contrast, vertical plane strain by north–south horizontal shortening and bulk vertical stretching must involve the Tibetan crust and supracrustals in substantial north–south shortening by thrusting and folding; doubling of crustal thickness would involve 50% north–south shortening. This model cannot predict, simply, the way in which the shortening is likely to occur, whether fairly homogeneous (figure 6, B1) or partitioned in upper crustal thrust sheets (figure 6, B2), but it is unlikely that simple homogeneous vertical plane strain would generate the widespread horizontal shear fabrics predicted by the underthrust model.

Many deeply eroded Precambrian terranes of high-grade metamorphic rocks, probably developed in collisional tectonic environments, show widespread flat or gently dipping axial surfaces and fabrics which would seemingly support the underthrust model for the origin of these terranes. However, Moho imbrication and thrust segmentation of the brittle upper crust either at a fine (figure 6, B1) or a coarse (figure 6, B2) scale is likely to generate gently dipping fabrics in adjacent crustal rocks. This raises, however, the problem of the great contrast in structural style between the Himalayas and Tibet, at least in the style observed at present erosion levels. The Himalayas have suffered some 80% shortening and are dominated by south-verging, gently northward dipping thrusts. By contrast, Tertiary structures in Tibet are thrust ramp basins containing folded red beds in a crust that has suffered a maximum 50% shortening. We suggest that the style contrast results from the presence or absence of pre-collisional lithospheric/crustal asymmetry. The Himalayas are, basically, a pile of basement-cored thrust sheets stacked on the northward-thinning crust of India above a northward thinning lithosphere; hence the thrust asymmetry was predetermined by the asymmetrical structure of the northern edge of India. In contrast, Tibet has resulted from the bulk homogeneous shortening of the Asian lithosphere, in which the thrust polarity within the brittle upper crust varies, although it is commonly to the south (Coward *et al.*, this volume).

Finally, the role of the lithospheric mantle cannot be ignored in discriminating among models. In general, convergence must thicken the lithosphere as it thickens the crust, whereas most underthrust solutions to crustal thickening avoid the problem of the Asian lithospheric mantle as India underthrusts. To slide the Indian crust neatly beneath the Tibetan–Asian crust involves the prior disposal or delamination of the Tibetan lithospheric mantle cleanly along the Moho (figure 6A) or a thrust ramp/flat model with a mega-flat along the Moho (figure 6A1) if a simple crustal doubling is to be achieved by this mechanism. Moreover, as argued above, it is clear that a thick underthrust Indian shield lithosphere does not underlie Tibet. If the Tibetan crust has been thickened by vertical plane strain, the underlying mantle lithosphere must have been similarly thickened. If, for example, the Tibetan lithosphere, prior to north–south shortening, was 125 km thick, it should now be 250 km following a 50% shortening. Simple thermal recovery to its present 150 km would take far too long and, hence, some form of rapid delamination or advective thinning seems to have been likely (England & Houseman 1988; Houseman, McKenzie & Molnar 1981). Rapid lithospheric thinning by delamination or stoping could also account for the rapid recent uplift of the Tibetan Plateau, its widespread recent volcanism and hot springs and its east–west extension (England & Houseman 1988). The deep earthquakes seen beneath the Tethyan collisional system in Rumania, southern Iberia, Iran and the Hindu Kush may be in sinking delaminated mantle lithosphere fragments. Many orogenic belts show a post-shortening morphotectonic (Hills 1956) phase of late uplift, synchronous with bimodal basaltic/silicic magmatism and

extensional tectonics, which could result from catastrophic thinning of a lithosphere thickened by shortening. Magmatism, particularly during advective lithospheric thinning, could contribute to crustal thickening and uplift by gabbroic underplating (Cox 1980; McKenzie 1984; Hildreth & Moorbath, in press) in the lower crust (figure 6C). It is remarkable that post-collisional intracontinental shortening is taken up principally by the Asian lithosphere north of the Indus–Zangbo Suture, excluding the strong Tarim and Qaidam enclaves; the Indian shield shows little post-Archaean deformation, except foreland basin flexure, south of the Himalayan Boundary Thrust. We suggest that this is the result of the collisional impingement of a strong Indian shield lithosphere, which has undergone secular thickening since the Archaean, with a complex collage of accreted Asian fragments with a thinner lithosphere north of the Indus–Zangbo Suture. Thus, the Indian lithosphere may be thought of as an indenting buttress with a thinner northern edge generated by Neotethyan Triassic/Jurassic rifting, which collapsed to form the Himalayan Zone of shortening. A thinner lithosphere along the northern edge of India is suggested by the gravity anomaly/flexural studies of Lyon-Caen & Molnar (1983, 1985) and Molnar & Lyon-Caen (in press) that show a northward-decreasing flexural rigidity of the Indian Shield beneath the Himalayas.

Present deformation of the Tibetan crust (figure 8) is principally by strike-slip and extension, seen in both seismic first motion solutions (Chen *et al.* 1981; Molnar & Chen 1983; Molnar & Deng 1984; Tapponnier & Molnar 1977) and in surface displacements (Armijo *et al.* 1982, 1986; Chang *et al.* 1986; Molnar *et al.* 1987*a*, *b*; Molnar & Tapponnier 1978; Ni & York 1978; Norin 1946; Shackleton 1981; Tapponnier *et al.* 1981*a*, *b*; Tapponnier & Molnar 1977). A widespread Miocene erosion surface is very gently warped and faulted across the width of the plateau (Shackleton & Chang, this volume). Roughly north–south grabens effect an approximately east–west extension, across steeply dipping normal faults. Along the eastern flank of the Nyainqentanglha, an inactive gently south-east dipping extensional detachment draws down early Tertiary volcanics across an older metamorphic and granitic basement. The uplift of the Nyainqentanglha may have resulted from footwall uplift during this phase of extensional detachment. Young north–south normal faulting continues south into the Himalayas but appears to be confined to elevations above 3 km. The grabens commonly control the positions and shape of lakes and are the sites of extensive hydrothermal activity.

Strike-slip faulting occurs on dextral NW-striking faults and on sinistral ENE-striking faults. The two sets appear to comprise a conjugate wrench regime (Rothery & Drury 1984) but with the bisector of the obtuse angle being the shortening direction. To the south in the Himalayas, a conjugate wrench regime consists of dextral NNW-striking faults and sinistral NE-striking faults (Dasgupta, Mukhopadhyay & Nandy 1987), a geometry in which the acute angle is bisected by the shortening direction as predicted if the faults developed on planes of maximum shear stress (Anderson 1948). The transition from the Tibetan to the Himalayan wrench geometry occurs roughly along the Yarlung–Zangbo suture, but it is not clear whether the transition is effected by a zone of intersection or by a gradual change of strike of individual faults. The strike-slip faults have, commonly, pull apart and, less commonly, transpressive segments. Several terminate at the ends of the north–south grabens, indicating that these at least have evolved synchronously with the graben.

There is little sign of active or recent thrusting in the Tibetan Plateau. Southwest of Amdo, Cretaceous or Palaeogene red sandstones and conglomerates are thrust southeastwards over Pleistocene–Holocene brown and yellow sandstones and conglomerates with frost-heave

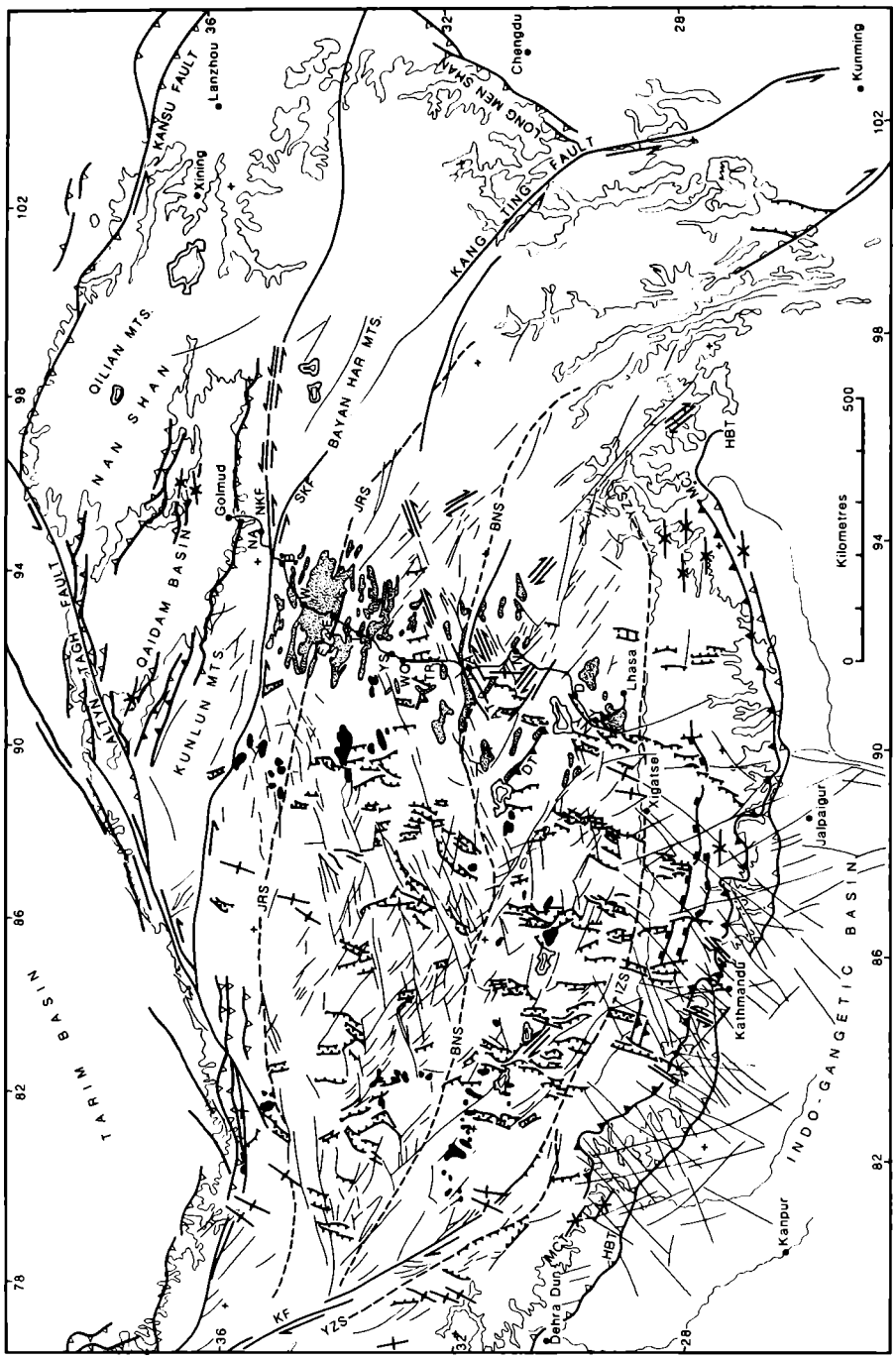

FIGURE 8. Map showing the principal neotectonic features of the Tibetan Plateau and adjacent regions. Himalayan low-angle extensional detachment zones from Burchfiel & Royden (1985). A – Amdo, AT – Amdo Thrust, B – Budongquan, BNS – Banggong-Nujiang Suture, D – Damxung, DT – Duba Thrust, E – Erdaogou, ET – Erdaogou Thrust, HBT – Himalayan Boundary Thrust, JRS – Jinsha River Suture, KF – Karakoram Fault, MCT – Main Central Thrust, N – Nagqu, NKF – North Kunlun Fault, NY – Nyainqentanglha, SKF – South Kunlun Fault, T – Tuo Tuo River, TP – Tanggula Pass, W – Wudaoliang, WQ – Wenquan, Y – Yangbajain, YS – Yanshiping, IZS – Indus–Zangbo Suture.

structures; the frost-heave structures are deformed below the thrust (Kidd & Molnar, this volume). South of Erdaogou, Palaeogene red sandstones are thrust to the south across Neogene lake beds. In both cases, young local relative uplift is indicated by antecedent drainage and incised meanders. These examples of thrusting do not appear to be characteristic of regional relationships and both instances of thrusting may be on transpressive segments of strike-slip faults. On the thrust plane, south of Erdaogou, striae pitch east at about 20° in the thrust surface indicating a dominant left-lateral strike-slip component on the thrust fault. Therefore, if north–south shortening is occurring today within the Tibetan crust, it is accommodated by strike-slip faulting, not by thrusting; this is supported by the dominant strike-slip first motion solutions. East-trending, thrust-bounded, basins involve Palaeogene red beds and appear to be of pre-Miocene age. Elevation, therefore, seems to be a critical factor in controlling tectonic style. Thrusting occurs at or just below 3 km, strike-slip faulting occurs at all elevations, whereas east–west extension occurs above 3 km. The way in which the present/Recent motion of India relative to Asia is partitioned into displacement and strain on, and to the north of, the Himalayan Boundary Thrust, has been examined by Molnar *et al.* (1987*a*). A modified version of their principal conclusions is shown in figure 9. A recent finite difference study of the Atlantic and Indian Oceans by S. Cande and W. C. Pitman III, pers. comm. has shown that a point on the Indian Plate just south of Kathmandu has moved northwards by about 2° since the time

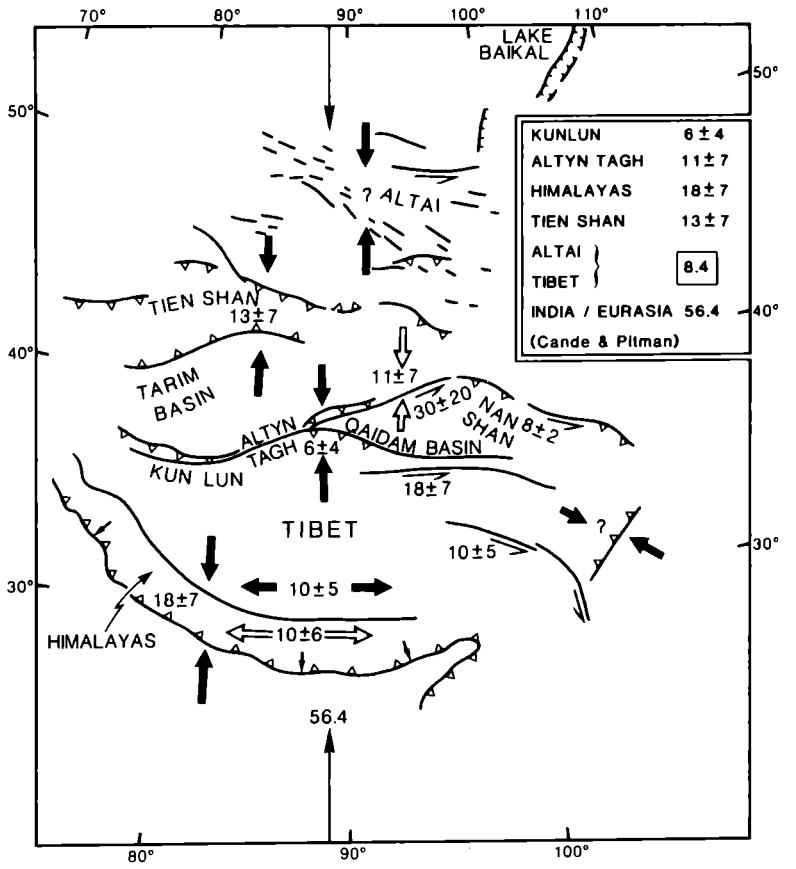

FIGURE 9. Neotectonic displacement in millimetres per year across and within the India–Eurasia convergent zone. Black arrows, shortening and extension values from thrust zones and graben zones respectively; open arrows, from strike-slip faults.

of Anomaly 3 (3.9 Ma), relative to 'stable' Eurasia, an average rate of 56.4 mm a^{-1}. 18 ± 7 mm a^{-1} is absorbed by thrusting in the Himalayas, 13 ± 7 mm a^{-1} by thrusting in the Tien Shan, 6 ± 4 mm a^{-1} by thrusting in the Kunlun and Altyn Tagh, and 11 ± 7 mm a^{-1} as the north–south convergent component of strike–slip faulting on the Altyn Tagh Fault (Molnar *et al.* 1987*a*). Excluding any possible shortening in Tibet, this gives a north–south shortening rate of 48 ± 25 mm a^{-1}, not identical to but consistent with the 56.4 mm a^{-1} deduced by Cande and Pitman, particularly if a small amount of shortening is absorbed by strike-slip faulting in Tibet. East–west extension of about 10 ± 6 mm a^{-1} is occurring within the Himalayas resulting from the curvature of the thrust belt (Armijo *et al.* 1986) in which fault plane solutions indicate a fanning of the slip direction everywhere normal to the thrust front as it changes strike. The continuation of the north–south grabens from the Himalayas across Tibet and the absence of a strike-slip boundary than would take up any differential motion between Tibet and the Himalayas suggest that Tibet is extending east–west at the same 10 mm a^{-1} rate with a small amount of north–south shortening contributed by the strike-slip faults.

The rate of eastward extrusion resulting from east–west extension in Tibet and left-lateral slip on the Kunlun Faults (*ca.* 18 mm a^{-1}; Kidd & Molnar, this volume) and Altyn Tagh Fault, (30 ± 20 mm a^{-1}; Molnar *et al.* 1987*a*) is uncertain. It is not known whether slip on the Kunlun Faults results from the compatibility termination of east–west extension in Tibet, or is in addition to it. It seems unlikely that the rate exceeds 10 mm a^{-1} because there is no obvious right-lateral slip zone at the southern edge of the Tibetan Plateau.

8. The history and timing of shortening, uplift and extrusion

That southern Tibet was at, or near, sea-level with a normal thickness continental crust during the mid-Cretaceous is indicated by widespread shallow water Albian limestones (Hennig 1915; Norin 1946), such as the Lingbuzong (figure 10). In southern Tibet, Albian limestones are succeeded by the Cenomanian–Turonian Takena Formation, a mostly fine-grained molasse derived principally from the north. The Takena was folded during the Campanian to early Palaeocene interval, but prior to the eruption of the Linzizong volcanics (figure 10), synchronously with the development of the Gangdese calc-alkaline arc, the development of the Xigaze flysch accretionary prism and the deposition of shallow water carbonates on a continental shelf on the northern edge of the Indian sub-continent. The obduction of the Spongtang ophiolite onto the northern edges of India during the Maastrichtian/Danian interval (Searle *et al.* 1987) was post-dated in the Indus–Zangbo Suture by the Palaeocene accumulation of ophiolitic conglomerates and late melanges. Therefore, until at least the late Cretaceous, the Neotethyan oceanic tract was subducted northwards beneath the Gangdise arc in southern Tibet. Northward oceanic subduction probably persisted until at least 50 Ma (Linzizong Volcanics). The Zongpu and Zhepure carbonates of the Zanskai shelf of northern India unconformably overlie the Spontang Ophiolite. We believe that all these events and sequences predate the terminal collision of India with Eurasia. We visualize a compressive Andean-style (Dewey 1980) Gangdise arc on the southern edge of Tibet in which intra-arc compression thickened the crust of the southern Lhasa Terrane (England & Searle 1986) and led to the pre-Linzizong folding of the Takena Formation. The obduction of the Spontang ophiolite is seen, therefore, as unrelated to the India–Eurasia collision and like other giant ophiolite nappes such as the Ordovician Bay of Islands Complex

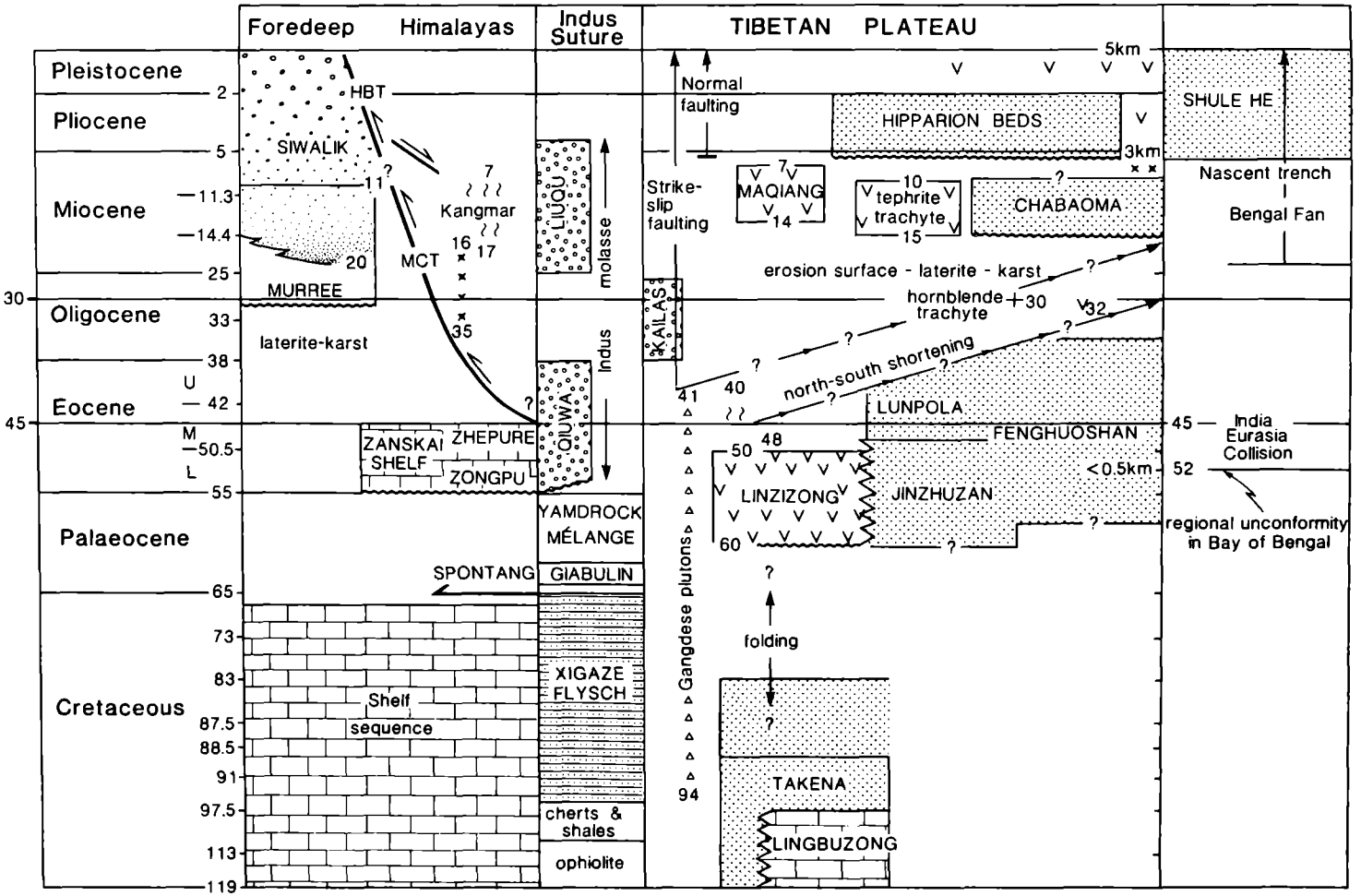

FIGURE 10. Simplified chronological chart for late Cretaceous to Present events in the Himalayas and Tibet. Triangles = calc-alkaline plutons, crosses = other plutons, V = volcanics, lazy S = metamorphism, bricks = marine carbonates, circles = coarse non-marine molasse, dots = non-marine clastics. Details from all papers in this volume; Allègre *et al.* 1984; Copeland *et al.* 1987; Le Fort 1975; Maluski *et al.* 1982; Searle *et al.* 1987; Xu, Schärer & Allègre 1985.

(Dewey & Bird 1971) was emplaced by the subduction of a rifted continental margin beneath the ophiolitic fore-arc of a primitive ensimatic arc. The obduction of the Spontang Ophiolite was part of a late Cretaceous obduction event that, although not precisely synchronous, occurred along the southern margin of Neotethys from Cyprus to India.

There is a widespread agreement that the collision of India with Eurasia occurred during the Eocene (e.g. Achache *et al.* 1983, 1984; Allègre *et al.* 1984; Burg & Chen 1984; Burg *et al.* 1983; Burke, Dewey & Kidd 1974; Klootwijk 1979; Molnar & Tapponnier 1975; Patriat & Achache 1984; Powell & Conaghan 1975; Sengör 1979; Tapponnier *et al.* 1981*a*). That the timing of the collision may be narrowed to the mid-Eocene at about 45 Ma is suggested by several lines of evidence.

First, relative plate motions deduced from finite difference studies using fracture zones and magnetic anomalies in the Atlantic and Indian Oceans indicate changes in the rate and direction of motion of India relative to Eurasia and changes in spreading rate in the Indian Ocean between Anomaly 22 (52 Ma) and Anomaly 20 (44.7 Ma) (McKenzie & Sclater 1971; Patriat & Achache 1984). The new detailed study by S. Cande and W. C. Pitman III (pers. comm.) of the motion of India relative to Eurasia, working the circuit from Eurasia to India through the spreading histories of the Atlantic and Indian Oceans, also shows a change in direction and rate of motion with a slowdown at about 52 Ma from 140 to 95 mm a^{-1}, a further slowdown to 71 mm a^{-1} and a sharp change in direction at about 45 Ma, and generally lower but roughly northward velocities since about 35 Ma combined with an anticlockwise rotation of 21°. We take the change of direction and slowdown at about 45 Ma as the approximate time during collision at which collisional buoyancy forces become sufficiently large to cause the beginning of 'indenter' tectonics (Molnar & Tapponnier 1975) and the beginning of collisional lithospheric thickening. This timing is supported by the cessation of the Gangdise magmatic arc between 50 and 41 Ma and the termination of the Zanskai carbonate shelf during the mid-Eocene (figure 10).

The kinematics, timing and amount of post-collisional north–south crustal shortening in Tibet is ill-defined and the subject of some disagreement among the authors of this paper. This is partly because there is little palaeontological control on the age of Palaeogene red-bed sequences, only the strongly deformed Fenghuoshan red-beds have yielded Eocene charophytes; we were unfortunately unable to examine much of the Palaeogene across the plateau. Also it is difficult or impossible to date, unequivocally, much of the deformation of the Mesozoic strata. There is, however, a clear contrast between virtually undeformed Neogene sequences and generally strongly deformed Palaeogene and older sequences. Flat-lying or gently dipping Lower Miocene and younger volcanics and sediments (Chabaoma, Majang, Hipparion beds) rest unconformably upon deformed older rocks, cut by a 30 Ma trachyte plug north of Erdaogou (Harris, Xu, Lewis, Hawkesworth & Zhang, this volume). The Neogene sequences mainly occupy faulted depressions or erosional hollows and form wide, flat, poorly exposed plains between gently undulating hill ranges that consist of older, more deformed, rocks. The widespread Tibetan erosion surface truncates pre-Neogene, but never Neogene, rocks and is believed to be Miocene in age (Shackleton & Chang, this volume; figure 10). Where Palaeogene red-bed sequences outcrop, they are folded and thrust. At Duba, Amdo and Erdaogou, red-beds occur in thrust-bounded ramp basins with both northward- and southward-directed thrusts. North–south shortening in the Fenghuo Shan ranges is a minimum of 50% and may be considerably more (Coward *et al.*, this volume). It is not considered likely that pre-

Miocene shortening is confined to areas of exposed Palaeogene and older rocks; shortened Palaeogene and older rocks probably lie beneath the Neogene basins because the basins close eastwards and westwards in places onto deformed Palaeogene rocks. Therefore we believe that an average figure of 50 % shortening is appropriate for the whole plateau, although it is clearly not homogeneously developed. Modelling suggests that the shortening and thickening of the Tibetan crust probably proceeded northwards from a pre-collisionally-thickened Gangdise crust (England & Searle 1986; England & Houseman 1988) rather than synchronously across the plateau. Evidence in support of this idea comes from Ulugh Muztagh (Molnar *et al.* 1987*b*) near the northern edge of the plateau. Here, an undeformed late Miocene two-mica granite intrudes a deformed basement overlain unconformably by undeformed Pliocene quartz sanidine tuffs, whereas just to the north, thrusting is extant suggesting a northward thrust migration.

In the authors' view, there is, as yet, no definitive evidence to determine the rate and timing of uplift of the Tibetan Plateau. However, several lines of evidence cumulatively suggest that the uplift was accomplished by at least two quite different mechanisms at different rates; a pre-Miocene uplift to about 3 km caused by northward-migrating crustal shortening and thickening and a very rapid Plio-Pleistocene uplift of some 2 km at an average rate of 0.4 mm a^{-1}. The second phase was accompanied by volcanism and east–west extension. Pedeplanation post-dated the pre-Miocene uplift and predated the Plio-Pleistocene uplift (Shackleton & Chang, this volume). First, floral evidence indicates evergreen broad-leaved forests growing in a hot and moist climate at less than 0.5 km during the Eocene (Li *et al.* 1981) succeeded by a later Eocene period of subdued low mean relief landscapes with sub-tropical grassland basins. By early Miocene times, broad-leaved evergreen forests had given way to coniferous alpine forests (Xu Ren 1981; Xu Shuying 1981). Miocene broad-leaved deciduous forests persisted into the early Pliocene (Axelrod 1981; Guo 1981; Song & Liu 1981). During the Pliocene, the Tibetan climate became rapidly drier, partly because of the increasing elevation of the Himalayas, with increasingly sparse deciduous vegetation (Xu Ren 1981; Xu Shuying 1981) culminating today in a plateau with an exceedingly sparse flora of diminutive plants. Second, coarse Pliocene to recent clastics (e.g. Shule He Formation, see figure 10) in basins around the plateau suggest fast late Tertiary–Quaternary uplift. Thirdly, terraces in the Kunlun and knickpoints in rivers at the edge of the plateau indicate fast recent uplift. Fourthly, fission track data in the Himalayas (Zeitler 1985) indicate a rapid acceleration of uplift rates during the last 5 Ma from about 0.2 mm a^{-1} to 0.9 mm a^{-1}; although uplift coupling between the Himalayas and Tibet cannot be proved, these high rates are too great to have resulted from thickening caused by crustal shortening and indicate a mechanism such as catastrophic lithospheric mantle thinning (England & Houseman 1988).

The time relationship between post-mid Eocene northward-migrating shortening in Tibet and southward-migrating thrusting in the Himalayas is not clear. The late Oligocene Murree sediments of the Indo–Gangetic foredeep are derived from the Indian Shield to the south, whereas the upwards-coarsening Siwalik sediments derived from the north began in the early Miocene (figure 10). Within the Himalayas, radiometric ages of structural, metamorphic and igneous events related to Tertiary–Quaternary shortening are mainly younger than 35 Ma (Le Fort 1975; Searle *et al.* 1987). Himalayan large rivers are antecedent from Tibet through the Himalayas (Seeber & Gornitz 1983; Wang, Shi & Zhou 1982) indicating that Tibet was a high area earlier than the Himalayas. Also, during the early Miocene, the Bengal Fan spread as a

coarsening upwards sequence of increasingly rapidly deposited sediments (Curray *et al.* 1980; Curray & Moore 1974; Cochran *et al.* 1987). Possibly the mid-Miocene development of a nascent trench in the Indian Ocean (Weissel, Anderson & Geller 1980) resulted from an increase in forces resisting the India–Asia convergence by collisional tightening in the Himalayas. We suggest that thrusting spread southwards in the Himalayas from early Miocene times as a consequence of the temporary 'blocking' of north-spreading deformation by the stronger lithosphere of the Tarim and Qaidam Basins. Thrusting and crustal thickening probably began in the northern Himalayas during late Eocene–Oligocene times (Maluski & Matte 1984), principally by the restacking of the thinned crust of the north Indian continental margin, the principal uplift of the Himalayas beginning in early Miocene times. However, the Gangdise belt underwent a phase of accelerating uplift during the early Miocene (Copeland *et al.* 1987, 1988), probably related to early Himalayan events, possibly to underthrusting of northern Himalayan basement beneath the Gangdise belt.

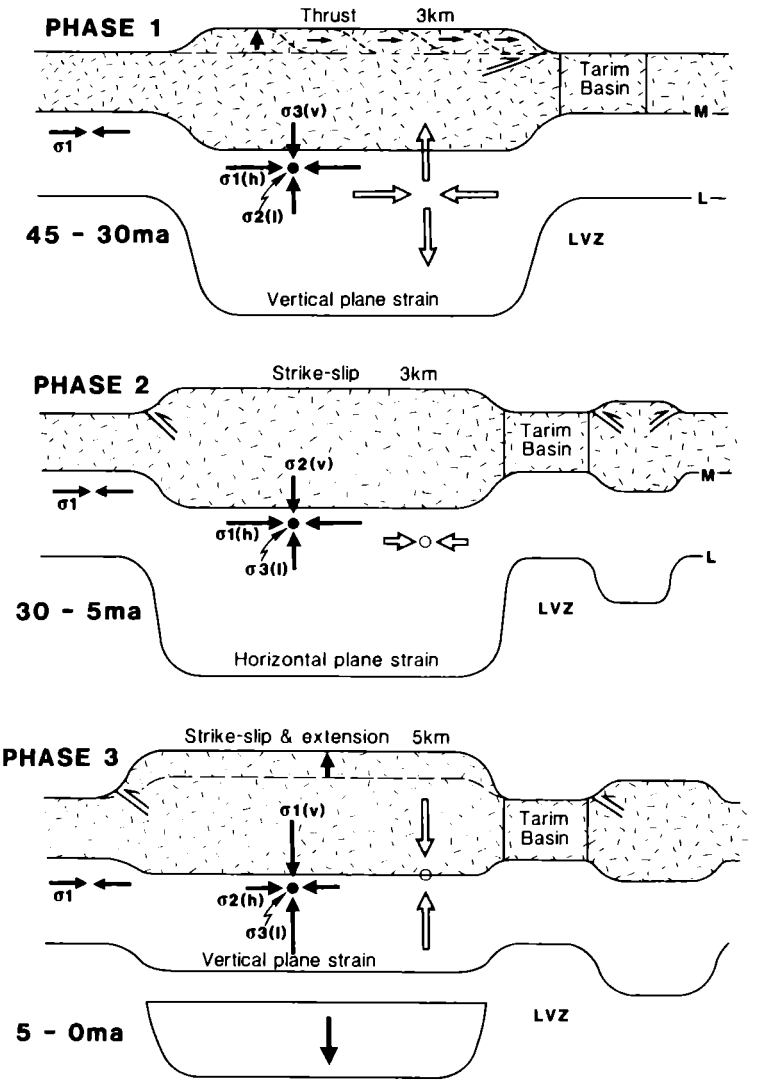

FIGURE 11. Three suggested phases of the Tertiary tectonic evolution of the Tibetan Plateau.

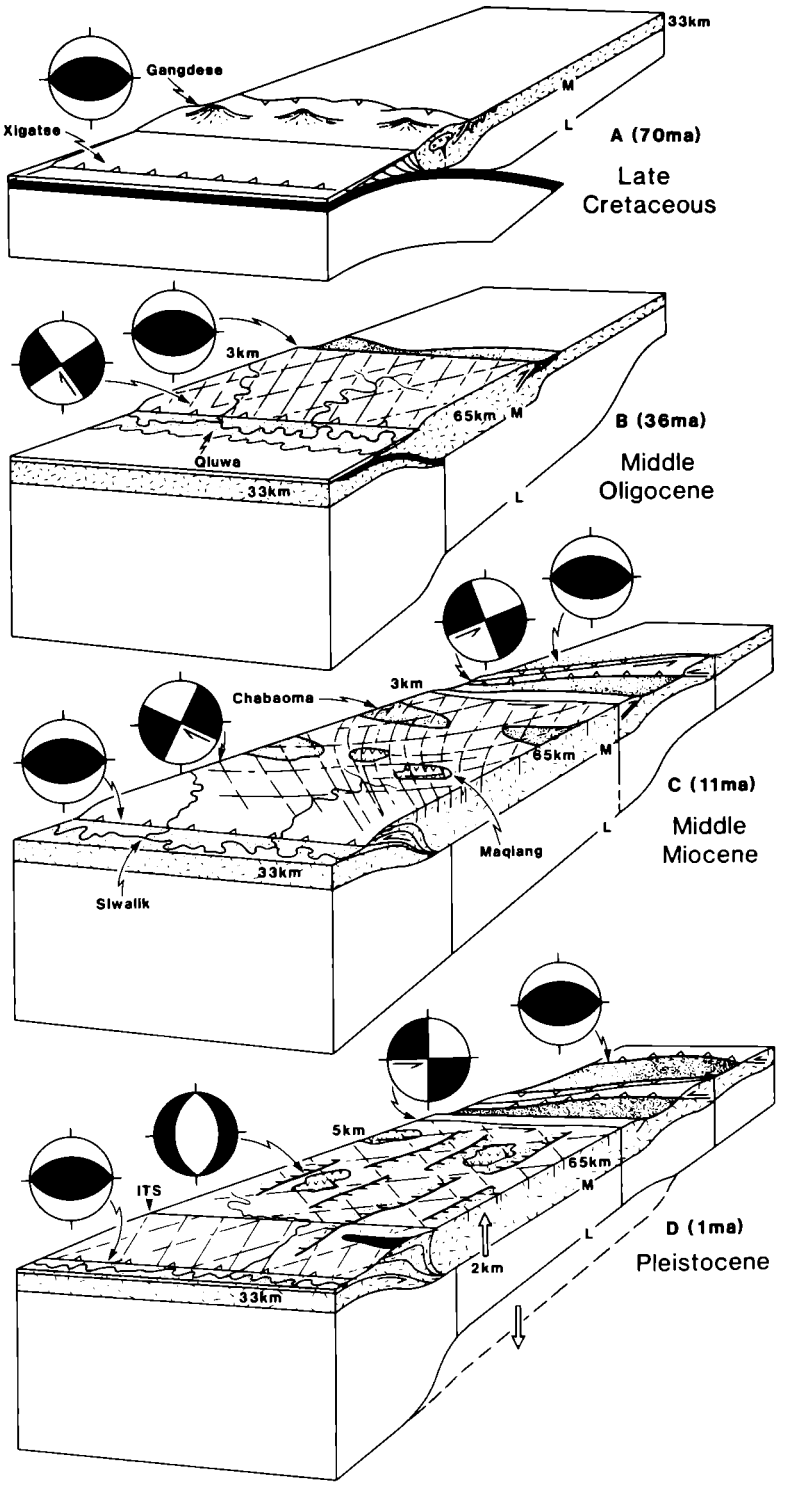

FIGURE 12. Schematic block diagrams illustrating suggested tectonic evolution of the Tibetan Plateau, the Himalayas, the Altyn Tagh and the Tarim Basin.

Lastly, we summarize our perception of the overall tectonic evolution of the Tibetan Plateau in the context of how finite displacements and strain in the India–Eurasia deforming zone since collision were partitioned in space and time, expressed as a tectonic facies sequence in figure 11 and as a series of four schematic block diagrams in figure 12. We wish to emphasize that this evolutionary model cannot be definitively substantiated but is more consistent than are other suggested models with geological and geophysical data currently available. From 45 to 30 Ma (mid-Eocene to late Oligocene) an India–Eurasia convergence of about 1000 km at an average rate of 66 mm a^{-1} was taken up in Tibet by a northward-propagating north–south crustal shortening and thickening and, in the northern Himalayas, by southward thrusting (Phase 1). Phase 1 was a plane strain, almost pure thrust, regime (figure 11, figure 12B) by the end of which the Tibetan crust between the Qaidam/Tarim Basins to the north and the Indus–Zangbo Suture to the south had doubled its thickness to about 65 km. As the crust/lithosphere progressively reached double thickness, thrusting ceased and a very slow north-south shortening was effected by strike-slip faulting. By about 30 Ma, shortening had reached, and was blocked by, the strong lithosphere of the Tarim and Qaidam Basins and, in Phase 2, spread southward to further develop the Himalayan thrust belt, and northwards into the Altyn Tagh and Tien Shan (figure 11, figure 12C). Phase 2 in Tibet was one of slow horizontal plane strain by strike-slip faulting, during which a very small amount of east–west extrusion occurred and the conjugate strike-slip fault system was shortened north–south to change the dihedral angle from acute to obtuse. In Phase 3, during the last 5 Ma (figure 11, figure 12D) north–south shortening has propagated into Asia north of the Tarim Basin and Tien Shan and southwards to involve more of the Indian subcontinent in the Himalayas. During Phases 2 and 3, some 1420 km of India–Eurasia convergence had been partitioned into about 440 km of shortening in the Himalayas and about 980 km north of Tibet. During Phase 3, a minimum of 50 km of eastward extrusion from Tibet is indicated by the 10 mm a^{-1} east–west extension; we do not believe that the total amount of extrusion during Phases 2 and 3 has exceeded 200 km, or about 15% of the east–west length of the Tibetan Plateau. Much of this 'extrusion' may have been taken up by thrusting in the Longmen Shan and we have not discovered, in Tibet, strains and displacements of the magnitude that would be needed to generate the huge amounts of eastward extrusion claimed by Tapponnier *et al.* (1982).

Phase 3 was a period of east–west extension across north–south grabens and of conjugate strike-slip faulting, when the Tibetan Plateau underwent an uplift of about 2 km (figure 11, figure 12D). Uplift was accompanied by volcanism and has been explained by the catastrophic delamination of the thickened lithospheric root beneath the Plateau (England & Houseman 1988). Late and rapid uplift, extension, bimodal magmatism, and post-orogenic minimum-melting granites superposed upon earlier phases of shortening, crustal thickening and prograde metamorphism is a feature common to many Palaeozoic and Cainozoic orogenic belts. It may be an important mechanism, generated by lithospheric delamination, by which orogenic zones weaken and extend, so as to return crustal thicknesses to normal without large amounts of denudation. In an extreme form, it may lead to total orogenic collapse and continental separation, a phenomenon pointed out by Wilson (1966) and inherent in the concept of the Wilson cycle of ocean opening and closing, where zones of crustal thickening in orogenic belts became weak zones susceptible to lithospheric extension (Dewey, in press).

References

Achache, J., Abtout, A. & Le Mouel, J. L. 1987 The downward continuation of Magsat Crustal Anomaly Field over Southeast Asia. *J. geophys. Res.* **92**, 11584–11596.

Achache, J., Courtillot, V. & Besse, J. 1983 Palaeomagnetic constraints on the late Cretaceous and Cenozoic tectonics of southeastern Asia. *Earth planet. Sci. Lett.* **63**, 123–136.

Achache, J., Courtillot, V. & Zhou Yaoxin 1984 Paleogeographic and tectonic evolution of southern Tibet since Middle Cretaceous time: new paleomagnetic data and synthesis. *J. geophys. Res.* **89**, 10311–10399.

Allègre, C. J. & 34 others, 1984 Structure and evolution of the Himalaya–Tibet orogenic belt. *Nature, Lond.* **307**, 17–22.

Anderson, E. M. 1948 *The Dynamics of Faulting*. Edinburgh: Oliver and Boyd.

Argand, E. 1924 La tectonique de l'Asie. *Proc 13th Int. Geol. Congr. Brussels* 1924. **7**, 171–372.

Armijo, R., Tapponnier, P., Mercier, J. L. & Han Tonglin 1982 A field study of Pleistocene rifts in Tibet. *Eos, Wash.* **63**, 1093.

Armijo, R, Tapponnier, P., Mercier, J. L. & Han Tonglin 1986 Quaternary extension in Southern Tibet: Field observations and tectonic implications. *J. geophys. Res.* **91**, 13803–13872.

Axelrod, D. I. 1981 Altitudes of Tertiary forests estimated from paleotemperature. *Geological and Ecological studies of Qinghai-Xizang Plateau* **1**, pp. 131–144. Beijing: Science Press.

Barazangi, M. & Ni, J. 1982 Velocities and propagation characteristics of Pn and Sn beneath the Himalayan arc and Tibetan Plateau: possible evidence for underthrusting of Indian continental lithosphere beneath Tibet. *Geology* **10**, 179–185.

Besse, J., Courtillot, V., Pozzi, J. P., Westphal, M. & Zhou Yaoxiu 1984 Palaeomagnetic estimates of crustal shortening in the Himalayan thrusts and Zangbo suture. *Nature, Lond.* **311**, 621–626.

Bingham, D. K. & Klootwijk, C. T. 1980 Palaeomagnetic constraints on Greater India's underthrusting of the Tibetan Plateau. *Nature, Lond.* **284**, 336–338.

Bird, P. 1978 Initiation of intracontinental subduction in the Himalayas. *J. geophys. Res.* **83**, 4975–4987.

Bird, P. & Toksoz, M. N. 1975 Structure and evolution of the Tibetan Plateau (abstract). *Eos, Wash.* **56**, 397.

Bird, P. & Toksoz, M. N. 1977 Strong attenuation of Rayleigh Waves in Tibet. *Nature, Lond.* **266**, 161–163.

Bird, P., Toksoz, M. N. & Sleep, N. H. 1975 Thermal and mechanical models of continent–continent convergence zones. *J. geophys. Res.* **80**, 4405–4416.

Brandon, C. & Romanowicz, B. 1986 A 'No-Lid' Zone in the central Chang–Tang Platform of Tibet: Evidence from Pure Path Phase Velocity Measurement of Long Period Rayleigh Waves. *J. geophys. Res.* **91**, 6547–6564.

Burchfiel, B. C. & Royden, L. H. 1985 North–south extension within the convergent Himalayan region. *Geology* **13**, 679–682.

Burg, J.-P. & Chen Guoming 1984 Tectonics and structural formation of southern Tibet, China. *Nature, Lond.* **311**, 219–223.

Burg, J.-P., Proust, F., Tapponnier, P. & Chen Guoming 1983 Deformation phases and tectonic evolution of the Lhasa Block (Southern Tibet, China). *Eclog. Geol. Helv.* **76**, 643–665.

Burke, K. C. A., Dewey, J. F. & Kidd, W. S. F. 1974 The Tibetan Plateau, its significance for tectonics and petrology. *Geol. Soc. Amer. Abstr. Programs* **6**, 1027–1028.

Carey, S. W. 1955 The orocline concept in geotectonics. *Royal Soc. Tasmania, Pap. Proc.* **89**, 255–288.

Chang Chengfa & Pan Yusheng 1981 A brief discussion on the tectonic evolution of the Qinghai-Xizang Plateau. *Geological and Ecological Studies of Qinghai-Xizang Plateau.* **1**, 1–18.

Chang Chengfa & Pan Yusheng 1984 The structure and evolution of the Qinghai-Xizang (Tibet) Plateau. *Academia Sinica Developments in Geoscience. Contribution to 27th International Geological Congress. 1984 Moscow.* Beijing: Science Press.

Chang Chengfa & Zheng Xilan 1973 Some tectonic features of the Mt. Jomo Lungma area, southern Tibet, China. *Sci. Sinica* **16**, 257–265.

Chang Chengfa & 26 others 1986 Preliminary conclusions of the Royal Society and Academia Sinica 1985 Geotraverse of Tibet. *Nature, Lond.* **323**, 501–507.

Chen Wanping & Molnar, P. 1975 Short period Rayleigh Wave dispersion across the Tibetan Plateau. *Bull. seismol. Soc. Amer.* **65**, 1051–1057.

Chen Wanping & Molnar, P. 1981 Constraints on the seismic wave velocity structure beneath the Tibetan Plateau and their tectonic implications. *J. geophys. Res.* **86**, 5937–5962.

Chen Wanping & Molnar, P. 1983 Focal depths of intracontinental and intraplate earthquakes and their implications for the thermal and mechanical properties of the lithosphere. *J. geophys. Res.* **88**, 4183–4214.

Chen Wanping, Nabalek, J. L., Fitch, T. J. & Molnar, P. 1981 An intermediate depth earthquake beneath Tibet: source characteristics of the event of September 14, 1976. *J. geophys. Res.* **86**, 2863–2876.

Choudhury, S. K. 1975 Gravity and crustal thickness in the Indo-Gangetic Plains and Himalayan region, India. *Geophys. Jl R. astr. Soc.* **40**, 441–452.

Chun, K. Y. & McEvilly, T. V. 1986 Crustal structure in Tibet: high seismic velocity in the lower crust. *J. geophys. Res.* **91**, 10405–10411.

Chun, K. Y. & Yoshii, T. 1977 Crustal structure of the Tibetan Plateau: a surface wave study by moving window analysis. *Bull. seismol. Soc. Amer.* **67**, 735–750.

Cochran, J. & 24 others. Leg 116 shipboard scientific party 1987 Collision in the Indian Ocean. *Nature, Lond.* **330**, 519–521.

Cohen, S. & Morgan, R. C. 1987 Propagating and quasi-static compressional straining in continental collisions. *Tectonophysics* **142**, 155–162.

Copeland, P., Harrison, T. M., Kidd, W. S. F., Xu Ronghua & Zhang Yuquan 1987 Rapid early Miocene uplift of southern Tibet. *Eos, Wash.* **68**, 432.

Copeland, P., Harrison, T. M., Kidd, W. S. F., Xu Ronghua & Zhang Yuquan 1988 Rapid early Miocene acceleration of uplift in the Gangdese Belt, Xizang (southern Tibet), and its bearing on accommodation mechanisms of the India-Asia collision. *Earth planet. Sci. Lett.* (in press).

Coulon, C., Maluski, H., Bollinger, C. & Wang, S. 1986 Mesozoic and Cenozoic volcanic rocks from central and southern Tibet $^{39}Ar/^{40}Ar$ dating, petrological characteristics and geodynamical significance. *Earth planet. Sci. Lett.* **79**, 281–302.

Coward, M. P. & Butler, R. W. H. 1985 Thrust tectonics and the deep structure of the Pakistan Himalayas. *Geology* **13**, 417–420.

Cox, K. 1980 A model for flood basalt vulcanism. *J. Petr.* **21**, 629–650.

Curray, J. R., Emmel, F. M., Moore, D. G. & Raitt, R. W. 1980 Structure, tectonics, and geological history of the northeastern Indian Ocean. In *The Ocean Basins and margins.* **6**, The Indian Ocean (ed. Nairn, A. E. M. & Stehli, F. G.). New York: Plenum Press.

Curray, J. R. & Moore, D. G. 1974 Sedimentary and tectonic processes in the Bengal deep-sea fan and geosyncline. In *The Geology of Continental Margins* (ed. C. A. Burk & C. L. Drake), pp. 617–628. New York: Springer-Verlag.

Dasgupta, S., Mukhopadhyay, M. & Nandy, D. R. 1987 Active transverse features in the central plateau of the Himalaya. *Tectonophysics* **136**, 255–264.

Deng Wanming 1978 A preliminary study on the petrology and petrochemistry of the Quaternary volcanic rocks of Northern Tibet Autonomous region. *Acta Geol. Sin. Eng. Ed.* **52**, 148–152.

Dewey, J. F. 1980 Episodicity, sequence and style at convergent plate boundaries. In *The Continental Crust and its Mineral Deposits* (ed. D. W. Strangway), Geol. Assoc. Can. Spec. Paper **20**, 553–573.

Dewey, J. F. (in press). Lithospheric stress, deformation, and tectonic cycles: the disruption of Pangaea and the closure of Tethys. In: *Gondwana and Tethys* (ed. M. G. Audley-Charles & A. Hallam). Oxford University Press.

Dewey, J. F. & Bird, J. M. 1970 Mountain belts and the new global tectonics. *J. geophys. Res.* **75**, 2625–2647.

Dewey, J. F. & Bird, J. M. 1971 The origin and emplacement of the ophiolite suite: Appalachian ophiolites in Newfoundland. *J. geophys. Res.* **76**, 3179–3206.

Dewey, J. F. & Burke, K. C. A. 1973 Tibetan, Variscan and Precambrian basement reactivation: products of a continental collision. *J. Geol.* **81**, 683–692.

England, P. C. & Houseman, G. A. 1985 The influence of lithospheric strength heterogeneities on the tectonics of Tibet and surrounding regions. *Nature, Lond.* **315**, 297–301.

England, P. C. & Houseman, G. A. 1986 Finite strain calculations of continental deformation. II: Application to the India-Asia plate collision. *J. geophys. Res.* **91**, 3664–3676.

England, P. C. & Houseman, G. A. 1988 The mechanics of the Tibetan Plateau. *Phil. Trans. R. Soc. Lond.* A (in press).

England, P. C. & McKenzie, D. P. 1982 A thin viscous sheet model for continental deformation. *Geophys. Jl R. astr. Soc.* **70**, 295–321.

England, P. C. & McKenzie, D. P. 1983 A thin viscous sheet model for continental deformation. *Geophys. Jl R. astr. Soc.* **70**, 295–321, 1982. (Correction to: A thin viscous sheet model for continental deformation, *Geophys. Jl R. astr. Soc.* **73**, 523–532, 1983).

England, P. C. & Searle, M. P. 1986 The Cretaceous-Tertiary deformation of the Lhasa Block and its implications for the crustal thickening of Tibet. *Tectonics* **5**, 1–14.

Francheteau, J. & 7 others 1984 High heat-flow in southern Tibet. *Nature, Lond.* **307**, 32–36.

Girardeau, J., Marcoux, J., Allègre, C. J., Bassoullet, J. P., Tang Youking, Xiao Xuchang, Zao Yougong & Wang Xibin 1984 Tectonic environment and geodynamic significance of the Neo-Cimmerian Dongqiao ophiolite, Banggong-Nujiang suture zone, Tibet. *Nature, Lond.* **307**, 27–31.

Guo Shuoangxing 1981 On the elevation and climatic changes of the Qinghai-Xizang Plateau based on fossil angiosperms. In *Geological and Ecological studies of Qinghai-Xizang Plateau.* **1**, 201–206. Beijing: Science Press.

Gupta, H. K. & Narain, H. 1967 Crustal structure in the Himalayan and Tibet Plateau region from surface wave dispersion. *Bull. seism. Soc. Amer.* **57**, 235–248.

Hennig, A. 1915 Zur Petrographie und Geologie von Sudwest Tibet. In *Southern Tibet* **5**. Kung Boktryckeriet, P. A. Stockholm: Norstedt. (220 pp).

Hildreth, W. & Moorbath, S. E. (in press). Crustal contributions to arc magmatism in the Andes of Central Chile. *Contr. Miner. Petr.*

Hills, E. S. 1956 A contribution to the Morphotectonics of Australia. *J. Geol. Soc. Austral.* **3**, 1–15.

Hirn, A. & 7 others 1984*a* Lhasa Block and bordering sutures – a continuation of 500-km Moho traverse through Tibet. *Nature, Lond.* **307**, 25–27.

Hirn, A. & 11 others 1984*b* Crustal structure and variability of the Himalayan border of Tibet. *Nature, Lond.* **307**, 23–25.

Hirn, A., Jobert, G., Wittlinger, G. Xu Xiongshao & Guo Enyuan 1984*c* Main features of the upper lithosphere in the unit between the high Himalayas and the Yarlung Zangbo suture. *Ann. Geophysicae* **2**, 113–117.

Holmes, A. 1965 *Principles of Physical Geology.* London: Nelson. 2nd edn. 1288pp.

Houseman, G. & England, P. 1986 Finite strain calculations of continental deformation. I: Method and general results for convergent zones. *J. geophys. Res.* **91**, 3651–3663.

Houseman, G. A., McKenzie, D. P. & Molnar, P. 1981 Convective instability of a thickened boundary layer and its relevance for the thermal evolution of continental convergent belts. *J. geophys. Res.* **86**, 6115–6135.

Jaupart, C., Francheteau, J. & Shen Xianjie 1985 On the thermal structure of the southern Tibetan crust. *Geophys. Jl R. astr. Soc.* **81**, 131–155.

Jobert, N., Journet, B., Jobert, G., Hirn, A. & Sun Kezhong 1985 Deep structure of southern Tibet inferred from the dispersion of Rayleigh waves through a long-period seismic network. *Nature, Lond.* **313**, 386–388.

Khramov, A. N., Petrova, G. N. & Pechersky, D. M. 1981 Paleomagnetism of the Soviet Union. In: *Paleoreconstruction of the Continents.* (ed. M. W. McElhinny & D. A. Valencio). Am. Geophys. Union, Geodynamics Series. **2**, 177–194.

Kidd, W. S. F. 1975 Widespread late Neogene and Quaternary alkaline vulcanism on the Tibetan Plateau (abstract). *Eos, Wash.* **56**, 453.

Klootwijk, C. T. 1979 A summary of palaeomagnetic data from eastern-peninsular Indo-Pakistan and south-central Asia: implications for collision tectonics. In *Structural Geology of the Himalaya* (ed. P. S. Salklani), pp. 307–360.

Klootwijk, C. T., Conaghan, P. J. & Powell, C. McA. 1985 The Himalayan Arc: large-scale continent subduction, oroclinal bending and back-arc spreading. *Earth planet. Sci. Lett.* **75**, 167–183.

Klootwijk, C. T. & Pierce, J. W. 1979 India's and Australia's pole path since the late Mesozoic and the India–Asia collision. *Nature, Lond.* **282**, 605–607.

Klootwijk, C. T., Sharma, M. D., Gergan, J., Tirkey, B., Shah, S. K. & Agarwal, V. 1979 The extent of Greater India. II. Palaeomagnetic data from the Ladakh intrusives at Kargil, Northwestern Himalayas. *Earth planet. Sci. Lett.* **44**, 47–67.

Le Fort, P. 1975 Himalayas: the collided ranges. Present knowledge of the continental arc. *Am. J. Sci.* **275A**, 1–44.

Li Chunyu, Liu Xueya, Wang Quan & Zhang Zhimeng 1979 A tentative contribution to plate tectonics of China. *Institute of Geology, Chinese Acad. Geol. Sci.* [mimeographed handout].

Li Jijun, Li Bingyuan, Wang Fubao, Zhang Qingsong, Wen Shixuan & Zheng Benxing 1981 The process of the uplift of the Qinghai-Xizang Plateau. In: *Geological and Ecological studies of Qinghai-Xizang Plateau.* **1**, 111–118. Beijing: Science Press.

Lyon-Caen, H. 1986 Comparison of the upper mantle shear wave velocity structure of the Indian Shield and the Tibetan Plateau and tectonic implications. *Geophys. Jl R. astr. Soc.* **86**, 727–749.

Lyon-Caen, H. & Molnar, P. 1983 Constraints on the structure of the Himalaya from an analysis of gravity anomalies and a flexural model of the lithosphere. *J. geophys. Res.* **88**, 8171–8191.

Lyon-Caen, H. & Molnar, P. 1984 Gravity anomalies and the structure of western Tibet and the southern Tarim Basin. *Geophys. Res. Lett.* **11**, 1251–1254.

Lyon-Caen, H. & Molnar, P. 1985 Gravity anomalies, flexure of the Indian plate, and the structure, support and evolution of the Himalaya and Ganga Basin. *Tectonics* **4**, 513–538.

Maluski, H. & Matte, P. 1984 Ages of Alpine tectonometamorphic events in the north western Himalayas by $^{39}Ar/^{40}Ar$ method. *Tectonics* **3**, 1–18.

Maluski, H., Proust, F. & Xiao, X. C. 1982 $^{39}Ar/^{40}Ar$ dating of the trans-Himalayan calc-alkaline magmatism of southern Tibet. *Nature, Lond.* **298**, 152–154.

Matthews, D. & Hirn, A. 1984 Crustal thickening in Himalayas and Caledonides. *Nature, Lond.* **308**, 497–498.

McKenzie, D. P. 1984 A possible mechanism for epeirogenic uplift. *Nature, Lond.* **307**, 616–618.

McKenzie, D. P. & Sclater, J. G. 1971 The evolution of the Indian Ocean since the late Cretaceous. *Geophys. Jl R. astr. Soc.* **24**, 437–528.

Min, Z. & Wu, F. T. 1987 Nature of the upper crust beneath Tibet. *Earth planet. Sci. Lett.* **84**, 204–210.

Molnar, P., Burchfiel, B. C., Liang K'uangyi & Zhao Ziyun 1987*a* Geomorphic evidence for active faulting in the Altyn Tagh and northern Tibet and qualitative estimates of its contribution to the convergence of India and Eurasia. *Geology* **15**, 249–253.

Molnar, P., Burchfiel, B. C., Zhao Ziyun, Liang K'uangyi, Wang Shuji & Huang Minmin 1987*b* Geological evolution of Northern Tibet: results of an expedition to Ulugh Muztagh. *Science, Wash.* **235**, 299–305.

Molnar, P. & Chen Wanping 1978 Evidence of large Cenozoic crustal shortening of Asia. *Nature, Lond.* **273**, 218–220.

Molnar, P. & Chen Wanping 1983 Focal depths and fault plane solutions of earthquakes under the Tibetan Plateau. *J. geophys. Res.* **88**, 1180–196.

Molnar, P. & Deng Quidong 1984 Faulting associated with large earthquakes and the average rate of deformation in central and eastern Asia. *J. geophys. Res.* **89**, 6203–6228.

Molnar, P. & Lyon-Caen, H. (in press) Some simple physical aspects of the support, structure and evolution of mountain belts. *Geol. Soc. Amer. Spec. Pap.*

Molnar, P. & Tapponnier, P. 1975 Cenozoic tectonics of Asia: effects of a continental collision. *Science, Wash.* **189**, 419–426.

Molnar, P. & Tapponnier, P. 1977 Relation of the tectonics of eastern China to the India–Eurasia collision: application of slip-line field theory to large-scale continental tectonics. *Geology* **5**, 212–216.

Molnar, P. & Tapponnier, P. 1978 Active tectonics of Tibet. *J. geophys. Res.* **83**, 5361–5375.

Nelson, M. R., McCaffrey, R. & Molnar, P. 1987 Source parameters for 11 earthquakes in the Tien Shan, Central Asia, determined by P And SH waveform inversion. *J. geophys. Res.* **92**, 12629–12648.

Ni, J. & Barazangi, M. 1983 High-frequency seismic wave propagation beneath the Indian Shield, Himalayan arc, Tibetan Plateau, and surrounding regions: high uppermost mantle velocities and efficient Sn propagation beneath Tibet. *Geophys. Jl R. astr. Soc.* **72**, 665–689.

Ni, J. & Barazangi, M. 1984 Seismotectonics of the Himalayan collision zone: geometry of the underthrusting Indian Plate beneath the Himalaya. *J. geophys. Res.* **89**, 1147–1163.

Ni, J. & York, J. E. 1978 Late Cenozoic extensional tectonics of the Tibetan Plateau. *J. geophys. Res.* **83**, 5377–5387.

Norin, E. 1946 Geological Explorations in Western Tibet. Reports of the Scientific Expedition to the Northwestern Provinces of China under the leadership of Dr. Sven Hedin, *Publ. 29* (III), *Geology* **7**, Tryckeri Aktiebolaget, Thule, Stockholm.

Patriat, P. & Achache, J. 1984 The chronology of the India-Eurasia collision. Implications for crustal shortening and the driving mechanism of plates. *Nature, Lond.* **311**, 615–621.

Pines, I., Teng, T. L., Rosenthal, R. & Alexander, S. 1980 A surface-wave dispersion study of the crustal and upper mantle structure of China. *J. geophys. Res.* **85**, 3829–3844.

Powell, C. M. 1986 Continental underplating model for the rise of the Tibetan Plateau. *Earth planet. Sci. Lett.* **81**, 79–94.

Powell, C. M. & Conaghan, P. J. 1973 Plate tectonics and the Himalayas. *Earth planet. Sci. Lett.* **20**, 1–12.

Powell, C. M. & Conaghan, P. J. 1975 Tectonic models of the Tibetan Plateau. *Geology* **3**, 727–731.

Pozzi, J.-P., Westphal, M., Zhou Yaoxiu, Xing Lishen & Chen Xianyao 1982 Position of the Lhasa Block, South Tibet, during the late Cretaceous. *Nature, Lond.* **297**, 319–321.

Romanowicz, B. A. 1982 Constraints on the structure of the Tibet Plateau from pure path phase velocities of Love and Rayleigh waves. *J. geophys. Res.* **87**, 6865–6883.

Rothery, D. A. & Drury, S. A. 1984 The neotectonics of the Tibetan Plateau. *Tectonics* **3**, 19–26.

Ruzaikeri, A. I., Nersesov, I. L. & Khaltevin, V. I. 1977 Propagation of Lg and lateral variations in crustal structure in Asia. *J. geophys. Res.* **82**, 307–316.

Scotese, C. R., Bambach, R. K., Barton, C., van der Voo, R. & Ziegler, A. M. 1979 Palaeozoic Base Maps. *J. Geol.* **87**, 217–277.

Searle, M. P. & 10 others 1987 The closing of Tethys and the tectonics of the Himalayas. *Bull. geol. Soc. Amer.* **98**, 678–701.

Seeber, L. & Gornitz, V. 1983 River profiles along the Himalayan arc as indicators of active tectonics. *Tectonophysics* **92**, 335–367.

Sengör, A. M. C. 1979 Mid-Mesozoic closure of Permo-Triassic Tethys and its implications. *Nature, Lond.* **279**, 590–593.

Shackleton, R. M. 1981 Structure of Southern Tibet: report on a traverse from Lhasa to Khatmandu organised by Academia Sinica. *J. Struct. Geol.* **3**, 97–105.

Shaw, P. & Orcutt, J. 1984 Propagation of PL and implications for the structure of Tibet. *J. geophys. Res.* **89**, 3135–3152.

Song Zhichen & Liu Gengwu 1981 Tertiary palynological assemblages from Xizang with reference to their paleogeographical significance. In *Geological and Ecological studies of Qinghai-Xizang Plateau.* **1**, 207–214. Beijing: Science Press.

Tapponnier, P. & 29 others 1981*a* The Tibetan side of the India-Eurasia collision. *Nature, Lond.* **294**, 405–410.

Tapponnier, P., Mercier, J. L., Armijo, R., Han Tonglin & Zhou J. 1981*b* Field evidence for active normal faulting in Tibet. *Nature, Lond.* **294**, 410–414.

Tapponnier, P. & Molnar, P. 1976 Slip-line field theory and large-scale tectonics. *Nature, Lond.* **264**, 319–324.

Tapponnier, P. & Molnar, P. 1977 Active faulting and tectonics in China. *J. geophys. Res.* **82**, 2095–2930.

Tapponnier, P., Peltzer, G., Le Dain, A. Y., Armijo, R. & Cobbold, P. 1982 Propagating extrusion tectonics in Asia: new insight from simple experiments with plasticine. *Geology* **10**, 611–616.

Teng Jiwen 1980 Characteristics of geophysical field and continental plate tectonics of the Qinghai-Xizang plateau and its neighbouring regions. In: *Proceedings of Symposium on Qinghai-Xizang (Tibet) Plateau* (abstracts), pp. 76–77. Beijing: Academia Sinica.

Teng Jiwen & 18 others 1981 Explosion seismological study for velocity distribution and structure of the crust and upper mantle from Damxung to Yadong of the Xizang plateau. In: *Geological and Ecological Studies of Qinghai-Xizang Plateau.* 691–709. Beijing: Science Press.

Teng Jiwen, Sun Kezhong, Xiong Shaobai, Yin Zhouxun, Yao Hung & Chen Lifang 1983 Deep seismic reflection waves and structure of the crust from Damxung to Yadong on the Xizang Plateau (Tibet). *Phys. Earth Planet. Int.* **31**, 293–306.

Van Ngoc Pham, Boyer, D., Therme, P., Xue Chengyuan, Li Li & Guo Yuanjin 1986 Partial melting zones in the crust in southern Tibet from magnetotelluric results. *Nature, Lond.* **319**, 310–314.

Vilotte, J. P., Daignières, M. & Madariaga, R. 1982 Numerical models of intraplate deformation: simple mechanical models of continental collision. *J. geophys. Res.* **87**, 10709–10728.

Vilotte, J. P., Daignières, M., Madariaga, R. & Zienkiewicz, O. C. 1984 The role of a heterogeneous inclusion during continental collision. *Phys. Earth Planet. Inter.* **36**, 236–259.

Vilotte, J. P., Madariaga, R., Daignières, M. & Zienkiewicz, O. C. 1986 Numerical study of continental collision: Influence of buoyancy forces and an initial stiff inclusion. *Geophys. Jl R. astr. Soc.* **84**, 279–310.

Wang, C. Y., Shi, Y. & Zhou, W. 1982 Dynamic uplift of the Himalaya. *Nature, Lond.* **298**, 553–556.

Watson, M. P., Hayward, A. B., Parkinson, D. N. & Zhang Zhouming 1987 Plate tectonic history, basic development and petroleum source rock deposition of onshore China. *J. mar. petr. Geol.* **4**, 205–225.

Weissel, J. K., Anderson, R. N. & Geller, C. A. 1980 Deformation of the Indo-Australian Plate. *Nature, Lond.* **287**, 284–291.

Westphal, M., Pozzi, J.-P., Zhou Yaoxiu, Xing Lisheng & Chen Xianyao 1983 Palaeomagnetic data about southern Tibet (Xizang) – I. The Cretaceous formations of the Lhasa Block. *Geophys. Jl R. astr. Soc.* **73**, 507–521.

Wilson, J. T. 1966 Did the Atlantic close and then re-open. *Nature, Lond.* **211**, 676–681.

Xu Ren 1981 Vegetational changes in the past and uplift of Qinghai-Xizang plateau. In *Geological and Ecological studies of Qinghai-Xizang Plateau.* **1**, 139–144. Beijing: Science Press.

Xu Shuying 1981 The evolution of the palaeogeographic environments in the Tanggula Mountains in the Pliocene-Quaternary. In *Geological and Ecological studies of Qinghai-Xizang Plateau.* **1**, 247–255. Beijing: Science Press.

Xu Ronghua, Schärer, U. & Allègre, C. J. 1985 Magmatism and metamorphism in the Lhasa Block (Tibet): a geochronological study. *J. Geol.* **93**, 41–57.

Zeitler, P. K. 1985 Cooling history of the NW Himalaya. *Tectonics* **4**, 127–151.

Zhang Shanzhen & He Yuanliang 1985 Late Palaeozoic palaeophytogeographic provinces in China and their relationships with plate tectonics. *Palaeontologica Cathayana* **2**, 77–86.

Zhang Zhouming, Liou J. G. & Coleman, R. G. 1984 An outline of the plate tectonics of China. *Bull. geol. Soc. Amer.* **95**, 295–312.

Zhao Wuling & Morgan, W. J. 1987 Injection of Indian crust into Tibetan lower crust: a two-dimensional finite element model study. *Tectonics* **6**, 489–504.

Zhou Wenhu, Yang Zhanshou, Zhu Hongbin & Wu Ligao 1981 Characteristics of the gravity field and the crustal structure in the eastern and central regions of the Xizang plateau. In *Geological and Ecological Studies of Qinghai-Xizang Plateau.* 673–682. Beijing: Science Press.

Maps

Geological map of the Qinghai-Xizang (Tibet) Plateau (1:1.5 M) 1980 Ministry of Geology & Natural Resources, Beijing.

Geological map of Qinghai Province (1:1 M) 1981 Qinghai Bureau of Geology & Mineral Resources, Xining.

Tectonic map of Asia (1:8 M) 1982 Research Inst. Geol., Chinese Acad. Geol. Sciences, Beijing. Cartographic Publishing House.

GEOLOGICAL MAP OF THE GEOTRAVERSE ROUTE

Relating to the paper by W.S.F. Kidd,
Pan Yusheng, Chang Chengfa, M.P. Coward, J.F. Dewey, F.R.S.,
A. Gansser, P. Molnar, R.M. Shackleton, F.R.S., and Sun Yiyin

Phil. Trans. R. Soc. Lond., volume 327

(Single-sided copies of these maps are available rolled in tubes from the Royal Society for £13.50 per pair in the U.K.; £19.00 per pair overseas.)

GEOLOGICAL MAP OF THE ACADEMIA SINICA–ROYAL SOCIETY GEOTRAVERSE ROUTE ACROSS THE XIZANG–QINGHAI (TIBETAN) PLATEAU

SOUTH SHEET – LHASA TO TANGGULA PASS

89 90 91 92 93

33 32 31 30 29

Tanggula Shan
Tanggula Pass 5200
TUMENGLA
Qixiang Co
Banggong Suture
Zarlar Zangbo
LUNPOLA
Xagor Co
Xiaqlong Co
Qiling Co (Zilling Tso)
DONGQIAO
Zige Tang Co
JK 4561
Co Nag 4588
NYAINRONG
XAGQUKA
Dunqagi Co
Pangkog Co
Dung Co
Daru Co
Kyiru Co
Jang Co
Pung Co
4522
Co Ngoin
NAGQU
Nag Qu (Nu Jiang River)
Nevi Pun Co
Bong Co
ZHAJUN GUNBAR
Bam Co 4555
GYANCO
BAINGOIN
XIONGMEI
DUBA
Gomang Co
Mujo Co
Yongzhu Zangbo
Zenco Gongma
Jeozu Co
Sen Co
SANGXUNG
GULU
NAMCO
Nam Co (Tengri-nor)
4718
Nyaindentanglha Shan
DEQEN
Bo Qu
DAMXUNG
Dam Qu
Zezhen
Zangbo River
NYINZHONG
JURULUNG
PANGDUO
QIBULUNG
YANGBAJAIN
QUESANG
Duilung Qu
LHUNZHUB FARM
PENGPO FARM
MAIZHOKUNGGAR
MAQU
GANDEN
LHASA
DOILUNGDEQEN
DAGZE
Gangdese Shan
DAZHUKE (ferry)
NYÊMO
QUXU
Yarlung Zangbo River
SAMYE
XIGAZE
Nyan Qu
RINBUNG
GONGGAR (Airport) 3572
Kamba-la 4720
Yangbajain Geothermal Field
Indus–Zangbo Suture
LHAZANG

geological contact
fault, age unspecified; normal or reverse or strike-slip displacement shown by ticks or triangles or half-arrows
fault; probable late Neogene or Quaternary movement; normal, or reverse, or strike-slip displacement
buried fault; (thrust margin of Qaidam basin) probable late Neogene – early Quaternary (but not Recent) displacement
lineament, mostly stratification: some faults/fractures
main road, arrow at pass
dirt road/track
dominantly volcanic rocks where ornament shown
■ KAIXINGLING settlement or highway depot
. 7162 elevation (metres)
latitude/longitude 1° intersections
hot spring
river; lake
boundary of ice field

0 25 50 75 100 kilometres
1 : 500,000

Compiled by W. S. F. Kidd; from field data of Geotraverse participants compiled by J. F. Dewey as field sheets during Geotraverse; interpretation of LANDSAT orbital images, supplemented in places by Shuttle large-format camera and Spacelab metric camera orbital images; Geological map of the Qinghai-Xizang Plateau, 1:1.5 m. (1980); Geological map of Qinghai, 1:1 m. (1985); Carte géologique du sud du Tibet, 1:1/2 m. CNRS (1983). See Kidd, Chang, Coward, Dewey, Gansser, Molnar, Shackleton, Sun (1988) – Geological mapping (this volume) for more details. For cross-sections, see Coward et. al. (this volume).

Base map from Defence Mapping Agency Operational Navigation Charts G-8 (ed. 3) and H-10 (ed. 7), modified with detail from orbital imagery and 1:100,000 topographic maps. Lambert conformal conic projection.

Geotraverse Participants; Chang Chengfa*, Chen Nansheng, M. P. Coward, Deng Wanming, J. F. Dewey, F.R.S.*+, A. Gansser, N. B. W. Harris, Jin Chengwei, W. S. F. Kidd, M. R. Leeder, Li Huan, Lin Jinlu, Liu Chenglie, Mei Houjun, P. Molnar, Pan Yun, Pan Yusheng, J. A. Pearce, R. M. Shackleton, F.R.S.*, A. B. Smith, Sun Yiyin, D. R. Watts, Xu Juntao, Xu Ronghua, Yin Jixiang+, Zhang Yuquan

*Expedition leader, +deputy leader

GEOLOGICAL MAP OF THE ACADEMIA SINICA–ROYAL SOCIETY GEOTRAVERSE ROUTE ACROSS THE XIZANG–QINGHAI (TIBETAN) PLATEAU

NORTH SHEET – TANGGULA PASS TO GOLMUD

0 25 50 75 100 kilometres

1 : 500,000

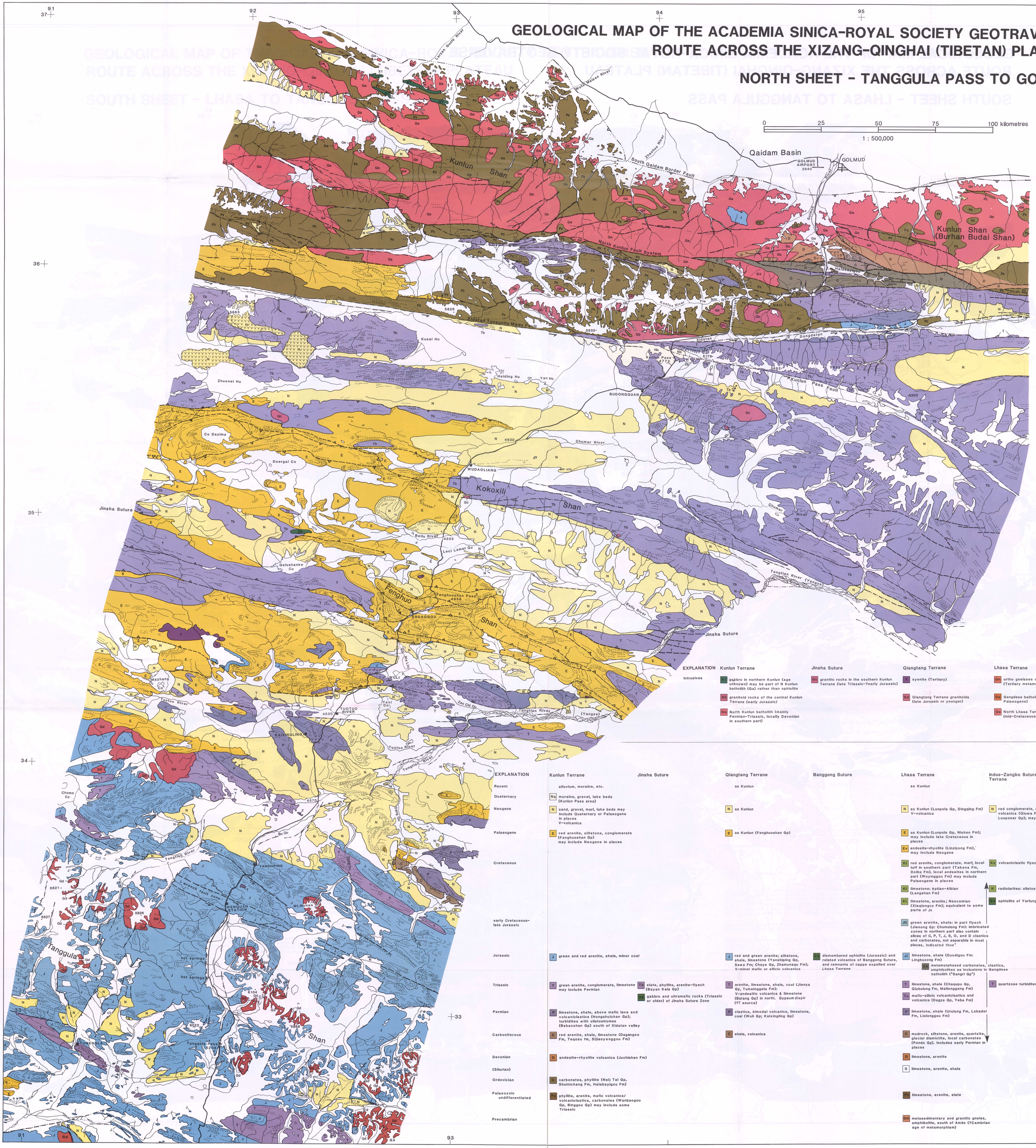

EXPLANATION

Intrusives

Kunlun Terrane

- Xi gabbro in northern Kunlun (age unknown) may be part of N Kunlun batholith (Ga) rather than ophiolite
- Gb granitoid rocks of the central Kunlun Terrane (early Jurassic)
- Ga North Kunlun batholith (mainly Permian–Triassic, locally Devonian in southern part)

Jinsha Suture

- Gc granitic rocks in the southern Kunlun Terrane (late Triassic–?early Jurassic)

Qiangtang Terrane

- Y syenite (Tertiary)
- Gd Qiangtang Terrane granitoids (late Jurassic or younger)

Lhasa Terrane

- Gn ortho gneisses of Nyainqentanglha (Tertiary metamorphism)
- Gg Gangdese batholith (late Cretaceous–Palaeogene)
- Ge North Lhasa Terrane granitoids (mid-Cretaceous)

EXPLANATION	Kunlun Terrane	Jinsha Suture	Qiangtang Terrane	Banggong Suture	Lhasa Terrane	Indus–Zangbo Suture and Himalayan Terrane
Recent	alluvium, moraine, etc.		as Kunlun		as Kunlun	
Quaternary	Nq moraine, gravel, lake beds (Kunlun Pass area)					
Neogene	N sand, gravel, mari, lake beds may include Quaternary or Palaeogene in places V–volcanics		N as Kunlun		N as Kunlun (Lunpola Gp, Dingqing Fm) V–volcanics	N red conglomerate, arenite, local volcanics (Qiuwa Fm; Liuqu Fm; Luoposar Gp); may include Oligocene
Palaeogene	E red arenite, siltstone, conglomerate (Fenghuoshan Gp) may include Neogene in places		E as Kunlun (Fenghuoshan Gp)		E as Kunlun (Lunpola Gp, Niubao Fm); may include late Cretaceous in places Ev andesite–rhyolite (Linzizong Fm), may include Neogene	
Cretaceous					Kt red arenite, conglomerate, marl; local tuff in southern part (Takena Fm, Doiba Fm), local andesites in northern part (Woynggou Fm) may include Palaeogene in places Kl limestone: Aptian–Albian (Langshan Fm) Ki limestone, arenite; Neocomian (Xiaqiongco Fm); equivalent to some parts of Jk	Ks volcaniclastic flysch (Xigaze Gp) K radiolarites: olistostromal shales Ko ophiolite of Yarlung Zangbo suture
early Cretaceous–late Jurassic					JK green arenite, shale: in part flysch (Jienong Gp; Chumulong Fm): imbricated zones in northern part also contain slices of C, P, T, J, S, O, and D clastics and carbonates, not separable in most places, indicated thus*	
Jurassic	J green and red arenite, shale, minor coal		J red and green arenite; siltstone, shale, limestone (Yanshiping Gp, Sewa Fm; Chaya Gp, Zhamunaqu Fm); V–minor mafic or silicic volcanics	Js dismembered ophiolite (Jurassic) and related volcanics of Banggong Suture, and remnants of nappe expelled over Lhasa Terrane	Jl limestone, shale (Duodigou Fm: Lingbuzong Fm) GM metamorphosed carbonates, clastics, amphibolites as inclusions in Gangdese batholith ("Sangri Gp")	
Triassic	T green arenite, conglomerate, limestone may include Permian	Tb slate, phyllite, arenite–flysch (Bayan Kala Gp) Xc gabbro and ultramafic rocks (Triassic or older) of Jinsha Suture Zone	T arenite, limestone, shale, coal (Jienza Gp, Tumaingqela Fm): V–andesitic volcanics & limestone (Batang Gp) in north. Gypsum diapir (?T source)		T limestone, shale (Chaqupu Gp, Qiubulung Fm, Mailonggang Fm) Tv mafic–silicic volcaniclastics and volcanics (Dagze Gp, Yeba Fm)	T quartzose turbidites and mudrocks
Permian	P limestone, shale, above mafic lava and volcaniclastics (Hongshuichan Gp); turbidites with olistostromes (Babaoshan Gp) south of Xidatan valley		P clastics, bimodal volcanics, limestone, coal (Wuli Gp; Kaixingling Gp)		P limestone, shale (Urulung Fm, Lobadoi Fm, Lielonggou Fm)	
Carboniferous	C red arenite, shale, limestone (Dagangou Fm, Teqosu fm, Sijiaoyanggou Fm)		C shale, volcanics		C mudrock, siltstone, arenite, quartzite, glacial diamictite, local carbonates (Pondo Gp). Includes early Permian in places	
Devonian	D andesite–rhyolite volcanics (Juchishan Fm)				D limestone, arenite	
(Silurian)					S limestone, arenite, shale	
Ordovician	O carbonates, phyllite (Naij Tal Gp, Shuinichang Fm, Halabayigou Fm)					
Palaeozoic undifferentiated	PZ phyllite, arenite, mafic volcanics/ volcaniclastics, carbonates (Wanbaogou Gp, Binggou Gp) may include some Triassic				PZ limestone, arenite, slate	
Precambrian					Gm metasedimentary and granitic gneiss, amphibolite, south of Amdo (?Cambrian age of metamorphism)	